Aghabi, Dana Ossama Nasief (2026) *Stealing metals like a pro(tozoan): ironing out metal acquisition and host manipulation in Toxoplasma gondii*. PhD thesis.

https://theses.gla.ac.uk/85811/

Copyright and moral rights for this work are retained by the author

A copy can be downloaded for personal non-commercial research or study, without prior permission or charge

This work cannot be reproduced or quoted extensively from without first obtaining permission from the author

The content must not be changed in any way or sold commercially in any format or medium without the formal permission of the author

When referring to this work, full bibliographic details including the author, title, awarding institution and date of the thesis must be given

Enlighten: Theses
https://theses.gla.ac.uk/
research-enlighten@glasgow.ac.uk



Stealing metals like a pro(tozoan): Ironing out metal acquisition and host manipulation in *Toxoplasma gondii*

By

Dana Ossama Nasief Aghabi
B.Sc. (Hons), M. Res.

Submitted in fulfilment of the requirements for the Degree of Doctor of Philosophy

School of Life Sciences
College of Medical, Veterinary & Life Sciences
Institute of Infection & Immunity
University of Glasgow

November 2025

Abstract

Transition metals, including iron and zinc, are indispensable metals for almost all life. They play essential roles as cofactors for enzymes involved in a range of biological processes, including DNA replication and metabolism. *Toxoplasma gondii* is a ubiquitous obligate intracellular apicomplexan parasite which requires iron and zinc for survival. However, in excess, these metals are toxic. Thus, *T. gondii* has to regulate the uptake of iron and zinc to maintain homeostasis and avoid metal toxicity. Many organisms acquire divalent metals, including iron and zinc, from the environment through an evolutionary conserved family of proteins; Zrt/Irt-like (ZIP) proteins. At the start of my PhD, the mechanisms by which *T. gondii* acquired these essential metals was not known. The main focus of this work is on the functional characterisation of TGME49_261720, one of the four ZIP-domain containing proteins predicted to be encoded by the *T. gondii* genome, which we called ZFT (Zn and Fe transporter).

In this thesis, I demonstrate that ZFT localises to the plasma membrane of the parasite and is essential for the replication of *T. gondii*. I found that the localisation and expression of ZFT is dynamic and dependent on iron and vacuolar-stage. I show that overexpression of ZFT leads to a growth defect, and parasites become hypersensitive to excess iron and zinc although protected from iron chelation. I demonstrate that loss of growth upon ZFT knockdown cannot be rescued by either excess iron or zinc, suggesting that ZFT's function is not redundant in the parasite. Loss of ZFT leads to altered morphology of the apicoplast - although function is maintained - and inhibits mitochondrial respiration, linked to decreased expression of the mitochondrial Fe-S cluster protein SDHB and activity of complex IV of the mitochondrial electron transport chain. ZFT knockdown triggers the partial differentiation of parasites to a more quiescent lifecycle stage. Importantly, I demonstrate that the expression of TgZFT in a yeast model complements the loss of zinc transporter activity, supporting the role of ZFT as a zinc transporter in *T. gondii*. Finally, I show that knocking down ZFT results in a decrease in parasite-associated iron and zinc, confirming ZFT transporter activity in *Toxoplasma gondii*.

However, as an intracellular pathogen, *Toxoplasma* acquires iron from its host cell. At the start of my PhD, little was known about the mechanisms by which *T. gondii* infection impacts host cell iron homeostasis. Thus, the second aim of my PhD project was to start to understand if and how *T. gondii* manipulates host cell iron homeostasis and trafficking by examining proteins involved in iron homeostasis in the host cell, in the context of infection.

Here, I found changes in expression of proteins involved in host iron acquisition (TfR and DMT1) upon infection in both human fibroblasts and murine macrophages, although no changes in iron storage (FTH1) were observed. I show that infected fibroblasts and macrophages take up significantly more transferrin following *T. gondii* infection. However, whether these changes are host- or parasite-driven is not yet known, and further work is required to elucidate this. In high iron conditions, I show that DMT1 expression levels are maintained in both cell types compared to uninfected/untreated. TfR expression levels are maintained in fibroblasts but are reduced in macrophages, suggesting differences in iron homeostasis between the two cell types. Finally, I demonstrate that the *T. gondii zft* 3' UTR confers iron responsiveness in fibroblasts but not in macrophages, further suggesting differences in iron handling between the two cell types.

Overall, I have characterised the first iron and zinc uptake transporter in *Toxoplasma gondii*, identifying the major pathway for the acquisition of these metals by the parasite. Moreover, I demonstrated that infection with *T. gondii* leads to changes in the expression of iron-related proteins in fibroblasts and macrophages. This work emphasises the importance of both iron and zinc to *Toxoplasma gondii* and for their ability to survive and persist within the host.

Table of contents

Abstract ..... **ii**

Table of contents ..... **iv**

List of tables ..... **xii**

List of figures ..... **xiii**

Figure copyright permissions ..... **xviii**

Acknowledgements ..... **xix**

Publications arising from this work ..... **xxi**

Conference proceedings ..... **xxi**

Author's declaration ..... **xxii**

Abbreviations ..... **xxiii**

Chapter 1 Introduction **26**

1.1 Chapter aims 27

1.2 The biology and importance of *Toxoplasma gondii* 28

1.2.1 The apicomplexan phylum and *Toxoplasma gondii* 28

1.2.2 Human and animal health impact of apicomplexan parasites 28

1.2.3 History of *Toxoplasma gondii* 30

1.2.4 Global prevalence and transmission of *Toxoplasma gondii* 31

1.2.5 Life cycle of *Toxoplasma gondii* 32

1.2.5.1 Sexual replication in the definitive host 34

1.2.5.2 Environmental stage 34

1.2.5.3 Asexual lytic cycle in the intermediate host 35

1.2.5.4 The switch from tachyzoites to bradyzoites, and the stresses that trigger differentiation 36

1.2.6 Pathogenesis and clinical features of toxoplasmosis 38

1.2.6.1 Toxoplasmosis in immunocompetent individuals 39

1.2.6.2 Toxoplasmosis in immunocompromised individuals 39

1.2.6.3 Toxoplasmosis in pregnant women 40

1.2.6.4 Clonal isolates and worldwide distribution 40

1.2.6.5 Impact of toxoplasmosis on animal health and the economy 41

1.2.6.6 Current treatments of toxoplasmosis 42

1.2.7 Importance of nutrient acquisition from the host for *Toxoplasma gondii* survival 43

1.2.8 Genetic manipulation of *Toxoplasma gondii* parasites 45
1.2.8.1 *Toxoplasma gondii* as a model organism 45
1.2.8.2 The genome of *Toxoplasma gondii* 45
1.2.8.3 Reverse genetics 46
1.2.8.4 Gene knockdown (Tetracycline-inducible system) 49
1.3 Transition metals and their importance in eukaryotic biology 51
1.3.1 Iron is essential for life 51
1.3.2 Zinc is essential for life 52
1.3.3 Metal toxicity 53
1.3.4 The role of transporters in metal uptake 54
1.3.4.1 Transport mechanisms 54
1.4 Zrt/Irt-like proteins (ZIPs): Their role in the transfer of divalent metals across biological membranes 57
1.4.1.1 Function and characteristics of ZIP proteins 57
1.4.1.2 ZIP family 57
1.4.1.3 Structure of ZIP proteins 58
1.4.1.4 Metal binding of ZIPs 60
1.4.1.5 Transport mechanism of ZIP proteins: Two-domain elevator-type mechanism 63
1.4.1.6 Substrate specificity of ZIP proteins 66
1.4.1.7 Dimerisation of ZIP proteins 67
1.4.1.8 Extracellular domain (ECD) of ZIPs 68
1.4.1.9 Regulation of ZIPs 69
1.4.1.10 ZIPs in yeast (*Saccharomyces cerevisiae)* 70
1.4.1.11 ZIPs in plants (*Arabidopsis thaliana*) 71
1.4.1.12 ZIPs in bacteria cells 72
1.4.1.13 ZIPs in mammalian cells 72
1.4.1.14 The role of ZIPs in protozoan parasites 75
1.4.1.15 Uncharacterised ZIP-domain containing proteins in *Toxoplasma gondii* 77
1.5 Transition metals and *Toxoplasma gondii* 78
1.5.1 Importance of iron in *Toxoplasma gondii* 78
1.5.2 Iron in haem biosynthesis in *Toxoplasma gondii* 79
1.5.3 Iron-sulphur (Fe-S) cluster biogenesis in *Toxoplasma gondii* 79
1.5.4 Organelles important for iron regulation and homeostasis in *Toxoplasma gondii* 80
1.5.4.1 Apicoplast 80
1.5.4.2 Mitochondria 83

1.5.4.3 Plant-like vacuolar compartment (PLVAC) 84
1.5.5 Role of zinc in *Toxoplasma gondii* 85
1.5.6 Chelation of transition metals 87
1.6 The battle for iron between host and pathogen 88
1.6.1 Macrophages: An overview 88
1.6.2 What is nutritional immunity? 89
1.6.3 Maintaining iron homeostasis: Iron uptake, storage, and trafficking in mammalian cells 90
1.6.3.1 Uptake of transferrin and non-transferrin bound iron 90
1.6.3.2 Divalent metal transporter 1 (DMT1) 91
1.6.3.3 The role of ferritin in iron storage 92
1.6.3.4 Ferroportin and iron export 93
1.6.4 Macrophages and iron sequestration during infection 95
1.6.5 Strategies employed by microbes to subvert macrophage iron sequestration to facilitate intracellular survival 96
1.6.5.1 Bacterial host iron manipulation 96
1.6.5.2 Protozoan parasite host iron manipulation 96
1.6.6 Antimicrobial strategies employed by macrophages in toxoplasmosis ... 98
1.6.7 Known strategies employed by *Toxoplasma gondii* to manipulate host iron stores 100
1.7 Thesis aims, significance and broader impact 102
Chapter 2 Materials and methods 103
2.1 Materials 104
2.1.1 Equipment 104
2.1.2 Software 105
2.1.3 Antibodies 106
2.1.3.1 Primary antibodies 106
2.1.3.2 Secondary antibodies 107
2.1.4 Kits 108
2.1.5 Buffers, media, and solutions 108
2.1.5.1 Bacteria 108
2.1.5.2 Yeast 109
2.1.5.3 Mammalian and *T. gondii* cell culture 109
2.1.5.4 DNA 110
2.1.5.5 Protein 111
2.1.6 Biological and chemical consumables 112
2.1.7 Drugs/agents 114

2.1.8 Oligonucleotide sequences 115
2.1.9 Plasmids 117
2.2 Cell biology 118
2.2.1 Cell strains 118
2.2.1.1 Mammalian and bacterial strains 118
2.2.1.2 *Toxoplasma gondii* strains 118
2.2.1.3 Yeast strains 119
2.2.2 Mammalian cell culture 119
2.2.2.1 Human foreskin fibroblasts (HFFs) 119
2.2.2.2 RAW 264.7 murine macrophages 119
2.2.2.3 RAW 264.7 murine macrophages cryopreservation and thawing of stabilates 120
2.2.3 *Toxoplasma gondii* cell culture 120
2.2.3.1 Mechanical release and filtering of intracellular parasites 120
2.2.3.2 *T. gondii* transfection and selection 120
2.2.3.3 Isolation of clonal *T. gondii* cell lines 121
2.2.3.4 *T. gondii* strain construction 121
2.2.3.5 Pre-treatment of HFFs before infection with *T. gondii* 123
2.2.3.6 Inducing the knockdown of ZFT 123
2.2.3.7 *T. gondii* cryopreservation and thawing of stabilates 123
2.3 Molecular biology 125
2.3.1 Polymerase chain reaction (PCR) 125
2.3.2 Agarose gel electrophoresis (AGE) 126
2.3.3 Restriction endonuclease digests 126
2.3.4 DNA Purification 126
2.3.5 Generation of chemically competent *E. coli* 127
2.3.6 Gibson assembly 127
2.3.7 Plasmid transformations into *E. coli* bacteria 128
2.3.8 Bacterial colony screening by PCR 128
2.3.9 Isolation of plasmid DNA from *E. coli* bacteria 128
2.3.10 DNA sequencing 129
2.3.11 Cryopreservation of transformed *E. coli* 129
2.3.12 Genomic DNA extraction from *Toxoplasma gondii* 129
2.3.13 Reverse transcriptase quantitative PCR (RT-qPCR) 130
2.4 Phenotypic characterisation 131
2.4.1 Immunofluorescence assay (IFA) 131
2.4.1.1 Intracellular *T. gondii* IFA 131
2.4.1.2 Extracellular *T. gondii* IFA 131

2.4.1.3 RAW MΦ IFA 132
2.4.1.4 Quantitative analysis of immunofluorescence assays 132
2.4.2 Plaque assay 133
2.4.3 Fluorescent growth assay 133
2.4.4 Seahorse assay 134
2.4.5 Flow cytometry 135
2.4.6 Luciferase assay 135
2.5 Protein biology 137
2.5.1 Sodium dodecyl sulphate polyacrylamide gel electrophoresis (SDS-PAGE) 137
2.5.2 Protein stability assay 137
2.5.3 Blue-native polyacrylamide gel electrophoresis (BN-PAGE) 138
2.5.4 Complex IV in gel oxidation assay 139
2.6 Microscopy 140
2.6.1 Light microscopy 140
2.6.2 Transmission electron microscopy (TEM) 140
2.6.3 Live cell microscopy 140
2.6.3.1 Ferro-orange dye 140
2.6.3.2 FluoZin™-3AM 141
2.7 Elemental analysis techniques 142
2.7.1 Inductively coupled plasma mass spectrometry (ICP-MS) 142
2.7.2 X-ray fluorescence microscopy (XFM) 143
2.8 Yeast 144
2.8.1 Generation of codon optimised sequences and cloning into yeast expression vector pDR195 144
2.8.2 Yeast transformations and selection 144
2.8.3 Drop test assay 145
2.9 Statistical analysis 146
Chapter 3 ZFT is the major iron and zinc transporter in *T. gondii* 147
3.1 Introduction and chapter aims 148
3.2 Iron transport in *Toxoplasma gondii* 149
3.3 ZFT localisation is dynamic and vacuolar stage dependent in F3ΔHX ZFT-3HA$_{sag1}$ 152
3.4 ZFT expression is regulated by the availability of iron in F3ΔHX ZFT-3HA$_{sag1}$ 155

3.5 ZFT localisation is dynamic and vacuolar stage dependent in F3ΔHX ZFT-3HA$_{zft}$ 158

3.6 ZFT expression is regulated by the availability of iron in F3ΔHX ZFT-3HA$_{zft}$. 164

3.7 ZFT protein stability is not altered under low iron conditions following cycloheximide treatment 168

3.8 Introducing a second copy of ZFT to overexpress: cell line validation 170

3.9 Overexpressing ZFT leads to a change in iron sensitivity 174

3.10 Generating a conditional knockdown of ZFT: T7S4-ZFT cell line validation .. 180

3.11 ZFT is essential for *T. gondii* survival 181

3.12 Tagging ZFT in the conditional knockdown T7S4-ZFT background: T7S4-ZFT3-HA$_{sag1}$ cell line validation 185

3.13 ZFT forms a complex under native conditions 189

3.14 ZFT knockdown alters apicoplast morphology and parasite replication, however function is maintained 190

3.15 ZFT knockdown alters mitochondrial organellar function 194

3.16 ZFT knockdown reduces expression of mitochondrial Fe-S cluster protein SDHB 195

3.17 ZFT knockdown reduces mitochondrial respiration at 48 h 199

3.18 ZFT knockdown triggers partial parasite differentiation 203

3.19 ZFT knockdown cannot be rescued by excess zinc 209

3.20 Parasites overexpressing ZFT are hypersensitive to excess zinc 213

3.21 ZFT expression depends on the availability of zinc 214

3.22 ZFT expression complements the lack of zinc transport in *S. cerevisiae* 217

3.23 ZFT knockdown leads to a decrease in parasite associated iron and zinc 220

3.24 Distribution of host iron and zinc is altered upon ZFT knockdown 231

3.25 Deletion of the Iron Responsive Element (IRE) in the 3' UTR of *zft* alters the responsiveness of ZFT to both iron and zinc availability at the protein level 233

3.26 Discussion and Summary 237

3.26.1 ZFT protein kinetics and substrate specificity 237

3.26.2 Unusual dynamic localisation of ZFT has not previously been reported in *T. gondii* 239

3.26.3 *zft* 3' UTR plays a critical role in ZFT expression under different iron conditions 241
3.26.4 Is ZFT being degraded and is the protein stabilised? 241
3.26.5 Overexpressing ZFT alters protein localisation and protein properties . 242
3.26.6 Parasites overexpressing ZFT are more sensitive to metal overload 244
3.26.7 ZFT is essential for the survival of *Toxoplasma gondii* as it cannot be rescued by the presence of exogenous substrate 245
3.26.8 Is iron critical for ZFT protein dimerisation in *Toxoplasma*? 248
3.26.9 ZFT knockdown triggers parasite differentiation, but is this an iron specific response or a general stress-induced one? 249
3.26.10 Absence of ZFT alters both mitochondrial and apicoplast organellar function in *T. gondii* 250
3.26.11 What is the role of zinc in *T. gondii* and how do the parasites respond to zinc starvation? 252
3.26.12 Yeast complementation experiments strongly support that ZFT is a zinc transporter in *Toxoplasma gondii*, but what about iron? 253
3.26.13 The limitations of ICP-MS and XFM as elemental analysis techniques in *Toxoplasma gondii* 254
3.26.14 Final summary and concluding remarks 256

Chapter 4 The battle for iron between the host and the bug: How *Toxoplasma gondii* modulates host iron homeostasis following infection ... 258

4.1 Introduction and chapter aims 259
4.2 *Toxoplasma gondii* modulates host iron homeostasis in fibroblast cells 260
4.2.1 Transferrin receptor is upregulated in *T. gondii* infected HFFs 260
4.2.2 DMT1 is upregulated in *T. gondii* infected HFFs 264
4.2.3 Ferritin heavy chain 1 (FTH1) expression is unaltered in *T. gondii* infected HFFs 269
4.3 *T. gondii* modulates host iron homeostasis in murine macrophage cells 272
4.3.1 Transferrin receptor expression is induced in *T. gondii* infected macrophages 272
4.3.2 DMT1 expression is induced in *T. gondii* infected macrophages 278
4.3.3 FTH1 expression in macrophages does not increase following infection, however, increases in excess iron conditions 281
4.3.4 The *zft* 3' UTR confers iron responsiveness in fibroblasts, but not in macrophages 284
4.4 Discussion and summary 286

4.4.1 Transferrin receptor expression is modulated following *T. gondii* infection in both fibroblasts and macrophages 286
4.4.2 DMT1 expression is modified in both fibroblasts and macrophages upon infection with *T. gondii* 290
4.4.3 Iron storage is not modulated in *T. gondii* infected host cells 295
4.4.4 What about iron export to maintain homeostasis? 297
4.4.5 The role of the *zft* 3' UTR in iron responsiveness is dependent on cell type 298
4.4.6 How is iron internalised at the parasitophorous vacuolar membrane (PVM)? 298
4.4.7 Limitations of the study 299
4.4.8 Final summary and concluding remarks 301

Chapter 5 Final discussion, summary, and future outlooks 307

References 310

List of tables

Table 2-1 - A list of equipment used in this study. 104
Table 2-2 - A list of software used in this study.....105
Table 2-3 - A list of primary antibodies used in this study. 106
Table 2-4 - A list of secondary antibodies used in this study. 107
Table 2-5 - A list of kits used in this study.....108
Table 2-6 - A list of buffers, media and solutions used for bacterial work in this study.....108
Table 2-7 - A list of buffers, media and solutions used for yeast work in this study. 109
Table 2-8 - A list of buffers, media and solutions used for mammalian and *T. gondii* cell culture work in this study.....110
Table 2-9 - A list of buffers and solutions used for DNA work in this study. 110
Table 2-10 - A list of buffers and solutions used for protein work in this study. 111
Table 2-11 - A list of biological and chemical consumables used in this study...113
Table 2-12 - A list of drugs and agents used in this study. 114
Table 2-13 - A list of the gRNA sequences used in this study. 115
Table 2-14 - List of primer sequences used in this study. 116
Table 2-15 - A list of plasmids either used or generated in this study. 117
Table 2-16 - A list of mammalian and bacterial strains used in this study. 118
Table 2-17 - A list of *Toxoplasma gondii* strains used in this study. 118
Table 2-18 - A list of yeast strains used in this study. 119
Table 2-19 - A list of freezing solution components used for *T. gondii* cryopreservation. 123
Table 2-20 - A list of PCR mixture components. 125
Table 2-21- PCR thermocycler conditions programme.....125
Table 2-22 – Components of BN-Page anode and cathode solutions. 138
Table 2-23- A list of yeast transformation mix components used in this study. .145
Table 3-1 - Table summarising known features including length, predicted localisation, phenotype score, TM domains, and ZIP domain E-values of the four predicted ZIP-domain containing proteins encoded by the *Toxoplasma* genome. 150

List of figures

Chapter 1

Figure 1.1 - The complex life cycle of *Toxoplasma gondii*. 33
Figure 1.2 - Lytic life cycle of *Toxoplasma gondii*. 36
Figure 1.3 - Tetracycline inducible knockdown system. 50
Figure 1.4 - Schematic of membrane topology of ZIP proteins. 60
Figure 1.5 - The binuclear metal centre in the transport pathway in BbZIP. 62
Figure 1.6 - Two-domain elevator-type transport mechanism of BpZIP. 64
Figure 1.7 - The proposed mechanism of zinc sensing and regulation by BpZIP via His149 and His151. 65
Figure 1.8 – Cellular localisation of Zrt/Irt-like (ZIP) transporter family proteins in mammalian cells. 74
Figure 1.9 - Summary of mammalian cellular iron homeostasis. 94
Figure 1.10 - Strategies employed by IFN-γ cytokine to eliminate *Toxoplasma gondii* in macrophages. 99

Chapter 3

Figure 3.1 - TgZFT protein alignment and predicted protein structure. 151
Figure 3.2 - F3ΔHX ZFT-3HA$_{sag1}$ strain construction and validation. 152
Figure 3.3 - ZFT localisation in the F3ΔHX ZFT-3HA$_{sag1}$ line is dynamic and dependent on vacuolar stage. 153
Figure 3.4 - ZFT-3HA$_{sag1}$ localisation is dynamic and dependent on vacuolar stage, localising basally in larger vacuoles. 154
Figure 3.5 - F3ΔHX ZFT-3HA$_{sag1}$ expression is reduced under low iron conditions. 156
Figure 3.6 - F3ΔHX ZFT-3HA$_{sag1}$ expression does not change under high iron conditions. 157
Figure 3.7 - F3ΔHX ZFT-3HA$_{zft}$ strain construction and validation. 159
Figure 3.8 - ZFT localisation in the F3ΔHX ZFT-3HA$_{zft}$ parasites is dynamic and dependent on vacuolar stage. 160
Figure 3.9 - ZFT-3HA$_{zft}$ lower bands are still detected post treatment with MG132 for 5 h, suggesting that the lower bands are nonspecific. 161

Figure 3.10 - ZFT peripheral localisation is significantly reduced in 4 and 8 parasite stage vacuoles at a high MOI compared to a low MOI. 163
Figure 3.11 - F3ΔHX ZFT-3HA$_{zft}$ expression is reduced under low iron conditions at 24 h but stabilised at 18 h. 165
Figure 3.12 - F3ΔHX ZFT-3HA$_{zft}$ expression is significantly reduced at 24 h compared to untreated but stabilised at 18 h. 167
Figure 3.13 - ZFT3HA$_{zft}$ protein stability is not altered post cycloheximide (CHX) treatment under high and low iron conditions. 169
Figure 3.14 - RHtdTomato pTUB8 ZFT-Ty DHFR strain construction and validation 171
Figure 3.15 - ZFT-Ty localisation is peripheral and also dispersed throughout the parasite 24 h post infection, with some puncta visible at the basal end when imaged with a super resolution microscope. 172
Figure 3.16 - ZFT-Ty localisation is more punctate and less dispersed throughout the parasite at 6 h compared to 24 h. 173
Figure 3.17 - Parasites overexpressing ZFT form fewer and smaller plaques compared to parental parasites. 174
Figure 3.18 - Parasites overexpressing ZFT are not more sensitive to excess iron compared to parental parasites by plaque assay. 176
Figure 3.19 - Overexpressing ZFT leads to a change in iron sensitivity. 178
Figure 3.20 - Overexpressing ZFT does not alter the parasite's sensitivity to oxidative stress. 179
Figure 3.21 - T7S4-ZFT strain construction and validation. 180
Figure 3.22 - Knockdown of ZFT blocks parasite replication. 181
Figure 3.23 - Excess iron does not rescue the growth defect observed upon ZFT knockdown. 183
Figure 3.24 - Excess iron and half the standard concentration of ATc is unable to rescue growth of ZFT knockdown parasites. 184
Figure 3.25 - T7S4-ZFT-3HA$_{sag1}$ strain construction and validation. 185
Figure 3.26 - Replacing the endogenous ZFT promoter with the T7S4 inducible promoter results in a significant overexpression of ZFT. 186
Figure 3.27 - ZFT-3HA$_{sag1}$ and ZFT-3HA$_{zft}$ expression levels at 24 h. 187
Figure 3.28 - Validation of ZFT knockdown in the F3ΔHX T7S4-ZFT-3HA$_{sag1}$ line by western blotting and immunofluorescence. 188

Figure 3.29 – T7S4-ZFT-3HA*sag1* forms a complex under native conditions. 189
Figure 3.30 - ZFT knockdown does not alter apicoplast morphology at 24 h and 48 h. 191
Figure 3.31 - ZFT knockdown parasites maintain apicoplast function at 48 h...192
Figure 3.32 – Parasites exhibit a delayed apicoplast phenotype following ZFT knockdown by altering apicoplast morphology and parasite replication. 193
Figure 3.33 - ZFT knockdown parasites show no changes in mitochondrial morphology. 194
Figure 3.34 Fe-S cluster protein SDHB expression is significantly reduced in ZFT knockdown parasites. 196
Figure 3.35 - Cytosolic Fe-S cluster protein ABCE1 expression levels remain unchanged following ZFT knockdown. 197
Figure 3.36 - ZFT knockdown parasites have reduced complex IV activity.....198
Figure 3.37 - ZFT knockdown does not alter mitochondrial respiration at 24 h.200
Figure 3.38 - ZFT knockdown reduces mitochondrial respiration at 48 h. 201
Figure 3.39 - ZFT knockdown does not affect mitochondrial cristae formation.202
Figure 3.40 - ZFT knockdown parasites exhibit asynchronous replication and large disorganised vacuoles. 205
Figure 3.41 - ZFT depletion increases expression of bradyzoite specific marker BAG1 and DBL, a lectin that binds to the cyst wall.....206
Figure 3.42 – 40 % of ZFT knockdown parasites initiate conversion to bradyzoites and are able to survive the transient loss of ZFT.....208
Figure 3.43 - Excess zinc is unable to rescue the growth phenotype upon ZFT knockdown. 210
Figure 3.44 - Fluorescent growth curve of ΔKu80:mNG parasites in the presence of increasing concentrations of Zn Ionophore 2-Mercaptopyridine N-oxide.....211
Figure 3.45 - Zinc ionophore 2-Mercaptopyridine N-oxide is unable to rescue the growth phenotype upon ZFT knockdown. 212
Figure 3.46 - ZFT overexpression parasites are hypersensitive to excess zinc. .213
Figure 3.47 - ZFT expression is dependent on the availability of zinc.....216
Figure 3.48 - TgZFT is able to complement the lack of zinc transport in the *Δzrt1/2* mutant by rescuing growth both in SD-Ura and SD-Ura + EGTA conditions.....218
Figure 3.49 - TgZFT does not complement the lack of manganese transport in the *Δsmf1* mutant in both in SD-Ura and SD-Ura + EGTA growth conditions. 219

Figure 3.50 - ZFT knockdown parasites have reduced parasite associated iron by live cell imaging using the FerroOrange live cell indicator. 221
Figure 3.51 - ZFT knockdown parasites have reduced parasite associated zinc by live cell imaging using the FluoZin™-3AM live cell indicator. 223
Figure 3.52 – Parasites have significantly reduced parasite associated zinc, but not iron, at both 24 h and 48 h post ZFT knockdown by ICP-MS. 224
Figure 3.53 - ZFT knockdown parasites have significantly reduced parasite associated iron by XFM at both 24 h and 48 h post induction. 226
Figure 3.54 - ZFT knockdown parasites have significantly reduced parasite associated zinc by XFM at both 24 h and 48 h post induction. 227
Figure 3.55 - XFM of extracellular untreated T7S4-ZFT parasites showing colocalisation of iron and zinc with phosphorous. 228
Figure 3.56 - Extracellular parasites have reduced sulphur and phosphorus 48 h post ZFT knockdown by XFM, however this decrease was modest when compared to the rate at which iron and zinc decrease upon knockdown of ZFT. 229
Figure 3.57 - ICP-MS elemental analysis techniques demonstrate that ZFT knockdown does not significantly change copper levels in the parasite. 230
Figure 3.58 - XFM of iron and zinc in intracellular infection conditions. 232
Figure 3.59 - F3ΔHX ZFT-3HA*zft* ΔIRE expression is not altered at 18 h in both low and high iron conditions, and at 24 h in high iron conditions, but significantly reduced in low iron conditions at 24 h. 234
Figure 3.60 - F3ΔHX ZFT-3HAzft ΔIRE expression significantly reduced in both high zinc and TPEN chelation conditions at 18 h post treatment, however not altered in both conditions at 24 h. 236

Chapter 4

Figure 4.1 – TfR expression is upregulated in *T. gondii* infected HFFs at 24 h. .261
Figure 4.2 - Fluorescent Tf-A488 binding increases on the surface of *T. gondii* infected HFFs at 24 h. 262
Figure 4.3 - TfR expression is upregulated in *T. gondii* infected HFFs at 48 h. .263
Figure 4.4 – DMT1 expression is upregulated in *T. gondii* infected HFFs at 24 h, and DMT1 localisation is altered in fibroblasts following infection. 265
Figure 4.5 - DMT1 expression is upregulated in *T. gondii* infected HFFs at 48 h. 266

Figure 4.6 – There is no significant difference in DMT1 expression in HFFs infected with ΔMYR1 compared to RHΔKu80 parasites at 24 h. 268
Figure 4.7- FTH1 expression is not altered in *T. gondii* infected HFFs at 24 h, however excess iron induces FTH1 expression. 270
Figure 4.8 - FTH1 expression is not altered in *T. gondii* infected HFFs at 48 h, however excess iron induces FTH1 expression. 271
Figure 4.9 - TfR expression is upregulated in *T. gondii* infected RAW 264.7 murine macrophages at 24 h. 274
Figure 4.10 - Fluorescent Tf-A488 binding increases on the surface of *T. gondii* infected RAW 264.7 murine macrophages at 24 h. 276
Figure 4.11 - TfR expression in RAW 264.7 murine macrophages does not significantly change following *T. gondii* infection at 48 h, however, significantly decreases in the presence of excess iron. 277
Figure 4.12 – DMT1 expression is upregulated in *T. gondii* infected RAW 264.7 murine macrophages at 24 h. 279
Figure 4.13 – DMT1 expression is upregulated in *T. gondii* infected RAW 264.7 murine macrophages at 48 h. 280
Figure 4.14 – FTH1 expression in RAW 264.7 murine macrophages does not significantly change following *T. gondii* infection at 24 h, however, FTH1 significantly increases in macrophages pretreated with excess iron. 282
Figure 4.15 – FTH1 expression in RAW 264.7 murine macrophages does not significantly change following *T. gondii* infection at 48 h, however, FTH1 significantly increases in macrophages pretreated with excess iron. 283
Figure 4.16 - The *zft* 3' UTR plays a role in iron responsiveness in iron deprivation conditions in fibroblasts but not in macrophages. 285
Figure 4.17 – Schematic representation of the changes in expression of iron-related proteins in both human fibroblasts and murine macrophages following infection with *Toxoplasma gondii* at 24 h compared to uninfected cells. 302
Figure 4.18 - Schematic representation of changes in the expression of iron-related proteins in fibroblasts and macrophages following *T. gondii* infection in excess iron conditions at 24 h compared to infected cells. 305
Figure 4.19 - Schematic representation of changes in the expression of iron-related proteins in fibroblasts and macrophages following *T. gondii* infection in excess iron conditions at 24 h compared to uninfected iron-treated cells. 306

Figure copyright permissions

Publisher	Journal	Title	Authors and year	Figure number in article	Figure number in thesis	Copyright licence
Springer Nature	Nature Reviews Microbiology	Modulation of innate immunity by *Toxoplasma gondii* virulence effector	Christopher A. Hunter and L. David Sibley, 2012	Figure 1	Figure 1.1	6133700012508
Annual Reviews	Annual Reviews of Microbiology	Lytic Cycle of *Toxoplasma gondii*: 15 Years Later	Ira Blader, Bradley Coleman, Chun-Ti Chen, and Marc-Jan Gubbels, 2015	Figure 1	Figure 1.2	1663974-1
John Wiley and Sons	FEBS Journal	Toward unzipping the ZIP metal transporters: structure, evolution, and implications on drug discovery against cancer	Jian Hu	Figure 2	Figure 1.5	6140850256717

Table 0.1 – A list of copyright permissions obtained from publications for figures reused in this thesis.

Acknowledgements

This thesis would not have been possible without the support of many people. First and foremost, I would like to thank my supervisor Dr. Clare Harding for giving me the opportunity to do this PhD, and for all the continuous support, guidance, and insightful discussions. I have thoroughly enjoyed being a part of the Harding Lab over the past five years. Your dedication, passion and enthusiasm for research has truly been an inspiration. I have learnt so much from you both professionally and personally that I hope to carry forward. I am also hugely appreciative for the many opportunities you gave me, particularly BoP, which I am very grateful for. Thank you for everything, and for creating such a safe, positive, and supportive environment for me to learn and grow in as a scientist, I will always treasure it.

Thank you to my second and third supervisors, Professor Kevin Maloy and Professor Lilach Sheiner for their helpful insights, discussions, and constructive feedback during my project. I also wish to acknowledge my PhD assessors Professor Richard McCulloch and Professor James Brewer for their advice, valuable suggestions, support, and kindness throughout my PhD. Thank you to Cecilia Gallego Rubio for your contribution to this project, particularly for generating some of the parasite lines that were essential to this work, and to Dr. Hiram Castillo Michel for all the XFM support and assistance during data collection and analysis at the ESRF. I would also like to thank members of SGDB, L6, and the wider parasitology department for making labs a fun and supportive working environment to be in. Thank you to Ruaraidh MacGregor for managing L6 and for always being so helpful, and to James Hurst and Andrew Boyd for making sure the building and TC stayed intact. Thank you to Susan Baillie and Dr. Leandro Lemgruber Soares from the imaging facility who always came to help and answered all my microscopy questions.

I am profoundly grateful to the Wellcome Trust for funding my PhD studentship, and the WT IIB management team in Glasgow, especially Dr. Megan MacLeod and Jacqueline Meiklejohn who helped me with all my questions and supported me throughout my PhD especially during unforeseen family circumstances. A special thank you also goes out to the WT IIB PhD students, especially Emma, Zaydah, Sofia, Chess, and Jonathon who always understood the challenges of a PhD. It was invaluable to have you there at every step along the way, relating, and bonding about all the ups and downs of a PhD together.

A truly heartfelt gratitude goes out to past and current members of the Harding Lab, especially Dr. Megan Sloan, Dr. Jack Hanna, Dr. Lucas Pagura and Lucia Mrvova. Thank you for your wisdom, stimulating discussions, and encouragement, but most importantly your friendship and kindness. There was never a dull moment in labs with you all there. You made coming into labs easy, and every day was so special, enjoyable, and full of laughter. It was such a privilege to work alongside you all. You are a true inspiration, both as scientists and as people, and I will really miss working with you all and seeing your faces every day. I am also grateful to past and current members of the Sheiner Lab, especially Shikha, Mariana, Jana, and Andrew for their day-to-day support in the lab and all the fun lunch clubs and coffee afternoons which meant a lot to me during my studies and made my PhD journey enjoyable. Thank you to Miguel Cortijo Martinez and Augustin Pouzache who were great students and made teaching an enjoyable experience.

I would like to express my sincere gratitude to Montana and Andrea Gaspare who I met at BoP. Your love and passion for science was so incredibly inspirational and infectious. I am so thankful that I met you both and got to spend three months with you in Woods Hole, it truly was a breath of fresh air. I have made friends for life and will always be grateful to Clare and BoP for allowing our worlds to collide.

I am deeply grateful for the unwavering support, love, and encouragement from my family. Thank you to my parents, Ossama and Nadia, and my sisters Cara and Yara who always encouraged me to pursue my passion. My academic journey would not have been possible without them. I would also like to thank my second family, Moira, Susan, and Sandra for their kindness, and for cheering me on and believing in me. Thank you to my cats Moss and Mavis for the unconditional love, purrs and cat cuddles when writing this thesis, you made my days much brighter.

Last but definitely not least, I would like to thank my fiancé Shaun for absolutely everything he has done for me. I will forever be grateful for your unconditional love, support, encouragement, kindness, and patience during all the moments of my PhD. Thank you for always being there for me, caring for me, and for giving me strength when I needed it most. Thank you for listening to all my practice presentations, driving me to labs on weekends and picking me up when I stayed late, and taking care of our home for us. Thank you for always knowing how to put a smile on my face and put me at ease. I love you and I can’t wait to marry you!

Publications arising from this work

The following published research papers contain work presented in this thesis:

Aghabi, D., Gallego Rubio, C., Cortijo Martinez, M., Pouzache, A., Gibson, E.J., Pagura, L., Harding, C.R., 2025. ZFT is the major iron and zinc transporter in Toxoplasma gondii. https://doi.org/10.7554/eLife.108666.1

Sloan, M.A., Scott, A., **Aghabi, D**., Mrvova, L., Harding, C.R., 2025. Iron-mediated post-transcriptional regulation in Toxoplasma gondii. PLoS Pathog 21, e1012857. https://doi.org/10.1371/journal.ppat.1012857

Conference proceedings

Part of this thesis has been presented at the following meetings and conferences:

- WCIP ISAB Retreat, Scotland, June 2023

Poster presentation: ZFT plays a role in iron acquisition in *Toxoplasma gondii*

- SPPIRIT ECR Symposium, Dundee, Scotland, October 2023

Poster presentation: ZFT plays a role in iron acquisition in *Toxoplasma gondii*

- Coccidia Day UK, Scotland, December 2023

Oral presentation: ZFT plays a role in iron acquisition in *Toxoplasma gondii*

- 17th International Congress on Toxoplasmosis, Berlin, Germany, May 2024

Oral presentation: ZFT plays a role in iron acquisition in *Toxoplasma gondii*

- SPPIRIT ECR Symposium, Edinburgh, Scotland, October 2024

Poster presentation: ZFT plays a role in iron acquisition in *Toxoplasma gondii*

Author's declaration

I, Dana Ossama Nasief Aghabi, hereby declare that this thesis is the result of my own work and has been written for the degree of PhD at the University of Glasgow. I am the sole author of this thesis and performed all the work presented in this study unless stated otherwise. Exceptions are listed below and contributions to the study have been specifically acknowledged in the text. All sources of information are also mentioned in the text. No part of this thesis has been previously presented for obtaining a degree at this or another university.

Signature:

Printed name: Dana Ossama Nasief Aghabi - November 2025

Chapter 3:

- Dr. Clare Harding designed the ImageJ macro for quantifying iron, zinc, phosphorous, and sulphur from the XFM data.
- Dr. Clare Harding generated the comparative analysis of the changes as a percentage of untreated cells (Figure 3.56c).
- Dr. Clare Harding prepared parasites by treating with DFO for 5 days for Dr. Leandro Lemgruber Soares for TEM (Figure 3.40d).
- Cecilia Gallego Rubio generated the ZFT-Ty and T7S4-ZFT parasite lines
- Cecilia Gallego Rubio quantified ZFT vacuolar organisation at 48 h in the T7S4-ZFT knockdown line (Figure 3.40b).
- Cecilia Gallego Rubio prepared and fixed samples for TEM of T7S4-ZFT knockdown parasites.
- Dr. Leandro Lemgruber Soares processed and imaged all TEM microscopy (Figure 3.39, Figure 3.40c, and Figure 3.40d).
- Dr. Lucas Pagura performed structural predictions of ZFT using ChimeraX (Figure 3.1b).
- Miguel Cortijo Martinez performed SAG1, BAG1 and DBL quantifications in T7S4-ZFT knockdown parasites under my supervision (Figure 3.41).
- Yeast spot assays were performed by Augustin Pouzache under my supervision during his undergraduate honours project (Figure 3.48 and 3.49)
- Dr. Megan Sloan generated the ZFT-3HAdIRE$_{zft}$ parasite line and performed western blots of this line under low and high conditions (Figure 3.59).

Chapter 4:

- Dr. Clare Harding performed and processed the flow cytometry experiment for fluorescent binding of Tf-A488 on the surface of *T. gondii* infected HFFs (Figure 4.2).
- Lucia Mrvova generated the nanoLuc$_{dhfr}$ and nanoLuc$_{zft}$ parasite lines used for the nanoluciferase assays in Figure 4.16.

Abbreviations

A	
aa	amino acid
AGE	agarose gel electrophoresis
AIDS	acquired immune deficiency syndrome
Amp	ampicillin
ApiAT	apicomplexan amino acid transporter
Ars	sodium arsenite
At *or A. thaliana*	*Arabidopsis thaliana*
ATc	anhydrotetracycline
ATP	adenosine triphosphate
ATQ	atovaquone
a.u.	arbitrary units
B	
BAG1	bradyzoite antigen 1
BCDH	branched-chain 2-oxo acid dehydrogenase
BFD1/2	bradyzoite formation deficient 1/2
BLAST	basic-local-alignment search
BMC	binuclear metal centre
BMDM	bone marrow derived macrophage
BN-PAGE	blue native polyacrylamide gel electrophoresis
bp	base pair
BSA	bovine serum albumin
C	
CAS9	CRISPR-associated gene 9
CAT	chloramphenicol acetyltransferase
Ca^{2+}	calcium
cDNA	complementary deoxyribonucleic acid
CDPK	calcium-dependent protein kinase
Cd^{2+}	cadmium
CHX	cycloheximide
CIA	cytosolic iron-sulphur assembly
CISMBI	2-(3-carbamimidoylsulfanylmethyl-benzyl)-isothiourea
CoA	coenzyme A
Co^{2+}	cobalt
Cp	ceruloplasmin
CPL	cathepsin L-like protease
CPN60	chaperonin 60
CRISPR	clustered regularly interspaced palindromic repeats
cRNA	CRISPR RNA
Cryo-EM	cryogenic electron microscopy
CTD	cytoplasmic domain
C-terminal	carboxy terminal
Cu or Cu^{2+}	copper
D	
D3	DMEM with 3 % FBS
D10	DMEM with 10 % FBS

DAB	3’3-diaminobenzidine tetrahydrochloride
DAPI	4’,6-diamidino-2-phenylindole
DBL	*Dolichos biflorus lectin*
DCYTB	duodenal cytochrome b
DFO	deferoxamine
DHFR	dihydrofolate reductase
DMEM	Dulbecco’s Modified Eagle Medium
DMSO	dimethyl sulfoxide
DMT1	divalent metal transporter 1
DNA	deoxyribonucleic acid
ds	double strand
DSB	double-strand break
E	
E. coli	*Escherichia coli*
e.g.	exempli gratia (for example)
EC_{50}	half maximal effective concentration
ECAR	extracellular acidification rate
ECD	extracellular domain
EDTA	ethylene diamine tetraacetic acid
EGTA	ethylene glycol tetraacetic acid
EM	electron microscopy
ER	endoplasmic reticulum
ESCRT	endosomal sorting complex required for transport
ESRF	European Synchrotron Radiation Facility
EtOH	ethanol
F	
FAC	ferric ammonium citrate
FACS	fluorescent activated cell sorting
FAS-II	type II fatty acid synthase complex
FBS	fetal bovine serum
FCCP	carbonyl cyanide-4-(trifluoromethoxy) phenylhydrazone
Fe^{2+}	ferrous iron
Fe^{3+}	ferric iron
Fe	iron
Fe-S	iron-sulphur
fM	femtomolar
FIJI	Fiji is just ImageJ
Fpn1	ferroportin
FTH1	ferritin heavy chain 1
FUDR	5-fluorodeoxyuridine
Fw	forward
G	
G	gauge
g	gram or gravity (dependent on context)
GAPDH	glyceraldehyde 3-phosphate dehydrogenase
GBP	guanylate-binding protein
gDNA	genomic deoxyribonucleic acid
GOI	gene of interest
GRA	dense granules
GSH	glutathione

H	
h	hour
H_2O	water
H_2O_2	hydrogen peroxide
HA	hemagglutinin
HFF	human foreskin fibroblast
His or H	histidine
HIV	human immunodeficiency virus
HRD	histidine rich domain
HRP	horseradish peroxidase
Hs	*Homo sapiens*
HSP	heat shock protein
Hx or HXGPRT	hypoxanthine-xanthine-guanine phosphoribosyl transferase
I	
ICP-MS	inductively coupled plasma mass spectrometry
IDO	indoleamine 2,3- dioxygenase
IDT	Integrated DNA Technologies
IFA	immunofluorescence assay
IFC	inward facing confirmation
IFN-γ	Interferon gamma
IL	interleukin
IMC	inner membrane complex
iNOS	inducible nitric oxide synthase
IRE	iron responsive element
IRG	immunity-related GTPase
IRP	iron regulatory protein
IRT1	iron-regulated transporter 1
ISC	iron-sulphur cluster assembly machinery
IVN	intravacuolar network
K	
KD	knockdown
kDa	kilo Dalton
L	
L. amazonensis	Leishmania amazonensis
L. donovani	*Leishmania donovani*
LAMP	lysosome-associated membrane protein
LB	Luria-Bertani
LFR1	*Leishmania* ferric reductase 1
LIP	labile iron pool
LipA	lipoic acid synthase
LIT1	*Leishmania* iron transporter 1
LOPIT	localization of organelle proteins by isotope tagging
LN2	liquid nitrogen
LPS	lipopolysaccharide
M	
M	molar
MΦ	macrophage
MFI	mean fluorescence intensity

mg	milligram
min	minute
MIT	mitochondrial iron transporter
ml	millilitre
mM	millimolar
Mn or Mn^{2+}	manganese
MOI	multiplicity of infection
MPA	mycophenolic acid
mRNA	messenger ribonucleic acid
MYR1	myc regulation 1
N	
nanoLuc	nanoluciferase
NCBI	National Centre for Biotechnology Information
NCOA4	nuclear receptor coactivator 4
ND	not determined
ng	nanogram
Ni^{2+}	nickel
NJEJ	non-homologous end joining
NK	natural killer
nm	nanometre
NO	nitric oxide
NRAMP2	natural resistance associated macrophage protein 2
NTBI	non-transferrin bound iron
NZY	NZ amine, yeast extract
O	
o/n	overnight
OCR	oxygen consumption rate
OD	optical density
OFC	outward facing confirmation
OGDH	2-oxo-glutarate dehydrogenase
P	
P	primer
Pb or P. berghei	*Plasmodium berghei*
Pf or P. falciparum	*Plasmodium falciparum*
PAL	proline-alanine-leucine
PAM	protospacer adjacent motif
PBS	phosphate buffered saline
PCBP	poly (rC)-binding protein
PCD	PAL motif containing domain
PCR	polymerase chain reaction
PDH	pyruvate dehydrogenase
PEG	polyethylene glycol
PFA	paraformaldehyde
PLVAC	plant-like vacuolar compartment
PM	plasma membrane
PV	parasitophorous vacuole
PVM	parasitophorous vacuolar membrane

Q	
qPCR	quantitative polymerase chain reaction
R	
RBC	red blood cell
RNA	ribonucleic acid
ROS	reactive oxygen species
rpm	revolutions per minute
RT	room temperature
RT-qPCR	reverse transcription - quantitative polymerase chain reaction
Rv	reverse
S	
s	second
SAG1	surface antigen 1
Sc. or *S. cerevisiae*	saccharomyces cerevisiae
SD	standard deviation or synthetic dropout (context dependent)
SD-Ura	synthetic dropout agar/media lacking uracil
SDHB	succinate dehydrogenase B
SDS	sodium dodecyl sulphate
SDS-PAGE	sodium dodecyl sulphate polyacrylamide gel electrophoresis
SEM	standard error of the mean
sgRNA	single guide RNA
SiN	poly-l-lysine nitride
SR-SIM	super resolution structured illumination microscopy
SLC	solute carrier
SOC	super optimal broth with catabolite repression
spp.	species
STEAP3	six-transmembrane epithelial antigen of the prostate 3
SUERC	Scottish Universities Environmental Research Centre
SUF	sulphur formation
T	
T. gondii or Tg	*Toxoplasma gondii*
TAE	tris-acetate-EDTA
TATi	tetracycline-regulated transactivator domain
Taq	thermos aquaticus
TBI	transferrin bound iron
TcIT	*Trypanosoma cruzi* iron transporter
TEM	transmission electron microscopy
TEMED	N,N,N',N'-tetramethylethylenediamine
TetO	tetracycline operator sequences
TfR	transferrin receptor
THP-1	Tohoku hospital pediatrics-1 cells
TM	transmembrane
TMD	transmembrane domain
TNF	tumour necrosis factor
TPEN	N,N,N',N'-tetrakis-(2- pyridylmethyl) ethylenediamine
TRE	tet-responsive promoter
TRPML1	transient receptor potential mucolipin 1

tTA	tetracycline-dependent transactivator
TUB	tubulin
U	
U	unit
UPRT	uracil phosphoribosyltransferase
UTR	untranslated region
UV	ultraviolet
V	
V	volt
v/v	volume/volume percentage
VIT	vacuolar iron transporter
W	
w/v	weight/volume percentage
WB	western blot
WHO	world health organisation
WT	wild-type
X	
Xan	xanthosine monophosphate
XFM	X-ray fluorescence microscopy
Y	
YPD	yeast peptone dextrose
Y2H	yeast two-hybrid
Z	
ZFT	zinc and iron transporter
ZIP	Zrt/Irt-like Protein
ZIPCO	ZIP domain-containing protein
Zn or Zn^{2+}	zinc
ZnT	zinc transporter
Zrt1/2	zinc-regulated transporter 1/2
µg	microgram
µl	microlitre
µm	micrometre
µM	micromolar
°C	degree Celsius

Chapter 1 Introduction

1.1 Chapter aims

In this chapter, I aim to introduce the biology of the apicomplexan parasite *Toxoplasma gondii*. I will highlight the importance of transition metals such as iron and zinc in biological systems, and specifically the role that they play in apicomplexan parasites. I will emphasise the importance of metal acquisition, specifically through the structure, function, transport mechanism, and substrate specificity of Zrt/Irt-like transporter proteins (ZIPs) and their role in metal uptake in diverse systems including yeast, plants, bacteria, mammalian cells and protozoan parasites. Furthermore, I will provide an introduction on the mechanisms of iron homeostasis in mammalian cells, and the concept of nutritional immunity: how host cells sequester metals to prevent pathogen replication. Finally, I will give some examples as to how pathogens, including bacteria and protozoan parasites, respond to this strategy by manipulating host iron homeostasis and trafficking to enable proliferation and survival: a story of tug-of-war between host and bug.

1.2 The biology and importance of *Toxoplasma gondii*

1.2.1 The apicomplexan phylum and *Toxoplasma gondii*

Apicomplexans, together with Dinoflagellates and Ciliate (Adl et al., 2005; Cavalier-Smith, 1993) are phylogenetically grouped in the supergroup of the Alveolate, and are characterised by the presence of a peripheral alveolar membrane system (Adl et al., 2019; Ruggiero et al., 2015). In apicomplexan parasites, this system is often referred to as the Inner Membrane Complex (IMC) (Blader et al., 2015; Morrissette and Sibley, 2002). The phylum Apicomplexa is a highly diverse group containing over 6,000 known species of unicellular, obligate protozoan parasites, and potentially many more yet to be identified (Adl et al., 2019, 2007). These species are often characterised by the presence of an apical complex that plays a role in parasite invasion into the host cell (Levine, 1973), and a complex parasitic life cycle (Levine et al., 1980; Levine, 1988). The Apicomplexa phylum consists of four subgroups: gregarines, cryptosporidia, hematozoa, and coccidia (Del Campo et al., 2019; Morrison, 2009). *Gregarina* spp. belongs to the gregarines subgroup, *Cryptosporidium* spp. are members of the cryptosporidia subgroup, *Plasmodium* spp., *Babesia* spp. and *Theileria* spp. are members of the hematozoa group, and *Eimeria* spp. and *Toxoplasma* are members of the coccidia subgroup of the Apicomplexa phylum. *Toxoplasma gondii* is the causative agent of the disease toxoplasmosis and is classified within the cyst-forming coccidia subclass of apicomplexan parasites, along with *Sarcocystis* (which form cysts in mammals, birds and reptiles), *Besnoitia* (which form cysts in brains of rodents), *Frenkelia* (which form cysts in rodents and reptiles), and *Neospora caninum* (which causes abortion in cattle) (Frenkel and Smith, 2003; Klevar, 2007). *T. gondii* is the only species in the genus *Toxoplasma* and will thus be referred to either as *Toxoplasma* or *T. gondii* for the remainder of this thesis.

1.2.2 Human and animal health impact of apicomplexan parasites

Parasites belonging to the Apicomplexa phylum cause severe disease and hold great veterinary and medical importance, imposing a significant health burden on both animal and human populations (Levine, 1988; Stelzer et al., 2019). Due to this burden, apicomplexan parasites impose a threat to the economy with significant financial losses every year. Of the parasites in this phylum, the

deadliest is the genus *Plasmodium* spp. from the hematozoa clade, the causative agent of malaria. *Plasmodium falciparum* is one of five species that cause malaria infections in humans and is responsible for most malaria-related deaths. These parasites are transmitted by the female *Anopheles* mosquito as a vector. Malaria remains a public health problem as it is one of the leading causes of morbidity and mortality in tropical regions of the world, mostly in Sub Saharan Africa and Southeast Asia. In 2023, the disease was responsible for approximately 263 million new clinical cases worldwide with an estimated mortality of 597,000, with the WHO African Region accounting for approximately 94 % of malaria cases and 95 % of deaths, primarily affecting children under the age of 5 (World Health Organisation (WHO), December 2023). Through increased prevention and control programmes, the incidence of malaria has experienced a 40 % decline between 2000 and 2015. However, despite this progress, the disease remains a global threat. WHO data has shown an increase in malaria cases from 252 million cases in 2022 to 263 million cases in 2023 (WHO, December 2023). Although this was largely due to the disruption of malaria intervention drives due to the COVID pandemic, the increase in drug resistant *P. falciparum* and *P. vivax* has also been a challenge (Björkman et al., 2024; Haldar et al., 2018; Hanboonkunupakarn and White, 2016; Ngwana-Joseph et al., 2024).

Other parasites belonging to the Apicomplexa phylum that have a large global burden through the loss of cattle (Trees et al., 1999) and poultry (Sharman et al., 2010) include *Eimeria* spp., *Neospora* spp., *Babesia* spp. and *Theileria* spp. *Eimeria* spp. is a member of the coccidia clade and is the causative agent for coccidiosis in poultry, with the avian disease affecting the production of eggs and successful offspring generation, resulting in a high economic burden through the loss of worldwide poultry production (Blake and Tomley, 2014). Both *Neospora* spp. and *Babesia* spp. lead to spontaneous abortions in cattle, also having a large global economic burden through the loss of livestock (Giles et al., 2014). *Babesia* spp. parasites are often carried though tick vectors and transported via blood following a tick bite. Some *Babesia* species, such as *Babesia microti*, are also known to infect immunocompromised individuals, and this can be lethal (Ortiz et al., 2020). Moreover, *Theileria* spp., which is also transmitted by ticks to both ruminants (Kiara et al., 2018) and equines (Mendoza et al., 2024), belongs to the

hematozoa clade and can also cause large economic burdens through the loss of livestock (Maharana et al., 2016; Morrison, 2015).

Another important human apicomplexan parasite is *Cryptosporidium* spp., the causative agent of cryptosporidiosis. *Cryptosporidium* can infect humans and has the potential be life threatening in immunocompromised individuals (Bouzid et al., 2013; Chalmers et al., 2019). Infection is opportunistic, through contaminated water or food sources (Franceschelli et al., 2022; Yamamoto et al., 2000). Infection with this parasite can lead to severe gastrointestinal illness and diarrhoea. In humans, cryptosporidiosis is implicated as the second major cause of diarrhoeal diseases and a main contributor to morbidity and mortality in developing countries, primarily affecting children (Checkley et al., 2015; Striepen, 2013). According to the WHO, it is estimated that in developing countries, approximately 20 % of diarrheal episodes in children are a result of infection with *Cryptosporidium* spp. compared to 9 % in developed countries. In addition to humans, C*ryptosporidium* can also infect ruminant livestock, particularly young calves, causing diarrheal disease, dehydration and in severe cases, death, imposing a large economic burden.

1.2.3 History of *Toxoplasma gondii*

T. gondii was first discovered and described simultaneously by two groups in 1908. French scientists Nicolle and Manceaux isolated the parasite in Charles Nicolle's research laboratory at the Pasteur Institute in Tunis from a North African hamster-like rodent, *Ctenodactylus gundi,* while researching leishmaniasis (Nicolle and Manceaux, 1908; Ferguson, 2009; Nicolle and Manceaux, 2009). Alfonso Splendore also isolated the parasite in a rabbit in Brazil (Splendore, 1908; Ferguson, 2009). It is named *Toxoplasma gondii* based on its morphology (in Greek toxon=arc/bow and plasma=form). However, its medical importance and clinical relevance to human health was not recognised until years later when *T. gondii* was identified within tissues of a congenitally infected infant, and the observation that *T. gondii* can be passed congenitally from mother to foetus was made in a newborn female in 1939 (Wolf et al., 1939; Cowen, 1942). A month following their birth, the female patient developed retinitis and encephalitis which eventually led to their death. It was not for another couple of years when the first fatal case in an adult was

recorded and reported (Pinkerton, and Weinman, 1944), and until 1957 when it was recognised to cause abortion in sheep (Hartley and Marshall, 1957).

1.2.4 Global prevalence and transmission of *Toxoplasma gondii*

Unlike most apicomplexan parasites which are only able to infect limited host or cell types, *Toxoplasma* is often regarded as the world's most successful and widespread parasite due to its wide host range and ubiquitous ability to infect all warm blooded species and nucleated cells (Carruthers, 2002; Tenter et al., 2000). Its success is supported by the statistic that approximately one third of the human population worldwide is infected with the parasite, with prevalence varying between countries and ranging anywhere between 10 – 90 % (Hill et al., 2005; Pappas et al., 2009). Despite its wide host range and worldwide distribution (Schlüter et al., 2014), exact estimations of infection rates are limited, particularly as there is no routine testing for toxoplasmosis diagnosis in the general population (Ybañez et al., 2020).

The most common route of infection in humans is through infection with either tissue cysts or environmentally resistant oocysts (De Moura et al., 2006; Jones and Dubey, 2012; Mead et al., 1999; Vieira et al., 2015). Sporulated oocysts are shed and excreted into the environment though felids, the definitive host. Most infections are linked to consumption of oocysts on unwashed fruits and vegetables (Pinto-Ferreira et al., 2019). Cysts can be shed by indoor felids into litter trays, and thus ingestion of oocysts through insufficient hygiene is another common route of infection in humans, an intermediate host (Dubey et al., 1998; Frenkel et al., 1970). Oocysts can also pass into open water, which is then used in irrigation or consumed directly. The cysts shed into the environment can then be ingested by other animals which act as intermediate hosts, where the parasite then forms as a tissue cyst. These tissue cysts are denatured upon cooking, however if the meat is undercooked, these tissue cysts are ingested, leading to infection (Plaza et al., 2020). Unlike the majority of other apicomplexan parasites, *T. gondii* can be transmitted orally between intermediate hosts as tissue cysts, omitting the need for the parasite to go through the sexual lifecycle in the definitive felid host before transmitting to a new host, driving the worldwide expansion of *Toxoplasma gondii* (Su et al., 2003). Transmission can also occur vertically during pregnancy. The parasite can cross the placenta from the mother to the developing foetus

(Chaudhry et al., 2014; Dubey, 2010). Another route of transmission is through human-human transfer via blood transfusions or organ transplantations from infected individuals (Botein et al., 2019; Yılmaz et al., 2021).

1.2.5 Life cycle of *Toxoplasma gondii*

The complete lifecycle of *Toxoplasma gondii* was first described in 1970 by Frenkel and colleagues (Dubey et al., 1970; Frenkel et al., 1970), with the discovery of the sexual stages in the intestine of the cat also described (Hutchison, 1965; Hutchison et al., 1970; Work and Hutchison, 1969). *T. gondii* goes through a complicated heteroxenous life cycle which consists of two main stages that occur in two different hosts; a sexual lifecycle stage which occurs within the definitive host (solely restricted to the intestines of the Felidae family) and an asexual lifecycle stage, also known as the lytic cycle, which occurs within the intermediate host (all warm-blooded species) (Dubey, 2009) (Figure 1.1).

During its lifecycle, *Toxoplasma* forms three infectious stages: tachyzoites (asexual fast-growing in the acute lytic stage), bradyzoites (asexual slow-growing and persistent cyst forming) and sporozoites (found within oocysts and shed by cat faeces in the sexual stages (Torrey and Yolken, 2013)). All these infectious stages can infect both the definitive or intermediate host through vertical (transplacental transfer of tachyzoites) or horizontal transmission (through ingestion of oocysts shed in the environment or ingestion of tissue cysts in undercooked meat). In the intermediate host, *T. gondii* tachyzoites invade host cells and replicate asexually. After multiple rounds of replication, the parasites egress from host cells, rupturing them and then invading nearby host cells. Some tachyzoites can convert into a slower-replicating form of the parasite termed bradyzoites which reside within tissue cysts where they can remain dormant until reactivated by a weakened immune system.

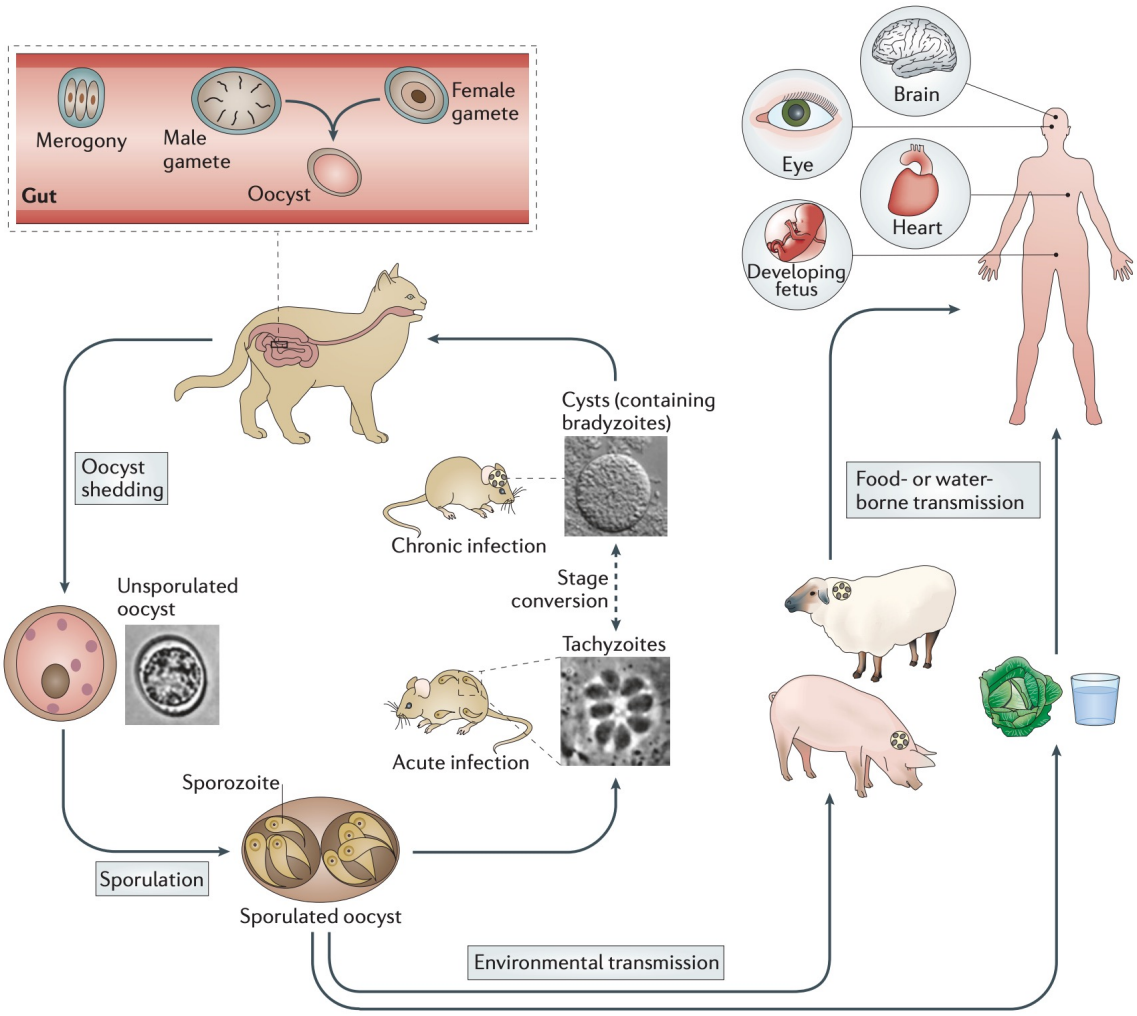


Figure 1.1 - The complex life cycle of *Toxoplasma gondii.*

Schematic of the life cycle of *T. gondii* including the sexual life cycle in the definitive host, the asexual cycle or lytic cycle in the intermediate host and the environmental stage. Felids shed oocysts into the environment which are then taken up by the intermediate host (any warm-blooded animal) where they undergo asexual replication. Ingestion of prey infected with *Toxoplasma* reintroduces the parasite to the definitive felid host where it can undergo sexual replication. Humans most often contract *T. gondii* through contaminated food or water sources. Infection with *T. gondii* can affect multiple organs including the eyes, brain, and heart of immunocompromised individuals and can also cause miscarriages and affect the developing foetus causing congenital defects in pregnant women. Figure taken from Hunter and Sibley, 2012. Republished by permission from the Springer Nature, Nature Reviews Microbiology, conveyed via Copyright Clearance Centre. License number: 6133700012508.

1.2.5.1 Sexual replication in the definitive host

Following the ingestion of sporulated oocysts or an intermediate host with a tissue cyst containing bradyzoites, *T. gondii* can now complete its sexual reproduction which only exclusively occurs in members that belong to the Felidae family (Dubey et al., 1998; Dubey and Frenkel, 1976). Once ingested, the cyst wall and tissues from the ingested intermediate host are digested by proteolytic enzymes in the small intestine and possibly the low pH of the stomach (Dubey et al., 1998). This in turn releases the parasites which mature to trophozoites and invade epithelial cells of the small intestine, where they replicate once via endodyogeny and then undergo a further three rounds of endopolygeny (where there are several rounds of nuclear division prior to budding) (Dubey et al., 1998; Tenter et al., 2000) and transform into schizonts. Schizogony is then followed by gametogony, a process of sexual development which results in the formation of male and female gametocytes, followed by the fusion of microgametocyes (male gametes) and macrogametes (female gametes) (Dubey et al., 1998). Following fertilisation, an oocyst is formed within an enterocyte which is then released as non-infective unsporulated oocysts within the intestinal lumen. These oocysts are then shed into the environment through felid faeces (Dubey et al., 1998; Frenkel et al., 1970; Robert-Gangneux and Dardé, 2012). Due to the thick multi-layered wall of the oocyst, it can remain in the environment and maintain infectivity for years until ingested by an intermediate host where the life cycle continues.

1.2.5.2 Environmental stage

Oocysts can be shed from the felid definitive host into the environment through faeces. Sporozoites can be formed within these oocysts in the environment via meiotic division, with each sporulated oocyst forming two sporocysts each with four haploid sporozoites (Dubey et al., 1970). This now makes the oocysts infective, which can then be taken up by the intermediate host via the consumption of contaminated food or water. As the oocyst is exposed to the environment, it is made resistant through a thick oocyst wall made from multiple layers (Dubey et al., 1998; Ferguson et al., 1975; Shapiro et al., 2019), protecting the sporozoites from the harsh environment outside the cat (Belli et al., 2006). Studies have also suggested that the oocyst wall is resistant to disinfectants and has a high rigidity. This allows the oocysts to survive outside the cat under both

drying and freezing conditions in the environment for over a year if humidity and temperature conditions are optimal, until they are ingested by an intermediate host (Dubey et al., 1998, 1970; Frenkel et al., 1975; Yilmaz and Hopkins, 1972).

1.2.5.3 Asexual lytic cycle in the intermediate host

Following the completion of the sexual cycle in the definitive host, sporulated oocysts are taken up by the intermediate host. During this stage, the parasites are rapidly growing, and multiplying (in Greek tachy=fast and zoite=living organism). In order for the parasites to divide and grow rapidly, parasites go through a repetitive set of processes known as the lytic cycle (Black and Boothroyd, 2000; Blader et al., 2015) (Figure 1.2). This begins with the parasite actively attaching to the host plasma membrane and re-orientating so that the apical end is facing the host cell, followed by active invasion. This leads to the formation of the parasitophorous vacuole membrane (PVM) during invasion, encapsulating the parasite. *T. gondii* then goes through several rounds of replication by endodyogeny (Black and Boothroyd, 2000). Endodyogeny is a process of asexual replication where two daughter cells are produced internally within a single mother cell, during which the mother cell is consumed. Following replication, the parasites lyse and egress the host cell, before invading neighbouring cells, a process which is regulated by calcium signalling (Hortua Triana et al., 2018). Tachyzoites can disseminate throughout the entire body and infect all tissues, until they are then recognised by the host's potent immune system. Upon this recognition, *T. gondii* then differentiates into the dormant bradyzoite stage (in Greek, brady=slow), where they replicate at a slower rate and persist in the host within cysts in tissues like the brain, heart and skeletal muscle (Blader et al., 2015; Cerutti et al., 2020; Dubey, 2020; Tomita et al., 2013).

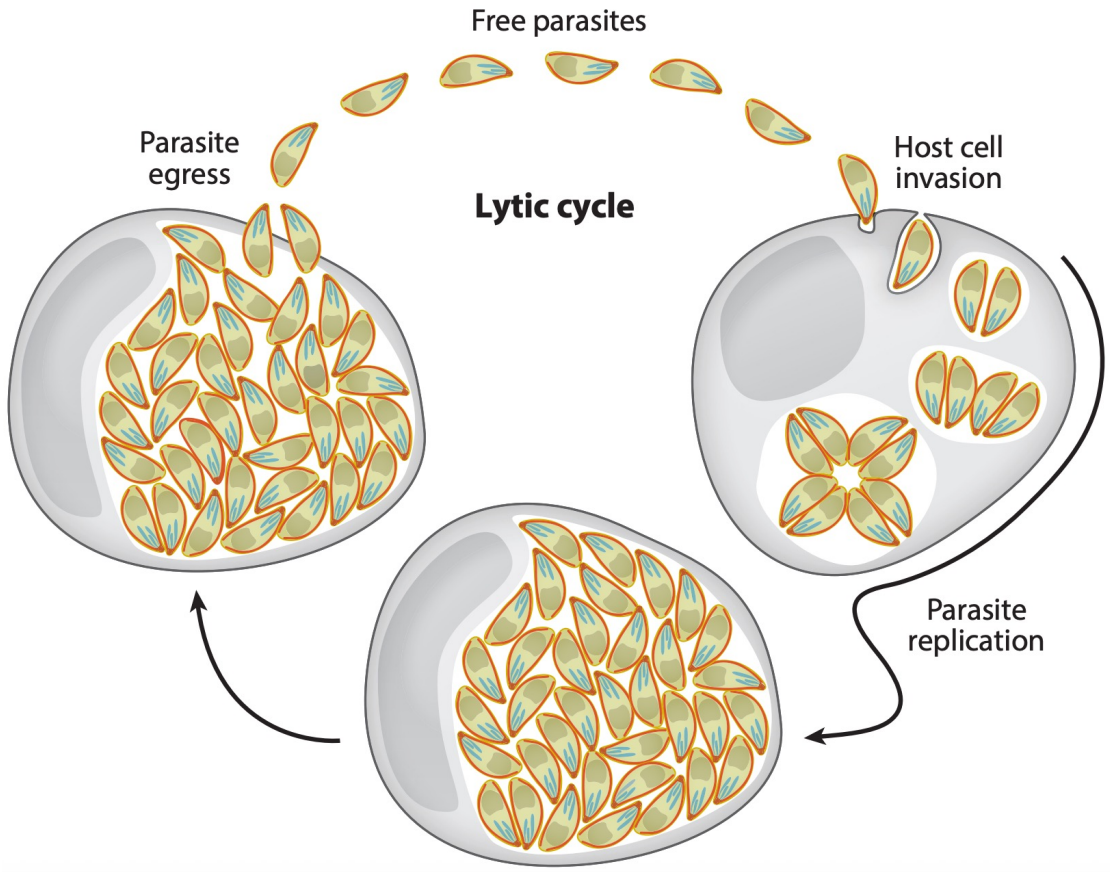


Figure 1.2 - Lytic life cycle of *Toxoplasma gondii.*

Lytic life cycle of *T. gondii* highlighting host cell invasion, formation of a parasitophorous vacuole, parasite replication within this vacuole, and finally parasite egress from the host cell. Following egress, the host cell bursts and free parasites infect nearby cells and the lytic cycle repeats. Figure taken from Blader et al., 2015. Republished by permission from the Annual Reviews of Microbiology, conveyed via Copyright Clearance Centre. License number: 1663974-1.

1.2.5.4 The switch from tachyzoites to bradyzoites, and the stresses that trigger differentiation

T. gondii tachyzoites differentiate upon encountering virtually any type of stress *in vitro*. Exogenous stress factors such as alkaline pH (Soete et al., 1994), drugs or chemicals, interferon-gamma (IFN-γ) (Bohne et al., 1994, 1993), pro-inflammatory cytokines such as IL-6 (Weiss et al., 1995), heat shock (Soete et al., 1994) and the deprivation of nutrients have all been shown to trigger bradyzoite differentiation *in vitro*.

Studies have shown that increasing the pH of the culture medium to a pH of 8.0-8.2, without CO_2 (to prevent any variations in pH) triggers the transition of tachyzoites into bradyzoites (Soete et al., 1994). Moreover, metabolic inhibitors that interfere with the function and activity of the parasite mitochondria including oligomycin, antimycin A and atovaquone have been shown to induce the expression of bradyzoite-specific markers. Sodium nitroprusside, which inhibits mitochondrial respiration also induces stage conversion (Bohne et al., 1994). This proposes that changes in the metabolism of *T. gondii* are also associated with parasite differentiation (Bohne et al., 1994; Tomavo and Boothroyd, 1995).

Finally, a potent inducer of tachyzoite to bradyzoite differentiation is the deprivation of nutrients, particularly as tachyzoites are fast replicating and have a higher need for nutrients when compared to the bradyzoite stage of the parasite which are slower replicating and thus don't have as much of a need for nutrients. *Toxoplasma gondii* is an arginine auxotroph and relies on uptake from the host cell. Starvation of arginine limits *T. gondii* replication, induces the differentiation to bradyzoites, and triggers the formation of cyst-like structures *in vitro* (Fox et al., 2004). Importantly, the deprivation of transition metals such as iron, an essential nutrient, has also been shown to promote bradyzoite stage conversion (Renaud et al., 2024; Sloan et al., 2025; Ying et al., 2024).

Notably, the process of bradyzoite differentiation *in vitro* is reversible, and differentiated bradyzoites can revert back to fast proliferating tachyzoites upon the removal of the stress factor that was used to induce the stage conversion (Soete et al., 1994). Collectively, these studies suggest that the factors that trigger the induction of bradyzoite differentiation can involve both exogenous and endogenous stresses, making the triggers of stage conversion multifactorial and complex.

Stress (as described above) triggers a transcriptional response in *T. gondii* via Bradyzoite Formation Deficient-1 (BFD1), the master regulator of *T. gondii* differentiation (Waldman et al., 2020). In response to stress, a cytosolic RNA-binding protein, BFD2, interacts with the BFD1 transcript. BFD1 then binds to the promoters of stage-specific genes (e.g. *bag1*) to promote stage conversion (Licon et al., 2023). This positive feedback loop between BFD1 and BFD2 controls stage conversion from tachyzoites to bradyzoites in *Toxoplasma gondii*. BFD1 can

activate the transcription of some apicomplexan AP2 proteins (ApiAP2) DNA binding proteins, including TgAP2IX-9, a known bradyzoite-linked transcription factor (Hong et al., 2017; Radke et al., 2013). Nevertheless, knockouts of these ApiAP2 transcription factors do not completely block differentiation, suggesting that *T. gondii* bradyzoite differentiation is regulated by multiple transcription factors. However, BFD1 is the master regulator of this switch and ApiAP2 proteins act as downstream mediators of bradyzoite programming (Jeffers et al., 2018; Waldman et al., 2020). Moreover, the phosphorylation state of the eukaryotic initiation factor-2 (eIF2α) has been shown to reprogramme the transcriptome of *T. gondii* to control translation and facilitate differentiation, driving and maintaining parasite latency (Holmes et al., 2017).

It is important to highlight that although several processes including translational and mitochondrial inhibition have been shown to trigger this transcriptional change in response to stress, the upstream sensors of this switch are not yet known.

1.2.6 Pathogenesis and clinical features of toxoplasmosis

The pathogenesis of *T. gondii* infection is characterised by the intracellular replication of the acute phase (tachyzoite form) which causes widespread infection. As mentioned previously in section 1.2.5, tachyzoites rapidly replicate within nucleated host cells until the host cell is ruptured and damaged upon the release of these intracellular parasites as they egress, actively causing tissue destruction and inflammation (Black and Boothroyd, 2000; Blader et al., 2015). This can lead to significant tissue damage and lesions most notably in the brain (encephalitis) and the retina (ocular toxoplasmosis) (Kijlstra and Petersen, 2014; Wang et al., 2017). To evade the host immune response, some of these tachyzoites transition to the chronic, latent stage (bradyzoite form) which are characterised by tissue cysts in the brain, skeletal and heart muscle (Blader et al., 2015; Cerutti et al., 2020; Dubey, 2020; Tomita et al., 2013).

Due to *T. gondii's* wide host range, toxoplasmosis is a widely distributed zoonotic infection worldwide. The outcome of the patient following infection with *T. gondii* is dependent on the pathogenicity of the parasite, host genetic profile, the susceptibility and immunocompetency of the host (Dubey et al., 2020).

1.2.6.1 Toxoplasmosis in immunocompetent individuals

Despite the high prevalence of *T. gondii* infection worldwide, the clinical manifestation is less than 20 % (Flegr et al., 2014; Hill et al., 2005; Remington, 1974). In healthy immunocompetent individuals, toxoplasmosis is often asymptomatic with little to no clinical manifestations, however cases could sometimes present mild flu-like symptoms including a fever, fatigue, muscle aches, a sore throat, or a headache. Ocular toxoplasmosis can affect immunocompetent individuals, where the parasite irreversibly damages the retina, leading to partial or complete visual loss (Ferreira et al., 2011; Gilbert et al., 2008; Montoya and Liesenfeld, 2004).

A correlation between *T. gondii* infection and behavioural changes in the host has been proposed. For example, studies have found that rats infected with *T. gondii* lose their natural fear of felids, and in some cases actually become attracted to cat urine, hypothesising that the parasite manipulates the behaviour of the host in order to survive and continue its reproductive cycle (Abdulai-Saiku and Vyas, 2017; Ingram et al., 2013; Vyas, 2015; Vyas et al., 2007; Webster, 2001). This has therefore led to the investigation as to whether infection with *T. gondii* correlates with changes in human neurological presentations or behaviour, specifically in relation to Alzheimer's disease (Nayeri et al., 2021; Yang et al., 2021), schizophrenia (Contopoulos-Ioannidis et al., 2022; Yang et al., 2024), depression (Kamal et al., 2022; Nasirpour et al., 2020), suicide (Soleymani et al., 2020) and obsessive compulsive disorders (Kazemi et al., 2022; Nayeri Chegeni et al., 2019). These studies suggest that *T. gondii* may manipulate the behaviour of the host; more specifically the neural pathways which may play a role in increased risk taking possibly to enhance the parasite's chance of transmission. It is important to note that correlation is not causation, and that proof of causation is complex and multifactorial.

1.2.6.2 Toxoplasmosis in immunocompromised individuals

Toxoplasma can cause debilitating complications with varying severity of clinical disease in immunocompromised individuals, including individuals with a compromised immune system following HIV/AIDs (Human immunodeficiency virus/Acquired immune deficiency syndrome), chemotherapy, a blood transfusion,

or organ transplant. Clinical manifestations could present as ocular disease, visual loss and blindness, pulmonary toxoplasmosis (Carme et al., 2002; De Souza Giassi et al., 2014; Leal et al., 2007), myocarditis, hydrocephalus or encephalitis caused by severe lesions which could be fatal if left untreated (Ambroise-Thomas and Pelloux, 1993; Maenz et al., 2014; Torrey and Yolken, 2013; Weiss and Dubey, 2009). As this parasite resides in intracellular cysts in tissues in the brain and muscle inside the host, should the immune system of an individual become compromised, these dormant parasites are then reactivated and become the acute tissue-damaging infectious forms called tachyzoites, causing lesions in the brain, muscles and retina, eventually leading to the development of ocular toxoplasmosis, inflammation of the retina or encephalitis (Kijlstra and Petersen, 2014; Wang et al., 2017). This reactivation can also lead to symptoms such as drowsiness, disorientation, headaches, muscle weakness, reflex changes and pneumonia (Wang et al., 2017).

1.2.6.3 Toxoplasmosis in pregnant women

Infection with *T. gondii* poses a significant risk during pregnancy to the foetus as the parasite can be vertically transmitted (Dubey, 2010). If infected within the first or second trimester of pregnancy or for the first time just before becoming pregnant, *T. gondii* can cause complications as the parasite can cross the placenta and infect the developing foetus. This can result in congenital toxoplasmosis and developmental defects to a developing foetus which often leads to miscarriages or still births (Desmonts and Couvreur, 1974; Dunn et al., 1999; Hohlfeld et al., 1989; Wong and Remington, 1994). In the case that the foetus survives, clinical manifestations can range from vision and hearing loss, developmental delays, seizures, cognitive issues, learning difficulties, hydrocephalus, liver or spleen enlargement and low birth weight (McAuley, 2014; Moncada and Montoya, 2012).

1.2.6.4 Clonal isolates and worldwide distribution

In addition to host susceptibility, virulence also varies with clonal strain type, as different isolates of *Toxoplasma* demonstrate varying levels of virulence in the host (Etheridge et al., 2014; Fentress et al., 2010; Khan et al., 2009; Taylor et al., 2006). Despite worldwide distribution and a wide host range, *Toxoplasma* has little genetic diversity and is considered genetically clonal at a population level. The

three main clonal lineages are known as Type I, II and III. Type I is the most virulent clonal strain of *T. gondii* and is mostly found in clinical isolates from North and South America. Type II is most commonly found in North America and Europe, compared to Type III which are comparatively slow growing and less virulent and found mostly in Central and South America (Fuentes et al., 2001; Grigg and Boothroyd, 2001; Sibley et al., 2009). RH is a typical Type I strain and is commonly used and manipulated in labs to understand the biology of *Toxoplasma*, particularly as it has fast growth and has an increased ability to survive extracellularly. Genetic analysis has revealed a fourth atypical *T. gondii* strain, haplogroup 12, revealing a fourth clonal lineage that is thought to be a result of genetic recombination in North America (Howe and Sibley, 1995; Khan et al., 2011). Atypical strains that genetically do not fit into either of these types are grouped into haplogroups 4-15 which have a worldwide distribution (Sibley et al., 2009; Yang et al., 2013). Strains from Europe and North America have low genetic diversity when compared to Africa and South America where extensive genetic diversity can be seen, correlating to both geographic area (Khan et al., 2007) as well as habitat (Khan et al., 2011). The difference in virulence is supported by ocular toxoplasmosis having the highest prevalence in Brazil and being associated with atypical or Type I strains in both North and South America (de-la-Torre et al., 2013; Glasner et al., 1992; Vallochi et al., 2005), whereas infections in Europe are more likely associated with Type II strains (Fernández-Escobar et al., 2022).

1.2.6.5 Impact of toxoplasmosis on animal health and the economy

As *T. gondii* is promiscuous and is able to infect all warm-blooded animals (Dubey, 2010; Schlüter et al., 2014; Tenter et al., 2000), infection with the parasite not only causes health burdens and implications in humans, but also greatly affects animal welfare, particularly livestock including pigs, sheep and goats. Infection with *T. gondii* can cause spontaneous abortions in pregnant sheep and goats, with outbreaks leading to a number of deaths and decimating animal numbers (Stelzer et al., 2019). A recent study in Italy found that 53.8 % of sheep sampled in two slaughterhouses between 2019 and 2021 tested positive for *T. gondii* seroprevalence. Another database demonstrates that the estimated prevalence of sheep infected with *T. gondii* in 2018 in the European Union was approximately 18 % (European Food Safety Authority (EFSA) and European Centre for Disease

Prevention and Control (ECDC), 2019). In cattle and poultry, reports of clinical toxoplasmosis is rare (Dubey, 2010). In addition to imposing a risk to animal welfare and health, the loss of sheep and goats in particular has caused economic burdens and resulted in large financial losses (Gutiérrez-Expósito et al., 2021; Stelzer et al., 2019; Torrey and Yolken, 2013).

1.2.6.6 Current treatments of toxoplasmosis

Treatment of toxoplasmosis is dependent on the status of the patient's immune system, the severity of the disease as well as the stage of pregnancy. For most immunocompetent and healthy individuals with no or mild flu-like symptoms, no treatment is required, and the immune system clears the acute form of infection, although bradyzoites are not eliminated. However, in more severe cases such as ocular toxoplasmosis or encephalitis, or in patients with a compromised immune system, a combination of prescription drugs including antifolates such as pyrimethamine and sulfadiazine are given to inhibit parasite growth and replication (Alday and Doggett, 2017; Dunay et al., 2018; Silva et al., 2021). As these drugs function by inhibiting folate metabolism typically through blocking enzymes such as dihydrofolate reductase (DHFR) which inhibits DNA synthesis, folinic acid is often simultaneously given to supply the host cells with a usable source of folate. As anti-folates are contraindicated during pregnancy, Spiramycin, a protein synthesis inhibitor, is often used to treat toxoplasmosis in pregnant women prior to the 20th week of pregnancy (Dunay et al., 2018; Rajapakse et al., 2013; Schoondermark-Van De Ven et al., 1994). However, many of these drugs have toxic side effects (Silva et al., 2021), and importantly, strain resistance to these drugs has been observed (Montazeri et al., 2018). Moreover, although there is a vaccine for *T. gondii* in sheep (Hiszczyńska-Sawicka et al., 2011), there are currently no vaccinations for *T. gondii* infection in humans (Mévélec et al., 2020). However, efforts continue to investigate different approaches to vaccination against *Toxoplasma* (Allahyari et al., 2020; Mamaghani et al., 2023). It is worth noting that these drugs act against the acute tachyzoite stage of *T. gondii* and there are currently no drugs or vaccines against the bradyzoite stage of the parasite. Further research is required to develop effective drugs to treat the cyst-forming dormant stage of *Toxoplasma*.

1.2.7 Importance of nutrient acquisition from the host for *Toxoplasma gondii* survival

T. gondii is an obligate intracellular parasite and thus requires a host cell to replicate and survive. *Toxoplasma* has evolved a range of strategies to efficiently promote the scavenging and acquisition of essential nutrients and metabolites from the mammalian host cell in order to meet its basic metabolic requirement (Coppens, 2014; Gazanion and Vergnes, 2018; Moreira et al., 2018), reviewed here (Van Dooren and McConville, 2025). When *T. gondii* first invades a host cell, it establishes the PVM which is initially composed of lipids from the host cell and is remodelled by the parasite following invasion to allow the uptake of nutrients. The PVM functions as a molecular sieve, being freely permeable and allowing the bidirectional diffusion of molecules <1.8 kDa to pass across the PVM (Schwab et al., 1994).

T. gondii tachyzoites are known to secrete over 200 dense granule (GRA) proteins which are either inserted into the PVM or the intravacuolar network (IVN) (connecting parasites with the PVM), retained within the lumen of the PV, or exported into the cytosol of host cells. Two of these GRA proteins, GRA17 and GRA24 have been shown to be major molecular components of this pore (Gold et al., 2015). Moreover, GRA1 forms a non-selective pore channel which allows for the passive transport and exchange of small parasite/host nutrients and metabolites including amino acids, sugars, lipids, vitamins and nucleotides (Fan et al., 2025). Studies have shown that GRA2 and GRA6 play a role in stabilising or generating the IVN which mediates the uptake of cytosolic host cell organelles and proteins including lysosomes and the direct transfer of lipids directly from host lipid bodies (Coppens et al., 2006). The recruitment of host cell organelles including the Golgi apparatus, endoplasmic reticulum (ER) as well as late endosomal/lysosomal vesicles also play a role in nutrient acquisition by the parasite through an exchange of lipids (Coppens et al., 2006; Deffieu et al., 2019; Nolan et al., 2017). GRA14 and GRA64 also play a role in the recruitment of the host endosomal sorting complex required for transport (ESCRT) machinery to the parasitophorous vacuole, which allows for the internalisation of organelles and host cell proteins to cross the PVM (Mayoral et al., 2022; Rivera-Cuevas et al., 2021; Romano et al., 2023).

Toxoplasma gondii are auxotrophic for many amino acids that must be salvaged from the host, either through the degradation of host proteins or by direct uptake of these molecules. Specific apicomplexan amino acid transporters (ApiAT) have been identified to mediate this uptake (Parker et al., 2019). *Toxoplasma* encodes 16 of these ApiAT transporters, with many shown to be essential for the parasite. *T. gondii* requires the uptake of the amino acid tryptophan from its host cell (Parker et al., 2019; Pfefferkorn, 1984), as well as tyrosine through the ApiAT5-3 (Marino and Boothroyd, 2017; Wallbank et al., 2019), arginine through the action of the ApiAT1and ApiAT6-1 transporters (Fairweather et al., 2021; Fox et al., 2004; Rajendran et al., 2021) and lysine through the general cationic amino acid transporter ApiAT6-1 (Fairweather et al., 2021). *Toxoplasma gondii* also utilises host-derived glucose as its major carbon source, however studies have been able to demonstrate that the parasites can also switch to the use of glutamine (or co-utilise other non-essential amino acids) as a carbon source in growth conditions where glucose is limited (Blume et al., 2009).

In addition to amino acids, *T. gondii* is also a purine auxotroph, a major nutrient that is required for the synthesis of nucleic acids. For example, the parasite imports adenosine and inosine through the low-affinity nucleoside transporter TgAT1 (Chiang et al., 1999) and the broad-spectrum high affinity nucleoside transporter TgAT2 (De Koning et al., 2003). *Toxoplasma gondii* also acquires several vitamins from the host cell which are required as co-factors for essential amino acids. Biotin is a co-factor for the acetyl-CoA carboxylase enzyme, which is required in the apicoplast for *de novo* fatty acid synthesis (Jelenska et al., 2002, 2001; Sidik et al., 2016). However, *Toxoplasma* lacks a biotin synthesis pathway and instead biotin is readily taken up from the host cell (Chen et al., 2015; Seeber and Soldati-Favre, 2010). Moreover, *T. gondii* scavenges lipoic acid from the host cell, an essential co-factor for a number of dehydrogenase enzymes, despite it being synthesised in the apicoplast of the parasite (Crawford et al., 2006). Finally, apicomplexan parasites including *Toxoplasma gondii* require haem, an essential cofactor for enzymes involved in the electron transport chain and energy generation including cytochromes.

1.2.8 Genetic manipulation of *Toxoplasma gondii* parasites

1.2.8.1 *Toxoplasma gondii* as a model organism

Toxoplasma gondii serves as an ideal and important model organism for studying conserved features of apicomplexan biology. This is mainly due to the straightforwardness of culturing the parasite *in vitro*, particularly to high numbers, and its fast replication due to the short lytic life cycle and high efficiency of both transient and stable transfections relative to other apicomplexan parasites (Kim and Weiss, 2004). This makes *T. gondii* experimentally tractable, particularly as growing, maintaining, and genetically manipulating these parasites (through the availability of tools for both forward and reverse genetics) under laboratory conditions is readily amenable. This is different from other apicomplexan parasites such as *Cryptosporidium* spp., where *in vitro* culturing of these parasites which accurately reproduces infection dynamics of the parasite is difficult and relied on repeated animal infections until very recently (Varegg et al., 2025). Although *in vitro* culture of *P. falciparum* was introduced almost fifty years ago (Haynes et al., 1976; Trager and Jenson, 1978), the process is relatively inefficient and demanding with low transfection efficiencies, and extended timescales. In addition, due to its promiscuity, *T. gondii* can be grown and maintained in almost any nucleated host cell, an advantage compared to *Plasmodium* species which are restricted to specific host cell types including erythrocytes and hepatocytes (Cowman and Crabb, 2006). *T. gondii* are also considered relatively large (2x7 µm) compared to other apicomplexan parasites such as *Plasmodium* merozoites (1.2x1 µm), making imaging and subcellular protein localisation more attractive.

1.2.8.2 The genome of *Toxoplasma gondii*

The *T. gondii* genome was completed and sequenced twenty years ago (Khan et al., 2005). *T. gondii* has a haploid genome, around 65 Mb in size with 13 chromosomes (Bunnik et al., 2019), with many genes occurring as single copies. Interestingly, despite having the same number of chromosomes, the genome size of *T. gondii* is double that of *P. falciparum* (Khan et al., 2005), which may be due to a higher number of introns per gene and a lower gene density. In *T. gondii*, the GC content is approximately between 52 – 56 % (Lau et al., 2016; Yucesan et al.,

2021), compared to *P. falciparum* where the GC content is closer to 19 % (Gardner et al., 2002; Musto et al., 1999; Pollack et al., 1982). Thanks to VEuPathDB, the *T. gondii* genome sequences as well as annotations of the different strains of *Toxoplasma* are constantly being updated on free-access online databases such as ToxoDB, enriching the understanding of the biology of this parasite and enhancing reverse genetic tools (Gajria et al., 2007; Harb and Roos, 2020; Kissinger, 2003).

1.2.8.3 Reverse genetics

Over the past twenty years, elucidating the functions of genes within *Toxoplasma gondii* has been made possible due to the development reverse genetics. Reverse genetics is a genetic molecular tool that is used to assess the function of a gene by manipulating the DNA sequence in a genome, particularly by gene knockouts, insertions, or modifications, and then examining the consequence this has on the phenotype. In *T. gondii*, transfection of a plasmid/DNA sequence through electroporation to overexpress or knock down a gene of interest (GOI) is an effective way of assessing and characterising a variety of proteins in the parasite. Both transient (expression of a gene that is not integrated into the genome) and stable (targeted or random insertion of the GOI into the genome of the parasite) transfections were first reported in 1993, with dihydrofolate reductase-thymidylate synthase (DHFR) used as a selectable marker (Donald and Roos, 1993; Soldati and Boothroyd, 1995).

Homologous recombination is not favoured in *Toxoplasma gondii*. It has a low frequency and is more challenging to achieve in the parasite, limiting the ability of site-specific and targeted insertions. Instead, random integration is favoured where the parasite integrates DNA into the genome via the non-homologous end joining (NHEJ) DNA repair pathway. However, although it is a crucial and fast repair mechanism, mutations such as insertions or deletions, or the loss of some nucleotides could occur throughout the repair process. The presence of this DNA repair pathway results in the random insertion of DNA, making the precise and direct modification of specific genes challenging. The proportion of homologous recombination in the parasite can be enhanced through the generation of a parental parasite strain that lacks the Ku80 gene (ΔKu80). Ku80 is an essential gene for the NHEJ DNA repair pathway which joins the broken ends of double-strand breaks (DSBs) made in the parasite's DNA. Knocking out the Ku80 gene

therefore disrupts and inactivates the NHEJ pathway, now favouring and increasing the efficiency of homologous recombination in *Toxoplasma gondii*. This significantly increases the efficiency of gene knockouts, inserting or deleting DNA sequences within a GOI and tagging endogenous loci in *T. gondii* (Fox et al., 2009; Huynh and Carruthers, 2009). The ΔKu80 strain has been a powerful tool to genetically manipulate *Toxoplasma gondii* and has been exploited to make many mutant *T. gondii* strains to assess gene function.

As *T. gondii* has a low transfection efficiency, selection markers can be used, this allows the creation of stable, drug resistant lines. Common selection markers include dihydrofolate reductase-thymidylate synthase (DHFR), an enzyme essential for nucleic acid synthesis, which confers resistance to pyrimethamine and hypoxanthine-xanthine-guanine phosphoribosyl transferase (HXGPRT), an enzyme in the purine salvage pathway which converts purine bases into nucleotides, which can be selected for in the presence of xanthine and mycophenolic acid (MPA) (Donald et al., 1996). Uracil phosphoribosyltransferase (UPRT), a non-essential enzyme of the pyrimidine salvage pathway, functions as a negative selection marker in *Toxoplasma gondii*. Parasites expressing UPRT convert 5-fluorodeoxyuridine (FUDR) into toxic metabolites and are thus drug sensitive. ΔUPRT parasites are in turn resistant to FUDR and can be selected for (Donald and Roos, 1995). Lastly, the chloramphenicol acetyltransferase (CAT) marker confers parasite resistance to the drug chloramphenicol through inactivation (Kim et al., 1993). *T. gondii* are sensitive to chloramphenicol in the first instance as this antibiotic inhibits protein synthesis by targeting the large ribosomal subunit in the apicoplast, which has retained features of bacterial origin (Beckers et al., 1995; Fichera and Roos, 1997; Roos, 1999). The apicoplast is an important endosymbiotic plastid organelle in apicomplexan parasites and is discussed in more detail in section 1.5.4.1.

Although the deletion of the Ku80 gene has advantages and increases the efficiency of homologous recombination in *T. gondii*, there is a limitation to what genetic background it can be deleted in (Fox et al., 2011, 2009). The more recent adaptation of CRISPR (clustered regularly interspaced palindromic repeats) more than ten years ago has proven most promising for effective genetic manipulation and efficient and targeted gene disruption in *Toxoplasma gondii*, as well as for site-specific insertion of selectable markers through homologous recombination

(Shen et al., 2014; Sidik et al., 2014). The progress in this technique to efficiently disrupt genes has been made by exploiting a DNA recognition system used as a natural defence mechanism by bacteria and archaea to protect them against mobile genetic elements such as plasmids and bacteriophages/viruses (Barrangou et al., 2007; Gasiunas et al., 2012; Jinek et al., 2012). The most commonly used system for genome editing across a variety of organisms is the type II CRISPR system from *Streptococcus pyogenes* (Jinek et al., 2012). The system has two main components, the single guide RNA (sgRNA) which is composed of the 20-nucleotide CRISPR RNA (crRNA) which consists of homology regions that are complementary and binds to a specific target DNA sequence in the genome, and the Cas9 (CRISPR-associated gene 9) nuclease enzyme which is expressed simultaneously with the sgRNA and forms a complex together. The sgRNA guides the Cas9 enzyme to the complementary DNA sequence in the genome and then following the binding of the gRNA to its target DNA sequence via homology sequences, the Cas9 enzyme then introduces double breaks in the DNA in a target sequence homologous to the CRISPR RNA. The sgRNA-Cas9 complex primarily targets genomic sequences that are complementary to the 20-bp gRNA, however mismatches can potentially result in off-target cleavage. The binding of the complex to the target sequence also requires the presence of a protospacer adjacent motif (PAM) sequence. The PAM sequence is composed of 5'-NGG-3' nucleotides which allows the sgRNA/Cas9 complex to distinguish between the crRNA-coding sequence and the target DNA sequence. Following the binding of Cas9 to the target site by complementation between the target DNA and the crRNA, the enzyme cleaves the DNA sequence. The Cas9 enzyme cuts the DNA sequence three bases upstream of the PAM site, creating blunt ends. These double stranded breaks can then be repaired either by NHEJ or by homologous recombination (Jinek et al., 2012). Through the availability of a repair template, these DSBs can be repaired via homologous recombination, allowing for the precise and accurate insertions of drug resistance cassettes, point mutations or epitope tags in the *T. gondii* genome (Di Cristina and Carruthers, 2018; Sidik et al., 2014).

The constitutive expression of CRISPR/Cas9 has been exploited in *T. gondii* where it was elegantly used for a genome wide CRISPR/Cas9-based genetic screen to identify the fitness conferring genes in *in vitro* growth conditions. This has been a valuable resource for the *Toxoplasma* community (Sidik et al., 2016). Overall,

CRISPR/Cas9 has been a crucial genetic research tool for understanding the biology of *Toxoplasma gondii* through functional gene studies.

1.2.8.4 Gene knockdown (Tetracycline-inducible system)

Beyond direct modification of the genome, conditional expression systems allow for the phenotypes of essential genes to be assessed. One important conditional approach is the use of a tetracycline-inducible system. Briefly, the endogenous promoter is replaced with an inducible T7S4 (tetracycline transactivator binding element) promoter, which can be inhibited with the addition of anhydrotetracycline (ATc) (Sheiner et al., 2011a). This is possible as a result of the generation of a parasite line where two modifications were made, firstly the insertion of the tetracycline-regulated transactivator domain, or TATi, which is constitutively expressed from a strong promoter (Meissner et al., 2002), and secondly, the deletion of the Ku80 locus (Sheiner et al., 2011a). This RHΔKu80 TATi line will be referred to as F3ΔHX during this thesis. The tetracycline-dependent transactivator (tTA) binds to tetracycline operator sequences, or TetO-sequences upstream of a tet-responsive promoter (TRE) which then activates the transcription of genes. The T7S4 inducible promoter can then be inserted upstream of the GOI by homologous recombination, replacing the endogenous promoter with this Tet-inducible promoter (Sheiner et al., 2011a). tTA then binds to the T7S4 promoter (a tet-responsive promoter) to express the gene. In the presence of ATc, this tetracycline homologue inhibits the binding of tTA to TetO, thus preventing the binding of TetO sequences to the tet-responsive T7S4 promoter, in turn inactivating the T7S4 promoter and knocking down gene expression levels (Figure 1.3). A drawback of this inducible system is that ATC-induced downregulation is not a complete knockout, and residual activity can still exist. In addition, the expression of the T7S4 promoter, the non-endogenous promoter, can potentially overexpress the GOI in the absence of ATc.

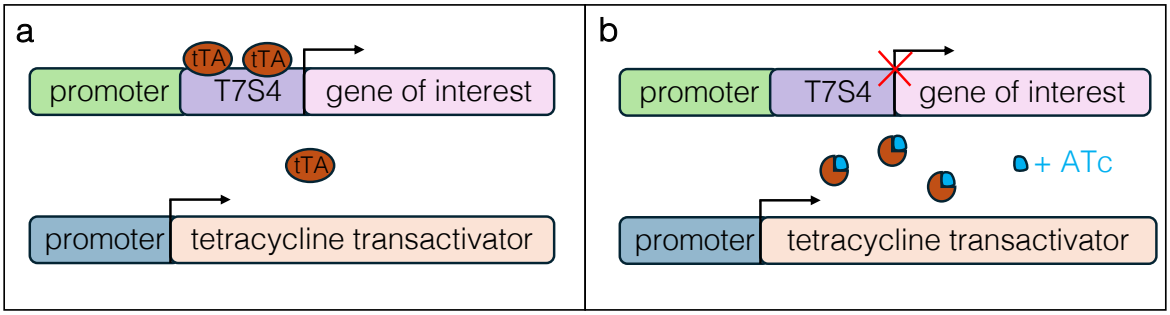


Figure 1.3 - Tetracycline inducible knockdown system.

a. Schematic of the tetracycline transactivator in the RHΔKu80 generating the RHΔKu80 TATi cell line, also referred to as F3ΔHX, which constitutively expresses a tetracycline-dependent transactivator, tTA. The endogenous promoter of the gene of interest is then replaced with a T7S4 promoter. Upon binding of tTA to the T7S4 promoter, the transcription of gene of interest is activated and the gene of interest is expressed. **b.** Upon the addition of the tetracycline homologue ATc, this binds to tTA and prevents it from binding to the T7S4 promoter. This inactivates the promoter and in turn results in the downregulation of gene expression levels.

1.3 Transition metals and their importance in eukaryotic biology

Transition metals, including iron and zinc, are essential and required nutrients for almost all eukaryotic life. They are essential co-factors in enzymes involved in the catalysis of many critical biochemical reactions in a range of biological systems. They play a critical role in a wide array of essential functions and metabolic processes including cellular respiration, translation, energy generation, metabolism and DNA replication (Teh et al., 2024).

1.3.1 Iron is essential for life

Iron is the most abundant element by mass on Earth, constituting around 32 % of the total mass and 80 % of the planet's inner and outer cores. It is also the fourth most abundant element on the surface of the Earth, making up approximately 6.3 % of the elemental composition in the crust (Frey and Reed, 2012). This ubiquity of iron and its versatile chemistry make it prevalent in many biological systems. Chemically, iron is redox active, with the two most common oxidation states of iron in biological systems being Fe (II) or Fe^{2+} in a complex (ferrous iron) and Fe (III) or Fe^{3+} in a complex (ferric iron). The ability and flexibility of iron to readily serve as an electron donor and acceptor and interconvert between oxidation states allows it to bind to oxygen and associate with proteins to shuttle electrons, mediating catalytic reactions (Aisen, 2001; Ganz, 2013). This underlies iron's critical role in biological systems under different physiological and environmental conditions.

Iron is an essential indispensable nutrient in almost all known life forms, serving as a co-factor for a number of essential enzymes such as involved in DNA synthesis, redox reactions, oxygen transport, energy production and metabolism (Cairo et al., 2006). Only a few prokaryotic species have been shown to not require iron (e.g. *Borrelia burgdorferi* (Posey and Gherardini, 2000), *Lactobac*illus *plantarum* (Archibald, 1983) and *Lactobacillus acidophilus* (Sabine and Vaselekos, 1967)) with all known eukaryotes requiring iron-bound enzymes. Approximately 2 % of the human genome encodes for proteins that contain iron. Out of these genes, 35 % encode for proteins that bind directly to iron ions (e.g. dioxygenase superoxide dismutase), 17 % are iron-sulphur (Fe-S) cluster-containing proteins (found

dispersed throughout cell, but are particularly found in the mitochondria in the TCA cycle where they play a critical role in energy generation) and 48 % encode for proteins that bind haem (Andreini et al., 2018). Haem-bound proteins including cytochromes and haemoproteins have a number of essential roles in metabolic processes, oxygen transport, and electron transfer in the mitochondrial electron transport chain for energy generation in biological systems.

Based on its toxicity (see section 1.3.3), iron-mediated regulation is vital for cellular health. A well-characterised mechanism for iron-dependent regulation in mammalian cells is the post-transcriptional iron-responsive element/iron regulatory protein (IRE/IRP) system. Genes involved in cellular iron homeostasis, such as the transferrin receptor (TfR), which mediates the primary pathway for iron uptake, contain short stem-loop structures known as iron-response elements (IREs) (Sanchez et al., 2011; Suárez-Quintana et al., 2025). Under low iron conditions, the metabolic enzyme aconitase (also known as iron-regulatory protein 1, IRP1) loses its Fe-S cluster cofactor. This loss inactivates aconitase's enzymatic function and enables aconitase to adopt an alternative role as an RNA-binding protein, where it interacts with IREs located in the UTRs of specific genes (Cho et al., 2021; Hentze et al., 1987; Koeller et al., 1989). Importantly, the position of an IRE within a transcript dictates whether translation is enhanced or whether the transcript is repressed. When IREs are located in the 3' UTR of a gene, they often act to stabilise the transcript and promote protein synthesis (Erlitzki et al., 2002; Koeller et al., 1989).

1.3.2 Zinc is essential for life

Another highly abundant metal is zinc. Although constituting a smaller percentage of the Earth's total mass when compared to iron, the stability of zinc as well as it's bioavailability in a range of environmental conditions make it an essential micronutrient for many biological systems. Chemically, zinc almost always exists in a 2+ oxidation state (Zn^{2+}) to form a stable ion and unlike other transition metals, it does not typically form a variety of other oxidation states and thus is not involved in reversible electron transfer.

Zinc is a ubiquitous transition metal essential in all living organisms, conferring a role in a wide range in physiological and cellular functions critical for many

biological processes. It is a defining feature of eukaryotic cells where approximately 3-10 % (~3000 proteins) of the human genome encodes for zinc-binding proteins (Andreini et al., 2006a; Maret, 2005, 2013; Rosenzweig, 2002), and 5-6 % of prokaryotic proteins contain Zn^{2+} (Andreini et al., 2009). Zinc is the second most abundant micronutrient in the human body after iron, and is an essential cofactor of a number of regulatory proteins and enzymes playing a critical role in maintaining redox balance and the catalysis of at many proteins including transcription factors and enzymes, playing a role in cellular control and signal transduction (Maret, 2013, 2009; Yamasaki et al., 2007). Zinc plays a critical role in the proliferation, differentiation and apoptosis of mammalian cells in addition to intercellular and extracellular communication signalling (Beyersmann and Haase, 2001; Chen et al., 2024; Maret, 2017). Zinc is also involved in the regulation of gene expression (through the stabilisation of zinc finger motifs in transcription factors), chromatin structure, antioxidant defences, immune responses, and DNA metabolism and synthesis in mammalian cells (Maret, 2013). Across all phyla and enzyme classes, over 300 zinc-dependent enzyme classes have been identified (Coleman, 1992).

1.3.3 Metal toxicity

Although the flexibility of the redox state of iron is critical in its role in many biological processes including the catalysis of enzymatic redox reactions and energy generation, this redox activity also poses a risk and could be deleterious if not controlled. In aerobic conditions, iron can act as catalysts for reactive oxygen species (ROS) and can be toxic to the cell (Galaris et al., 2019; Imlay et al., 1988). Free ferrous iron (Fe^{2+}) can catalyse the Fenton reaction by reacting with hydrogen peroxide H_2O_2 in the cell to catalyse the generation of reactive oxygen and nitrogen species including highly reactive radicals like hydroxyl radicals (OH) (Graf et al., 1984; Winterbourn, 1995). This can be toxic by causing DNA damage and can often lead to cell death (Dixon and Stockwell, 2014). Thus, free intracellular Fe^{2+} has to be tightly regulated through specialised acquisition/uptake, storage, utilisation and export pathways to minimise the risk of metal toxicity (Hentze et al., 2004).

In addition to iron, zinc levels also have to be tightly regulated as studies have shown that both an excess and deficiency of zinc can be deleterious to cells,

causing protein misfolding and apoptosis (Choi and Koh, 1998; Kim et al., 2000; Sheline et al., 2000). Studies have found that an increase in zinc concentrations is toxic to cells due to mitochondrial impairment, oxidative stress, an increase in the generation of ROS and eventually cell death (Slepchenko et al., 2017; Stork and Li, 2016). In HeLa cells (Knies and Li, 2021) and H9c2 cardiomyocytes (Turan et al., 2024; Yang et al., 2023), exposure to excess zinc causes mitochondrial disfunction and eventually cell death. Given the wide range of biological processes that require zinc, levels are also tightly controlled within cells to avoid zinc toxicity and thus levels are maintained at low physiological concentrations (Krężel and Maret, 2016; Lu et al., 2016). Similar to iron, the uptake, export, storage and subcellular distribution of zinc is tightly regulated, mainly through metallothioneins, zinc transporters (ZnT) as well as Zrt/Irt-like (ZIP) zinc importer proteins (Kambe et al., 2021, 2017, 2014) which will be discussed in detail in section 1.4.

1.3.4 The role of transporters in metal uptake

The majority of transporter substrates, e.g. glucose or sodium cations are able to diffuse down concentration gradients across biological membranes. However, the chemical properties of essential trace elements such as iron and zinc, means that they cannot passively diffuse across membranes, and require specific molecular mechanisms for their transport across biological membranes. As these metals are essential for almost all eukaryotic life, many organisms have established a range of approaches to acquire and uptake metals from the environment. Metal acquisition also has to be regulated and coordinated alongside storage, detoxification, and efflux methods within cells to maintain cellular metal homeostasis. Therefore, metal transporters are found both at the plasma membrane and internal membranes such as the mitochondria. Understanding the molecular mechanisms of metal uptake therefore gives a crucial insight into physiological metal homeostasis.

1.3.4.1 Transport mechanisms

In cellular systems, the movement of molecules across biological membranes can be divided into two mechanisms: passive and active transport (Baldwin, 2000). Passive transport does not require energy, instead it relies on the second law of

thermodynamics to drive the movement of ions from a high concentration to a low concentration. Passive transport is broken down into simple passive diffusion or facilitated diffusion, also known as carrier-mediated diffusion (Stillwell, 2016). Passive diffusion is where small uncharged molecules move from a high to low concentration across the membrane, and this is solely governed by the differences in concentration gradient (Sadée et al., 1995). If molecules are too charged or large to pass across the membrane by simple diffusion, they are able to cross the membrane via channel proteins which are embedded in the membrane. In facilitated diffusion, particles are still moving from a high to low concentration gradient and also do not require cellular energy (Sadée et al., 1995). Uniport, symport and antiport transport are all mechanisms of facilitated diffusion and are mainly distinguished by the number of molecules and the direction of the transport (Goswitz and Brooker, 1995; Yan, 2015). Uniport transports a singular molecule across a membrane and in one direction and often relies on a carrier protein. Symport is a form of secondary active transport, and transports two molecules across a membrane in the same direction by using the movement of one ion down its concentration gradient across the membrane to then provide for an “uphill” movement of another ion against its concentration gradient. Finally, antiport transport two molecules across a membrane in opposite directions. Similar to symport transport, antiport also relies on the movement of one ion down it’s concentration gradient and the opposite movement of another molecule against its concentration gradient (Goswitz and Brooker, 1995; Yan, 2015).

On the contrary, active transport describes the process of the movement of ions across a cell membrane from a low concentration gradient to a higher concentration gradient (Stillwell, 2016). As the transport of these ions is across the concentration gradient, the process of active transport requires energy, often in the form of adenosine triphosphate (ATP). In active transport, molecules bind to one side of a carrier protein embedded within the cellular membrane, which then undergoes morphological changes and transports the molecule to the other side of the membrane. The conformation change in the carrier protein in active transport is what requires energy. An example of an active transport protein are P-Type ATPases which use the hydrolysis of ATP for the transport of metal ions across membranes (Bublitz et al., 2011; Keeran et al., 2021; Solioz and Vulpe, 1996; Zhitnitsky and Lewinson, 2014). The hydrolysis of ATP leads to the transfer

of a phosphate group to an aspartate residue on the enzyme, forming a phosphorylated intermediate. This then leads to a conformational change in the protein, altering its structure and changing the sites where ions can bind, allowing them to transport across the membrane. The phosphate intermediate is then released, allowing the transporter to then return to its original confirmation ready to bind another ATP (Apell, 2004; Rosenzweig and Argüello, 2012) .

Transporters have differing levels of selectivity and redundancy, with either a single transporter transporting multiple metals, or the same metal having multiple transporters it can cross biological membranes through. In addition, metal transporters often lack a high level of specificity, and sometimes metals of a similar valency, size or chemical properties can be transported across the membrane by the same protein. For example, Cd^{2+}, although toxic with no biological role, is often transported across membranes via the ZIP family of transporters (discussed in section 1.4) which play a role in acquiring Zn^{2+} from the extracellular environment into the cytoplasm of cells (Yang et al., 2025).

1.4 Zrt/Irt-like proteins (ZIPs): Their role in the transfer of divalent metals across biological membranes

In this section, I will focus on the structure, function, transport mechanisms, substrate specificity, and regulation of Zrt/Irt-like protein (ZIP) transporters, also known as the solute carrier family 39A (SLC39A) in mammalian cells (Eide, 2004). Further, I will give some detail on the current knowledge of ZIPs in organisms including yeast, plants, mammalian cells, and protozoan parasites.

1.4.1.1 Function and characteristics of ZIP proteins

ZIPs are ubiquitous metal transporters, and since their discovery in 1996 in yeast, have been identified across all kingdoms of life including bacteria, plants, fungus, archaea, protozoans, prokaryotes and eukaryotes (Eide, 2004; Gaither and Eide, 2001a). ZIPs play a critical role in the uptake, compartmentalisation, and cellular homeostasis of transition metals including zinc, iron, and manganese. A key feature of the ZIP family is that they play a central role in the uptake of these metals from the extracellular environment, as well as regulating their release from intracellular organellar compartments such as the endoplasmic reticulum, mitochondria, and Golgi apparatus into the cytosol of cells.

1.4.1.2 ZIP family

Since their identification in 1996, ZIP family proteins have been discovered across various organisms. As such, the classification of the mammalian ZIP metal transport family of proteins has been evolving (Gaither and Eide, 2001a; Guerinot, 2000). Currently, the widely accepted classification of ZIPs based on phylogenetic analysis, sequence similarity, functional characteristics and structural motifs divides the family into four known subfamilies – ZIPI, ZIPII, GufA and LIV-1, although there may be more (Hu, 2021; Hu and Jiang, 2024). Subfamilies ZIPI, ZIPII and GufA are more closely phylogenetically related compared to LIV-1, which is mainly found in mammals and is associated with LIV-1, an oestrogen-regulated gene (Taylor and Nicholson, 2003). The LIV-1 subfamily of ZIP proteins has a conserved motif (HEXPHEXGD) in transmembrane protein 5 (TM5), and has been shown to be a site for zinc ion transport within the transmembrane domain of the protein (Taylor and Nicholson, 2003). The length of the extracellular domain (ECD) has also been shown to be variable depending on the subfamilies. For example,

the ECD is very small or non-existent in subfamilies ZIPI, ZIPII and GufA (Fukada and Kambe, 2011), however exhibits diverse lengths at the N-terminal domain of the ECD in the LIV-1 subfamily of ZIP proteins (Taylor and Nicholson, 2003; Zhang et al., 2016). In mammalian cells, 14 ZIPs have been identified. ZIP9 belongs to the ZIPI subfamily, ZIP11 belongs to the GufA subfamily, and ZIP1,2, and 3 belong to the ZIPII subfamily. The remaining mammalian ZIPs (ZIP4-8, ZIP10, and ZIP12-14) belong to the LIV-1 subfamily of ZIP proteins.

1.4.1.3 Structure of ZIP proteins

ZIP transporters are integral membrane proteins (Hu and Jiang, 2024) typically ranging between 309 and 476 amino acids and are approximately 2-4 kilobases in length, with most ZIP genes containing at least three exons (Ajeesh Krishna et al., 2020). Two ZIP transport protein structures have been characterised. The bacterial ZIP from *Bordetella bronchiseptica* (BbZIP) (Pang et al., 2023; Zhang et al., 2017) revealed that the structure of ZIPs is evolutionary conserved across eukaryotes, as the structure closely aligns with the computationally predicted human ZIP protein HsZIP4 (Antala et al., 2015). The second structure was from the extracellular domain of ZIP4 in the black fruit bat *Pteropus alecto*, which was shown to have 68 % homology with the human HsZIP4 protein (Zhang et al., 2016).

The X-ray crystal structure of BbZIP revealed the architecture of the transmembrane domains, which is predicted to be conserved across all ZIP family proteins (Zhang et al., 2017). The ZIP protein families are predicted to have eight transmembrane (TM) helices (TM1-TM8, also referred to as α1-α8), with both the N-terminus soluble domain and short C-terminus of the protein exposed to the extracellular environment (Hu and Jiang, 2024). This was confirmed through the X-ray structure of BbZIP (Zhang et al., 2017). The TMD of ZIP proteins play a core role in directly mediating metal uptake across the membrane, compared to the N-terminus in the extracellular domain and intracellular loops which mostly play a regulatory role. In BbZIP, the core TMD transport channel across the membrane contains TM2, TM4, TM5 and TM7, and the extracellular outer helices consist of TM1, TM3, TM6 and TM8 (Zhang et al., 2017). In human ZIPs, the C-terminal sequences are short, ranging from a single residue in ZIP1, 5 and 11, to ten residues in ZIP6 (Wang et al., 2025). Short C-terminal sequences contain short linear motifs (SLiMs), or minimotifs that serve as a site for protein-protein

interactions (Sharma and Schiller, 2019), possibly suggesting their functional involvement in targeting ZIPs to specific cellular compartments and highlights the possibility of their involvement in post-translational modifications.

Another unique feature of ZIPs among other transporters is the transmembrane domain architecture known as the 3+2+3 architecture. This is where TM1-TM3 can be superimposed on TM6-TM8 following a 180° rotation, and TM4 and TM5 are related symmetrically and sandwiched in the middle between the two three-transmembrane domains on either side (Zhang et al., 2017). TM4 and TM5 domains of ZIPs form the core transport pathway, and often contain conserved residues including histidine, aspartate and glutamate, facilitating the binding and translocation of metals (Antala and Dempski, 2012; Lin et al., 2010).

Moreover, the structure of BbZIP was revealed as a monomer with an inward facing confirmation and conserved residues in the binuclear metal centres (BMC) in the transmembrane pore of the protein/centre of the transport pathway. The BMC consists of two bridged metal binding sites M1 and M2 within the transmembrane helices α4 and α5, which can be occupied by zinc or cadmium (Zhang et al., 2017) (see section 1.4.1.4). Another defining feature of ZIP proteins is the extended intracellular cytoplasmic domain loop (IL2) between TM3 and TM4, where a histidine-rich cluster is often found, which plays an important role in sensing intracellular zinc levels and regulating zinc uptake and maintaining intracellular zinc homeostasis (Milon et al., 2006; Pang et al., 2023). Studies have shown that the histidine-rich cluster in the cytoplasmic domain (CTD) of HsZIP4 in mammalian cells mediates the ubiquitination and degradation of this transporter to protect against zinc toxicity (Mao et al., 2007). However, not much is known about the CTD of ZIPs and further research is required to understand their role in the function of ZIP transport proteins. Finally, the presence of α helices in the extracellular loops is also a key features of ZIP proteins, playing a critical role in zinc and iron metal coordination (Hu and Jiang, 2024; Potocki et al., 2014; T. Zhang et al., 2019). A basic schematic of the membrane topology of ZIP proteins is represented in Figure 1.4.

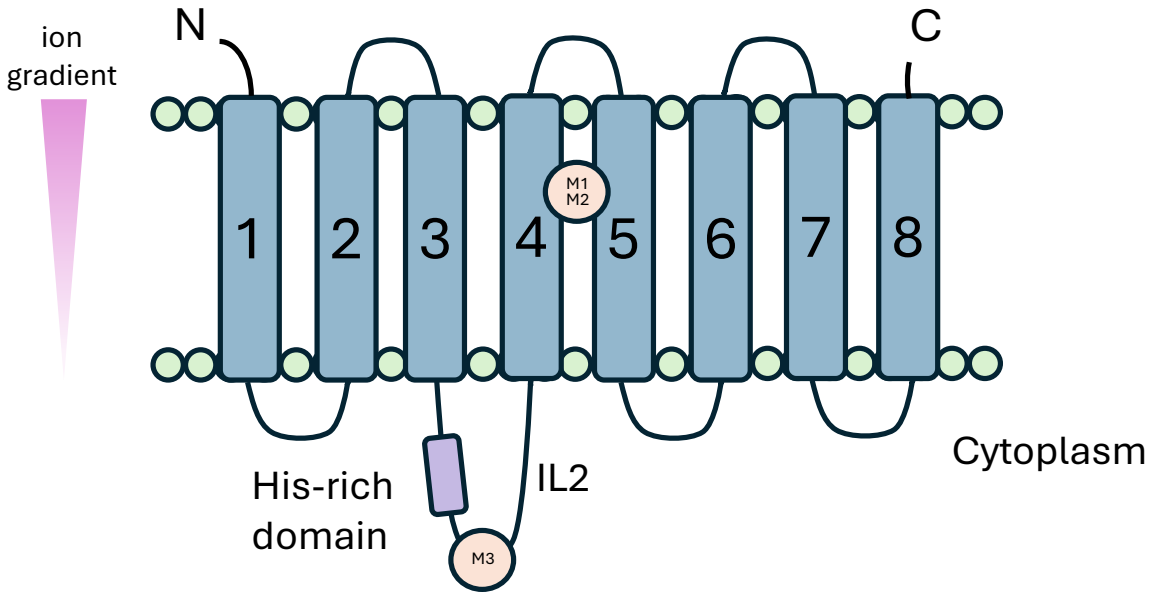


Figure 1.4 - Schematic of membrane topology of ZIP proteins.

Schematic of the topology of a ZIP protein, containing eight transmembrane domains (TM1-TM8) highlighted in blue, with both the N-terminus extracellular domain and C-terminus facing the extracellular environment. The histidine rich domain between TM3 and TM4 in the intracellular loop 2 (IL2) is highlighted in purple. The metal binding sites M1, M2 and M3 are also highlighted in orange. Adapted from Hu and Jiang, 2024.

1.4.1.4 Metal binding of ZIPs

The ability of ZIP transporters to selectively import divalent metal ions is dependent on the metal binding sites in the protein. This step is critical in the ZIP-mediated functional transport of metals across membranes. The presence of the BMC located within transmembrane domains TM4 and TM5 of ZIPs is central to the function of metal binding sites. This forms the metal transport site which is composed of both the M1 and M2 metal binding sites which mediate substrate specificity and metal transport (Zhang et al., 2017), and have been shown to be required for metal binding (Wiuf et al., 2022). The conserved sequence motif HEXXHE for example, is a LIV-1 specific motif in TM5 which serves as the BMC in BbZIP (Zhang et al., 2017). The presence of a histidine rich domain in the N-terminal extracellular domain of the human HsZIP4 has been shown to be essential for the high affinity binding of zinc ions and functional zinc transport (T. Zhang et al., 2019). Histidine residues within the TMD have also been identified as important for the binding of zinc as well as substrate selectivity and transport efficiency (Hu and Jiang, 2024; T. Zhang et al., 2019). Both ZIP6 and ZIP10 have

also shown to have conserved histidine residue motifs that are required for the binding and transport of zinc (Taylor, 2023; Taylor and Nicholson, 2003). The conserved motif histidine-asparagine-proline (HNP) in TM2 of ZIPs and the conserved motif HXXHXDH in TM4 have also both been implicated in the binding and translocation of metals in ZIP proteins efficiency (Hu and Jiang, 2024; T. Zhang et al., 2019).

The metal binding site M1 in the BMC of TM4 and TM5 has been shown to be crucial in metal binding in ZIPs. The M1 site in BbZIP is formed by residues between TM2, TM4 and TM5; M99 on TM2, H177 and E181 on TM4, and Q207 and E211 on TM5 (Pang et al., 2023; Sharma and Merz, 2021) (Figure 1.5). The M1 site has been shown to often be conserved and is essential for the activity of HsZIP4 (Sharma and Merz, 2021; Zhang et al., 2020). Mutagenesis of HsZIP4 demonstrated that the M1 binding site is essential for zinc transport activity. The M1 binding site in the resolved structure of BbZIP constitutes of amino acid residues Glu177, His181 and Gln207, and in the outward facing confirmation, zinc ions have access to and can bind to the M1 metal binding site. Residues in the M1 binding site have been shown to be more highly conserved than M2, supporting that this metal binding site has an essential role in the transport of zinc (Kambe et al., 2021; Zhang et al., 2017).

The specific amino acid residues of the M2 binding site are less conserved but in BpZIP are commonly located on TM4, TM5 and TM6, and often by the following residues: N178 and E181 on TM4, D208 and E211 on TM5 and either E239 or E240 on TM6 (Pang et al., 2023; Sharma and Merz, 2021; Zhang et al., 2017) (Figure 1.5). The BbZIP structure showed significantly less site occupancy at the M2 site compared to the M1 site (Pang et al., 2023; Zhang et al., 2023), and mutagenesis of the M2 metal binding site in BbZIP demonstrated that this site is not essential for the transport activity of zinc (Zhang et al., 2017). Compared to the M1 binding site in HsZIP4, the M2 site is less conserved, more variable and can be dispensable for metal binding. M2 mutagenesis did not completely diminish zinc transport activity and did not affect the substrate specificity of HsZIP14 (Sharma and Merz, 2021; Zhang et al., 2020). The M2 metal binding site in HsZIP4 has instead been shown to maintain its activity in a broad range of pH (Zhang et al., 2020). Studies have also shown the importance of the M2 metal binding site. Examination of the M2 site of HsZIP2 has demonstrated that a lysine residue replaces the metal

chelating residue which prevents the binding of a second metal ion. This was shown to be crucial for the transport activity (Gyimesi et al., 2019).

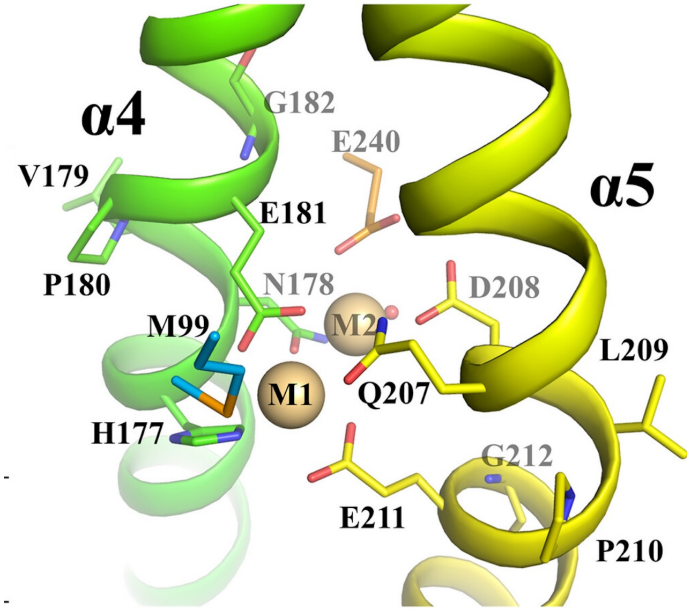


Figure 1.5 - The binuclear metal centre in the transport pathway in BbZIP.

Figure demonstrates the binuclear metal centre (BMC) in helices α4 and α5 in the middle of the transport pathway in BbZIP. Both M1 and M2 metal binding sites with conserved residues involved in metal binding highlighted as sticks. Figure taken from Hu, 2021. Republished by permission from John Wiley and Sons, FEBS Journal, conveyed via Copyright Clearance Centre. License number: 6140850256717.

The conserved histidine residues in the intracellular loop 2 (IL2) between TM3 and TM4 have also been shown to harbour two high affinity zinc binding sites in the mammalian ZIP4 (Bafaro et al., 2019). The recent cryo-EM structure of the bacterial BbZIP shows that these histidine residues in the intracellular loop IL2 are able to form a high affinity metal binding site, M3, which is near the cytoplasmic surface and is formed by Asp144 on TM3, Glu276 on TM7, and the histidine residues in the IL2 including His149 and His151 between TM3 and TM4, critical for sensing intracellular zinc levels and facilitating zinc transport activity (Pang et al., 2023).

1.4.1.5 Transport mechanism of ZIP proteins: Two-domain elevator-type mechanism

Now that the metal is bound to the metal binding sites in the transport pathway between helices α4 and α5 of ZIP, how does this lead to translocation of the metal across the lipid bilayer? It has been proposed that BbZIP functions as a Zn^{2+}/H^{+} antiporter (Pang et al., 2023). It was originally proposed to be an ion channel forming a pore and that its uptake mechanism of zinc is pH sensitive (Lin et al., 2010). Although passive influx of zinc ions across the membrane is possible down the electrochemical gradient, both secondary active transporters as well as channel transport mechanisms have been proposed for ZIPs. The transport of metals via ZIPs has been proposed to be coupled to the transportation of other solutes. For example, $Zn^{2+}/HCO3^{-}$ transport has been proposed in human ZIP1, ZIP2, ZIP8, and ZIP14 (Gaither and Eide, 2001b, 2000; Girijashanker et al., 2008, 2008; Liu et al., 2008). Zn^{2+}/H^{+} symport (Hoch et al., 2020) for HsZIP4 as well as passive transport for HsZIP2, which prefers a low pH, (Gyimesi et al., 2019) have also been proposed. However, until recently, the mechanisms by which ZIPs transport metals across biological membranes have remained elusive.

Recent structural, evolutionary and mutagenesis studies in the bacterial BbZIP have outlined the unique transport mechanism employed by ZIP proteins for the transfer of metal ions across a membrane, pointing to an elevator-type transport mechanism likely conserved across ZIP proteins (Wiuf et al., 2022; Zhang et al., 2023). This two domain elevator model of the dimer was proposed as a mechanism of metal ion transport by ZIP proteins which has a static scaffolding domain and a more dynamic transport domain (Wiuf et al., 2022; Zhang et al., 2023). The studies propose that ZIP transporter proteins form stable scaffold domain-based dimers that exploit an oscillating elevator type mechanism which allow the transition of transmembrane domains between an outward facing confirmation (OFC) and an inward facing confirmation (IFC) (Wiuf et al., 2022; Zhang et al., 2023) (Figure 1.6). Firstly, the opening between TM2 and TM8 in the OFC which is likely due to the highly conserved S106 on α4, D305 and surface facing D113 amino acid residues, allows for the recruitment of ion from the extracellular space into the negatively charged cavity. The S106 residue acts as a gating residue at the entrance of the pore. This in turn provides access to the functional and conserved amino acid residues E181, E211 and Q207 of the M1 metal binding site, the

selectivity filter. The binding of metals at the M1 site then triggers a slight confirmational change; a rotation in an “elevator-like” translocation from an outward facing confirmation slightly towards the intracellular side along the scaffold domain, with the metal ion still bound at the M1 site almost exclusively through the side chains of the transmembrane domains α4 and α5. In low intracellular metal conditions, the release of the metal ion across the membrane in the inward open metal-bound state is then facilitated by the delivery of the metal ions to conserved residues in transmembrane proteins TM2, TM3 and TM7: D144 (on TM3), H275 (on TM2) and E276 (on TM7) (Pang et al., 2023; Wiuf et al., 2022). E276 changes its side chain to permit the receival of the metal ion from the M1 metal binding site and is then passed on to D144 and then released into the cytosol. The transport domain then reverts back to the original metal free outward facing confirmation and the cycle continues.

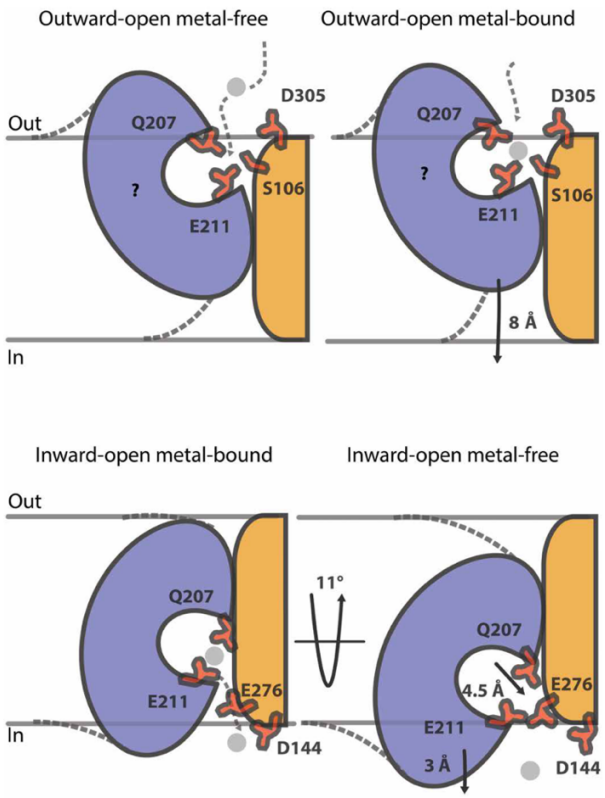


Figure 1.6 - Two-domain elevator-type transport mechanism of BpZIP.

Schematic diagram of the proposed two-domain elevator type transport mechanism of BpZIP showing key functioning residues in red. Metal ions are represented in grey. TM5 is represented in purple and TM7 is shown in orange. ZIP dimers allow for the formation of a stable scaffold which transforms between an outward-open metal free state where the metal ion then binds, to an inward-open state where the ions are then released into the cytoplasm. Image taken from Wiuf et al., 2022.

The histidine residues His149 and His151 in the IL2 loop of BpZIP have been shown to be involved in sensing intracellular zinc levels, particularly when the intracellular zinc threshold is reached (Pang et al., 2023). Together with Asp144 on TM3, a third inhibitory metal binding site M3 is formed in some ZIPs such as HsZIP8 and HsZIP14. This inhibits the release of any further zinc into the cell and prevents the conformational change from an inward facing confirmation to an outward facing confirmation, blocking transport activity until intracellular zinc levels are restored (Pang et al., 2023). This is demonstrated in Figure 1.7 below.

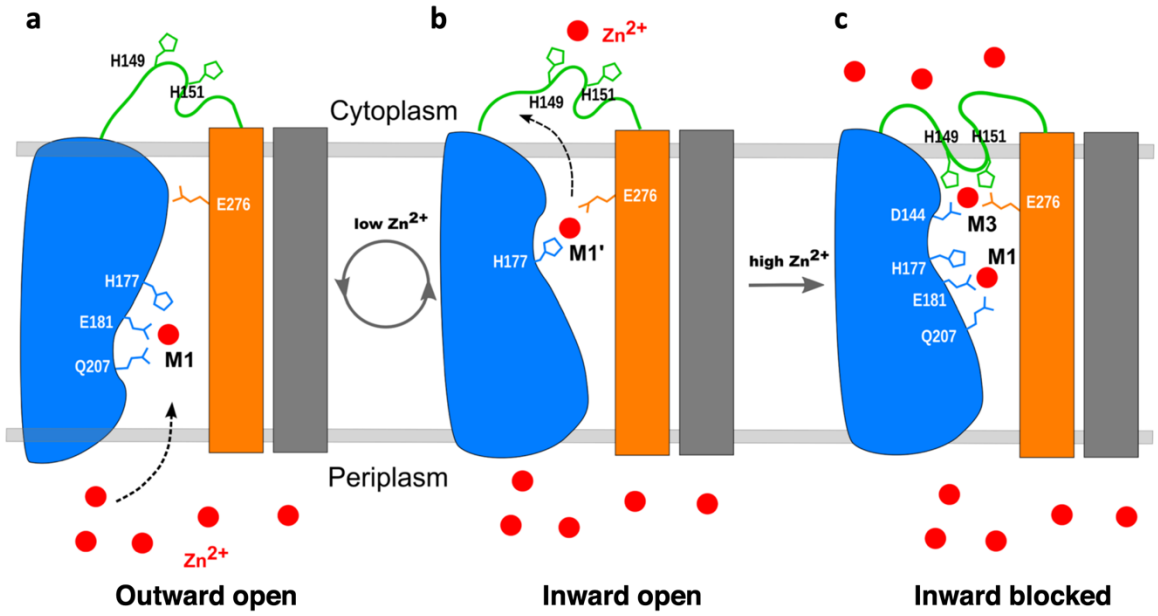


Figure 1.7 - The proposed mechanism of zinc sensing and regulation by BpZIP via His149 and His151.

In the outward open confirmation, conserved amino acid residues E181 and H177 on TM4, and Q207 on TM5 form the M1 binding site in the active transport pathway between TM4 and TM5, and under low zinc conditions zinc is transported across the lipid bilayer into the cytoplasm in the inward open confirmation. H149 and H151 conserved histidine amino acid residues are able to sense the intracellular zinc conditions, and under high zinc concentrations interact with D144 on TM3 to form a third metal binding site which is inhibitory; blocking the transport of zinc across the membrane. Figure taken from Pang et al., 2023.

1.4.1.6 Substrate specificity of ZIP proteins

When first discovered in yeast in 1996, it was thought that ZIP proteins only transported zinc. However, since then, the substrate spectra of members of the ZIP family have been shown to extend beyond zinc, to Fe^{2+}, Mn^{2+}, Cd^{2+}, Co^{2+}, Cu^{2+} and Ni^{2+}. Each ZIP transporter has a specific affinity and specificity for different metals (Gaither and Eide, 2001a; Guerinot, 2000). The differences observed between the affinity of ZIP proteins to different metals and the kinetics of metal transport is dependent on the selectivity for metal ions and the concentrations of the substrates. This is supported by the ZIP transporter in *E. coli*, ZupT, which has been shown to transport a broad spectrum of substrates including zinc, iron, cobalt and possibly manganese (Grass et al., 2005). Although the promiscuity of some ZIPs has been retained throughout evolution (for example AtIrt1 in plants and HsZIP8 and HsZIP14 in humans), other ZIPs, such as HsZIP4, have evolved to have a tighter and narrower substrate spectrum, becoming more specific transporters, mostly for zinc. Zrt1 in yeast and Irt1 in *A. thaliana* have been shown to selectively transport iron and zinc but can transport other transition metals in cases of metal deprivation. For example, Zrt1 in yeast has been shown to transport cadmium and to a lesser extent cobalt and manganese (H Zhao and Eide, 1996). AtIrt1 in plants primarily takes up iron, however has also been shown to transport zinc, cadmium, manganese, cobalt and nickel (Korshunova et al., 1999). Mammalian ZIP8 and ZIP14 have also been shown to play a role in cellular cadmium uptake to avoid cadmium induced toxicity within cells (Jenkitkasemwong et al., 2012). Notably, both mammalian ZIP8 and ZIP18 have been shown to transport a broad spectrum of substrates compared to other members of the LIV-1 subfamily ZIP members, including iron and manganese in addition to zinc, demonstrating the range of functional diversity of ZIP proteins (Aydemir and Cousins, 2018; C.-Y. Wang et al., 2012).

The promiscuity of these ZIP is often largely dependent on variations in conserved metal binding motifs, often histidine residues in TM4 and TM5 which are important in the binding and translocation of metal ions (Eide, 2006; Jeong and Eide, 2013). In HsZIP8 and HsZIP14, the first histidine residue, which is highly conserved in LIV-1 ZIPs, is replaced with a glutamate in the second motif in the transport site. This substitution of amino acid residues (E343 in the human HsZIP8) is likely to be linked to the broader substrate specificity of both HsZIP8 and HsZIP14. Mutations

in residues (E343H or E343A) in the TM5 of the human HsZIP8 prevent transport of manganese and cadmium (Fujishiro et al., 2022), highlighting its role in substrate specificity. Moreover, studies demonstrated that the E343H variant also did not demonstrate any zinc transport activity (Jiang et al., 2023), further implicating the importance of this residue in the substrate specificity and transport activity of HsZIP8 in iron, zinc and manganese acquisition. Interestingly, the substitution of residue Q180H, which localises at the beginning of the metal transport pathway, with a histidine that is conserved amongst other LIV-1 ZIP proteins was able to rescue the E343 variant and also demonstrated an increase in zinc selectivity over cadmium (Jiang et al., 2023). Other mutations with substituted C310A and N357H as well as Q180H and E343H resulted in a variant which demonstrated increased activity of zinc transport and reduced the activity of iron, manganese and cadmium uptake (Jiang et al., 2023). This study highlights the importance of the Q180 and E343 residues within the transport pathway in substrate specificity of HsZIP8 by forming a selectivity filter and screening for metals before entering the transport site. Unlike other LIV-1 proteins where there is a HNXXD sequence motif in TM4 of the protein, it is switched in ZIP13 where the sequence motif is DNXXH instead. Mutations that swap the D/H residues in this distinct sequence motif in TM4 in the BMC of ZIP13 reduce iron uptake activity, altering the substrate specify and preference of ZIP13 in *Drosophila melanogaster* (Zhao and Zhou, 2020). Although many ZIPs exhibit similar architectures, subtle variations in amino acid residues in the metal binding regions as well as structural differences underpin their substrate specificity, selectivity and affinity depending on the need and availability for the metal ions in the environment. The presence of the M1 selectivity filter creates a metal binding pocket that plays an important role in coordinating metal binding and is critical for avoiding the transport of non-specific metals across membranes, ensuring that the correct metals are efficiently acquired to maintain metal homeostasis within cells.

1.4.1.7 Dimerisation of ZIP proteins

Both bacterial and mammalian ZIPs can form either homodimers or hetero-dimers, thought to stabilise the transporters or facilitate confirmational changes to allow the transport of metal ions across the membrane (Bin et al., 2011; Lin et al., 2010; Liu et al., 2022; Taylor et al., 2016; Zhang et al., 2016). In bacteria, studies on the ZIP-family transporter BbZIP from the prokaryote *Bordetella bronchiseptica,*

also sometimes referred to as ZIPB, have confirmed the formation of a dimer. BbZIP ran as a homodimer on size exclusion columns, and crystallisation interestingly demonstrated both a monomeric and dimeric state (Zhang et al., 2017). This was further supported when the structure of the BbZIP was determined by cryo-EM studies, providing direct evidence of dimer formation. In BbZIP, the dimer interface has been shown to be stabilised via interactions between TM2, TM3 and TM7 (Pang et al., 2023). In eukaryotic cells, the biochemical characterisation of the mammalian ZIP13 has shown that the purified zinc transporter functions as a homodimer, although sometimes ran as a monomer on a blue native page analysis (Bin et al., 2011). In addition to ZIP13, ZIP6 and ZIP10 in mammalian cells have been shown to form a heterodimer critical for their function, suggesting that the existence of ZIPs in dimeric states may have a role in downstream cellular processes such as signal transduction (Taylor et al., 2016). Studies have also predicted that the human HsZIP4 also exists and functions as a homodimer *in vivo*, with the extracellular domain shown to be essential for the dimerisation of this transporter (Liu et al., 2022).

1.4.1.8 Extracellular domain (ECD) of ZIPs

The N-terminus in the extracellular domain (ECD) of ZIPs is highly variable in eukaryotes and is thought to also contribute to substrate specificity. In prokaryotes, this ECD is often short, non-conserved and unstructured. In eukaryotic cells, particularly in the LIV-1 subfamily of ZIP proteins, the ECD have evolved to be longer, folded and more highly conserved. The only crystal structure of the ZIP ECD is the ZIP4 protein from *Pteropus alecto*, a black fruit bat (Zhang et al., 2016). The ECD of ZIP4 has 14 α helices and an N-terminal histidine rich domain (HRD) (T. Zhang et al., 2019), which is stabilised by four conserved disulfide bonds (Zhang et al., 2016), and has a conserved proline-alanine-leucine (PAL)-motif containing domain (PCD) in the C-terminal domain. The PCD is only present in the LIV-1 subfamily of mammalian ZIP proteins (ZIP5, 6, 8, 10, 12 and 14) and plays a role in mediating the dimerisation of the ZIP4 ECD. However, studies have shown that the extracellular domain of ZIP4 is not essential for its dimerisation (Liu et al., 2022), and thus the role of the PCD in ZIP dimerisation remains unclear. Deleting this domain led to a loss of transport activity by approximately 75 %, emphasising and highlighting the importance of the ECD in the function of ZIP4 in zinc acquisition (Zhang et al., 2016). However, this was

challenged in a later study which showed that the depletion of the ECD of ZIP4 did not alter the transport of zinc (Liu et al., 2022) and thus the exact function remains unclear. A recent study has shown that the absence of the ECD reduced the rate of zinc transport of ZIP4 by more than half, in addition to confirming the role of histidine rich domain in playing an important role in maintaining optimal zinc transport activity (Jiang et al., 2024). Other studies observed an increase in cell surface expression in HEK293 cells following the deletion of the ECD of ZIP4, and have therefore suggested that ZIP4-ECD plays a role in regulating the trafficking of ZIP4 (Chun et al., 2019; Zhang et al., 2020, 2016). Recently, AlphaFold3 has allowed the prediction and analysis of the 14 human ZIPs (Wang et al., 2025). ZIP1, ZIP2, ZIP3, ZIP9 and ZIP11 do not have an extracellular domain. ZIP8, ZIP13, ZIP6 ZIP10 and ZIP5 only have a single ECD in each monomer. ZIP4 and ZIP12 have two ECDs in each monomer. The existence of multiple histidine and glutamine residues in the extracellular domain has been predicted to attract zinc ions, particularly in the human HsZIP7 (Wang et al., 2025) and HsZIP4 (Chun et al., 2019).

1.4.1.9 Regulation of ZIPs

ZIP transporters are regulated both translationally and post translationally (Eide, 2020; Guerinot, 2000). For example, ZIP4 in mammalian cells has been shown to be regulated by intracellular zinc levels through the histidine rich cluster between TM3 and TM4 in the cytoplasmic domain. In high zinc conditions, HsZIP4 senses intracellular zinc levels and is regulated by endocytosis where in the histidine rich domain (Zhang et al., 2020) is targeted for ubiquitination and degradation in order to maintain intracellular zinc homeostasis (Mao et al., 2007). A similar mechanism was suggested for *Arabidopsis thaliana* Irt1 (Eide et al., 1996). Disrupting this loop resulted in an accumulation of intracellular zinc, and the binding of zinc to this loop promoted the ubiquitination, endocytosis and degradation of AtIrt1 (Dubeaux et al., 2018). The histidine-rich domain in the intracellular loop between TM3 and TM4 is therefore important in regulating the expression of ZIPs and its transport activity in response the availability of intracellular zinc.

1.4.1.10 ZIPs in yeast (*Saccharomyces cerevisiae)*

The identification and expansion of the ZIP metal transporter superfamily over the past three decades was sparked in 1996 by the discovery of the zinc-regulated transporter 1 and 2 (Zrt1/Zrt2) in the yeast *Saccharomyces cerevisiae* (Hui Zhao and Eide, 1996; H Zhao and Eide, 1996). There are two separate pathways for the uptake of zinc in S*accharomyces cerevisiae*. Zrt1 is a high affinity zinc transporter and is induced upon zinc deficiency, and Zrt2 is a low affinity zinc transporter that is not tightly regulated by the availability of zinc. Studies have found that the overexpression of Zrt1 increased zinc uptake, and the absence of this gene resulted in growth defects of yeast in zinc-deficient conditions, suggesting that Zrt1 is regulated by the intracellular availability of zinc (H Zhao and Eide, 1996).

Zrt2 is a low affinity zinc transporter and was shown to have a higher substrate specificity for zinc compared to other metals, with homology to both Zrt1 in *S. cerevisiae* and Irt1 in *A. thaliana*. Overexpression of Zrt2 increases the low affinity uptake of zinc, and the absence of this gene inhibits the activity of this low affinity uptake pathway of zinc without having any effect on the high affinity uptake system of zinc. This suggests that both pathways are independent of each other (Hui Zhao and Eide, 1996). Zrt3 is another protein that belongs to the ZIP family of transporters in *S. cerevisiae* that increases in expression in zinc deprivation conditions and plays an important role in mediating the mobilisation of zinc from intracellular vacuolar stores into the cytosol (MacDiarmid et al., 2000).

These studies emphasise the importance of ZIP proteins in transition metal acquisition in yeast. The generation of these mutant yeast strains have allowed for multiple characterisation studies to be conducted to confirm the functional role of other predicted ZIP proteins in zinc acquisition in other organisms. This is performed via heterologous expression and assessing whether the ZIP protein expressed is able to rescue/complement the mutant growth phenotype of yeast lacking the major high and low affinity zinc transporters.

1.4.1.11 ZIPs in plants (*Arabidopsis thaliana*)

Yeast complementation studies using the *zrt1*/*zrt2* mutants have allowed for the identification and functional characterisation of the first ZIP proteins in the model plant *Arabidopsis thaliana,* AtZIP1-4 (Grotz et al., 1998; Guerinot, 2000). Since the discovery of the first ZIP protein in *A. thaliana*, a total of 15 ZIPs have been identified, including the three iron responsive transporters (IRTs). AtZIP1-3, AtZIP7, AtZIP11 and AtZIP12 all complemented *zrt1*/*zrt2* mutant yeast strains in zinc deprivation conditions (Milner et al., 2013), confirming zinc transport activity of these proteins. Seeds overexpressing AtZIP1 have been shown to have an enhanced accumulation of zinc and an increased rate of zinc transport, particularly in zinc deprivation conditions (Skuza et al., 2022). These ZIPs have different substrate specificities, where AtZIP1 and AtZIP3 play a role in zinc uptake (Ochoa Tufiño et al., 2025), AtZIP8 is important for the acquisition of iron and AtZIP2 important in copper uptake (Robe et al., 2025). Moreover, they exhibit different affinities to iron, with AtZIP1 being a low affinity iron transporter and AtZIP2 being a high affinity iron transporter. In *Arabidopsis thaliana*, ZIPs often exhibit redundancy/compensatory roles. For example, a study found that AtIRT3, AtZIP4, AtZIP6 and AtZIP9 (all highly expressed in seed development and upregulated in zinc deficient environments) exhibit redundant roles in maintaining zinc homeostasis in the plant (Lee et al., 2021). Single or double mutations of these ZIPs demonstrated no growth defects in both standard and zinc deficient conditions. However, triple and quadruple mutants of these ZIPs demonstrated an impaired growth defect of *A. thaliana* regardless of zinc availability (Lee et al., 2021). More recently, AtZIP3 and AtZIP5, which play an important role in being the major zinc uptake transporters in *A. thaliana*, act redundantly in zinc deficiency (Ochoa Tufiño et al., 2025). In addition to zinc, three ZIPs in *A. thaliana* have been shown to play a role in iron acquisition; AtIRT1, AtIRT2 and AtIRT3 (Lin et al., 2009; Vert et al., 2002, 2001). AtIrt1 was the first iron transporter to be identified and investigated in the plant (Eide et al., 1996; Korshunova et al., 1999). Studies have demonstrated its essential role in *Arabidopsis* in iron uptake from the soil (Vert et al., 2002) and have shown that it has a broad substrate range, complementing a yeast strain defective in the high affinity manganese uptake (Δ*smf1*) (Korshunova et al., 1999). A number of ZIPs have also been identified and characterised in other plants including maize, rice and wheat, which have been reviewed in great detail by Ajeesh Krishna et al., 2020.

1.4.1.12 ZIPs in bacteria cells

Iron and zinc homeostasis must also be maintained and regulated in bacteria. ZupT, a member of the prokaryotic ZIP family of proteins, is a bacterial metal ion transporter protein. It is the first characterised bacterial member of the ZIP protein family and was first identified in *Escherichia coli*, shown to play a role in zinc uptake (Grass et al., 2002). ZupT has been shown to transport a broad range of divalent metal cations including iron, zinc, manganese, cadmium as well as cobalt (Grass et al., 2005). ZupT, similar to ZIP proteins in other organisms, plays a critical role in maintaining ion homeostasis and is important for the survival and pathogenicity of bacteria in the context of infection. This has been demonstrated across a range of bacterial species including *Salmonella enterica* (Cerasi et al., 2014; Karlinsey et al., 2010), *Clostridioides difficile* (Zackular et al., 2020) and *Escherichia coli* (Sabri et al., 2009). The structure of the bacterial ZIP transporter in *Bordetella bronchiseptica* (BbZIP) was determined by X-ray crystallography to start to understand the mechanisms of how these transporters function (Pang et al., 2023; Zhang et al., 2017). This was discussed in more detail in sections 1.4.1.3, 1.4.1.4 and 1.4.1.5.

1.4.1.13 ZIPs in mammalian cells

As zinc plays a critical role in a range of cellular functions, the disruption of zinc cellular homeostasis has been shown to disrupt biological systems in mammalian models (Hara et al., 2017; Hojyo and Fukada, 2016a, 2016b). Thus, ZIP proteins play an important role in maintaining zinc homeostasis in mammalian cells by taking up zinc from the extracellular environment into the cytosol, or mobilisation from within intracellular compartments within the cell into the cytosol. In the human genome, 14 ZIPs have been identified (named ZIP1-ZIP14), with localisation in different tissues and distribution on both the plasma membrane of cells as well as intracellular organellar compartments including endosomes, lysosomes, endoplasmic reticulum, Golgi apparatus, and the mitochondria (Figure 1.8). The majority of HsZIPs, including ZIPs1-6, ZIP8, ZIP10, ZIP12 and ZIP14 have been shown to localise to the plasma membrane of mammalian cells and are important in zinc acquisition/uptake into cells (Chowanadisai et al., 2013; Girijashanker et al., 2008, 2008; Hogstrand et al., 2013; Leung et al., 2012; Taylor et al., 2016; C.-Y. Wang et al., 2012; Wang et al., 2004b, 2004a). ZIP1 expression is ubiquitous

in mammalian cells and tissues of humans and mice, particularly in K562 erythroleukemia cells and in prostate cells (Costello et al., 1999; Franklin et al., 2003; Gaither and Eide, 2001b).

Human HsZIP4 localises to the plasma membrane of mammalian cells and has been proposed to be a Zn^{2+}/H^{+} symporter (Hoch et al., 2020). As previously stated, the expression and abundance of HsZIP4 on the surface of cells is regulated by the availability of the substrate zinc. Studies suggest that in addition to transporting zinc, HsZIP4 is able to senses the levels of intracellular zinc to regulate its endocytosis, internalisation and proteasomal and lysosomal degradation in high zinc extracellular conditions, maintaining zinc homeostasis and protecting against zinc cytotoxicity (Mao et al., 2007; Weaver et al., 2007). Studies have also demonstrated that zinc deficiency results in an increase in expression of HsZIP4 on the surface membrane of mammalian cells (Dufner-Beattie et al., 2003b; Kim et al., 2004; Mao et al., 2007; Wang, 2004; Weaver et al., 2007).

Another ZIP transporter protein with unique localisation is ZIP7, which localises to secretory pathways within mammalian cells including the endoplasmic reticulum and the Golgi apparatus (Huang et al., 2005; Taylor et al., 2004). ZIP7 has been shown to maintain zinc homeostasis within these intracellular compartments, tightly controlling the movement of zinc stored in the ER and Golgi to the cytosol. Studies have demonstrated that the transport of zinc via ZIP7 is dependent upon the phosphorylation of this protein by a protein kinase CK2 to activate it, triggering cytosolic zinc signalling pathways (Taylor et al., 2012). ZIP9, ZIP11 and ZIP13 have also been shown to localise to the Golgi (Bin et al., 2011; Kelleher et al., 2012; Taniguchi et al., 2013), with ZIP11 also predicted to be the only ZIP protein localised in the nucleus, regulating nuclear zinc homeostasis (Alyssa B. et al., 2013; Olea-Flores et al., 2022).

Both ZIP8 and ZIP14 are predicted to have eight transmembrane domains (He et al., 2006; Taylor et al., 2005) and have been shown to transport a range of metals including zinc, iron, manganese and cadmium in mammalian cells (Beker Aydemir et al., 2012; He et al., 2006; Liu et al., 2008; Liuzzi et al., 2006; Pinilla-Tenas et al., 2011; C.-Y. Wang et al., 2012; Zhao et al., 2010). In fact, studies have shown that ZIP8 has a higher affinity for Mn compared to Zn (He et al., 2006). In addition to localising on the plasma membrane and taking up metals from the extracellular

environment, ZIP8 and ZIP14 also localise on the surface of endosomes/lysosomes within cells (Aydemir et al., 2009), with ZIP8 also shown to localise to mitochondrial membranes (Riley et al., 2017).

Studies have further suggested that the expression of some mammalian ZIPs, e.g. ZIP2, is dependent on the membrane potential in addition to the extracellular pH, with increased activity at a lower pH (Franz et al., 2018; Gyimesi et al., 2019). Studies also suggest that many human ZIPs form homodimers in their native state including ZIP4, ZIP5, ZIP6, ZIP10 and ZIP13 (Ahern et al., 2020; Bin et al., 2011; Hogstrand et al., 2013; Hojyo et al., 2014; Pocanschi et al., 2013), with ZIP6 forming a functional heteromeric complex with ZIP10 (Taylor et al., 2016).

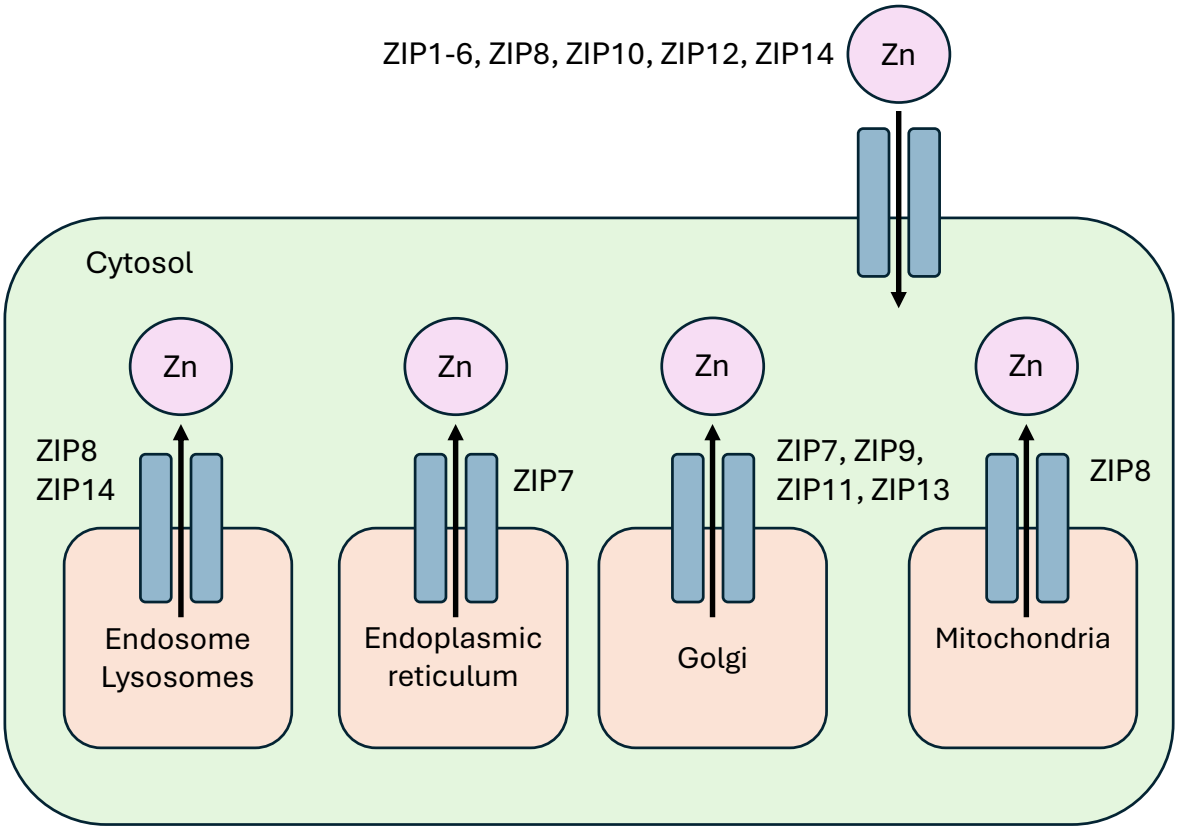


Figure 1.8 – Cellular localisation of Zrt/Irt-like (ZIP) transporter family proteins in mammalian cells.

Schematic diagram of the localisation of ZIP proteins that control zinc/metal homeostasis in mammalian cells. ZIP transporters are highlighted in blue, zinc ions highlighted in pink, the cytosol in green and the intracellular organellar compartments highlighted in orange. Black arrows represent the direction of zinc transport in both the plasma membrane of the cell as well as organellar membranes. Adapted from Takagishi et al., 2017.

1.4.1.14 The role of ZIPs in protozoan parasites

ZIP-domain containing proteins are also a common strategy exploited by protozoan parasites to acquire iron and zinc from their environment. For example, ZIPs have been shown to play a role in iron uptake in *Leishmania,* a genus of kinetoplastid parasites. This protozoan parasite resides within acidic phagolysosomes within macrophages which allows the parasite to directly take up iron in the form of transferrin that has been endocytosed from the host. A study demonstrated that ferric iron released from host transferrin is reduced to ferrous Fe^{2+} by the *Leishmania* ferric reductase 1, or LFR1. LFR1 is localised to the plasma membrane and is essential for the generation of vertebrate infective forms of the parasite. Under iron deprivation conditions, LFR1 is upregulated in *Leishmania amazonensis*, one of the causative agent of cutaneous leishmaniasis (Flannery et al., 2011). LFR1 works alongside another protein involved in iron acquisition in *L. amazonensis,* the *Leishmania* iron transporter (LIT1). LIT1 is a ferrous iron transporter belonging to the ZIP-domain containing family of proteins. It was identified based on homology with the ferrous iron transporter AtIrt1 in *Arabidopsis thaliana*. Parasites lacking LIT1 are unable to replicate intracellularly and are also unable to form lesions *in vivo*. Finally, LIT1 expression is increased under iron deprivation conditions, highlighting the essential role that this ZIP protein plays in intracellular iron acquisition in *Leishmania* (Huynh et al., 2006; Jacques et al., 2010). In *L. infantum*, one of the causative agent of visceral leishmaniasis, LiZIP3, a ZIP-domain containing protein, has been identified as the first mediator of zinc homeostasis via heterologous complementation rescue in yeast strains deficient in zinc acquisition (Carvalho et al., 2015, 2012). LiZIP3 is a cellular zinc transporter, playing an important role in the import of zinc into the parasites. The expression of LiZIP3 is tightly regulated by the availability of zinc, decreasing in the presence of excess zinc and increasing in metal chelation conditions using EDTA. The study also highlights that the expression of LiZIP3 in *Xenopus laevis* oocytes stimulates the uptake of zinc, and demonstrates that zinc is the preferred substrate for this transporter compared to other metals (Carvalho et al., 2015, 2012). The protein localises to the plasma membrane of the parasites and studies have shown that the overexpression of LiZIP3 results in an increase in zinc internalisation. In high zinc conditions, both the expression and localisation of LiZIP3 are lost, highlighting its role in zinc import (Carvalho et al., 2015, 2012).

In *Trypanosoma cruzi*, the causative agent of Chagas disease, the mechanisms of iron/zinc acquisition are not well understood. Recently, a study has identified TcIT, an iron transporter with a highly conserved domain corresponding to the ZIP superfamily, with homology to iron transporters in both *Leishmania amazonensis* (LIT1) and *Arabidopsis thaliana* (AtIRT1) (Dick et al., 2022). The study found that TcIT localised to the plasma membrane of the parasite, and that TcIT transcription increased in iron deprivation conditions. Further, following overexpression of this transporter, the concentrations of intracellular iron within epimastigotes was increased (Dick et al., 2022). This study identifies TcIT as the first ZIP protein in *Trypanosoma cruzi*, highlighting its role in iron transport in the parasite.

In *Trichomonas vaginalis,* the anaerobic parasite that causes trichomoniasis, eight ZIP-domain containing proteins were bioinformatically identified following a genome-wide analysis. However, only two (TvZIP2 and TvZIP4) are transcriptionally iron regulated (Fernández-Martín et al., 2017). TvZIP2 is upregulated under high iron conditions, compared to TvZIP4 which, in contrast, is upregulated under iron deprivation conditions (Fernández-Martín et al., 2017). This suggests that TvZIP2 may play a role in the export of iron, where TvZIP4 uptakes iron. In the presence of excess zinc, the expression of TvZIP1, 3, 5 and 7 were downregulated, suggesting that these ZIP proteins encoded by the *Trichomonas vaginalis* genome may play an important role in iron and zinc acquisition in the parasite (Fernández-Martín et al., 2017).

ZIP-domain containing proteins also play an important role in iron and zinc acquisition in the protozoan apicomplexan parasite *Plasmodium*, the causative agent of malaria. For example, PbZIPCO, belonging to the ZIP family of transport proteins, has been identified as a putative metal iron transporter in *Plasmodium berghei* (Sahu et al., 2014). The study demonstrated that PbZIPCO localises to the plasma membrane of the parasite and highlights the importance of PbZIPCO in the development of the liver stage of the parasite within hepatocytes. The study also showed that both iron and zinc supplementation were able to rescue PbZIPCO mutant deficiency, supporting its role as an iron and zinc transporter in *P. berghei* (Sahu et al., 2014). In *P. falciparum,* a study has identified PfZIP1 as a selective zinc transporter belonging to the ZIP domain superfamily (Shrivastava et al., 2024). The study found that PfZIP1 has a dynamic and stage-dependent localisation, initially targeting to the apicoplast in trophozoites and then localising

to the plasma membrane of the parasite in schizonts and gametocytes. PfZIP1 expression was shown to increase in zinc chelation conditions, and that although it also binds to iron, this ZIP transporter exhibits preferential binding to zinc (Shrivastava et al., 2024).

1.4.1.15 Uncharacterised ZIP-domain containing proteins in *Toxoplasma gondii*

Although iron and zinc have been shown to be essential for the survival and proliferation of *T. gondii*, at the start of my PhD, the mechanisms by which this parasite acquired divalent metals were unknown. The *Toxoplasma* genome encodes four predicted ZIP domain containing proteins: TGME49_261720, TGME49_254080, TGME49_500163 and TGME49_225530. However, before my PhD, none of these were functionally characterised in the parasite and their functional role in iron and zinc acquisition remained elusive.

1.5 Transition metals and *Toxoplasma gondii*

1.5.1 Importance of iron in *Toxoplasma gondii*

Toxoplasma gondii, an obligate intracellular apicomplexan parasite, requires iron for essential cellular processes, making up approximately 5 % of the total element content within the parasite (Al-sandaqchi et al., 2018). Iron plays a critical role for a number of essential cellular processes during *T. gondii* infection such as iron-sulphur (Fe-S) cluster biogenesis pathways (Aw et al., 2021; Pamukcu et al., 2021; Renaud et al., 2022), the production of ATP, energy generation and transfer (Henkel et al., 2022), haem biosynthesis (Akuh et al., 2022; Bergmann et al., 2020; Kloehn et al., 2021; Tjhin et al., 2020) and the regulation of iron-dependent redox reactions (Akuh et al., 2022; Henkel et al., 2022; Song et al., 2023). The source of iron taken up is also important. Although the genome of other species encode a ferric reductases which reduces ferric Fe^{3+} to ferrous Fe^{2+} (Andrews et al., 2003; Zaidi et al., 2017; X. Zhang et al., 2019), there is no evidence that apicomplexan genomes code for any ferric reductase genes, suggesting that apicomplexan parasites may directly take up iron in its ferrous form.

Multiple studies have demonstrated that iron is required for the growth of *T. gondii,* as iron deprivation using chelators restricts parasite growth and replication both *in vitro* and *in vivo* (Aghabi et al., 2023; Mahmoud, 1999; Renaud et al., 2024; Sloan et al., 2025). This is also observed in other apicomplexan parasites such as *Plasmodium* (Ferrer et al., 2012; Raventos-Suarez et al., 1982). It is also important to emphasise that a balance of iron is important in order to avoid metal toxicity, as excess iron is also toxic to the parasite and leads to death (Aghabi et al., 2023; Ying et al., 2024). To further support the dependency of *T. gondii* replication on iron, one of the strategies employed by IFN-γ in host cells following infection to inhibit parasite replication is to limit the availability of iron to the parasites (Dimier and Bout, 1998). Studies have also demonstrated that iron deprivation through chelation triggers the initiation of stage conversion of tachyzoites to bradyzoites, with an increased expression of bradyzoite specific markers observed (Renaud et al., 2024; Sloan et al., 2025; Ying et al., 2024).

1.5.2 Iron in haem biosynthesis in *Toxoplasma gondii*

Toxoplasma gondii requires iron for essential processes including haem biosynthesis (Bergmann et al., 2020a; Kloehn et al., 2021; Tjhin et al., 2020). Haem is a ubiquitous iron-containing porphyrin organic ring molecule (Poulos, 2014). It serves as an essential prosthetic group and is a cofactor for several enzymes involved in a range of cellular functions including DNA replication and repair, mitochondrial respiration, transcriptional and translational control and detoxification across archaea, bacteria and eukaryotes (Andreini et al., 2018). The ability of haem to alternate between an oxidised and reduced state allows for the transfer of electrons in the mitochondrial electron transport chain for energy generation and the redox reactions of haem-containing proteins. In apicomplexan parasites, both complex III and complex IV of the mitochondrial electron transport chain contain haem or haem-containing proteins, such as cytochrome c, which aid in the transfer of electrons between the complexes and energy generation (Hayward and Van Dooren, 2019; Kořený et al., 2013; Sigala and Goldberg, 2014). In *T. gondii*, the enzymes of the haem biosynthesis pathway are localised to the cytosol, mitochondrion and the apicoplast (Seeber et al., 2008; Van Dooren et al., 2012) and synthesis has been shown to be important for parasite fitness (Bergmann et al., 2020a; Krishnan et al., 2020; Tjhin et al., 2020). To date, no haem transporters have been identified in *T. gondii*. Impaired growth following the deletion of a haem-biosynthesis enzyme in the parasite could not be rescued in the presence of exogenous haem, suggesting that *Toxoplasma* is unable to efficiently salvage haem and instead encodes a functional *de novo* haem biosynthesis pathway (Bergmann et al., 2020a; Krishnan et al., 2020).

1.5.3 Iron-sulphur (Fe-S) cluster biogenesis in *Toxoplasma gondii*

Iron is also required by *Toxoplasma gondii* for essential processes such as iron-sulphur cluster biogenesis pathways (Aw et al., 2021; Leonard et al., 2023; Renaud et al., 2025, 2022). Iron-sulphur (Fe-S) clusters are essential for all eukaryotes, being central molecules in proteins within cells that play important roles in a range of cellular processes (Andreini et al., 2018). Fe-S clusters are ubiquitous cofactors that are required by a number of enzymes involved in essential cellular processes and metabolic pathways such as cellular respiration, DNA replication and repair, tRNA modification, transcriptional and translational control, amino

acid biosynthesis and protein translation (Netz et al., 2014). They are involved in essential cellular pathways, including the storage of iron, regulation of gene expression, electron transfer, as well as oxygen and nitrogen sensing (Lill, 2009). Fe-S clusters are made up of a geometric arrangement and assembly of inorganic sulphur/sulphide ions (S^{2-}) and ferrous (Fe^{2+}) or ferric (Fe^{3+}) iron which can then be delivered to their respective enzymes (Braymer et al., 2021).

It is predicted that *Toxoplasma gondii* encodes 70 Fe-S cluster containing proteins (Renaud et al., 2025). Fe-S clusters in *T. gondii* cannot be scavenged from the environment/host cell and must be synthesised *de novo* within the parasite. Thus, *Toxoplasma* encodes three dedicated Fe-S cluster biogenesis pathways localised to a number of cellular compartments including the apicoplast, mitochondria and the cytosol (Pamukcu et al., 2021; Renaud et al., 2022). These pathways include the mitochondrial iron-sulphur cluster assembly machinery pathway (ISC pathway) used for the synthesis of Fe-S clusters in the mitochondria, the sulphur formation pathway (SUF pathway) for Fe-S cluster biogenesis in the plastid apicoplast, and the cytosolic iron-sulphur assembly pathway (CIA pathway) for Fe-S cluster biogenesis in the cytoplasm (Pamukcu et al., 2021; Renaud et al., 2025). The SUF pathway in the apicoplast is independent of the cytosolic (CIA) and mitochondrial (ISC) Fe-S cluster biogenesis pathways (Pamukcu et al., 2021). However, the cytosolic CIA pathway highly depends on the mitochondrial ISC pathway for providing a sulphur-containing precursor (Lill et al., 2014). The disruption of these Fe-S cluster biogenesis pathways in the apicoplast and mitochondrion of *Toxoplasma gondii* has been shown to cause destabilisation of Fe-S cluster containing proteins, highlighting the importance of iron in these organelles (Maclean et al., 2024; Pamukcu et al., 2021; Renaud et al., 2022).

1.5.4 Organelles important for iron regulation and homeostasis in *Toxoplasma gondii*

1.5.4.1 Apicoplast

Iron is required for proteins essential in the apicoplast of *Toxoplasma gondii*. The apicoplast is an endosymbiotic plastid organelle of the Apicomplexa originating from the secondary endosymbiosis of a photosynthetic red alga (Janouškovec et al., 2010; McFadden and Yeh, 2017; Striepen, 2011; Van Dooren and Striepen,

2013). Although the apicoplast has lost photosynthetic functions, it harbours vital fitness-conferring metabolic pathways, many of which rely on iron-dependent enzymes. These processes include replication, transcription, translation, fatty acid biogenesis, isoprenoid, and haem intermediate biosynthesis, as well as maintaining redox potential, many of which incorporate Fe-S cluster proteins as cofactors. Studies have supported the importance of iron to this organelle, as iron deprivation affects the segregation of the apicoplast in daughter cells in *T. gondii*, although no fragmentation or major collapse of the organelle was observed (Renaud et al., 2024). This was further supported as iron depletion did not affect the morphology and integrity of the apicoplast (Ying et al., 2024). *Toxoplasma gondii* encodes a functional haem biosynthesis pathway, and the apicoplast has been shown to be involved in the production of haem which is essential for the replication, growth and survival of the parasite (Bergmann et al., 2020). Moreover, the characterisation of TgUroD, an apicoplast localised enzyme, further highlights the importance of the apicoplast in haem biosynthesis (Tjhin et al., 2020). The apicoplast harbours essential enzymes that have reducing power. For example, the apicoplast expresses enzymes that are essential for the biosynthesis of isoprenoid through the 2C-methyl-D-erythritol 4-phosphate (MEP) pathway. A study has found that ferredoxin, a redox carrier that is also a small iron-sulphur cluster containing protein, is essential for the transfer of electrons for both isoprenoid, lipoate and Fe-S biosynthesis pathways, as well as the modification of tRNAs in the apicoplast. This ferredoxin was shown to be essential for *T. gondii* tachyzoite growth and replication, without affecting the ultrastructure and morphology of the organelle (Akuh et al., 2022; Henkel et al., 2022).

In addition, the apicoplast harbours its own machinery for a key metabolic pathway that plays a vital role in the synthesis and assembly of Fe-S clusters. This pathway facilitates the biogenesis and transfer of Fe-S clusters to enzymes that are localised in the apicoplast of *T. gondii*. Particularly, the sulphur utilisation factor (SUF) pathway for the biogenesis of Fe-S clusters in the apicoplast is important for the synthesis of fatty acids and isoprenoid, and to maintain the function and sustainability of the organelle. The depletion of components of the SUF pathway in the apicoplast, for example the scaffold protein, TgSUFC, has been shown to block *in vitro T. gondii* tachyzoite replication irreversibly. This led to defects in the parasite membranes during cell division, apicoplast loss following

reinvasion, and impacted Fe-S pathways in the apicoplast including the lipoylation of the pyruvate dehydrogenase enzyme PDH-E2 (Renaud et al., 2022). Studies have also shown that the cysteine desulfurase, TgNFS2 (TGGT1_216170), which plays a role in the first steps of the SUF pathway to provide the inorganic sulphur portion of Fe-S cluster proteins, is essential for the growth and survival of intracellular *T. gondii* tachyzoites (Pamukcu et al., 2021; Renaud et al., 2022). Disruption of components of the SUF pathway have also been shown to result in defects in fatty acid synthesis within the apicoplast. As the supplementation with exogenous fatty acids did not fully recover parasite growth, the generation of isoprenoid-derived precursors in the SUF pathway in the apicoplast has also been shown to affect other important cellular pathways downstream of the apicoplast. This includes the targeting of GPI anchored proteins for the motility of *Toxoplasma,* as the knockdown of both TgNFS2 and TgSUFC resulted in the mislocalisation of the GPI-anchored surface antigen (Renaud et al., 2022). The depletion of TgNFS2 altered the SUF Fe-S cluster biogenesis pathway in the apicoplast and initiated an upregulation of expression of bradyzoite specific markers, although did not trigger a full stage conversion into bradyzoites (Pamukcu et al., 2021). The biosynthesis of lipoic acid synthase, LipA, an essential Fe-S cluster protein, is dependent on the SUF pathway. LipA is essential in the modification and lipoylation of the E2 subunit on the dehydrogenase enzymes pyruvate dehydrogenase (PDH-E2), the only known substrate of lipoylation which localises in the apicoplast (Crawford et al., 2006; Pamukcu et al., 2021). This enzyme plays an important role in converting pyruvate to acetyl-CoA which is a precursor required for type II fatty acid synthase complex (FAS-II) for the synthesis of fatty acids in the apicoplast, an essential metabolic pathway for organellar biogenesis and survival of *T. gondii* (Mazumdar et al., 2006). Studies have also shown a decrease in lipoylation of PDH-E2 following the knockdown of TgNFS2 in the SUF pathway, supporting the importance of the role of iron in the apicoplast (Pamukcu et al., 2021). Collectively, these studies highlight the importance of iron in the apicoplast of *T. gondii*, particularly in the SUF iron-sulphur cluster biogenesis pathway, essential for the integrity, maintenance, and function of this organelle and in turn the survival of *Toxoplasma gondii*.

1.5.4.2 Mitochondria

The mitochondrion also harbours essential iron-containing proteins in the parasite. *Toxoplasma gondii* and *Plasmodium* spp. parasites harbour a single large mitochondrion, a double membrane-bound endosymbiotic organelle, which is central to energy generation and cellular metabolism (Mathur et al., 2021). The mitochondria originally originated from free-living prokaryotic cells (such as aerobic bacteria) that were once engulfed by an ancestral eukaryotic host cell (Archibald, 2015; Gray, 2012). Iron is required for proteins that are essential in the mitochondria, playing a critical role in the electron transport chain for cellular respiration and energy generation. Studies have shown that iron deprivation reduces mitochondrial respiration as well as alters mitochondrial morphology in *T. gondii* (Hanna et al., 2025). This supports the functional role and importance for iron in this organelle, as the disruption of the function has often been suggested to lead to morphological changes within the organelles (Mallo et al., 2021; Wu et al., 2022). Further, the expression of a putative mitochondrial iron transporter, MIT (TGGT1_277090), increases in parasites lacking the vacuolar iron transporter (ΔVIT). VIT has previously been shown to localise to the plant-like vacuolar compartment (PLVAC) and plays an important role in the storage and detoxification of excess iron in *Toxoplasma gondii* (Aghabi et al., 2023). The increase in MIT expression in the absence of VIT is possibly in an attempt to increase the storage of iron in the mitochondria to remove excess iron from the cytosol and avoid iron toxicity. MIT is also increased in iron limiting conditions (Hanna et al., 2025), demonstrating close regulation of mitochondrial iron to support cellular respiration. This mechanism has been proposed in other systems including yeast (Li et al., 2010) and in mammalian cells, where the overexpression of iron transporters in the mitochondria has been shown to rescue the effects of iron depletion (Unlu et al., 2022). Studies have also previously shown that the inhibition of cellular respiration has been linked to bradyzoite stage conversion (Tomavo and Boothroyd, 1995), however the factors that directly link iron or mitochondrial respiration directly to parasite differentiation are not yet well known.

Iron is also incorporated into Fe-S cluster proteins which are required for a range of cellular pathways. The mitochondria host many iron-containing proteins, including iron-sulphur (Fe-S) cluster proteins within the electron transport chain

which are involved in energy generation and cellular respiration (Aw et al., 2021; Maclean et al., 2021; Pamukcu et al., 2021). A study has highlighted the importance of a mitochondrial transporter, ABCB7L, an ATP-binding cassette transporter, in the biogenesis of both nuclear and cytosolic Fe-S cluster proteins, as well as metabolism and DNA replication, further supporting the role and importance for iron-related metabolism in the mitochondria of *T. gondii* (Maclean et al., 2024). Another study has demonstrated a role of a scaffold protein, TgNBP35 (TGME49_280730), which despite localising in the outer mitochondrial membrane, is important for cytosolic Fe-S cluster biogenesis and was shown to be essential for parasite proliferation (Aw et al., 2021). Another scaffold protein important for the iron-sulphur cluster (ISC) pathway in the mitochondria is TgISU1 (TGGT1_237560), which was shown to be essential for parasite replication. Inducible knockdown of this protein resulted in the depletion of components of the electron transport chain impairing cellular respiration, and the activation of the expression of bradyzoite specific markers, initiating stage conversion (Pamukcu et al., 2021).

Within the mitochondria, succinate dehydrogenase B (SDHB) (TGME49_215280) is a key protein containing three iron sulphur clusters. SDHB has essential roles in the electron transport chain as part of complex II as well as the TCA cycle for energy generation (Maclean et al., 2021; Silva et al., 2023). TgRieske (TGGT1_320220) is another Fe-S cluster protein, part of complex III of the mitochondrial electron transport chain in *T. gondii*, important for electron transfer to cytochrome *c* and energy generation (Hayward et al., 2021; Maclean et al., 2021). Moreover, the Fe-S clusters of the protein TgApiCox13 (TGME49_254030) are essential for the activity, integrity and stability of the cytochrome *c* oxidase complex (Complex IV), critical for the functioning of the mitochondrial electron transport chain in *T. gondii* (Leonard et al., 2023). Collectively, these studies emphasise the importance of iron in the mitochondria of *T. gondii*, particularly highlighting the role that Fe-S cluster biogenesis pathways in this organelle play in parasite replication and survival.

1.5.4.3 Plant-like vacuolar compartment (PLVAC)

Toxoplasma gondii possesses a lysosomal-like membrane-bound vesicular organelle termed the plant-like vacuolar compartment (PLVAC) (Liu et al., 2014;

Miranda et al., 2010; Parussini et al., 2010; Stasic et al., 2022). In extracellular parasites, the PLVAC exists as a single large vacuole. However upon intracellular replication, the vacuole becomes fragmented throughout the parasite (Miranda et al., 2010; Parussini et al., 2010). In *T. gondii*, the PLVAC expresses transporters on its surface enabling the storage of toxic ions including zinc, where the zinc transporter TgZnT localises and protects the parasite from zinc toxicity (Chasen et al., 2019), and iron, where the vacuolar iron transporter TgVIT localises to store and detoxify excess iron (Aghabi et al., 2023). *T. gondii* also expresses a H+-ATPase (V-ATPase) and a cathepsin L-like protease (TgCPL), which are often used as markers for the PLVAC. The vacuolar -H(+) -pyrophosphatase TgVP1 also localises to the PLVAC and has been shown to be required for host cell invasion, microneme secretion and the extracellular survival of *T. gondii* (Liu et al., 2014). VP1 is another common marker used for the PLVAC in *Toxoplasma*. The organelle is a site for the transport of calcium and sodium, and has also been linked to the storage of calcium (Miranda et al., 2010). During the acute stage of infection, the PLVAC is also a site for ingestion and digestion of host cytosolic proteins (Dou et al., 2014), as well as protein trafficking, where the vacuolar proton H+ -ATPase localises and plays an important role in regulating the intracellular pH, in turn protecting the parasites against toxic ions and also impacting the maturation of essential secretory proteins (Stasic et al., 2019).

1.5.5 Role of zinc in *Toxoplasma gondii*

The role of other transition metals in *T. gondii* beyond iron such as zinc is less well understood. However, based on other eukaryotic genomes, it is predicted that at least 800 proteins in *T. gondii* require zinc, with many shown to be essential. These include TgZFP2, a zinc finger protein shown to play a role in coordinating mitosis and budding in the parasite (Semenovskaya et al., 2020) as well as TgZNF2, an evolutionary conserved zinc protein shown to be involved in mRNA nuclear export in *T. gondii* (Gissot et al., 2017). Moreover, a recent study has found that TgZnT, a vacuolar zinc transporter, protects the parasite from zinc toxicity, proposing its role in zinc homeostasis during the lytic infection stages of *Toxoplasma gondii* (Chasen et al., 2019). The study showed that this zinc transporter is important for the growth and replication of *T. gondii*. This was supported as mutant parasites lacking this transporter have reduced viability in *in vitro* growth assays, suggesting that a loss of ability to store zinc leads to mild

parasite growth defects. To further support the role of zinc, this phenotype was exacerbated in excess zinc conditions and was rescued following the chelation of zinc (Chasen et al., 2019). The expression of TgZnT restored zinc tolerance in yeast strains that were sensitive to high concentrations of zinc (Chasen et al., 2019), confirming its role as a zinc transporter. However, at the beginning of my PhD, the uptake, acquisition, and transport of zinc into *T. gondii*, and the effects of zinc chelation on the parasite were not known or investigated.

Several zinc-binding proteins in apicomplexan parasites are highly conserved, although the majority of these proteins have yet to be functionally characterised. Some have been shown to play an important role in the life cycle of the parasites. Zinc finger proteins such as the C2H2 zinc finger protein (PbZFP) in *P. berghei* has been demonstrated to regulate the transition of life cycle stages of the parasite and play a role in histone modifications and the transmission of malaria (Gopalakrishnan et al., 2017). Studies have also shown that zinc is essential for the progression of intraerythrocytic stages of the parasite, and inhibiting the acquisition of zinc prevents the replication of *P. falciparum*, and that these parasites accumulate zinc during their life cycle (approximately 400 % of the levels of zinc found in uninfected erythrocytes), suggesting an important role for zinc in parasite growth and survival (Marvin et al., 2012). Moreover, a putative metal ion transporter in *P. berghei*, PbZIPCO has been shown to localise to the plasma membrane of parasites and shown to be essential in liver stages of parasite development (Sahu et al., 2014). Based on partial rescue experiments with excess iron and zinc, this protein was identified as an iron and zinc transporter in *P. berghei* (Sahu et al., 2014). More recently, a zinc-selective transporter in *P. falciparum*, ZIP1, has been found to play a role in zinc and to a lesser extent, iron, acquisition in the parasite. PfZIP1 exhibits a dynamic localisation, localising to the plasma membrane in the schizont and gametocyte stages and in the apicoplast of the trophozoite stages of the parasite, suggesting a stage-specific role of PfZIP1 (Shrivastava et al., 2024).

1.5.6 Chelation of transition metals

Chelating agents play a critical part of functionally characterising proteins involved in transition metal sequestration and transport. Chelators are electron donors and are able to bind to metal ions to form a ring-structured complex and block the reactivity of the ion. This inactivates the metal ion, in turn reducing their reactivity. Deferoxamine, or DFO, is a high affinity iron chelating agent often used to chelate iron from cells as it effectively outcompetes many biological ligands for ferric iron (Bellotti and Remelli, 2021). It is a siderophore molecule produced by *Streptomyces pilosus* (Barona-Gómez et al., 2004) which chelates iron by binding to various forms of iron including ferric iron (Fe^{3+}), iron stored in ferritin, NTBI and the free LIP through six oxygen donor atoms. A stable hexadentate complex is then formed with the ferric form of iron at a 1:1 ratio (Hershko et al., 2001). Once bound, iron is unavailable for redox reactions. Studies in mammalian cells have also shown that DFO treatment induces the release of iron from ferritin stores via autophagy within the cytoplasm, before being degraded via proteasomal degradation (De Domenico et al., 2009). Iron is then excreted by the cell through the iron exporter ferroportin. Although non-cell permeable (Kicic et al., 2001; Kwiatkowski, 2011; Lloyd et al., 1991), there is evidence that DFO can be internalised within cells (Glickstein et al., 2005), allowing its access to intracellular iron pools.

N,N,N',N'-tetrakis-(2- pyridylmethyl) ethylenediamine (TPEN) is a membrane permeable chelating agent. Although TPEN can chelate other divalent transition metal ions such as iron, copper, cobalt, nickel, and to a lesser extent manganese, it has the highest affinity for zinc and is thus the most commonly used selective zinc chelator in biological studies (Cho et al., 2007; Schaefer-Ramadan et al., 2019). It chelates metals by forming a highly stable complex with the metal ions as it has four pyridyl and two amine nitrogen donors. Ethylene glycol-bis(2-aminoethyl ether)-N,N,N,N-tetraacetic acid (EGTA) is another chelating agent used to chelate divalent ions, although it has a higher affinity for calcium over other metals and to a lesser extent magnesium (Durham, 1983; Sorour et al., 2016). However it is also known to bind zinc and is thus often used to chelate zinc (de Jesus et al., 2019; Hsu and Anderson, 1995; Schröder et al., 2021).

1.6 The battle for iron between host and pathogen

The chemical properties of iron which allow it to donate and accept electrons in redox reactions are beneficial to many cellular systems, however, also pose a challenge. As mentioned in section 1.3.3, excess iron in cells could be toxic through the generation of ROS via the Fenton reaction (Winterbourn, 1995). As iron is an essential nutrient for almost all forms of life and is critical for the growth, proliferation, and survival of many microbes during infection, mammalian iron homeostasis must be tightly regulated. In this section, I will describe cellular iron uptake, storage, and trafficking pathways in mammalian cells as a strategy to maintain iron homeostasis and avoid iron toxicity, how macrophages sequester iron to control infection, and finally and how pathogens including bacteria and parasites subvert this to support their growth and persistence.

1.6.1 Macrophages: An overview

Macrophages, or MΦ, are a type of white blood cell. They are an immune phagocytic cells that originate from bone-marrow-derived-monocytes that migrate to essentially all tissues where they are then able to differentiate into resident macrophages (Epelman et al., 2014; Guan et al., 2025). They play a critical role in a nonspecific defence response, innate immunity, but also act as a bridge to the adaptive immune response by recruiting other immune cells such as lymphocytes. Macrophages have important roles in engulfing invaders, killing pathogens and clearing apoptotic cells (Pandey et al., 2022; Park and Hunter, 2020; Su et al., 2020). In addition to their role in engulfing pathogens, macrophages play a key role in tissue homeostasis and regulating inflammation. They release cytokines, small soluble proteins such as tumour necrosis factors (TNF), interleukins (IL), interferons (IFN) to communicate with other cells to trigger an immune response (Arango Duque and Descoteaux, 2014). Classically, it has been demonstrated that IFN-γ and microbial products such as lipopolysaccharide (LPS) trigger the activation of M1 macrophages, which produce pro-inflammatory cytokines such as TNFα, IL-1β and IL-6, resulting in the production of ROS or nitric acid (NO) to actively kill microbes (Khojah et al., 2016). On the other hand, M2 macrophages are stimulated by exposure to cytokines including IL-4, IL-10 or IL-13, and unlike M1 macrophages, are anti-inflammatory, and instead focus on promoting tissue damage, repair, and healing (Atri et al.,

2018; Chen et al., 2023; Martinez and Gordon, 2014; Wang et al., 2014). Beyond their critical immune response in clearing pathogens and maintaining tissue homeostasis, macrophages are at the forefront of systemic iron homeostasis, actively employing iron sequestration to resist infection, being central to innate pathogen control and iron recycling (Nairz et al., 2017). They play a central role in regulating essential iron transfer pathways to restrict the availability of nutrients such as iron to microbes, limiting their proliferation and survival (Recalcati and Cairo, 2021; Soares and Hamza, 2016). Intracellular pathogens employ several mechanisms and strategies to acquire iron from host macrophages to grow and survive, whereas macrophages actively employ iron sequestration strategies to resist infection resulting in a battle for iron.

1.6.2 What is nutritional immunity?

The strategy employed by macrophages to sequester nutrients such as the transition metal iron is known as nutritional immunity. Nutritional immunity is a strategy of the immune system where host resistance following infection is dependent on the ability of the host to restrict access of essential nutrients to pathogens, in turn limiting pathogen proliferation and survival (Hood and Skaar, 2012; Martins et al., 2019; Gerner et al., 2020; Monteith and Skaar, 2021). Iron is a critical determinant for host-pathogen interactions. Due to the intrinsic toxicity of iron, cells have developed robust mechanisms to acquire, traffic, store and excrete iron. However, this compartmentalisation and sequestration of iron brings rise to challenges to intracellular pathogens, which require and rely on the sufficient availability of iron for their intracellular proliferation, survival and pathogenicity (Ganz, 2009; James E. Cassat and Skaar, 2013; Weiss and Carver, 2018). To counteract invading pathogens, the immune system actively restricts iron availability to inhibit microbe growth and survival. Macrophages are involved by altering iron regulatory pathways and sequestering iron in order to restrict iron availability to pathogens, inhibiting their proliferation and survival (Haschka et al., 2021a; Nairz et al., 2010, 2014; Pandey et al., 2022).

1.6.3 Maintaining iron homeostasis: Iron uptake, storage, and trafficking in mammalian cells

Here, I will highlight some important iron proteins and mechanisms employed by mammalian cells to maintain iron homeostasis under physiological conditions. This will provide the basis to then explore how macrophages respond following infection and sequester iron to control pathogen proliferation and survival. A schematic of mammalian cellular iron homeostasis is represented in Figure 1.9.

1.6.3.1 Uptake of transferrin and non-transferrin bound iron

There are two major routes of cellular iron uptake, transferrin (Tf)-bound iron uptake, and non-Tf-bound iron uptake (NTBI). However under physiological conditions, the majority of iron is bound to transferrin (Lawen and Lane, 2013; Richardson and Ponka, 1997). Iron uptake in mammalian cells is primarily mediated by the transferrin receptor (TfR) binding to transferrin (Dautry-Varsat, 1986). Transferrin-bound iron is maintained in a Fe^{3+} oxidation state until delivered to tissues where it binds to the extracellular part of the transferrin receptor (Qian et al., 1997; Qian and Tang, 1995), a type 2 transmembrane glycoprotein that is expressed as a homodimer on the surface of cells that is approximately 97 kDa (Kühn et al., 1984; McClelland et al., 1984; Schneider et al., 1984). This complex is then endocytosed via clathrin-mediated endocytosis (Lawrence et al., 1999), before being acidified and dissociated in the endosome. The pH of the endosome is decreased to approximately 6.5 through the action of the vacuolar H+-ATPase (V-ATPase) (Nelson and Harvey, 1999) which then triggers the release of Fe^{3+} from transferrin. Next, Fe^{3+} is reduced to Fe^{2+} most likely by the six-transmembrane epithelial antigen of the prostate 3 (STEAP3), an endosomal ferrireductase required for the efficient uptake of transferrin-bound iron (Ohgami et al., 2005). Fe^{2+} is then transported across the membrane of the endosome into the cytosol mediated by the divalent metal transporter 1 (DMT1) (see section 1.6.3.2 below). Non-transferrin bound iron can also directly be taken up by mammalian cells through DMT1 as well as the zinc transporters ZIP8 (SLC39A8) (C.-Y. Wang et al., 2012) and ZIP14 (Liuzzi et al., 2006). Cytosolic Fe^{2+} makes up part of the labile iron pool (LIP) (Qian et al., 1997). Iron from the LIP is then mobilised by the chaperone poly(rC)-binding protein 1 (Protchenko et al., 2021) which transports iron into the mitochondria via mitoferrin-1 (Shaw et al.,

2006). Iron-free transferrin that is still associated with TfR in the endosomes is then recycled and transported back to the cell surface where transferrin is then released (De Domenico et al., 2008). Transferrin receptor expression is regulated by the IRE/IRP system, containing an IRE in the 3' UTR of the gene that most likely affects the stability of *TfR* mRNA (Rouault, 2006; Wallander et al., 2006). Binding of IRPs to the IRE of TfR increases levels of cytosolic iron in limited iron conditions by increasing the uptake of iron through TfR (Erlitzki et al., 2002; Pantopoulos, 2004).

1.6.3.2 Divalent metal transporter 1 (DMT1)

Following the release of iron from transferrin in the acidified endosomes and the reduction of Fe^{3+} to Fe^{2+}, iron is transported across the endosomal membrane into the cytosol of various cell types through the divalent metal transporter 1 (DMT1) (Bogdan et al., 2016; Gunshin et al., 1997). DMT1 (previously known as NRAMP2) is a member of the SLC group of membrane transport proteins, SLC11A2. DMT1 was the first mammalian iron transporter identified (Gruenheid et al., 1995). The mRNA of DMT1 is alternatively spliced, giving rise to four different isoforms of DMT1 (Fleming et al., 1999; Hubert and Hentze, 2002; Lee et al., 1998). These four isoforms have 12 transmembrane domains (Czachorowski et al., 2009; Gunshin et al., 1997; Wessling-Resnick, 2015), and range between 61-65 kDa in humans. Iron transport mediated via DMT1 is also known to be coupled to proton symport and is pH dependent. In addition to iron, other ions/divalent metals including Mn^{2+}, Zn^{2+}, Co^{2+}, Cd^{2+}, Cu^{2+} and Ni^{2+} have also been shown to be transported by DMT1 (Gunshin et al., 1997). Non-transferrin bound iron can also be taken up into mammalian cells, particularly duodenal enterocytes, by DMT1 from the plasma membrane after being reduced by ferric reductases such as duodenal cytochrome b (DCYTB), which reduces ferric Fe^{3+} iron to ferrous Fe^{2+} iron (D. Lane et al., 2015). Iron can also cross the outer membrane of the mitochondria via DMT1 (Wolff et al., 2014). Similar to the transferrin receptor, the expression of DMT1 is also regulated by the IRE/IRP system (Lee et al., 1998). The existence of an IRE in the 3' UTR of two out of the four isoforms suggests that the expression of DMT1 is post-transcriptionally controlled by intracellular iron concentrations (Gunshin et al., 2001). The presence of an IRE in the 3' UTR of DMT1 stabilises the expression of this transporter in iron deprivation conditions to promote iron uptake and maintain iron homeostasis.

1.6.3.3 The role of ferritin in iron storage

In human serum and within cells, iron is tightly bound to the iron storage protein ferritin to keep the bioavailability of free intracellular Fe (II) iron levels or non-transferrin bound iron (NTBI) low, avoiding metal toxicity and regulating oxidative damage to maintain cellular iron homeostasis (Arosio et al., 2009; Chasteen, 1998; Harrison and Arosio, 1996). Human poly (rC)-binding protein 1 (PCBP1) acts as an iron chaperone, facilitating the delivery and loading of iron into ferritin. It also controls the sensing, trafficking, and chemical reactivity or iron (Patel et al., 2021). Studies have demonstrated that the depletion of PCBP1 increases cytosolic iron pools and inhibits ferritin loading, emphasising the role as a cytosolic iron chaperone (Shi et al., 2008). Ferritin is also regulated by the IRE/IRP system, where IRPs can bind to a single IRE within the 5' untranslated region, inhibiting translation and thereby reducing the sequestration of iron into ferritin storage in iron deprivation conditions, thus maintaining cellular iron homeostasis (Eisenstein and Blemings, 1998; Hentze et al., 2010; Muckenthaler et al., 1998; Pantopoulos, 2004).

Iron stored within protein cages of ferritin is released upon degradation through ferritinophagy (Mancias et al., 2015). Ferritinophagy is mediated by the nuclear receptor coactivator 4 (NCOA4), a selective cargo receptor that targets it to autophagosomes for degradation, releasing the stored iron for cellular usage (Santana-Codina and Mancias, 2018; Le et al., 2024). Studies have found that NCOA4 is required for the delivery of ferritin to lysosomes, and depleting NCOA4 from cells prevented the degradation of ferritin, resulting in a decrease in intracellular iron availability (Mancias et al., 2014). NCOA4 plays a critical role in maintaining iron homeostasis levels by controlling the rate of ferritin degradation depending on the demand, balancing the iron levels within the cells, and thus preventing iron overload and toxicity.

1.6.3.4 Ferroportin and iron export

To date, ferroportin (FPN1), also known as SLC40A1, is the only known Fe^{2+} ferrous iron exporter in mammalian cells. After export, ferrous iron is re-oxidised to Fe^{3+} ferric iron by the ferroxidase enzyme hephaestin (Heph), shown to physically interact with ferroportin on the cell surface (Yeh et al., 2009), or by ceruloplasmin (Cp) in macrophages which, coupled with ferroportin, exports Fe^{2+} and re-oxidises Fe^{2+} to Fe^{3+} (Jeong and David, 2003). The efflux of ferrous iron from macrophages and enterocytes through ferroportin into the plasma is crucial for maintaining systemic iron homeostasis. Studies have shown that although the deletion of ferroportin *in utero* resulted in viable mice, these mice exhibited anaemia and stunted growth after birth and resulted in the accumulation of iron in iron-exporting tissues (Zohn et al., 2007). Other studies have also found that conditional inactivation of ferroportin results in iron accumulation and retention in cells including macrophages, enterocytes and hepatocytes (Donovan et al., 2005), supporting that essential role of FPN1 in cellular iron export.

Ferroportin-mediated efflux of iron is negatively regulated by hepcidin, a peptide hormone derived in the liver. Hepcidin binds to ferroportin promoting it's phosphorylation and in turn its internalisation and lysosomal degradation, preventing iron overload (Hentze et al., 2010; Nemeth and Ganz, 2009). In low iron conditions, hepcidin expression is repressed, reducing the degradation of FPN1 and increasing the levels of available iron to meet iron demands and maintain homeostasis. In addition to its regulation post-translational regulation via hepcidin, ferroportin can also be subjected to post-transcriptional regulation. Studies have shown that IFN-γ and LPS downregulate ferroportin mRNA expression levels (Ludwiczek et al., 2003). Ferroportin mRNA is also expressed in two alternatively spliced isoform transcripts and regulated by the IRE-IRP system. FPN1 expresses an IRE in the 5' UTR of one of its isoforms (Zhang et al., 2009), ensuring that in iron-deficient conditions, translation of FPN1 is repressed by IRP1 and IRP2, preventing iron export in order to maintain cellular iron homeostasis (Abboud and Haile, 2000; Liu et al., 2002; Lymboussaki et al., 2003; McKie et al., 2000).

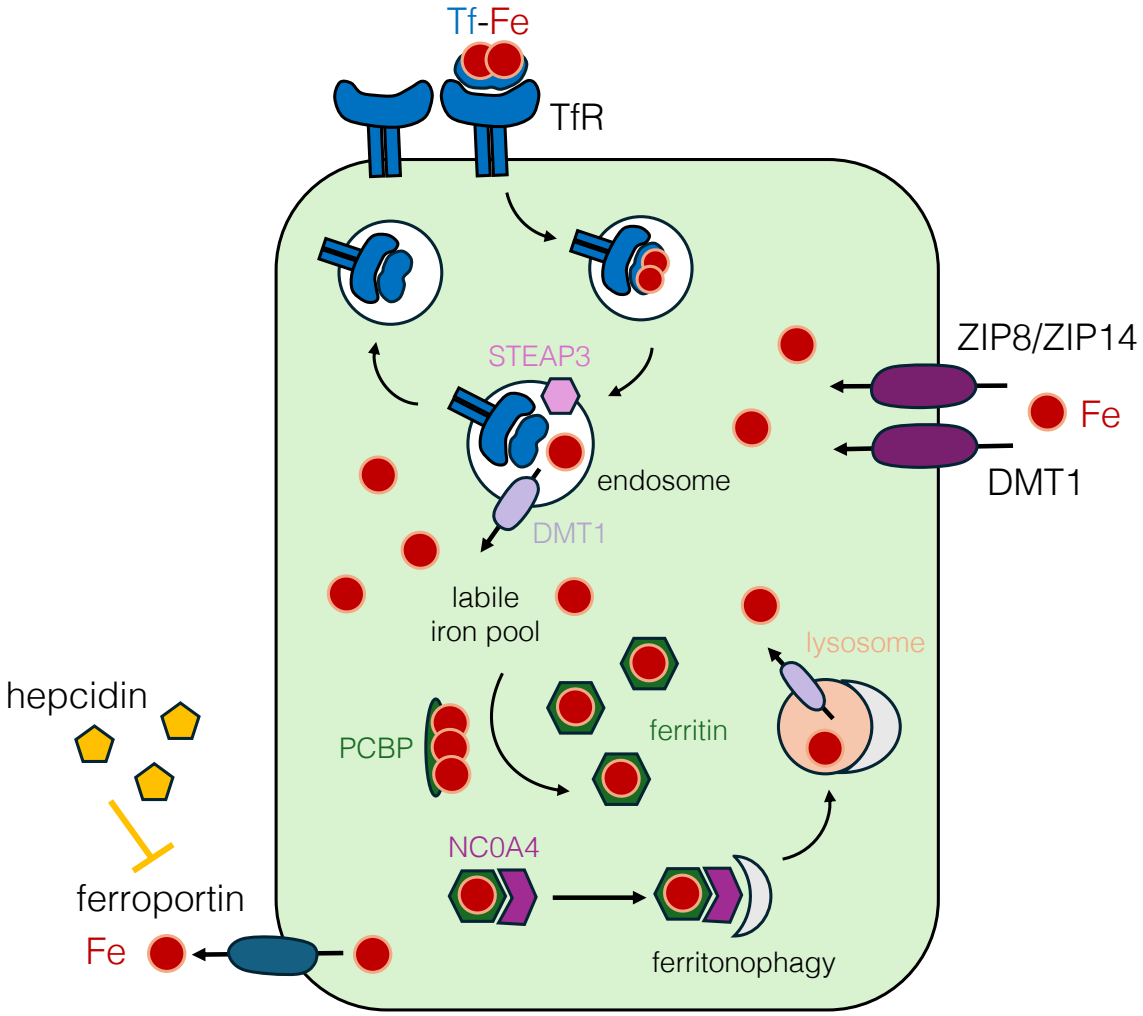


Figure 1.9 - Summary of mammalian cellular iron homeostasis.

Schematic summarising mammalian cellular iron homeostasis. Iron can be bound to transferrin and taken up in its ferric Fe^{3+} form via the transferrin receptor which is then endocytosed via clathrin mediated endocytosis. In endosomes, the ferric reductase STEAP3 reduces ferric Fe^{3+} to ferrous Fe^{2+} iron which is then exported out of the endosome via DMT1. Non-transferrin bound iron can also be taken up by transporter such as ZIP8/ZIP14 and DMT1 on the cell surface. Free iron is now available in the labile iron pool which can be utilised in the cell. Iron is stored within protein cages of ferritin which is mediated by the chaperone PCBP. In low iron conditions, the enzyme NCOA4 targets ferritin for degradation via ferritinophagy in lysosomes. In high iron conditions, iron is exported out of the cell via the iron exporter ferroportin, maintaining iron homeostasis. Hepcidin binds to ferroportin and triggers its degradation, reducing iron export from the cell and maintaining systemic iron homeostasis.

1.6.4 Macrophages and iron sequestration during infection

Upon infection, mammalian iron homeostasis is actively shifted and reshaped. Macrophages play a central role controlling infection by sequestering iron following the invasion of pathogens. They restrict the availability of this essential nutrient and in turn limit the proliferation and survival of the pathogen. For example, studies have highlighted how the regulation of the hepcidin-ferroportin axis in *Plasmodium* infection plays a central role in regulating the availability of iron in red blood cells (RBC). Following *Plasmodium berghei* infection, the iron exporter ferroportin is upregulated, reducing the levels of iron in the RBC and thus limiting the supply of iron to the parasite. On the contrary, an increase in iron levels leads to an upregulation of hepcidin which inhibits ferroportin by binding to it and triggering its downregulation. This increases the availability of iron within the RBC and promotes parasite growth (Wunderlich et al., 2024; Zhang et al., 2018). This phenomenon is also observed in murine macrophages following infection with the intracellular, gram-negative bacteria *Salmonella typhimurium* which resides within phagosomes. Infection leads to an increase in expression of the principal iron exporter ferroportin, reducing the cytoplasmic LIP and iron storage via ferritin, limiting the availability of iron and limiting microbial proliferation and survival (Nairz et al., 2007). Studies in *Salmonella typhimurium* demonstrated that mice lacking ferritin display impaired iron storage capacities as well as an increase in bacterial burden, highlighting the role that ferritin plays in controlling *Salmonella* infection in macrophages (Haschka et al., 2021b). The role of DMT1 in sequestering host iron stores following infection has also been highlighted upon *Salmonella typhimurium* infection which showed that macrophages deficient in DMT1 have an impaired control of infection. They observed an increase in the availability of iron which in turn leads to the proliferation, survival, and persistence of *Salmonella typhimurium* within macrophages (Grander et al., 2022). Finally, iron regulatory proteins (IRPs) have also been shown to play a key role in iron transport and sequestration in macrophages, restricting the growth and survival of *Salmonella typhimurium*. Mutations in both IRP1 and IRP2 in mice led to an increase in *Salmonella* bacteria burden in both the spleen and liver, and *ex vivo* experiments supported the role that IRPs play in restricting bacterial growth (Nairz et al., 2015).

1.6.5 Strategies employed by microbes to subvert macrophage iron sequestration to facilitate intracellular survival

Although macrophages actively sequester iron to restrict nutrient availability to pathogens and control infection, intracellular pathogens employ mechanisms to subvert this sequestration to acquire iron from the host to sustain infection and survival. Here, I will highlight a few examples of how pathogens manipulate host iron homeostasis following infection to allow for their proliferation and persistence.

1.6.5.1 Bacterial host iron manipulation

Klebsiella pneumoniae manipulates its host cell to acquire iron by inducing the expression of transferrin receptor, the main cellular iron importer in macrophages. This increases the availability of iron and allows persistence of the bacteria in THP1 macrophage cells *in vitro* (Grubwieser et al., 2023). *Mycobacterium tuberculosis* has been shown to hijack host ferritin metabolism in a TRIM21 and NCOA4-dependent manner to mediate the degradation of ferritin and increase the availability of iron for the survival of the pathogen (Dai et al., 2023). In *Salmonella typhimurium* infection, studies have demonstrated a repression of ferroportin expression via a hepcidin-independent mechanism to increase iron availability for bacterial persistence (Willemetz et al., 2017). This was further proposed in *Salmonella enterica* where an increase in ferroportin expression levels inhibited bacterial growth, and the downregulation of ferroportin by hepcidin enhanced the survival of the pathogen (Chlosta et al., 2006). Finally, the intracellular bacteria *Francisella tularensis* induces TfR expression as a result of an increase in IRP1 and IRP2 which regulate TfR mRNA stability. Infection also increases the expression of the ferrireductase STEAP3 and the iron uptake transporter DMT1. This increases iron uptake into macrophages, increasing the levels of intracellular iron and supporting the survival and growth of *Francisella tularensis* (Pan et al., 2010).

1.6.5.2 Protozoan parasite host iron manipulation

In addition to the manipulation of host iron stores by bacteria, studies have also demonstrated mechanisms by which protozoan parasites, particularly *Leishmania* and *Plasmodium*, subvert host iron sequestration. *Leishmania donovani* inhibits

the translation and expression of ferroportin in host macrophages in a hepcidin-independent manner, increasing the availability of iron for the parasite (Das et al., 2018). Another study highlighted that *Leishmania donovani* directly scavenges and depletes the host macrophage LIP for persistence. This decrease in labile iron pool then triggers the activation of the iron sensors IRP1 and IRP2 which then bind to the 3' UTR of the transferrin receptor gene, in turn increasing its expression, exploiting the iron uptake capacity of macrophages and increasing the availability of the LIP for *L. donovani* growth and survival (Das et al., 2009). A study in *L. amazonensis* demonstrated that infection triggers the upregulation of hepcidin, which then binds to and triggers degradation of the iron exporter ferroportin. This inhibits the export of iron, leading to an increase in the availability of iron within macrophages and promoting parasite replication (Ben-Othman et al., 2014). In addition to ferroportin, *Leishmania* infection triggers the hepcidin-mediated degradation of NRAMP1, accompanied with an increase in iron availability and in turn enhanced intracellular proliferation rate of the parasite (Banerjee and Datta, 2020). Studies have also shown that *Leishmania donovani* infection can trigger the cleavage of chaperones poly(rC)-binding proteins 1 and 2 (PCBP1 and PCBP2) in macrophages, reducing iron loading into ferritin and increasing the levels of intracellular iron for the proliferation and survival of the parasite within macrophages (Sen et al., 2022).

The role of apicomplexan parasites in modulation of host iron homeostasis, particularly in macrophages, is less well understood. Despite this, some studies in *Plasmodium* have demonstrated that these parasites are able to manipulate host iron stores. Following infection, *Plasmodium* parasites digest approximately up to 80 % of the haemoglobin in RBC host cells, liberating haem and converting it to haemozoin important for parasite growth and survival (Hackett et al., 2009). In *Plasmodium falciparum*, a homologue of the mammalian iron transporter DMT1 was identified and shown to be vital for cellular iron metabolism in the parasite (Loveridge and Sigala, 2024). PfDMT1 localises to the food vacuole membrane and was shown to be essential, with knockdown of PfDMT1 exhibiting defects in a range of iron-dependent functions including mitochondrial polarisation and impairment of apicoplast biogenesis in the parasite. Supplementation with exogenous iron, but not other metals, was shown to selectively rescue the growth of DMT1 (Loveridge and Sigala, 2024). In *P. yoelii*, a study has shown that the iron

transporter PyDMT1 interacts with host ferritin and this is required for disease pathogenesis, as knockout ferritin cells which increases cytosolic LIP, led to a significant inhibition of WT but not mutant PyDMT1 parasites, supporting the interaction between PyDMT1 and host ferritin (Zhong and Zhou, 2023). *P. falciparum* has been shown to increase the LIP in infected RBCs from early ring to late schizont stages, and that the addition of either ferric citrate or transferrin to the culture medium increases the labile iron pool in RBCs at the trophozoite stages of the parasite, suggesting that *Plasmodium* parasites can access iron in the source of serum, or iron bound to transferrin, in addition to the LIP (Clark et al., 2013).

1.6.6 Antimicrobial strategies employed by macrophages in toxoplasmosis

Toxoplasma gondii resides within macrophages and is able to invade and replicate within these immune cells. Although they play a central role in the proliferation and spread of the parasite through the regulation of immunity and metabolism, they are also able to restrict parasite growth and produce inflammatory cytokines that contribute to parasite clearance. This makes macrophages important regulatory cells in the fight against toxoplasmosis. During early stages of infection, the cell-mediated immune response to *T. gondii* is controlled by natural killer (NK) cells which prime processes including antigen presentation and cytokine production (Poncet et al., 2019). This includes the production of the cytokine IFN-γ, crucial for the survival of the host cell following infection with *Toxoplasma*. The production of IFN-γ by NK cells is triggered by the recognition of *T. gondii* profilin by Toll-like receptors 11 and 12 (TLR11 and TLR12) by dendritic cells. A study more than 40 years ago has shown that the presence of IFN-γ eliminates *T. gondii* in macrophages, emphasising the importance of this cytokine as a major effector molecule in the resistance of the host against the parasite and control of infection (Nathan et al., 1983).

At least three different protective mechanisms that are IFN-γ mediated have been identified, highlighted in Figure 1.10. Firstly, the presence of IFN-γ enhances the expression of indoleamine 2,3- dioxygenase (IDO) (Pfefferkorn et al., 1986). These are inhibitory proteins which then deplete the essential amino acid tryptophan, required for the growth and survival of *T. gondii* (Pfefferkorn, 1984). IFN-γ also induces the inducible nitric oxide synthase (iNOS) enzyme, which then generates

nitric oxide (NO), a highly toxic metabolite that triggers NO-mediated toxicity and kills the parasite. An increase in iNOS also depletes the essential amino acid arginine required by *T. gondii*, in turn limiting its growth and persistence (Takács et al., 2012). Finally, IFN-γ also upregulates the expression of immunity-related GTPases (IRGs) as well as guanylate-binding proteins (GBPs). These effector proteins play a role in the destruction of the parasitophorous vacuole where *T. gondii* are protected and reside, making the intracellular parasites more susceptible to elimination in the cytoplasm of macrophages (Takács et al., 2012).

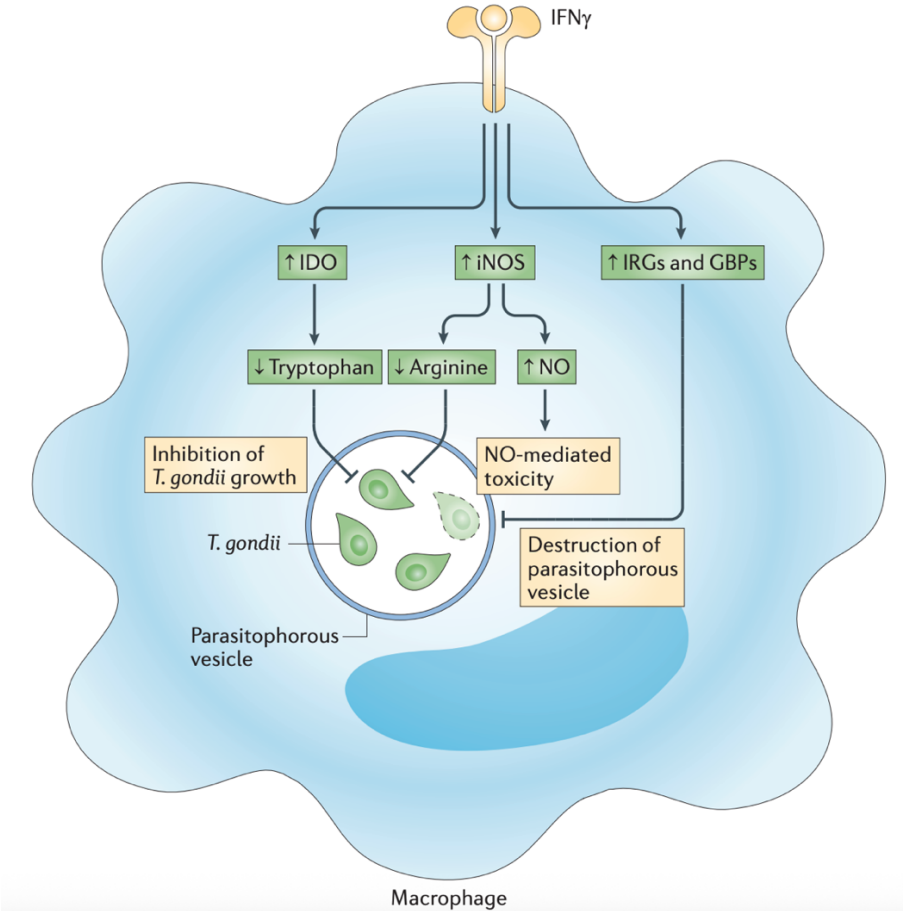


Figure 1.10 - Strategies employed by IFN-γ cytokine to eliminate *Toxoplasma gondii* in macrophages.

Schematic showing the three mechanisms of IFN-γ mediated elimination of *T. gondii* parasites in infected macrophages, including an increase in IDO expression which reduces the essential amino acid tryptophan, and an increase in iNOS which increases NO toxicity and decreases the essential amino acid arginine for parasite survival. Finally, IFN-γ increases IRGs and GBPs which play a role in the destruction of the parasitophorous vacuole, making the parasites more vulnerable in the cytoplasm of macrophages for elimination. Figure taken from Yarovinsky, 2014. Republished by permission from the Springer Nature, Nature Reviews Immunology, conveyed via Copyright Clearance Centre. License number: 6140831461689.

The immune functions of macrophages to control infection are often closely linked with the regulation of cellular iron homeostasis. In addition to the mechanisms of IFN-γ control of *Toxoplasma* infection mentioned above, this cytokine also controls infection by altering the availability of nutrients to the parasite, including restricting the availability of iron. For example in the context of bacterial infections, IFN-γ has been shown to promote the export of iron from human macrophages, limiting the replication of intracellular bacteria (Abreu et al., 2020). It has also been shown to restrict the availability of intracellular iron from *Salmonella typhimurium* in macrophages, controlling infection (Nairz et al., 2008). This has also been proposed in *T. gondii* where IFN-γ activated rat enterocytes and peritoneal macrophages cells inhibited the replication of *Toxoplasma gondii* by restricting the levels of intracellular iron available to the parasite (Dimier and Bout, 1998). Macrophages also employ iron dependent mechanisms to control *T. gondii* infection. A study has highlighted the role of Fam96, a conserved protein that is highly expressed in macrophages in controlling infection. The deletion of Fam96 led to an increase in parasite burden in mice by disrupting iron homeostasis and inhibiting immune effector molecules, emphasising its role in controlling infection. Fam96 does so through the regulation of macrophage cell polarisation which is dependent on the modification of intracellular iron homeostasis (Liu et al., 2024). Although macrophages are one of the first type of immune cells that *T. gondii* encounter following infection, the parasites are still able to persist and replicate within them, suggesting that these parasites are able to remodel macrophage cell physiology to allow for their survival.

1.6.7 Known strategies employed by *Toxoplasma gondii* to manipulate host iron stores

A key aspect of remodelling macrophages following infection involves manipulating host iron metabolism to allow for parasite growth and survival. However, at the beginning of my PhD, little was known about the mechanisms by which *Toxoplasma gondii* infection affects host iron handling. Gene-array hybridisation assays to determine the transcriptional role of *T. gondii* infection has revealed an upregulation of transferrin receptor expression levels in infected fibroblasts, which was further supported by western blot analysis (Gail et al., 2001). Later studies have attributed this induction in transferrin receptor

expression in infected cells to an increase in the activity of IRP1 which binds to the 3' UTR of the transferrin receptor mRNA, stabilising it and preventing it from degradation (Gail et al., 2004). The study further highlighted that this increase in TfR expression was not due to the direct interaction of parasite factors with the iron uptake machinery, but was mediated indirectly by host cell or parasite-derived secreted factors (Gail et al., 2004).

More recently, the mechanisms by which *Toxoplasma* interferes in host iron metabolism by interfering with ferroptosis have started to become better understood. A study has demonstrated that *T. gondii* infection triggers the activation of ferroptosis-related signalling pathways, which resulted in pathological damage in the hippocampus of mice. Treatment with an iron chelator led to ferroptosis resistance and prolonged the survival of the host by decreasing the burden of *T. gondii* (Wang et al., 2023). This was further supported by a study which highlighted that infection with *T. gondii* induces ferroptosis hallmarks in murine macrophages, including increasing the expression of lactate dehydrogenase, the levels of labile iron, the generation of ROS and the accumulation of lipid peroxidases. This has been shown to be important for the replication and virulence of *T. gondii* both *in vitro* and *in vivo*, and suggests that the parasite hijacks iron-lipid metabolism in macrophages to aid in its survival (Li et al., 2025). However, at the start of my PhD, the expression of other host iron associated proteins including the divalent metal transporter 1 (DMT1), ferritin heavy chain 1 (FTH1) and ferroportin (FPN1) in the context of *Toxoplasma gondii* infection were not known.

1.7 Thesis aims, significance and broader impact

Aim 1: Uncovering how *Toxoplasma gondii* acquires iron and zinc through the identification and functional characterisation of a ZIP domain containing protein, ZFT.

Motivation 1: Transition metals such as iron and zinc are essential nutrients for almost all eukaryotic life. They have been shown to be essential for the ubiquitous parasite *Toxoplasma gondii*, and the uptake of these ions must be carefully balanced and regulated to avoid metal toxicity and cellular death. Despite their importance in many cellular and biological systems, when I started my PhD research studies, the mechanisms by which *T. gondii* acquired iron and zinc were not yet known. Therefore, the main aim of my PhD was to identify and characterise the first metal uptake transporter in the parasite and to further signify the importance of iron and zinc to *T. gondii*. Understanding the transporters required for the uptake of these metals into the parasite will advance the understanding of how *T. gondii* acquires nutrients from its host and allow for future experiments to investigate the metallobiology of these parasites. This will further our understanding on how these metals are used in cellular and biological processes within the parasite and the important role that they play in apicomplexan parasite biology and possibly open up avenues to iron chelation as a potential strategy to control *T. gondii* infection.

Aim 2: Understanding if and how *Toxoplasma gondii* modulates and manipulates host iron homeostasis following infection.

Motivation 2: Although iron is required by *T. gondii* both *in vitro* and *in vivo* (Bergmann et al., 2020; Renaud et al., 2024; Sloan et al., 2025), and some host iron-related proteins were shown to be modulated in infection, the full picture on how *T. gondii* hijacks host iron trafficking was not fully understood at the beginning of my studies. I therefore aimed to investigate how the parasite modulates the host iron homeostasis and subverts host cell processes for nutrient acquisition following infection to ensure sufficient iron availability and parasite growth and survival.

Chapter 2 Materials and methods

2.1 Materials

2.1.1 Equipment

Manufacturer	Equipment
Agilent	Seahorse XF HS Mini Analyzer
Applied Biosystems	7500 Fast Real-Time PCR System
Avidity Science	Alto™ I Type 1 Ultrapure Water System
BD Bioscieces	25G needles, FACs tubes, BD FACSCelesta™ Cell Analyzer
BioRad	Agarose gel electrophoresis equipment, T100™ Thermal Cycler, GenePulser Xcell™ electroporator, SDS-PAGE equipment
BMG LabTech	PHERAstar FS microplate reader
Denver Instruments	pH meter, analytical balance
Eppendorf	miniSpin tabletop centrifuge, biophotometer, New Brunswick™ Innova® 44/44R Shaker
FisherBrand	Syringes, vacuum system, mini-centrifuge
Gallenkamp	Yeast cell incubator
Gilson	Pipettes
Grant Instruments	GD100 water bath, SUB Aqua 12 Plus water bath, CVP-2 centrifuge vortex for PCR plates, block heater
Hanna Instruments	Multiparameter Digital Ph Meter
Heidolph	Rotamax 120 shaker, REAX top vortex
Heraeus Instruments	Orbital mixer, bacterial incubator
Invitrogen	SDS-PAGE equipment
Kern	ADB analytical balance
Kühner Switzerland	ISF-1-W Incubator shaker temperature controls
Labtech	G-Storm PCR machine
Leica Microsystems	Inverted DiM8 microscope
Li-COR	Odyssey CLx
Navigator	Analytical balance
Nikon Instruments inc	A1-R inverted microscope
PHCbi	Cell culture incubators
Premier Laboratory Systems	Fume hoods
Scotsman	Ice machine
SLS Lab Basics	Orbital shaker
Starlab	Pipettes, pipette guns, heating magnetic stirrer, vortex mixer, multichannel pipettes
Stuart	Block heater SBH130D, orbital shaker, roller mixer, rotary shaker
Syngene	PXi GelDoc reader
ThermoFisher Scientific	Heraeus Pico 21 tabletop centrifuge, Heraeus Fresco 21 cooling centrifuge, iBrightFL100, SL 16R centrifuge, Nanodrop spectrophotometer, pipette guns, tissue culture hoods, UVP UV transilluminator
ZEISS	Primovert inverted cell culture microscope, ELYRA 7 with Lattice SIM^2 microscope

Table 2-1 - A list of equipment used in this study.

2.1.2 Software

Software	Version	Supplier
Adobe Acrobat Reader	2025.001.20476	Adobe Systems, Inc.
Basic Local Alignment search tool (BLAST)	2.16.0	National Institute for Biotechnology Information (NCBI)
Benchling	NA	Saji Wickramasekara & Ashu Singhal (MIT)
ChimeraX	1.10	Resource for Biocomputing, Visualization, and Informatics (RBVI) at UCSF
Clustal Omega	1.2.4	EMBL-EBI
Codon Optimisation Tool	NA	Integrated DNA Technologies (IDT)
(Fiji is Just) ImageJ	2.14.0/1.54p	National Institutes of Health (NIH) (Schindelin et al., 2012)
FlowJo	10.10.0	Becton Dickinson & Company (BD)
GraphPad Prism	10.5.0	GraphPad Software, Inc.
Image Lab	6.1.0	BioRad
Image Studio	5.2.5	Li-COR
Inkscape	1.4.2	Open source vector graphics editor
InterPro	105.0	EMBL
Leica Application Suite (LAS) X Core	3.7.5.24914	Leica Microsystems
MARS (Microplate Analysis and Reporting Software)	3.20 R2	BMG LabTech Data Analysis Software for PHERAstar
Microsoft	16.97.2	Microsoft Corporation
NanoDrop 1000	1.6.198	ThermoFisher Scientific
Orange	3.38.1	Bioinformatics Laboratory at the University of Ljubljana
PHERAstar software	5.30 R3	BMG LabTech
PyMca	5.9.4	European Synchrotron Radiation Facility (ESRF)
SnapGene	8.1	GSL Biotech LLC
T-coffee	13.46.1. b8b01e06	Multiple sequence alignment tool (Notredame et al., 2000)
Tm Calculator	1.16.7	New England Biolabs
VEuPathDB (ToxoDB, PlasmoDB, HostDB)	Release 68	National Institute of Allergy and Infectious Disease (NIAID)
XF HS Mini Controller Software	V3.0.0.41	Agilent
Zen Blue	3.12	Carl Zeiss Microscopy
Zotero	7.0.15	Reference manager - Corporation for Digital Scholarship
7500 System Software	2.0.6	Applied Bioscience

Table 2-2 - A list of software used in this study.

2.1.3 Antibodies

2.1.3.1 Primary antibodies

Epitope	Antibody Species	Target Species	Dilution		Source
			IFA	Western Blot	
α-HA	Rat		1:500	1:500	Merck 11867423001
α-Ty	Mouse		1:1000	1:2000	Sebastian Lourido
α-GAP45	Rabbit	*T. gondii*	1:5000	ND	Dominique Soldati
α-IMC1	Rabbit	*T. gondii*	1:2000	ND	Dominique Soldati
α-SAG1	Mouse	*T. gondii*	1:500	ND	Sebastian Lourido
α-BAG1	Rabbit	*T. gondii*	1:500	ND	Lilach Sheiner
α-CDPK1	Guinea Pig	*T. gondii*	1:5000	1:10,000	Sebastian Lourido
α-TOM40	Rabbit	*T. gondii*	1:1000	1:1000	Giel Van Dooren
α-CPN60	Rabbit	*T. gondii*	1:1000	1:2000	Lilach Sheiner
α-lipoic acid	Rabbit	*T. gondii*	ND	1:1000	Abcam ab58724
α-GAPDH	Mouse	Human/ Mouse	1:1000	1:1000	Merck G8795
α-TfR	Rabbit	Rabbit	1:1000	1:1000	Abcam ab214039
α-DMT1/ SLC11A2	Rabbit	Human	1:1000	1:1000	Cell Signalling Technology D3V8G
α-DMT1/ SLC11A2	Rabbit	Mouse	1:1000	1:1000	Merck ABS983
α-FTH1	Rabbit	Human/ Mouse	1:1000	1:1000	Cell Signalling Technology 3998S
α-FPN1/ SLC40A1	Rabbit	Human/ Mouse	1:1000	1:1000	Novus Biologicals NBP1-21502

Table 2-3 - A list of primary antibodies used in this study.

ND = Not Determined

2.1.3.2 Secondary antibodies

Name	Antibody Species	Dilution		Source
		IFA	Western Blot	
Alexa Fluor 488 α-mouse IgG	Goat	1:1000	-	Invitrogen A11001
Alexa Fluor 594 α-mouse IgG	Goat	1:1000	-	Invitrogen A11005
Alexa Fluor 488 α-rabbit IgG	Goat	1:1000	-	Invitrogen A11008
Alexa Fluor 594 α-rabbit IgG	Goat	1:1000	-	Invitrogen A11012
Alexa Fluor 488 α-guinea pig IgG	Goat	1:1000	-	Invitrogen A11073
Alexa Fluor 594 α-guinea pig IgG	Goat	1:1000	-	Invitrogen A11076
Alexa Fluor 488 α-rat IgG	Chicken	1:1000	-	Invitrogen A21470
Alexa Fluor 594 α-rat IgG	Goat	1:1000	-	Invitrogen A1107
α-guinea pig IgG DyLight 680	Goat	-	1:10,000	Invitrogen SA5-19989
IRDye 800Cw α-guinea pig	Donkey	-	1:10,000	LI-COR 925-32411
α-rat IgG DyLight 680	Donkey	-	1:10,000	Invitrogen SA5-10032
IRDye 680RD α-rat	Goat	-	1:10,000	LI-COR 926-68076
IRDye 680RD α-mouse	Goat	-	1:10,000	Abcam ab216776
α-rabbit IgG DyLight 680 conjugated	Goat	-	1:10,000	Abcam ab216776
α-rabbit IgG DyLight 800Cw	Goat	-	1:10,000	Abcam ab216773
α-mouse IgG HRP conjugate	Goat	-	1:1000	Promega W4021
α-rabbit IgG HRP conjugate	Goat	-	1:5000	Promega W4011
α-rat IgG HRP conjugate	Goat	-	1:5000	Abcam ab6845
Dolichos Biflorus Agglutinin (DBA) 488	*Dolichos biflorus*	-	1:1000	Vectorlabs, FL-1031

Table 2-4 - A list of secondary antibodies used in this study.

- = no reaction

2.1.4 Kits

Kit	Source
QIAprep® Spin Miniprep Kit	QIAGEN, 27106
QIAGEN® Plasmid Plus Midi Kit	QIAGEN, 12943
DNeasy® Blood and Tissue Kit	QIAGEN, 69506
MinElute® PCR Purification Kit	QIAGEN, 28004
MinElute® Gel Extraction Kit	QIAGEN, 28604
QIAEX®II Gel Extraction Kit	QIAGEN, 20021
RNeasy® Mini Kit	QIAGEN, 74104
High-Capacity cDNA Reverse Transcription Kit	Applied Biosystems, 4368814
Nano-Glo® Luciferase Assay	Promega, N1110

Table 2-5 - A list of kits used in this study.

2.1.5 Buffers, media, and solutions

2.1.5.1 Bacteria

Solution	Components
LB medium	10 g/l tryptone, 5 g/l yeast extract, 5 g/l NaCl
LB agar	1.5 % (w/v) agar in LB medium
NZY broth medium	5 g/l NaCl, 2 g/l $MgSO_4*7H_2O$, 5 g/l yeast extract, 10 g/l casein hydrolysate, pH adjusted to 7.5
Ampicillin 1000X	10 % (w/v) ampicillin in distilled water for a final concentration of 100 mg/mL. Filter sterilise with a 0.2 µM filter
Transformation buffer I (TB-I)	60 mM potassium acetate, 80 mM $MnCl_2$, 100 mM $CaCl_2$ and 15 % (w/v) glycerol in distilled water. Filter sterilise and store up to 1 year at 4 °C
Transformation buffer II (TB-II)	10 mM MOPS pH 7.0, 10 mM RbCl, 100 mM $CaCl_2$ and 15 % (w/v) glycerol in distilled water. Filter sterilise and store at 4 °C
Glycerol stock freezing solution	40 % (v/v) glycerol and 2 % (w/v) peptone in LB medium

Table 2-6 - A list of buffers, media and solutions used for bacterial work in this study.

2.1.5.2 Yeast

Solution	Components
$PEG_{3000-5000}$	50 % (w/v) in distilled water. Autoclaved to sterilise and stored at 4 °C
1 M Lithium Acetate (LiAc)	1 M Lithium Acetate (w/v) in distilled water (2.04 g LiAc in 20 mL water). Autoclaved to sterilise and stored at 4 °C. Used at 100 mM for transformations
20 % Glucose	100 g glucose in 500 mL distilled water. Filter sterilise and use at 1:10 dilution
YPD (Yeast Peptone Dextrose) Medium	1 % yeast extract (w/v), 2 % peptone (w/v) in distilled water and autoclave. Before use, add 2 % glucose solution (v/v)
YPD Agar	1 % yeast extract (w/v), 2 % peptone (w/v) and 2 % agar (w/v) in distilled water and autoclave. Before use, add 2 % glucose solution (v/v)
SD (-Ura) Medium	0.078 % dropout supplement -ura (w/v) in distilled water and autoclave. Before use, add 2 % glucose solution (v/v)
SD (-Ura) Agar	0.078 % dropout supplement -ura (w/v) and 2 % agar (w/v) in distilled water and autoclave. Before use, add 2 % glucose solution (v/v)

Table 2-7 - A list of buffers, media and solutions used for yeast work in this study.

2.1.5.3 Mammalian and *T. gondii* cell culture

Solution	Components
D10 Media	Dulbecco's Modified Eagle Medium (DMEM) supplemented with 10 % heat-inactivated foetal bovine serum (FBS), 2 mM L-glutamine and 50 U/mL Penicillin/Streptomycin
D3 Media	Dulbecco's Modified Eagle Medium (DMEM) supplemented with 3 % heat-inactivated foetal bovine serum (FBS), 2 mM L-glutamine and 50 U/mL Penicillin/Streptomycin
10x PBS	137 mM NaCl, 2.7 mM KCl, 8 mM Na_2HPO_4, 1.8 mM KH_2PO_4 (pH 7.4)
Cytomix electroporation buffer	10 mM KPO_4, 120 mM KCL, 5 mM $MgCl_2$, 0.15 mM $CaCl_2$, 25 mM HEPES, 2 mM EGTA
100 mM ATP	1 g ATP (Sigma-Aldrich A6419-1G) in 18 mL distilled water. Adjust pH to 7 and sterilise using a 0.2 µM filter
250 mM GSH	1 g glutathione (GSH) (Sigma-Aldrich G6013-5G) in 12.8 mL distilled water. Sterilise using a 0.2 µM filter
Buffer A Extracellular Solution	116 mM NaCl, 5.4 mM KCL, 0.8 mM $MgSO_4$, 5.5 mM glucose, 50 mM HEPES in distilled water, adjusted to pH 7.2 and filter sterilised

Proteinase K	Prepare 10 mg/mL in 1x PBS (Sigma-Aldrich P2308-100MG)
Coomassie	0.3 % Coomassie brilliant blue R-250 (w/v), 45 % methanol (v/v), and 10 % glacial acetic acid (v/v) in distilled water
Coomassie Destain Solution	40 % methanol (v/v), 10 % glacial acetic acid (v/v) in distilled water
FACS buffer	1 % FBS, 25 mM HEPES and 5 mM EDTA in 1x PBS
Ringer's solution	155 mM NaCl, 3 mM KCL, 2 mM $CaCl_2$, 1 mM $MgCl_2$, 3 mM Na_2HPO_4, 10 mM HEPES, 10 mM Glucose and 1 % FBS in distilled water, pH to 7.4 and filter sterilised
Paraformaldehyde (PFA) fixative	4 % PFA (v/v) in 1x PBS
Transmission electron microscopy (TEM) fixative solution	2.5 % glutaraldehyde (w/v) and 4 % PFA (w/v) in 0.1 M cacodylate buffer
IFA permeabilisation and blocking solution	2 % BSA (w/v), 0.2 % Triton X-100 (v/v) in 1x PBS
Crystal Violet	49 mM crystal violet, 20 % ethanol (v/v), 70 mM ammonium oxalate
Ammonium acetate	100 mM ammonium acetate in distilled water
Poly-L-Lysine (Sigma-Aldrich)	0.1 % Poly-L-Lysine (w/v) in distilled water

Table 2-8 - A list of buffers, media and solutions used for mammalian and *T. gondii* cell culture work in this study.

2.1.5.4 DNA

Solution	Components
50x TAE Buffer	2 M Trizma® base, 5.71 % glacial acetic acid (v/v), 50 mM EDTA (pH 8) in distilled water
1 kb plus DNA Ladder (Invitrogen)	100 µL 1kb plus DNA ladder, 83 µL 6x gel loading dye (Biolabs) and 317 µL distilled water
6x Gel Loading Dye Purple (New England Biolabs)	1x Buffer components: 2.5 % Ficol®-400, 10 mM EDTA, 3.3 mM Tris-HCL, 0.08 % SDS, 0.02 % Dye 1, 0.001 % Dye 2, pH 8 @ 25 °C
10x hybridisation buffer	1 M KAc, 300 mM HEPES, pH 7.5

Table 2-9 - A list of buffers and solutions used for DNA work in this study.

2.1.5.5 Protein

Solution	Components
RIPA lysis buffer	150 mM NaCl, 1 % Triton X-100 (v/v), 0.5 % sodium deoxycholate (w/v), 0.1 % SDS (w/v), 50 mM Trizma® base in distilled water, adjusted to pH 8
5x Laemmli sample buffer	10 % SDS (w/v), 50 % glycerol (v/v), 300 mM TrisHCL pH 6.8, 0.05 % bromophenol blue (w/v) in distilled water
10 % APS	1 g ammonium persulfate in 10 mL distilled water
4x resolving gel buffer	1.5 M Trizma® base and 0.4 % SDS (w/v) in distilled water, adjusted to pH 8.8
10 % Resolving gel	33.33 % of Bis-acrylamide 30 % solution (v/v), 25 % of 4x resolving gel (v/v),1 % of 10% SDS (v/v), 0.05 % TEMED, and 1 % of 10 % APS (v/v) in distilled water
4x stacking gel buffer	0.5 M Trizma® base, 0.4 % SDS (w/v), adjusted to pH 6.8 in distilled water
5 % Stacking gel	16.67 % of Bis-acrylamide 30 % solution (v/v), 13.33 % of 4x stacking gel (v/v), 0.1 % of 10 % SDS (v/v), 0.05 % TEMED, and 0.1 % of 10 % APS (v/v) in distilled water
10x SDS protein gel running buffer	0.25M Trizma® base, 1.92 M glycine and 1 % SDS (w/v) in distilled water
10x transfer buffer	25 mM Trizma® base and 192 mM glycine in distilled water
1x transfer buffer	48 mM Trizma® base, 39 mM glycine and 20 % methanol (v/v)
PBST washing solution	10 % 10x PBS (v/v) in distilled water and 0.1 % Tween 20 (v/v)
Protein blocking solution	10 % 10x PBS (v/v) in distilled water, 0.1 % Tween 20 (v/v) and 5 % skimmed milk powder (w/v)
PageRuler prestained protein ladder	62.5 mM Tris-H_3PO_4 (pH 7.5 at 25 °C), 1 mM EDTA, 2 % SDS, 10 mM DTT, 1 mM sodium azide and 33 % glycerol
1x Blue Native (BN) PAGE running buffer	30 mL 20x running buffer solution and 570 mL distilled water
1x BN-PAGE dark cathode buffer	10 mL 20x cathode buffer solution, 10 mL 20x running buffer solution and 180 mL distilled water
1x BN-PAGE light cathode buffer	1 mL 20x cathode buffer, 10 mL 20x running buffer solution and 189 mL distilled water
Digitonin (Sigma-Aldrich)	5 % (w/v) digitonin in distilled water
1x BN-PAGE lysis buffer	25 % 4x Native PAGE buffer (v/v) (Invitrogen), 2 % protease inhibitors (v/v), 1 % digitonin (v/v) in distilled water
NativeMark unstained protein ladder	Bis/Tris-HCl, pH 7.0; NaCl; glycerol; Ponceau S
Complex IV oxidation buffer	50 mM KH_2PO_4 pH 7.2 in distilled water

Table 2-10 - A list of buffers and solutions used for protein work in this study.

2.1.6 Biological and chemical consumables

Reagent	Source
Acetic acid glacial	vwr chemicals, 20104.334
ACK lysis buffer	ThermoFisher Scientific, A1049201
Acrylamide/Bis-acrylamide 30 % solution	Sigma-Aldrich, A3699
Amersham™ Hyperfilm ECL film	Cytiva, 28906837
Amersham™ Protan™ Nitrocellulose Blotting Membrane 0.45 µm NC	Cytiva, 10600002
Ammonium Acetate	Sigma-Aldrich, A1542
Ammonium Persulfate	Sigma-Aldrich, A3678
Bacteriological agar for microbiology	vwr chemicals, 84609.0500
Beta-mercaptoethanol	ThermoFisher Scientific, 31350010
Bovine Serum Albumin	Sigma-Aldrich, A7030
Bradford Reagent	Sigma-Aldrich, B6916
Chelex® 100 sodium form	Sigma-Aldrich, 95577
Crystal Violet	Sigma-Aldrich, 61135
Cytochrome *c*	Sigma-Aldrich, C7752
DAPI Fluoromount-G®	SouthernBiotech, 0100-20
D-Glucose Anhydrous	ThermoFisher Scientific, G/0500/53
Digitonin	Sigma-Aldrich, D141
Dimethyl Sulfoxide	Sigma-Aldrich, D4540
DNase I Amplification Grade	ThermoFisher Scientific, 1806801
DO Supplement-Ura	TaKaRa Bio, 630416
Dulbecco's Modified Eagle Medium (DMEM 1x)	Gibco, 41965-039
Dulbecco's Phosphate Buffered Saline (DPBS 1x)	Gibco, 14190-094
Ethylenediaminetetraacetic acid (EDTA)	ThermoFisher Scientific, 15575020
Ethanol	Merck, 1.00983.2500
Ethylene glycol-bis(2-amino-ethylether)-N,N,N', N' tetraacetic acid (EGTA)	Sigma-Aldrich, E3889
Fetal Bovine Serum (Head Inactivated)	Gibco, A5256801
Gel Loading Dye Purple (6X)	New England Biolabs, B7024A
Glycerol	Sigma-Aldrich, G5516, ThermoFisher Scientific, G/0650/17
Glycine	Sigma-Aldrich, G7126
GoTaq® G2 Hot Start Green Master Mix	Promega, M742A
Herring Sperm DNA	Promega, D181A
Immersol™ 518F Immersion Oil	Zeiss, 433802-9010-000
1 Kb Plus DNA Ladder	ThermoFisher Scientific, 10787018

1.0 and 1.5 mm cassettes	Life technologies, NC2015
3'3-Diaminobenzidine Tetrahydrochloride (DAB)	Sigma-Aldrich, D5637
0.05 % Trypsin-EDTA (1x)	Gibco, 25300-054
NativeMark™ Unstained Protein Standard	ThermoFisher Scientific, LC0725
NEBuilder® HiFi DNA Assembly Master Mix	New England Biolabs, E2621S
L-Glutamine Solution	Sigma-Aldrich, G7513
Lithium Acetate Dyhydrate	Sigma-Aldrich, L4158
M-CSF	BioLegend, 576404
Methanol	Sigma-Aldrich, 34860
Minimal SD Base	TakaRa Bio, 630411
NativePAGE™ 4x Sample Buffer	ThermoFisher Scientific, BN20032
NativePAGE™ 3-12 % Bis-Tris Gel	ThermoFisher Scientific, BN2011BX10
Nitric Acid 67-69 % for trace metal analysis	vwr chemicals, 83872.270
N, N, N', N'-Tetramethyl-ethylenediamine	Sigma-Aldrich, T9281
PageRuler™ Plus Prestained Protein Ladder	ThermoFisher Scientific, 26619
Penicillin-Streptomycin	Sigma-Aldrich, P0781
Peptone	Formedium, PEP02
Pierce™ ECL Western Blotting Substrate	ThermoFisher Scientific, 32106
Poly-L-lysine Solution	Sigma-Aldrich, P8920
Ponceau S Staining Solution	ThermoFisher Scientific, A40000278
PowerSYBR Green PCR Master Mix	ThermoFisher Scientific, 4367659
Proteinase K from *Tritirachium album*	Sigma-Aldrich, P2308
Q5® High-Fidelity 2X Master Mix	New England Biolabs, M0492S
rCutSmart Buffer	New England Biolabs, B6004S
Recombinant Mouse IFN-γ	BioLegend, 575306
RPMI 1640 Medium	ThermoFisher Scientific, 31870025
Skim Milk Powder	Sigma-Aldrich, 70166
Sodium Chloride	vwr chemicals, 27810.295
Sodium Deoxycholate	Sigma-Aldrich, D6750
Sodium Dodecyl Sulphate	Sigma-Aldrich, 75747
SYBR™ Safe DNA Gel Stain	ThermoFisher Scientific, S33102
Triton™ X-100	Sigma-Aldrich, X100
Trizma® base	Sigma-Aldrich, T6066
TWEEN® 20	Sigma-Aldrich, P1379
UltraPure™ Agarose	Life Technologies, 16500
Yeast Extract Powder	Formedium, YEA02

Table 2-11 - A list of biological and chemical consumables used in this study.

2.1.7 Drugs/agents

Drug/Agent	Concentration	Solvent/Diluent	Source
Ampicillin (sodium salt)	100 mg/mL	Distilled water	Cayman Chemical, CAY14417
Chloramphenicol	40 mg/mL	Distilled water	Sigma-Aldrich, C3175
Cycloheximide	100 mg/mL	DMSO	Sigma Aldrich, 01810
Pyrimethamine	1 mM	Ethanol	Sigma-Aldrich, 46706
Ferric ammonium citrate (FAC)	500 mM	1x PBS	Sigma-Aldrich, F5879
Ferric chloride	10 mM	Distilled water	Sigma-Aldrich, F1513
Deferoxamine mesylate salt (DFO)	100 mM	1x PBS	Sigma-Aldrich, D9533
Zinc sulphate ($ZnSO_4$)	100 mM	Distilled water	Sigma-Aldrich, 307491
Sodium Arsenate (Ars)	5 mM	1x PBS	Sigma-Aldrich, S7400
2-Mercaptopyridine N-oxide sodium salt (Zn Ionophore)	10 mM	Distilled water	Sigma-Aldrich, H3261
N,N,N',N'-tetrakis-(2-pyridylmethyl) ethylenediamine (TPEN)	5 mM	DMSO	Merck, 616394
Anhydrotetracycline hydrochloride (ATc)	1 mM	Ethanol	Abcam, ab145350
MG132 Proteasome Inhibitor	10 mM	DMSO	Sigma-Aldrich, M8699
FCCP	50 mM	DMSO	Sigma-Aldrich, C2920
Atovaquone	1 mM	DMSO	ThermoFisher Scientific, 17565545
FluoZin™-3AM	2 mM	DMSO	ThermoFisher Scientific, F24195
FerroOrange	1 mM	DMSO	Dojindo, F374-10
Hoechst 33342, trihydrochloride, trihydrate	16.2 mM	Distilled water	ThermoFisher Scientific, H3570
Transferrin From Human Serum, Alexa Fluor™ 488 Conjugate	25 mg/mL	Distilled water	ThermoFisher Scientific, T13342
CISMBI	500 µM	DMSO	Sigma-Aldrich, S312630

Table 2-12 - A list of drugs and agents used in this study.

2.1.8 Oligonucleotide sequences

gRNA Sequences	
Name	**Sequence (5' – 3')**
ZFT 3'	TGAACTGTTGCACAACCTAC
ZFT 5'	CCTTGAGACCTTTCCTCCCG
SDHB 3'	CGAGCCGAGGTTACGCAGCG
ABCE1 3'	GCTCGACGACGCTTGAAGCG

Table 2-13 - A list of the gRNA sequences used in this study.

Primer Sequences		
Name	**Sequence (5' – 3')**	**Purpose**
P1	ggtactcggtcttaccctggtggatctggctctagacg ctTACCCGTACGACGTCCCGGA	Repair template for generation of ZFT-3HA Fw sequence
P2	tcgccacactgtctacagagagctgactagaaagtta cacCTGATAGCTGTCTTGTGTAT	Repair template for generation of ZFT-3HA Rv sequence
P3	CCTGATCTACTGCCTAGGGGCCAGC	Fw sequence for ZFT-3HA$_{zft}$ and ZFT-3HA$_{sag1}$ PCR validation
P4	GGATCCGAGCACGCGCAGTAAAG	Rv sequence for ZFT-3HA$_{sag1}$ PCR validation
P5	ctttataatggggcacatgc	Rv sequence for ZFT-3HA$_{zft}$ PCR validation
P6	ctcgttggcatttttttcttgATGGCGACGGTCGC AGAC	ZFT amplification from cDNA Fw
P7	tgagcacaacggtgattaatttaatcgagcgggtcct ggttcgtgtggacctcAGCGTCTAGAGCCAGAT CCAC	ZFT amplification from cDNA and Ty tag Rv
P8	CTCGGTCTTACCCTGGTGGATCTGGCTCT AGACGCaGAGGTCCACACGAACCAGGACC CGCTCGATAGCGGAGCTACTAACTTCAGC	P2A-DHFR amplification Fw
P9	GTGATTAATTTAATCGAGCGGGTCCTGGT TCGTGTGGACCgctaGACAGCCATCTCCAT CTGGAT	P2A-DHFR amplification Rv
P10	ctcgttggcatttttttcttgatggcgacggtcgcagac	TUB8 ZFT-Ty DHFR integration verification Fw
P11	tgagcacaacggtgattaatttaatcgagcgggtcct ggttcgtgtggacctcagcgtctagagccagatccac	TUB8 ZFT-Ty DHFR integration verification Rv
P12	accgaacagggcgacgatttttccccttgagaccttt cctCTTCGCCAGGCTGTAAATCC	ZFT T7S4 Fw
P13	agctggcagcagacatcacatcgtctgcgaccgtcg ccatTGGTTGAAGACAGACGAAAGCAGTT G	ZFT T7S4 Rv
P14	cctgataggttctggacctccctcgc	ZFT T7S4 5' integration Fw
P15	cgtagagcagaaacgcactactaaag	ZFT T7S4 5' integration Rv

P16	gcaaagccagagggatatatgctcc	ZFT T7S4 3' integration Fw
P17	cgaggtcgacgtatcgataagcttacg	ZFT T7S4 3' integration Rv
P18	AAATAGGATGGTACATCCCCC	HA integration test Rv
P19	gaaacacacttcgtgcagc	CAT integration test Fw
P20	CTTTTCTTTTGTGGGTTGTGC	SDHB-3HA Fw
P21	CGACATTTGCATGTACATACC	SDHB-3HA UTR Rv
P22	ATCTCGTCAGCGGCATGAACC	ABCE1-3HA Fw
P23	CATACACGGACACAGATACGC	ABCE1-3HA UTR Rv
P24	aaaaaaaatataccccagcctcgagATGGCCACC GTCGCTGATGAC	Amplification of ZFT for yeast expression Fw
P25	aagtccaaagctggatccgcctcgagTTAGTCAA GAGGGTCTTGGTTAG	Amplification of ZFT for yeast expression Rv
P26	GGGACGACATGGAGAAAATC	Actin RT-qPCR Fw
P27	AGAAAGAACGGCCTGGATAG	Actin RT-qPCR Rv
P28	CGGACAACCGAATAGTGGCT	ZFT RT-qPCR Fw
P29	CGCCAACGATCATTCCTTCG	ZFT RT-qPCR Rv

Table 2-14 - List of primer sequences used in this study.

2.1.9 Plasmids

Plasmid	Antibiotic resistance	Source
U6-sgRNA-Cas9-DHFR	Ampicillin	Sebastian Lourido
pU6-ZFT 3'-sgRNA		This study
pU6-ZFT 5'-sgRNA		This study
pLIC-3xHA-CAT		Lilach Sheiner
LIC-3HA-zftUTR-CAT		This study
tub-ZFT-Ty-HX		This study
tub-ZFT-Ty-P2A-DHFR		This study
T7S4-G13-DHFR		Lilach Sheiner
pU6- SDHB 3' sgRNA		Andrew Maclean
pU6-ABCE1 3’ sgRNA		Giel Van Dooran
pDR195		AddGene, #36028
pDR195-scZFT-Ty Full Length		This study

Table 2-15 - A list of plasmids either used or generated in this study.

2.2 Cell biology

2.2.1 Cell strains

2.2.1.1 Mammalian and bacterial strains

Cells	Organism	Source
Human Foreskin Fibroblasts (HFFs)	*Homo Sapiens*	ATCC® SCRC-1041™
RAW 264.7 murine macrophages	*Mus musculus*	ATCC® TIB-71 ™
DH5α	*E. coli*	Home-made chemically competent

Table 2-16 - A list of mammalian and bacterial strains used in this study.

2.2.1.2 *Toxoplasma gondii* strains

Strain	Reference
F3ΔHX	(Sheiner et al., 2011)
RHΔKu80ΔHXG	(Fox et al., 2009; Huynh and Carruthers, 2009)
RHΔKu80:mNeonGreen	(Aghabi et al., 2023)
RHΔKu80:tdTomato	
RHtdTomato	(Elati et al., 2023)
RHtdTomato pTUB8-ZFT-Ty-DHFR	this study
F3ΔHX ZFT-3HA$_{zft}$	
F3ΔHX ZFT-3HA$_{sag1}$	
F3ΔHX T7S4-ZFT	
F3ΔHX T7S4-ZFT-3HA$_{sag1}$	
F3ΔHX T7S4-ZFT SDHB-3HA	
F3ΔHX T7S4-ZFT ABCE1-3HA	
nanoLuc$_{dhfr}$	(Sloan et al., 2025)
nanoLuc$_{zft}$	

Table 2-17 - A list of *Toxoplasma gondii* strains used in this study.

2.2.1.3 Yeast strains

Strain	Reference
Δzrt1/2	(Ullah et al., 2018)
Δfet3/4	
Δsmf1	
Δzrt1/2:TgZFT	This study
Δzrt1/2:pDR195	This study

Table 2-18 - A list of yeast strains used in this study.

2.2.2 Mammalian cell culture

2.2.2.1 Human foreskin fibroblasts (HFFs)

Primary human foreskin fibroblasts (HFFs) were the cells used to grow and maintain *T. gondii* tachyzoites. HFFs were cultured in Dulbecco's Modified Eagle Medium (DMEM) supplemented with 10 % (D10) heat-inactivated foetal bovine serum (FBS), 2 mM L-glutamine and 50 U/mL Penicillin/Streptomycin and maintained at 37 °C with 5 % CO_2. HFFs were maintained in culture until approx. passage 24. HFFs were split 1:4 by removing the media, washing the cells once with 1x PBS, adding 4 mL of trypsin and incubating at 37°C for 8 minutes to detach the cells from the culture flask. Following this, D10 media was added to the cells and split into tissue culture dishes/plates. When split 1:4, HFFs reached confluency after approximately 7 days, and are ready to infect with *Toxoplasma gondii* parasites at this point.

2.2.2.2 RAW 264.7 murine macrophages

RAW 264.7 murine macrophages were cultured in DMEM media supplemented with 10 % (D10) heat-inactivated foetal bovine serum (FBS), 2 mM L-glutamine and 50 U/mL Penicillin/Streptomycin and maintained at 37 °C with 5 % CO_2. Macrophages were sub-cultured every 2-3 days, never reaching more than 70-80 % confluency. This was done by changing the media, gently scraping the cells to detach them from the surface, and then splitting 1:10 in a T75 flask.

2.2.2.3 RAW 264.7 murine macrophages cryopreservation and thawing of stabilates

To cryopreserve RAW 264.7 murine macrophages, media was replaced on the cells with fresh D10. Macrophages were then gently scraped to detach from the culture flask, counted, and resuspended to 5 x 10^6 cells/mL in FBS and 10 % dimethyl sulfoxide (DMSO). 1 mL of cells were pipetted into a labelled cryovial and placed into a freezing container at -80 °C. The following day, cells were moved to liquid nitrogen (LN2) for long term storage. To thaw RAW 264.7 murine macrophages, cells are thawed in a 37 °C incubator and added to 10 mL of prewarmed D10 media. Cells were spun down at 1500 x g for 5 minutes and resuspended in 12 mL of prewarmed D10 media and seeded into a T75 vented flask.

2.2.3 *Toxoplasma gondii* cell culture

T. gondii tachyzoites were grown in HFFs cultured in DMEM supplemented with 3 % (D3) heat-inactivated FBS, 2 mM L-glutamine and 50 U/mL Penicillin/Streptomycin and maintained at 37 °C with 5 % CO_2, until they lysed approximately 80-90 % host cell monolayer. Once lysed, parasites were then inoculated onto a fresh host cell monolayer to maintain. *T. gondii* parasites were disposed of by disinfecting in 5 % chemgene for 4 hours before being autoclaved.

2.2.3.1 Mechanical release and filtering of intracellular parasites

To mechanically release intracellular *T. gondii* parasites from HFFs, the media was removed, cells were gently washed twice in 1x PBS before adding 5 mL 1x PBS and gently scraping the cells to detach them from the surface of the dish. Cells were then passed 3-4 times through a 25 G needle attached to a 5 mL syringe to mechanically release the parasites from the fibroblast cells. Cells were then passed through a 3 µM filter to allow parasites to pass through, leaving behind larger host cell debris.

2.2.3.2 *T. gondii* transfection and selection

Approximately 5x10^6 parasites were used per transfection. If intracellular, parasites were mechanically released by scraping and syringing. Parasites were collected by centrifugation at 1500 x g for 10 minutes. Supernatant was then

removed, and parasite pellets were resuspended in 520 µL cytomix, 65 µL ATP (100 mM) and 65 µL GSH (100 mM) and transferred to an electroporation cuvette. 100 µL of DNA (70 µg) was then added to the cuvette and mixed. Parasites were electroporated using the Bio-Rad© electroporator at 1700 V, 0.2 ms pulse length, 2 pulses with 5 second intervals and then inoculated onto HFF cells. The media was replaced 6 hours later or the following morning. Stable integration of plasmids into the *Toxoplasma* genome was selected for by culturing the transfected pool of parasites with selection markers. The chloramphenicol acetyltransferase (CAT) gene was selected for with 40 µg/mL chloramphenicol. The dihydrofolate reductase (DHFR) resistance gene was selected for using 1 µM pyrimethamine.

2.2.3.3 Isolation of clonal *T. gondii* cell lines

Following the crash and recovery of parasite pools after transfection and drug selection pressure, the stable pool was tested by PCR (see section 2.3.1) for integration of transfected plasmid DNA. If positive, single positive clones were isolated. To do so, 2-3 parasites of the stable mixed pool population were seeded into each well of clear 96-well plate and cultured at 37 °C and 5 % CO_2 for 6-7 days undisturbed in the presence of the appropriate selection marker to allow plaque formation. After a week, each well of the plates were checked for single plaque formation (arising from a single parasite), indicating a clonal parasite line. Once the plaques were large enough, parasites were validated either by polymerase chain reaction (PCR) (see section 2.3.1) or an immunofluorescence assay (IFA) (see chapter 2.4.1) before expanding and making stocks.

2.2.3.4 *T. gondii* strain construction

For the generation of the ZFT-3HA$_{sag1}$ strain, a fragment containing the 3HA epitope sequences and chloramphenicol resistance gene was amplified by PCR from plasmid LIC-3HA-CAT (Sheiner et al., 2011) to generate the repair template (using primers P1 and P2) which includes the upstream homologous region of ZFT and downstream homologous regions around the stop codon. F3ΔHX parasites were then transfected using a Gene Pulse BioRad electroporator with 30 µg of the purified repair template PCR product and 40 µg of a plasmid containing Cas9 guide targeting the 3' end of the genomic sequence of ZFT (Table 2-13). Transgenic

parasites were selected with chloramphenicol and cloned out as described in section 2.2.3.3. Clones were validated by PCR using primers P3 and P4.

For the generation of the ZFT-3HA$_{zft}$ strain, a fragment containing the 3HA epitope sequences, *zft* 3' UTR and chloramphenicol resistance gene was amplified by PCR from plasmid LIC-3HA$_{zft}$-CAT (modified plasmid from (Sheiner et al., 2011) to generate the repair template (using primers P1 and P2) which includes the upstream homologous region of ZFT and downstream homologous regions around the stop codon. F3ΔHX parasites were then transfected using a Gene Pulse BioRad electroporator with 30 µg of the purified repair template PCR product and 40 µg of a plasmid containing Cas9 guide targeting the 3' end of the genomic sequence of ZFT (Table 2-13). Transgenic parasites were selected with chloramphenicol, cloned by limiting serial dilution. Clones were validated by PCR using primers P3 and P5.

To generate RHtdTomato pTUB8 ZFT-Ty-DHFR parasites, ZFT was amplified from cDNA, and a Ty tag was inserted at the 3' end of the gene by PCR using primers P6 and P7. The tubulin promoter TUB8 plasmid was digested with EcoRI and PacI and then assembled with the ZFT-Ty PCR product to generate the new plasmid. The DHFR sequence was amplified using primers P8 and P9. The TUB-ZFT-Ty plasmid was then digested using BbvC1 enzyme then the DHFR sequence was inserted into the plasmid. TUB8-ZFT-Ty-DHFR plasmid was linearised using enzyme ScaI and the transfected into RHtdTomato parasites using a Gene Pulse BioRad electroporator. Parasites were selected using pyrimethamine and cloned by limiting dilution. Clones were confirmed using primers P10 and P11. For the generation of the F3ΔHX T7S4-ZFT strain, the T7S4 promoter was amplified from the G13m5 plasmid (Sheiner et al., 2011) using primers P12 and P13. F3ΔHX parasites were transfected using a Gene Pulse BioRad electroporator with 30 µg of the purified repair template T7S4-ZFT PCR product and 40 µg of a plasmid containing Cas9 guide targeting the 3' end of the genomic sequence of ZFT (Table 2-13). Parasites were selected with pyrimethamine and cloned by limiting dilution. Clones were screened for 3' integration using primers P14 and P15, and 5' integration using primers P16 and P17. For the generation of the F3ΔHX T7S4-ZFT-3HA$_{sag1}$ line, ZFT was tagged as previously described in F3ΔHX T7S4-ZFT parasites, selected for with chloramphenicol, and cloned by limiting dilution. The T7S4-ZFT SDHB-3HA and T7S4-ZFT ABCE1-3HA parasite strains were generated by

tagging SDHB and ABCE1 as previously described (Maclean et al., 2024, 2021) in the F3ΔHX T7S4-ZFT parasites, selected for with chloramphenicol, and cloned by limiting dilution. T7S4-ZFT SDHB-3HA clones were screened for 5' integration using primers P18 and P20, and 3' integration using primers P19 and P21. T7S4-ZFT ABCE1-3HA clones were screened for 5' integration using primers P18 and P22, and 3' integration using primers P19 and P23. Parasite lines were selected using either chloramphenicol, made up in MiliQ water and used at 40 µg/ml or pyrimethamine, made up in ethanol and used at 2 µM. All sgRNA sequences (Table 2-13) and primers (Table 2-14) used in the study are listed above.

2.2.3.5 Pre-treatment of HFFs before infection with *T. gondii*

HFFs were pretreated with either ferric ammonium citrate (FAC), deferoxamine (DFO), $ZnSO_4$, TPEN or CISMBI at concentrations indicated in the text for 24 hours by replacing the media of the HFFs with D3 media complemented with the metal supplement, chelator, or inhibitor. After 24 h, HFFs were infected with *T. gondii* for a further 18 h, 24 h or 48 h or as indicated in the text, continuously under metal supplementation, chelation, or inhibition.

2.2.3.6 Inducing the knockdown of ZFT

Knockdown of ZFT was induced by the addition of 0.5 ATc µM, unless indicated otherwise, to the cell culture media to either the T7S4-ZFT, T7S4-ZFT-3HA$_{sag1}$, T7S4-ZFT SDHB-3HA or T7S4-ZFT ABCE1-3HA parasite lines. The induction lasted for either 24, 48, 72 or 96 h, as indicated in the text.

2.2.3.7 *T. gondii* cryopreservation and thawing of stabilates

T. gondii parasites were frozen down ideally when intracellular in vacuoles. Freezing solution was prepared as follows:

Solution	Components
Solution A	50 % FBS (v/v) and 50 % D3 media (v/v)
Solution B	20 % DMSO (v/v) and 80 % D3 media (v/v)

Table 2-19 - A list of freezing solution components used for *T. gondii* cryopreservation.

Briefly, media was removed from parasites and cells were washes twice with 1x PBS. 250 µL trypsin was added to each dish, swirled and incubated at 37 °C for 2 minutes. Dishes were then vigorously tapped to aid in cell detachment, before adding 1 mL of solution A to each dish, and then 1 mL of solution B to each dish and gently pipetting the cells to mix. 1 mL of the solution was then aliquoted into each of two precooled cryovials, keeping as cool as possible. Cryovials were then placed in a CoolCell freezing container in the -80 °C freezer overnight before being transferred to liquid nitrogen for long term storage.

To thaw *Toxoplasma gondii,* the cryovial was placed in an incubator for approximately 2-5 minutes until thawed. In the meantime, the media was replaced on a confluent HFF host cell dish with D10 media. After the vial thawed, the parasites were then transferred onto the new host cell dish with the appropriate selection and incubated at 37 °C and 5 % CO_2. Media was changed on the parasites at least three hours later or the next morning.

2.3 Molecular biology

2.3.1 Polymerase chain reaction (PCR)

Polymerase chain reaction (PCR) was performed to amplify DNA fragments from a variety of DNA templates, either for molecular cloning, bacterial colony PCR screening, or *T. gondii* parasite pool and clonal verification. GoTaq® G2 Hot Start Master Mix (Promega, M7422) or Q5® High-Fidelity 2X Master Mix (New England Biolabs, M0492S) were both used in this study. The GoTaq polymerase was used for more analytical purposes such as verifying DNA integration in parasite and bacterial clones, and the high fidelity polymerase was used during molecular cloning to avoid the introduction of mutations during the amplification of DNA fragments. The components of each PCR reaction were as follows (Table 2-20) for a 25 µL reaction: DMSO was used to enhance amplification by inhibiting secondary structures.

Component	Volume	Final concentration
GoTaq® G2 Hot Start Green Master Mix, 2X or Q5® High-Fidelity 2X Master Mix	12.5 µL	1x
Forward primer (10 µM)	1 µL	0.4 µM
Reverse primer (10 µM)	1 µL	0.4 µM
DMSO	1 µL	4 % (v/v)
DNA template	1 – 5 µL	< 250-1000 ng
Nuclease-Free Water	(8.5 µL / to a final volume of 25 µL)	NA

Table 2-20 - A list of PCR mixture components.

NA = Not Applicable

Once the above components were mixed by pipetting up and down, they were transferred to a 0.2 mL PCR tube and transferred to a PCR thermal cycler machine (Bio-Rad) and PCR was performed using the following cycling conditions:

Temperature	Time	Step	Cycles
95 °C	5 minutes	Initial denaturation	1
95 °C	30 seconds	Denaturation	25 – 32
50 – 72 °C	30 seconds	Annealing	
72 °C	30 seconds / kb	Extension	
75 °C	5 minutes	Final extension	1
4-10 °C		Storage	Hold

Table 2-21- PCR thermocycler conditions programme.

2.3.2 Agarose gel electrophoresis (AGE)

PCR products were run on an agarose gel to separate DNA fragments based on size and confirm size of the amplified DNA segment. To do so, either a 1 %, 1.5 % or 2 % agarose gel was made depending on the size of DNA fragment by dissolving agarose (Invitrogen, 16500-500) in 1x TAE buffer (see Table 2-9) and gently heating in the microwave until dissolved. Once cooled down, SYBR Safe (Invitrogen, S33102) was added at a dilution of 1:10,000 to visualise the DNA, before being poured into a plastic cassette and adding the appropriate combs. Once the agarose gel set, the gel was placed in an electrophoresis chamber. DNA was prepared by adding the appropriate amount of 6x purple gel loading dye (New England Biolabs, B7024A) to each sample. 7 µL of 1 Kb plus DNA ladder (ThermoFisher Scientific, 10787018) and DNA samples were loaded onto the gel. The gel was then run at either 80 V for 60 minutes or at 100 V for 25 minutes until the dye is approximately 75 % - 80 % way down the gel before imaging under UV light on a Syngene PXi GelDoc reader.

2.3.3 Restriction endonuclease digests

DNA was digested with endonucleases either for molecular cloning of an insert into a plasmid, a diagnostic tool for plasmid verifications, or to linearise plasmids prior to transfecting. Approximately 100 ng of DNA was used to verify DNA isolated from bacterial cultures for diagnostic purposes. Approximately 60 µg vector DNA was linearised using a single restriction enzyme prior to stable transfection. Restriction digests were performed using enzymes and their respective buffers (New England Biolabs) according to the manufacturers protocol, often at 37°C for 2-4 h and then ran on an agarose gel (see section 2.3.2) to verify.

2.3.4 DNA Purification

DNA was purified from a PCR reaction using the MinElute® PCR Purification Kit (Qiagen, 28004) following the manufacturer's protocol, eluting the DNA in distilled water. DNA was also purified from an agarose gel by cutting out the desired bands from the gel using a scalpel blade over a UV transilluminator and then purified using the MinElute® Gel Extraction Kit (Qiagen, 28604) following the manufacturer's protocol. DNA was eluted in distilled water.

2.3.5 Generation of chemically competent *E. coli*

Briefly, a single colony of *E. coli* was taken from a streaked solid LB agar plate, inoculated into 2 mL of LB broth, and grown overnight shaking at 37 °C. 20 µL of overnight culture was diluted into 10 mL of LB broth and grown at 37 °C while shaking to early log phase (OD_{600} = 0.3) by measuring approximately every hour. The culture was then transferred into a 50 mL centrifuge tube and incubated for 20 minutes at 4 °C in an ice water bath. Cells were then pelleted by centrifugation at 2000 x g for 10 minutes at 4 °C. Supernatant was decanted and 3.3 mL of TB-1 buffer (see Table 2-6) was added to the cells, gently swirling in the 4 °C water bath to resuspend cells. Repeated gentle pipetting of cells was also used to resuspend cells if necessary. The cell resuspension was incubated in the ice cold water bath for 2 h. Cells were centrifuged at 2000 x g for 10 minutes at 4 °C. Supernatant was gently decanted and cells were resuspended in 1.1 mL of TB-II buffer (see Table 2-6). 100 µL aliquots of the resuspension were transferred into prechilled 1.5 mL Eppendorf tubes and immediately stored at -80 °C.

2.3.6 Gibson assembly

Gibson assembly will assemble multiple DNA fragments into a single plasmid. Firstly, primers were designed such that the PCR product will have between 15 and 25 bp of homology with the ends of the plasmid being cloned into. The PCR fragment is then amplified using the standard PCR protocol described in section 2.3.1, ideally with a high fidelity enzyme such as Q5. The PCR products (plasmid backbone and insert) were either cleaned up directly as described in section 2.3.4 or alternatively were then ran on an agarose gel as described in section 2.3.2 and purified as described in 2.3.4 using a gel extraction kit. To clone sgRNA into plasmids, duplex primers (reverse complements) were set up by adding 5 µL 100 nM primer 1, 5 µL 100 nM primer 2, 5 µL 10x hybridisation buffer (see Table 2-9) and 35 µL distilled water. The duplex primers were then denatured at 95 °C for 2 minutes before being allowed to gradually cool down to room temperature, allowing them to anneal together. The fragments were then assembled on ice by mixing 50-100 ng of vector with a 2-10 fold molar excess of insert compared to vector, 10 µL of NEBuilder® HiFi DNA Assembly Master Mix (New England Biolabs, E2621S) and distilled water to a final volume of 20 µL. The reaction was then

incubated in a thermocycler at 50 °C for 15 minutes. The assembled plasmids were then transformed into competent cells as described below in section 2.3.7.

2.3.7 Plasmid transformations into *E. coli* bacteria

DH5α chemically competent *E. coli* bacterial cells stored at -80 °C were thawed on ice. DNA was then added to 50 µL bacteria and mixed gently by pipetting up and down. Cells were then incubated on ice for 30 minutes before being heat shocked at 42 °C for 30 seconds. Cells were then incubated on ice for a further 2 minutes before adding 500 µL of room temperature NZY medium to promote bacterial recovery. Cells were allowed to recover for 1 hour at 37 °C with shaking before being plated onto LB Agar plates with 100 µg/mL ampicillin for selection. Plates were cultured overnight at 37 °C for ~16 hours. Transformed bacterial colonies were then screened for by performing a colony PCR (see section 2.3.8) or sequencing (see section 2.3.10).

2.3.8 Bacterial colony screening by PCR

When testing multiple colonies to validate successful plasmid transformation, a bacterial colony PCR screen was performed. Primers were designed upstream and downstream of the target to allow the differentiation between colonies transformed with the plasmid that has the insert vs. colonies that have been transformed with empty plasmids without the insert. A PCR mastermix was made as previously described in section Table 2-20 and 25 µL was aliquoted into each PCR tube. Single bacterial colonies were then picked off an LB agar plate, gently resuspended into the respective PCR tube with the PCR mastermix and then streaked onto a fresh LB agar plate with 100 µg/mL ampicillin. The PCR reaction was performed as previously described in section 2.3.1 with the thermocycler conditions listed in Table 2-21.

2.3.9 Isolation of plasmid DNA from *E. coli* bacteria

Bacterial culture (either from a single colony on an agar plate or a swab from a glycerol stock) was inoculated in either 5 mL (small scale miniprep) or 50 mL (large scale midiprep) LB medium with 100 µg/mL ampicillin overnight at 37 °C shaker for ~16 hours. Plasmid DNA from overnight liquid culture was then isolated following either the QIAprep Spin Miniprep Kit (Qiagen, 27106) manufacturers

protocol for a miniprep or the QIAGEN Plasmid Plus Midi Kit (Qiagen, 12943) manufacturers protocol for a midiprep. DNA was eluted either in 30 µL (miniprep) or 200 µL (midiprep) distilled water at room temperature (RT) for 5 minutes to achieve maximum elusion efficiency, followed by centrifugation at 17,900 x g for 1 minute. DNA concentration and purity was measured using a Nanodrop™ spectrophotometer following the manufacturer's instructions and stored at -20 °C.

2.3.10 DNA sequencing

Plasmid DNA was sent for sequencing at Eurofins Genomics and was prepared following the company's protocol by adding 5 µL of 5 µM primer, 2.5 µL distilled water and 2.5 µL of DNA in an Eppendorf tube labelled with a sequencing barcode.

2.3.11 Cryopreservation of transformed *E. coli*

DH5α *E. coli* bacterial cells successfully transformed with a plasmid of interest were cryopreserved by growing the bacteria originating from a single colony overnight in LB medium with ampicillin (100 µg/mL) at 37 °C overnight while shaking. Cells were cryopreserved by taking 1 mL of a freshly grown liquid bacterial culture and mixing it with 1 mL of glycerol stock freezing solution containing 40 % glycerol and 2 % peptone in LB medium in a 1:1 ratio. Stocks were then preserved at -80 °C for long term storage.

2.3.12 Genomic DNA extraction from *Toxoplasma gondii*

To isolate genomic DNA (gDNA) from *T. gondii* parasites, 500 µL of parasites from a fully lysed dish or 50 µL from a single well in a 96 well plate were centrifuged at 7000 rpm for 10 minutes at RT in a microcentrifuge. The supernatant was then carefully removed, cells washed once with 1x PBS, then resuspended in 80 µL distilled water, 10 µL 10x Thermo Pol Buffer and 10 µL of Proteinase K (10 mg/mL). Samples were then placed in a thermocycler at 60 °C for 90 minutes followed by 95 °C for 20 minutes before being stored at -20 °C for long term storage.

2.3.13 Reverse transcriptase quantitative PCR (RT-qPCR)

To validate the T7S4-ZFT parasites, RT-qPCR was performed to confirm successful knockdown of ZFT mRNA levels. HFFs were infected with T7S4-ZFT with and without ATc for 24, 48, 72 and 96 h before being mechanically lysed and filtered through a 3 µm filter to remove any host cell debris. Parasites were then harvested by centrifugation at 2000 x g for 10 minutes, supernatant was removed, pellet was washed once in 1x PBS before centrifuging at 7000 rpm for 10 minutes. Supernatant was removed and pellets were frozen at -20 °C overnight. RNA was then extracted from the pellets using the RNeasy Mini Kit (Qiagen, 74104). 1 µg RNA was then treated with DNAse I 1 U/µL (ThermoFisher Scientific, 18068015) at RT for 15 minutes before inactivating the DNAse with 25 mM EDTA followed by DNase denaturation at 65 °C for 10 minutes. Using 1 µg of DNase I treated RNA, cDNA synthesis was then performed using the High-Capacity cDNA Reverse Transcription Kit (Applied Biosystems, A48571) according to manufacturer's instructions. RT-qPCR was carried out on the Applied Biosystems 7500 Real Time PCR machine using PowerSYBR green PCR master mix (ThermoFisher Scientific 4367659) and 2 ng of 1:10 diluted cDNAs per reaction. Primers P26 and P27 were used for actin as a housekeeping control gene and primers P28 and P29 were used for ZFT (Table 2-14). The results are from three independent biological replicates; performed in technical triplicate. Relative fold changes were calculated using the Pfaffl method (Pfaffl, 2001) using actin as a housekeeping gene control. GraphPad Prism 10 was used to perform statistical analysis.

2.4 Phenotypic characterisation

2.4.1 Immunofluorescence assay (IFA)

Indirect immunofluorescence assays (IFA) were performed on both infected HFF monolayers or naturally egressed extracellular tachyzoites, as well as infected and uninfected RAW 264.7 murine macrophages.

2.4.1.1 Intracellular *T. gondii* IFA

Cells were washed twice with 1x PBS to remove extracellular parasites. Intracellular *T. gondii* parasites were then fixed with 4 % paraformaldehyde (PFA) at room temperature for 20 minutes, before being washed twice with 1x PBS. Cells were permeabilized and blocked in blocking buffer (PBS/0.2 % Triton X-100/2 % Bovine Serum Albumin (BSA)) for 30 minutes at room temperature, or at 4°C overnight. Coverslips were then incubated in the plate itself in a wet chamber (a damp blue roll over the plate to prevent evaporation) with primary antibodies (as indicated) diluted accordingly in 30-40 µL of blocking buffer for 1 hour at room temperature. Coverslips were then washed three times with PBST (0. 2 % Triton X-100 in 1x PBS), 5 minutes each. After washing, slides were incubated in a wet chamber with the secondary antibodies (1:1000) accordingly in 30-40 µL blocking buffer for 45 minutes to 1 h at room temperature in the dark. Coverslips were then washed three times with PBST (0.2 % Triton X-100 in 1x PBS) for 5 minutes each and mounted onto glass slides with 10 µL Fluoromount with 4′,6-diamidino-2-phenylindole (DAPI) (Southern Biotech, 0100-20) to stain DNA. Primary and secondary antibody species and dilutions are detailed in Table 2-3 and Table 2-4 respectively.

2.4.1.2 Extracellular *T. gondii* IFA

Extracellular parasites for immunofluorescence assays were gently spun onto poly-L-lysine (Sigma-Aldrich, P8920) coated coverslips at 400 x g for 5 minutes and fixed with 4 % PFA for 20 minutes at room temperature and washed once in PBS. Cells were permeabilized, fixed, and stained as described above in section 2.4.1.1.

2.4.1.3 RAW MΦ IFA

RAW 264.7 murine macrophages were gently scraped and counted, and 5 x 10^5 cells were seeded per well of an IFA plate for 4 hours-overnight before infection with *T. gondii* at an MOI of 2. Fixing, permeabilising, and staining was performed as described above.

2.4.1.4 Quantitative analysis of immunofluorescence assays

Percentage of peripheral or basal ZFT-3HA$_{zft}$ localisation was quantified in respect to number of parasites per vacuole. 100 vacuoles were counted for each condition. Results are mean of three independent experiments, ± SD. The mean fluorescence intensity (MFI) of ZFT-3HA$_{zft}$ parasites was also quantified in relation to the number of parasites per vacuoles. For this, a Z projection of approximately 20 slices for each image was generated with a "sum slices" projection type. Areas around each of 100 vacuoles were drawn manually, and the mean fluorescence of the HA signal was measured on FIJI. This value was then normalised by subtracting it from an average background fluorescence of each respective image. The MFI per parasite was then calculated by dividing the normalised mean fluorescence by the number of parasites in each respective vacuole measured. Each point represents individual MFI/parasite values from three independent experiments.

For the MFI of both Ferro-orange and FluoZin™-3AM extracellular parasites, parasite in focus were manually drawn around using FIJI and the mean fluorescence of the 546 and 495 signals was measured for Ferro-orange and FluoZin™-3AM respectively on FIJI. The values were then normalised to background fluorescence as described above. Points represented the MFI of FerroOrange/FluoZin-3AM parasites from four or three independent experiments respectively. To determine the number of parasites per vacuole upon ZFT knockdown, 100 vacuoles for each condition (parental and T7S4-ZFT parasites in the presence and absence of ATc 48 h) were counted and the number of parasites and organisation per vacuole was noted. Results are the mean of four independent experiments.

To quantify the percentage of vacuoles expressing either tachyzoite or bradyzoite specific markers following ZFT knockdown, 100 vacuoles for each condition (parental and T7S4-ZFT parasites in the presence and absence of ATc 48 h) were counted and the number of vacuoles expressing either SAG1, BAG1 or DBL staining was determined as a percentage. The mean of three independent experiments is represented in this study.

2.4.2 Plaque assay

Briefly, confluent monolayers of HFFs in a 6-well plate were infected with either 100, 500 or 1000 parental of indicated parasites, either in standard or supplemented D3 media, or D3 media supplemented with 200 µM FAC, 25 µM $ZnSO_4$, 2 µM zinc ionophore, or both 200 µM FAC and 25 µM $ZnSO_4$ combined. For T7S4-ZFT plaque assays, parasites were cultured in the absence or presence of 0.5 µM ATc unless indicated otherwise in the text. Parasites were left undisturbed to replicate for 6-7 days, unless stated otherwise. For the ATc washout experiment, cells were treated with ATc for three days, before being washed and replaced with standard D3 to allow recovery, before being fixed and stained as standard protocol. Cells were washed three times with 1x PBS before being fixed with ice cold methanol at room temperature for 20 minutes. Cells were stained using a crystal violet stain for at least 3-4 hours at room temperature, before being washed with distilled water and dried overnight on the bench. Images were taken on a smart phone camera, and plaque numbers and size were quantified using FIJI software and normalised to the appropriate controls as indicated.

2.4.3 Fluorescent growth assay

Growth assays of fluorescent cells were performed using tdTomato-expressing parasites in black, clear bottomed 96 well plates, pre-seeded with HFFs. Host cells were infected with 1,000 RHtdTomato or RHtdTom TUB8 ZFT-Ty-DHFR tachyzoites per well and were allowed to invade for 2 hours at 37 °C with 5 % CO_2 . After 2 hours, the media was supplemented with either FAC, DFO, Ars or $ZnSO_4$ at appropriate concentrations and incubated at 37°C with 5 % CO_2 for 4 days. Fluorescence for each well was recorded at 4 days using a PHERAstar FS microplate reader (BMG LabTech). Experiments were performed in three wells, each representing a technical replicate, and at least three independent biological

experiments were performed. Fluorescence values were normalised to wells with untreated but infected wells, with uninfected wells serving as blanks. Dose-response curves and EC_{50} values were generated using GraphPad Prism 10 using the log(drug) vs. response model.

2.4.4 Seahorse assay

A seahorse assay was performed as previously described (Hayward et al., 2022). T7S4-ZFT parasites were incubated in the presence or absence of ATc for either 24 h or 48 h. A day before the experiment, distilled water was added to each well of a fresh assay plate before replacing the sensor lid. The plate was left at 37 °C with atmospheric CO_2. The Seahorse culture plate was treated with poly-L-lysine by incubating for 30 minutes at RT before being washed with sterile autoclaved water and stored in the fridge to dry overnight at 4 °C. 15 mL of Seahorse XF medium was prepared by supplementing the base medium with 5 mM glucose (75 µL) and 1 mM glutamine (15 µL), and left to prewarm at 37 °C. Next, the required drugs were prepared in the supplemented Seahorse medium. 1 µM carbonyl cyanide-4-(trifluoromethoxy) phenylhydrazone FCCP (Sigma-Aldrich, C2920) was prepared by adding 0.8 µL of a 50 mM stock to 5 mL supplemented medium. 1 µM atovaquone (ATQ) (ThermoFisher Scientific, 17565545) was prepared by adding 0.9 µL of a 1 mM stock to 1 mL supplemented medium. Cells were washed once with 1x PBS to remove any extracellular parasites. Intracellular parasites were then scraped and syringed to mechanically release them, before being filtered to remove any host cell debris. Parasites were then resuspended in prewarmed 37 °C Seahorse XF media (Agilent) supplemented with 5 mM glucose and 1 mM glutamine and pelleted by centrifugation. During this harvesting spin, the water in the assay plate was replaced with the calibration solution. 25 µL of drugs were added into each port of the plate, with FCCP going into port A and ATQ going into port B. The assay plate with the filled ports and calibration solution was then placed into the Seahorse machine and left to calibrate. After spinning, media was gently removed and pelleted parasites were resuspended in 1 mL supplemented media to wash. 10 µL of this was taken for counting. 175 µL was then added to each well of a poly-L-lysine treated seahorse XFp cell culture miniplate (Agilent), with each well having 1.5 x 10^6 parasites total. The parasites were then gently centrifuged at 300 x g for 5 minutes. The basal oxygen consumption rate (OCR) and the extracellular acidification rate (ECAR) was quantified using the Seahorse

XF HS Mini Analyser (Agilent Technologies). The non-mitochondrial OCR was determined after the addition of 1 µM atovaquone and subtracted as background. Basal mitochondrial OCR values were calculated by subtracting this background from raw OCR readings obtained before the addition of 1 µM FCCP. Maximal mitochondrial OCR values were calculated by subtracting this background from raw OCR readings obtained after the addition of 1 µM FCCP, and basal ECAR values were reported as raw values.

2.4.5 Flow cytometry

RAW 264.7 murine macrophages were seeded 1:4 onto 6 cm dishes and counted. After 3-4 hours, macrophages were then infected with ΔKu80:tdTomato parasites at an MOI of 1 for 24 h. Uninfected cells were used as a control. RAW macrophages were also left uninfected but stimulated with IFN-γ (20 ng/mL) and LPS (1 µg/mL) for 24 h to assess whether the responses observed are *Toxoplasma gondii* specific or a general pathogen response. The next day, cells were washes once with 1x PBS and starved using serum free media (DMEM media supplemented with L-glutamine and Pen/Strep without FBS) for 30 minutes at 37 °C with 5 % CO_2. Cells were then kept on ice for 10 minutes before adding transferrin from human serum, Alexa Fluor® 488 conjugate (T13342, Life technologies) 1:1000 on ice for a further 5 minutes. Cells were gently scraped to detach from the surface and centrifuged at 500 x g for 5 minutes at 4 °C and then resuspended in 2 mL of FACS buffer (see Table 2-8) before being analysed on the BD FACSCelesta™ Cell Analyzer.

2.4.6 Luciferase assay

A nanoLuciferase assay was performed on parasites infecting both HFFs and RAW 264.7 murine macrophages. Macrophages were seeded 1:10 onto 6 cm dishes and counted, either untreated D10 media or in the presence of 100 µM DFO. Media was replaced on HFFs with either untreated D3 media or in the presence of 100 µM DFO. 24 h later, HFFs were infected with either F3ΔHX, nanoLuc$_{zft}$ or nanoLuc$_{dhfr}$ as a control, at a density of 7 x 10^6 cells per dish for 24 h. RAW macrophages were infected with the same parasite lines at an MOI of 3. 0.5 µM of CISMBI, a DMT1 specific inhibitor, was added to half of the untreated HFFs and macrophages for 24 h along with infection. After 24 h, cells were washed once with 1x PBS and parasites were mechanically released and filtered. Uninfected HFFs and

macrophages in DFO and CISMBI conditions were used as a negative control. Parasites were then harvested by centrifugation at 1500 x g for 15 minutes before the supernatant being gently removed and the pellet resuspended in 150 µL media. For each line and condition, 50 µL of parasites were added into each of three wells in a white-bottom 96-well plate. Uninfected HFFs and macrophages were prepared in the same way and used as background fluorescence and luminescence. Parasite fluorescence was measured using the PHERAstar FS microplate reader (BMG LabTech). Following fluorescence measurement, the nanoLuciferase assay was performed following the manufacturer's protocol using the Nano-Glo® Luciferase Assay System (Promega). To do so, the Nano-Glo® Luciferase Assay substrate was diluted 1:50 in the Nano-Glo® Luciferase Assay buffer, before adding 50 µL in each well and mixing well. This was left to incubate for at least five minutes before luminescence was measured in lumens using the PHERAstar FS microplate reader (BMG LabTech). Initially, the average fluorescence of each sample from each technical replicate/well was subtracted from the fluorescence values of respective uninfected HFFs or macrophages in the appropriate conditions to give a corrected fluorescence. The same method was used to obtain a corrected luminescence for each sample. The normalised luminescence was then calculated by dividing the corrected luminescence by the corrected fluorescence for each sample and then plotted relative to untreated infected conditions.

2.5 Protein biology

2.5.1 Sodium dodecyl sulphate polyacrylamide gel electrophoresis (SDS-PAGE)

Parasites were mechanically released, filtered, and harvested by centrifugation at 1500 x g for 10 minutes, and lysed with RIPA lysis buffer (see Table 2-10) on ice for 30 minutes. Samples were then resuspended with 5x Laemmli buffer (see Table 2-10) and boiled at 95 °C for 5 minutes (unless stated otherwise). Proteins were separated on a 10 % SDS-PAGE gel (see Table 2-10), initially at 120 V for 20 minutes then 175 V for 60 minutes. PageRuler Prestained Protein Ladder (ThermoFisher Scientific, 26619) was used as a molecular weight marker. Proteins were then wet transferred to nitrocellulose membrane in Towbin buffer (see Table 2-10) for 60-120 minutes at 250 mA. The membrane was then stained with Ponceau S staining solution for 20 minutes at RT to visualise the presence of proteins and validate successful transfer. The membrane was then blocked for at least 1 h at room temperature in blocking buffer (5 % milk in 0.1 % Tween/PBS). Blots were stained with primary antibodies overnight at 4°C followed by secondary fluorescent antibodies at room temperature for 1 h. ZFT, ABCE1, SDHB, CPN60, and lipoic acid were all detected using Pierce ECL Western Blotting Substrate and imaged using the Invitrogen iBright 1500 Imaging System. All other antibodies were detected using the LI-COR Odyssey LCX system.

RAW 264.7 murine macrophages were seeded 1:4 onto 6 cm dishes and counted. After 3-4 hours, macrophages were then infected with RHΔKu80 parasites, unless stated otherwise, at an MOI of 2 for either 24 h or 48 h. Cells were then gently scraped and collected by centrifugation at 1500 x g for 10 minutes and processed for western blotting as described.

2.5.2 Protein stability assay

Briefly, HFFs were either untreated or pretreated 100 µM DFO for 24 h before infection with ZFT-3HA$_{zft}$ for a further 24 h. Parasites were then incubated with 100 µM cycloheximide (CHX) (Sigma Aldrich, 01810) for 1, 3, 5 and 7 h before being harvested and processed for immunoblotting and detection as previously described (2.5.1).

2.5.3 Blue-native polyacrylamide gel electrophoresis (BN-PAGE)

Firstly, the following solutions were prepared and stored in the cold room at 4 °C:

	20x Cathode Buffer (BN2002)	20x Running Buffer (BN2001)	Water (up to 200 mL)
Anode/Running buffer	0	10	190
Light cathode buffer	1	10	189
Dark cathode buffer	10	10	180

Table 2-22 – Components of BN-Page anode and cathode solutions.

For Blue native (BN) PAGE, 1 x 10^7 parasites were mechanically released, filtered, and harvested by centrifugation at 1500 x g for 10 minutes. The parasite pellet was then resuspended in 5 µL BN lysis buffer (see Table 2-10) and incubated on ice for 30 minutes before being centrifuged at 4 °C for 30 minutes at 18,000 x g. The 5 µL supernatant containing the solubilised membrane proteins was then transferred to a new tube and added to 15 µL of blue solution (loading buffer containing 1 µL 5 % Coomassie G-250 Coomassie sample additive, 59 µL Native PAGE 4x sample buffer) with the final concentration being 0.0625 % Coomassie G250 and 0.25 % DDM. The gel tank was then filled with cold dark cathode buffer (inside) and anode buffer/running buffer (outside). To visualise the lanes more clearly, some of the dark blue buffer was taken out from the inside of the chamber until the samples were loaded. This was then added back when ready to run. Before loading the samples, every well was cleaned by briefly pipetting up and down the dark blue buffer (to ensure even distribution of the sample in the wells). 1 x 10^7 parasites in a total volume of 15-20 µL were loaded onto a 3-12 % Native PAGE Bis-Tris gel (ThermoFisher Scientific, NP0301PK2) at 80 V, 10 mA for 1 hour. NativeMark™ was used as the molecular marker. The dark cathode solution was removed and replaced with the light cathode solution. The samples were then run for a further 2 hours at 250 V, 6 mA until the dye front was at the bottom. Proteins were then transferred onto a PVDF membrane (0.45 µM, Cytiva, 10600023) via wet transfer in Towbin buffer (see Table 2-10) at 100 V for 60-120 minutes. Immunoblotting and chemiluminescence detection were performed as above in section 2.5.1.

2.5.4 Complex IV in gel oxidation assay

Intracellular *T. gondii* tachyzoites were scraped, syringed, and filtered through a 3 µM to remove any large host cell debris, and counted using a haemocytometer. Parasites were centrifuged at 1500 x g for 10 minutes at 4 °C. The supernatant was removed gently without disrupting the pellet, and parasites were washed once with 1x PBS to remove any residual media before being transferred to a new 1.5 mL Eppendorf tube and centrifuged at 12,000 x g for 1 minute at 4 °C to pellet the parasites. PBS was gently removed, and the pellets were then resuspended in BN-PAGE lysis buffer (see Table 2-10) to a final concentration of 2.5 x 10^5 parasites/µL. Samples were then kept on ice for 30 minutes, occasionally mixing to allow for cell lysis and solubilisation. Samples were then spun at 20,000 x g for 30 minutes at 4 °C to pellet any unsolubilised cell debris. The supernatant was transferred to a fresh labelled 1.5 mL Eppendorf tube. Samples were stored at -80 °C until the assay was ready to run.

Samples were thawed on ice and kept on ice for the entire duration of the experiment. 15 µL of sample per well was aliquoted, and then ¼ of G250 additive (5 % stock) as the detergent % in the sample was added. For example, 1.5 µL of G250 additive stock was added to 30 µL of protein sample. The anode/running buffer, dark and light cathode buffers were prepared as described in Table 2-22 and kept at 4 °C to chill. Samples were run on a 4-16 % BN-PAGE gel (Novex-Life technologies) in the cold room at 4 °C with the dark cathode buffer in the centre of the rank at 150 V for 60 minutes. The dark cathode buffer was then replaced with the light cathode buffer and run for a further 90 minutes at 250 V until the dye has reached the bottom of the gel. To perform the in gel enzyme stain, the oxidation buffer was prepared as previously described in Table 2-10. 1 mg/mL cytochrome *c* and 0.1 % (w/v) 3'3-diaminobenzidine tetrahydrochloride (DAB) were added to the oxidation buffer. The gel was then gently removed from the plastic cassette and incubated in the staining solution overnight at room temperature for complex IV to be visualised.

2.6 Microscopy

2.6.1 Light microscopy

Fluorescent images were obtained using an inverted DiM8 microscope (Leica Microsystems) by acquiring stacks of ~20 with 0.15 µm increments between each stack. Images were acquired using the LAS X Core software. Super resolution structured illumination microscopy (SR-SIM) was performed on an ELYRA 7 with Lattice SIM^2 microscope (Zeiss) using the ZEN Blue software. Confocal microscopy was used to image infected and uninfected RAW 264.7 murine macrophages using the Nikon A1-R inverted microscope. Images were processed using NIS-Elements software. All images were processed using FIJI software (Schindelin et al., 2012).

2.6.2 Transmission electron microscopy (TEM)

HFF monolayers were infected with T7S4-ZFT parasites with or without ATc as indicated and processed and imaged by TEM by Dr. Leandro Lemgruber Soares at the University of Glasgow. Infected cells were fixed in a solution containing 2.5 % glutaraldehyde and 4 % paraformaldehyde prepared in 0.1 M cacodylate buffer. After several washes in 0.1 M cacodylate buffer, the samples were post-fixed in 1 % osmium tetroxide (OsO_4) and 1.25 % potassium ferrocyanide ($K_4[Fe(CN)_6]$) for 1 hour in the dark. En bloc staining was then performed using 0.5 % aqueous uranyl acetate at room temperature for 1 hour in the dark. The specimens were dehydrated through a graded acetone series and embedded in epoxy resin. Ultrathin sections (60 nm) were cut using a Leica Ultramicrotome UC6 and examined with a Jeol 1200EX transmission electron microscope (Jeol, Japan).

2.6.3 Live cell microscopy

To assess the amount of parasite associated metal following ZFT knockdown, live cell microscopy was performed using both iron and zinc live cell indicators.

2.6.3.1 Ferro-orange dye

To assess iron levels in the parasites, FerroOrange (Dojindo, F374-10) was used. To validate the indicator, parental parasites were treated with 200 µM FAC for 48 h. T7S4-ZFT parasites were either left untreated or treated with ATc for 48 h.

Following treatment, intracellular parasites from a 6 cm dish were mechanically released, and 2 mL were harvested by centrifugation at 1500 x g 10 minutes and resuspended in 1 mL DMEM containing 1 µM FerroOrange (Dojindo, F374-10) and 10 µM Hoechst 33342 (ThermoFisher Scientific, H3570). The entire suspension was then transferred onto poly-L-lysine–coated live-cell dishes (Cellvis, D29-20-1.5-N) and incubated at 37 °C for 10 min prior to imaging. Images were acquired, processed and analysed with FIJI as described in sections 2.6.1 and 2.4.1.4.

2.6.3.2 FluoZin™-3AM

To assess the levels of zinc in the parasites, FluoZin™-3AM (ThermoFisher Scientific, F14201), a Zn^{2+} selective indicator, was used. To validate the indicator, parental parasites were treated with 50 µM $ZnSO_4$ for 24 h. T7S4-ZFT parasites were either untreated or treated with ATc for 48 h. Following treatment, intracellular parasites from a 6 cm dish were mechanically released, and 2 mL were harvested by centrifugation at 1500 x g 10 minutes and resuspended in 1 mL DMEM supplemented with 2 µM FluoZin™-3AM (ThermoFisher Scientific, F14201) and 10 µM Hoechst 33342 (ThermoFisher Scientific, H3570). The entire suspension was then transferred onto poly-L-lysine–coated live-cell dishes (Cellvis, D29-20-1.5-N) and incubated at 37 °C for 10 min prior to imaging. Images were acquired, processed, and analysed with FIJI as described in sections 2.6.1 and 2.4.1.4.

2.7 Elemental analysis techniques

2.7.1 Inductively coupled plasma mass spectrometry (ICP-MS)

Total parasite associated iron, zinc and copper were quantified using ICP-MS. The day before the collection and sample processing, metal free 15 mL falcon tubes were washed with 3 mL 65 % nitric acid then washed with distilled water before drying overnight. Confluent HFFs cells in T150 flasks were infected with T7S4-ZFT parasites for 24 h before the addition of ATc for a further 24 h or infected with T7S4-ZFT parasites and ATc simultaneously for 48 h to ensure efficient knockdown. Untreated (-ATc) parasites were used as a control. 5-6 x T150s were infected for each condition. Uninfected HFFs were used as a blank control. Cells were washed once with 1x PBS to discard any extracellular parasites. Intracellular parasites were then mechanically released and filtered either through 0.3 µM filters or PD-10 columns (Cytiva, 17085101). Parasites were harvested by centrifugation at 2000 x g for 10 minutes. Supernatant was gently removed, and parasite pellets were resuspended in 10 mL of 1x PBS treated with 6 % Chelex 100 sodium form (Merck, C7901) to wash, combining the five flasks for each condition together. Parasites were then counted using a haemocytometer. 1 x 10^9 parasites for each condition is ideal. Parasites were then washed a further two times with chelexed PBS, once with 10 mL 1 mM EDTA and then resuspended in 5 mL chelexed PBS before being transferred to a 15 mL falcon tube. 500 µL was taken for Bradford assay analysis and centrifuged at 7000 rpm for 10 minutes in a tabletop centrifuge before removing the supernatant and resuspending in 500 µL distilled water for protein quantification via Bradford. The remaining 4.5 mL of parasites was centrifuged at 2000 x g for 10 minutes and supernatant was gently removed. Each parasite sample was then digested by resuspending the pellets in 687 µL distilled water, transferring to a 2 mL Eppendorf tube, and adding 1.3 mL of 65 % nitric acid (vwr chemicals, 83872.270) and 13 µL 10 % Triton X-100 stock in water. Samples were boiled at 85 °C for 5 hours. 500 µL of each sample was then taken and added to three metal free tubes, each with 4.5 mL of 2 % nitric acid and 12 µL 10 % Triton X-100 (final concentration 0.025 %). A blank sample containing 500 µL of water instead of parasite samples was used as a control. Samples were stored at -20 °C before all biological replicates were ready to be sent. Samples were quantified at the Scottish Universities Environmental Research Centre (SUERC) and processed by Dr Valerie Olive.

Samples were analysed using an Agilent 7500ce ICP-MS, equipped with a double-pass spray chamber and a self-aspiring nebulizer, optimised for a flow rate of 0.1 mL/min. A 3 ppb indium standard (^{115}In) was used as an internal standard to correct for sensitivity loss due to the sample matrix. Copper and zinc were measured at masses 63 and 66, respectively, with results reported as the mean of 10 replicates. Calibration curves were generated from three concentrations (5, 10, and 20 ppb) using Cu and Zn mono-element Specpure® solutions. Iron was measured at mass 56 using a collision cell with a hydrogen flow of 4 mL/min to suppress interference from $^{40}Ar^{16}O$. Calibration for Fe was performed using 200 ppb and 300 ppb mono-element Specpure® solutions, and results represent the mean of 20 repeats.

2.7.2 X-ray fluorescence microscopy (XFM)

T7S4-ZFT parasites were cultured in the absence or presence of ATc for 24 h or 48 h. Following host cell lysis, parasites were harvested by filtration, pelleted by centrifugation, and resuspended in 5 mL of extracellular buffer A solution (see Table 2-8). Approximately 500 µL of resuspended parasites were then transferred onto 2 x 2 mm poly-l-lysine nitride (SiN) windows (Norcada, X5200D). Samples were then gently centrifuged at 200 x g for 2 minutes and then incubated at room temperature for 20 minutes. Following adhesion or infection, cells were washed twice with 1x chelexed PBS before being fixed in 4 % PFA prepared in 1x chelexed PBS at room temperature for 20 minutes. Samples were then initially washed twice in 1x chelexed PBS, before being washed twice in 100 mM ammonium acetate and finally twice in MiliQ H_2O and then left to dry overnight. Elemental mapping was carried out at the European Synchrotron Radiation Facility in Grenoble, France at beamline ID21 under proposal number LS-3419. The data is available at https://doi.esrf.fr/10.15151/ESRF-DC-2119497225. Data analysis was conducted using PyMca5.9.2 (Solé et al., 2007) and FIJI (Schindelin et al., 2012). The 48 h time point represents two independent biological experiments, while the 24 h time point represents one independent biological experiment. We thank Dr. Hiram Castillo Michel for all the support and assistance during data collection and analysis.

2.8 Yeast

2.8.1 Generation of codon optimised sequences and cloning into yeast expression vector pDR195

The full length native coding sequence of ZFT (TGME49_261720) was obtained from ToxoDB and codon-optimised using the Integrated DNA Technologies (IDT) Codon Optimisation Tool (https://eu.idtdna.com/CodonOpt) to enhance heterologous expression in *Saccharomyces cerevisiae*. The codon-optimised gene was synthesised as a double-stranded DNA fragment (gBlock® Gene Fragment, IDT). The codon optimised sequence of full length ZFT was then amplified by PCR as described in section 2.3.1 using P24 and P25, cloned into the yeast expression vector pDR195 (AddGene, #36028) and transformed into *Escherichia coli* DH5α for plasmid amplification. Correct insertion of full length ZFT into the yeast expression vector pDR195 was confirmed by colony PCR and sequencing.

2.8.2 Yeast transformations and selection

Δzrt1/2, *Δfet3/4* and *Δsmf1* (Ullah et al., 2018) strains, a kind gift from Jim Dunwell (University of Reading), were transformed as previously described (Gietz and Schiestl, 2007). Briefly, 5 mL of YPD media was inoculated with the yeast strain to transform and shaken overnight at 30 °C. The next day, the OD_{600} of the overnight culture was measured and inoculated to a final OD_{600} of 0.2. 10 mL of YPD was used for each transformation. Cells were harvested by centrifuging at 3000 rpm for 5 minutes at room temperature. Supernatant was then gently removed, and cells were washed by resuspending the pellet in half the volume of sterile distilled water. Cells were centrifuged again at 3000 rpm for 5 minutes at RT. The supernatant was then gently removed, and pellets were resuspended in 1 mL of 100 mM lithium acetate (LiAc) for each transformation and aliquoted into 1 mL Eppendorf tubes. Samples were then centrifuged at maximum speed for 30 seconds – 1 minute in a tabletop centrifuge. The transformation mix (detailed in Table 2-23) was then added to the pellet and pipetted up and down and vortexed vigorously until the cells were completely resuspended in the transformation mix:

Component	Volume per transformation
50 % $PEG_{3000-5000}$	240 µL
1 M LiAc	36 µL
ssDNA/Herring Sperm DNA (2 mg/µL) (Promega, D181A)	25 µL
DNA (~500 ng plasmid DNA) + sterile distilled water	50 µL

Table 2-23- A list of yeast transformation mix components used in this study.

The yeast were incubated at 30 °C for 30 minutes in a water bath, before being heat shocked at 42 °C for 20 minutes. Cells then recovered for a further 30 minutes at 30 °C in a water bath. Cells were centrifuged at 8000 rpm for 1 minute, and the supernatant was gently removed without disrupting the pellet. Finally, the pellet was resuspended in 200 µL sterile distilled water and gently spread onto synthetic dropout agar lacking uracil (SD-Ura) to select for positive transformations. Plates were incubated at 30 °C for 2-3 days.

2.8.3 Drop test assay

Colonies were grown overnight in SD-Ura media at 30 °C shaker. The OD_{600} of the overnight cultures were measured and then diluted 1:5 four times in SD-Ura media to final concentrations of 0.2, 0.04, 0,008 and 0.0016 OD_{600}. 7 µL of each dilution was gently spotted onto SD-Ura agar, or SD-Ura agar supplemented with 5 mM EGTA plates and allowed to dry for 2-3 hours at RT. Plates were incubated at 30 °C for 4 days, and pictures were taken using a smart phone.

2.9 Statistical analysis

All data was initially entered into Microsoft Excel to calculate simple analysis such as averages, means, and percentages. The data was then transferred to GraphPad Prism® V10 to be processed further. Statistical analysis was also all performed in GraphPad Prism® V10. For analysis of group comparisons, either unpaired or paired t-tests were performed to calculate the *p* values. For multiple comparisons, either one-way or two-way ANOVA tests were performed to determine the *p* value accompanied with Tukey's multiple test. Each statistical analysis test performed for each experiment is described in the respective figure legend.

Chapter 3 ZFT is the major iron and zinc transporter in *T. gondii*

3.1 Introduction and chapter aims

Although both iron and zinc are essential for *Toxoplasma gondii*, how the parasite acquires these transition metals from the environment was unknown and not yet established at the beginning of my PhD studies. Many organisms use ZIP (Zrt/Irt-like)-domain containing proteins, a highly conserved family of metal transporters (Guerinot, 2000) to acquire metals. *T. gondii* encodes four genes encoding ZIP-domain containing proteins. During my PhD, my main aim was to characterise one of these ZIP-domain containing proteins TGME49_261720 and assess its role as a functional iron and zinc transporter in *T. gondii*. In this chapter, I characterise TGME49_261720, named **Z**n and **F**e **T**ransporter (ZFT), in detail. To do so, I utilised genetic manipulation strategies such as CRISPR-Cas9, molecular and protein biology techniques, microscopy as well as elemental analysis techniques including ICP-MS and XFM.

3.2 Iron transport in *Toxoplasma gondii*

To initially start to understand how *T. gondii* acquires iron from its environment, four genes encoding predicted ZIP-domain containing proteins were identified from the *Toxoplasma* genome on ToxoDB/VEuPathDB (Amos et al., 2022) (Table 3-1). Out of the four predicted genes, the ZIP domain of TGME49_500163 was predicted to contain only three transmembrane domains instead of the typical 8-9 found in ZIP-domain containing transporters. Moreover, the ZIP-domain of TGME49_254080 was poorly conserved when compared to the other genes encoding ZIP domain containing proteins in *T. gondii* and only had 6 out of the typical 8-9 transmembrane domains. As a result, both genes were excluded from further analysis. The two remaining candidates in *T. gondii*, TGME49_261720 and TGME49_225530, encode ZIP-domain containing proteins with high predicted confidence (E value < $7x10^{-30}$), and are predicted to both have eight transmembrane domains. Both proteins share limited sequence similarity (21 % and 26 % respectively) with the *Plasmodium* ZIP-domain containing protein, PfZIPCO. This suggests they are not direct orthologs of the *Plasmodium* gene.

To assess functional conservation, a multiple sequence alignment was performed. Residues at the binuclear metal centres (BMC) M1 and M2 within transmembrane helices α4 and α5 were then examined, as these have previously been shown to be essential for metal binding in the bacterial ZIP homolog BbZIP (Wiuf et al., 2022). Several key residues which are required for transport activity, including E181 and E211 (Wiuf et al., 2022), were found to be conserved in the *Toxoplasma* ZIP-domain containing proteins (Figure 3.1a). Interestingly, TGME49_261720 carries a distinctive HGxxEG motif at the M1 binuclear metal centre. This motif is observed only in coccidian ZIPs and a few marine species such as *Branchiostoma floridae*, although its functional impact remains unclear (Figure 3.1a). In contrast, the second predicted ZIP domain containing protein TGME49_225530, which shares a 36 % protein sequence similarity to TGME49_261720, possessed a HAxxEG motif instead, also present in ZIP9-like prokaryotic proteins (Hu, 2021).

Interestingly, at the M2 binuclear metal centre, all apicomplexan ZIP-domain containing proteins analysed contained a conserved HK motif, including sequences from the digenic gregarine *Porospora* and *Cryptosporidium* (Figure 3.1a). However, in free-living alveolate such as *Chromera*, this HK motif is not

conserved. This motif is characteristic of the ZIPI family of ZIP proteins, and is also present in human ZIP proteins HsZIP1 and HsZIP2 (Dufner-Beattie et al., 2003a). The lysine at this site is thought to inhibit metal binding but has nonetheless been shown to be important in HsZIP2 for transport activity, potentially contributing to a role in the transporter's response to a change in pH (Gyimesi et al., 2019).

Structural prediction of TGME49_261720 as a dimer (consistent with other ZIP-domain containing proteins) was constructed by Dr. Lucas Pagura using ChimeraX. The predicted structure revealed that TGME49_261720 has eight transmembrane domains, as well as a large unstructured loop between helices 3 and 4. This unstructured extracellular loop is predicted to be on the outer lumen, however, its role, if functional, remains unknown. This extracellular loop does contain a His-rich region which has previously been shown to play a role in metal binding in HsZIP4 in mammalian cells (T. Zhang et al., 2019). Moreover, H314 and E318, known conserved metal binding residues, are located within the core of the predicted protein structure and sequence (Figure 3.1b).

Next, the structural prediction of TGME49_261720 was aligned with HsZIP1, the human ZIP-domain transporter which functions as a zinc importer (Gaither and Eide, 2001b). Although TGME49_261720 has the large, extracellular unstructured loop, good alignment was observed between TGME49_261720 and HsZIP1 (Figure 3.1c). Given the conserved motif of TGME49_261720, its predicted plasma membrane localisation and essentiality in tachyzoites, this gene was selected for functional characterisation for the duration of my PhD studies.

ID	Length (aa)	Predicted localisation (Barylyuk et al., 2020)	Phenotype score (Sidik et al., 2016)	TM domains	ZIP domain (E value)
TGME49_261720 (ZFT)	488	PM-integral	-4.31	8	5.9E-34
TGME49_225530	717	n/a	-2.94	8	7.2E-30
TGME49_254080	490	rhoptries 2	1.41	6	4.4E-16
TGME49_500163	1347	n/a	-1.4	3	5.9E-30

Table 3-1 - Table summarising known features including length, predicted localisation, phenotype score, TM domains, and ZIP domain E-values of the four predicted ZIP-domain containing proteins encoded by the *Toxoplasma* genome.

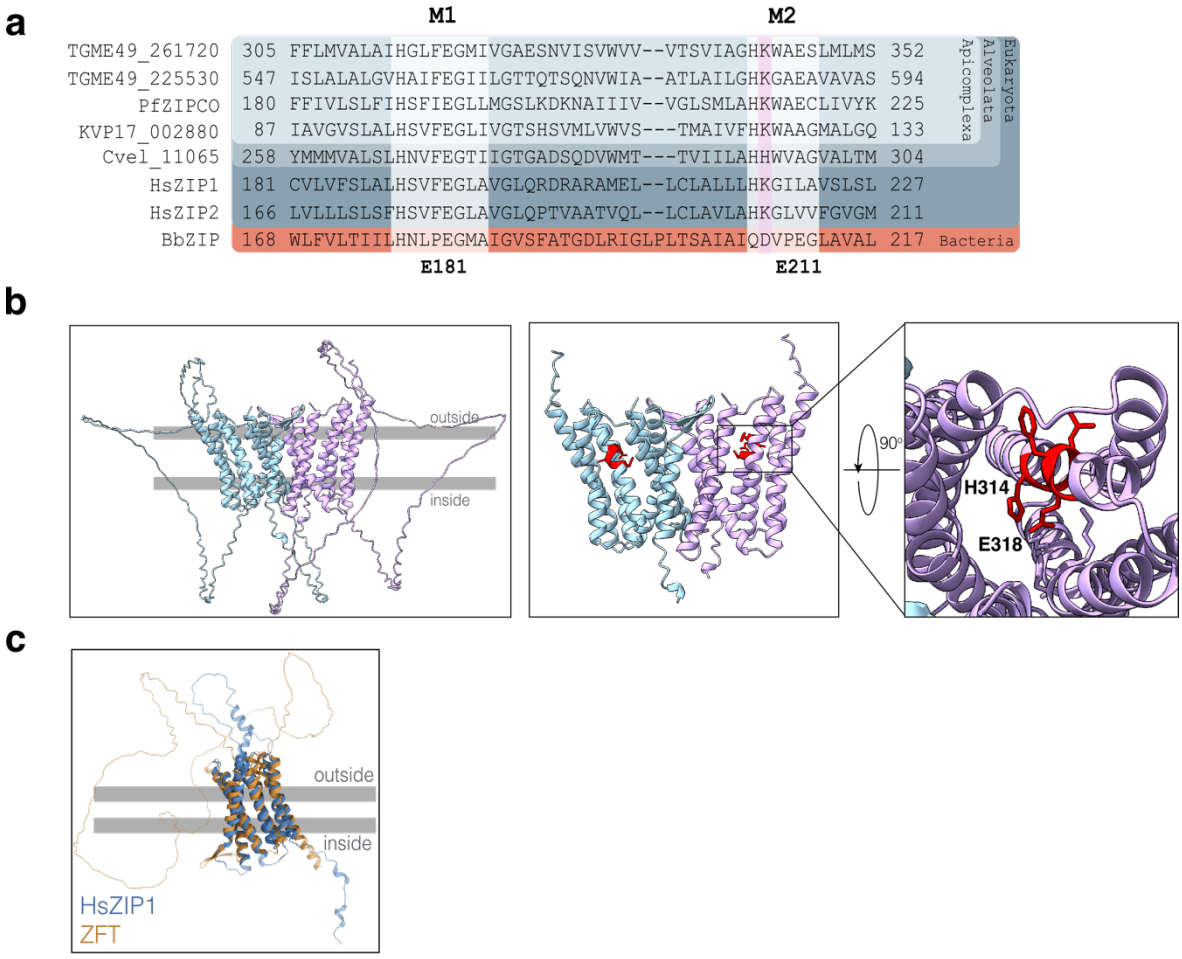


Figure 3.1 - TgZFT protein alignment and predicted protein structure.

a. Multiple sequence alignment of ZIP-domain containing proteins from *T. gondii* (TGME49_261720), *T. gondii* (TGME49_266800), *P. falciparum* (PF3D7_1022300), *Porospora cf. gigantea* (KVP17_002880), *Chromera vella* (Cvel_11065), *H. sapiens* HsZIP1 and HsZIP2 and *Bordetella bronchiseptica* (BbZIP). Key conserved residues E181 and E211 in the M1 and M2 BMCs respectively in transmembrane domains α4 and α5 which have been shown to be required for metal binding are highlighted. The KH motif found in HsZIP1 and HsZIP2 and Apicomplexa are also highlighted. **b.** Structural prediction of TGME49_261720 as a dimer, showing eight transmembrane domains, as well as a large unstructured loop between helices 3 and 4. The conserved metal binding residues H314 and E318, are located within the core of the predicted protein structure and sequence. **c.** Predicted protein structural alignment of the human ZIP transporter HsZIP1 (blue) with TGME49_261720 (ZFT) (orange).

3.3 ZFT localisation is dynamic and vacuolar stage dependent in F3ΔHX ZFT-3HA*sag1*

In *Plasmodium falciparum*, PfZIP1 localises to the parasite plasma membrane (Shrivastava et al., 2024). To investigate where ZFT localises in *T. gondii*, ZFT was tagged in F3ΔHX parasites by integrating a sequence coding for a 3xHA epitope tag at the C terminal under the endogenous promoter with the *sag1* 3' UTR (F3ΔHX ZFT-3HA*sag1*) as demonstrated in the schematic in Figure 3.2a. Successful integration was verified by PCR with an expected size of 572 bp (Figure 3.2b). Parental F3ΔHX parasites were used as a control. The ZFT-3H*sag1* line was further verified by western blotting, demonstrating that the tagged protein ran at the expected size of 50 kDa (Figure 3.2c). It is worth noting that multiple, non-specific lower bands (marked with asterisks) were observed, some of these were also seen in the untagged parental control. CDPK1 was used as a loading control.

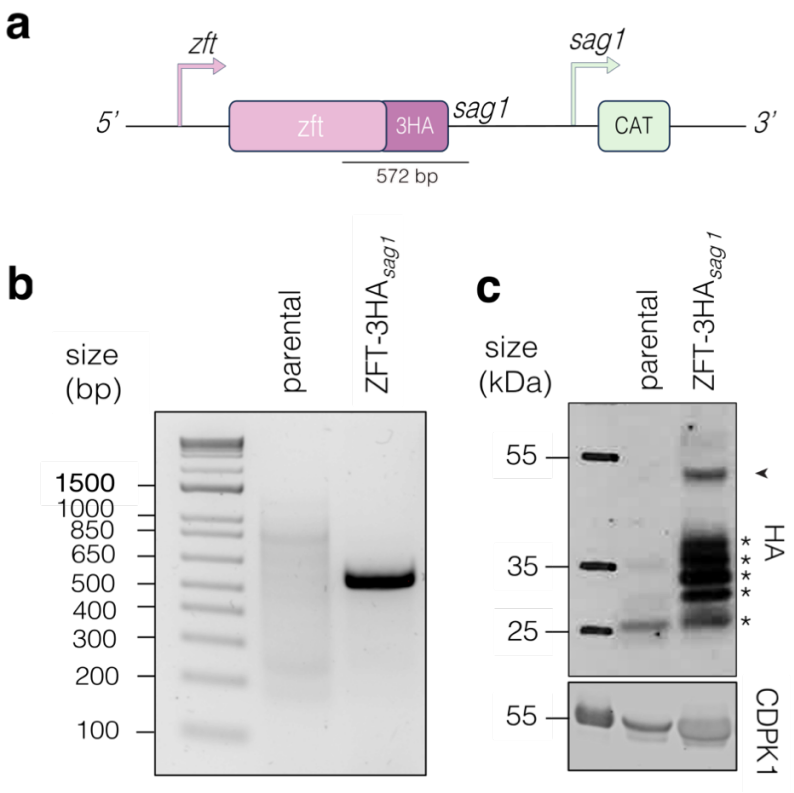


Figure 3.2 - F3ΔHX ZFT-3HA*sag1* strain construction and validation.

a. Schematic of F3ΔHX ZFT-3HA*sag1* strain construction to tag ZFT with a 3xHA epitope tag at the C terminal under the endogenous promoter at the *sag1* 3' UTR. **b.** PCR confirming successful integration, with an expected band size of 572 bp as indicated in (a). **c.** Western blotting of ZFT-3HA*sag1* confirming ZFT is successfully tagged and runs at the expected band size (50 kDa). Non-specific bands are marked with asterisks. CDPK1 was used as a loading control.

To assess the localisation of ZFT, an immunofluorescence assay (IFA) was performed by infecting HFFs with ZFT-3HA*sag1* parasites for 24 h before fixing and staining with an anti-HA antibody, and an anti-GAP45 antibody as a control to stain for GAP45, a component of the inner membrane complex of *T. gondii*. As predicted from the LOPIT (localization of organelle proteins by isotope tagging) data, ZFT localises to the periphery of the parasites. However interestingly, this localisation is dynamic and ZFT-3HA*sag1* is also seen at puncta the basal end of the parasite (Figure 3.3a). Further, this localisation is highly dependent on the number of parasites per vacuole. In early stages of replication (2-4 parasites/vacuole), ZFT localises mostly to the periphery of the parasites. However, in the larger vacuoles (8-8+ parasites/vacuole), ZFT localisation shifts and becomes more basal in the parasite (Figure 3.3b).

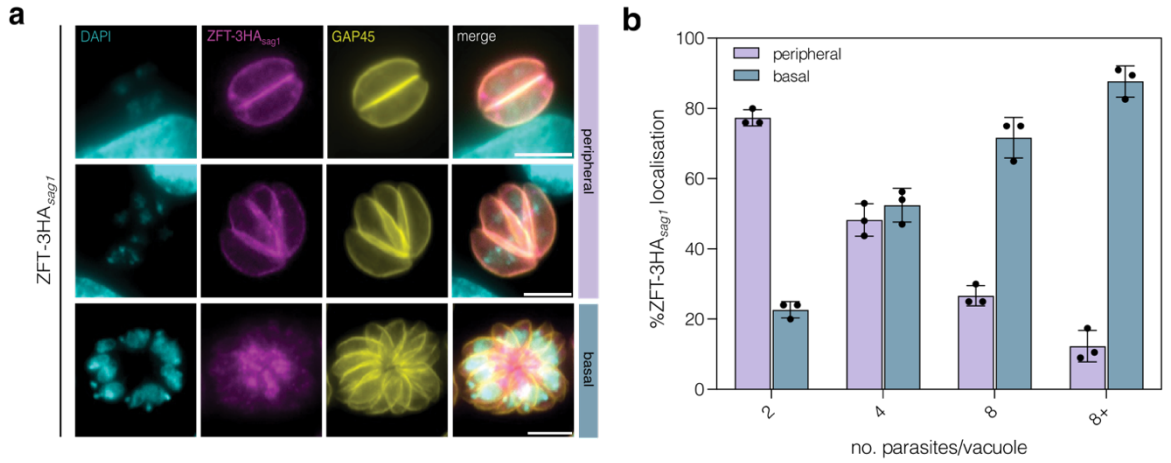


Figure 3.3 - ZFT localisation in the F3ΔHX ZFT-3HA*sag1* line is dynamic and dependent on vacuolar stage.

a. Immunofluorescence assay of F3ΔHX ZFT-3HA*sag1* demonstrating dynamic peripheral and basal localisation at 24 h. Scale bar 5 µm. **b.** Percentage of ZFT-3HA*sag1* localisation (peripheral or basal) in respect to the number of parasites/vacuole. 100 vacuoles were counted for each of three biological replicates. Bars represent the mean of three independent biological experiments ± SD. ZFT-3HA*sag1* localisation is more peripheral in vacuoles were fewer number of parasites and shifts to a more basal localisation the larger the vacuoles get.

To examine this change in localisation in more detail at a higher resolution, F3ΔHX ZFT-3HA*sag1* parasites were imaged 24 h post infection by super resolution microscopy using the ELYRA microscope. Figure 3.4 shows the dynamic localisation of ZFT-3HA*sag1* at a higher resolution.

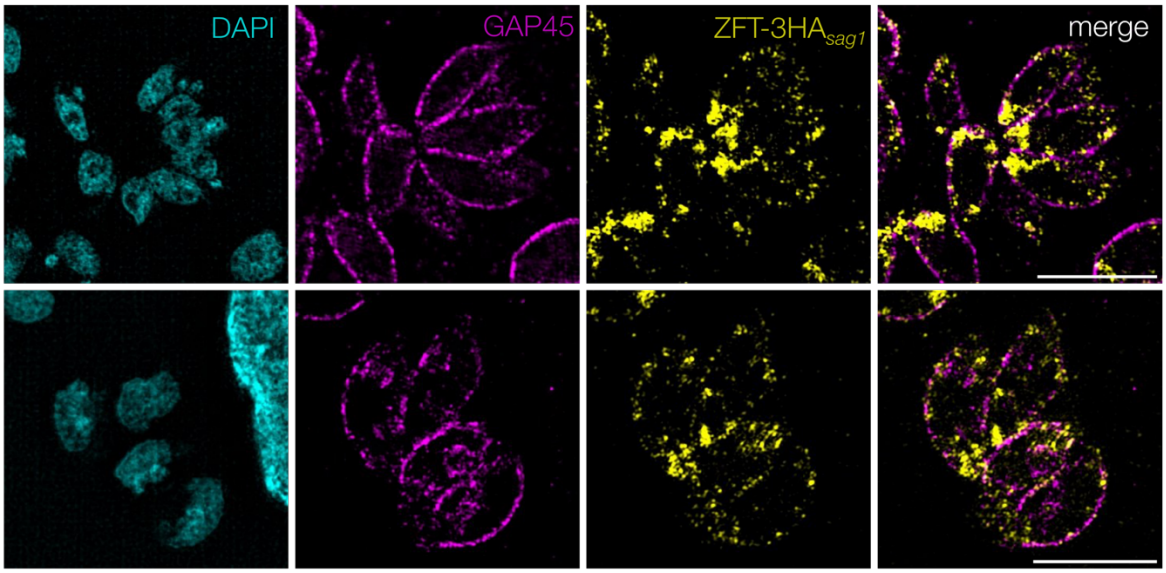


Figure 3.4 - ZFT-3HA*sag1* localisation is dynamic and dependent on vacuolar stage, localising basally in larger vacuoles.

Immunofluorescence assay of F3ΔHX ZFT-3HA*sag1* imaged by super resolution microscopy for a higher resolution. Results demonstrate dynamic peripheral and basal localisation at 24 h. Scale bar 5 µm.

3.4 ZFT expression is regulated by the availability of iron in F3ΔHX ZFT-3HA*sag1*

The localisation and expression of transporters is often regulated by the availability of the substrate (Conte and Walker, 2011; Gao and Dubos, 2021; Lee et al., 2020). Previously, I showed that the iron transporter VIT involved in iron storage and detoxication in *T. gondii* is also regulated by iron availability (Aghabi et al., 2023). To assess if ZFT expression in the F3ΔHX ZFT-3HA*sag1* parasites changes in low iron conditions, I chelated the iron from the host cells for 24 h before infection using the chelator deferoxamine (100 μM DFO) and then infected the cells with F3ΔHX ZFT-3HA*sag1* for either 18 h or 24 h before harvesting cells for western blot analysis. At 18 h post treatment, ZFT-3HA*sag1* levels were significantly reduced to around 36 % of the untreated (p = 0.0204, two-tailed paired t test) (Figure 3.5a, b). By 24 h post treatment, ZFT-3HA*sag1* expression was reduced further to around 27 % of the untreated (p = 0.0116, two-tailed paired t test) (Figure 3.5c, d). Loss of ZFT-3HA*sag1* expression under low iron conditions at 24 h was further confirmed by immunofluorescence by pre-treating host cells with DFO for 24 h before infecting with F3ΔHX ZFT-3HA*sag1* for 24 h and fixing and staining with anti-HA and anti-GAP45 antibodies (Figure 3.5e). These data demonstrate that ZFT-3HA*sag1* expression is significantly reduced under low iron.

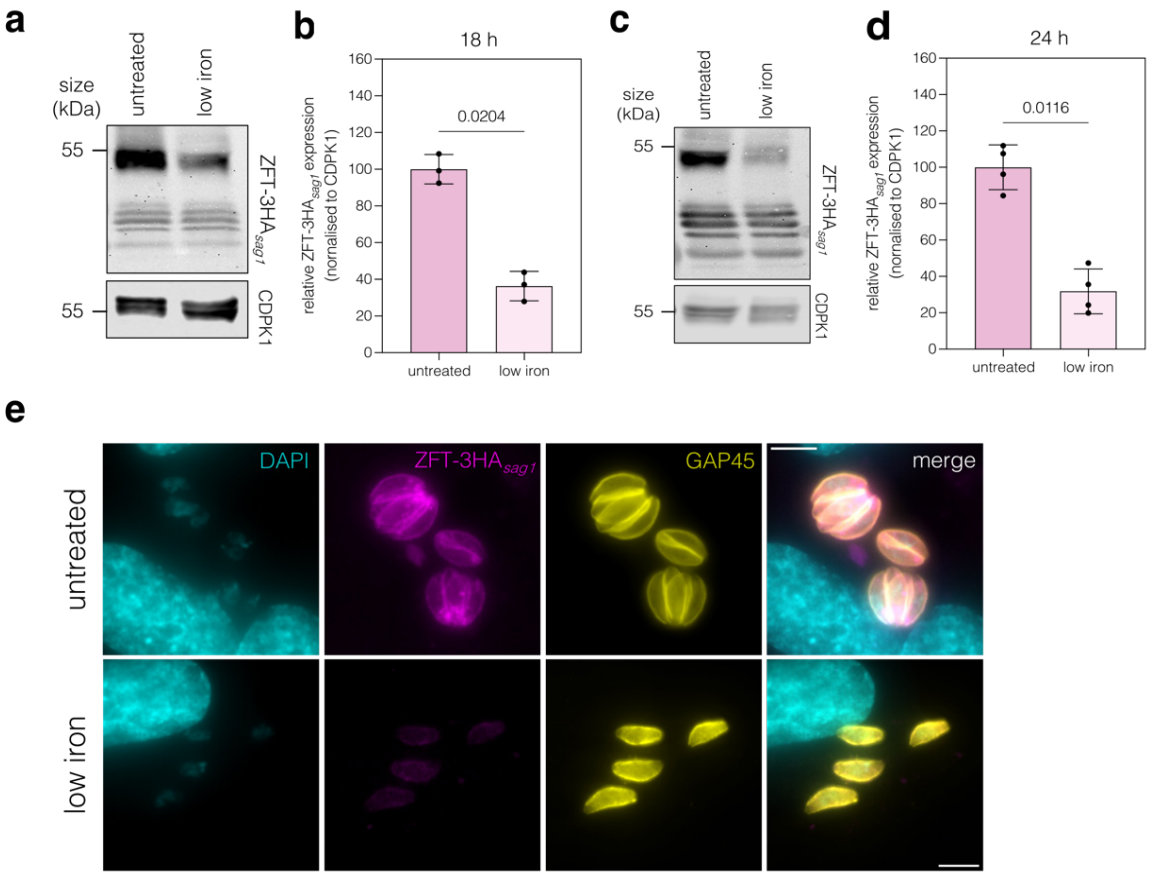


Figure 3.5 - F3ΔHX ZFT-3HA$_{sag1}$ expression is reduced under low iron conditions.

a. Western blot analysis of ZFT-3HA$_{sag1}$ expression in untreated and low iron conditions (100 µM DFO) at 18 h post infection. CDPK1 used as a loading control. **b.** Quantification of ZFT-3HA$_{sag1}$ levels at 18 h in untreated and low iron conditions from three independent biological experiments. Bars are at mean ± SD. *p* values from two-tailed paired t test. **c.** Western blot analysis of ZFT-3HA$_{sag1}$ expression in untreated and low iron conditions (100 µM DFO) at 24 h post infection. CDPK1 used as a loading control. **d.** Quantification of ZFT-3HA$_{sag1}$ levels at 24 h in untreated and low iron conditions from four independent biological experiments. Bars are at mean ± SD. *p* values from two-tailed paired t test. **e.** Immunofluorescence assay of ZFT-3HA$_{sag1}$ at 24 h post infection in untreated and low iron (100 µM DFO) conditions confirming that that ZFT-3HA$_{sag1}$ expression levels are reduced under low iron conditions. Scale bars 5 µm.

To assess if ZFT expression in the F3ΔHX ZFT-3HA$_{sag1}$ parasites changes in high iron conditions, I treated the host cells with exogenous iron for 24 h before infection using ferric ammonium chloride (FAC) (500 µM FAC) and then infected the cells with F3ΔHX ZFT-3HA$_{sag1}$ for either 18 h or 24 h before harvesting cells for western blot analysis. Interestingly, at both 18 h and 24 h post infection, ZFT-3HA$_{sag1}$ levels did not significantly change in high iron conditions compared to untreated conditions (Figure 3.6a, b, c, d). ZFT-3HA$_{sag1}$ expression under high iron conditions

at 24 h was further confirmed by immunofluorescence by pre-treating host cells with FAC for 24 h before infecting with F3ΔHX ZFT-3HA*sag1* for 24 h and fixing and staining with anti-HA and anti-GAP45 antibodies (Figure 3.6e). These data demonstrate that ZFT-3HA*sag1* expression does not significantly change under excess iron conditions.

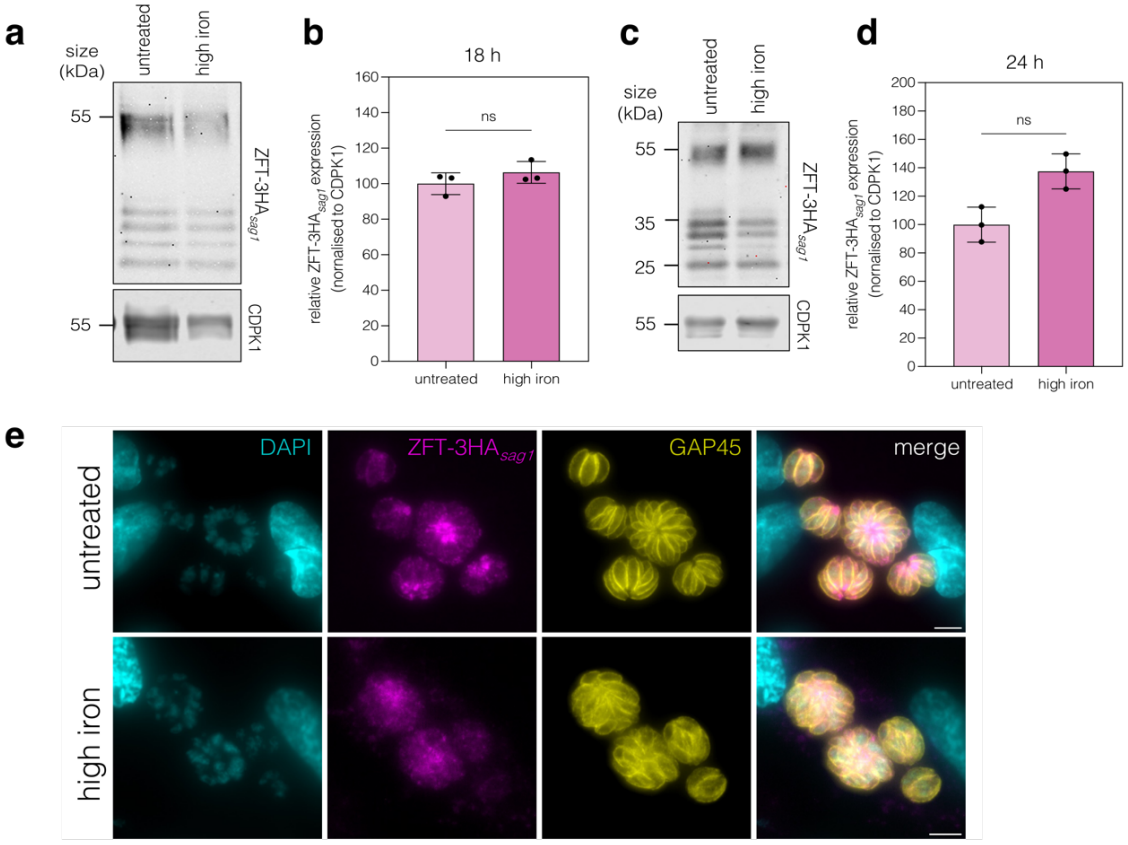


Figure 3.6 - F3ΔHX ZFT-3HA*sag1* expression does not change under high iron conditions.

a. Western blot analysis of ZFT-3HA*sag1* expression in untreated and high iron conditions (500 µM FAC) at 18 h post infection. CDPK1 used as a loading control. **b.** Quantification of ZFT-3HA*sag1* levels at 18 h in untreated and high iron conditions from three independent biological experiments. Bars are at mean ± SD. *p* values from two-tailed paired t test. **c.** Western blot analysis of ZFT-3HA*sag1* expression in untreated and high iron conditions (500 µM FAC) at 24 h post infection. CDPK1 used as a loading control. **d.** Quantification of ZFT-3HA*sag1* levels at 24 h in untreated and high iron conditions from three independent biological experiments. Bars are at mean ± SD. *p* values from two-tailed paired t test. **e.** Immunofluorescence assay of ZFT-3HA*sag1* at 24 h post infection in untreated and high iron (500 µM FAC) conditions confirming that that ZFT-3HA*sag1* expression levels are not changed under excess iron. Scale bars 5 µm.

3.5 ZFT localisation is dynamic and vacuolar stage dependent in F3ΔHX ZFT-3HA$_{zft}$

It has previously been shown that the 3' UTR of *zft* plays an important role in iron mediated regulation, particularly under low iron conditions (Sloan et al., 2025). To determine if changing the UTR affected ZFT localisation and expression in low and high iron conditions, I also tagged it with a 3xHA epitope tag at the C terminal under the endogenous promoter followed by the endogenous 3' UTR (F3ΔHX ZFT-3HA$_{zft}$) as demonstrated in the schematic in Figure 3.7a. Successful integration was verified by PCR with an expected size of 3600 bp (Figure 3.7b). Parental parasites were used as a control. The ZFT-3HA$_{zft}$ line was further verified by western blotting, demonstrating that the tagged protein ran at the expected size of 50 kDa (Figure 3.7c). The multiple, non-specific lower bands (marked with asterisks) were also observed. Parental parasites were used as a control, and CDPK1 was used as a loading control.

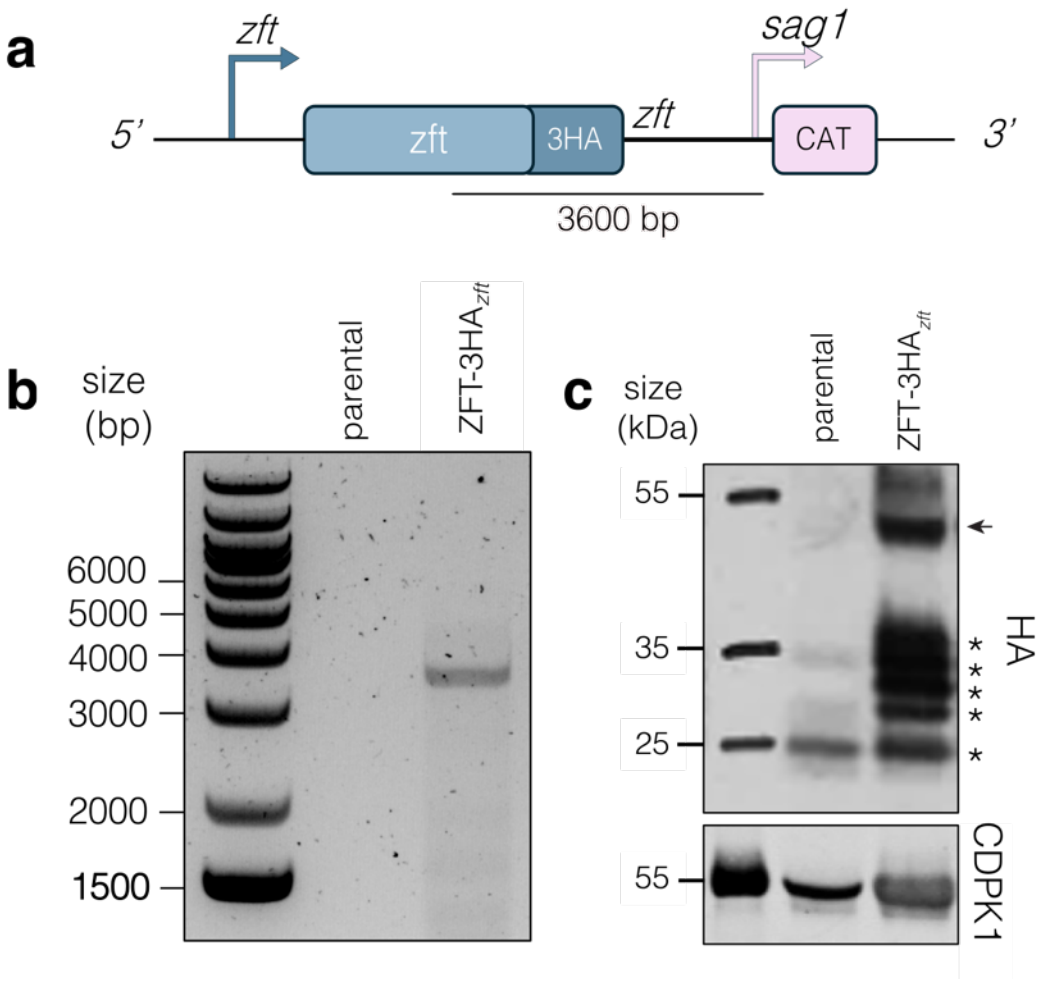


Figure 3.7 - F3ΔHX ZFT-3HA$_{zft}$ strain construction and validation.

a. Schematic of F3ΔHX ZFT-3HA$_{zft}$ strain construction to tag ZFT with a 3xHA epitope tag at the C terminal under the endogenous promoter at the endogenous 3' UTR. **b.** PCR confirming successful integration, with an expected band size of 3600 bp as indicated in (a). **c.** Western blotting of ZFT-3HA$_{zft}$ confirming ZFT is successfully tagged and runs at the expected band size (50 kDa). Non-specific bands are marked with asterisks. CDPK1 was used as a loading control.

To assess the localisation of ZFT in the endogenous 3' UTR tagged line, an IFA was performed by infecting HFFs with ZFT-3HA$_{zft}$ parasites for 24 h before fixing and staining with anti-HA and anti-GAP45 antibodies. Similar localisation was observed to ZFT-3HA$_{sag1}$ parasites where ZFT localises to the periphery of the parasites however is also seen at puncta at the basal end of the parasite (Figure 3.8a). Similarly to the ZFT-3HA$_{sag1}$ parasites, this localisation is dynamic and also highly dependent on the number of parasites per vacuole, where ZFT is localised more peripherally in vacuoles with fewer number of parasites and then shifts to a more basal localisation in vacuoles with 8 or more parasites (Figure 3.8b). To further expand on this observation, I quantified the amount of ZFT-3HA$_{zft}$ by quantifying the mean fluorescence intensity (MFI) of ZFT-3HA$_{zft}$ per parasite. I found that the MFI of ZFT/parasite is higher in vacuoles with fewer parasites compared to larger vacuoles of 8 or more parasites ($p < 0.001$, one-way ANOVA, Tukey corrected for multiple comparisons) (Figure 3.8c). This data suggests that ZFT is being degraded in a vacuolar stage-dependent manner.

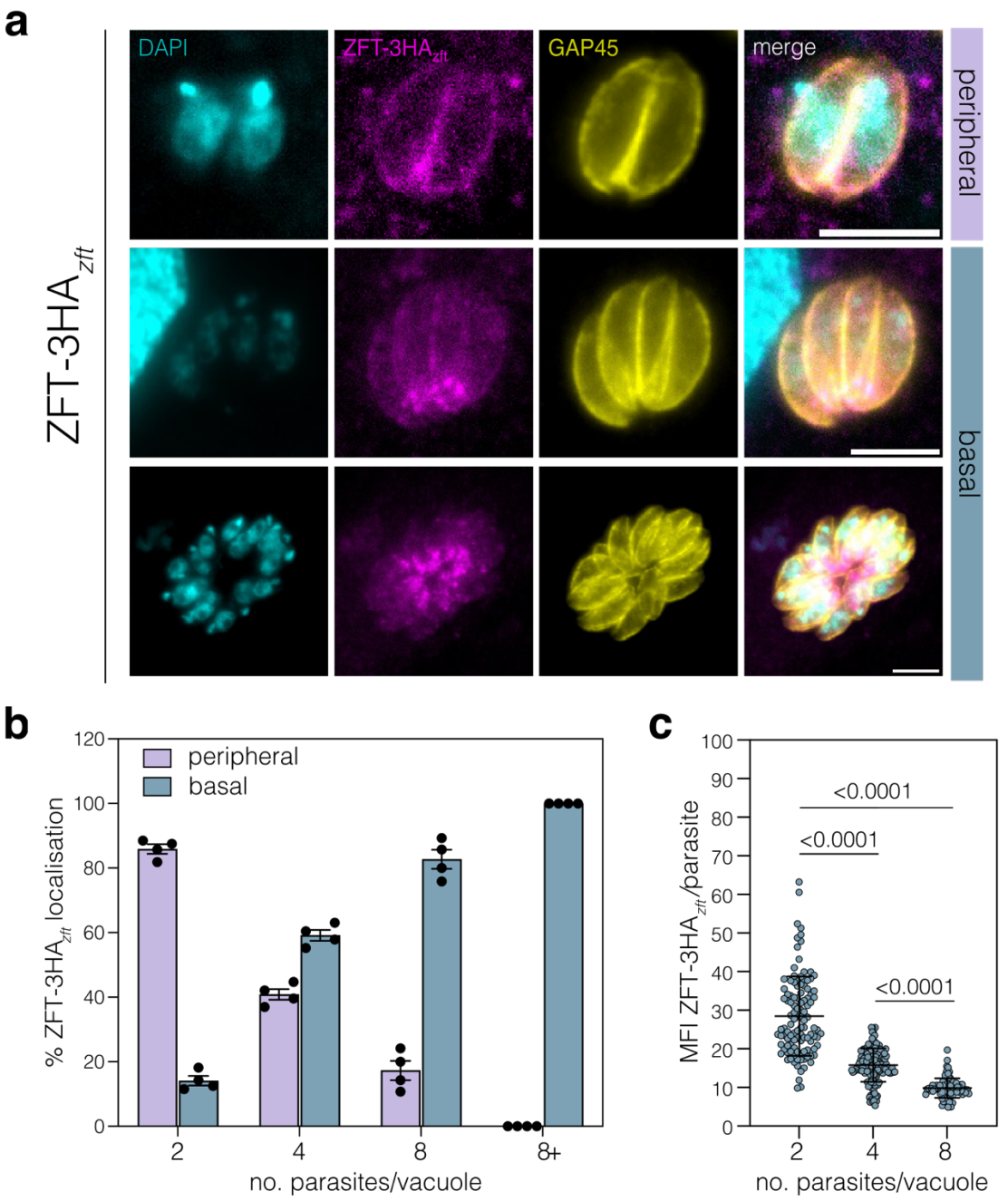


Figure 3.8 - ZFT localisation in the F3ΔHX ZFT-3HA$_{zft}$ parasites is dynamic and dependent on vacuolar stage.

a. Immunofluorescence assay of F3ΔHX ZFT-3HA$_{zft}$ demonstrating dynamic peripheral and basal localisation at 24 h. Scale bar 5 µm. **b.** Percentage of ZFT-3HA$_{zft}$ localisation (peripheral or basal) in respect to the number of parasites/vacuole. 100 vacuoles were counted for each of four biological replicates. Bars represent the mean of four independent biological experiments ± SD. Similar to ZFT-3HA$_{sag1,}$ ZFT-3HA$_{zft}$ localisation is more peripheral in vacuoles were fewer number of parasites and shifts to a more basal localisation in larger vacuoles. **c.** MFI of ZFT-3HA$_{zft}$/parasite in relation to the number of parasites per vacuoles. Each point represents individual MFI/parasite values from three independent biological experiments. Bars at the mean ± SD. *p* values from ordinary one-way ANOVA, Tukey corrected for multiple comparisons.

I hypothesised that the "non-specific" lower bands observed on the western gel may be ZFT degradation products. I have also previously shown in Figure 3.8c that the MFI of ZFT was higher in 2 parasite vacuoles compared to larger vacuoles, suggesting that ZFT may possibly be being degraded in a vacuolar stage dependent manner. One way to examine whether ZFT is being degraded by proteasomal degradation is by blocking the proteasome using an inhibitor, MG132 (Brown et al., 2017). If ZFT was targeted for degradation by the proteasome, MG132 would block this. I found that the lower bands on the western blot were still detected following MG132 treatment for 5 hours (Figure 3.9), suggesting that either these bands are nonspecific, or it may be possible that ZFT is being degraded in another manner.

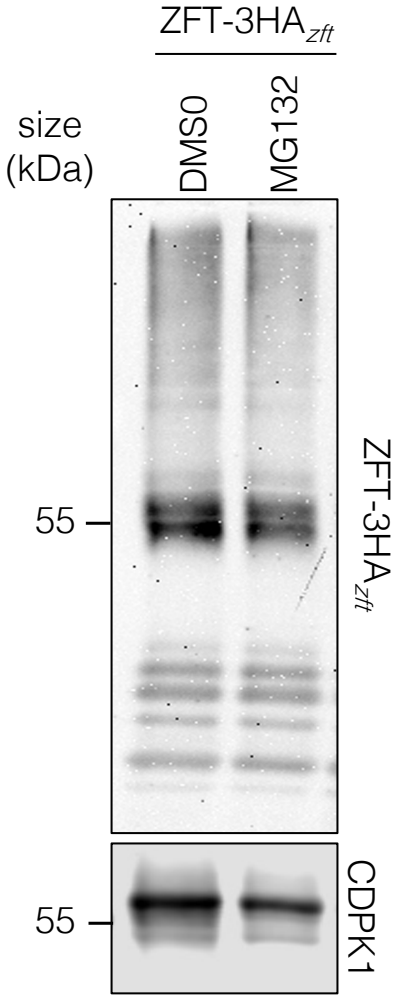


Figure 3.9 - ZFT-3HA$_{zft}$ lower bands are still detected post treatment with MG132 for 5 h, suggesting that the lower bands are nonspecific.

Western blot analysis of ZFT-3HA$_{zft}$ in the presence of MG132 treatment for 5 hours. Parasites were also treated with DMSO as a control. CDPK1 used as a loading control.

Given that the localisation of ZFT is highly dynamic and dependent on vacuolar stage, I was next curious to test whether the infection density may also possibly influence the localisation of ZFT. To test this, fibroblasts were infected with either a low multiplicity of infection (MOI) with 2.5 x 10^4 cells, or with a high MOI with 4 x 10^5 cells for 24 h and then fixed. I then performed an immunofluorescence assay and quantified the percentage of peripheral/basal localisation of ZFT depending on the number of parasites per vacuole as above. Interestingly, the data shows that for both 4 and 8 parasites per vacuole stage, there is a significant (p = 0.0332 and p < 0.0001 respectively, two-way ANOVA with Tukey correction) decrease in the percentage of peripheral localisation of ZFT at a high MOI compared to a low MOI (Figure 3.10a). I also quantified the percentage of vacuoles exhibiting the different number of parasites to ensure that this remained consistent and was therefore not likely affecting the change in peripheral localisation observed at the different MOIs. The data shows that the percentage of vacuoles expressing 2, 4, 8 and 8+ parasites/vacuole does not significantly change between low and high MOI. (Figure 3.10b). This suggests that the distribution and localisation of ZFT is affected by infection density. It is possible that an increased MOI increases the parasite burden and alters iron availability and homeostasis in the host, reducing the need for ZFT to accumulate at the periphery of the parasite. It is possible that at a low MOI there is less competition, so ZFT localises to the periphery to ensure efficient access to host derived iron. In contrast, at a high MOI, host iron may be depleted at a faster rate and localising ZFT to the periphery of the cell is no longer advantageous, and parasites may therefore internalise ZFT to access iron stores from within the parasite.

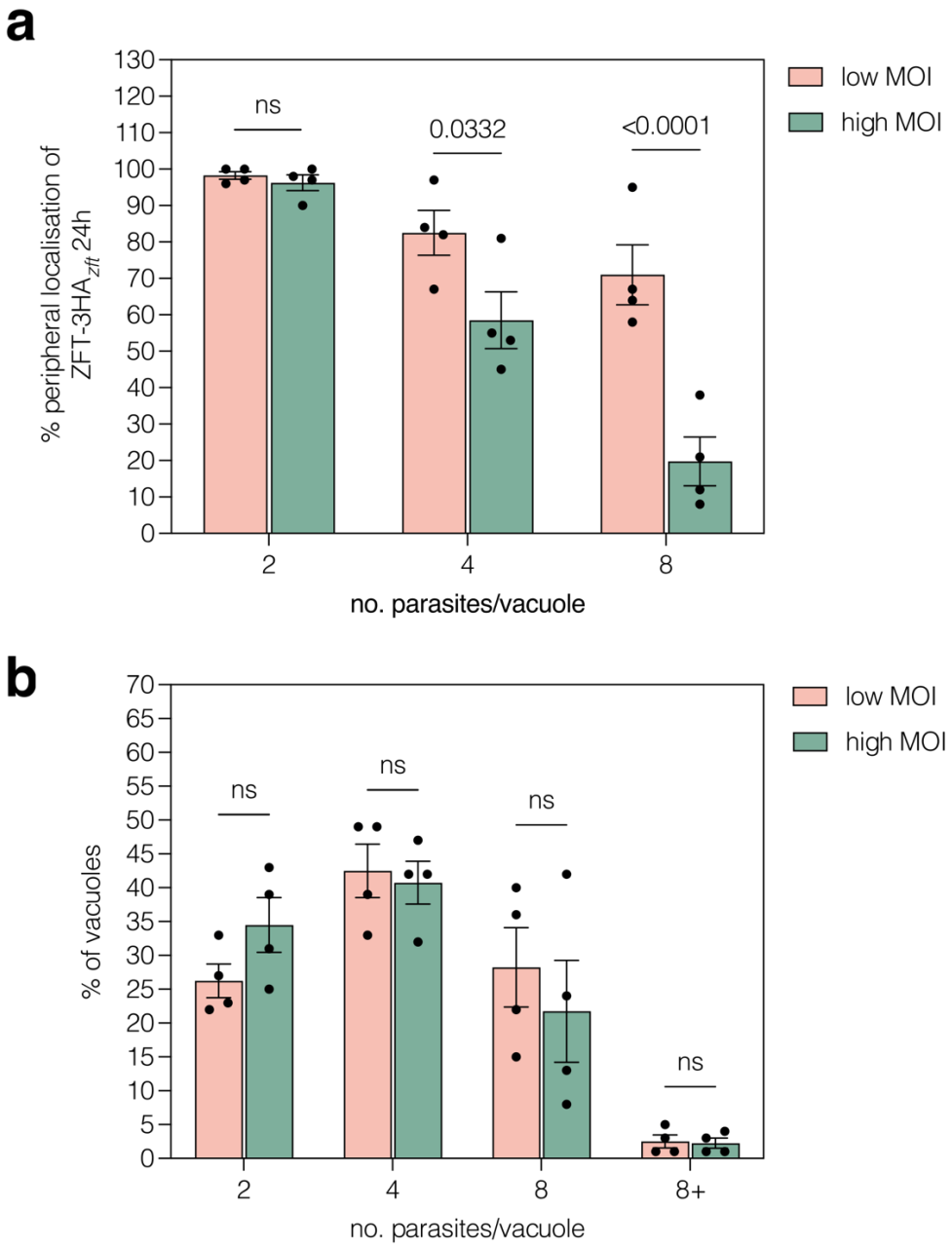


Figure 3.10 - ZFT peripheral localisation is significantly reduced in 4 and 8 parasite stage vacuoles at a high MOI compared to a low MOI.

a. Percentage of peripheral ZFT-3HA$_{zft}$ localisation in respect to the number of parasites/vacuole at both a low MOI (2.5 x 10^4 cells) and a high MOI (4 x 10^5 cells). 100 vacuoles were counted for each of four biological replicates. Bars represent the mean of four independent biological experiments ± SD. Data shows that the percentage of peripheral localisation of ZFT is significantly reduced in 4 and 8 stage parasites/vacuole at a high MOI compared to a low MOI. **b.** Percentage of vacuoles with either 2, 4, 8 or 8+ parasites per vacuole at both a low MOI (2.5 x 10^4 cells) and a high MOI (4 x 10^5 cells). 100 vacuoles were counted for each of four biological replicates. Bars represent the mean of four independent biological experiments ± SD. Data shows that the percentage of vacuoles expressing 2, 4, 8 and 8+ parasites/vacuole does not significantly change between low and high MOI.

3.6 ZFT expression is regulated by the availability of iron in F3ΔHX ZFT-3HA*zft*

To assess if ZFT expression in the F3ΔHX ZFT-3HA*zft* parasites changes in low iron conditions, I chelated the iron from the host cells for 24 h before infection using the chelator deferoxamine (100 μM DFO) and then infected the cells with F3ΔHX ZFT-3HA*zft* for either 18 h or 24 h before harvesting cells for western blot analysis. At 18 h post treatment, ZFT-3HA*zft* levels were slightly but significantly reduced to around 80 % of the untreated (p = 0.0019, two-tailed paired t test) (Figure 3.11a, b). This is distinct to ZFT-3HA*sag1* expression under low iron conditions at 18 h, where ZFT-3HA*sag1* expression levels are reduced to 40 % (Figure 3.5a, b). By 24 h post treatment, ZFT-3HA*zft* expression was reduced further to around 25 % of the untreated (p = 0.0007, two-tailed paired t test) (Figure 3.11c, d), similar to ZFT-3HA*sag1* expression under low iron conditions (Figure 3.5c, d). To determine if the localisation of ZFT was affected under iron starvation, I treated the parasites with 100 μM DFO for 24 h. Under low iron conditions (100 μM DFO), ZFT-3HA*zft* localisation was maintained at the parasite periphery, although some intracellular vesicles could be observed (Figure 3.11e). To further confirm this phenotype, an immunofluorescence assay was performed using a lower dose of DFO (20 μM DFO) (Figure 3.11f). Previous work in the lab has demonstrated that these conditions limit parasite replication without being too high/severely affecting replication (Hanna et al., 2025). The data demonstrates that under these low iron (20 μM DFO) conditions, the peripheral localisation of ZFT is significantly (p = 0.0021, two- way ANOVA, Fisher LSD) more common compared to basal localisation (Figure 3.11g), confirming the hypothesis that the localisation of ZFT is both vacuolar stage dependent and also dependent on the availability of iron.

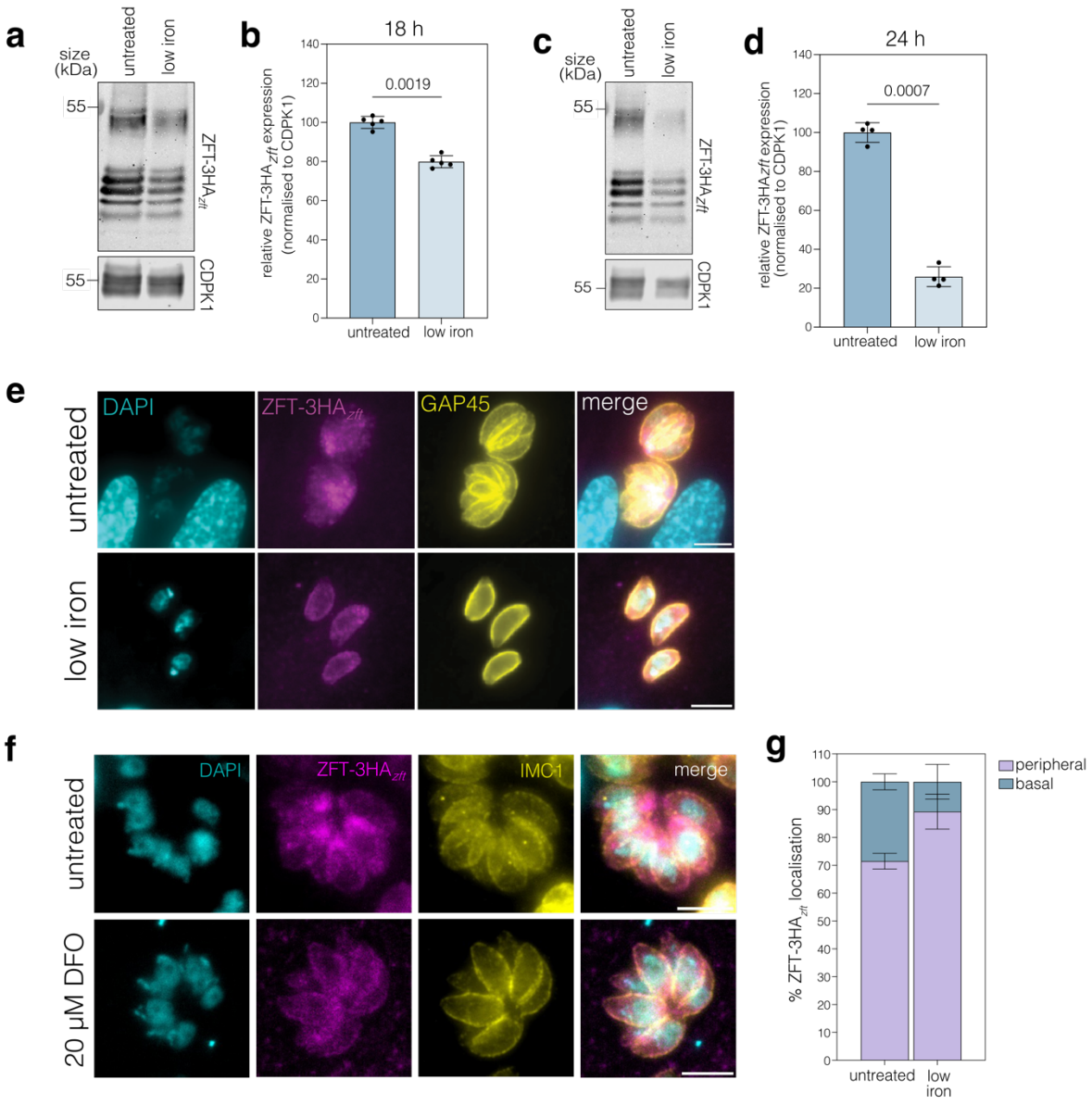


Figure 3.11 - F3ΔHX ZFT-3HA$_{zft}$ expression is reduced under low iron conditions at 24 h but stabilised at 18 h.

a. Western blot analysis of ZFT-3HA$_{zft}$ expression in untreated and low iron conditions (100 µM DFO) at 18 h post infection. CDPK1 used as a loading control. **b.** Quantification of ZFT-3HA$_{zft}$ levels at 18 h in untreated and low iron conditions from five independent biological experiments. Bars are at mean ± SD. *p* values from two-tailed paired t test. **c.** Western blot analysis of ZFT-3HA$_{zft}$ expression in untreated and low iron conditions (100 µM DFO) at 24 h post infection. CDPK1 used as a loading control. **d.** Quantification of ZFT-3HA$_{zft}$ levels at 24 h in untreated and low iron conditions from four independent biological experiments. Bars are at mean ± SD. *p* values from two-tailed paired t test. **e.** Immunofluorescence assay of ZFT-3HA$_{zft}$ at 24 h post infection in untreated and low iron (100 µM DFO) conditions. **f.** Immunofluorescence assay of ZFT-3HA$_{zft}$ at 24 h post infection in untreated and 20 µM DFO conditions. **g.** Quantification of ZFT-3HA$_{zft}$ localisation (peripheral/basal) in untreated and 20 µM DFO low iron conditions. Bars are mean of three independent biological experiments, ± SD.

To assess if ZFT expression in the F3ΔHX ZFT-3HA$_{zft}$ parasites changes in high iron conditions, I treated the host cells with exogenous iron for 24 h before infection using 500 μM FAC and then infected the cells with F3ΔHX ZFT-3HA$_{zft}$ for either 18 h or 24 h before harvesting cells for western blot analysis. At 18 h post treatment, ZFT-3HA$_{zft}$ levels were slightly (to around 87 % of the untreated) but significantly (p = 0.028, two-tailed paired t test) reduced (Figure 3.12a, b). Interestingly, this is distinct to ZFT-3HA$_{sag1}$ expression under high iron conditions at 18 h, where ZFT-3HA$_{sag1}$ expression levels are not significantly altered (Figure 3.6a, b). However, by 24 h post treatment, ZFT-3HA$_{zft}$ expression was reduced to around 40 % of the untreated (p = 0.0041, two-tailed paired t test) (Figure 3.12c, d). This is also distinct to ZFT-3HA$_{sag1}$ expression under high iron conditions at 24 h, where ZFT-3HA$_{sag1}$ expression levels are not significantly changed (Figure 3.6c, d). I further validated the loss of ZFT-3HA$_{zft}$ expression under excess iron at 24 h by immunofluorescence (Figure 3.12e, f). These data demonstrate that ZFT-3HA$_{zft}$ expression levels are significantly reduced under excess iron conditions.

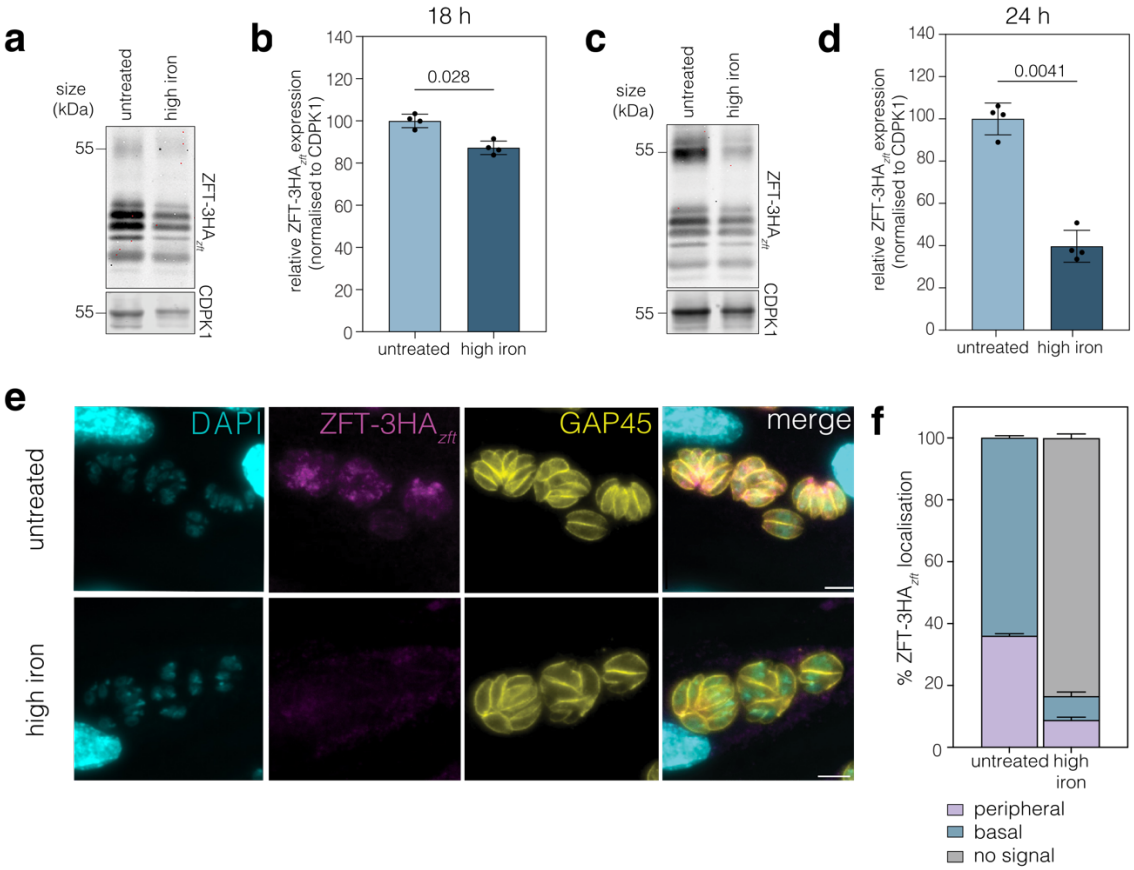


Figure 3.12 - F3ΔHX ZFT-3HA*zft* expression is significantly reduced at 24 h compared to untreated but stabilised at 18 h.

a. Western blot analysis of ZFT-3HA*zft* expression in untreated and high iron conditions (500 µM FAC) at 18 h post infection. CDPK1 used as a loading control. **b.** Quantification of ZFT-3HA*zft* levels at 18 h in untreated and high iron conditions from four independent biological experiments. Bars are at mean ± SD. *p* values from two-tailed paired t test. **c.** Western blot analysis of ZFT-3HA*zft* expression in untreated and high iron conditions (500 µM FAC) at 24 h post infection. CDPK1 used as a loading control. **d.** Quantification of ZFT-3HA*zft* levels at 24 h in untreated and high iron conditions from four independent biological experiments. Bars are at mean ± SD. *p* values from two-tailed paired t test. **e.** Immunofluorescence assay of ZFT-3HA*zft* at 24 h post infection in untreated and high iron (500 µM FAC) conditions confirming that that ZFT-3HA*zft* expression levels are significantly reduced under excess iron. Scale bars 5 µm. **f.** Quantification of ZFT-3HA*zft* localisation (peripheral/basal/no signal) in untreated and high iron (500 µM FAC) conditions. Bars are mean of three independent biological experiments, ± SD.

3.7 ZFT protein stability is not altered under low iron conditions following cycloheximide treatment

Many proteins are often either stabilised or degraded depending on the availability of their substrate or cofactor. More specifically, iron-mediated changes in protein stability have previously been documented in mammalian cells (Chen et al., 2009; De Domenico et al., 2007; Garza et al., 2020). Previous work in the lab has shown that the *zft* 3' UTR demonstrates mRNA levels stability that is iron-dependent, showing stabilisation of the transcript under iron deprivation conditions (Sloan et al., 2025). However, protein stability has not previously been examined. I have previously shown that ZFT-3HA$_{zft}$ expression levels are stabilised under both low (Figure 3.11a, b) and high (Figure 3.12a, b) iron conditions at 18 h compared to untreated parasites. To further examine this phenotype and assess whether the accumulation of ZFT protein is driven by a change in protein stability under different iron conditions, parasites cultured in untreated D3, 500 µM FAC or 100 µM DFO for 24 h were treated with cycloheximide (CHX) to inhibit all new cytosolic protein translation for 0, 1, 3, 5 and 7 h. Following treatment, parasites were harvested for western blot analysis (Figure 3.13a, b, c).

I found that ZFT demonstrated a rapid drop in abundance between 1-3 h post translation inhibition, demonstrating that significant new translation is required to maintain ZFT levels (Figure 3.13d). However, for all time points, there is no significant difference in the rate of decay of ZFT between untreated, high iron and low iron conditions following CHX treatment (Figure 3.13d), although it is clear that both FAC and DFO alter the kinetics of degradation of ZFT. The data further suggests that under high iron conditions, ZFT is most likely being internalised rather than being degraded. CDPK1 was used as a control and is also degraded following CHX treatment in untreated, high, and low iron conditions (Figure 3.13e). Furthermore, when plotting the proportion of both ZFT and CDPK1 remaining following CHX treatment under different iron conditions, the shape of the curves are not significantly different. This data suggests that excess iron and iron deprivation do not significantly enhance the stability of ZFT protein. ZFT remaining stable under both high and low iron conditions and not degrading at a slower rate than untreated conditions suggests that the accumulation of ZFT observed at 18 h under low iron conditions is most likely due to regulation of at

either the transcriptional or translational level, rather than by decreased protein turnover.

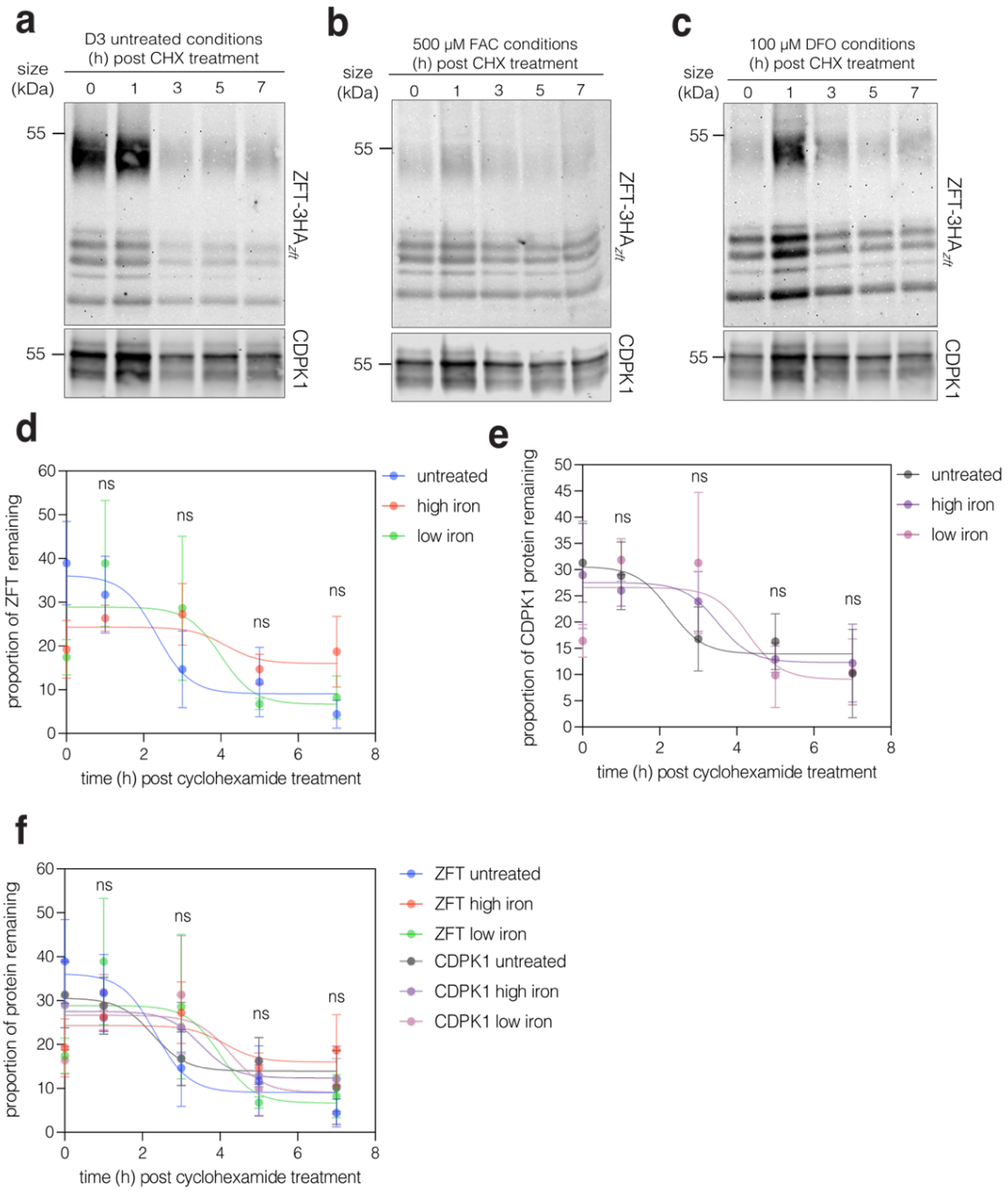


Figure 3.13 - ZFT3HA$_{zft}$ protein stability is not altered post cycloheximide (CHX) treatment under high and low iron conditions.

a. Western blot analysis of ZFT-3HA$_{zft}$ grown in D3 conditions for 24 h then treated with 100 µM cycloheximide (CHX) for 1, 3, 5 and 7 h. CDPK1 used as a loading control. **b.** Western blot analysis of ZFT-3HA$_{zft}$ grown in 500 µM FAC conditions for 24 h then treated with 100 µM cycloheximide (CHX) for 1, 3, 5 and 7 h. **c.** Western blot analysis of ZFT-3HA$_{zft}$ grown in 100 µM DFO conditions for 24 h then treated with 100 µM cycloheximide (CHX) for 1, 3, 5 and 7 h. Quantifications of western blots showing the proportion of ZFT **(d)**, CDPK1 **(e)**, and both ZFT and CDPK1

together **(f)** remaining following CHX treatment for 1, 3, 5 and 7 h compared to no CHX treatment cultured in untreated, 500 µM FAC and 100 µM DFO conditions. Bars are at the mean of n=3 for untreated and 500 µM FAC conditions and n=2 for 100 µM DFO conditions, ± SD. *p* values from two-tailed paired t test corrected for multiple comparisons by two-stage step-up (Benjamini, Krieger, and Yekutieli).

3.8 Introducing a second copy of ZFT to overexpress: cell line validation

To examine the function of ZFT in more detail and assess the sensitivity of ZFT to iron, ZFT was stably overexpressed. Initial attempts were unsuccessful, possibly due to toxicity. However, by coupling a second copy of ZFT with a C-terminal Ty tag expressed from a strong pTUB8 promoter (Frénal et al., 2010) with DHFR using a P2A-slip peptide (Markus et al., 2019), and maintaining the line in pyrimethamine, expression can be maintained (Figure 3.14a). Cecilia Gallego Rubio generated this line. I validated this line by PCR to confirm the presence of the gene (Figure 3.14b) and by western blotting to validate the presence of the protein (Figure 3.14c). Interestingly, and distinct from ZFT-3HA$_{sag1}$ and ZFT-3HA$_{zft}$, ZFT-Ty was only visible by western blot when the lysates were not boiled.

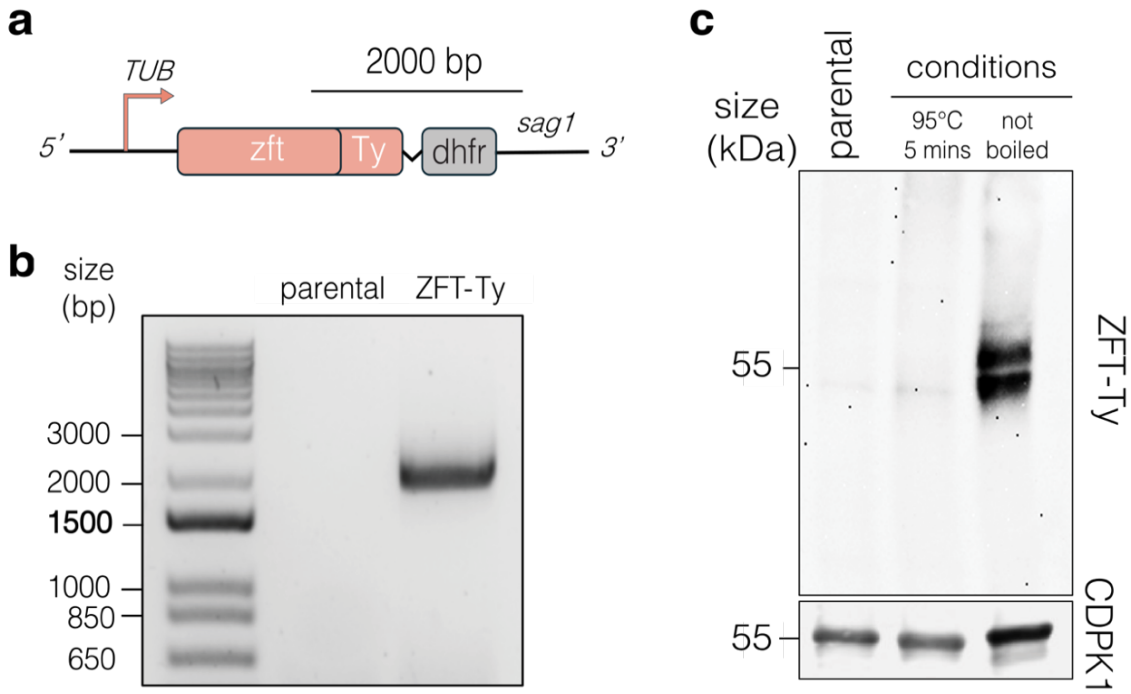


Figure 3.14 - RHtdTomato pTUB8 ZFT-Ty DHFR strain construction and validation

a. Schematic of RHtdTomato pTUB8 ZFT-Ty DHFR strain construction to overexpress a second copy of ZFT coupled to a Ty tag under the strong pTUB8 promoter with DHFR using a P2A slip peptide at the *sag1* 3' UTR. **b.** PCR confirming the presence of the second copy of ZFT-Ty gene with an expected band size of 2000 bp as indicated in (a). **c.** Western blotting of ZFT-Ty under different boiling conditions confirming ZFT is successfully tagged and overexpressed, running at the expected band size (50 kDa). CDPK1 was used as a loading control.

To further validate the ZFT-Ty parasite line, an immunofluorescence assay was performed at 24 h, before being fixed and stained with an anti-Ty antibody (Figure 3.15a). The data shows that ZFT is successfully tagged, however the localisation is neither peripheral or basal, and seems to be dispersed throughout the cell, with some puncta visible. To examine this in more detail at a higher resolution, an immunofluorescence assay was performed with ZFT-Ty parasites 24 h post infection and imaged using the super resolution ELYRA microscope (Figure 3.15b). At this resolution, the ZFT-Ty signal still seems to be dispersed throughout the cell but with a focus of signal at the basal end of the parasites.

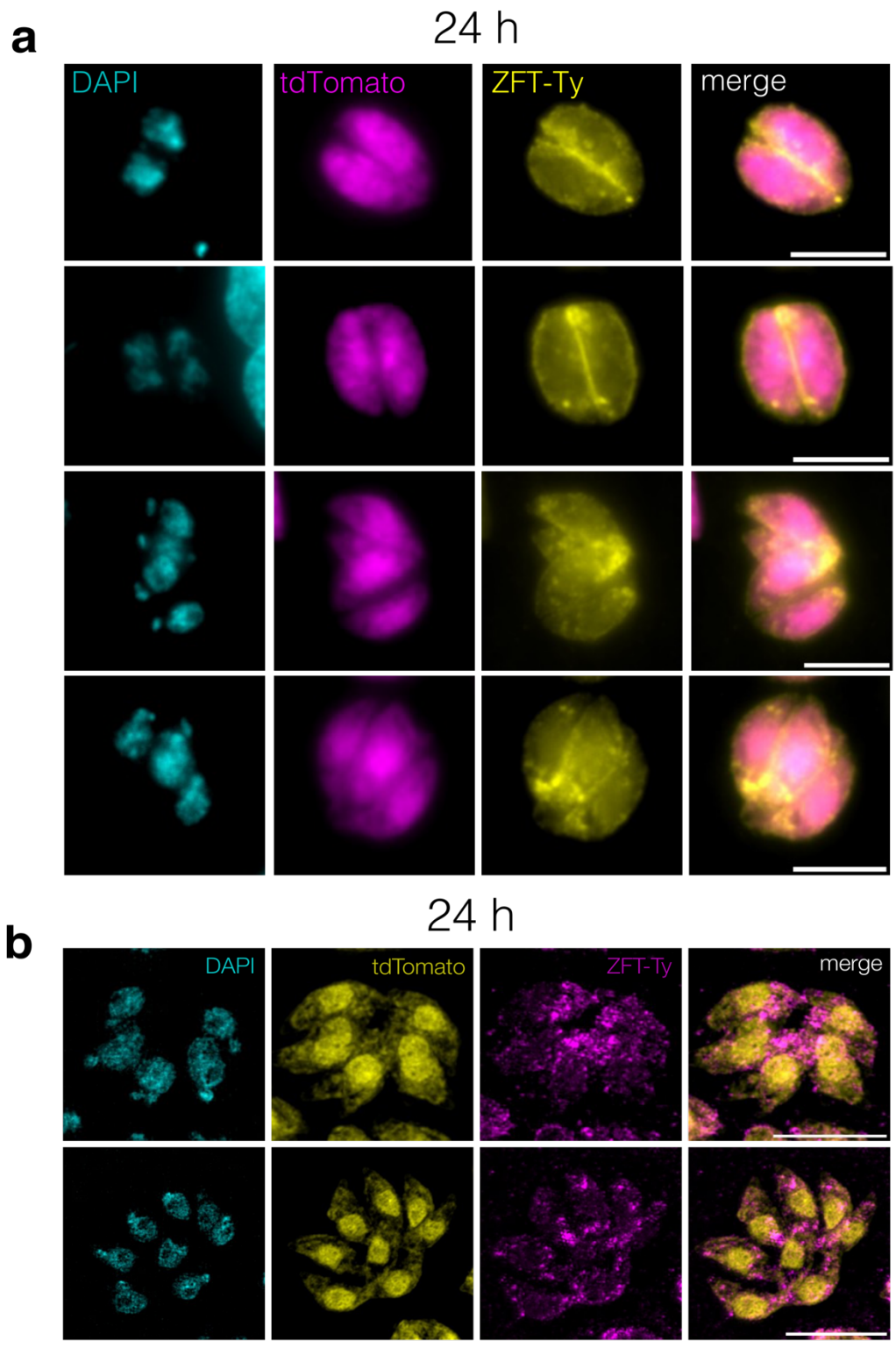


Figure 3.15 - ZFT-Ty localisation is peripheral and also dispersed throughout the parasite 24 h post infection, with some puncta visible at the basal end when imaged with a super resolution microscope.

a. Immunofluorescence assay of RHtdTomato TUB8 ZFT-Ty DHFR 24 h demonstrating dispersed signal. Scale bar 5 µm. **b.** Immunofluorescence assay of RHtdTomato TUB8 ZFT-Ty DHFR 24 h imaged using a super resolution ELYRA microscope demonstrating dispersed signal with notable puncta at the basal end of the parasites. Scale bar 5 µm.

It is possible that the localisation and protein expression of ZFT seen at 24 h is a compensatory change or a secondary adaptation to the overexpression. ZFT-Ty protein levels, localisation and post-translational modifications may change over a 24 h time period. As the overexpression of ZFT may be toxic to the parasite and cells may have adapted at 24 h, I was next curious to examine an earlier time point, 6 h, to investigate more primary effects and initial targeting of ZFT when it is overexpressed. Interestingly, I observed that ZFT-Ty localises more as puncta/foci within the parasite and is less dispersed within the cell at 6 h compared to 24 h (Figure 3.16).

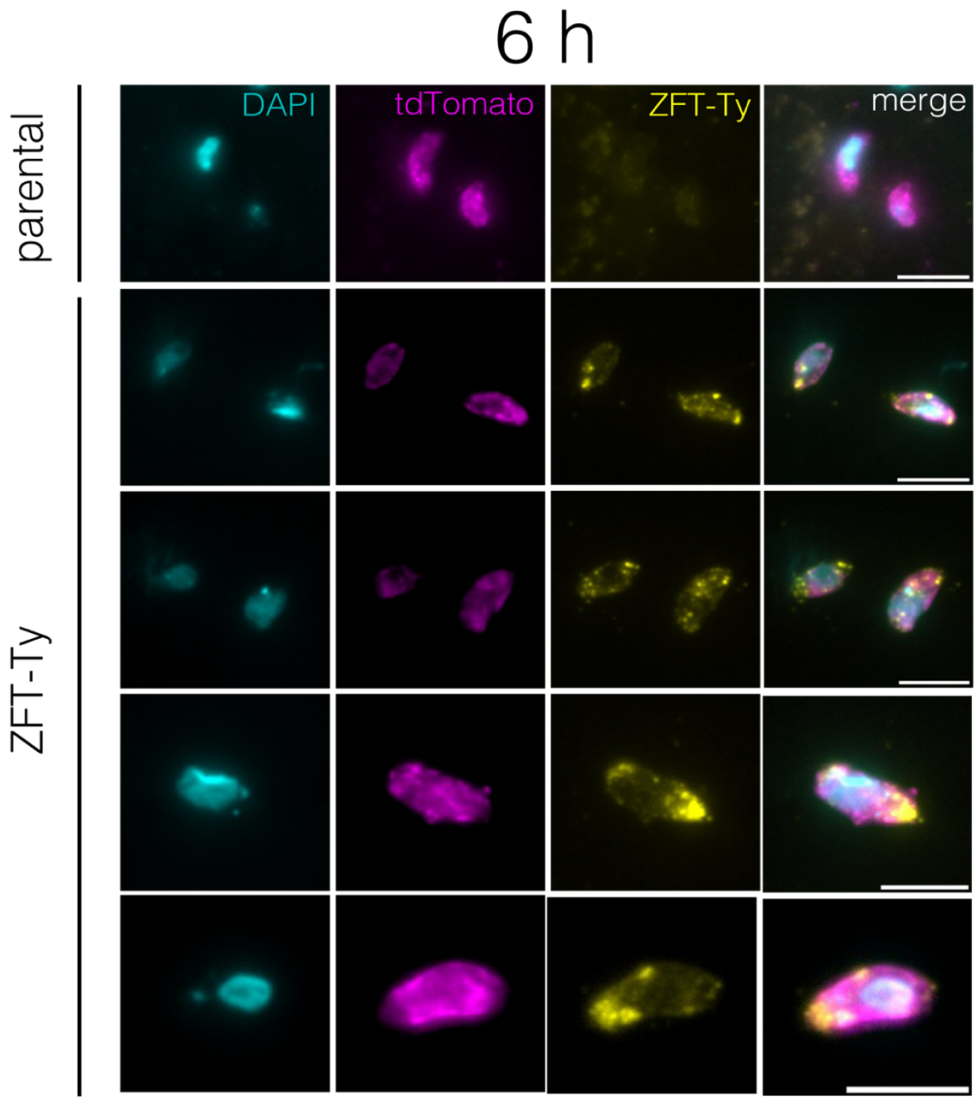


Figure 3.16 - ZFT-Ty localisation is more punctate and less dispersed throughout the parasite at 6 h compared to 24 h.

Immunofluorescence assay of RHtdTomato TUB8 ZFT-Ty DHFR 6 hpi demonstrating more punctate ZFT-Ty expression and localisation compared to 24 h post infection. Scale bar 5 μm.

3.9 Overexpressing ZFT leads to a change in iron sensitivity

To further examine the effect of overexpressing ZFT on parasite fitness, a plaque assay of both parental RHtdTomato and ZFT-Ty parasites was performed (Figure 3.17a). The data demonstrates that parasites overexpressing ZFT form significantly (p = 0.0027, unpaired two-tailed t test) fewer plaques compared to parental parasites (Figure 3.17b), with significantly smaller area (p < 0.0001, two-tailed unpaired t test with Welch's correction) (Figure 3.17c). This data suggests that overexpressing ZFT inhibits parasite replication.

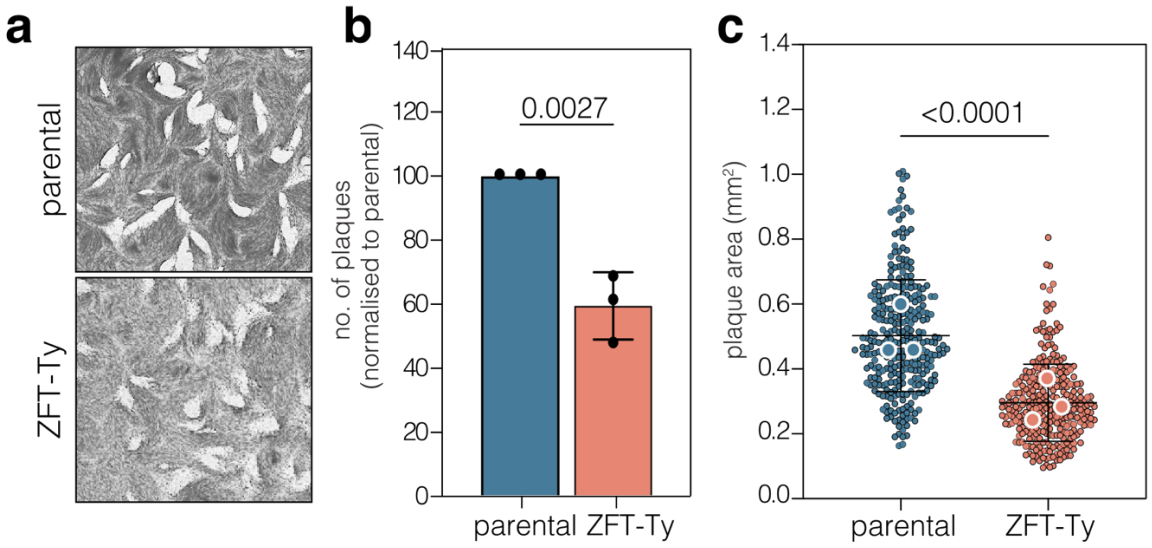


Figure 3.17 - Parasites overexpressing ZFT form fewer and smaller plaques compared to parental parasites.

a. Plaque assay of parental RHtdTomato and ZFT-Ty parasites in untreated conditions. **b.** Quantification of plaque numbers for parental RHtdTomato and ZFT-Ty parasites, p values are unpaired two-tailed t test. **c.** Quantification of plaque areas for parental RHtdTomato and ZFT-Ty parasites. Points represent individual plaque areas from three independent biological experiments. Bars are at the mean ± SD. p values from two-tailed unpaired t test with Welch's correction. Average of plaque areas from each of three biological replicates represented as larger overlayed points. Data shows that overexpressing ZFT inhibits parasite replication.

The sensitivity to metal conditions in the environment can be changed following the overexpression of metal transporters (Aghabi et al., 2023; Connolly et al., 2002; Li and Kaplan, 1998). To assess whether overexpressing ZFT makes the parasites more sensitive to excess iron, I performed a plaque assay of both parental RHtdTomato parasites and parasites overexpressing ZFT in untreated and high iron (500 μM FAC) conditions (Figure 3.18a). I found that in both parental and ZFT-Ty parasite strains, treatment with excess iron significantly reduces the number of plaques and plaque area compared to untreated, supporting the idea that excess iron is toxic and inhibits parasite replication (Figure 3.18b, c). However, there was no significant differences between plaque numbers in high iron conditions for parasites overexpressing ZFT compared to the parental parasites when normalised to the untreated for each line, suggesting that parasites overexpressing ZFT are no more sensitive to excess iron compared to the parental line (Figure 3.18d).

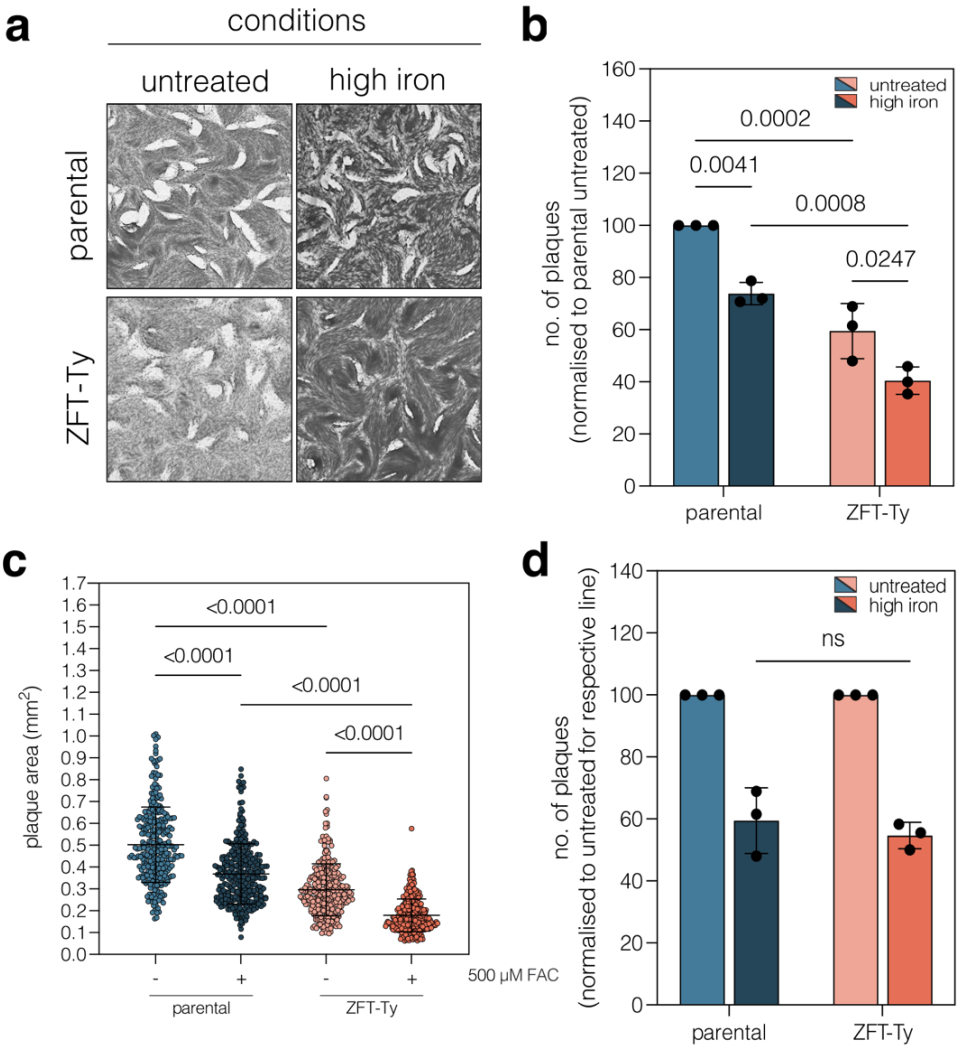


Figure 3.18 - Parasites overexpressing ZFT are not more sensitive to excess iron compared to parental parasites by plaque assay.

a. Plaque assay of parental RHtdTomato and ZFT-Ty parasites in untreated and high iron (500 µM FAC) conditions. **b.** Quantification of plaque numbers from (a) for parental RHtdTomato and ZFT-Ty parasites in untreated and high iron conditions, normalised to parental untreated. Bars are at the mean of three independent experiments, ± SD. *p* values from two-way ANOVA, Tukey corrected for multiple comparisons. **c.** Quantification of plaques area in mm^2 from (a) of parental RHtdTomato and ZFT-Ty parasites in untreated and high iron conditions. Points represent individual plaques from three independent biological experiments. Bars show the mean ± SD. p values from ordinary one-way ANOVA, Tukey corrected for multiple comparisons. **d.** Quantification of plaque numbers from (a) for parental RHtdTomato and ZFT-Ty parasites in untreated and high iron conditions, normalised to untreated for the respective line. Bars are at the mean of three independent experiments, ± SD. *p* values from two-way ANOVA, Tukey corrected for multiple comparisons.

To further examine the effects of overexpressing ZFT on the parasite's sensitivity to excess iron, host cells in a black opaque 96-well plate were infected with parental RHtdTomato or RHtdTomato TUB8 ZFT-Ty DHFR parasites and then treated with an increasing concentration of excess iron (FAC), or DFO. After four days, parasite fluorescence was quantified as a proxy for parasite survival. Data shows that parasites that overexpress ZFT-Ty are significantly (p = 0.0027, two-tailed unpaired t test) more sensitive (EC_{50} = 0.386 mM, 95 % C.I. 0.315 to 0.479 mM) to excess iron compared to the parental line (EC_{50} = 1.29 mM, 95 % C.I. 0.813 to 2.01 mM) (Figure 3.19a, b). To test the effect of ZFT-Ty overexpression on iron starvation, I treated parasites with the iron chelator, DFO. The results demonstrate that parasites overexpressing ZFT are significantly (p = 0.0246, two-tailed unpaired t test) more resistant (EC_{50} = 22.81 µM, 95 % C.l. 16.8 to 30.6 µM) to iron chelation, compared to the parental line (EC_{50} = 8.18 µM, 95 % C.l. 6.94 to 9.71 µM) (Figure 3.19c, d). These data suggest that overexpression of ZFT leads to alterations in parasite iron sensitivity – they are hypersensitive to excess iron compared to parental parasites, however the overexpression of ZFT provides a protective effect against iron chelation.

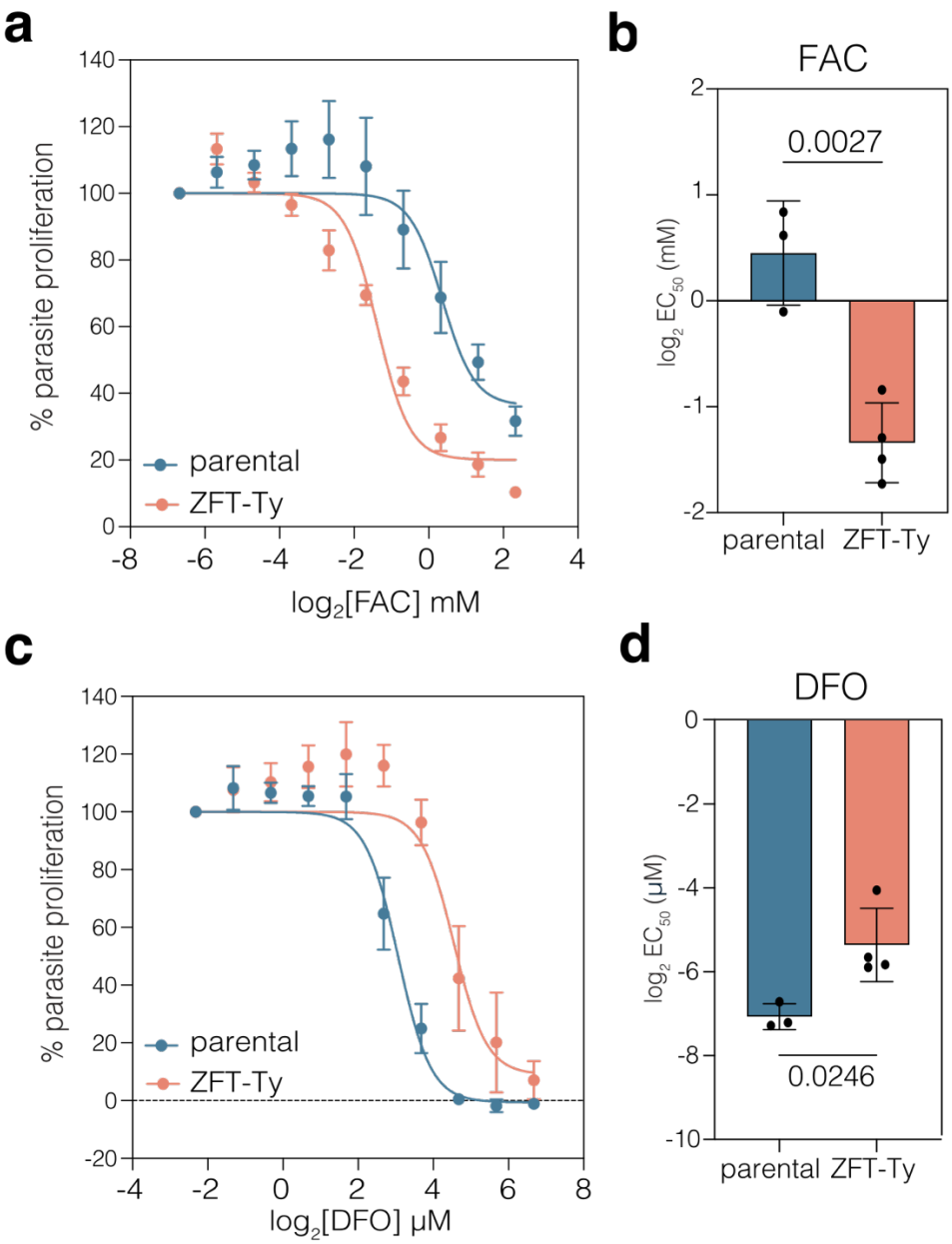


Figure 3.19 - Overexpressing ZFT leads to a change in iron sensitivity.

a. Dose response curve showing the percentage of parental and ZFT-Ty parasite survival in the presence of increasing concentrations of excess iron (FAC). **b.** Graphs demonstrating the mean parasite EC_{50} for FAC for parental RHtdTomato and ZFT-Ty parasites. Each point represents an independent experiment. Bars at mean of three independent biological experiments for parental and four independent biological experiments for ZFT-Ty, ± SD. *p* values from two-tailed unpaired t test. **c.** Dose response curve showing the percentage of parental and ZFT-Ty parasite survival following iron depletion using the chelator DFO. **d.** Graphs demonstrating the mean parasite EC_{50} for DFO for parental RHtdTomato and ZFT-Ty parasites. Each point represents an independent experiment. Bars at mean of three independent biological experiments for parental and four independent biological experiments for ZFT-Ty, ± SD. *p* values from two-tailed unpaired t test.

It is possible that parasites overexpressing ZFT are more sensitive to excess iron based on a non-specific increased sensitivity to oxidative stress, as was seen upon disruption of iron storage (Aghabi et al., 2023). To test whether overexpressing ZFT leads to a change in increased sensitivity to oxidative stress, parasites were treated with sodium arsenite (Ars), which has previously been used to induce oxidative stress in *T. gondii* (Aghabi et al., 2023; Augusto et al., 2021). However, the data suggests that the phenotype is specific to iron as the overexpression of ZFT does not lead to any significant change in oxidative stress sensitivity (Figure 3.20a, b).

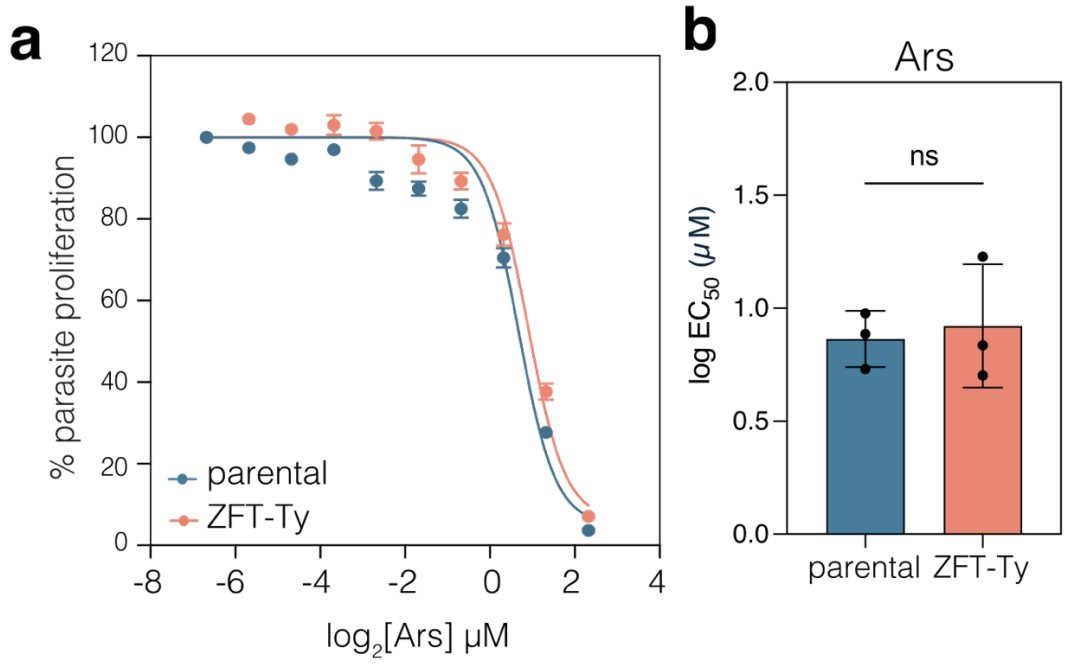


Figure 3.20 - Overexpressing ZFT does not alter the parasite's sensitivity to oxidative stress.

a. Fluorescent growth curves showing the percentage of parental and ZFT-Ty parasite survival in the presence of sodium arsenite (Ars). **b.** Graphs demonstrating the mean EC_{50} for Ars for RHtdTomato parental and ZFT-Ty parasites. Each point represents an independent experiment. Bars at mean of three independent biological experiments, ± SD. *p* values from two-tailed unpaired t test.

3.10 Generating a conditional knockdown of ZFT: T7S4-ZFT cell line validation

Based on the genome wide essentiality screen study by Sidik et al., 2016, ZFT is predicted to be essential, with a fitness conferring score of -4.3, for the survival of *T. gondii*. To assess whether ZFT is essential for parasite replication, an inducible knockdown line was generated where the endogenous promoter of ZFT was replaced with the T7S4 promoter. Cecilia Gallego Rubio generated this line. The presence of the drug anhydrotetracycline (ATc) inhibits the T7S4 promoter (Sheiner et al., 2011a), triggering the inducible downregulation of ZFT expression. A schematic of the T7S4-ZFT strain construction is demonstrated in Figure 3.21a. I performed a PCR to confirm both the 5' and 3' integration of the DHFR-T7S4 (Figure 3.21b). To verify conditional knockdown of ZFT, I performed RT-qPCR to examine the relative *zft* mRNA expression levels (normalised to actin) following the addition of ATc. I found that the relative *zft* mRNA expression levels are significantly reduced by approximately 60 % by 24 h post induction with ATc (p = 0.0032, two-tailed unpaired t-test with Welch's correction), confirming the inducible knockdown of ZFT (Figure 3.21c).

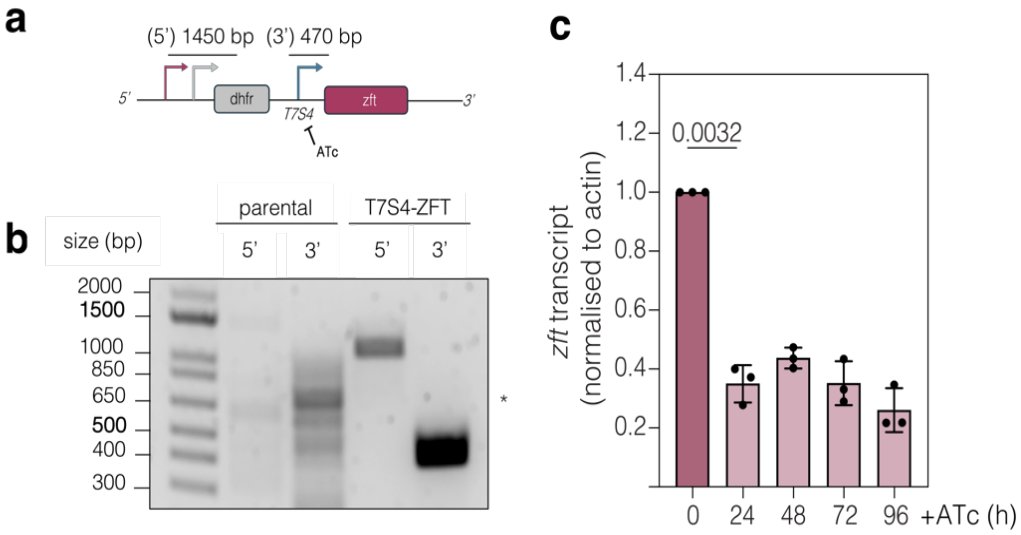


Figure 3.21 - T7S4-ZFT strain construction and validation.

a. Schematic of F3ΔHX T7S4-ZFT strain construction under the T7S4 inducible promoter which is inhibited in the presence of ATc. **b.** PCR validating successful integration of the T7S4-DHFR cassette at both the 5' and 3' with the expected band sizes shown in (a). Parental F3ΔHX parasites were used as a control. **c.** RT-qPCR showing *zft* mRNA transcript levels following the addition of ATc, relative to 0 h ATc and normalised to actin. Bars at mean of three independent biological experiments, ± SD. *p* values from two-tailed unpaired t test.

3.11 ZFT is essential for *T. gondii* survival

To examine the essentiality of ZFT in parasite survival and replication, a plaque assay was performed in the presence and absence of ATc to examine parasite growth upon the depletion of ZFT (Figure 3.22a). Interestingly, the replacement of the ZFT promoter alone from the endogenous promoter to the T7S4 promoter led to a significant (p = 0.0052, two-way ANOVA, Tukey corrected for multiple comparisons) growth defect by plaque number (Figure 3.22a, b). The area of the plaques was also subsequently measured in mm^2 (Figure 3.22c). I found that swapping promoters resulted in significantly smaller plaques compared to the parental line. This suggests that the correct expression of ZFT plays an important role in the fitness of *Toxoplasma gondii*. The data further demonstrates that the addition of ATc to knock ZFT down renders the T7S4-ZFT parasites unable to form plaques in the host cell monolayer compared to the parental line (Figure 3.21a, b, c), confirming that the expression of ZFT is essential for parasite survival.

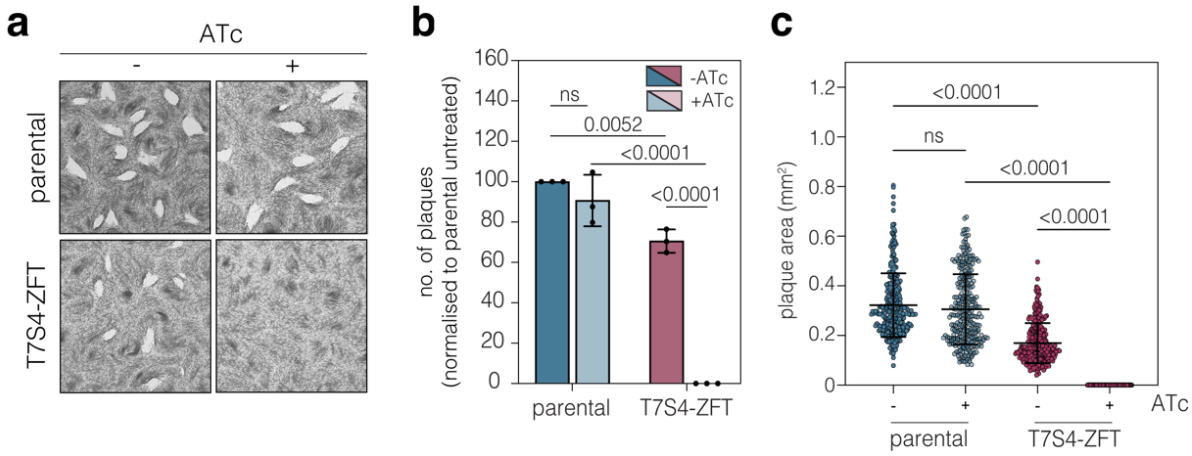


Figure 3.22 - Knockdown of ZFT blocks parasite replication.

a. Plaque assay of parental and T7S4-ZFT parasites in the absence and presence of ATc for 6 days, showing that ZFT knockdown parasites are unable to form any plaques in a host cell monolayer. **b.** Quantification of number of plaques in (a) formed by parental and T7S4-ZFT parasites in the absence and presence of ATc, normalised to parental untreated. Bars are at mean of three independent biological experiments, ± SD. *p* values from two-way ANOVA, Tukey corrected for multiple comparisons. **c.** Quantification of plaque area in mm^2 from (a) of parental and T7S4-ZFT plaques in the absence and presence of ATc. Points represent individual plaques from three independent biological experiments. Bars show the mean ± SD. p values from ordinary one-way ANOVA, Tukey corrected for multiple comparisons.

In *Plasmodium*, the loss of DMT1 (Loveridge and Sigala, 2024) or ZIPCO (Sahu et al., 2014) results in a growth defect which is rescued by the addition of exogenous substrate. To test if excess iron could rescue the growth defect observed upon ZFT knockdown, I treated T7S4-ZFT parasites with both ATc and 200 µM FAC and performed a plaque assay (Figure 3.23a). I found that replacing the ZFT promoter alone from the endogenous promoter to the T7S4 promoter led to a significant reduction in plaque area (p < 0.0001, two-tailed unpaired t test with Welch's correction) in high iron conditions (200 µM FAC) compared to untreated conditions (Figure 3.23b), reminiscent of the overexpression results above (Figure 3.19a, b). Interestingly however, the data demonstrated that exogenous iron was unable to rescue the growth defect observed upon ZFT knockdown, both by plaque number and plaque area (Figure 3.23c, d).

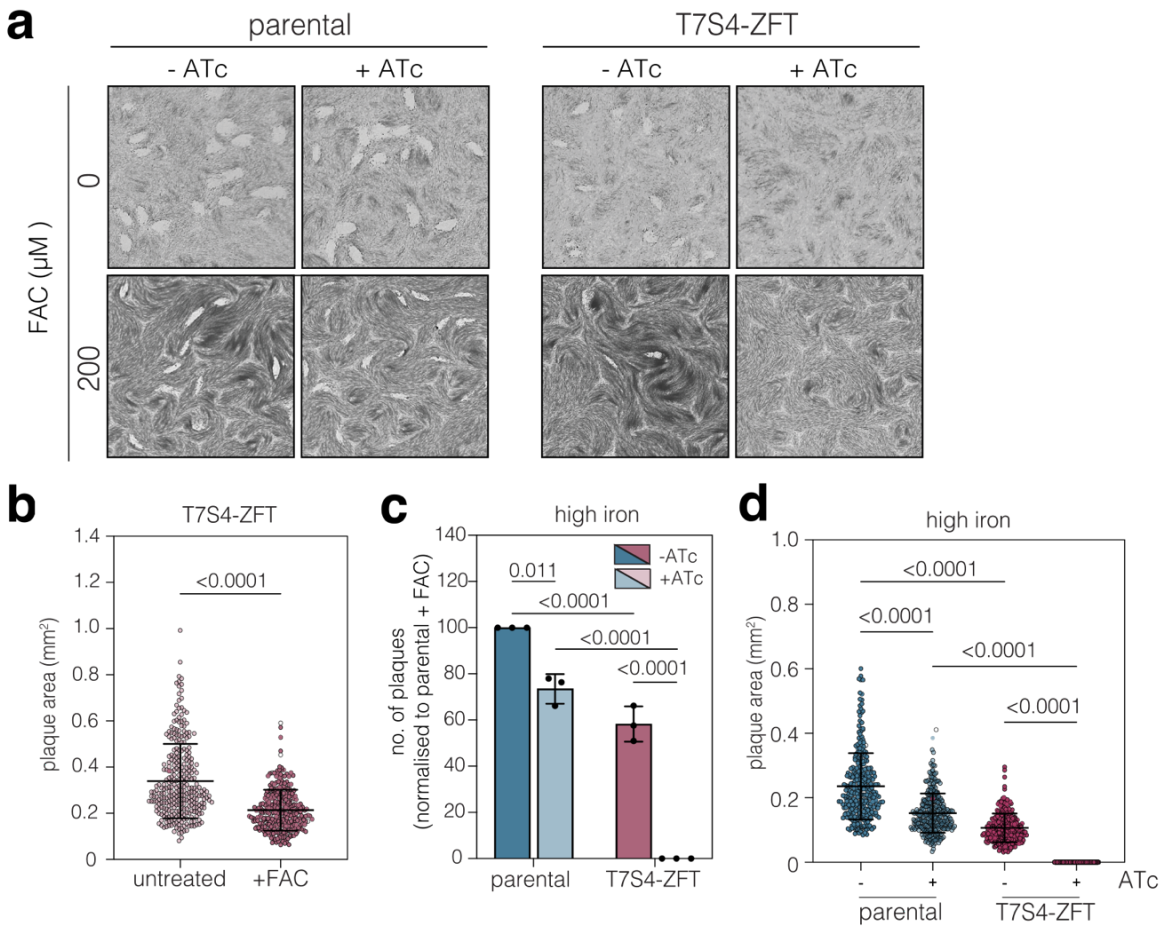


Figure 3.23 - Excess iron does not rescue the growth defect observed upon ZFT knockdown.

a. Plaque assay of parental and T7S4-ZFT parasites with the addition of 200 μM FAC in the absence and presence of ATc for 6 days, showing that excess iron does not rescue growth of ZFT knockdown parasites. **b.** Quantification of plaque area in mm^2 from (a) generated by T7S4-ZFT plaques in untreated and high iron (200 μM FAC) conditions, showing that replacing the promoter alone makes parasites more sensitive to excess iron. Points represent individual plaque areas from three independent biological experiments. Bars show mean ± SD. p values are from two-tailed unpaired t test with Welch's correction. **c.** Quantification of number of plaques in (a) formed by parental and T7S4-ZFT parasites in the absence and presence of ATc, in the presence of excess iron (200 μM FAC) normalised to parental untreated. Bars are at mean of three independent biological experiments, ± SD. *p* values from two-way ANOVA, Tukey corrected for multiple comparisons. **d.** Quantification of plaque area generated by parental and T7S4-ZFT parasites with and without ATc, in the presence of excess iron (200 μM FAC). Points represent individual plaque areas from three independent biological experiments. Bars show the mean ± SD. *p* values from ordinary one-way ANOVA, Tukey corrected for multiple comparisons.

Previous studies have shown that partial knockdown of DMT1 in *P. falciparum* resulted in residual PfDMT1 expression. This led to a less severe growth defect which was then rescued by the addition of exogenous metal supplementation transported by residual PfDMT1 (Loveridge and Sigala, 2024). I was therefore curious to assess whether excess iron could possibly restore growth of ZFT knockdown parasites if some ZFT remained. To do so, I performed a plaque assay with half the standard concentration of ATc (0.25 μM) instead (Figure 3.24a). The data demonstrated that under these conditions, ZFT knockdown parasites are still unable to form any plaques, even in the presence of excess iron (200 μM FAC) (Figure 3.24a, b, c). This data suggests that the growth defect upon ZFT knockdown is strong and irreversible, further emphasising the importance and essentiality of the role that ZFT plays as the major iron transporter.

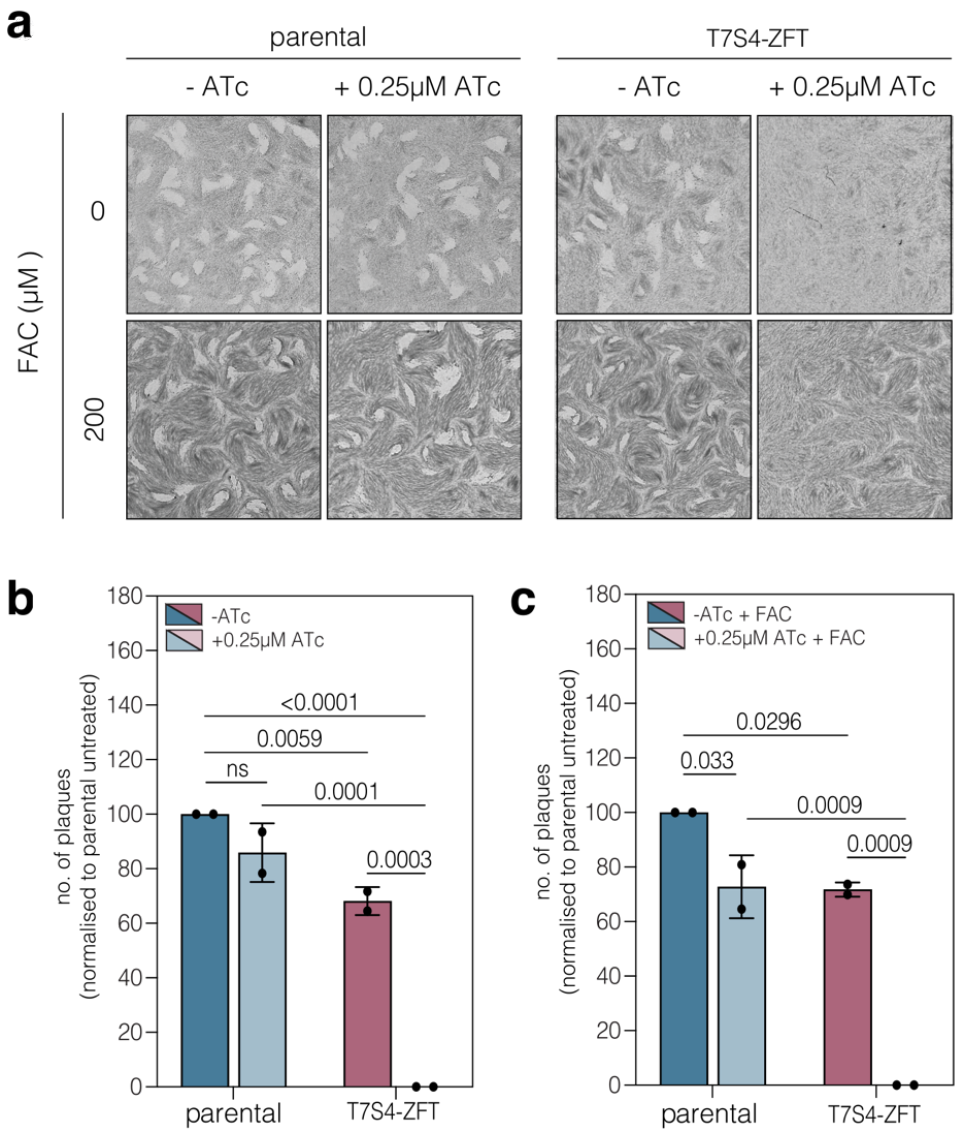


Figure 3.24 - Excess iron and half the standard concentration of ATc is unable to rescue growth of ZFT knockdown parasites.

a. Plaque assays of parental and T7S4-ZFT parasites with and without 0.25 μM ATc instead of the standard 0.5 μM ATc and excess iron (200 μM FAC) for 6 days showing the inability of ZFT knockdown parasites from forming plaques in the host cell monolayer. Quantification of plaque numbers formed by parental and T7S4-ZFT parasites with and without 0.25 μM ATc in untreated conditions **(b)** or high iron (200 μM FAC) conditions **(c)**, normalised to parental without ATc in untreated (b) or high iron (c) conditions. Bars are at the mean of two independent biological experiments, ± SD. *p* values from two-way ANOVA, Tukey corrected for multiple comparisons.

3.12 Tagging ZFT in the conditional knockdown T7S4-ZFT background: T7S4-ZFT3-HA*sag1* cell line validation

I next epitope tagged ZFT with a 3xHA epitope tag in the background of the T7S4-ZFT promoter replacement line at the *sag1* 3' UTR. Figure 3.25a shows the schematic of the F3ΔHX T7S4-ZFT-3HA*sag1* parasite strain construction. This line was validated by PCR confirming the successful integration in the T7S4-ZFT background (Figure 3.25b). I further confirmed this line by western blotting under different boiling conditions (Figure 3.25c).

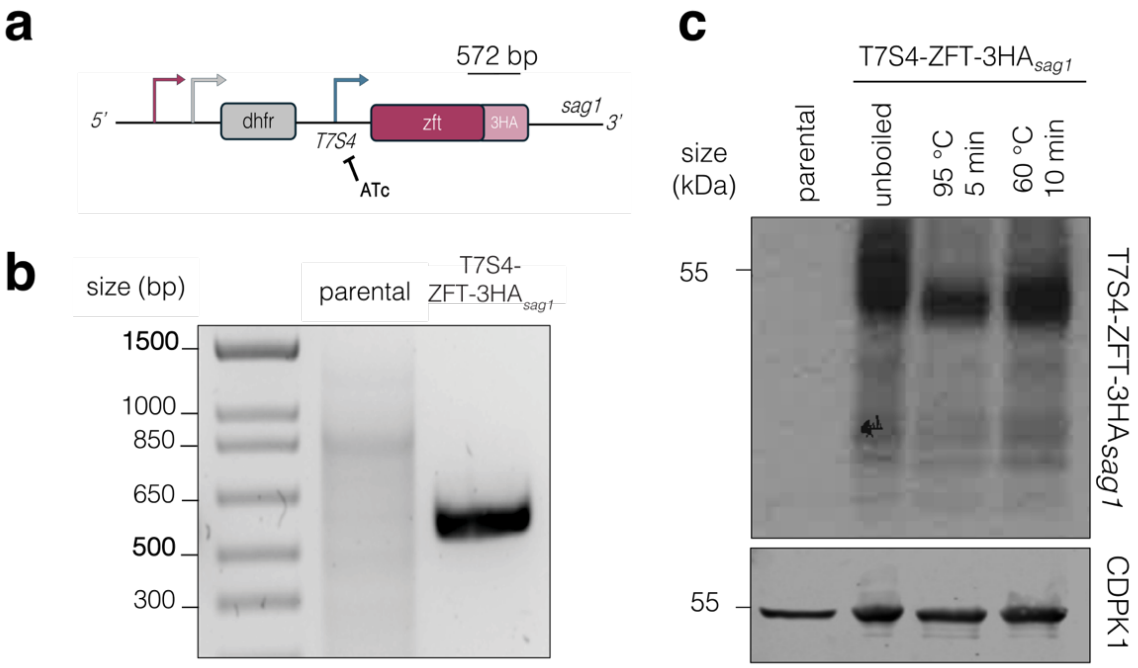


Figure 3.25 - T7S4-ZFT-3HA*sag1* strain construction and validation.

a. Schematic of F3ΔHX T7S4-ZFT-3HA*sag1* strain construction to tag ZFT with a 3xHA epitope tag at the C terminal under the T7S4 inducible promoter, where ZFT is endogenously tagged with a 3xHA epitope tag at the C-terminal at the *sag1* 3' UTR. **b.** PCR confirming successful integration in the T7S4-ZFT background, with an expected band size of 572 bp as indicated in (a). **c.** Western blotting of F3ΔHX T7S4-ZFT-3HA*sag1* under different boiling conditions confirming ZFT is successfully tagged and runs at the expected band size (50 kDa). CDPK1 was used as a loading control.

Next, I was intrigued to examine the effect of replacing the promoter alone from the endogenous ZFT promoter to the T7S4 inducible promoter on ZFT expression. This was particularly intriguing as previous plaque assay data in Figure 3.23a and b suggest that swapping of the promoter altered the sensitivity of the parasites to excess iron. I performed western blot analysis (Figure 3.26a) and found that changing the promoter to a T7S4 inducible promoter led to a significant (~5 times more) overexpression of ZFT in the F3ΔHX T7S4-ZFT-3HA$_{sag1}$ cell line compared with the endogenous promoter in F3ΔHX ZFT-3HA$_{zft}$ cell line (Figure 3.26b).

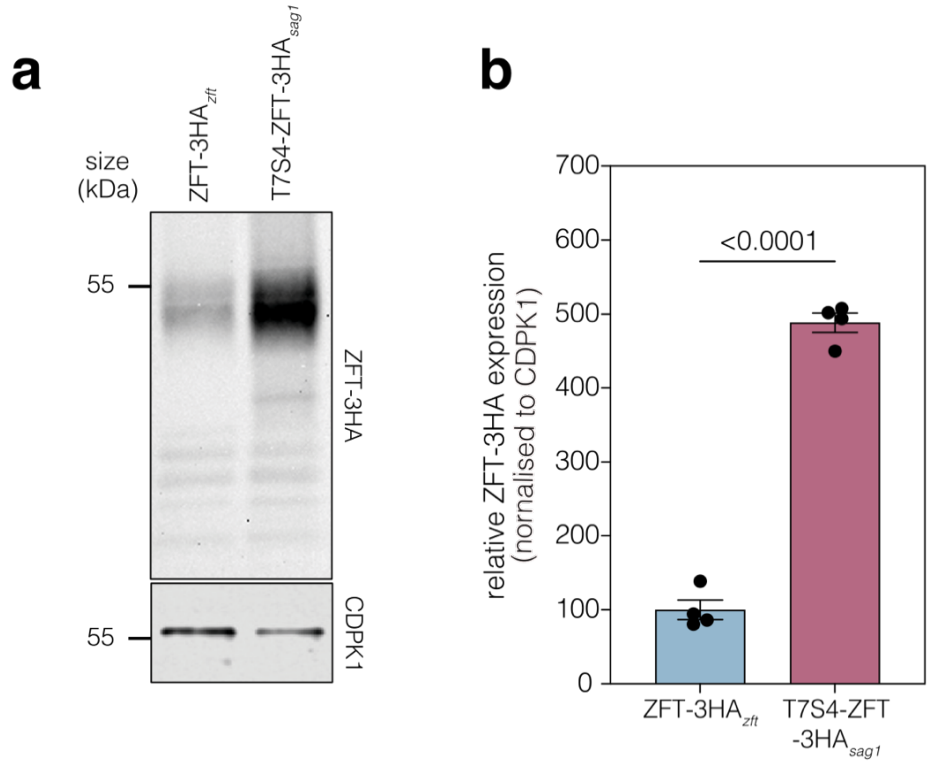


Figure 3.26 - Replacing the endogenous ZFT promoter with the T7S4 inducible promoter results in a significant overexpression of ZFT.

a. Western blot analysis of ZFT expression levels in both the F3ΔHX ZFT-3HA$_{zft}$ parasites under the endogenous promoter and the F3ΔHX T7S4-ZFT-3HA$_{sag1}$ parasites under the T7S4 inducible promoter at 24 h post infection. CDPK1 used as a loading control. **b.** Quantification of ZFT-3HA expression levels at 24 h in F3ΔHX ZFT-3HA$_{zft}$ and F3ΔHX T7S4-ZFT-3HA$_{sag1}$ parasites relative to the endogenous promoter and normalised to CDPK1. Bars are at mean of four independent biological experiments ± SD. p values from two-tailed unpaired t test.

However, in addition to the difference in promoters, it is important to note that the 3' UTRs between the two cell lines are also different, with ZFT-3HA$_{zft}$ being tagged retaining the endogenous *zft* 3' UTR and T7S4-ZFT-3HA$_{sag1}$ being tagged using the *sag1* 3' UTR. To ensure that the difference in expression levels observed is due to the promoter replacement rather than the 3' UTR, I performed a western blot of both ZFT-3HA$_{zft}$ and ZFT-3HA$_{sag1}$ parasites at 24 h, both with the endogenous promoter. I show that although based on one biological replicate, the expression levels of ZFT-3HA$_{zft}$ and ZFT-3HA$_{sag1}$ appear qualitatively similar with no clear differences observed (Figure 3.27).

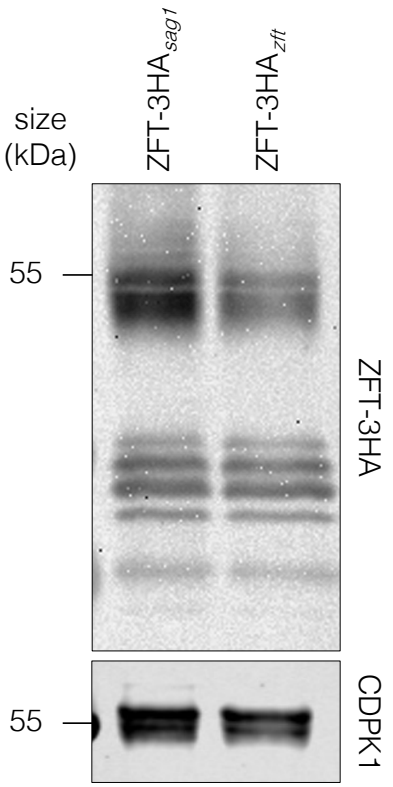


Figure 3.27 - ZFT-3HA$_{sag1}$ and ZFT-3HA$_{zft}$ expression levels at 24 h.

Western blot analysis of ZFT expression levels in both the F3ΔHX ZFT-3HA$_{zft}$ and F3ΔHX ZFT-3HA$_{sag1}$ parasites at 24 h post infection. CDPK1 used as a loading control.

Knockdown of ZFT in the F3ΔHX T7S4-ZFT-3HA$_{sag1}$ line was further validated by western blot analysis in the absence and presence of ATc at 24 h, 48 h 72 h and 96 h post induction (Figure 3.28a). I found that 24 h after the addition of ATc, there is a significant ~70 % drop ($p < 0.0001$, two-tailed paired t-test) in T7S4-ZFT-3HA$_{sag1}$ expression levels (relative to uninduced, normalised to CDPK1). 48 h after

adding ATc, there is only approximately 10 % of the protein remained (p = 0.0131, two-tailed paired t-test) (Figure 3.28b). To further confirm successful generation of this parasite line, an immunofluorescence assay was performed where host cells were infected with F3ΔHX T7S4-ZFT-3HA$_{sag1}$ parasites in the absence and presence of ATc. 48 h post induction, the parasites were fixed and then stained for anti-HA and anti-GAP45. I found that ZFT-3HA$_{sag1}$ was undetectable by IFA, validating successful knockdown of ZFT 48 h post induction with ATc (Figure 3.28c).

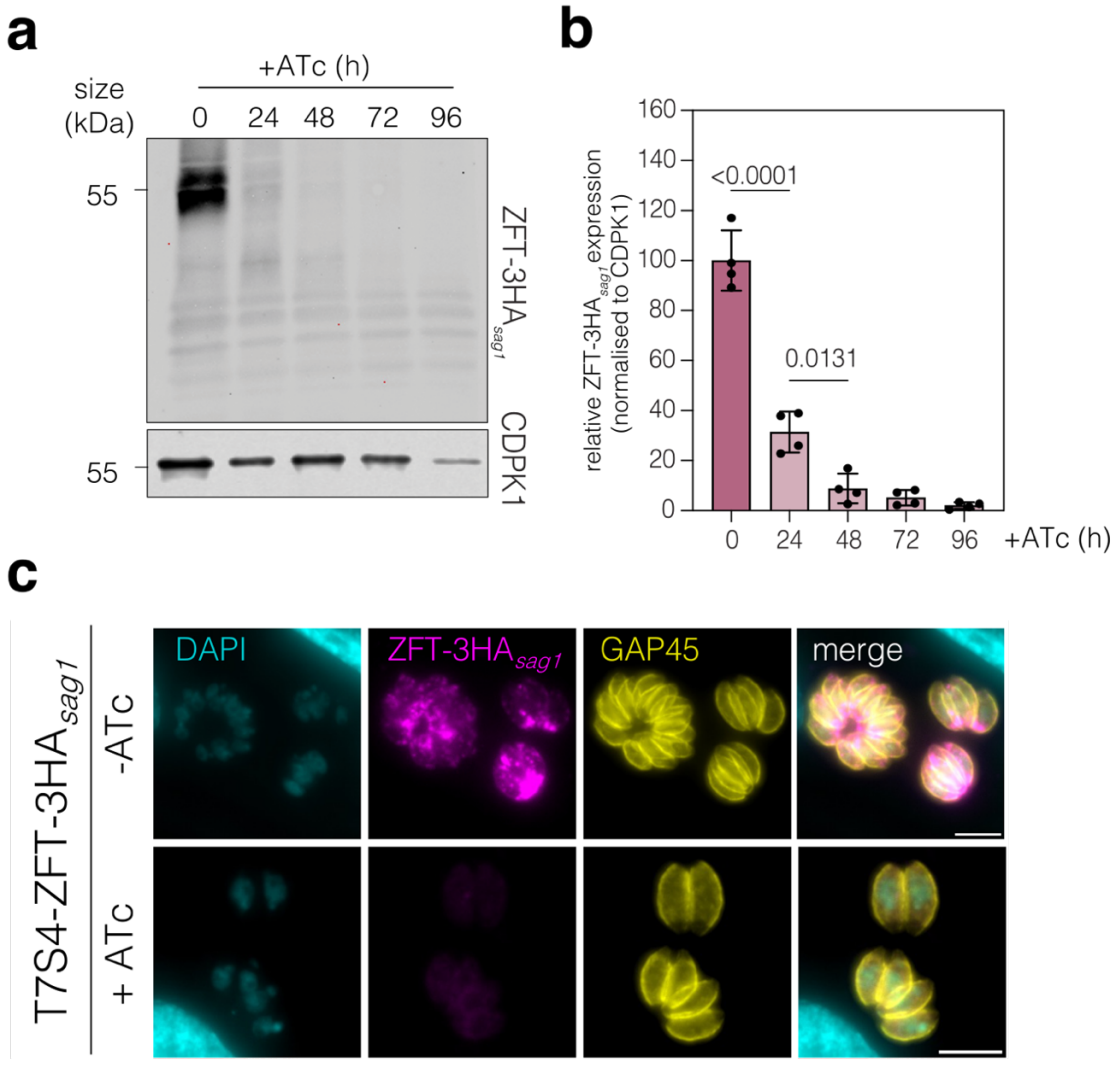


Figure 3.28 - Validation of ZFT knockdown in the F3ΔHX T7S4-ZFT-3HA$_{sag1}$ line by western blotting and immunofluorescence.

a. Western blot analysis confirming successful knockdown of ZFT at 24, 48, 72 and 96 h post induction with ATc. CDPK1 used as a loading control. **b.** Quantification of ZFT-3HA$_{sag1}$ expression levels following knockdown relative to 0 h ATc, normalised to CDPK1. Bars at mean of four independent biological experiments, ± SD. p values from two-way ANOVA, Tukey corrected for multiple comparisons. **c.** immunofluorescence assay showing ZFT-3HA$_{sag1}$ expression in untreated parasites and parasites induced with ATc for 48 h to knock ZFT down. Scale bar 5 µm.

3.13 ZFT forms a complex under native conditions

Studies in bacteria and eukaryotes have previously suggested that ZIPs function either as homodimers or heterodimers (Ahern et al., 2020; Bin et al., 2011; Lin et al., 2011; Taylor et al., 2016). To examine whether ZFT-3HA$_{sag1}$ forms a complex under native conditions in *Toxoplasma gondii*, a Blue native PAGE (BN-PAGE) was performed, and results show that ZFT-3HA$_{sag1}$ forms a complex of approximately 100 kDa. This complex is then lost upon 48 h knockdown, suggesting that ZFT forms a dimer (Figure 3.29).

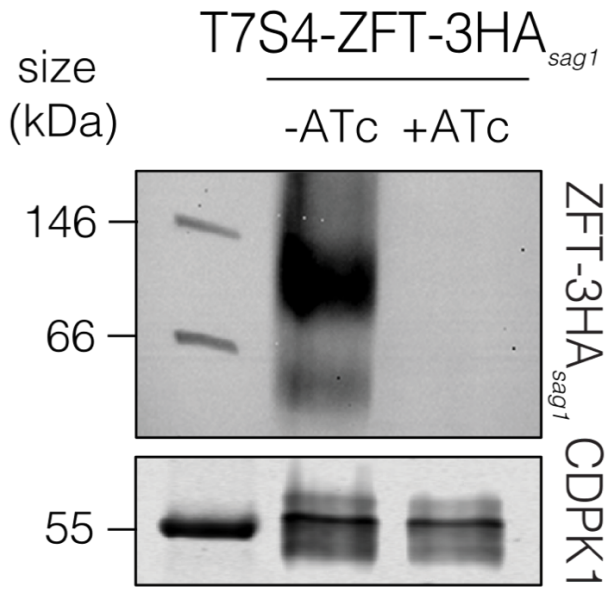


Figure 3.29 – T7S4-ZFT-3HA$_{sag1}$ forms a complex under native conditions.

Blue native PAGE (BN-PAGE) of F3ΔHX T7S4-ZFT-3HA$_{sag1}$ with and without ATc induction for 48 h demonstrating a ZFT-3HA$_{sag1}$ complex at around 100 kDa. CDPK1 used as a loading control. Representative of two independent biological experiments.

3.14 ZFT knockdown alters apicoplast morphology and parasite replication, however function is maintained

Iron plays an important role in the apicoplast of *Toxoplasma gondii* (Maclean et al., 2024; Pamukcu et al., 2021; Renaud et al., 2022), and the disruption of organellar function often leads to morphological changes of the organelle (Jacot et al., 2013; Sanchez et al., 2025). To assess if knockdown of ZFT affects the morphology of the apicoplast, an immunofluorescence assay was performed on T7S4-ZFT knockdown parasites in the absence and presence of ATc for 24 and 48 h to induce ZFT knockdown. Parasites were then stained with an anti-SAG1 antibody and an anti-CPN60 antibody. CPN60, or chaperonin 60, is an essential protein in the apicoplast which is nuclear encoded. It functions as part of a larger chaperone complex and plays a vital role in maintaining protein stability and protein folding, ensuring proper organellar function. CPN60 is targeted to the apicoplast by a bipartite signal which is then cleaved during its import into the organelle (Agrawal et al., 2009). I saw no clear morphological defects in the parasite's apicoplast under these conditions following ZFT knockdown (Figure 3.30).

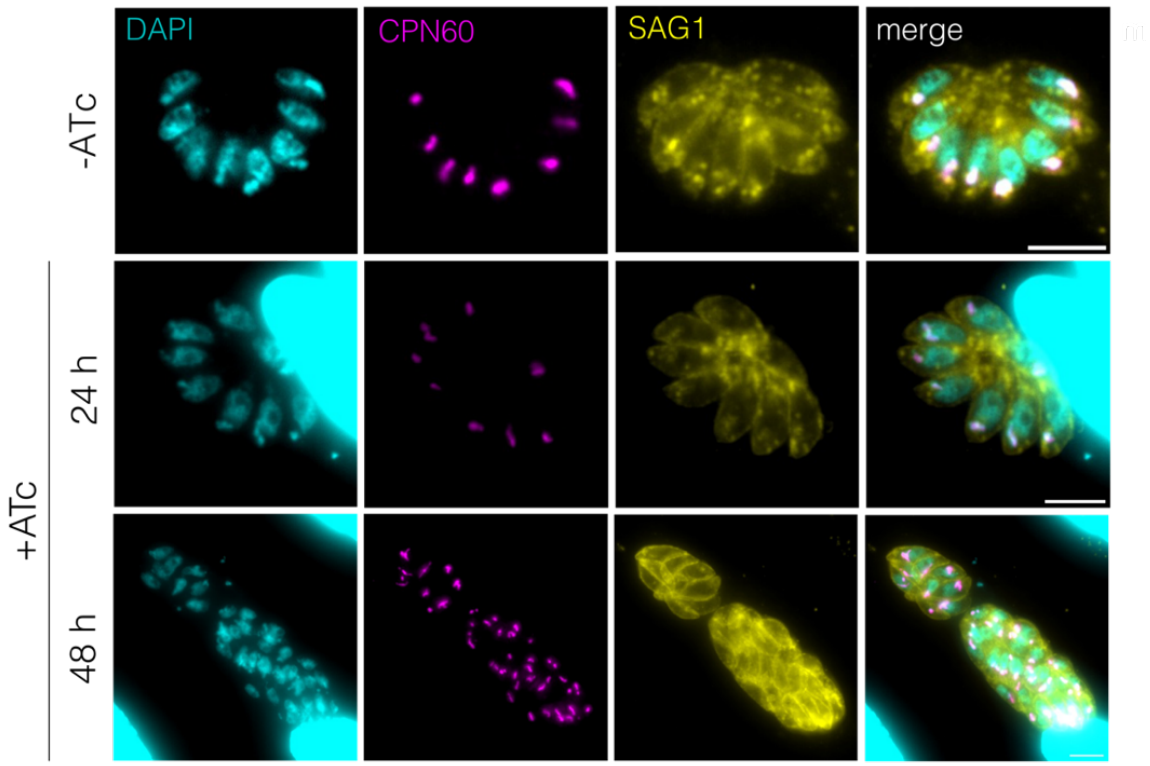


Figure 3.30 - ZFT knockdown does not alter apicoplast morphology at 24 h and 48 h.

Immunofluorescence assay of T7S4-ZFT parasites with and without ATc for 24 and 48 h, staining for CPN60 (apicoplast marker) and SAG1, showing no clear morphological apicoplast changes. Scale bar 5 µm.

Next, to assess whether there is a functional defect in the apicoplast following knockdown of ZFT, the processing of CPN60 was examined by western blotting following 48 h of ATc induction. No change was observed in CPN60 processing post ZFT depletion, with both the pre-processed (p) and mature (m) forms of CPN60 detected (Figure 3.31a). To further determine if there is an apicoplast functional defect, protein lipoylation was examined. The apicoplast in *T. gondii* contains the protein LipA, an essential Fe-S cluster protein which is essential for lipoylation and modification of the E2 subunits of the apicoplast localised enzyme pyruvate dehydrogenase (PDH-E2) (Crawford et al., 2006; Pamukcu et al., 2021). The enzyme PDH is essential for the conversion of pyruvate to acetyl-CoA, which is then further utilized for fatty acid biosynthesis in the apicoplast. To examine protein lipoylation in the parasite, a western blot was performed on T7S4-ZFT parasites with and without ATc 48 h using an anti-lipoic acid antibody. Lipoylated TgPDH-E2 was detected 48 h post ZFT knockdown (Figure 3.31b), and no significant change in TgPDH-E2 lipoylation was observed (Figure 3.31c). This data suggests that at the time point following the knockdown of ZFT, the apicoplast function is maintained in *T. gondii*.

Two mitochondrially-localised lipoylated enzymes were also detected, 2-oxo-glutarate dehydrogenase (TgOGDH-E2) and branched-chain 2-oxo acid dehydrogenase-E2 (TgBCDH-E2) (Figure 3.31b). TgOGDH is predicted to be an essential enzyme for *T. gondii* and functions in providing a precursor of the haem biosynthetic pathway, succinyl-CoA, and TgBCDH is an essential enzyme involved in the breakdown of branched-chain amino acids including valine, leucine, and isoleucine. Lipoylation of enzymes in the mitochondria occurs via the scavenging of lipoic acid in an iron-independent mechanism (Crawford et al., 2006). Although the lipoylation of TgOGDH-E2 was not significantly altered following the knockdown of ZFT (Figure 3.31d), interestingly, the lipoylation of TgBCDH-E2 significantly (p = 0.027, two tailed unpaired t test) increased upon the depletion of ZFT (Figure 3.31e).

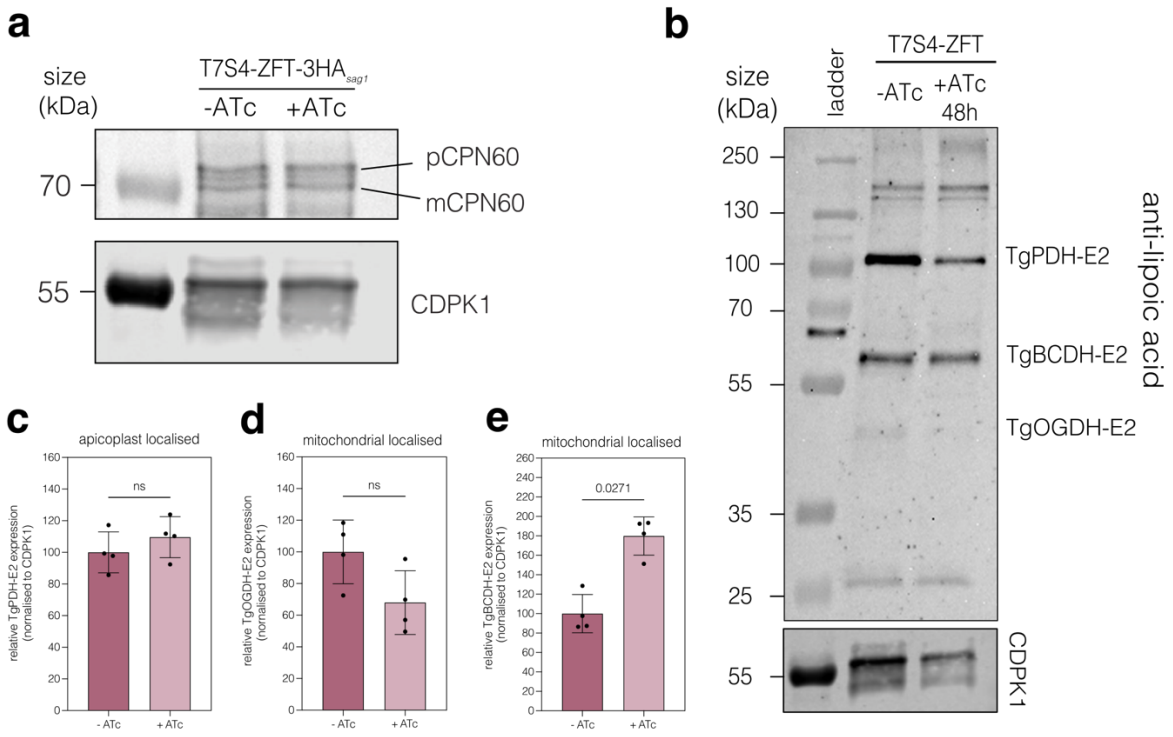


Figure 3.31 - ZFT knockdown parasites maintain apicoplast function at 48 h.

a. Western blot demonstrating both pre-processed (p) and mature (m) forms of CPN60 48 h post ZFT knockdown in the T7S4-ZFT-3HA$_{sag1}$ line. CDPK1 used as a loading control. **b.** Western blot of anti-lipoic acid in T7S4-ZFT parasites demonstrating the presence of both TgPDH-E2 and TgOGDH-E2 in induced conditions, suggesting apicoplast function is maintained following ZFT knockdown. Quantification of TgPDH-E2 **(c)**, TgOGDH-E2 **(d)** and TgBCDH-E2 **(e)** expression relative to untreated normalised to CDPK1 following knockdown of ZFT 48 h. Bars represent the mean of four independent experiments, ± SD. *p* values are two-tailed paired *t* test.

To further determine whether ZFT knockdown parasites experience a delayed phenotype, I performed another immunofluorescence assay where the parasites were treated with ATc for 24 h, before mechanically releasing them and allowing them to reinvade new host cells under ATc conditions for a further 24 h (Figure 3.32a). The parasites were fixed and stained as before and apicoplast morphology was assessed by counting 100 vacuoles per condition and determining whether the apicoplast appeared normal or elongated in morphology. The data shows that ZFT knockdown parasites have slightly, but significantly (p = 0.04, two-way ANOVA with Tukey correction) more elongated apicoplast (Figure 3.32b). In addition to the apicoplast morphological defects under these conditions, I also observe a defect in parasite replication by examining the number of parasites/vacuole. I found a significant (p < 0.0054 at the 1, 2, 4 and 8 parasites/vacuole, two-way

ANOVA with Šidák correction) decrease in the number of parasites per vacuole after induction of ZFT knockdown with ATc in the second round of invasion, with more than 80 % of the vacuoles having 1 or 2 vacuoles, compared to approximately 30 % in untreated conditions (Figure 3.32c). These data suggest that ZFT knockdown alters apicoplast morphology and parasite replication after a further round of mechanical release and invasion.

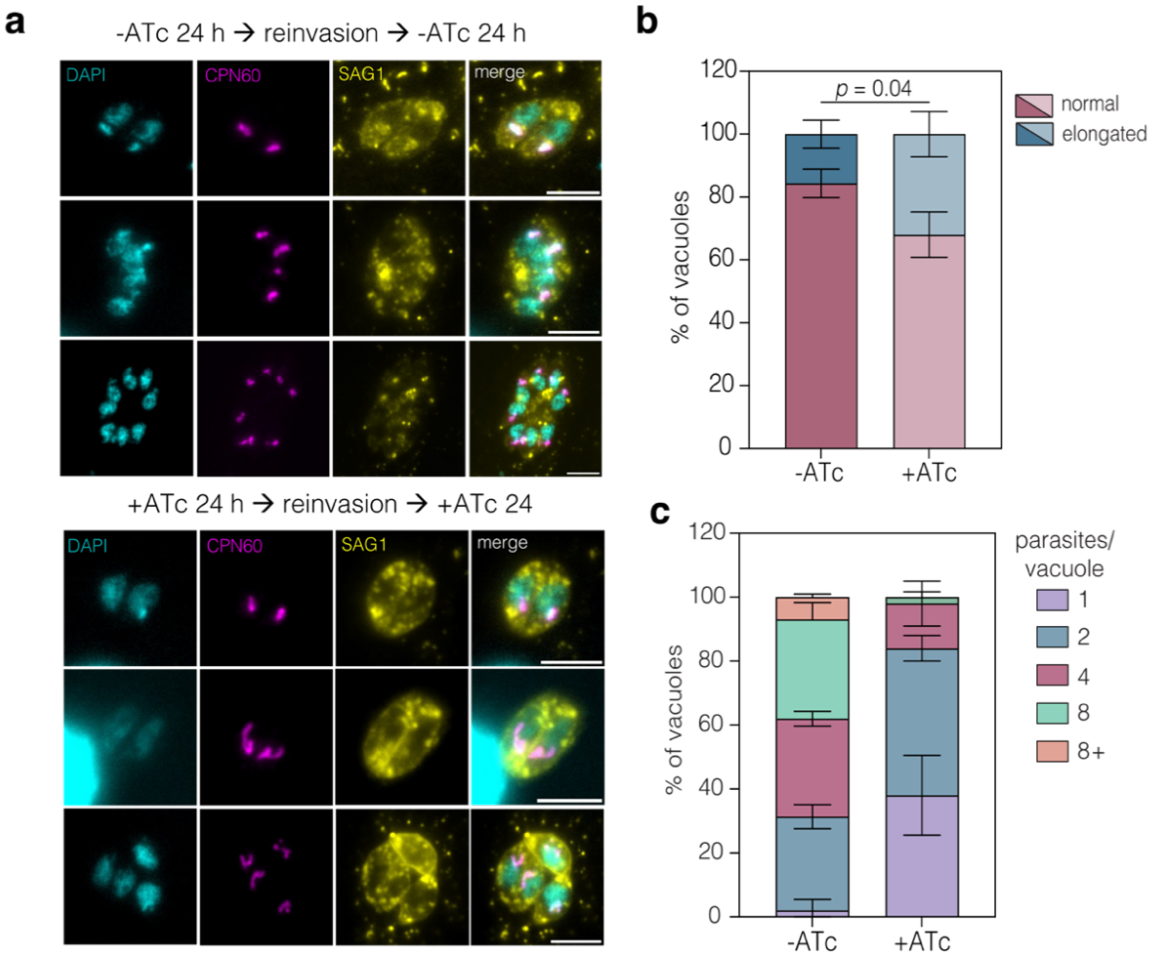


Figure 3.32 – Parasites exhibit a delayed apicoplast phenotype following ZFT knockdown by altering apicoplast morphology and parasite replication.

a. Immunofluorescence assay of T7S4-ZFT parasites following ATc treatment for 24 h, mechanical release and invasion for a further 24 h under ATc conditions. Parasites stained with CPN60 (apicoplast marker) and SAG1. Scale bar 5 µm. **b.** Quantification of % of T7S4-ZFT apicoplast from (a) that appeared normal or elongated in untreated and ATc conditions. 100 vacuoles for each condition were counted. Bars are at the mean of three independent biological experiments, ± SD **c.** Quantification of the percentage of parasites/vacuole in T7S4-ZFT parasites with and without ATc for 48 h following mechanical release and invasion. 100 vacuoles for each condition were counted. Bars at mean of three independent biological experiments, ± SD.

3.15 ZFT knockdown alters mitochondrial organellar function

Iron serves as a cofactor for several enzymes involved in energy production within the parasite, particularly within the electron transport chain in the mitochondria (Maclean et al., 2021). Iron serves as the central molecule in haem, and haem bound proteins have numerous essential roles in the electron transport chain and energy generation. I was therefore curious to assess whether the phenotype observed following ZFT knockdown was due to any changes in mitochondrial organelle morphology, as well as mitochondrial respiration. To assess whether knockdown of ZFT influences gross mitochondrial morphology, an immunofluorescence assay was performed on T7S4-ZFT parasites with and without ATc for 24 h and 48 h, staining for TOM40, a protein on the outer membrane of the mitochondria, and imaged by light microscopy. After both 24 and 48 h ATc, I saw no gross morphological defects in the mitochondria (Figure 3.33).

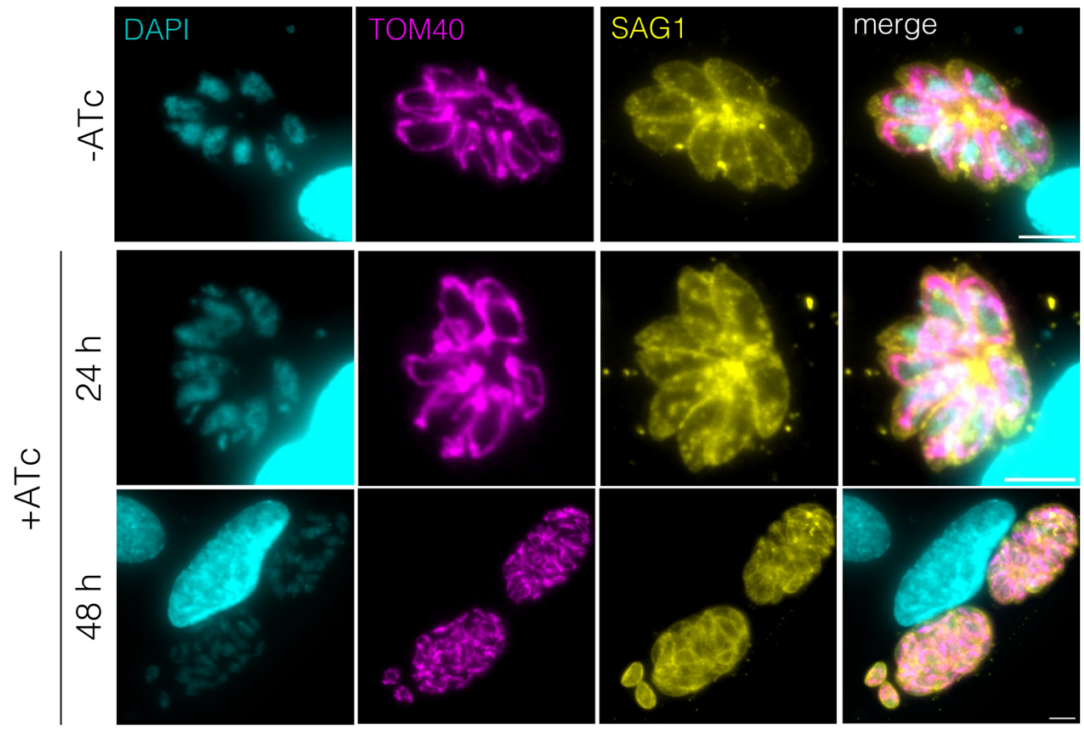


Figure 3.33 - ZFT knockdown parasites show no changes in mitochondrial morphology.

Immunofluorescence assay of T7S4-ZFT parasites with and without ATc for 24 and 48 h, staining for TOM40 (mitochondrial marker) and SAG1 showing no clear mitochondrial morphological changes. Scale bar 5 μm.

3.16 ZFT knockdown reduces expression of mitochondrial Fe-S cluster protein SDHB

Iron is also incorporated in Fe-S cluster proteins, which are found in the electron transport chain and the TCA cycle in the mitochondria where they play an important role in energy production. To assess the effect of ZFT depletion on the expression of Fe-S cluster proteins in the mitochondria, I tagged the key mitochondrial protein succinate dehydrogenase (SDHB) (TGME49_215280) with a 3xHA epitope tag in the T7S4-ZFT background (Figure 3.34a). SDHB has essential roles in the TCA cycle and in complex II of the mitochondrial electron transport chain and contains three Fe-S clusters (Maclean et al., 2021; Silva et al., 2023). Successful tagging of SDHB in the T7S4-ZFT background was validated by PCR (Figure 3.34b). To assess SDHB-3HA expression levels following the knockdown of ZFT, I treated the parasites with ATc for 48 h to induce ZFT knockdown and then performed western blot analysis to quantify protein levels. Upon depletion of ZFT, SDHB-3HA expression levels are significantly (p = 0.0205, two-tailed paired t-test) reduced to around 34 %, compared to untreated parasites (Figure 3.34c, d).

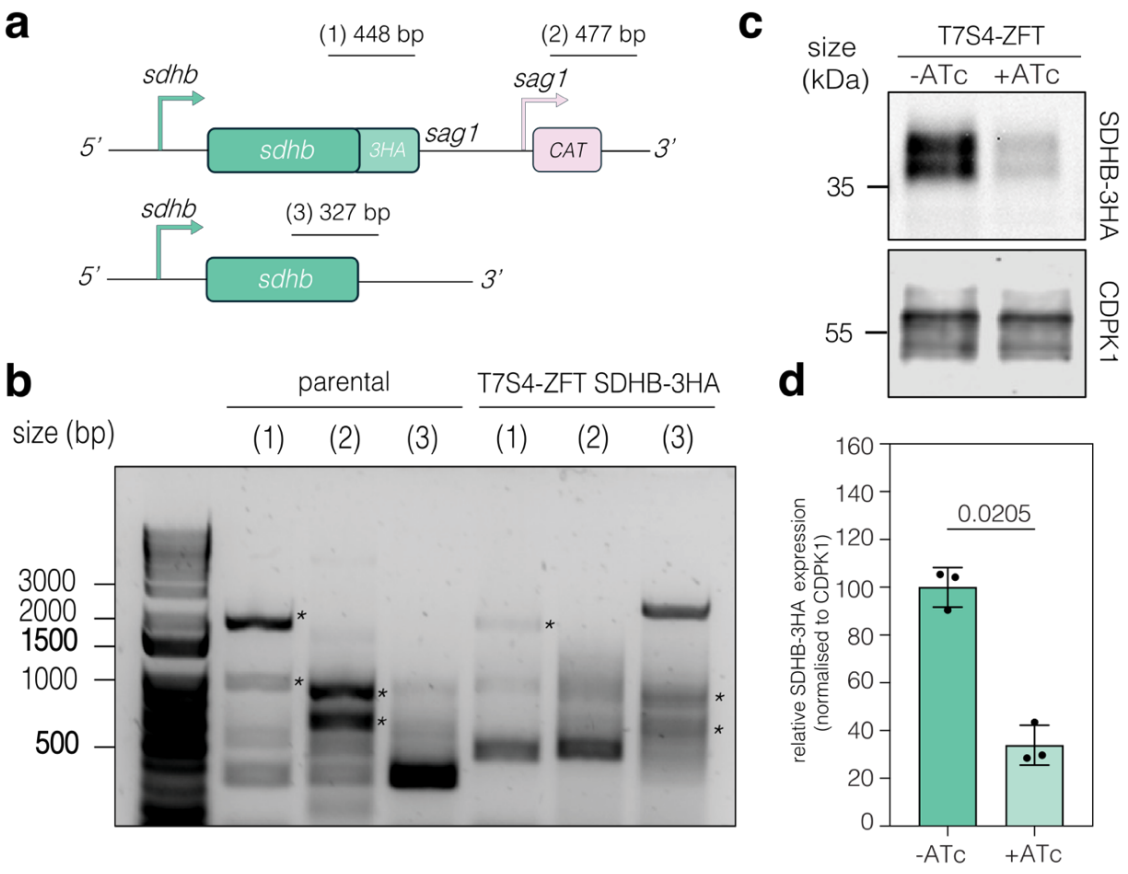


Figure 3.34 Fe-S cluster protein SDHB expression is significantly reduced in ZFT knockdown parasites.

a. Schematic of F3ΔHX T7S4-ZFT SDHB-3HA strain construction to endogenously tag SDHB with 3xHA epitope tags at the C-terminal under the endogenous promoter in the T7S4-ZFT background. **b.** PCR validating successful integration of the 3xHA epitope tag and the CAT selection cassette into the endogenous locus in the T7S4-ZFT SDHB-3HA line. (1) represents the 5' integration, (2) represents the 3' integration and (3) represents the endogenous locus. Non-specific bands marked with asterisks. **c.** Western blot of T7S4-ZFT SDHB-3HA in the absence and presence of ATc 48 h. CDPK1 used as a loading control. **d.** Quantification of SDHB-HA expression relative to untreated normalised to CDPK1 following knockdown of ZFT. Bars represent the mean of three independent experiments, ± SD. *p* values are two-tailed paired *t* test.

As a control, an essential cytosolic Fe-S cluster protein, ABCE1 (TGME49_216790) (Barthelme et al., 2007; Maclean et al., 2024; Renaud et al., 2025), was also tagged with a 3xHA epitope tag in the T7S4-ZFT background (Figure 3.35a). Successful tagging of ABCE1 in the T7S4-ZFT background was validated by PCR (Figure 3.35b). To assess ABCE1-3HA expression levels following the knockdown of ZFT, I treated the parasites with ATc for 48 h to induce ZFT knockdown and then performed western blot analysis to quantify protein levels. Interestingly, I found that ABCE-1 expression levels remain unchanged following the knockdown of ZFT (p = 0.1758, two-tailed paired t-test) compared to untreated parasites (Figure 3.35c, d).

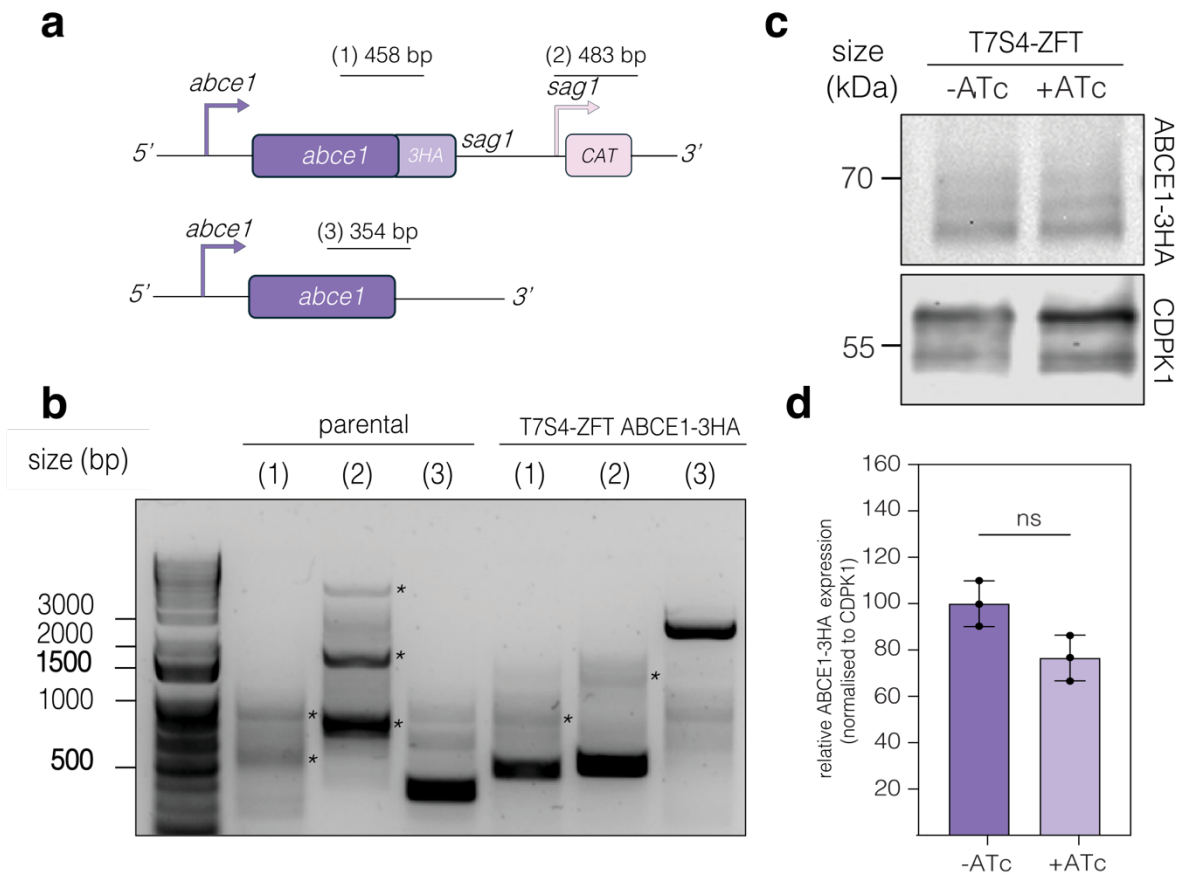


Figure 3.35 - Cytosolic Fe-S cluster protein ABCE1 expression levels remain unchanged following ZFT knockdown.

a. Schematic of F3ΔHX T7S4-ZFT ABCE1-3HA strain construction to endogenously tag ABCE1 with 3xHA epitope tags at the C-terminal under the endogenous promoter in the T7S4-ZFT background. **b.** PCR validating successful integration of the 3xHA epitope tag and the CAT selection cassette into the endogenous locus in the T7S4-ZFT ABCE1-3HA line. (1) represents the 5' integration, (2) represents the 3' integration and (3) represents the endogenous locus. Non-specific bands marked with asterisks. **c.** Western blot of T7S4-ZFT ABCE1-3HA in the absence and presence of ATc 48 h. CDPK1 used as a loading control. **d.** Quantification of ABCE1-HA expression relative to untreated normalised to CDPK1 following knockdown of ZFT. Bars represent the mean of three independent experiments, ± SD. *p* values are two-tailed paired *t* test.

As the expression of SDHB, a component of complex II in the mitochondrial electron transport chain was significantly reduced, I aimed to further assess the effects of ZFT knockdown on the mitochondrial electron transport chain, by examining the activity of complex IV by an in gel activity assay (Lacombe et al., 2019; Silva et al., 2023). Complex IV of the electron transport chain is predicted to contain both Fe-S proteins and haemoproteins (Leonard et al., 2023). The data demonstrates that 48 h post ATc induction, ZFT knockdown parasites have reduced complex IV activity (Figure 3.36).

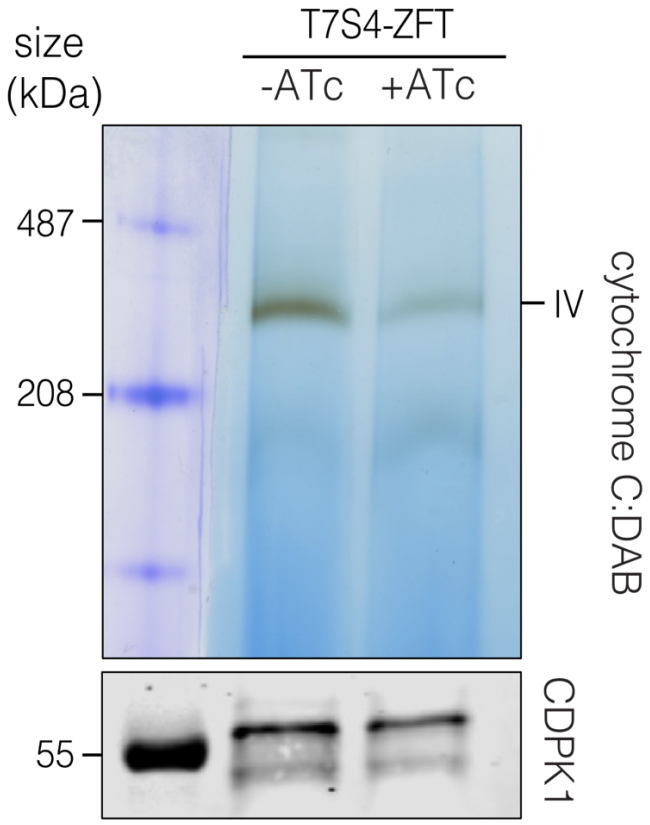


Figure 3.36 - ZFT knockdown parasites have reduced complex IV activity.

Complex IV in gel activity assay of T7S4-ZFT parasites with and without ATc 48 h, showing that ZFT knockdown parasites have reduced complex IV activity. CDPK1 used as a loading control. Representative of four independent biological experiments.

3.17 ZFT knockdown reduces mitochondrial respiration at 48 h

The reduction of SDHB expression levels, a component of complex II, and depletion of complex IV activity following ZFT knockdown, may result in changes in mitochondrial respiration. In other organisms, iron deprivation can result in mitochondrial respiration defects which can be assessed by quantifying the oxygen consumption rate using a Seahorse assay (Hayward et al., 2022) (Figure 3.37a, b). In the first 20 minutes, the basal mitochondrial oxygen consumption rate (mOCR) is measured. FCCP is then added, which uncouples the proton gradient across the inner mitochondrial membrane thus uncoupling electron transport from ATP synthesis and allowing protons to freely cross the inner mitochondrial membrane, allowing measurement of the maximal respiratory capacity of the parasite. Atovaquone, a complex III inhibitor, is then added which blocks the electron transport chain, allowing the measurement of mitochondrial oxygen consumption rate that is electron transport chain dependent. The spare capacity is the difference between the maximal and basal mOCR. Extracellular acidification rate (ECAR) is also measured and can be used to interpret a measure of glycolytic activity. This is because protons are dissociated from lactic acid to form lactate, an end product of glycolysis, thereby acidifying the medium.

24 h following ZFT knockdown, no significant changes were observed in basal (Figure 3.37b) or maximal (Figure 3.37c) mOCR. Furthermore, there was no significant change in basal ECAR following ZFT knockdown (Figure 3.37d). The metabolic map suggests that 24 h post knockdown of ZFT does not make the parasites more or less glycolytic than untreated parasites (Figure 3.37e).

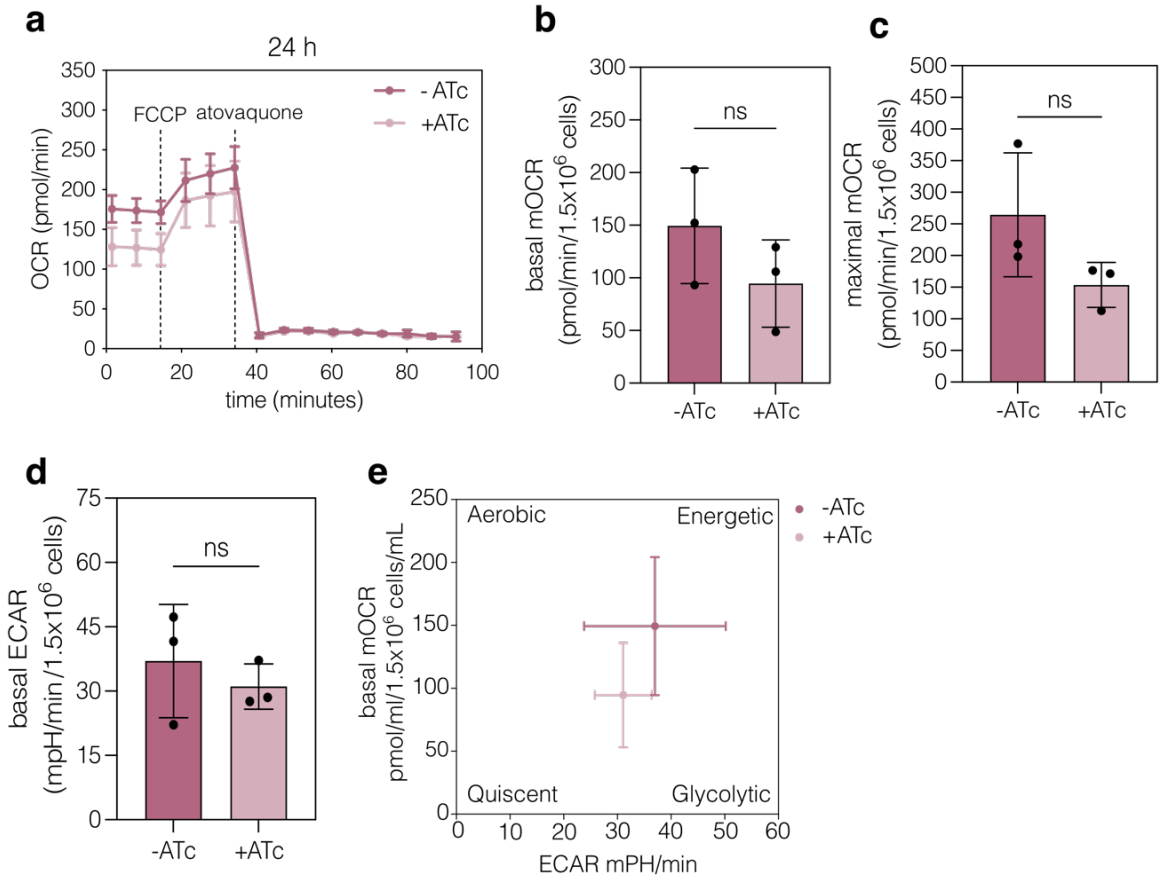


Figure 3.37 - ZFT knockdown does not alter mitochondrial respiration at 24 h.

a. Trace of mitochondrial oxygen consumption rate (mOCR) of T7S4-ZFT in the absence or presence of ATc for 24 h via Seahorse assay. Quantification of basal mOCR showing that ZFT knockdown does not significantly change basal mOCR **(b)**, maximal mOCR **(c),** or basal ECAR **(d)** compared to untreated parasites. Bars represent the mean of three independent experiments, ± SD. *p* values are from two-tailed unpaired t test with Welch's correction. **e.** Metabolic map demonstrating that knocking down ZFT does not make the parasites more or less glycolytic compared to untreated parasites. Points are at the mean of three independent biological experiments, ± SD.

As there is still approximately 30 % of ZFT protein remaining at 24 h following ZFT knockdown, I was next interested to assess mitochondrial respiration 48 h post ZFT knockdown, as at this timepoint only approximately 10 % of ZFT protein remains. A representative seahorse trace for T7S4-ZFT parasites 48 h upon ZFT knockdown is shown in Figure 3.38a. At 48 h post ZFT knockdown, I found reduced basal mitochondrial oxygen consumption rates (p = 0.0238, two-tailed unpaired t test with Welch's correction) (Figure 3.38b), as well as reduced maximal mitochondrial oxygen consumption rates (p = 0.0054, two-tailed unpaired t test with Welch's correction) (Figure 3.38c), compared to untreated parasites. Interestingly, I found that knocking down ZFT does not significantly change the

extracellular acidification rate (ECAR), a proxy for glycolysis (Figure 3.38d). The metabolic map suggests that knocking down ZFT for 48 h renders the parasites less glycolytic and having a more quiescent phenotype than untreated parasites. It also demonstrates that ZFT knockdown leads to a reduction in oxidative phosphorylation (Figure 3.38e).

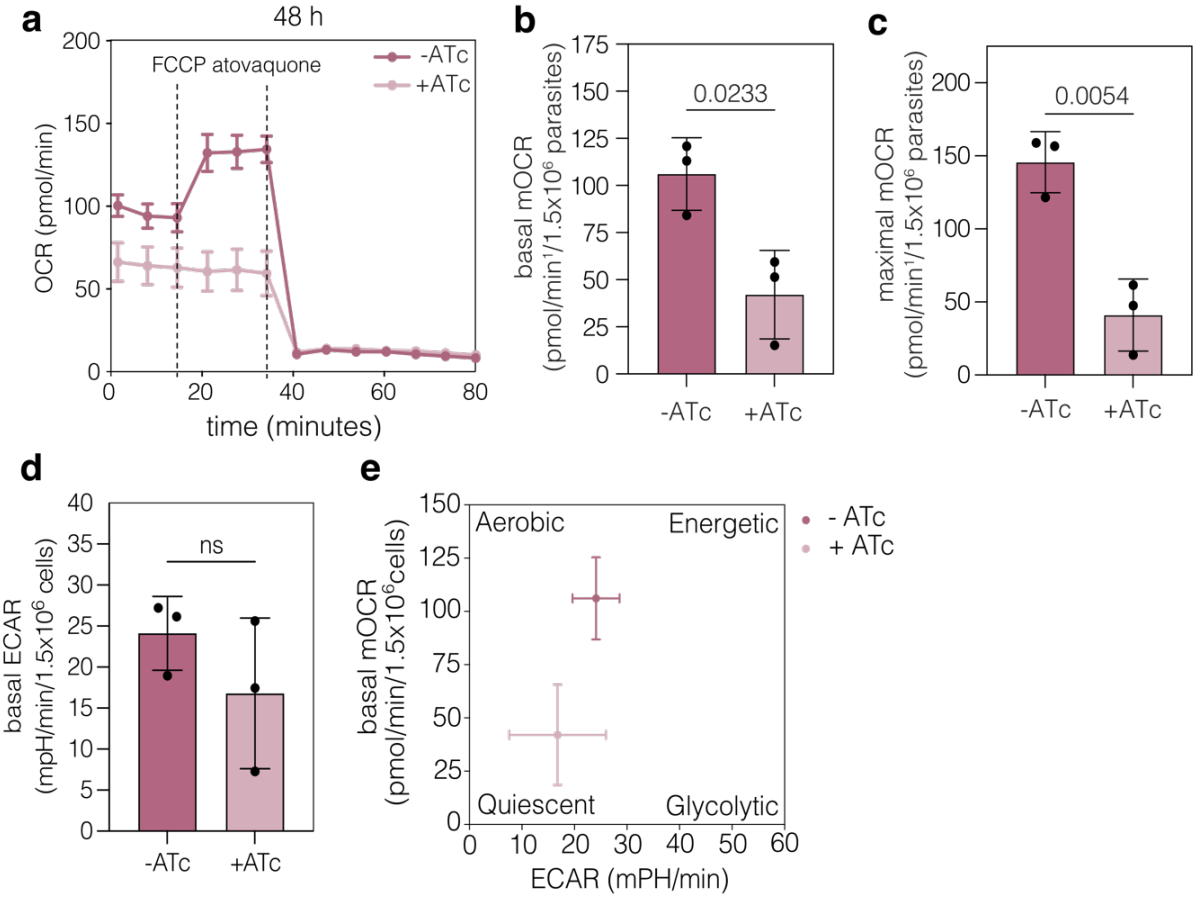


Figure 3.38 - ZFT knockdown reduces mitochondrial respiration at 48 h.

a. Trace of mitochondrial oxygen consumption rate (mOCR) of T7S4-ZFT in the absence or presence of ATc for 48 h via Seahorse assay. Quantification of basal mOCR showing that ZFT knockdown results in a significant decrease in basal mOCR **(b)** and maximal mOCR **(c)** compared to untreated parasites. Bars represent the mean of three independent experiments, ± SD. *p* values are from two-tailed unpaired *t* test with Welch's correction. **d.** Quantification of basal extracellular acidification rate (ECAR) showing no significant change upon ZFT knockdown. Bars represent the mean of three independent experiments, ± SD. *p* values are from two-tailed unpaired *t* test with Welch's correction. **e.** Metabolic map demonstrating that knocking down ZFT leads to more quiescent parasites with less oxidative phosphorylation. Points are at the mean of three independent biological experiments, ± SD.

Previous studies have linked changes in mitochondrial respiration with changes in the formation and morphology of mitochondrial cristae (Baker et al., 2019; Huet et al., 2018). Cristae formation was examined in more detail by transmission electron microscopy (TEM) imaging 72 h post ATc induction to knock ZFT down. This work was done by Cecilia Gallego Rubio, and images were taken and processed by Dr. Leandro Lemgruber Soares. We saw no clear defects in the morphology or cristae formation in ZFT knockdown parasites compared to untreated parasites (Figure 3.39).

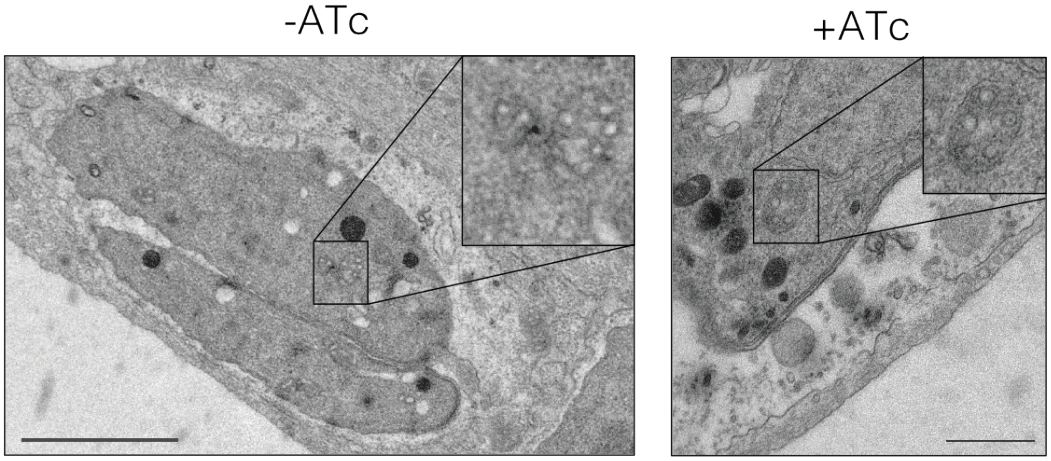


Figure 3.39 - ZFT knockdown does not affect mitochondrial cristae formation.

TEM of T7S4-ZFT parasites with and without ATc induction for 72 h, showing no alterations in mitochondrial cristae formation following ZFT knockdown. Scale bar = 2 µM and 500 nM respectively.

These data demonstrate that ZFT knockdown reduces mitochondrial respiration rates in the parasite, although morphologically the organelle seems to be unaffected. The data also shows that knocking down ZFT results in a significant reduction in the expression of the Fe-S cluster protein SDHB, while ABCE1 remains unaffected.

3.18 ZFT knockdown triggers partial parasite differentiation

To further examine the effects of knocking down ZFT, parasite replication was examined by immunofluorescence, counting the number of parasites per vacuole. At 48 h post ATc induction, parasite replication did not appear to be inhibited following ZFT knockdown (Figure 3.40a). However, large vacuoles were observed, containing many nuclei. These large vacuoles did not appear to egress from the host cell monolayer. Upon ZFT knockdown at 48 h, there is a significant (p < 0.0001, two-way ANOVA with Tukey correction) increase in vacuoles (~50 %) which appeared to be disorganised, losing their vacuolar organisation (Figure 3.40b). Cecilia Gallego Rubio performed this quantification. Moreover, asynchronous replication was frequently observed, with vacuoles only containing single parasites with daughter cell scaffolds (Figure 3.40a, inset).

I examined this phenotype further. One life cycle stage in *T. gondii* where the parasites no longer grow synchronously and lose their organisation within the vacuole are bradyzoites – these parasites are cyst forming, persist in tissues, grow slowly, and lose tachyzoite specific markers such as SAG1. To examine the effect of loss of ZFT in more detail, transmission electron microscopy (TEM) was performed. To do so, T7S4-ZFT parasites were treated in the presence and absence of ATc for five days to induce the knockdown of ZFT and the parasites were visualised by TEM. Samples were processed and images were taken by Dr. Leandro Lemgruber Soares.

Although no obvious morphological changes were observed upon ZFT knockdown, I observed a heavily vesiculated PVM and the accumulation of small vesicles in close proximity in the intravacuolar space. This is different from untreated parasites, where a smooth PVM is observed with no accumulation of vesicles (Figure 3.40c). Furthermore, upon ZFT knockdown, a number of enlarged electron-lucent vesicles are also observed, which were not present in untreated cells (Figure 3.40c). Such large vesicles have previously been reported to contain materials that form the cyst wall (Tomita et al., 2013), a characteristic of *Toxoplasma gondii* transitioning from tachyzoites to bradyzoites.

Previous studies have shown that iron depletion can be sufficient to drive the conversion of tachyzoites to bradyzoites (Renaud et al., 2024; Sloan et al., 2025; Ying et al., 2024). I was thus intrigued to assess whether the depletion of iron itself could be sufficient to trigger this differentiation phenotype of tachyzoites to bradyzoites. To examine this, Dr. Clare Harding treated parental parasites with the iron chelator, DFO, for 5 days before fixing and imaging by TEM, performed and processed by Dr. Leandro Lemgruber Soares. Similarly to ZFT knockdown parasites, parental parasites also exhibit similar large vesicles in close proximity to the PVM when iron is depleted (Figure 3.40d), suggesting that iron depletion also triggers this differentiation from tachyzoite to bradyzoite parasites.

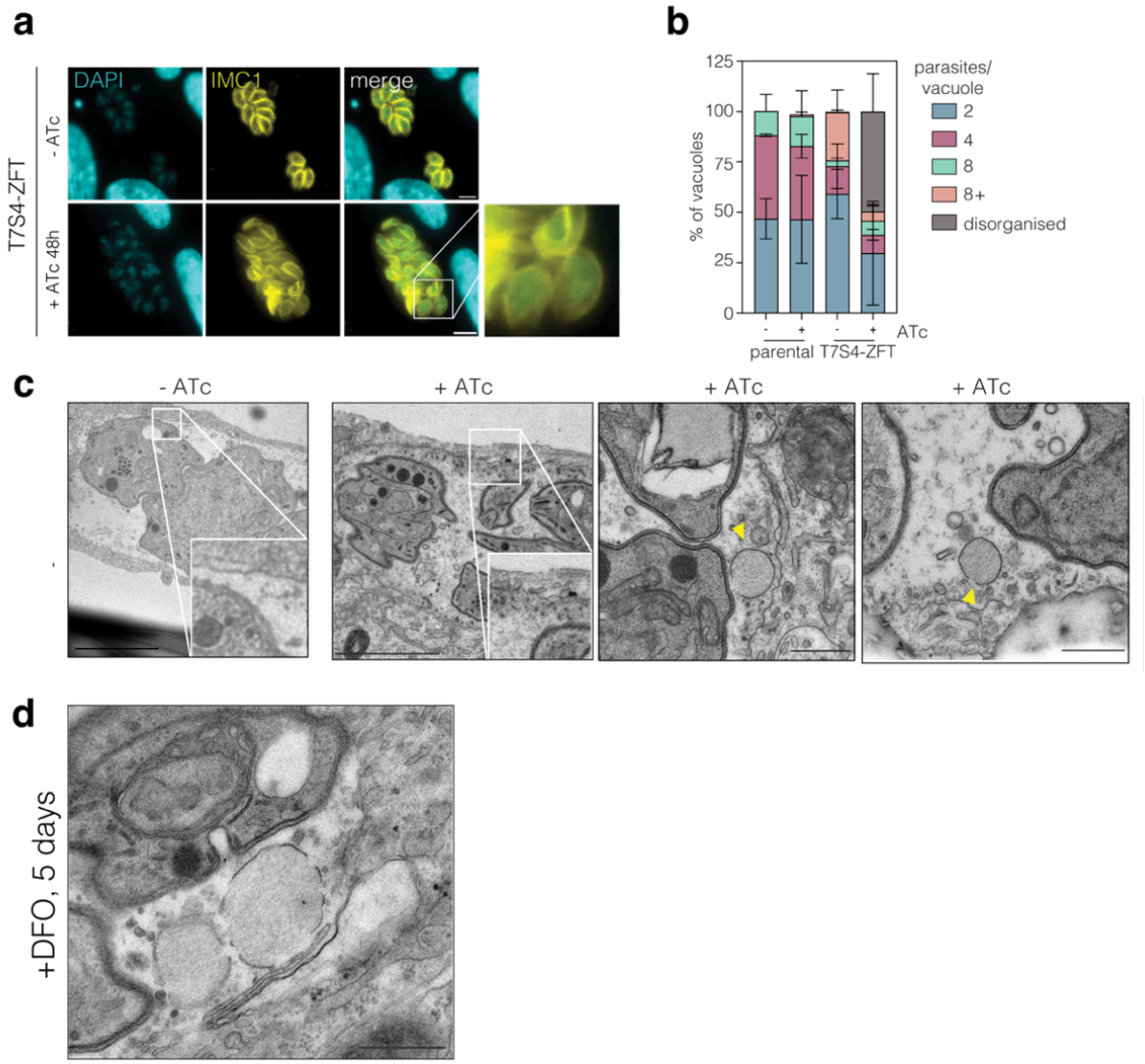


Figure 3.40 - ZFT knockdown parasites exhibit asynchronous replication and large disorganised vacuoles.

a. Immunofluorescence assay of T7S4-ZFT parasites with and without ATc induction for 48 h. Parasites stained for IMC1. Inset highlights a region where the parasites are disorganised and asynchronously replicating within the vacuole upon ZFT knockdown. Scale bar 5µm. **b.** Quantification of number of parasites/vacuole in parental and T7S4-ZFT parasites with and without ATc for 48 h. 100 vacuoles for each condition were counted. Bars represent the mean of four independent replicates, ± SD. **c.** TEM microscopy images of T7S4-ZFT parasites untreated and ATc induced for 5 days. Highlighted regions detail regions of the PVM. Yellow arrows indicate large electron-lucent vesicles in the parasitophorous vacuolar space. Scale bar 500 nm. **d.** Immuno-electron microscopy of parental parasites treated with the iron chelator, DFO for 5 days, indicating enlarged vesicles in the parasites close to the PV space. Scale bar 500 nm.

To further determine if depleting ZFT is sufficient to induce tachyzoite to bradyzoite stage conversion, the expression of bradyzoite specific markers upon the knockdown of ZFT was examined. To do so, an immunofluorescence assay was performed on T7S4-ZFT parasites in the absence and presence of ATc at 48 h and 96 h respectively. The parasites were stained with SAG1 antibody, a tachyzoite specific marker, BAG1 antibody, a bradyzoite specific protein marker (Kannan et al., 2019) and DBL, a lectin which binds to the heavily glycosylated cyst wall of the parasites (Tomita et al., 2013). At 72 h post ZFT knockdown, BAG1 expression was observed in some vacuoles (Figure 3.41a), and at 96 h post ZFT knockdown, vacuoles with DBL staining the periphery of the vacuoles was observed (Figure 3.41b).

The percentage of vacuoles expressing BAG1, DBL and SAG1 was then quantified by counting the number of vacuoles expressing these markers in 100 vacuoles for each condition. This work was performed by Miguel Cortijo Martinez, under my supervision. The data shows significantly higher percentage of vacuoles expressing BAG1 (p = 0.0013, two-way ANOVA, Tukey corrected for multiple comparisons) (Figure 3.41c) and DBL (p = 0.0001, two-way ANOVA, Tukey corrected for multiple comparisons) (Figure 3.41d) upon ZFT knockdown, compared to untreated parasites. However, the data further demonstrates that SAG1 expression was not significantly altered in ZFT knockdown parasites compared to the untreated parasites (Figure 3.41e).

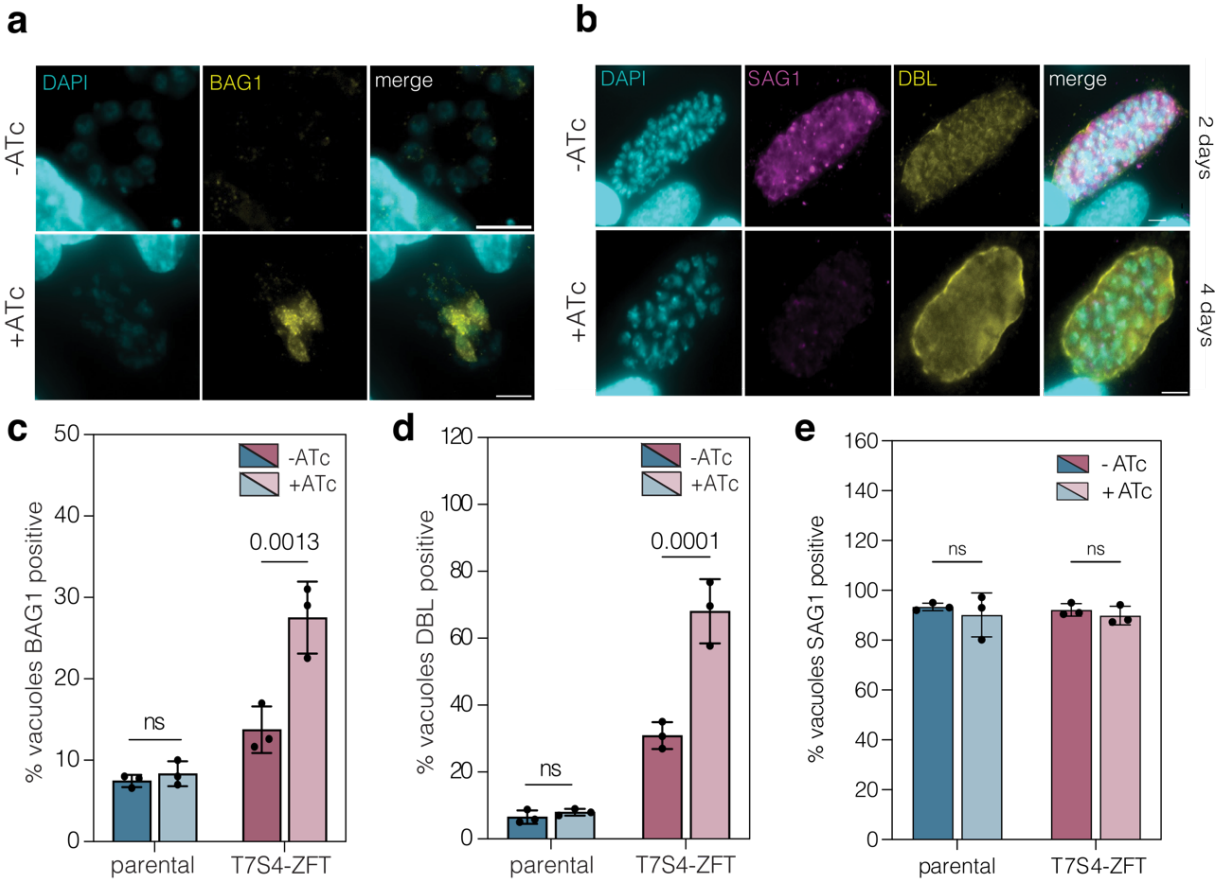


Figure 3.41 - ZFT depletion increases expression of bradyzoite specific marker BAG1 and DBL, a lectin that binds to the cyst wall.

a. Immunofluorescence assay of T7S4-ZFT untreated without ATc for two days and with ATc for 72 h days. Parasites stained for BAG1, a bradyzoite specific marker. Scale bar 5 µm. **b.** Immunofluorescence assay of T7S4-ZFT untreated without ATc for two days and with ATc for 96 h. Parasites stained for DBL, a lectin which binds to the cyst wall of the parasite. Scale bar 5 µm. Quantification of the percent of vacuoles expressing BAG1 **(c)**, DBL **(d)** and SAG1 **(e)**. 100 vacuoles for each condition were counted. Bars are the mean of three independent biological experiments, ± SD. p values from two-way ANOVA, Tukey corrected for multiple comparisons.

These data demonstrate that loss of ZFT results in an increase in the expression of bradyzoite specific marker BAG1, as well as an increase in cyst wall production, highlighted by an increase in DBL expression. Altogether, the data suggests that the partial parasite differentiation is triggered upon the depletion of ZFT.

Previous studies have demonstrated that differentiation of *T. gondii* from tachyzoites to bradyzoites can allow the parasites to survive stresses that would otherwise be fatal. Studies have also shown that parasites are able to reactivate and convert back to tachyzoites from bradyzoites if the stress is removed (Cerutti et al., 2020; Soete et al., 1993; Sullivan and Jeffers, 2012). To assess whether parasites that initiated stage conversion after ZFT depletion actually remain viable, parasite survival was quantified by plaque assay. Parasites were treated with ATc for 72 h, then washed and incubated with DMEM in the absence of ATc and left for a further 6 days. I found that that following ATc washout, T7S4-ZFT parasites are now able to form plaques in the host cell monolayer, indicating that some parasites remained viable (Figure 3.42a).

Upon quantification, approximately 40 % of T7S4-ZFT parasites were able to reestablish growth after 72 h ZFT knockdown ($p < 0.0001$, two-tailed unpaired *t* test) (Figure 3.42b). Interestingly, this is a similar proportion to those expressing the bradyzoite marker BAG1 (Figure 3.41c). The data suggests that although parental parasites are unable to survive a transient depletion of ZFT, approximately 40 % of the vacuoles initiate the conversion and transition from tachyzoites to bradyzoites and are able to survive the transient absence of ZFT.

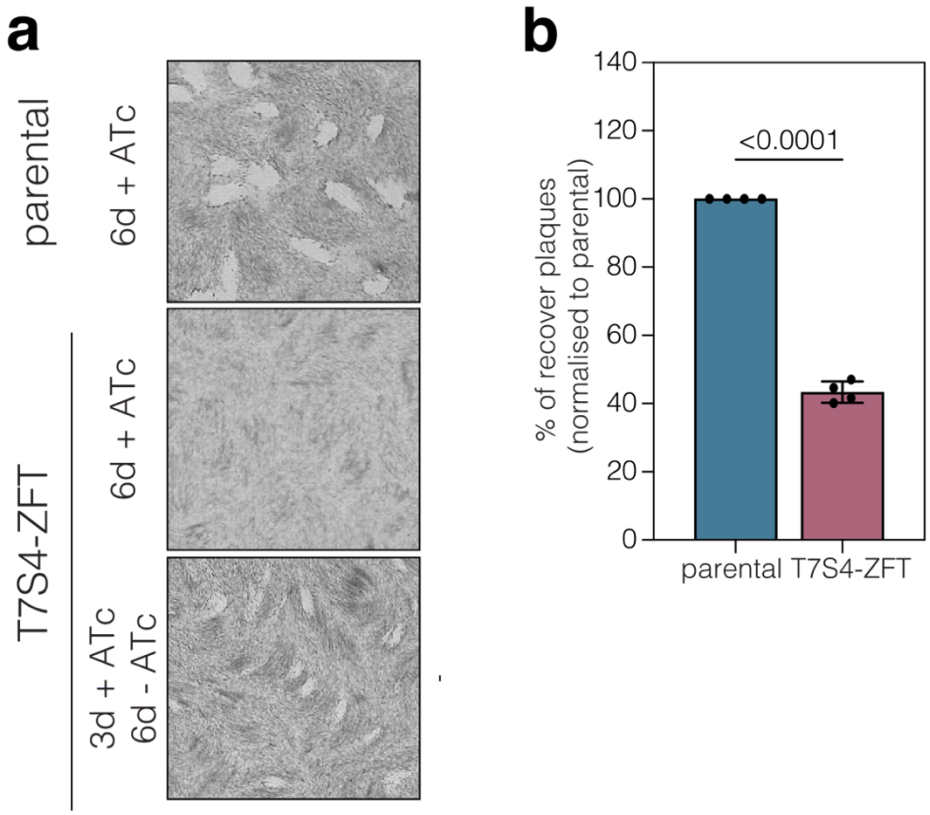


Figure 3.42 – 40 % of ZFT knockdown parasites initiate conversion to bradyzoites and are able to survive the transient loss of ZFT.

a. Plaque assays of parental line treated with ATc for 6 days, and T7S4-ZFT parasites, treated either with ATc for six days, or for three days following ATc washout and six days recovery. **b.** Quantification of plaque number recovery following ATc washout, normalised to parental parasites. Bars at mean of four independent experiments, ± SD. *p* values from two-tailed unpaired *t* test.

Altogether, the data demonstrates that loss of ZFT results in an increase in the expression of bradyzoite specific marker BAG1, as well as an increase in cyst wall production, highlighted by an increase in DBL expression. This suggests that partial parasite differentiation is triggered upon the depletion of ZFT. This and other published data also show that removing iron from parental parasites also causes these parasites to differentiate into the cyst forming stage of the parasite. The data further demonstrates that approximately 40 % of parasites were able to reestablish growth following ZFT knockdown, suggesting that they differentiated into bradyzoites upon ZFT knockdown and were able to convert back to tachyzoites following the removal of ATc.

3.19 ZFT knockdown cannot be rescued by excess zinc

Previous studies have shown that ZIP proteins also transport zinc (Gaither and Eide, 2001b; C.-Y. Wang et al., 2012; Jeong and Eide, 2013; Hu, 2021; Kambe et al., 2021) and to date, no zinc importers have been identified in *T. gondii*. To determine if ZFT in *T. gondii* also plays a role in zinc uptake in addition to iron, I was first curious to assess whether excess zinc could rescue the growth phenotype following ZFT knockdown. To do so, T7S4-ZFT parasites with and without ATc were treated with high zinc (25 μM $ZnSO_4$) conditions for 6 days and a plaque assay was performed (Figure 3.43a). Similar to excess iron, I found that excess zinc also does not rescue the growth phenotype following ZFT knockdown, both by plaque number (Figure 3.43b) and area (Figure 3.43c). I found that exposure of both the parental and T7S4-ZFT parasites to high zinc conditions makes the plaque areas significantly smaller compared to untreated cells, suggesting that the zinc is being internalised by the parasites, as too much zinc can be toxic to parasite survival. Interestingly, as with iron, I found that solely changing the promoter significantly ($p < 0.0001$, ordinary one-way ANOVA, Tukey corrected for multiple comparisons) leads to a reduction in plaque size compared to untreated parasites in high zinc conditions (Figure 3.43d).

As the role of iron in ZFT knockdown parasites was previously examined, I was next curious to test if the addition of both excess iron (200 μM FAC) and zinc (25 μM $ZnSO_4$) could rescue the growth phenotype following the knockdown of ZFT by plaque assay (Figure 3.43a). However, the results demonstrate that the addition of both excess iron and zinc was also unable to rescue to growth defect (Figure 3.43b). Intriguingly, similar to excess iron and zinc alone, I found that changing the promoter alone to the T7S4 inducible promoter results in a significant ($p < 0.0001$, two-way ANOVA, Tukey corrected for multiple comparisons) decrease in number of plaque numbers (to approximately 20 %) compared to parental parasites in conditions with both excess iron and zinc (Figure 3.43e). These data suggest that overexpressing ZFT by changing the promoter alone makes the parasites more sensitive to both iron and zinc.

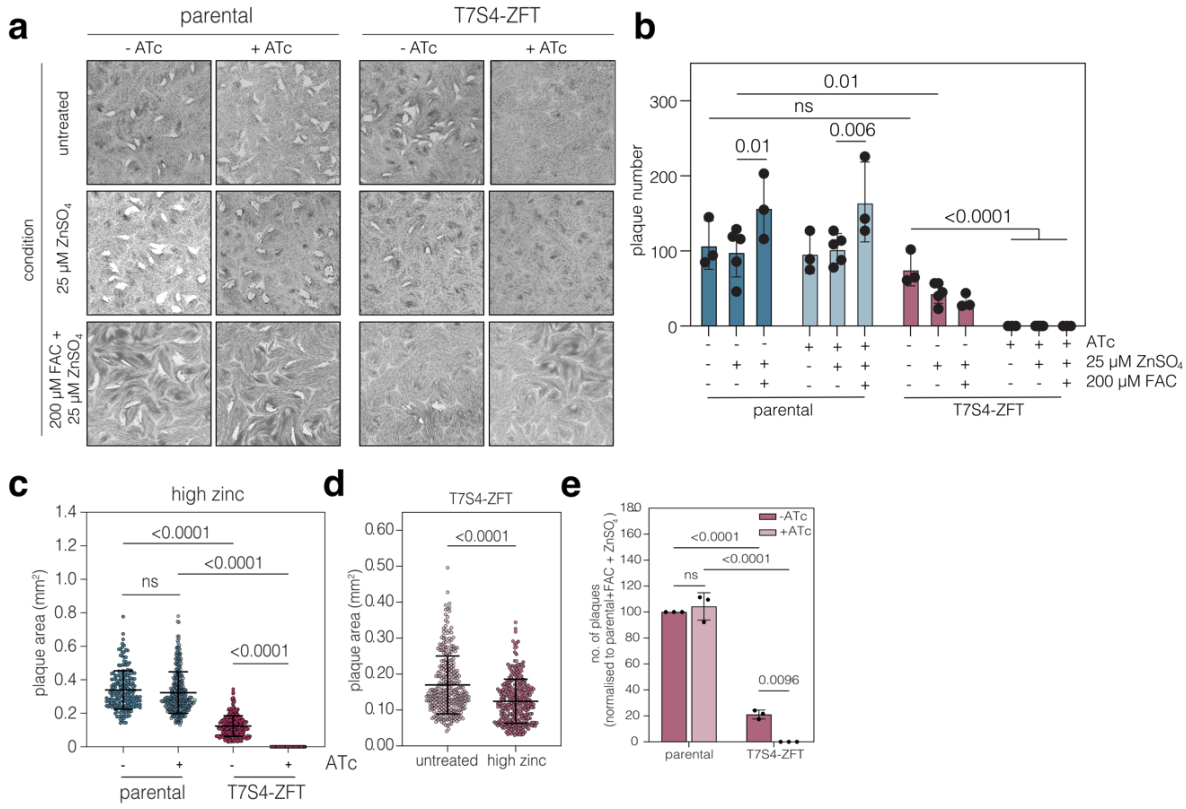


Figure 3.43 - Excess zinc is unable to rescue the growth phenotype upon ZFT knockdown.

a. Plaque assay of parental and T7S4-ZFT parasites with and without ATc, in untreated, high zinc (25 µM $ZnSO_4$) and high iron and zinc combined (200 µM FAC and 25 µM $ZnSO_4$) conditions, showing that the ZFT knockdown phenotype cannot be rescued. **b.** Bar graph quantifying the plaque numbers from (a) of parental and T7S4-ZFT parasites under different conditions. Bars are at mean ± SD. *p* values from two-way ANOVA, Tukey corrected for multiple comparisons. **c.** Plaque areas in mm^2 from (a) of parental and T7S4-ZFT parasites with and without ATc under high zinc (25 µM $ZnSO_4$) conditions. Points represent individual plaque areas from two (parental -ATc) or three (all other conditions) independent biological experiments. Bars show the mean ± SD. *p* values from ordinary one-way ANOVA, Tukey corrected for multiple comparisons. **d.** Plaque areas in mm^2 of T7S4-ZFT parasites in untreated and high zinc (25 µM $ZnSO_4$) conditions showing that changing the promoter alone makes the parasites more sensitive to excess zinc. Points represent individual plaque areas from three independent biological experiments. Bars show the mean ± SD. *p* values are from two-tailed unpaired t test with Welch's correction. **e.** Quantification of plaque numbers from (a) of parental and T7S4-ZFT parasites with and without ATc in high iron and zinc conditions (200 µM FAC and 25 µM $ZnSO_4$) combined, normalised to parental under these conditions. Bars are at the mean of three independent biological experiments, ± SD. *p* values from two-way ANOVA, Tukey corrected for multiple comparisons.

I was next interested to assess whether the addition of a zinc ionophore could rescue the growth phenotype, to ensure direct intracellular delivery into the parasite. An ionophore is a molecule that specifically and reversibly binds to a specific ion and facilitates their transport across the lipid bilayer cell membrane. To initially identify what concentrations to use, a fluorescent growth assay was performed with ΔKu80:mNG parasites to identify what concentrations are toxic to the parasite and what concentrations to use (Figure 3.44). The concentration used for the following experiments was 2 μM Zn Ionophore 2-Mercaptopyridine N-oxide, which would kill approximately ~40 - 50 % of the parasites.

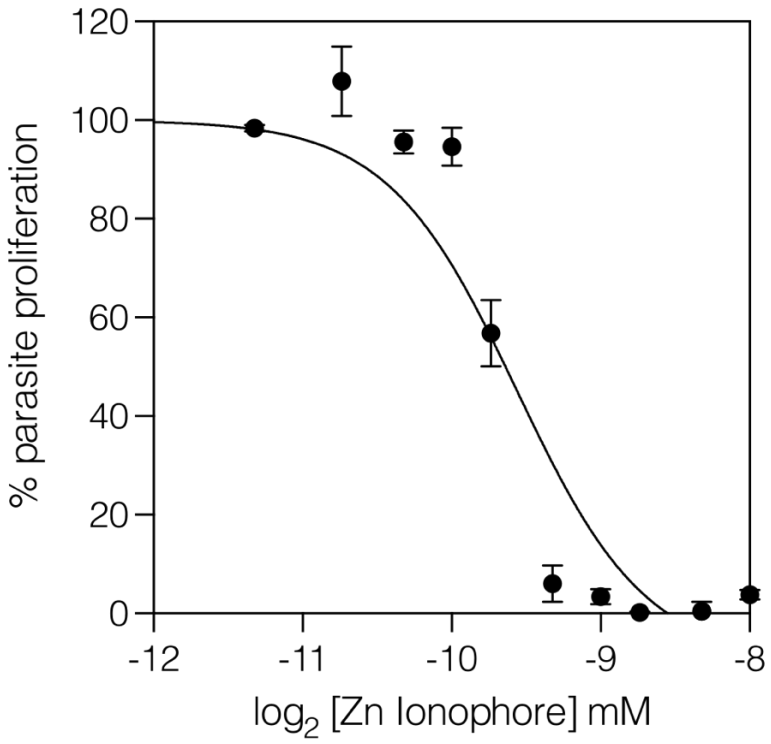


Figure 3.44 - Fluorescent growth curve of ΔKu80:mNG parasites in the presence of increasing concentrations of Zn Ionophore 2-Mercaptopyridine N-oxide.

Dose response curve showing the percentage of parental ΔKu80:mNG parasite survival in the presence of increasing concentrations of zinc ionophore 2-Mercaptopyridine N-oxide. Bars represent the mean of two independent biological experiments ± SEM.

To determine if the presence of a zinc ionophore would rescue the ZFT knockdown phenotype, a plaque assay of parental and T7S4-ZFT parasites was performed with and without ATc in the presence and absence of a zinc ionophore 2-Mercaptopyridine N-oxide (Figure 3.45a). Similar to conditions used before, I found that the presence of a zinc ionophore was also unable to rescue the growth phenotype following the knockdown of ZFT by plaque number (Figure 3.45b).

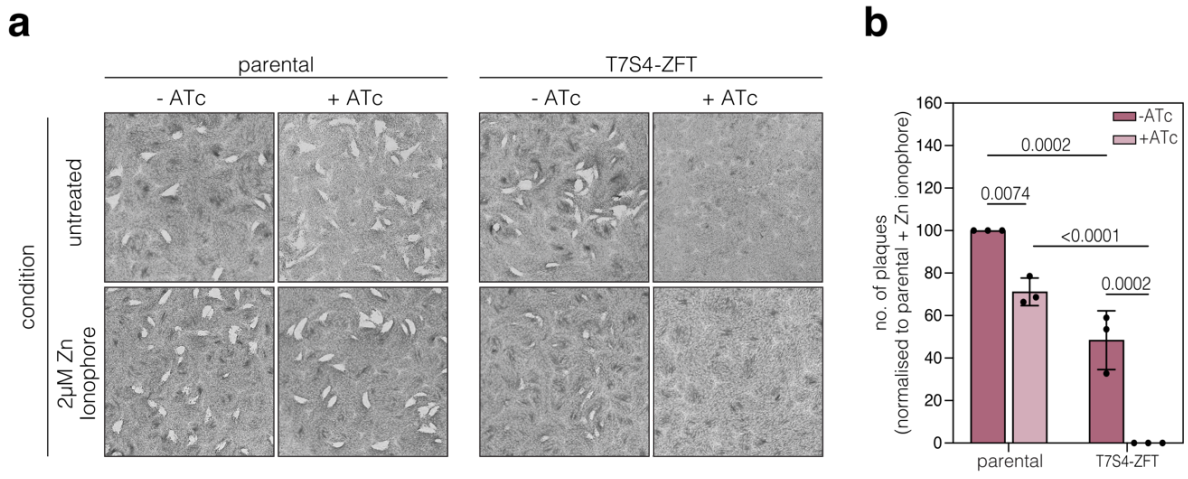


Figure 3.45 - Zinc ionophore 2-Mercaptopyridine N-oxide is unable to rescue the growth phenotype upon ZFT knockdown.

a. Plaque assay of parental and T7S4-ZFT parasites with and without ATc, in untreated and zinc ionophore (2 μM) conditions, showing that the ZFT knockdown phenotype cannot be rescued. **b.** Quantification of plaque numbers from (a) of parental and T7S4-ZFT parasites with and without under zinc ionophore conditions, normalised to parental parasite treated with Zn ionophore. Bars are at the mean of three independent biological experiments, ± SD. *p* values from two-way ANOVA, Tukey corrected for multiple comparisons.

3.20 Parasites overexpressing ZFT are hypersensitive to excess zinc

Previously, I showed that parasites overexpressing ZFT are hypersensitive to excess iron compared to parental parasites (Figure 3.19a, b). The plaque assays represented in Figure 3.43a suggest that an overexpression of ZFT leads to a reduction in plaque number and area under high zinc conditions. To further support this and assess the sensitivity of parasites overexpressing ZFT to excess zinc, I performed a fluorescent growth assay with the ZFT-Ty overexpression line under increasing concentrations of $ZnSO_4$. I found that overexpressing ZFT leads to a slight but significant (p = 0.01, two-tailed paired t-test) increase in zinc sensitivity compared to parental parasites (Figure 3.46a, b). The plaque assay and fluorescent growth assay data both support and suggest that the overexpression of ZFT renders *T. gondii* parasites more sensitive to excess zinc.

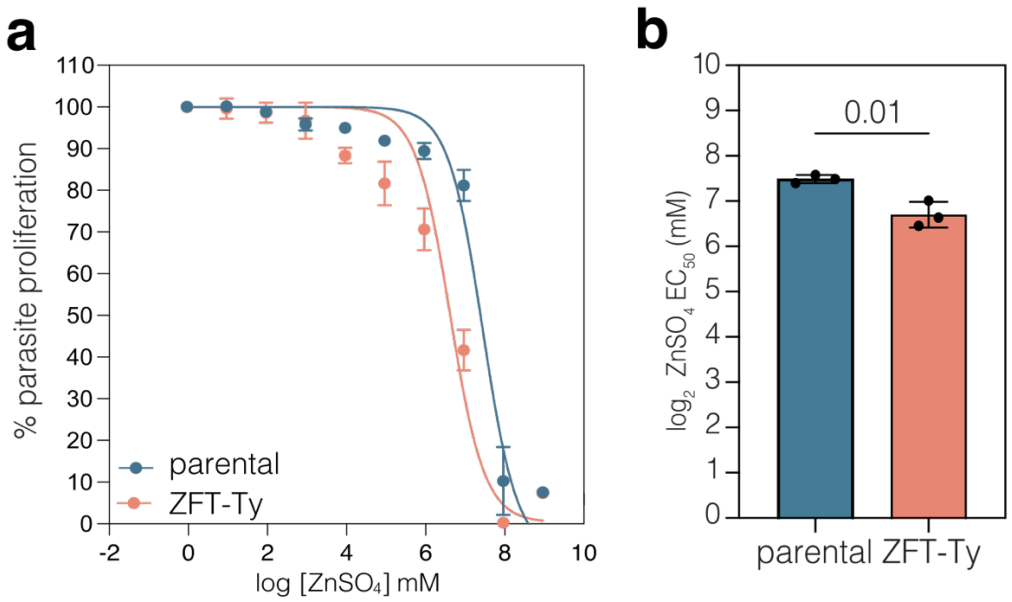
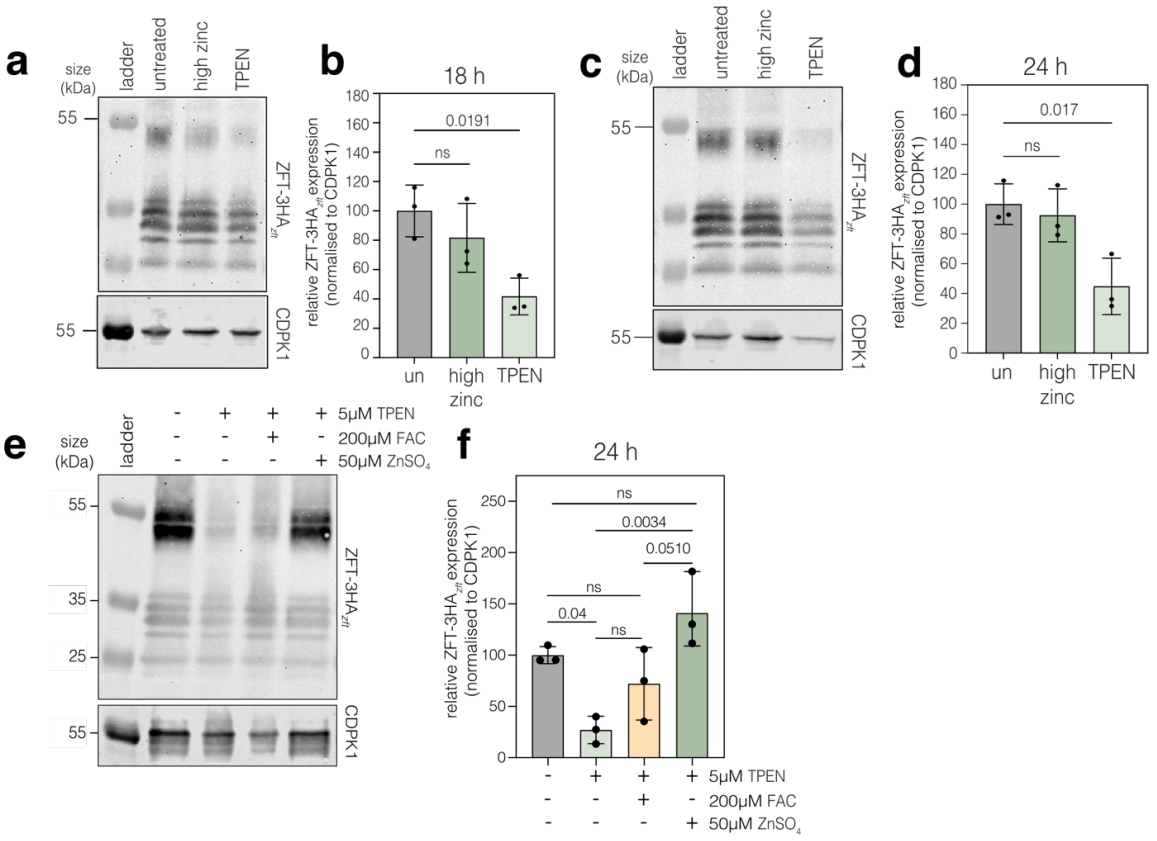


Figure 3.46 - ZFT overexpression parasites are hypersensitive to excess zinc.

a. Dose response curve showing the percentage of parental and ZFT-Ty parasite survival in the presence of increasing concentrations of excess zinc ($ZnSO_4$). **b.** Bar graph demonstrating the mean parasite EC_{50} for $ZnSO_4$ for parental RHtdTomato and ZFT-Ty parasites. Each point represents an independent experiment. Bars at mean of three independent biological experiments, ± SD. p values from two-tailed unpaired t test.

3.21 ZFT expression depends on the availability of zinc

Previously in this chapter, I showed that ZFT expression is dependent on the availability of iron. To assess if ZFT expression is dependent on the availability of zinc, I treated ZFT-3HA$_{zft}$ parasites in the presence of either 50 µM $ZnSO_4$, or 5 µM TPEN, a cation chelator often used to reduce zinc levels (Schaefer-Ramadan et al., 2019), for 18 h and 24 h, and quantified ZFT-3HA$_{zft}$ abundance. Interestingly, and distinct from iron treatment, excess zinc did not significantly change ZFT-3HA$_{zft}$ expression at both 18 h (Figure 3.47a, b) and 24 h (Figure 3.47c, d). However, upon TPEN chelator treatment for both the 18 h and 24 h timepoints, I found a significant decrease in ZFT-3HA$_{zft}$ expression levels (p = 0.0191, and p = 0.017, one-way ANOVA, Tukey corrected for multiple comparisons) (Figure 3.47b, d). While TPEN is often used to reduce the levels of zinc, I was curious to assess whether its presence also has an effect on the levels of iron, as it is a possibility that the reduction of ZFT following TPEN chelation treatment could be a result of a reduction in iron levels. To examine this, I treated ZFT-3HA$_{zft}$ parasites in the presence of either 5 µM TPEN, 5 µM TPEN and 200 µM FAC, and finally, 5 µM TPEN and $ZnSO_4$ for 24 h. Untreated ZFT-3HA$_{zft}$ parasites were used as a control. I then performed a western blot analysis (Figure 3.47e) and quantified the abundance of ZFT-3HA$_{zft}$. I found that ZFT-3HA$_{zft}$ expression is not significantly changed in TPEN and FAC conditions compared to TPEN only conditions (Figure 3.47e, f). However, ZFT-3HA$_{zft}$ expression levels were significantly (p = 0.0034, one-way ANOVA, Tukey corrected for multiple comparisons) increased in TPEN and $ZnSO_4$ conditions compared to TPEN only treatment (Figure 3.47e, f), supporting that the reduction in ZFT expression levels observed following TPEN treatment is more likely due to a reduction of zinc rather than a reduction of iron. This expression of ZFT under high iron conditions was further verified by an immunofluorescence assay where I treated the parasites with high zinc (50 µM $ZnSO_4$) conditions for 24 h. I show that there is no change in expression or localisation of ZFT under excess zinc conditions in ZFT-3HA$_{zft}$ parasites (Figure 3.47e)


a
size (kDa)
ladder
untreated
high zinc
TPEN
55
55
ZFT-3HA$_{zft}$
CDPK1
b
18 h
relative ZFT-3HA$_{zft}$ expression (normalised to CDPK1)
0.0191
ns
un
high zinc
TPEN
c
size (kDa)
ladder
untreated
high zinc
TPEN
55
55
ZFT-3HA$_{zft}$
CDPK1
d
24 h
relative ZFT-3HA$_{zft}$ expression (normalised to CDPK1)
0.017
ns
un
high zinc
TPEN
e
size (kDa)
ladder
5μM TPEN
200μM FAC
50μM ZnSO$_4$
55
35
25
55
ZFT-3HA$_{zft}$
CDPK1
f
24 h
relative ZFT-3HA$_{zft}$ expression (normalised to CDPK1)
ns
0.0034
0.0510
ns
0.04
ns
5μM TPEN
200μM FAC
50μM ZnSO$_4$

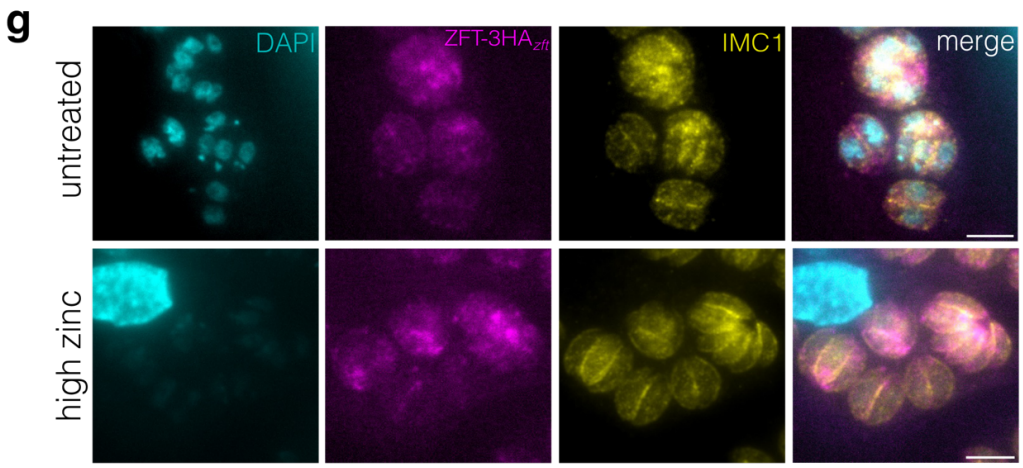

g
untreated
high zinc
DAPI
ZFT-3HA$_{zft}$
IMC1
merge

Figure 3.47 - ZFT expression is dependent on the availability of zinc.

a. Western blot analysis of ZFT-3HA$_{zft}$ expression in untreated, high zinc (50 µM $ZnSO_4$) and 5 µM TPEN chelation conditions at 18 h post infection. CDPK1 used as a loading control. **b.** Quantification of ZFT-3HA$_{zft}$ levels at 18 h in untreated, high zinc (50 µM $ZnSO_4$) and 5 µM TPEN chelation conditions from three independent biological experiments. Bars are at mean ± SD. *p* values from two-tailed paired t test. **c.** Western blot analysis of ZFT-3HA$_{zft}$ expression in untreated, high zinc (50 µM $ZnSO_4$) and 5 µM TPEN chelation conditions at 24 h post infection. CDPK1 used as a loading control. **d.** Quantification of ZFT-3HA$_{zft}$ levels at 24 h in untreated, high zinc (50 µM $ZnSO_4$) and 5 µM TPEN chelation conditions from three independent biological experiments. Bars are at mean ± SD. *p* values from two-tailed paired t test. **e.** Western blot analysis of ZFT-3HA$_{zft}$ expression in untreated, 5 µM TPEN, 5 µM TPEN and 200 µM FAC conditions and 5 µM TPEN and 50 µM $ZnSO_4$ conditions at 24 h post infection. CDPK1 used as a loading control. **f.** Quantification of ZFT-3HA$_{zft}$ levels at 24 h in untreated, 5 µM TPEN, 5 µM TPEN and 200 µM FAC conditions and 5 µM TPEN and 50 µM $ZnSO_4$ conditions from three independent biological experiments. Bars are at mean ± SD. *p* values from two-way ANOVA, Tukey corrected for multiple comparisons. **g.** Immunofluorescence assay of ZFT-3HA$_{zft}$ at 24 h post infection in untreated and high zinc (50 µM $ZnSO_4$), conditions confirming that that ZFT-3HA$_{zft}$ expression levels are not altered under excess zinc. Scale bars 5 µm.

3.22 ZFT expression complements the lack of zinc transport in *S. cerevisiae*

I next aimed to investigate whether ZFT has a functional role in zinc uptake in *T. gondii*. To do so, *T. gondii* ZFT was codon optimised for *Saccharomyces cerevisiae*. Codon optimisation can enhance the expression of heterologous genes by replacing codons used less frequently with more frequently used codons without modifying the encoded amino acid sequence (Burgess-Brown et al., 2008; Gustafsson et al., 2004; Maertens et al., 2010; Plotkin and Kudla, 2011). The full length codon optimised ZFT sequence was synthesised and amplified by PCR. This was then cloned into the yeast expression vector pDR195 and transformed into either a parental yeast strain (DY1457) or a yeast strain lacking both the low and high affinity zinc transporters, *Δzrt1/2* (Ullah et al., 2018) for constitutive expression and selected by growth on synthetic defined agar lacking uracil (SD-Ura). The plasmids contain a functional URA3 gene, which codes for an essential enzyme for synthesising uracil in yeast. This selection therefore then allows the transformed yeast to now grow in uracil-deficient conditions. The empty yeast expression vector was also transformed as a control. To assess if TgZFT is able to complement the *Δzrt1/2* mutant, a spot assay was performed of both parental WT DY1457 and *Δzrt1/2* yeast strains, transformed with either the empty yeast expression plasmid as a control, or the yeast expression plasmid cloned with full length TgZFT. This was performed under standard SD-Ura conditions and SD-Ura + 5 μM EGTA; a cation chelator which chelates zinc. The spot assays were performed by Augustin Pouzache, under my supervision. The data demonstrates that under standard selection dropout SD-Ura conditions, the TgZFT complemented the mild growth defect of the *Δzrt1/2* mutant (Figure 3.48a). Upon zinc removal by EGTA, the *Δzrt1/2* mutant does not grow, however this is rescued by the expression of TgZFT (Figure 3.48b). These data demonstrate that the *T. gondii* ZFT can complement zinc transport in the *Δzrt1/2* mutant yeast strain, supporting the role of ZFT as a functional zinc transporter.

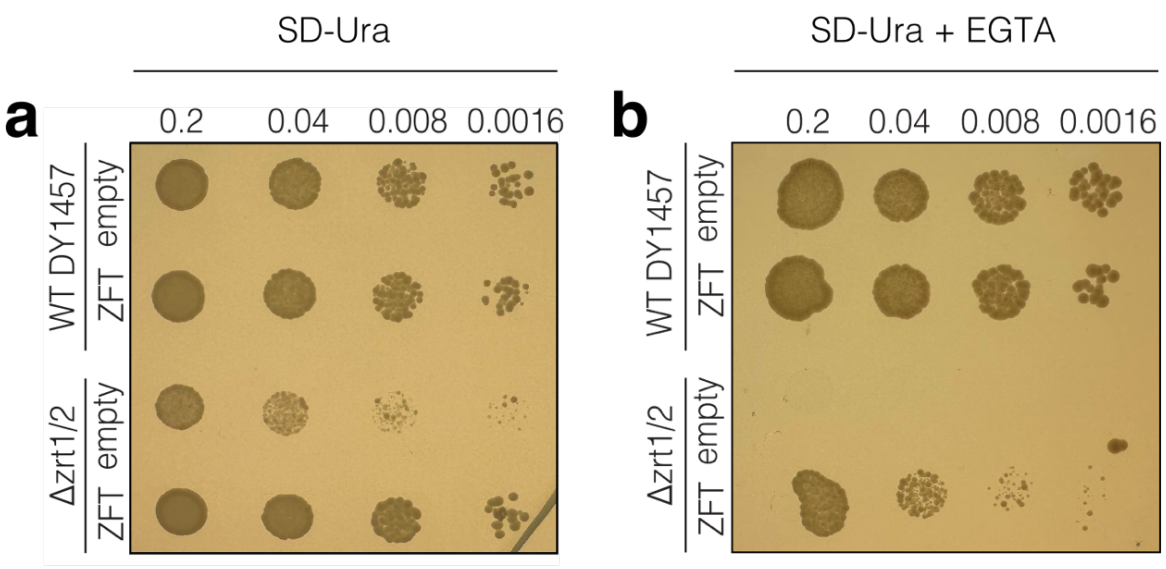


Figure 3.48 - TgZFT is able to complement the lack of zinc transport in the *Δzrt1/2* mutant by rescuing growth both in SD-Ura and SD-Ura + EGTA conditions.

a. Yeast spot test assay in SD-Ura showing a dilution of both WT DY1457 parental and *Δzrt1/2* mutant strains transformed with either an empty expression vector or an expression vector expressing the codon optimised TgZFT. This demonstrates that TgZFT expression rescues the growth of the *Δzrt1/2* yeast under normal conditions. Representative of two independent biological experiments. **b.** Yeast spot test assay in SD-Ura supplemented with 5 mM EGTA showing a dilution of both WT DY1457 parental and *Δzrt1/2* mutant strains transformed with either an empty expression vector or an expression vector expressing the codon optimised TgZFT, demonstrating that TgZFT rescues *Δzrt1/2* growth under zinc chelation conditions. Representative of two independent biological experiments.

To investigate whether ZFT has a functional role in iron uptake in addition to zinc in *T. gondii*, I next aimed to express the codon optimised ZFT in a *S. cerevisiae* iron transporter mutant that lacks both the low and high affinity iron transporter *Δfet3/4* (Ullah et al., 2018). However, despite six attempts, no viable transformants were recovered. These transformations were performed both by myself and by Augustin Pouzache.

To further validate the role and substrate specificity of ZFT as the major zinc transporter in *Toxoplasma gondii*, codon optimised ZFT was additionally transformed into *Δsmf1*, a mutant yeast strain lacking the high affinity manganese transporter (Ullah et al., 2018). Functional complementation was then assessed by performing a spot assay in standard SD-Ura growth conditions as well as 5 mM EGTA chelation conditions. The spot assays were performed by Augustin Pouzache,

under my supervision. In contrast to the *Δzrt1/2* transformations, TgZFT was unable to rescue the growth of *Δsmf1* both under standard SD-Ura conditions (Figure 3.49a) as well as EGTA conditions (Figure 3.49b), suggesting that ZFT does not transport manganese and has a substrate specificity for zinc. However, it is important to note that it may be possible that TgZFT is either mislocalised following the transformations, or that expression of ZFT in this background is toxic or mis-expressed, and that failure may not only be due to substrate specificity.

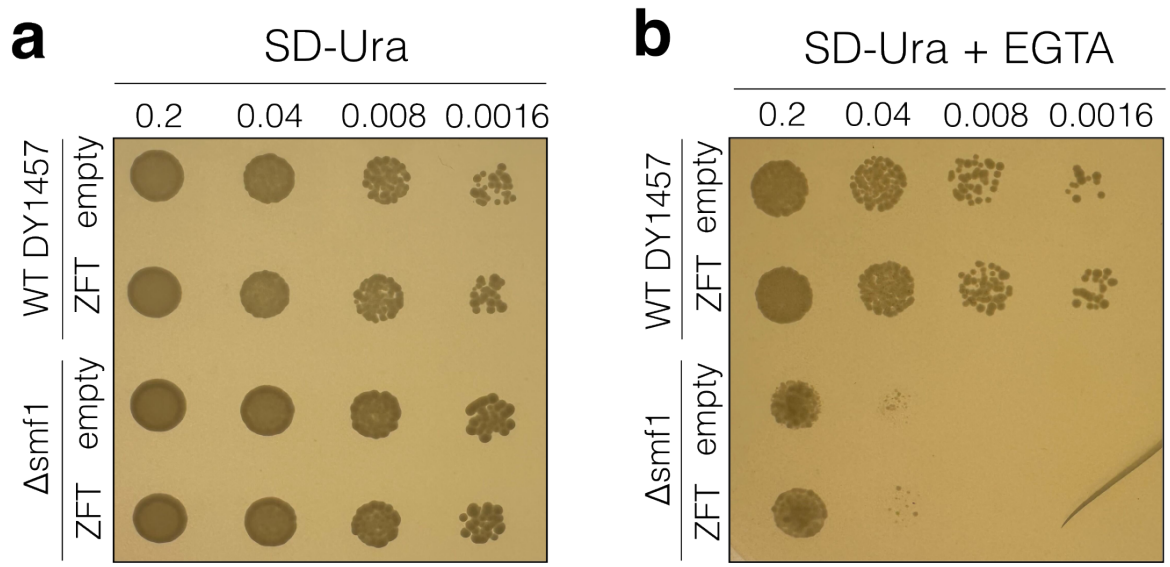


Figure 3.49 - TgZFT does not complement the lack of manganese transport in the *Δsmf1* mutant in both in SD-Ura and SD-Ura + EGTA growth conditions.

a. Yeast spot test assay in SD-Ura showing a dilution of both WT DY1457 parental and *Δsmf1* mutant strains transformed with either an empty expression vector or an expression vector expressing the codon optimised TgZFT. This demonstrates that TgZFT expression does not rescue or complement the growth of the *Δsmf1* yeast under normal conditions. Representative of two independent biological experiments. **b.** Yeast spot test assay in SD-Ura supplemented with 5 mM EGTA showing a dilution of both WT DY1457 parental and *Δsmf1* mutant strains transformed with either an empty expression vector or an expression vector expressing the codon optimised TgZFT, demonstrating that TgZFT does not rescue or complement *Δsmf1* growth under chelation conditions. Representative of two independent biological experiments.

3.23 ZFT knockdown leads to a decrease in parasite associated iron and zinc

Next, to assess whether ZFT knockdown parasites have less parasite associated iron, live cell imaging was performed on T7S4-ZFT parasites with and without ATc induction for 48 h using an iron (FerroOrange) indicator. FerroOrange works by specifically detecting labile ferrous (Fe^{2+}) iron ions in live cells and increases fluorescence in the presence of labile iron (Weber et al., 2020; Yu et al., 2022). However, before doing so, the indicator was initially validated in *T. gondii*. To do so, I pre-treated parental parasites with excess iron (200 µM FAC) for 48 h before live imaging (Figure 3.50a). I found that parental parasites exposed to excess iron have a significantly (p < 0.0001, two-tailed unpaired t test with Welch's correction) higher FerroOrange MFI compared to untreated parasites (Figure 3.50b). This data thus validates the sensitivity of FerroOrange as an iron live cell indicator in *Toxoplasma gondii*. As the iron live cell indicator has now been verified in the parasite, I performed live cell imaging on T7S4-ZFT parasites with and without ATc induction for 48 h (Figure 3.50c). The data shows that ZFT knockdown parasites have significantly (p = 0.0027, two-tailed unpaired t test with Welch's correction) reduced FerroOrange MFI compared to untreated parasites (Figure 3.50d), suggesting that upon knockdown of ZFT for 48 h, parasites have significantly reduced parasite associated iron.

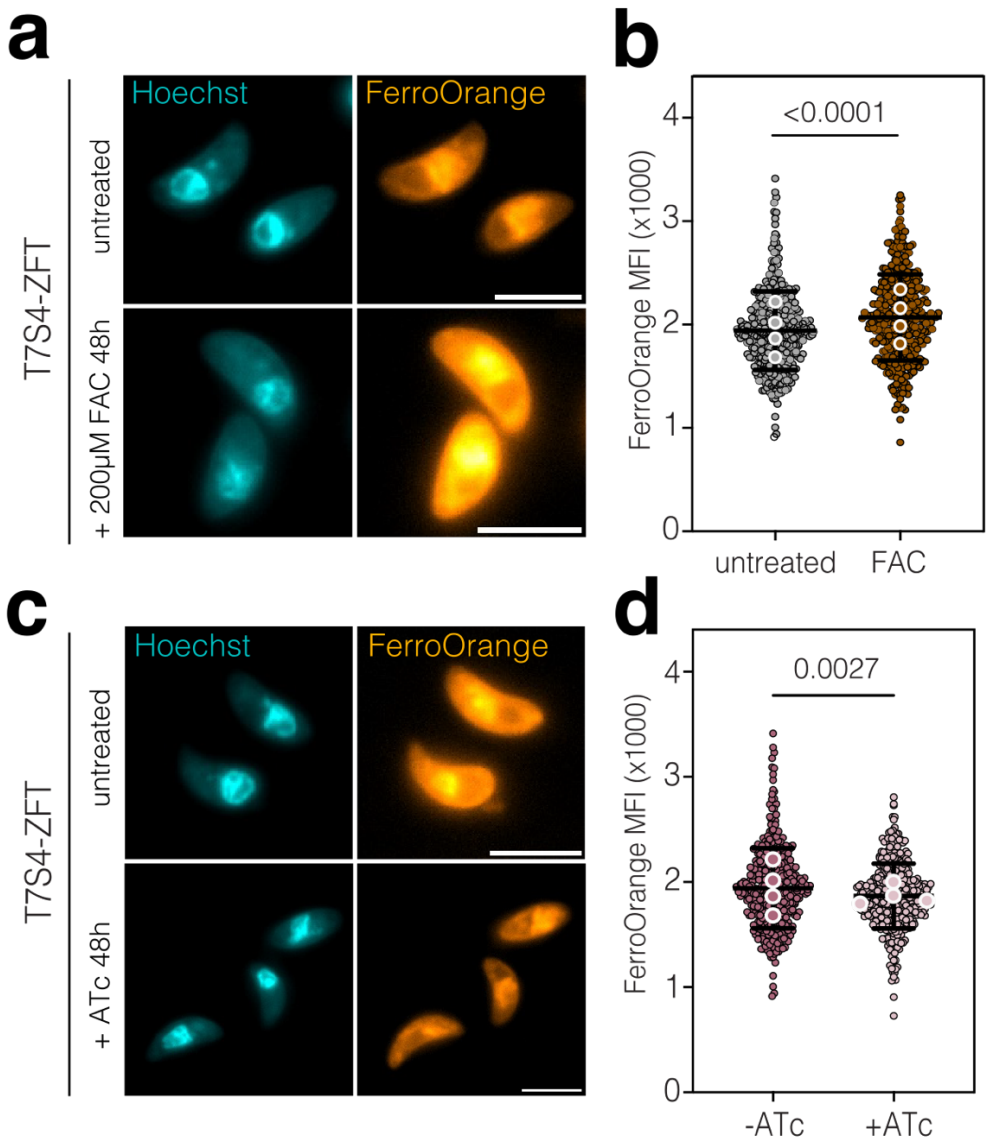


Figure 3.50 - ZFT knockdown parasites have reduced parasite associated iron by live cell imaging using the FerroOrange live cell indicator.

a. Live cell imaging of parental T7S4-ZFT parasites in untreated and high iron (200 µM FAC) conditions for 48 h to validate the indicator. Parasites stained with Hoechst to stain DNA, and FerroOrange, the iron live cell indicator. Scale bar 5 µm. **b.** Quantification of FerroOrange MFI of parental T7S4-ZFT parasites in untreated and high iron (200 µM FAC) conditions for 48 h. Points represent the MFI of FerroOrange/parasite from four independent biological experiments. Average FerroOrange MFI from each of four biological replicates represented as larger overlayed points. Bars at mean ± SD. *p* value from two-tailed unpaired t test with Welch's correction. **c.** Live cell imaging of parental T7S4-ZFT parasites with and without ATc for 48 h to induce ZFT knockdown. Parasites were stained with Hoechst to stain DNA, and FerroOrange, the iron live cell indicator. Scale bar 5 µm. **d.** Quantification of FerroOrange MFI of parental T7S4-ZFT parasites with and without ATc for 48 h. Points are MFI of FerroOrange/parasite from four independent experiments. Average FerroOrange MFI from each of four biological replicates represented as larger overlayed points. Bars at mean ± SD. *p* value from two-tailed unpaired t test with Welch's correction.

Next, to assess whether ZFT knockdown parasites have less parasite associated zinc, live cell imaging was performed on T7S4-ZFT parasites with and without ATc induction for 24 h using a zinc (FluoZin™-3AM) indicator which increases fluorescence in the presence of zinc (Li et al., 2009; Rajapakse et al., 2017). However, as with the FerroOrange indicator, the FluoZin™-3AM indicator was initially validated in *T. gondii*. To do so, I pre-treated parental parasites with excess zinc (50 μM $ZnSO_4$) intracellularly for 24 h before live imaging (Figure 3.51a). Similar to iron, I found that parental parasites exposed to excess zinc also have a significantly ($p < 0.0001$, two-tailed unpaired t test with Welch's correction) higher FluoZin™-3AM MFI compared to untreated parasites (Figure 3.51b). This data thus validates the sensitivity of FluoZin™-3AM as a zinc live cell indicator in *Toxoplasma gondii*. I then performed live cell imaging on T7S4-ZFT parasites with and without ATc induction for 24 h (Figure 3.51c). Similar to iron, the data shows that ZFT knockdown parasites have significantly ($p < 0.0001$, two-tailed unpaired t test with Welch's correction) reduced FluoZin™-3AM MFI compared to untreated parasites (Figure 3.51d), suggesting that in the absence of ZFT, parasites have significantly reduced parasite associated zinc.

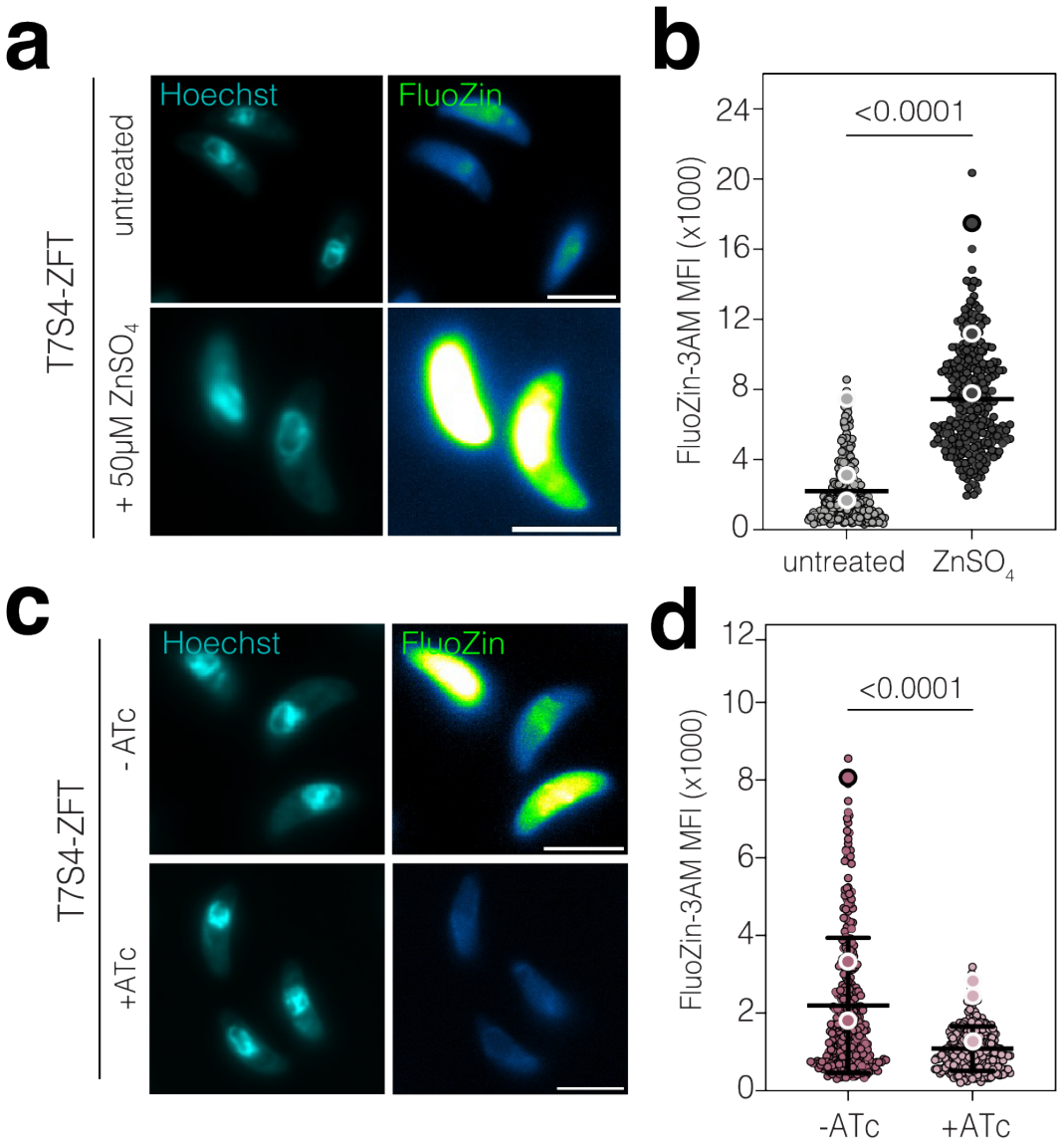


Figure 3.51 - ZFT knockdown parasites have reduced parasite associated zinc by live cell imaging using the FluoZin™-3AM live cell indicator.

a. Live cell imaging of parental T7S4-ZFT parasites in untreated and high zinc (50 µM $ZnSO_4$) conditions for 24 h to validate the indicator. Parasites stained with Hoechst to stain DNA, and FluoZin™-3AM, the zinc live cell indicator. Scale bar 5 µm. **b.** Quantification of FluoZin™-3AM MFI of parental T7S4-ZFT parasites in untreated and high zinc (50 µM $ZnSO_4$) conditions for 24 h. Points represent the MFI of FluoZin™-3AM /parasite from three independent experiments. Average FluoZin™-3AM MFI from each of three biological replicates represented as larger overlayed points. Bars at mean ± SD. *p* value from two-tailed unpaired t test with Welch's correction. **c.** Live cell imaging of parental T7S4-ZFT parasites with and without ATc for 24 h to induce ZFT knockdown. Parasites were stained with Hoechst to stain DNA, and FluoZin™-3AM, the zinc live cell indicator. Scale bar 5 µm. **d.** Quantification of FluoZin™-3AM MFI of parental T7S4-ZFT parasites with and without ATc for 24 h. Points are MFI of FluoZin™-3AM /parasite from three independent experiments. Average FluoZin™-3AM MFI from each of three biological replicates represented as larger overlayed points. Bars at mean ± SD. *p* value from two-tailed unpaired t test with Welch's correction.

To further assess the effect of ZFT knockdown on parasite associated metal, I performed inductively coupled plasma-mass spectrometry (ICP-MS). This is an elemental technique which has been used to quantify the abundance of elements in cells and complex environments (Al-sandaqchi et al., 2018; Hare et al., 2012). I performed this experiment on T7S4-ZFT parasites with and without ATc for 24 h and 48 h to induce ZFT knockdown and measured both iron and zinc levels in the parasites using ICP-MS. Uninfected HFFs were also filtered and used a control and normalised against. Samples were sent to the Scottish Universities Environmental Research Centre and quantified by Dr Valerie Olive. I found that at both 24 h and 48 h post ZFT knockdown, parasite-associated iron was not significantly different in the ZFT knockdown parasites compared to untreated, although with large variation between experiments (Figure 3.52a). However, iron detection via ICP-MS can often be challenging due to interference, and even in the untreated cells, the iron levels were very close to the limit of detection. In contrast, I found that for both 24 h and 48 h post ZFT knockdown, parasite associated zinc levels are significantly (p = 0.0062, and p = 0.0073, two-tailed paired t test respectively) reduced in the absence of ZFT compared to untreated cells (Figure 3.52b).

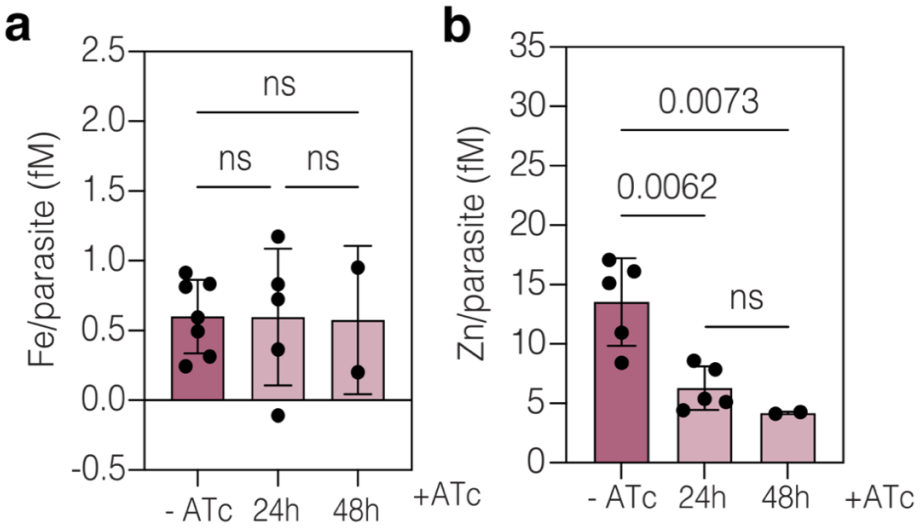


Figure 3.52 – Parasites have significantly reduced parasite associated zinc, but not iron, at both 24 h and 48 h post ZFT knockdown by ICP-MS.

a. Iron/parasite (fM) quantification by ICP-MS in T7S4-ZFT parasites with and without ATc for 24 h and 48 h. Bars at mean (n = 7 for – ATc, n = 5 for + ATc 24 h and n = 2 for + ATc 48 h) ± SD. *p* values from one-way ANOVA, Tukey corrected for multiple comparisons. **b.** Zinc/parasite (fM) quantification by ICP-MS in T7S4-ZFT parasites with and without ATc for 24 h and 48 h. Bars at mean (n = 5 for – ATc and + ATc 24 h and n = 2 for + ATc 48 h) ± SD. *p* values from one-way ANOVA, Tukey corrected for multiple comparisons.

Metals such as iron and zinc can also be quantified at a subcellular resolution using X-Ray fluorescence microscopy (XFM). This elemental analysis technique allows both spatial and quantitative analysis of elements within cells and complex environments (Aghabi et al., 2023; Miller and Ralle, 2024; Paunesku et al., 2021). To perform XFM, I utilised the ID21 beamline at the European Synchrotron Radiation Facility (ESRF) in Grenoble, France. I would like to thank Dr. Hiram Castillo-Michel, the beamline scientist at ID21, for all of his support and assistance during our time there. I was able to detect iron in extracellular, parental T7S4-ZFT parasites, which seemed to localise at distinct foci within the parasites, possibly at the PLVAC, based on our previous observations (Aghabi et al., 2023) (Figure 3.53a). However, at 48 h post ZFT knockdown, iron was no longer detected in the parasites. Parasite associated iron was then quantified by XFM in FIJI using a macro written by Dr. Clare Harding in untreated T7S4-ZFT parental parasites as well as both 24 h and 48 h ATc induction to deplete ZFT. I found that ZFT knockdown parasites have significantly ($p < 0.0001$, ordinary one-way ANOVA, Tukey corrected for multiple comparisons) less parasite associated iron at both timepoints, from ~250 nM in untreated, to ~150 nM at 24 h and ~95 nM at 48 h (Figure 3.53b).

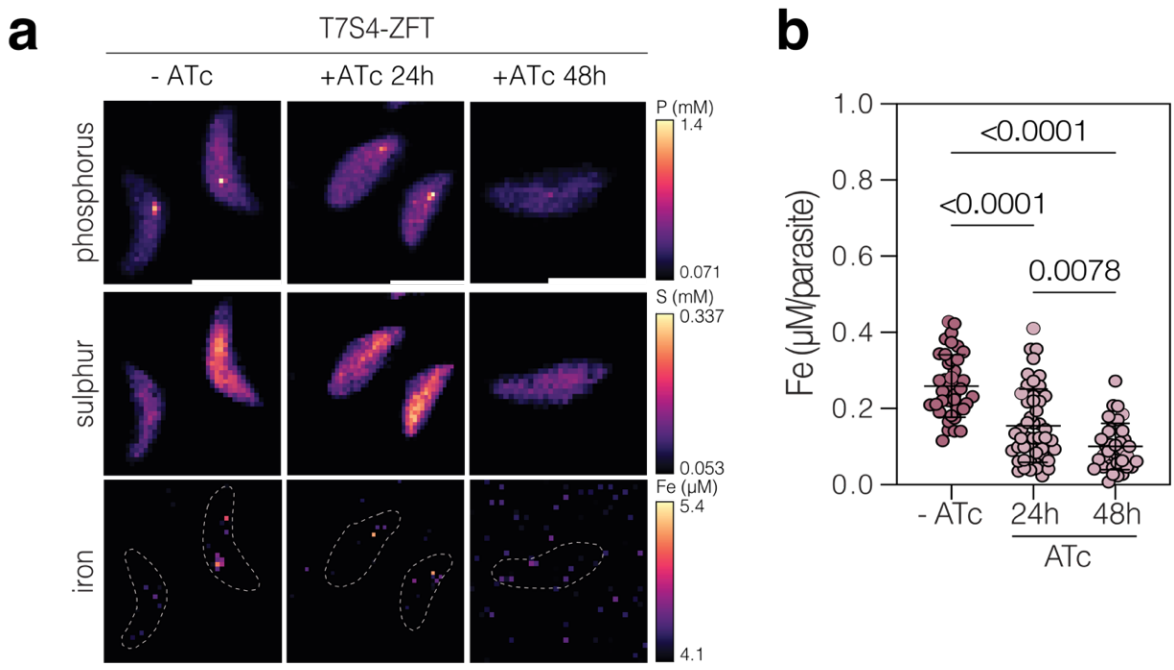


Figure 3.53 - ZFT knockdown parasites have significantly reduced parasite associated iron by XFM at both 24 h and 48 h post induction.

a. XFM of extracellular T7S4-ZFT parasites with and without ATc treatment for 24 and 48 h showing phosphorous, sulphur and iron. Scale bar 5 μm **b.** Quantification of iron by XFM in T7S4-ZFT parasites before and after ZFT knockdown at 24 and 48 h. Bars at mean ± SD. *p* values from one-way ANOVA, Tukey corrected for multiple comparisons.

Next, I assessed the localisation and abundance of zinc in T7S4-ZFT parasites, as above. In extracellular parasites, zinc mostly localises in what is believed to be the parasite nucleus, as has been observed in other organisms (Olea-Flores et al., 2022). Zinc also localises in specific foci within the parasite, which I believe to be the PLVAC based on previous studies (Chasen et al., 2019). Furthermore, I found that zinc frequently colocalises with iron as well as phosphorous within extracellular parasites. Similar to iron, the depletion of ZFT results in a decrease in parasite associated zinc at both 24 and 48 h ATc, both in the foci and within the nucleus. This decrease in parasite associated zinc was particularly prominent following 48 h of ZFT knockdown (Figure 3.54a). Parasite associated zinc was then quantified by XFM in FIJI using a macro written by Dr. Clare Harding in untreated T7S4-ZFT parental parasites as well as both 24 h and 48 h ATc induced parasites to deplete ZFT. I found that ZFT knockdown parasites have significantly ($p < 0.0001$, ordinary one-way ANOVA, Tukey corrected for multiple comparisons) less parasite associated zinc at both timepoints, from ~6 μM in untreated, to ~3.5 μM at 24 h and ~1.7 μM at 48 h (Figure 3.54b).

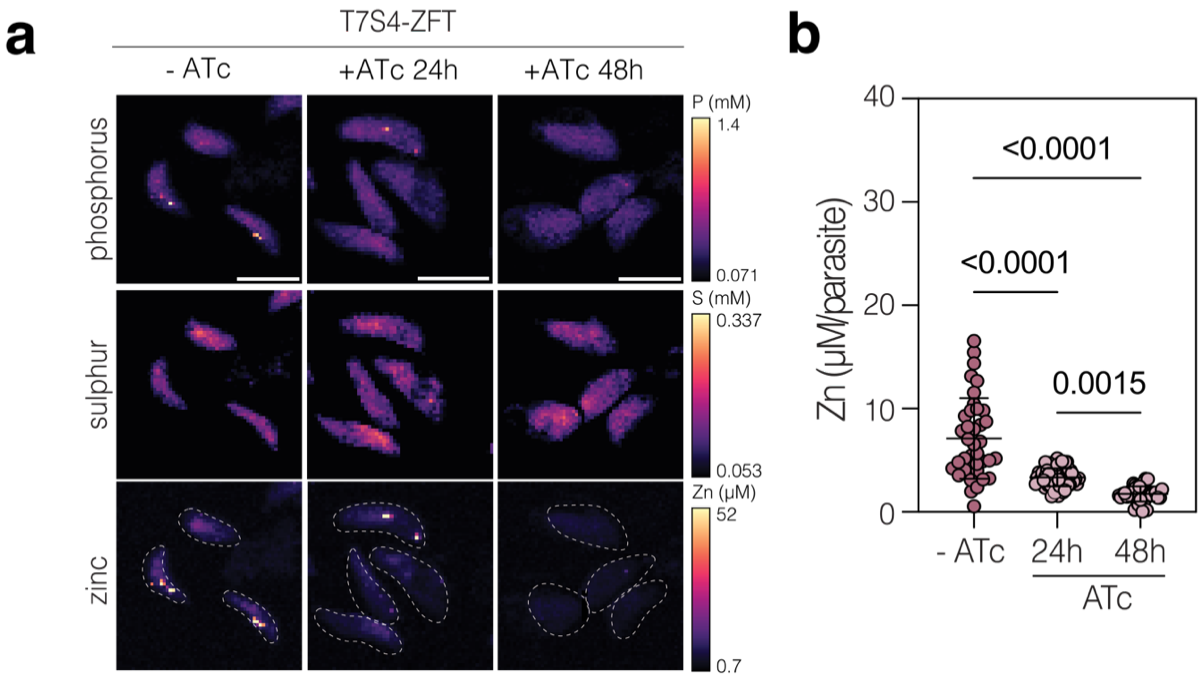


Figure 3.54 - ZFT knockdown parasites have significantly reduced parasite associated zinc by XFM at both 24 h and 48 h post induction.

a. XFM of extracellular T7S4-ZFT parasites with and without ATc treatment for 24 and 48 h showing phosphorous, sulphur and zinc. Scale bar 5 µm. **b.** Quantification of zinc by XFM in T7S4-ZFT parasites before and after ZFT knockdown at 24 and 48 h. Bars at mean ± SD. *p* values from one-way ANOVA, Tukey corrected for multiple comparisons.

Consistent with previous observations (Chasen et al., 2019), frequent co-localisation of both iron and zinc with phosphorus was also observed in extracellular parasites (Figure 3.55). Dr. Clare Harding processed these images.

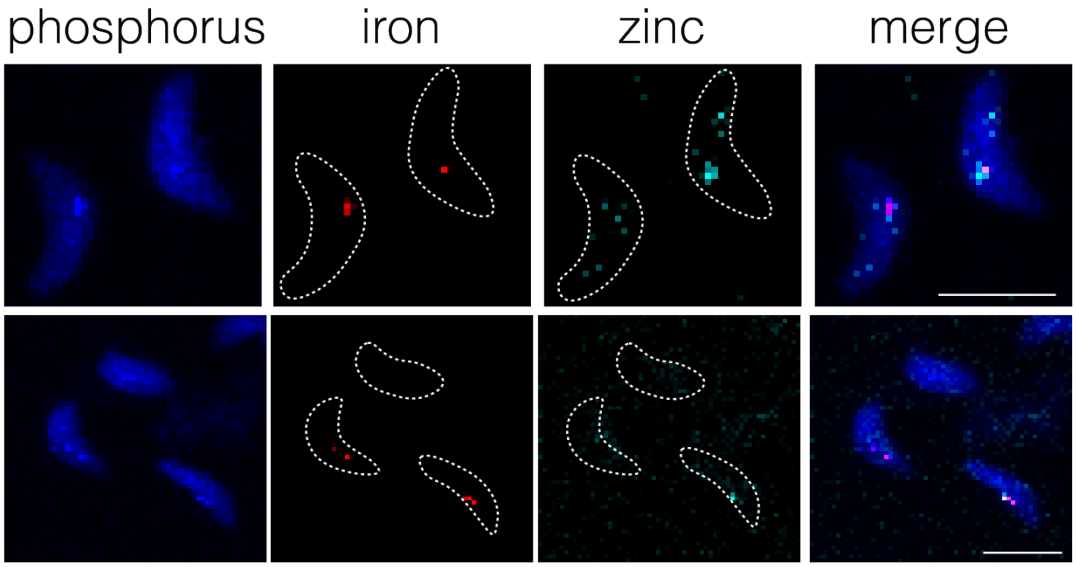


Figure 3.55 - XFM of extracellular untreated T7S4-ZFT parasites showing colocalisation of iron and zinc with phosphorous.

XFM images of untreated extracellular T7S4-ZFT parasites prior to ZFT knockdown, demonstrating that iron, along with zinc, colocalise with phosphorous foci within the parasite. Scale bar 5 µm.

Next, I quantified the amount of sulphur and phosphorous by XFM in parasites by XFM. Interestingly, I observed that both sulphur and phosphorus concentrations were also significantly (p = 0.0014 and p = 0.008 respectively, ordinary one-way ANOVA, Tukey correction for multiple comparisons) reduced at 48 h post knockdown of ZFT (Figure 3.56a, b). However, the magnitude of the decrease was much less. Comparative analysis of the changes as a percentage of untreated cells, performed by Dr. Clare Harding, indicated a strong, time-dependent depletion of iron and zinc, accompanied by a more modest smaller decrease (approximately 10–20 %) in both sulphur and phosphorus (Figure 3.56c). Given that sulphur and phosphorus are both highly abundant components of cellular macromolecules, these modest decreases may reflect impairments in protein synthesis or DNA replication following the knockdown of ZFT. Collectively, these findings confirm and support the role of ZFT as the principal iron and zinc transporter in *T. gondii*.

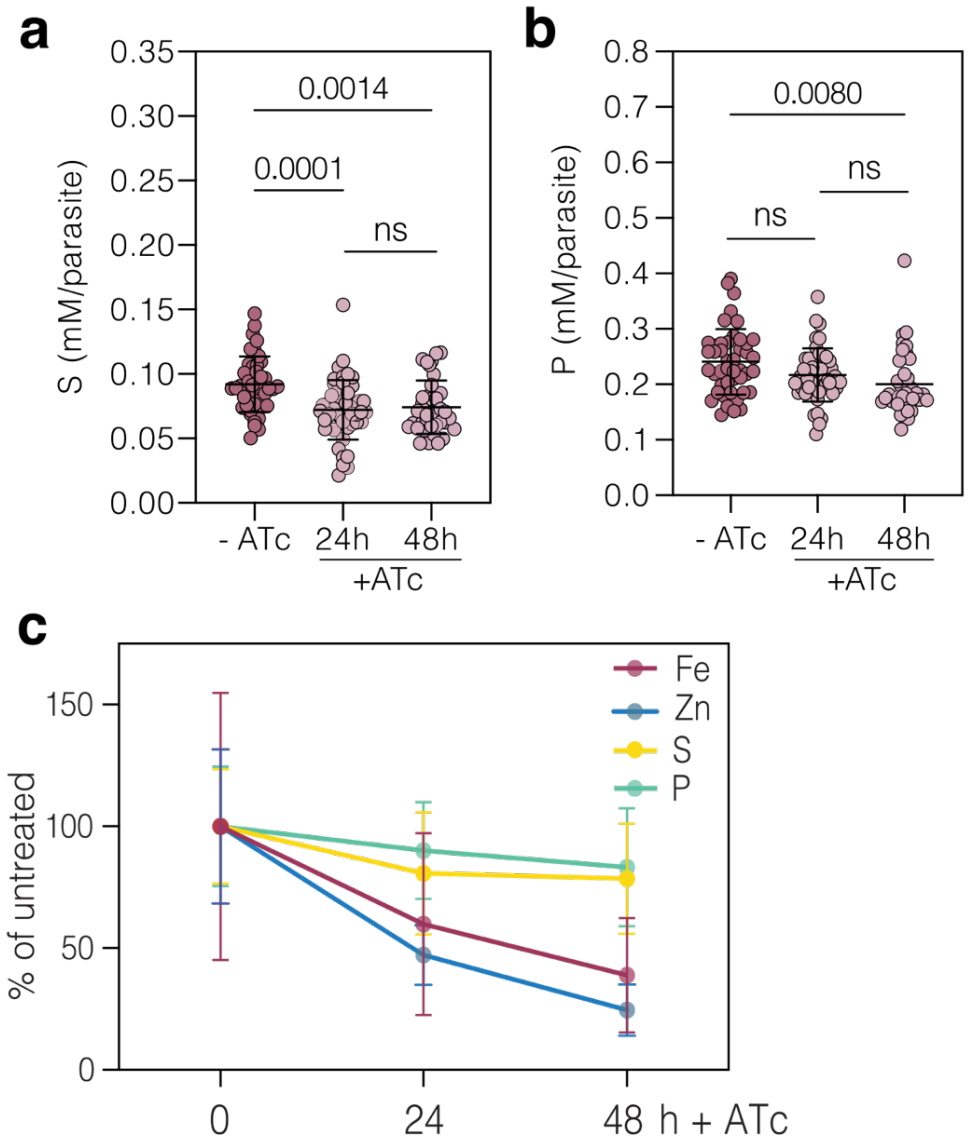


Figure 3.56 - Extracellular parasites have reduced sulphur and phosphorus 48 h post ZFT knockdown by XFM, however this decrease was modest when compared to the rate at which iron and zinc decrease upon knockdown of ZFT.

a. Quantification of sulphur by XFM in T7S4-ZFT parasites before and after ZFT knockdown at 24 and 48 h. Bars at mean ± SD. *p* values from one-way ANOVA, Tukey corrected for multiple comparisons. **b.** Quantification of phosphorus by XFM in T7S4-ZFT parasites before and after ZFT knockdown at 24 and 48 h. Bars at mean ± SD. *p* values from one-way ANOVA, Tukey corrected for multiple comparisons. **c.** Quantification of changes in iron, zinc, sulphur, and phosphorus following the addition of ATc as a percentage of untreated cells. Bars at mean ± SD.

Next, I was curious to investigate if other metals such as copper were affected upon knockdown of ZFT. To do so, I used ICP-MS to quantify the amount of parasite associated copper in T7S4-ZFT parasites before and after induction with ATc to knock ZFT down at 24 and 48 h. I demonstrate that by ICP-MS analysis, there is no significant difference in parasite associated copper before and after ZFT knockdown (Figure 3.57), supporting that ZFT is a transporter specific to iron and zinc, and suggesting the possibility that the knockdown of ZFT does not result in the overexpression of copper transporters to compensate for the loss of ZFT.

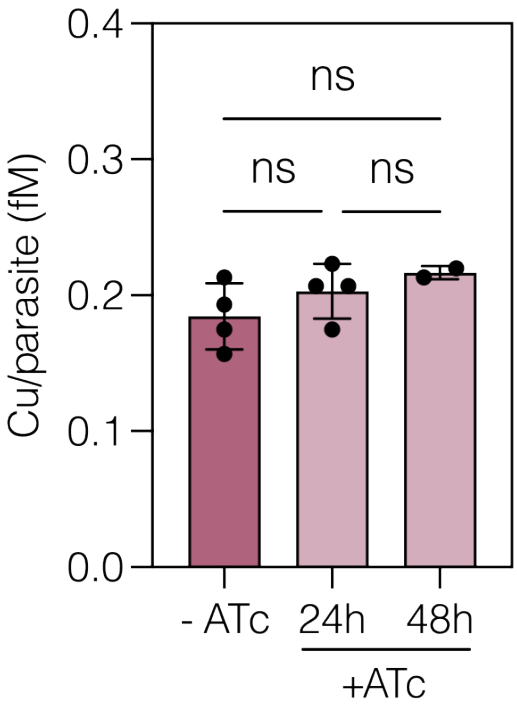


Figure 3.57 - ICP-MS elemental analysis techniques demonstrate that ZFT knockdown does not significantly change copper levels in the parasite.

Cu/parasite (fM) quantification by ICP-MS in T7S4-ZFT parasites with and without ATc for 24 h and 48 h. Bars at mean (n = 4 for – ATc and + ATc 24 h, and n = 2 for + ATc 48 h) ± SD. *p* values from one-way ANOVA, Tukey corrected for multiple comparisons.

3.24 Distribution of host iron and zinc is altered upon ZFT knockdown

Having established both the iron and zinc content of *T. gondii* in the extracellular state before and after ZFT knockdown, I was next curious to examine how these metal levels change during intracellular infection by XFM elemental analysis. To do this, HFFs were infected with either RHΔKu80:tdTomato or T7S4-ZFT parasites induced with ATc for 24 h to knock ZFT down. I observed clear intracellular foci of iron in approximately 90 % of the RHΔKu80:tdTomato intracellular parasites, however only approximately 50 % in the T7S4-ZFT +ATc 24 h parasites. The nuclear zinc also appeared to be significantly more prominent qualitatively by eye in the control RHΔKu80:tdTomato intracellular parasites compared to the T7S4-ZFT +ATc 24 h parasites (Figure 3.58a). To investigate this in more detail, I quantified the MFI of intravacuolar zinc in both RHΔKu80:tdTomato and T7S4-ZFT +ATc 24 h parasites. I found that the intravacuolar zinc levels in the T7S4-ZFT +ATc 24 h parasites have a significantly (p = 0.0193 , two-tailed unpaired t test with Welch's correction) lower intravacuolar zinc MFI compared to RHΔKu80:tdTomato (Figure 3.58b). This data further supports the role of ZFT in zinc acquisition in *Toxoplasma gondii*, particularly in intracellular infection conditions within fibroblast host cells.

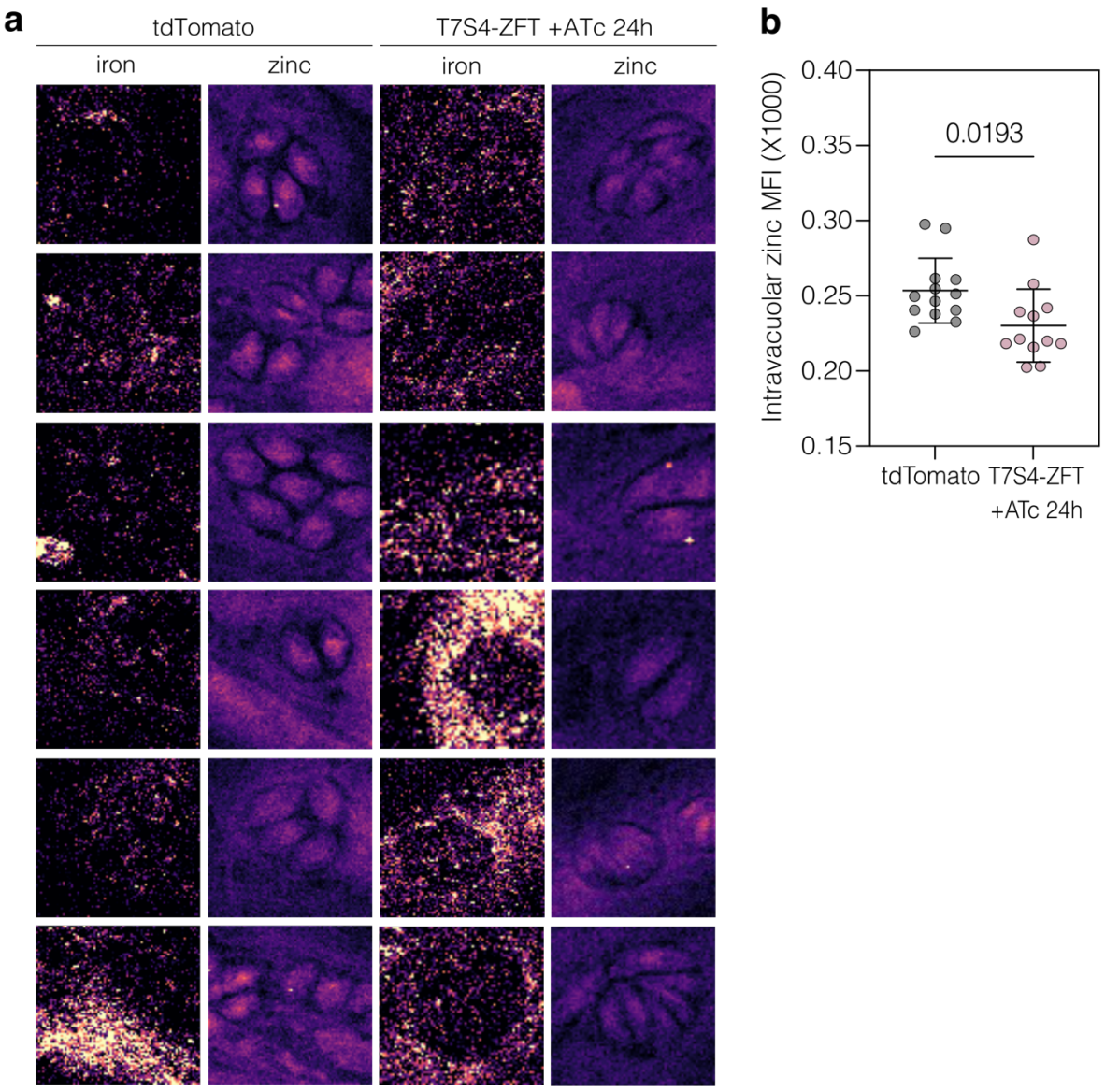


Figure 3.58 - XFM of iron and zinc in intracellular infection conditions.

a. Intracellular XFM elemental analysis of both iron and zinc in HFFs infected with either RHΔKu80:tdTomato or T7S4-ZFT + ATc 24 h parasites. **b.** Quantification of the MFI of intravacuolar zinc of RHΔKu80:tdTomato and T7S4-ZFT +ATc 24 h vacuoles. Points represent the MFI of zinc/vacuole from 13 vacuoles for RHΔKu80:tdTomato and 12 vacuoles for T7S4-ZFT +ATc 24 h. Bars at mean ± SD. *p* value from two-tailed unpaired t test with Welch's correction.

3.25 Deletion of the Iron Responsive Element (IRE) in the 3' UTR of *zft* alters the responsiveness of ZFT to both iron and zinc availability at the protein level.

Finally, a well-characterised mechanism for iron-dependent regulation in mammalian cells is the post-transcriptional IRE/IRP system. Importantly, the position of an IRE within a transcript dictates whether translation is enhanced or whether the transcript is repressed. When IREs are located in the 3' UTR of a gene, they often act to stabilise the transcript and promote protein synthesis (Koeller et al., 1989; Erlitzki et al., 2002).

To determine if the predicted IRE sequence in the 3' UTR of *zft* plays an important role in conferring iron-responsiveness, Dr. Megan Sloan deleted bases 2-25 from the predicted IRE sequence (18 nucleotides) and confirmed that its removal from the 3' UTR of *zft* reduced iron responsiveness (Sloan et al., 2025). Once validated, the same 18 nucleotide sequence were then deleted from the predicted IRE sequence in the *zft* 3' UTR in the background of ZFT-3HA$_{zft}$. I was curious to assess whether the deletion of these nucleotides in the IRE affected the responsiveness of ZFT to iron availability at the protein level. To do so, western blot analysis was performed on ZFT-3HA$_{zft}$ ΔIRE parasites either untreated (D3 only) or treated with iron chelation (100 μM DFO), or excess iron (500 μM FAC) conditions for 18 h (Figure 3.59a) and 24 h (Figure 3.59c). The iron responsiveness westerns were performed and quantified by Dr. Megan Sloan. We found that at 18 h post treatment, ZFT-3HA$_{zft}$ ΔIRE expression is not significantly altered in both high and low iron conditions (Figure 3.59a, b), similar to ZFT-3HA$_{zft}$ expression in the same conditions (Figure 3.11a, b and Figure 3.12a, b)

At 24 h post treatment, we found that ZFT-3HA$_{zft}$ ΔIRE expression is significantly (p = 0.0473, two-tailed paired t test) reduced to approximately 20 % compared to untreated cells in low iron conditions (Figure 3.59c, d), similar to ZFT-3HA$_{zft}$ expression in iron chelation conditions as well (Figure 3.11c, d). Interestingly, we found that in high iron conditions at 24 h, there is no significant difference in ZFT-3HA$_{zft}$ ΔIRE expression levels compared to untreated. This is different from the expression of ZFT-3HA$_{zft}$ in high iron conditions at 24 h post treatment, where I observed a significant reduction in expression (p = 0.0041, two-tailed paired t test) compared to untreated cells (Figure 3.12c, d).

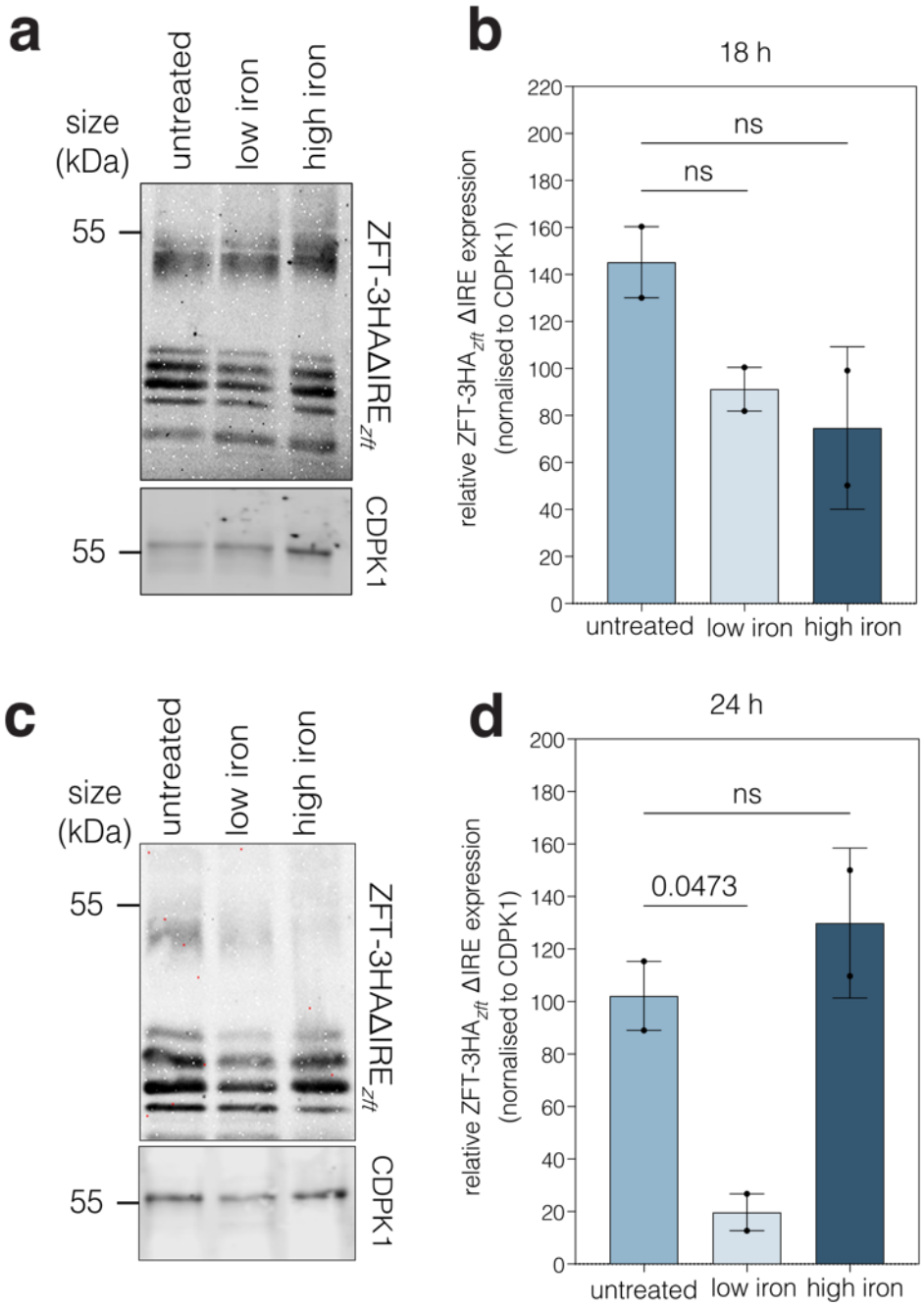


Figure 3.59 - F3ΔHX ZFT-3HA$_{zft}$ ΔIRE expression is not altered at 18 h in both low and high iron conditions, and at 24 h in high iron conditions, but significantly reduced in low iron conditions at 24 h.

a. Western blot analysis of ZFT-3HA$_{zft}$ ΔIRE expression in untreated, low iron (100 µM DFO) and high iron (500 µM FAC) conditions at 18 h post infection. CDPK1 used as a loading control. **b.** Quantification of ZFT-3HA$_{zft}$ ΔIRE levels at 18 h in untreated, low iron and high iron conditions from two independent biological experiments. Bars are at mean ± SD. *p* values from two-tailed paired t test. **c.** Western blot analysis of ZFT-3HA$_{zft}$ ΔIRE expression in untreated, low iron (100 µM DFO) and high iron (500 µM FAC) conditions at 24 h post infection. CDPK1 used as a loading control. **d.** Quantification of ZFT-3HA$_{zft}$ levels ΔIRE at 24 h in untreated, low iron and high iron conditions from two independent biological experiments. Bars are at mean ± SD. *p* values from two-tailed paired t test.

Next, I aimed to assess whether the deletion of these nucleotides in the IRE affected the responsiveness of ZFT to zinc availability instead at the protein level. To do so, western blot analysis was performed on ZFT-3HA$_{zft}$ ΔIRE parasites either untreated (D3 only) or treated with excess zinc (50 μM $ZnSO_4$) or 5 μM TPEN for 18 h (Figure 3.60a) and 24 h (Figure 3.60c).

At 18 h post treatment, ZFT-3HA$_{zft}$ ΔIRE expression is significantly reduced in both high zinc (p = 0.0260, two-tailed paired t test) and TPEN (p = 0.0137, two-tailed paired t test) conditions (Figure 3.60a, b). In high zinc conditions at 18 h, the expression of ZFT-3HA$_{zft}$ ΔIRE is different from ZFT-3HA$_{zft}$ expression which is not significantly changed (Figure 3.47a, b). Similar to ZFT-3HA$_{zft}$ expression at 24 h post treatment (Figure 3.47c, d), I found that ZFT-3HA$_{zft}$ ΔIRE expression is not significantly altered at 24 h in high zinc conditions (Figure 3.60c, d). However interestingly in TPEN chelation conditions, there is also no significant difference in ZFT-3HA$_{zft}$ ΔIRE expression levels compared to untreated (Figure 3.60c, d). This is different from the expression of ZFT-3HA$_{zft}$ in low zinc conditions at 24 h post treatment, where I observed a significant reduction in expression (p = 0.017, two-tailed paired t test) compared to untreated cells (Figure 3.47c, d). However, this experiment was only performed in two biological replicates and the second replicate demonstrated around an 80 % reduction in ZFT-3HA$_{zft}$ ΔIRE expression levels compared to untreated (Figure 3.60c, d). More biological replicates need to be performed to further explore this phenotype.

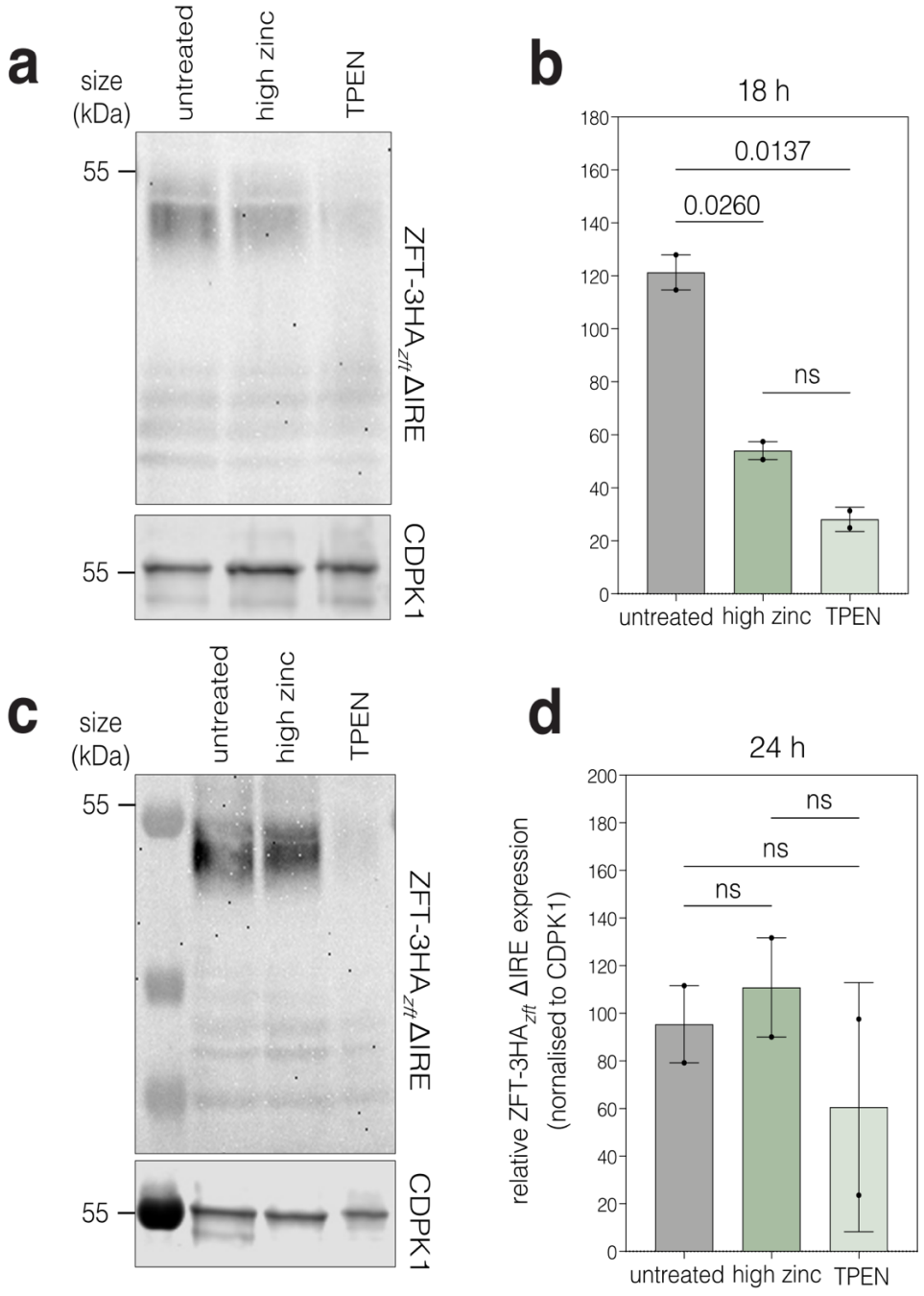


Figure 3.60 - F3ΔHX ZFT-3HAzft ΔIRE expression significantly reduced in both high zinc and TPEN chelation conditions at 18 h post treatment, however not altered in both conditions at 24 h.

a. Western blot analysis of ZFT-3HA$_{zft}$ ΔIRE expression in untreated, high zinc (50 μM $ZnSO_4$) and 5 μM TPEN conditions at 18 h post infection. CDPK1 used as a loading control. **b.** Quantification of ZFT-3HA$_{zft}$ ΔIRE levels at 18 h in untreated, high zinc and TPEN conditions from two independent biological experiments. Bars are at mean ± SD. *p* values from two-tailed paired t test. **c.** Western blot analysis of ZFT-3HA$_{zft}$ ΔIRE expression in untreated, high zinc (50 μM $ZnSO_4$) and 5 μM TPEN conditions at 24 h post infection. CDPK1 used as a loading control. **d.** Quantification of ZFT-3HA$_{zft}$ levels ΔIRE at 24 h in untreated, high zinc and TPEN conditions from two independent biological experiments. Bars are at mean ± SD. *p* values from two-tailed paired t test.

3.26 Discussion and Summary

3.26.1 ZFT protein kinetics and substrate specificity

Before the beginning of my PhD studies, the mechanisms by which *Toxoplasma gondii* acquired transition metals such as iron and zinc from its environment were unknown. In this chapter, I have characterised the first ZIP-domain containing protein in *T. gondii*, named ZFT. I have demonstrated for the first time, that this transporter is the major iron and zinc importer in the parasite, and is essential for its survival.

The analysis has revealed conserved residues (E181 and E211) in predicted *T. gondii* ZIP-domain containing proteins that have been shown to play a key role in metal binding and transport activity (Wiuf et al., 2022). Moreover, the analysis for the first time has identified a novel motif within the M1 metal binding centre which is conserved amongst coccidian parasites. However, further studies will be required to start to understand the role it plays in transition metal transport and substrate specificity.

Different ZIP subfamilies demonstrate different substrate specificities. TgZFT belongs to the ZIPI subfamily of ZIP transporters. Both ZIP founding members Zrt1/2 from *S. cerevisiae* and Irt1 in *A. thaliana* also belong to this subfamily of ZIP proteins. For example, AtIrt1 mainly plays a role in iron uptake, however, has also been shown to play a role in the uptake of other metals including zinc, manganese, cobalt and cadmium (Korshunova et al., 1999). Zrt1 and Zrt2 are high and low affinity zinc transporters respectively, however, have been shown to also transport manganese (H Zhao and Eide, 1996). The absence of the metalloprotease-like motif found in the LIV-1 subfamily of ZIPs is a further indication of this broader substrate specificity. Proteins belonging to the ZIPI subfamily have conserved metal binding residues including histidine, aspartate, and glutamate in the M1 and M2 metal binding sites in TM4 and TM5 of the transporter. These residues have been shown to play an important role in facilitating the binding and the translocation of metal ions across a lipid bilayer (Antala and Dempski, 2012; Lin et al., 2010). In human HsZIP8 and HsZIP14, a highly conserved histidine residue in the transport site is actually replaced by a glutamate residue and has been shown to likely be responsible for the broader

substrate specificity of these ZIPs (Aydemir and Cousins, 2018; C.-Y. Wang et al., 2012). In *Arabidopsis*, residues D108 and E111 play a role in determining the substrate specificity of AtIrt1. The replacement of glutamic acid with alanine inhibited zinc transport, and the replacement of aspartic residues with alanine also eliminated both manganese and iron transport (Rogers et al., 2000). These studies highlight the importance of the selectivity filter of the ZIPI subfamily of proteins in determining substrate specificity of ZIPs and could help inform or suggest possible residues that may play a functional role in metal binding and substrate specificity of ZFT in *Toxoplasma*. Moreover, the HK motif in the M2 metal binding site is also characteristic of the ZIPI subfamily of ZIP proteins, and is also shared in human HsZIP1 and HsZIP2 (Dufner-Beattie et al., 2003a). Although the presence of this lysine most likely prevents the binding of metals at the site, studies in HsZIP2 have shown that this motif is required for the transport activity. The analysis of the ZFT sequence and predicted protein structure confirmed the presence of a conserved residue leucine at position 403. This further supports the role of ZFT in iron and zinc transport, as this residue has previously been linked to broad substrate specificity in related transporters (Gyimesi et al., 2019).

Structure-function analysis could be investigated to test these assumptions and determine what residues are important for what substrate specificity (iron vs. zinc). Site directed mutagenesis to mutate the conserved amino acid residues in the metal binding sites in TM4 and TM5 of ZFT (e.g. H314 and E318) could possibly shift the substrate preference between metal ions and predict what amino acid residues are critical for the transport of iron and zinc. Finally, mutating the HK motif in the M2 metal binding site could elucidate whether this motif plays a role in ZFT transporter activity and substrate specificity. Following mutagenesis, transport activity of different substrates could be measured either by live-cell indicator dyes, radioactive metal uptake assays using radiolabelled $^{55/59}$Fe and ^{65}Zn, or elemental analysis techniques such as XFM and ICP-MS which would enable the simultaneous measurement of multiple metal substrates. This would allow us to further elucidate the residues that have an important role in the substrate specificity of ZFT in *Toxoplasma gondii*.

In this chapter, I have shown that ZFT is the major iron and zinc transporter. However, further studies could be performed to start to understand the substrate specificity and kinetics of ZFT by measuring uptake rates and kinetics of both iron

and zinc across a range of concentrations. For example, fitting Michaelis–Menten kinetics to obtain Km would allow us to investigate ZFT's affinity to these metals, as well as Vmax to examine ZFT's efficiency at transporting iron and zinc. Radioactive metal uptake assays could also be used to test whether ZFT has a higher affinity for zinc over iron, or vice versa, providing mechanistic insights into the physiological relevance of this transporter in *T. gondii*. A previous study has shown that in mouse ZIP8-expressing cells, a 10-fold molar excess of zinc inhibited 90 % of the uptake of ^{59}Fe (C.-Y. Wang et al., 2012). It would be interesting to further study ZFT's substrate specificity and assess whether there is any competition between the two metals and if one metal is inhibited by the presence of another by performing radioactive metal uptake competition assays. Moreover, some studies have described other ZIP family members to function as proton-coupled symporters (Girijashanker et al., 2008; Liu et al., 2008). Experiments involving measuring pH dependence, changes in membrane potential, or ion substitution, would elucidate whether ZFT also functions as a proton-coupled symporter in *T. gondii*.

3.26.2 Unusual dynamic localisation of ZFT has not previously been reported in *T. gondii*

In this chapter, I show that the localisation of ZFT is highly dynamic and dependent on vacuolar stage and intracellular replication, localising peripherally at the plasma membrane in vacuoles with fewer parasites, then moving to what I believe are vesicles clustered at the basal end of the larger vacuoles. This vacuolar stage dependent change in localisation is unusual and novel as it has not previously been reported in *Toxoplasma gondii*. Previous attempts by Cecilia Gallego Rubio and Dr. Clare Harding to fluorescently tag ZFT were unfortunately unsuccessful as they led to mislocalisation of ZFT to the endoplasmic reticulum (ER). This meant that tracking of ZFT trafficking in live cells was not possible. My current working hypothesis is that at early stages of replication, *T. gondii* requires transition metals such as iron and zinc, and thus expresses ZFT on the periphery at the plasma membrane. As the parasites go through 2-3 rounds of replication, the parasites may no longer require iron and zinc for replication purposes, and to avoid toxic metal overload (Aghabi et al., 2023), ZFT is then internalised possibly by endocytosis and is then either degraded, recycled, or trafficked into endosomal vesicles at the basal end of the parasite. This hypothesis may be supported by the

peripheral localisation of ZFT under low iron conditions (Figure 3.11), and the significant reduction of ZFT expression following degradation in high iron conditions (Figure 3.12).

In addition to ZIP-domain containing proteins transporting metal across the plasma membrane, some studies have shown that ZIP proteins also mediate transport from intracellular vesicles into the cytosol of cells (Hara et al., 2017; Jeong and Eide, 2013; Takagishi et al., 2017). For example, in mammalian cells, ZIP9 (Matsuura et al., 2009) and ZIP13 (Fukada et al., 2011; Jeong et al., 2012) are localised at the Golgi. ZIP8 localises to the plasma membrane, as well as to lysosomes and the mitochondria within the cells (Besecker et al., 2008). Furthermore, a ZIP protein that localises to the ER in mammalian cells is ZIP7 (Ohashi et al., 2016). Although the LOPIT data predicts ZFT to be localised to the plasma membrane (Barylyuk et al., 2020), the possibility of ZFT being localised to intracellular organelles and compartments within the cell should not be ruled out. It is possible that *T. gondii* uptakes materials from the extracellular environment in digestive vesicles, and then ZFT may possibly transport free metals from these digested vesicles into the cytosol. HaloTag labelling has previously been used to track proteins in live cells (Chang and Dickinson, 2022; Couturier et al., 2022), and this has previously been used to label proteins in *T. gondii* (Singer et al., 2023). Future work could attempt labelling ZFT with a HaloTag and tracking it in live cells throughout intracellular replication to track the trafficking of this protein. Moreover, previous studies have shown that alternative splicing regulates the subcellular localisation of the divalent metal transporter 1 (DMT1) isoforms (Tabuchi et al., 2002). It is interesting to note that ZFT is alternatively spliced, and there is a variant of the gene where exon 3 is completely absent. It may be possible that the different variants of ZFT are expressed in different cell cycle stages, which may explain the changes in localisation that I observe. Further work is required to further examine the highly dynamic localisation of ZFT in intracellular parasites.

3.26.3 *zft* 3' UTR plays a critical role in ZFT expression under different iron conditions

I examined the expression of ZFT in both the *sag1* 3' UTR tagged line as well as in the endogenous *zft* 3' UTR tagged line. The data shows that in the ZFT-3HA$_{sag1}$ line, ZFT expression is significantly reduced at both 18 and 24 h under low iron conditions (Figure 3.5). Interestingly, under low iron conditions, ZFT expression in the ZFT-3HA$_{zft}$ line was significantly reduced at 24 h however stabilised at 18 h (Figure 3.11). Previous work in the lab has shown that the important role that the 3' UTR of *zft* plays in iron sensing within the parasite, and that the *zft* mRNA transcript levels are stabilised under low iron conditions 18 h post treatment (Sloan et al., 2025). The data in this chapter further confirm the role of the 3' UTR of *zft* in stabilising ZFT protein levels at 18 h. Interestingly, under high iron conditions in the ZFT-3HA$_{sag1}$ line, ZFT expression is not significantly altered compared to untreated cells at both 18 and 24 h (Figure 3.6). However, in the ZFT-3HA$_{zft}$ line, ZFT expression levels are significantly reduced at 18 h and even more so at 24 h post treatment (Figure 3.12). This further elucidates to the important role that the 3' UTR of *zft* plays in iron sensing. It would be interesting to perform RT-qPCR experiments to investigate ZFT expression levels in both these lines in untreated, low, and high iron conditions at multiple time points close together throughout infection to better understand the dynamic expression of this protein in different iron availability environments.

3.26.4 Is ZFT being degraded and is the protein stabilised?

When I initially attempted to visualise ZFT protein levels by western blot analysis, the appearance of the multiple lower bands intrigued me. As they appeared to clear and distinct, I hypothesised that these lower bands are specific and may be degradation products of ZFT, and I was aiming to assess the predicted cleavage sites of ZFT to investigate if the size of these lower bands matched the degradation products of ZFT following cleavage. Before doing so, I treated the parasites with MG132, a proteosome inhibitor, for 5 h to examine whether blocking this would eliminate the lower bands, however the lower bands were still detected (Figure 3.9). This suggested to me that either the lower bands were non-specific, or that ZFT is being degraded in a non-proteasomal dependent manner. However, other lab members also observed these lower bands in HA tagged proteins.

Further, when tagging ZFT with a Ty tag in the overexpression line ZFT-Ty, the lower bands on the western blots were absent (Figure 3.14), suggesting that the lower bands observed in the ZFT-3HA parasites were nonspecific. Some anti-HA antibodies detect endogenous proteins that have HA-like motifs, giving reproducible lower bands. Mass spectrometry analysis of these fragments would give a definitive answer of what the lower bands actually are. The protein stability assay in Figure 3.13 shows that ZFT protein is not more stable under high iron and iron deprivation conditions compared to untreated conditions. This suggests that although ZFT expression is stabilised by western blot analysis under these iron conditions, possibly because the transcript is being stabilised (Sloan et al., 2025), the degradation rate/half-life of ZFT is not changed after CHX treatment in high and low iron conditions compared to untreated, reflecting differences between ZFT protein synthesis and protein degradation.

3.26.5 Overexpressing ZFT alters protein localisation and protein properties

To further assess the role that ZFT plays in iron acquisition in *T. gondii*, an overexpression line under the tubulin promoter was generated. When validating the line via western blotting, two distinct closely migrating bands were apparent. The presence of two distinct bands may point to some post-translational modifications of ZFT which are amplified by overexpressing ZFT. Moreover, some proteins are synthesised as a precursor and then cleaved to form the mature form. Overexpressing ZFT may have saturated the processing maturity, and the two bands observed may be both the precursor and the mature form. Previous studies have shown that ZIP proteins can form stable homodimers under native conditions (Bin et al., 2011; Lin et al., 2010; Liu et al., 2022; Taylor et al., 2016; Zhang et al., 2016). In this chapter, I performed a BN-PAGE and show that ZFT possibly forms a homodimer under native conditions (Figure 3.29). It is possible that the two distinct bands visible are homodimers, even more so as this is an overexpression system so the relative abundance of the dimers may be higher.

Interestingly, ZFT was detectable in western blots when expressed at endogenous levels in the ZFT-3HA$_{sag1}$ and ZFT-3HA$_{zft}$ tagged lines and subjected to boiling at 95° C for 5 minutes. However, when overexpressing ZFT, boiling the sample led to a loss of detectable signal, whereas omitting the boiling step restored ZFT

detection. This is likely due to heat-induced aggregation at high ZFT concentrations in the overexpression line. Overexpressing a protein can often lead to protein misfolding or make ZFT more prone to forming aggregates, which upon boiling, are insoluble. They either fail to enter the gel, or the aggregation can often mask the epitopes on the protein that are required for antibody recognition. This has also been observed with other transmembrane proteins, where exposure to heat treatment rendered proteins undetectable on a western blot (Tsuji, 2020).

To further validate the ZFT-Ty line, an immunofluorescence assay was performed initially at 24 hpi. In both the ZFT-3HA$_{sag1}$ and ZFT-3HA$_{zft}$ lines, ZFT localises at the plasma membrane of the parasites in small vacuoles at early stages of replication before moving to a basal localisation in larger vacuoles. However, at 24 h, the localisation of ZFT in the overexpression ZFT-Ty line appeared to be localised at the basal end, and also dispersed throughout the cytoplasm, with little to no localisation at the plasma membrane of the parasites (Figure 3.15). This observation is consistent with the possibility that the parasite limits excessive metal uptake by internalising or degrading ZFT, particularly when it is overexpressed, thereby preventing metal toxicity. It is possible that the overexpression of ZFT overwhelms the trafficking and folding machinery in the parasite, and that excess ZFT may get misfolded or stuck in compartments such as the Golgi or the ER which may explain the dispersed signal. As this is an overexpression line and metal toxicity is a concern, I looked at an earlier time point, 6 hpi to see if there were any changes to the localisation. Here, although no peripheral localisation was observed, I observed less dispersion throughout the cell cytoplasm and more visible puncta, possibly the plant-like vacuolar compartment (PLVAC) (Aghabi et al., 2023) as well as clear basal localisation. As too much iron is toxic for the parasite, ZFT may be being retained in the ER or trafficked for degradation via endosomal vesicular compartments or recycled, which may explain the distinct puncta and basal localisation observed. It would have been interesting to assess the localisation of ZFT in the overexpression line in low iron conditions using DFO. Moreover, it would have been interesting to perform an immunofluorescence assay on ZFT-Ty with an antibody against cathepsin protease L (CPL), which resides within the dynamic acidified organelle PLVAC (Dou et al., 2014; Stasic et al., 2022), to confirm whether or not ZFT colocalises with this compartment when it is overexpressed.

In this chapter, I have demonstrated that the overexpression of ZFT alters the localisation and protein properties of ZFT. Protein phosphorylation, a post-translational modification (PTM) is also likely to play a central role in the regulation of ZIP transporter activity. On ToxoDB, there is some evidence of the phosphorylation of ZFT, which would possibly explain some of the small changes visible by western blotting. An *in silico* analysis predicts that all human ZIPs are phosphorylated, emphasising the importance of this PTM in regulating ZIP transporter activity (Thingholm et al., 2020). Phosphorylation of ZIPs has been previously documented and plays an important role as a post translational regulation mechanism for the control of metal uptake. For example, the phosphorylation of the cytoplasmic IL-2 loop in the mammalian ZIP7 has been shown to increase ZIP transporter activity. The release of zinc from intracellular zinc stores such as the ER has been linked to the phosphorylation of Ser275 and Ser276 of mammalian ZIP7, which results in the phosphorylation of tyrosine kinases, activating intracellular signalling pathways in the cell and potentially phosphorylating other ZIPs to increase zinc uptake in low zinc conditions (Taylor et al., 2012; Thingholm et al., 2020). More recently, S294 and T294 have been shown to be phosphorylation sites in ZIP7, playing a critical role in the activity of the transporter (Nimmanon et al., 2017). Moreover, ZIP6, ZIP10 and ZIP14 have multiple tyrosine phosphorylation sites within this IL-2 loop (Taylor, 2023). In plants, the phosphorylation of this loop in AtIrt1 has been shown to be required for the endocytosis of this transporter in high zinc conditions (Dubeaux et al., 2018). Collectively, these studies support that possibility of ZFT phosphorylation, however further work is required to elucidate this and to understand the role that this would play in the control of metal uptake and the regulation of ZFT in different metal conditions in *Toxoplasma gondii*.

3.26.6 Parasites overexpressing ZFT are more sensitive to metal overload

The overexpression of metal transporters can be toxic to cells. In this chapter, I demonstrate that parasites overexpressing ZFT form fewer and smaller plaques compared to parental parasites, suggesting that overexpressing ZFT inhibits parasite replication, potentially due to increased metal uptake and toxicity. As anticipated, I demonstrate that in high iron conditions, parental parasites form fewer and smaller plaques compared to untreated cells, as too much iron can be

toxic and inhibit parasite replication. Parasites overexpressing ZFT have a growth defect compared to those untreated in high iron, however, this defect was not proportionally greater than the defect in the parental parasites under similar circumstances. This was intriguing, particularly as by a fluorescent growth assay, I show that parasites overexpressing ZFT are more sensitive to both excess iron (Figure 3.19) and zinc (Figure 3.46). A possible reason for this may be due to incubation times. The plaque assays were incubated for 6-7 days, compared to the fluorescent growth curves which were incubated for 3-4 days. It is possible that for the plaque assays, parasites overexpressing ZFT have had more time to compensate for the increased availability of iron by storing them within vacuolar compartments in the cell more efficiently to avoid metal toxicity. I also demonstrate that overexpressing ZFT provides a protective effect against the removal of iron, strongly supporting the role of ZFT in iron uptake in *T. gondii*. I performed plaque assays under low iron conditions using 100 µM DFO, however this was toxic to the host cells for a prolonged period of time (6-7 days) and almost completely disrupted the host cell monolayer. Thus, I was unable to quantify any plaque formation under these conditions. Future work could involve performing some plaque assays of parental and ZFT-Ty parasites under possibly 1-5 µM DFO to assess if ZFT-Ty parasites form more and larger plaques under iron chelation conditions compared to parental parasites. Moreover, I show that overexpressing ZFT does not alter parasite sensitivity to oxidative stress. Preliminary ICP-MS data shows that parasites overexpressing ZFT have significantly more parasite associated zinc but not iron. This could possibly be due to *T. gondii* enhancing mechanisms by which they store and detoxify excess iron, possibly through the vacuolar iron transporter VIT (Aghabi et al., 2023), as too much iron is toxic to the parasite. I would be intrigued to overexpress ZFT in the ΔVIT parasites and assess if this is toxic to the parasites, and if an increase in iron is observed by ICP-MS.

3.26.7 ZFT is essential for the survival of *Toxoplasma gondii* as it cannot be rescued by the presence of exogenous substrate

An inducible knockdown line, T7S4-ZFT, was generated to functionally assess the role of ZFT in iron and zinc transport, and to test its essentiality for parasite survival. Although *zft* transcript levels are reduced to around ~40 % compared to uninduced, this remains even after 96 h treatment with ATc (Figure 3.21). This is different from protein levels, where approximately ~30 % of the protein remained

after 24 h ATc, and ~10 % at 48 h. At both 72 and 96 h post ATc induction, ZFT protein is undetectable (Figure 3.28). This suggests that the transcript is stable, but the protein is being translationally modified and repressed, suggesting the protein is unstable and has a rapid turnover rate, being degraded at a fast rate. Moreover, it has been predicted that ZFT also has low translational efficiency being at the bottom of 20-40 % of all genes (Peters et al., 2025), which would further support this. Another possible explanation is experimental sensitivity. RT-qPCR is significantly more sensitive than western blotting. The 40 % transcript remaining may still be producing protein, however this may be below the detection limit of a western blot, particularly as ZFT is a low abundance protein. Another explanation is that the remaining RT-qPCR signal may be coming from an alternatively spliced isoform that the HA antibody is unable to detect. Interestingly at 96 h following ATc induction, the ZFT band at ~55 kDa is no longer detectable however the lower bands that were initially thought to be due to degradation of ZFT are still present, further supporting that these bands are non-specific and an artifact of the HA antibody. Further work is required to better understand how ZFT expression is regulated and modified, particularly translationally at the protein level.

In this chapter, I demonstrate that ZFT is essential for parasite survival as knocking down ZFT renders the parasites unable to form plaques in a host cell monolayer (Figure 3.22). I demonstrate that changing the promoter to a T7S4 promoter resulted in an overexpression of ZFT (Figure 3.26), and this alone made the parasites more sensitive to excess iron (Figure 3.23) and zinc (Figure 3.43). Other studies in *Plasmodium* were able to rescue the mutant phenotype by the addition of excess substrate (Chasen et al., 2019; Loveridge and Sigala, 2024). However, I show that the addition of excess iron, zinc, zinc ionophore, and iron and zinc combined were all unable to rescue the growth of ZFT knockdown parasites. Initially, I suspected that this may be due to the inability of the metals reaching the parasites, however I have shown from the live cell indicator dye FerroOrange and FluoZin-3AM verification experiments that the exogenous metals are able to reach the parasites. It may be possible that the concentrations of iron and zinc used were too high, particularly in the background of ZFT knockdown. It may be interesting to repeat these experiments with a lower concentration to examine if this rescues the phenotype, although the lower concentrations of metals may be

sequestered by host cells. I also attempted reducing the amount of ATc and adding excess iron; however, this also did not rescue the growth of ZFT knockdown parasites (Figure 3.24). It is possible that 0.25 µM ATc is still sufficient to efficiently knock down ZFT. RT-qPCR analysis could be performed to assess how much ZFT is present under half the standard concentration of ATc. However, I have shown that even after using 0.5 µM standard ATc concentrations, some ZFT remained both by quantifying mRNA levels (Figure 3.21) and protein levels (Figure 3.28), and it was not sufficient enough to rescue with the addition of excess iron (Figure 3.23).

The most compelling argument for the inability to rescue parasite growth following ZFT knockdown is that there is no other transporter in *Toxoplasma gondii* that is able to complement for the loss of ZFT. This raises the question of the role of the remaining three ZIP-domain containing proteins in *T. gondii* metal acquisition. The affinity of these transporters may be significantly lower for iron and zinc, and as we suspect ZFT is the major iron and zinc transporter, even excess iron and zinc is not sufficient to be taken up by other transporters on the surface to a level ample enough to rescue the growth of ZFT knockdown parasites. It is also a possibility that the other three predicted ZIP-domain containing proteins in *T. gondii* localise only inside the parasite rather than on the cell surface. Future work is required to further elucidate the roles of the remaining ZIP proteins in *Toxoplasma*. It would be intriguing to examine the expression of other ZIP proteins in *T. gondii* in the absence of ZFT, either by performing proteomic analysis on ZFT knockdown parasites to assess the general proteome response following ZFT knockdown, or by tagging the remaining ZIP proteins in the T7S4-ZFT background and assess what happens to their expression when ZFT is knocked down. Dr. Clare Harding and Elena Hartmann made some attempts to tag TGME49_225530, the second ZIP domain containing protein in *T. gondii,* predicted to be essential with 8 transmembrane domain containing proteins, however unfortunately this was unsuccessful.

To try and understand why the other predicted ZIP domain containing protein, TGME49_2255300 does not complement ZFT, I examined the percent identity between the two sequences using BLAST and looked at conserved residues. I found a 36 % protein sequence similarity. Interestingly, H314, E318 and E181 in the M1 metal binding site are all conserved between ZFT and TGME49_2255300. Both E211

and the lysine residue in M2 are also conserved in TM5, excluding the possibility of a second metal binding site. The main difference is that in contrast to ZFT which has a HGxxEG motif at the M1 BMC, TGME49_2255300 has a HAxxEG motif instead. Interestingly, this HAxxEG motif present in TGME49_2255300 is also present in ZIP-9 like prokaryotic proteins (Hu, 2021). Both glycine and alanine are aliphatic amino acids. As Ala (A) has a methyl side chain and is less flexible compared to Gly (G) which has a small neutral side chain, it is possible that the presence of an alanine instead of a glycine after the histidine restricts the conformation of the transporter. This would restrict the flexibility of the backbone and may result in a subtle misposition of the His residue which is essential for the binding of metals in ZIP proteins. This may in turn possibly reduce the binding affinity of TGME49_2255300 to iron and zinc compared to ZFT. Similarly, the presence of an Ile (I) instead of Met (M) in the M1 binding side in TGME49_2255300 removes the flexible side chain and replaces it with a more bulky and branched hydrophobic side chain (Hu, 2021). This may affect the binding affinity of iron and zinc by altering the metal coordination geometry at the BMC metal binding pocket. Another amino acid difference in the M1 binding site between these two ZIP sequences is the presence of an isoleucine instead of a leucine in TGME49_2255300. Both these amino acids are aliphatic; with non-polar, uncharged, and hydrophobic side chains. It is possible that the differences in branching may affect side-chain orientation and combined with other amino acid substitutions, this may change the geometry and confirmation of the structure, impairing metal binding, and transport. It is plausible that iron and zinc bind to TGME49_2255300, however possibly at a lower affinity. The amino acid substitutions may affect the confirmation changes required for the transport of these metals across the lipid bilayer.

3.26.8 Is iron critical for ZFT protein dimerisation in *Toxoplasma*?

ZIP-domain containing proteins have previously been shown to form homodimers or heterodimers (Ahern et al., 2020; Bin et al., 2011; Lin et al., 2011; Taylor et al., 2016). In this chapter, I performed a BN-PAGE and demonstrate that ZFT forms a complex of approximately 100 kDa, and that this complex is lost 48 h post knockdown, suggesting that ZFT forms a dimer (Figure 3.29). However, the role that iron plays in protein dimerisation, particularly in *T. gondii*, has not been

examined. The observation that ZFT forms a dimer may have functional relevance, as oligomerisation is often critical for transporter stability or activity. Some studies suggest a strong coupling between protein dimerisation and metal binding (Chou et al., 2004; Ghosh et al., 2015). Further experiments could investigate whether dimerisation of ZFT affects iron and zinc transport in *Toxoplasma gondii* by mutagenesis of predicted interfaces of ZFT in the context of metal transport in the parasite. Whether the dimerisation of ZFT is required for protein function and the relative abundance of ZFT in the monomer and dimer forms is also currently unknown and requires further studies. Performing an immunoprecipitation and mass spectrometry analysis is also required to identify binding partners and interactors of ZFT. A yeast two-hybrid (Y2H) assay could also be performed to identify protein-protein interactions.

3.26.9 ZFT knockdown triggers parasite differentiation, but is this an iron specific response or a general stress-induced one?

In this chapter, I demonstrated that ZFT knockdown parasites exhibit asynchronous replication and exhibit large, disorganised vacuoles (Figure 3.40). Moreover, 48 h post ZFT knockdown, parasites express significantly more bradyzoite specific marker, BAG1, and DBL, a lectin which binds to the cyst wall of the parasites (Figure 3.41), suggesting that knocking down ZFT may trigger initiation of stage conversion into bradyzoites. Parasites exposed to iron chelation via DFO also exhibit similar phenotypes, supporting that this transition is linked to iron deprivation. This phenotype has also been seen under iron chelation conditions in other studies (Renaud et al., 2024; Ying et al., 2024). Furthermore, I demonstrated that ~40 % of ZFT knockdown parasites initiate conversion to bradyzoites and don't actually die, and are able to survive the transient loss of ZFT, as their growth could be rescued by removing ATc (Figure 3.42). However, whether this trigger of differentiation is directly linked and specific to iron deprivation, or whether this is a general stress response that the parasites resort to for dormancy following nutrient deprivation, remains unknown. This phenotype has previously been observed in other mitochondrial mutants, for example of translation, transport, or of the electron transport chain (Maclean et al., 2024; Pamukcu et al., 2021; Silva et al., 2023). However, the metabolic or environmental cues that drive bradyzoite conversion in *Toxoplasma gondii* are not

completely understood. It is possible that knocking down ZFT could trigger metabolic signals derived in response to sensing a lack of iron and zinc which are essential for parasite survival. Previous studies have shown that inhibition of translation in *T. gondii* has previously been linked to stage conversion (Gastens and Fischer, 2002; Holmes et al., 2024, 2017; Wang et al., 2024). A puromycin incorporation assay (Maclean et al., 2024) could be performed to assess global protein translation and new protein synthesis following the knockdown of ZFT to understand if iron and zinc availability affects protein translation. Recent studies from the lab have shown that iron deprivation causes a significant decrease in global puromycin incorporation in the parasites, demonstrating an inhibition of translation, which can be rescued by the addition of excess iron (Hanna et al., 2025). It is therefore likely that ZFT knockdown may reduce global protein translation in the parasite, which is supported by the small decrease in sulphur and phosphorus seen by XFM, and this could in turn induce parasite differentiation.

3.26.10 Absence of ZFT alters both mitochondrial and apicoplast organellar function in *T. gondii*

In this chapter I demonstrate that although the mitochondrial morphology (Figure 3.33) and cristae formation (Figure 3.39) appear to be normal, knocking down ZFT reduces mitochondrial respiration at 48 h by Seahorse assay (Figure 3.38). Moreover, I found a significant reduction in the complex II Fe-S cluster protein SDHB (Maclean et al., 2021) expression levels (Figure 3.34), as well as reduced complex IV activity (Figure 3.36) within the mitochondrial electron transport chain, which would explain a reduction in mitochondrial respiration. Interestingly, we do not observe a reduction in mitochondrial respiration 24 h post ZFT knockdown – however there is still approximately 30 % of ZFT expression present at this time, and potentially this is not enough time to sufficiently deplete iron stores in the parasite. It would have been interesting to assess both SDHB and complex IV activity at this time point as well, which would strengthen the hypothesis that mitochondrial respiration at 48 h post ZFT knockdown is reduced due to the reduction in mitochondrial electron transport chain complex activity and complex II iron-bound protein SDHB.

Interestingly, the expression of ABCE1, a cytoplasmic Fe-S cluster protein, is not significantly altered post ZFT knockdown. This confirms that there is a lack of a global effect on all Fe-S cluster proteins in *T. gondii* upon knockdown of ZFT. This may also highlight differences in the role of Fe-S cluster proteins in different compartments within the parasite i.e. the mitochondria vs. the cytoplasm. It is possible that knocking down ZFT preferentially affects mitochondrial Fe-S cluster proteins before cytosolic ones, suggesting that the mitochondrial iron demand may be being prioritised.

Finally, previous studies have linked a reduction of mitochondrial respiration as well as the biogenesis of mitochondrial Fe-S cluster proteins to bradyzoite differentiation (Pamukcu et al., 2021; Tomavo and Boothroyd, 1995). It is possible that this may explain the trigger in bradyzoite conversion that is observed following ZFT knockdown. However, at this moment in time, the link between iron, zinc, and mitochondrial function with the stage conversion of tachyzoites to bradyzoites is currently not yet known.

Another organelle *in T. gondii* where iron is known to be required is the apicoplast (Renaud et al., 2022). Initially, the data shows that at 48 h post ZFT knockdown, no clear changes in apicoplast morphology (Figure 3.30) or function (Figure 3.31) were observed. However, although no change in apicoplast lipoylation was observed, there was a significant increase in the lipoylation of TgBCDH-E2, which localises in the mitochondria. This suggests an increase in mitochondrial lipoic acid scavenging from the host following the depletion of iron (Hanna et al., 2025). Moreover, upon ZFT depletion, a delayed phenotype is observed on the apicoplast, with a significantly higher proportion of apicoplast exhibiting an elongated morphology, in concert with a decrease in parasite replication (Figure 3.32), suggesting that knocking down ZFT results in a delayed phenotype on the apicoplast. This data further supports that metal import is required for the apicoplast in *Toxoplasma*. PfZIP1, a fitness conferring zinc transporter in *P. falciparum*, has been predicted to contain an apicoplast targeting sequence, transiently localising in the apicoplast (Sayers et al., 2018; Shrivastava et al., 2024), suggesting that zinc is also very likely to be essential and play an important role in the apicoplast. Further investigation is required to elucidate the role of zinc in the apicoplast of *T. gondii*. Moreover, in addition to zinc, no apicoplast-specific metal transporters have previously been characterised in *Toxoplasma*

gondii. Previous attempts in the lab by Grace Gill and Dr. Clare Harding have been made to characterise DMT2, a predicted apicoplast iron transporter, however unfortunately this was unsuccessful. I would have liked to repeat the CPN60 and lipoic acid assays following mechanical release and forced invasion of ZFT knockdown parasites to assess if a defect is observed in apicoplast function, which would support the elongated morphology observed.

3.26.11 What is the role of zinc in *T. gondii* and how do the parasites respond to zinc starvation?

ZIP-domain containing proteins are known to play an important role in zinc acquisition in mammalian cells (Besecker et al., 2008; Gaither and Eide, 2001b; Hara et al., 2017; Matsuura et al., 2009; Wang et al., 2004b), as well as in *Plasmodium* (Sahu et al., 2014; Shrivastava et al., 2024). Moreover, it has been observed in other organisms that ZIP-protein degradation can be mediated by excess zinc (Pang et al., 2023). However, interestingly in this chapter, I demonstrate that at both 18 and 24 h post treatment with excess zinc, ZFT expression levels are not significantly different compared to untreated cells (Figure 3.47). This is a different response to the availability of iron, where we observe a significant reduction in ZFT expression levels under high iron conditions at 24 h, and this expression is stabilised at 18 h (Figure 3.12). A possible explanation for this is that excess iron is maybe more toxic than other metals, and the parasite needs to regulate iron levels more efficiently when compared to zinc to avoid iron toxicity and cell death. Zinc fluctuations may be being buffered, and the parasite may rely more heavily on zinc storage and sequestration mechanisms in the parasite rather than uptake and transporter regulation. It is a possibility that *T. gondii* relies more heavily on iron uptake via ZFT to maintain iron homeostasis in the parasite and is possibly not as efficient or effective at sequestering or storing iron in the parasite in high iron conditions, compared to zinc. This would explain the significant decrease in ZFT transporter expression levels in excess iron. Further, there is evidence from other systems that excess zinc can modulate iron uptake (Blaby-Haas and Merchant, 2013; Xu et al., 2019) as well as copper homeostasis in *E. coli* (Xu et al., 2019). It is also possible that excess zinc results in a decrease in iron acquisition, which would support the stabilisation of ZFT expression under these conditions.

In this chapter, I also show that at both time points, ZFT expression is significantly reduced under low zinc conditions following chelation using TPEN (Figure 3.47). This is a similar response to the availability of iron, where a significant reduction in ZFT expression under low iron conditions at 24 h is observed (Figure 3.11). Previously, the lab has shown that ZFT expression is stabilised under iron chelation conditions (Sloan et al., 2025). However, ZFT expression is stabilised under low iron at 18 h (Figure 3.11), and this effect is not observed under zinc chelation conditions using TPEN (Figure 3.47). As the potential of zinc-mediated regulation in *T. gondii* has not yet been assessed, it is unclear to establish whether the lack of stabilisation of ZFT under TPEN conditions at 18 h is due to the inability of the parasites to sense and respond to zinc in the same way as iron. It may also be due to the length of time the parasites were treated, or the treatment concentrations and conditions, as these may have been insufficient to trigger such pathway as seen with iron. Future work is needed to establish zinc sensing in the parasite. Moreover, while the importance and role of iron in *T. gondii* has previously been established, more studies are required to examine the role that zinc plays in *Toxoplasma* and how these parasites respond to zinc starvation conditions.

3.26.12 Yeast complementation experiments strongly support that ZFT is a zinc transporter in *Toxoplasma gondii*, but what about iron?

One way to evaluate the functionality of a transporter is through yeast heterologous complementation experiments. In this chapter, I show that TgZFT is able to complement the lack of zinc transport in the *Δzrt1/2* mutant by rescuing growth both in SD-Ura and SD-Ura + EGTA chelation conditions, strongly supporting the functional role of TgZFT as a zinc transporter (Figure 3.48). I further suggest the substrate specificity of ZFT, as it was unable to complement the lack of a high affinity manganese transporter in the *Δsmf1* mutant (Figure 3.49). To investigate whether ZFT has a functional role in iron uptake in addition to zinc in *T. gondii*, I aimed to express the codon optimised ZFT in a *S. cerevisiae* iron transporter mutant that lacks both the low and high affinity iron transporter *Δfet3/4* (Ullah et al., 2018). However, despite six attempts, no viable transformants were recovered. This may be because the expression of ZFT in the *Δfet3/4* mutant may be toxic to the yeast in this background, or that *Δfet3/4* was unable to survive the transformation protocol.

Another way to confirm the direct role of ZFT in iron uptake is by ectopically expressing ZFT on the surface of *Xenopus laevis* oocytes. This work was done by Dr. Lucas Pagura in the lab of Giel van Dooren with the help of Dr. Steven Fairweather at the Australian National University. To assess whether the expression of ZFT on the surface of the oocytes mediated the uptake of iron, oocytes were incubated in the presence of radioactive iron, $^{55}Fe^{2+}$, and the uptake of iron by each individual oocyst was measured. Although the uninjected control oocytes did not take up iron over time, oocytes expressing ZFT on their surface showed saturable iron uptake over time. We were next curious to assess whether ZFT also mediates the uptake of zinc in *Xenopus laevis* oocytes and demonstrated that iron uptake is significantly inhibited/outcompeted in the presence of excess zinc. This has also been proposed for HsZIP8 and HsZIP14 in humans (Pinilla-Tenas et al., 2011; C.-Y. Wang et al., 2012). In addition to the yeast complementation experiments, these data strongly support that ZFT mediates both iron and zinc uptake in *T. gondii*.

3.26.13 The limitations of ICP-MS and XFM as elemental analysis techniques in *Toxoplasma gondii*

Both elemental analysis techniques ICP-MS and XFM have been instrumental to characterising ZFT as the major iron and zinc transporter in *Toxoplasma gondii*. However, although the data demonstrated a significant reduction in parasite associated zinc following ZFT knockdown at both 24 and 48 h by ICP-MS (Figure 3.52), no significant decrease in parasite associated iron was observed at both time points (Figure 3.52). A possible explanation for this is that iron levels within the parasite, even in untreated cells, are very close to the limit of detection. Studies have shown that the detection of iron in cells by ICP-MS can also be challenging due to interference (Segura et al., 2003). In contrast, zinc levels within the parasite are notably significantly higher and therefore more readily detected by ICP-MS analysis. Further, I found that parasite associated copper levels do not significantly change following ZFT knockdown by ICP-MS analysis (Figure 3.57), suggesting that ZFT does not have any substrate specificity for copper, and that the knockdown of ZFT does not trigger any other pathways to increase copper uptake within the parasite.

XFM analysis showed that parasites have significantly reduced iron (Figure 3.53) and zinc (Figure 3.54) at both 24 and 48 h following ZFT knockdown, strongly supporting that ZFT is the major iron and zinc transporter in *Toxoplasma gondii*. I demonstrated that by XFM, the percentage of zinc in ZFT knockdown parasites compared to untreated cells is lower than that of iron – suggesting the rate at which zinc is depleted upon knockdown of ZFT is faster than that of iron. It may be possible that ZFT has a higher affinity for zinc compared to iron, however kinetic studies are needed to further assess this. Moreover, it may most likely be that ZFT is the only and major zinc transporter in *T. gondii*. This may also result in the parasite releasing iron from stores such as the PLVAC and the mitochondrion to balance out the reduction of iron levels following knockdown of ZFT. Differences in how these metals are stored within the parasite could also be a possible explanation, where iron can be sequestered with haem and Fe-S cluster proteins, whereas zinc may rely more heavily on continuous import from the environment. A possible explanation is that zinc may be more labile within the parasite and possibly primarily buffered by zinc-binding enzymes and proteins such as zinc finger transcription factors and metalloproteins, supporting a more dramatic decrease in zinc levels within the parasite following ZFT knockdown. In prokaryotic cells, approximately 5-6 % of the proteome are zinc-binding proteins (Andreini et al., 2006b). Moreover, a study in *P. falciparum* has demonstrated that the parasite accumulates substantial labile/free zinc pools, and the dynamic fluxes in these pools has been shown to be essential for parasite growth in erythrocytes (Marvin et al., 2012). Iron regulation and balance within *Toxoplasma gondii* may be more tightly controlled and regulated when compared to zinc, however future work is required to fully elucidate and support this.

Further, due to technical reasons, XFM in this study was performed on chemically fixed parasites using 4 % paraformaldehyde (PFA). It is important to consider that this may have altered the distribution of metals within the parasite and may have caused metals to diffuse out of their native compartments, leading to an underestimation of metal concentration within the parasite (Jin et al., 2017). Despite limitations of chemical fixation methods, this technique still provided direct evidence of changes in elemental composition in *Toxoplasma gondii* upon knockdown of ZFT. For future studies and higher fidelity XFM, cryofixation/cryogenic preparation of parasites will be performed instead to

preserve metals such as iron and zinc in a near-native hydrated state within the parasite for a more accurate representation of metal concentrations.

3.26.14 Final summary and concluding remarks

In this chapter, I show that both zinc and iron often appear as specific localised foci or puncta in extracellular parasites by XFM, which I believe to be the PLVAC where these metals are stored based on previous observations (Aghabi et al., 2023; Chasen et al., 2019). Beyond the localised foci, the data also demonstrates that zinc appears to be concentrated to the nucleus of the parasites, where it plays a role in gene expression as well as DNA replication (Olea-Flores et al., 2022). It would be interesting and informative to combine organellar localisation with XFM to more clearly start to understand where these metals are localised within the parasites. It would also be interesting to localise ZFT by XFM and examine how this correlates with both iron and zinc localisation within the parasite.

Future work is required to optimise such experiments and conditions. Recently, the development of X-ray sensitive tags allows for the visualisation of specific organelles or protein of interest (POI) by XFM. These X-ray sensitive probes are most commonly made up of an X-ray fluorophore that is conjugated to an affinity tag. Some examples of these fluorophores include gold nanoparticles and quantum dots which when conjugated to a secondary antibody can target a particular antigen within the cell as long as an organelle-specific peptide is attached to it (Corezzi et al., 2009; McRae et al., 2006; H. Wang et al., 2012). For example, cells can be treated with primary antibodies specific to the intracellular organelles such as the mitochondria, ER or Golgi apparatus. A commercial secondary antibody, FluoroNanogold, is then added and conjugated to the primary antibody. This antibody is composed of a gold cluster as well as a fluorescent tag. This allows for the visualisation of subcellular organelles using XFM as gold binds specifically to the target organelles (McRae et al., 2006). Finally, a metal binding peptide can be genetically encoded with a protein of interest to visualise subcellular localisation (Victor et al., 2020). The addition of 12 his-tags to ZFT could possibly allow for the visualisation of ZFT by XFM, as nickel has a high binding affinity to his-tagged proteins. Combining these X-ray sensitive metal probes with X-ray fluorescence microscopy allows for the correlation of a POI /organelle with its chemical environment.

In summary, in this chapter, I characterise the first metal importer in *Toxoplasma gondii*. The data validates that ZFT, a ZIP-domain containing protein, is indispensable, highlighting the critical role of both iron and zinc in the parasite. The findings presented in this chapter are novel and advance the field by expanding on the knowledge of how these obligate intracellular parasites acquire nutrients from its environment, and the impact this in turn has on parasite survival and replication within its host.

Chapter 4 The battle for iron between the host and the bug: How *Toxoplasma gondii* modulates host iron homeostasis following infection

4.1 Introduction and chapter aims

In the chapter, I aim to investigate if and how *Toxoplasma gondii* infection modulates iron homeostasis and subverts host cell iron trafficking following infection to enable replication within its host cell in two different cell types: fibroblasts and macrophages. To do so, I will examine the expression and localisation of key proteins involved in iron homeostasis including TfR, DMT1 and FTH1. Understanding the effects of *Toxoplasma* infection on these proteins will demonstrate a mechanistic insight into host-pathogen interactions, highlighting the availability of iron as a bottleneck for *T. gondii* growth and broadening the field of nutritional immunity. The parasite-driven disruption of cellular iron homeostasis is a virulence trait that could be a potential therapeutic target.

4.2 *Toxoplasma gondii* modulates host iron homeostasis in fibroblast cells

4.2.1 Transferrin receptor is upregulated in *T. gondii* infected HFFs

In mammalian cells, iron can be acquired by the ubiquitous transferrin-transferrin receptor (TfR) pathway (Theurl et al., 2005). This complex is often internalised into the cell via clathrin-mediated endocytosis, these are trafficked to lysosomes where iron is then released from transferrin and resulting intracellular free iron joins the labile iron pool (LIP). Transferrin receptors are recycled back up to the cell surface. A study on gene-array hybridisation assays to determine the transcriptional role of *T. gondii* infection has demonstrated an upregulation of transferrin receptor expression levels in infected fibroblasts. This was also further supported by western blots (Gail et al., 2001, 2004).

To confirm if infection with *Toxoplasma* increases TfR expression levels in fibroblasts, I infected HFFs with RHΔKu80 parasites for 24 h before harvesting cells and performing a western blot analysis (Figure 4.1a). To determine whether availability of iron affected the expression of TfR, particularly in the context of infection, I pretreated HFFs with 500 μM FAC for 24 h before infecting with RHΔKu80 tachyzoites for a further 24 h (Figure 4.1a). I found that transferrin receptor expression levels are significantly ($p < 0.001$, one-way ANOVA, Tukey corrected for multiple comparisons) increased following *T. gondii* infection at 24 h (Figure 4.1b). There is no significant change in TfR expression levels in uninfected cells even in the presence of excess iron (Figure 4.1b). I found that in the presence of excess iron, infected HFFs have significantly ($p < 0.001$, one-way ANOVA, Tukey corrected for multiple comparisons) increased TfR expression levels compared to uninfected HFFs treated with excess iron (Figure 4.1b). The data further demonstrates that in the presence of excess iron and infection for 24 h, the TfR expression levels are significantly ($p = 0.0161$, one-way ANOVA, Tukey corrected for multiple comparisons) reduced when compared to untreated infected cells (Figure 4.1b).

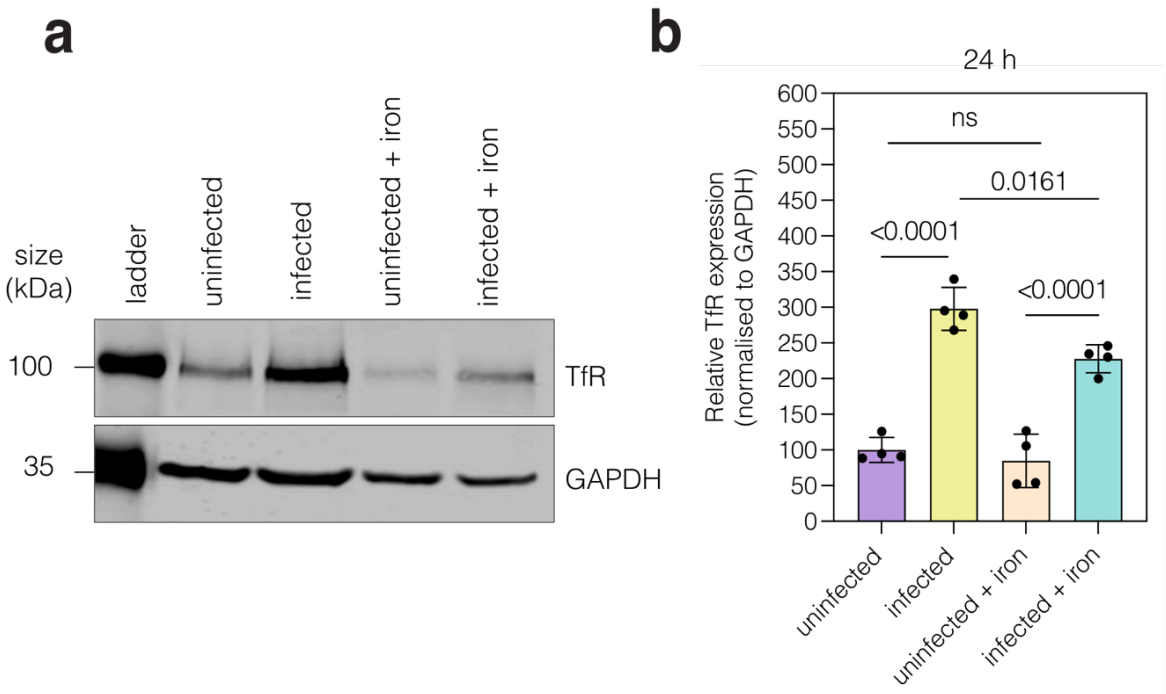


Figure 4.1 – TfR expression is upregulated in *T. gondii* infected HFFs at 24 h.

a. Western blot analysis of TfR expression in uninfected and RHΔKu80 infected HFFs in both untreated and high iron (500 μM FAC) conditions at 24 h. GAPDH used as a loading control. **b.** Quantification of TfR expression levels in uninfected and infected HFFs in both untreated and high iron (500 μM FAC) conditions at 24 h, relative to uninfected untreated, from four independent biological experiments. Bars are at mean ± SD. *p* values from ordinary one-way ANOVA, Tukey corrected for multiple comparisons.

Following the confirmation of an increase in transferrin receptor expression levels at 24 h, this was further validated by examining the levels of transferrin binding on the surface of infected fibroblasts. This work was done by Dr. Clare Harding. To do so, HFFs were infected with RHΔKu80:tdTomato parasites for 24 h before staining with fluorescent transferrin (Tf-A488) and analysing on a flow cytometer. The data demonstrates that there is a significant (p = 0.0035, one-way ANOVA, Tukey corrected for multiple comparisons) increase in Tf-A488 binding on the surface of infected HFFs at 24 h, compared to uninfected cells (Figure 4.2). Using cells with no red signal as uninfected, bystander cells within the infected sample showed no significant change in Tf-A488 binding when compared to uninfected cells (Figure 4.2). This data further supports the increase in transferrin receptor expression and suggests that fibroblast cells take up significantly more transferrin following infection with *T. gondii*.

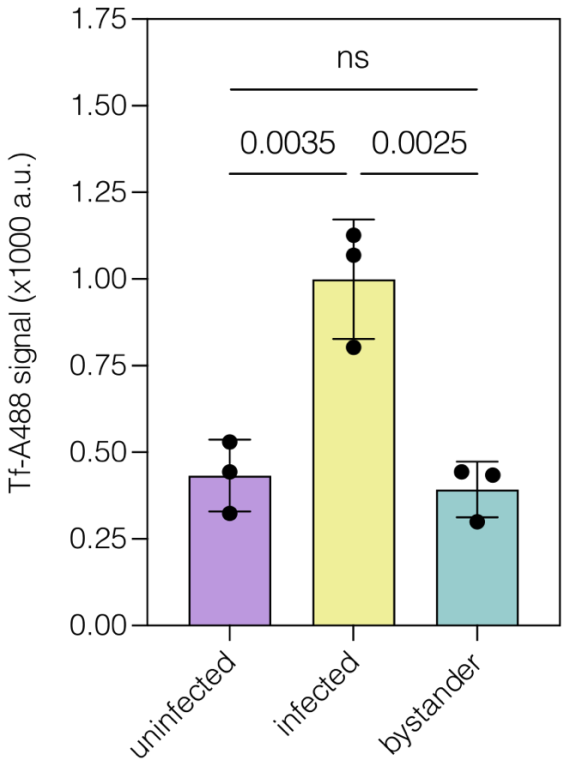


Figure 4.2 - Fluorescent Tf-A488 binding increases on the surface of *T. gondii* infected HFFs at 24 h.

Quantification of Tf-A488 fluorescent signal from three independent biological replicates from fibroblasts infected with RHΔKu80:tdTomato parasites for 24 h. Bars are at mean ± SD. *p* values from ordinary one-way ANOVA, Tukey corrected for multiple comparisons.

To assess if infection with *Toxoplasma* maintains increased TfR expression late in infection, I infected HFFs with RHΔKu80 parasites for 48 h before harvesting the cells and performing a western blot as above (Figure 4.3a). I found that similar to 24 h, transferrin receptor expression levels are significantly (p = 0.0007, one-way ANOVA, Tukey corrected for multiple comparisons) increased following *T. gondii* infection at 48 h (Figure 4.3b). Similar to 24 h, there is also no significant change in TfR expression levels in uninfected cells even in the presence of excess iron (Figure 4.3b). Moreover, I found that in the presence of excess iron, infected HFFs have no significant change in TfR expression levels compared to uninfected HFFs treated with excess iron (Figure 4.3b). Interestingly, the data further demonstrates that in the presence of excess iron and infection for 48 h, the TfR expression levels are significantly (p = 0.0110, one-way ANOVA, Tukey corrected

for multiple comparisons) reduced when compared to untreated infected cells (Figure 4.3b).

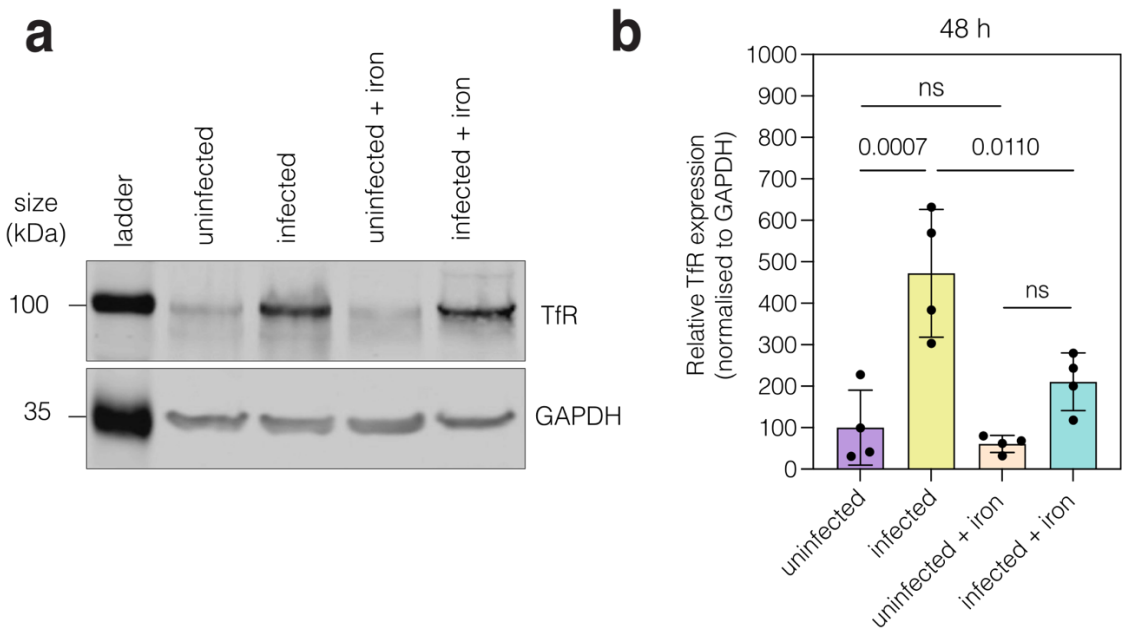


Figure 4.3 - TfR expression is upregulated in *T. gondii* infected HFFs at 48 h.

a. Western blot analysis of TfR expression in uninfected and RHΔKu80 infected HFFs in both untreated and high iron (500 μM FAC) conditions at 48 h. GAPDH used as a loading control. **b.** Quantification of TfR expression levels in uninfected and infected HFFs in both untreated and high iron (500 μM FAC) conditions at 48 h, relative to uninfected untreated, from four independent biological experiments. Bars are at mean ± SD. *p* values from ordinary one-way ANOVA, Tukey corrected for multiple comparisons.

4.2.2 DMT1 is upregulated in *T. gondii* infected HFFs

Mammalian cells can also acquire non-transferrin bound iron through a divalent metal transporter 1 (DMT1) (SLC11A2) (Yanatori and Kishi, 2019). DMT1 also functions as a transporter to release iron from endosomal compartments, particularly lysosomes, within the cell into the cytoplasm (Weber et al., 2020). STEAP3, a six-transmembrane epithelial antigen of the prostate 3, an endosomal reductase, reduces iron from the ferric Fe^{3+} form to the ferrous Fe^{2+} form (Galy et al., 2024; Ohgami et al., 2006, 2005), which joins the LIP within the cytosol of the cell.

To assess the effect of *T. gondii* infection on DMT1 expression in fibroblast cells, I infected HFFs with RHΔKu80 parasites for 24 h before harvesting the cells and performing a western blot (Figure 4.4a). I show that DMT1 expression levels are significantly (p = 0.0110, one-way ANOVA, Tukey corrected for multiple comparisons) increased following *T. gondii* infection at 24 h (Figure 4.4b). In the presence of excess iron, DMT1 expression in HFFs is significantly (p = 0.0053, one-way ANOVA, Tukey corrected for multiple comparisons) increased, and this was exacerbated in infected cells (Figure 4.4b). Interestingly, the data further demonstrates that in the presence of excess iron and infection for 24 h, the DMT1 expression levels are significantly (p = 0.0361, one-way ANOVA, Tukey corrected for multiple comparisons) increased when compared to untreated infected cells (Figure 4.4b). I next performed an immunofluorescence assay whereby I infected HFFs with RHΔKu80:tdTomato parasites for 24 h before fixing and staining. I found that DMT1 localisation is altered following *Toxoplasma gondii* infection at 24 h (Figure 4.4c). In uninfected fibroblasts, DMT1 seems to localise near the nucleus, particularly near the endosomes and the Golgi apparatus. However, after infection with *T. gondii*, DMT1 localisation seems to change and is now being redirected and recruited to around the parasitophorous vacuole.

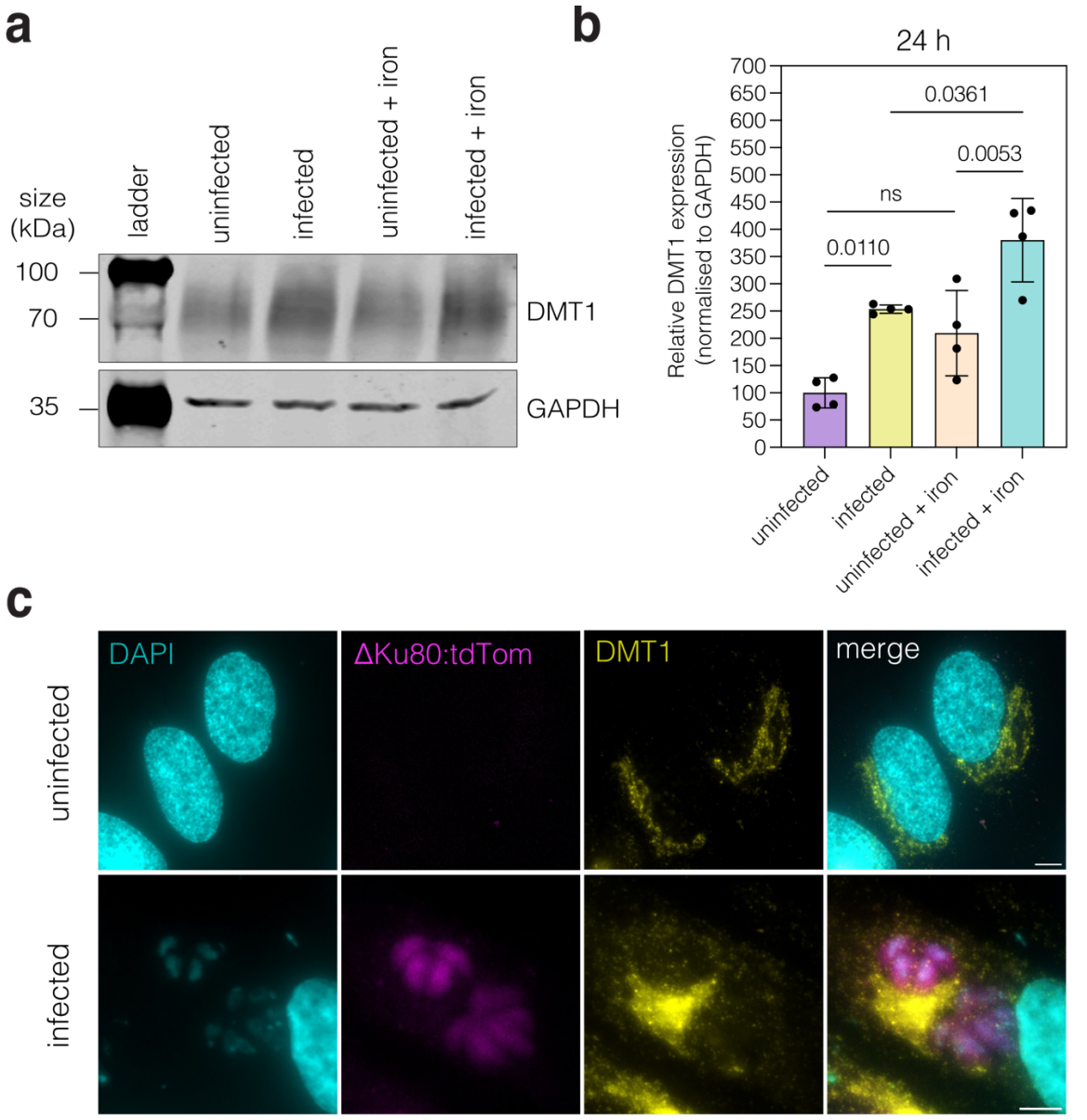


Figure 4.4 – DMT1 expression is upregulated in *T. gondii* infected HFFs at 24 h, and DMT1 localisation is altered in fibroblasts following infection.

a. Western blot analysis of DMT1 expression in uninfected and RHΔKu80 infected HFFs in both untreated and high iron (500 μM FAC) conditions at 24 h. GAPDH used as a loading control. **b.** Quantification of DMT1 expression levels in uninfected and infected HFFs in both untreated and high iron (500 μM FAC) conditions at 24 h, relative to uninfected untreated, from four independent biological experiments. Bars are at mean ± SD. *p* values from ordinary one-way ANOVA, Tukey corrected for multiple comparisons. **c.** Immunofluorescence assay of uninfected and infected HFFs at 24 h showing a change in DMT1 localisation upon *T. gondii* infection. Scale bar 5 μM.

To investigate if infection with *Toxoplasma* increases DMT1 expression levels in fibroblasts at a later time point, I collected samples as described above. Increased DMT1 expression following infection was maintained at 48 h post infection compared to 24 h, still significantly *(p* = 0.0269, one-way ANOVA, Tukey corrected for multiple comparisons) increasing following *T. gondii* infection (Figure 4.5a, b). DMT1 expression levels are also maintained as 24 h in the presence of excess iron in uninfected cells, with no significant change in expression levels (Figure 4.5a, b). DMT1 expression levels are also maintained in the presence of excess iron and infection as 24 h, significantly (*p* = 0.0018, one-way ANOVA, Tukey corrected for multiple comparisons) increasing in infected HFFs in the presence of excess iron compared to uninfected HFFs also treated with excess iron (Figure 4.5a, b). Finally, in the presence of excess iron and infection for 48 h, DMT1 expression levels maintained as 24 h, also significantly (*p* = 0.0258, one-way ANOVA, Tukey corrected for multiple comparisons) higher when compared to untreated infected cells (Figure 4.5a, b).

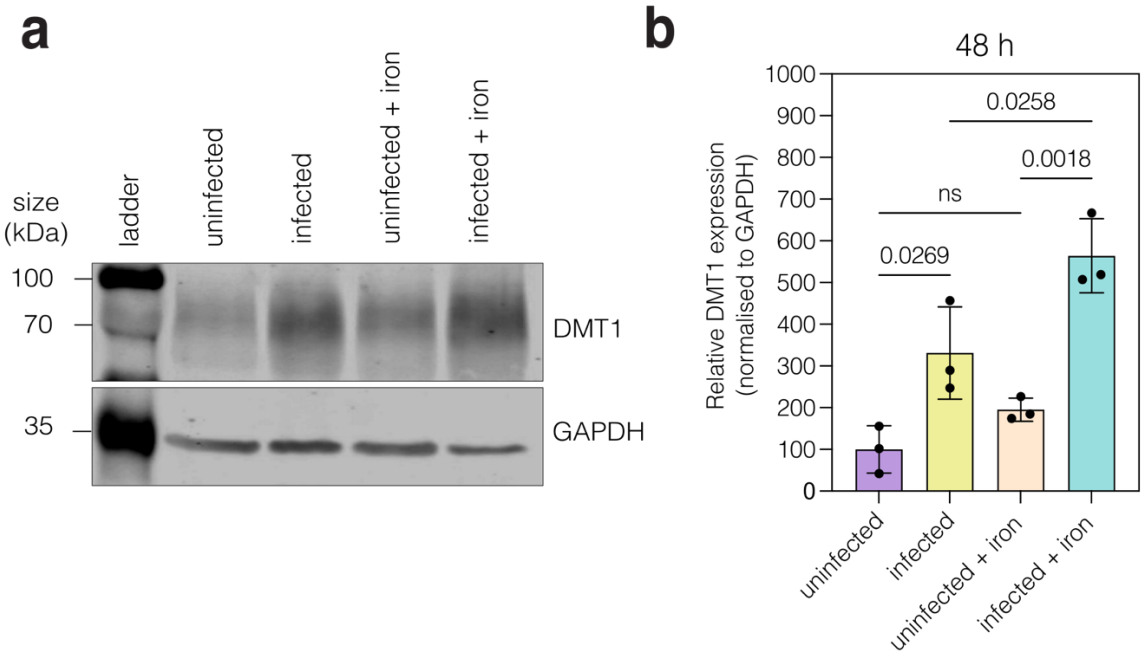


Figure 4.5 - DMT1 expression is upregulated in *T. gondii* infected HFFs at 48 h.

a. Western blot analysis of DMT1 expression in uninfected and RHΔKu80 infected HFFs in both untreated and high iron (500 μM FAC) conditions at 48 h. GAPDH used as a loading control. **b.** Quantification of DMT1 expression levels in uninfected and infected HFFs in both untreated and high iron (500 μM FAC) conditions at 48 h, relative to uninfected untreated, from three independent biological experiments. Bars are at mean ± SD. *p* values from ordinary one-way ANOVA, Tukey corrected for multiple comparisons.

The change in expression levels and localisation of DMT1 following *T. gondii* infection may be a host driven response to combat infection by increasing iron levels in the cell to kill the parasite, or it may potentially equally be a parasite driven response where *Toxoplasma* actively manipulates host iron handling. One way *T. gondii* would be able to do this is through secreted proteins, as has been established for other organisms (Christenson et al., 2019; Sen et al., 2022). To assess whether DMT1 expression in fibroblasts is modulated by secreted proteins following infection, I infected HFFs with a mutant parasite strain, defective in effector secretion, ΔMYR1 (c-myc regulation 1) and assessed DMT1 protein expression (Figure 4.6a). MYR1 localises to the parasite PV membrane and forms part of a multiprotein complex which plays a role in mediating the release of secreted effector proteins, including GRA16 and GRA24, across the PV membrane of the parasite into the host cell, in turn controlling important signaling pathways within the host (Bougdour et al., 2013; Franco et al., 2016; Marino et al., 2018). However, I observe no significant difference in DMT1 expression in HFFs infected with ΔMYR1 parasites compared to RHΔKu80 parasites at 24 h (Figure 4.6b), suggesting that DMT1 expression is most likely not regulated by *T. gondii* MYR1-dependent secreted proteins.

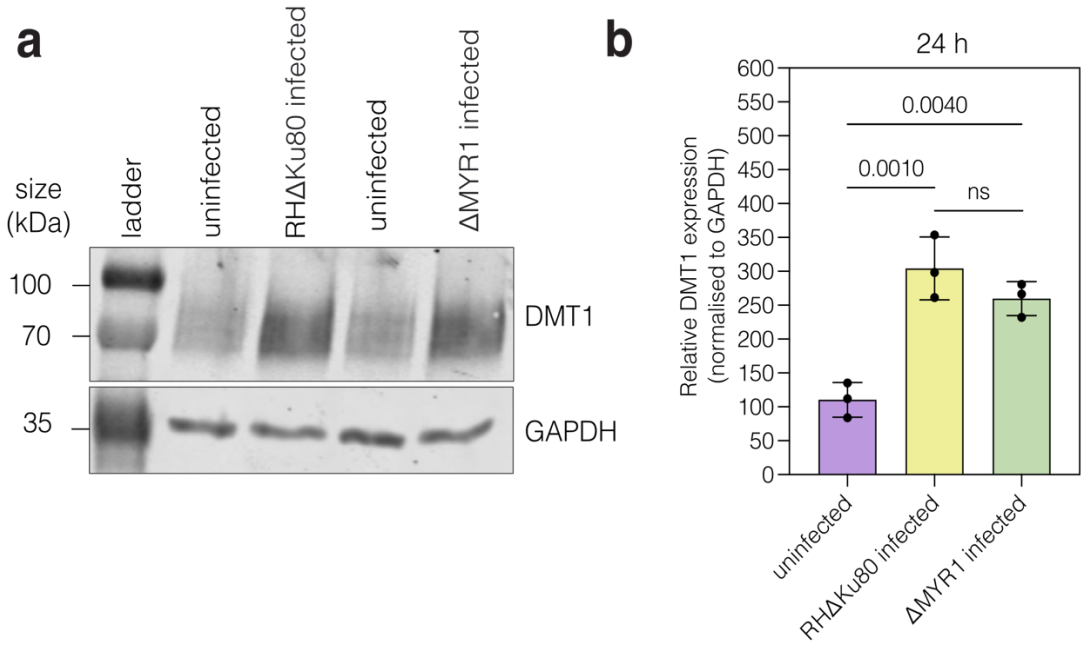


Figure 4.6 – There is no significant difference in DMT1 expression in HFFs infected with ΔMYR1 compared to RHΔKu80 parasites at 24 h.

a. Western blot analysis of DMT1 expression in uninfected, RHΔKu80 infected and ΔMYR1 infected at 24 h. GAPDH used as a loading control. **b.** Quantification of DMT1 expression levels in uninfected and infected HFFs at 24 h, relative to uninfected, from three independent biological experiments. Bars are at mean ± SD. *p* values from ordinary one-way ANOVA, Tukey corrected for multiple comparisons.

4.2.3 Ferritin heavy chain 1 (FTH1) expression is unaltered in *T. gondii* infected HFFs

As free labile iron is toxic, in mammalian cells approximately 75 % of iron is stored within protein cages of ferritin within the cytoplasm (D. J. R. Lane et al., 2015). When iron is required in the cell, it is released from ferritin through autophagic degradation/ferritinophagy via lysosomes (Mancias et al., 2014; Zhu et al., 2024).

To assess the effect of *T. gondii* infection and iron treatment on ferritin heavy chain 1 (FTH1) expression levels in fibroblast cells, I infected HFFs with RHΔKu80 parasites for 24 h before harvesting the cells and performing a western blot analysis (Figure 4.7a). Interestingly, I found that FTH1 expression levels in infected HFFs do not significantly change compared to uninfected HFFs at 24 h (Figure 4.7b). As expected, I show that there is a significant ($p < 0.0001$, one-way ANOVA, Tukey corrected for multiple comparisons) increase in FTH1 expression levels in uninfected cells in the presence of excess iron compared to uninfected untreated cells. Moreover, the data shows that there is a significant ($p < 0.0001$, one-way ANOVA, Tukey corrected for multiple comparisons) increase in FTH1 expression levels in infected cells in the presence of excess iron compared to infected untreated cells. The data further demonstrates that in the presence of excess iron and infection for 24 h, there is no significant change in FTH1 expression levels when compared to untreated, infected cells (Figure 4.7b).

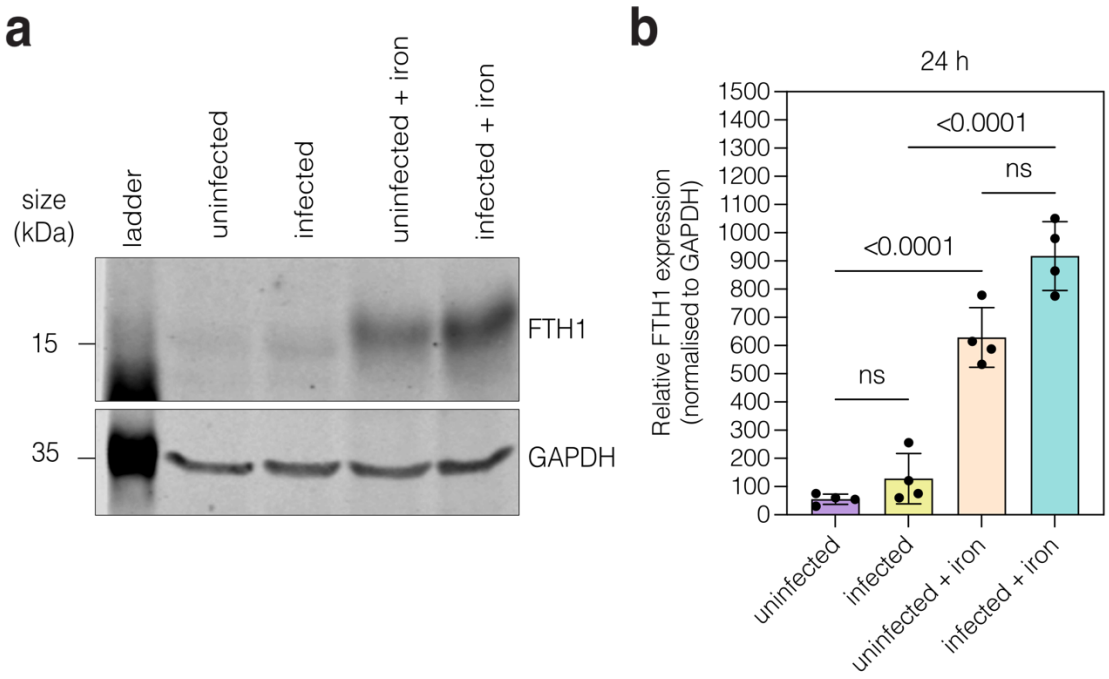


Figure 4.7- FTH1 expression is not altered in *T. gondii* infected HFFs at 24 h, however excess iron induces FTH1 expression.

a. Western blot analysis of FTH1 expression in uninfected and RHΔKu80 infected HFFs in both untreated and high iron (500 μM FAC) conditions at 24 h. GAPDH used as a loading control. **b.** Quantification of FTH1 expression levels in uninfected and infected HFFs in both untreated and high iron (500 μM FAC) conditions at 24 h, relative to uninfected untreated, from four independent biological experiments. Bars are at mean ± SD. *p* values from ordinary one-way ANOVA, Tukey corrected for multiple comparisons.

At 48 h post infection, I found that FTH1 expression levels in uninfected HFFs exposed to excess iron for 48 h are approximately twice the expression of that at 24 h. Further, the data demonstrates that in the presence of excess iron, FTH1 expression levels are significantly ($p < 0.0001$, one-way ANOVA, Tukey corrected for multiple comparisons) increased in infected HFFs in the presence of excess iron compared to uninfected, iron-treated HFFs (Figure 4.8b). In the presence of excess iron and infection for 48 h, FTH1 expression levels are significantly ($p < 0.0001$, one-way ANOVA, Tukey corrected for multiple comparisons) increased when compared to untreated infected cells (Figure 4.8b), and this is approximately double the expression levels compared to 24 h, where no significant change in FTH1 expression is observed in these conditions.

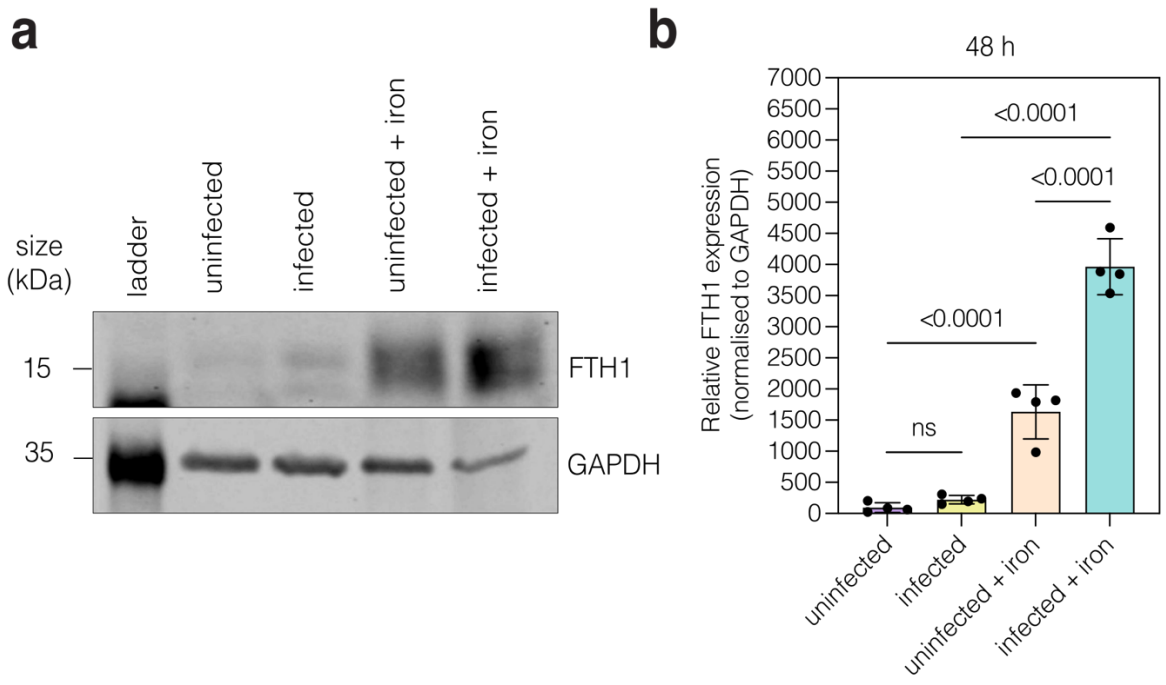


Figure 4.8 - FTH1 expression is not altered in *T. gondii* infected HFFs at 48 h, however excess iron induces FTH1 expression.

a. Western blot analysis of FTH1 expression in uninfected and RHΔKu80 infected HFFs in both untreated and high iron (500 μM FAC) conditions at 48 h. GAPDH used as a loading control. **b.** Quantification of FTH1 expression levels in uninfected and infected HFFs in both untreated and high iron (500 μM FAC) conditions at 48 h, relative to uninfected untreated, from four independent biological experiments. Bars are at mean ± SD. *p* values from ordinary one-way ANOVA, Tukey corrected for multiple comparisons.

4.3 *T. gondii* modulates host iron homeostasis in murine macrophage cells

Previously in this chapter, I investigated how *T. gondii* alters host iron homeostasis following infection in fibroblast cells. However, fibroblasts cells are non-professional phagocytic cells that mainly play a role in the production of the extracellular matrix and structural support, and lack specialised iron-trafficking mechanisms that play a large role in antimicrobial responses *in vivo* (Plikus et al., 2021; Romana-Souza et al., 2021). Studies, particularly in *Leishmania*, have investigated how pathogens alter iron homeostasis in the macrophages following infection (Ben-Othman et al., 2014; Goto et al., 2024; Sen et al., 2022). Macrophages are critical for innate immunity and are important in the front line control of *T. gondii* infection by engulfing invaders and initialising the inflammatory immune response (Park and Hunter, 2020). Moreover, the cytokine IFNγ is critical for the control of *T. gondii* in macrophages (Lykens et al., 2010; Nathan et al., 1983; Suzuki et al., 1988). However, little is known about if and how *Toxoplasma gondii* triggers changes and reprograms iron handling in professional phagocytic cells following infection. Therefore, my next aim was to assess how *Toxoplasma gondii* infection remodels host iron homeostasis in macrophages and compare this to fibroblasts. To investigate this, I examined the protein expression levels of key proteins involved in iron metabolism including TfR, DMT1 and FTH1 in RAW 264.7 murine macrophages at both 24 and 48 h.

4.3.1 Transferrin receptor expression is induced in *T. gondii* infected macrophages

To assess the effect of *T. gondii* infection on TfR expression in macrophages, I infected RAW 264.7 murine macrophages with RHΔKu80 parasites with an MOI of 2 for 24 h and/or treated with 500 μM FAC before harvesting the cells and performing a western blot analysis (Figure 4.9a). I found that TfR expression levels in macrophages are slightly but significantly (p = 0.0377, one-way ANOVA, Tukey corrected for multiple comparisons) increased following *T. gondii* infection at 24 h (Figure 4.9b). I show that there is a significant (p < 0.0001, one-way ANOVA, Tukey corrected for multiple comparisons) decrease in TfR expression levels in uninfected cells in the presence of excess iron when compared to uninfected, untreated macrophages (Figure 4.9b). Interestingly, I show that in the presence

of excess iron, there is no significant change in TfR expression in macrophages following infection when compared to uninfected macrophages treated with excess iron (Figure 4.9b). The data further demonstrates that in the presence of excess iron and infection for 24 h, TfR expression levels are significantly ($p < 0.0001$, one-way ANOVA, Tukey corrected for multiple comparisons) reduced when compared to untreated infected cells (Figure 4.9b). To test how receptor localisation was affected in infection, I infected RAW 264.7 murine macrophages with RHΔKu80:mNG parasites at an MOI of 2 for 24 h before fixing and staining. I found that TfR expression increases in *T. gondii* infected macrophages compared to uninfected (Figure 4.9c), as above, although no clear changes in localisation could be observed.

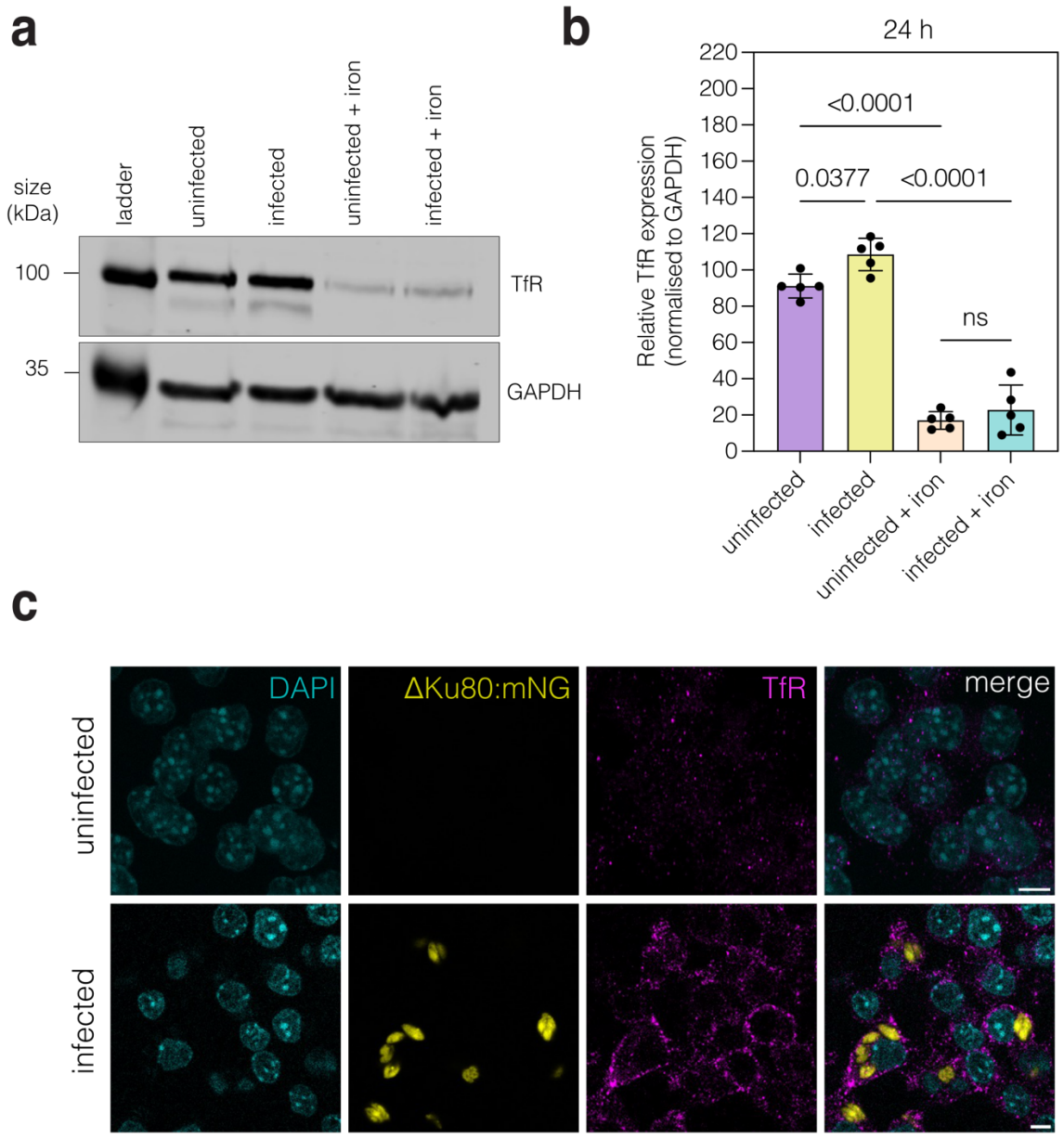


Figure 4.9 - TfR expression is upregulated in *T. gondii* infected RAW 264.7 murine macrophages at 24 h.

a. Western blot analysis of TfR expression in uninfected and RHΔKu80 infected RAW 264.7 murine macrophages in both untreated and high iron (500 µM FAC) conditions at 24 h. GAPDH used as a loading control. **b.** Quantification of TfR expression levels in uninfected and infected macrophages in both untreated and high iron (500 µM FAC) conditions at 24 h, relative to uninfected untreated, from five independent biological experiments. Bars are at mean ± SD. *p* values from ordinary one-way ANOVA, Tukey corrected for multiple comparisons. **c.** Immunofluorescence assay of uninfected and infected macrophages at 24 h showing an increase in TfR expression upon *T. gondii* infection. Scale bar 5 µM.

As macrophages upregulate TfR expression following infection with *T. gondii*, I next aimed to further validate this by assessing whether there was also increased transferrin binding on the surface of infected macrophages. To do so, RAW 264.7 macrophages were infected with RHΔKu80:tdTomato parasites at an MOI of 2 for 24 h before staining with a fluorescent transferrin (Tf-A488) and analysed. An unstained control was also included. The data demonstrates that there is a significant (p = 0.03, one-way ANOVA, Tukey corrected for multiple comparisons) increase in Tf-A488 binding on the surface of infected macrophages at 24 h compared to uninfected cells (Figure 4.10a, b). Uninfected cells in the infected sample (bystander) cells showed no significant change in Tf-A488 binding when compared to the uninfected population (Figure 4.10b). Interestingly, there was no significant difference in Tf-A488 binding in IFNγ/LPS induced macrophages compared to uninfected cells, however there is a significant (p = 0.04, one-way ANOVA, Tukey corrected for multiple comparisons) decrease in Tf-A488 binding in IFNγ/LPS induced macrophages when compared to *T. gondii* infected cells (Figure 4.10b). Although whether this represents more efficient killing of the parasites by these primed macrophages was not investigated further.

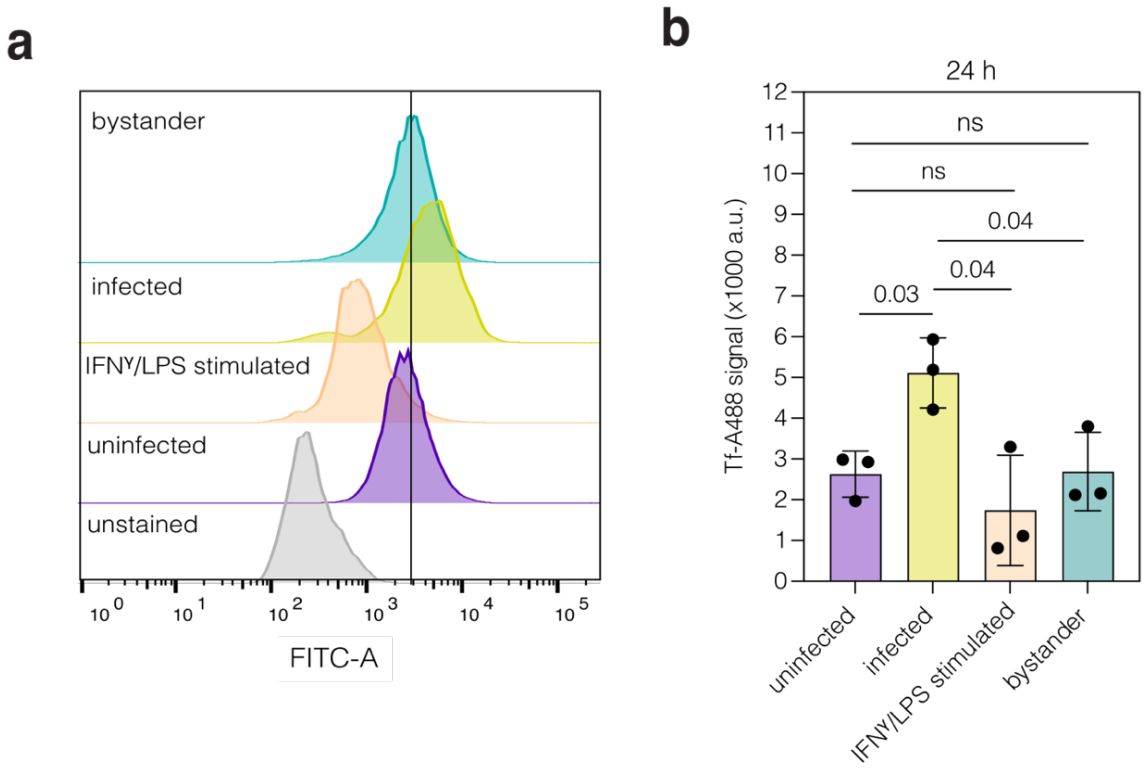


Figure 4.10 - Fluorescent Tf-A488 binding increases on the surface of *T. gondii* infected RAW 264.7 murine macrophages at 24 h.

a. Representative histogram of fluorescent Tf-A488 surface staining bystander, infected, IFNγ/LPS induced, uninfected and unstained RAW 264.7 murine macrophages at 24 h. **b.** Quantification of Tf-A488 fluorescent signal from three independent biological replicates. Bars are at mean ± SD. *p* values from ordinary one-way ANOVA, Tukey corrected for multiple comparisons.

As above, TfR abundance was also assessed at 48 h. Interestingly, I found that there is no longer a significant difference in TfR expression levels at 48 h in infected macrophages compared to uninfected macrophages (Figure 4.11b). Similar to 24 h, the data demonstrates that TfR expression is significantly (p = 0.0007, one-way ANOVA, Tukey corrected for multiple comparisons) reduced in uninfected cells pretreated with excess iron when compared to uninfected untreated macrophages at 48 h (Figure 4.11b). I also show that, similar to 24 h, there is no significant difference in TfR expression levels in infected macrophages in the presence of excess iron compared to uninfected cells also pretreated with excess iron at 48 h (Figure 4.11b). Moreover, the data demonstrates that similar to 24 h, TfR expression levels are significantly ($p < 0.0027$, one-way ANOVA, Tukey corrected for multiple comparisons) decreased in infected macrophages in the presence of excess iron compared to infected untreated macrophages at 48 h (Figure 4.11b).

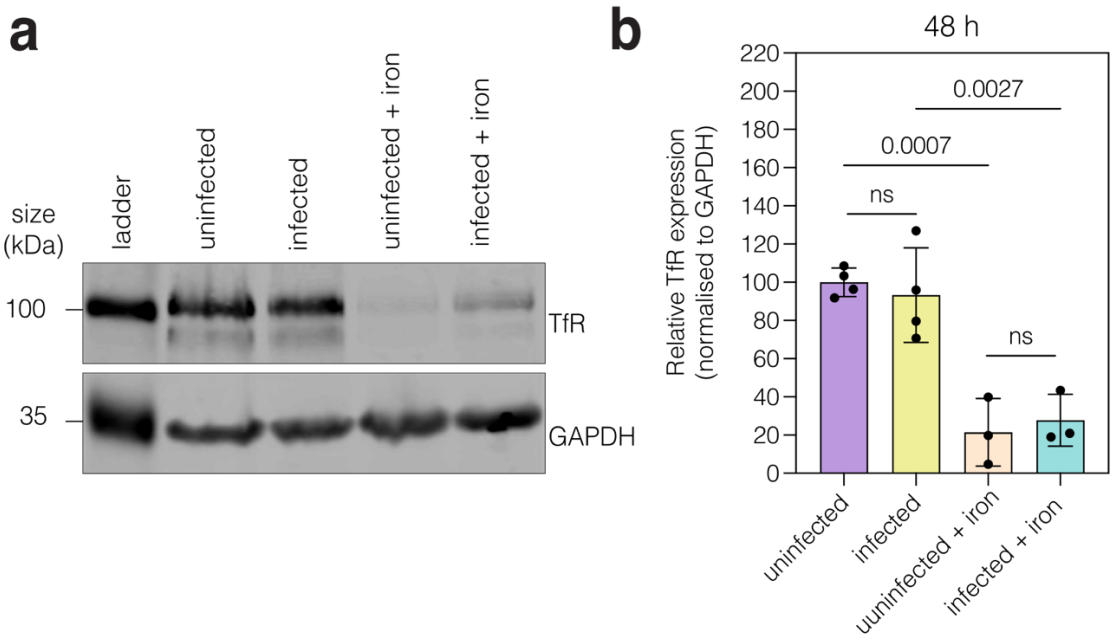


Figure 4.11 - TfR expression in RAW 264.7 murine macrophages does not significantly change following *T. gondii* infection at 48 h, however, significantly decreases in the presence of excess iron.

a. Western blot analysis of TfR expression in uninfected and RHΔKu80 infected RAW 264.7 murine macrophages in both untreated and high iron (500 μM FAC) conditions at 48 h. GAPDH used as a loading control. **b.** Quantification of TfR expression levels in uninfected and infected macrophages in both untreated and high iron (500 μM FAC) conditions at 48 h, relative to uninfected untreated, from four independent biological experiments. Bars are at mean ± SD. *p* values from ordinary one-way ANOVA, Tukey corrected for multiple comparisons.

4.3.2 DMT1 expression is induced in *T. gondii* infected macrophages

To assess if DMT1 expression levels following *T. gondii* infection differ in macrophages when compared to HFFs, I infected as above and demonstrate that DMT1 expression levels in macrophages are significantly (p = 0.0102, one-way ANOVA, Tukey corrected for multiple comparisons) increased following *T. gondii* infection at 24 h (Figure 4.12b). Similar to HFFs, the data demonstrates that there is no significant change in DMT1 expression levels in uninfected, iron-treated cells when compared to uninfected untreated macrophages at 24 h (Figure 4.12b). Moreover, I found that in the presence of excess iron, there is no significant change in DMT1 expression in macrophages at 24 h following infection when compared to uninfected macrophages treated with excess iron (Figure 4.12b). Intriguingly, the data further demonstrates that in the presence of excess iron and infection for 24 h, DMT1 expression levels are not significantly altered when compared to untreated infected cells (Figure 4.12b). Looking at the localisation of DMT1 in RAW macrophages, I show that DMT1 expression is increased in *T. gondii* infected macrophages compared to uninfected macrophages at 24 h, although unlike HFFs, no clear change in localisation was observed (Figure 4.12c).

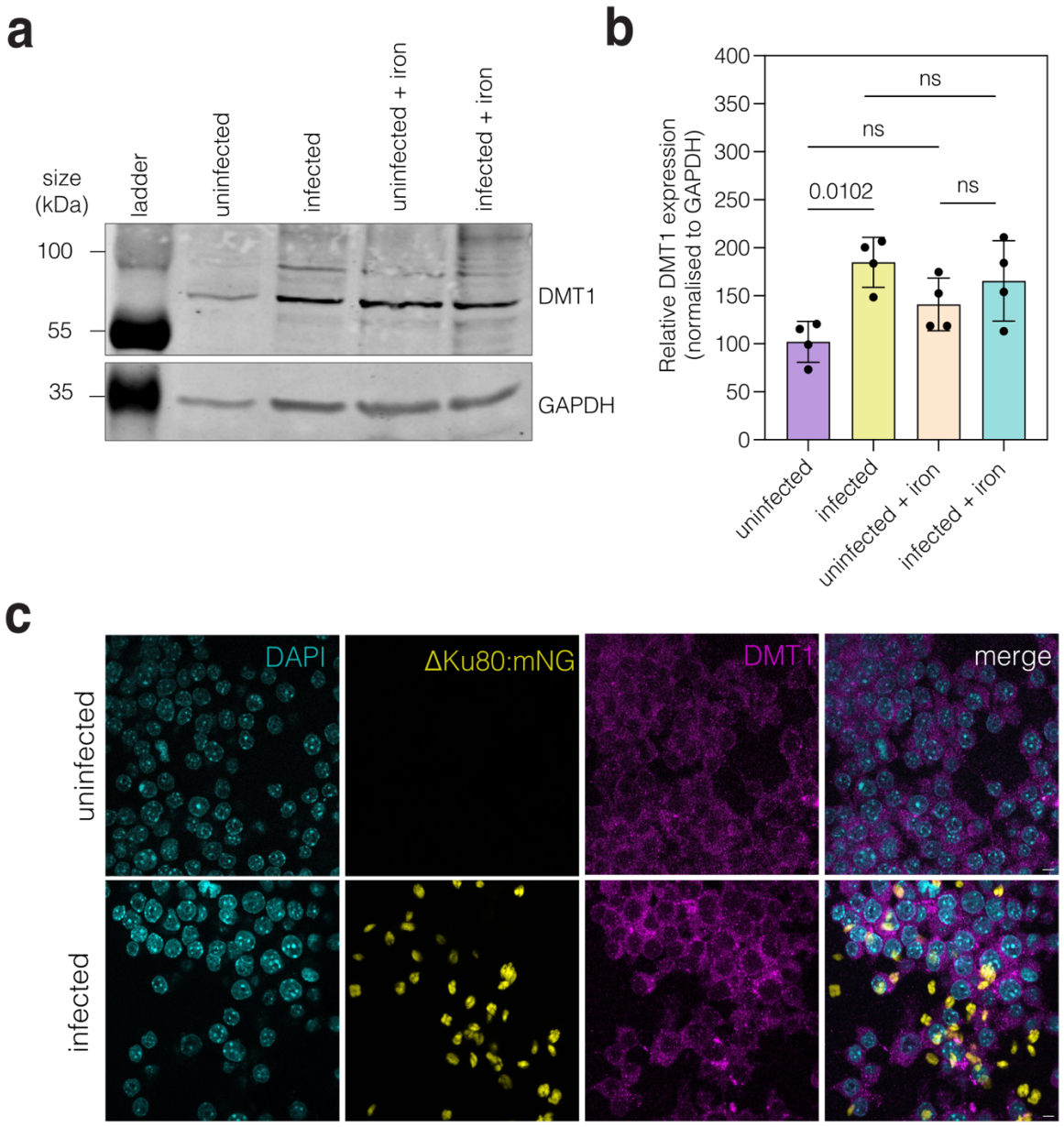


Figure 4.12 – DMT1 expression is upregulated in *T. gondii* infected RAW 264.7 murine macrophages at 24 h.

a. Western blot analysis of DMT1 expression in uninfected and RHΔKu80 infected RAW 264.7 murine macrophages in both untreated and high iron (500 µM FAC) conditions at 24 h. GAPDH used as a loading control. **b.** Quantification of DMT1 expression levels in uninfected and infected macrophages in both untreated and high iron (500 µM FAC) conditions at 24 h, relative to uninfected untreated, from four independent biological experiments. Bars are at mean ± SD. *p* values from ordinary one-way ANOVA, Tukey corrected for multiple comparisons. **c.** Immunofluorescence assay of uninfected and infected macrophages at 24 h showing an increase in DMT1 expression upon *T. gondii* infection. Scale bar 5 µM.

I then tested how DMT1 expression was maintained later in infection. Similar to at 24 h, I show that there is a significant (p = 0.0153, one-way ANOVA, Tukey corrected for multiple comparisons) increase in DMT1 expression levels at 48 h upon infection (Figure 4.13b). Iron treatment alone did not lead to a change in DMT1 expression (Figure 4.13b) and there is no significant change in DMT1 expression in macrophages at 48 h following infection when compared to infected untreated macrophages (Figure 4.13b). Interestingly, and different from 24 h, I found that DMT1 expression levels are significantly (p = 0.0228, one-way ANOVA, Tukey corrected for multiple comparisons) increased in infected, iron-treated macrophages compared to uninfected macrophages also treated with excess iron at 48 h (Figure 4.13b).

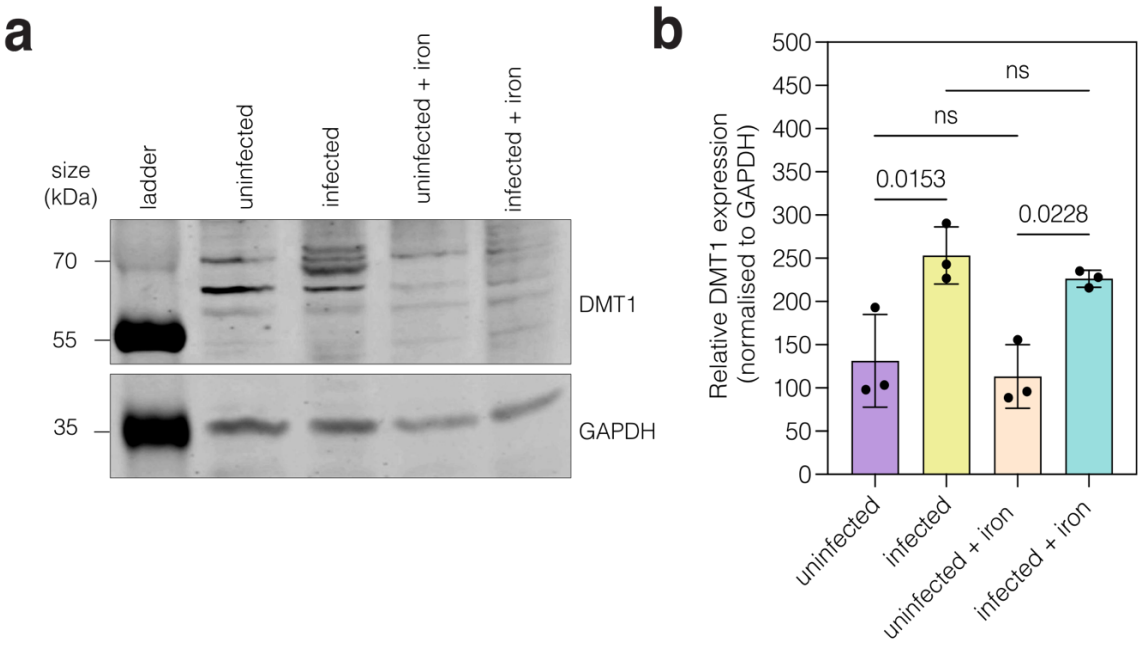


Figure 4.13 – DMT1 expression is upregulated in *T. gondii* infected RAW 264.7 murine macrophages at 48 h.

a. Western blot analysis of DMT1 expression in uninfected and RHΔKu80 infected RAW 264.7 murine macrophages in both untreated and high iron (500 µM FAC) conditions at 48 h. GAPDH used as a loading control. **b.** Quantification of DMT1 expression levels in uninfected and infected macrophages in both untreated and high iron (500 µM FAC) conditions at 48 h, relative to uninfected untreated, from three independent biological experiments. Bars are at mean ± SD. p values from ordinary one-way ANOVA, Tukey corrected for multiple comparisons.

4.3.3 FTH1 expression in macrophages does not increase following infection, however, increases in excess iron conditions

To assess if FTH1 expression levels following *T. gondii* infection differ in macrophages when compared to HFFs, I infected and analysed cells as above (Figure 4.14a). I show that FTH1 expression levels in macrophages do not significantly change following *T. gondii* infection at 24 h (Figure 4.14b). However, as expected, iron treatment led to a significant ($p < 0.0001$, one-way ANOVA, Tukey corrected for multiple comparisons) increase in FTH1 expression levels. Moreover, I show that in the presence of excess iron, there is no significant change in FTH1 expression in macrophages at 24 h following infection, when compared to uninfected, iron-treated macrophages (Figure 4.14b). I was next curious to assess whether infection with *T. gondii* results in a change in FTH1 localisation and expression levels following infection by immunofluorescence. I observed no clear changes in FTH1 localisation and expression in *T. gondii* infected macrophages, compared to uninfected macrophages at 24 h (Figure 4.14c).

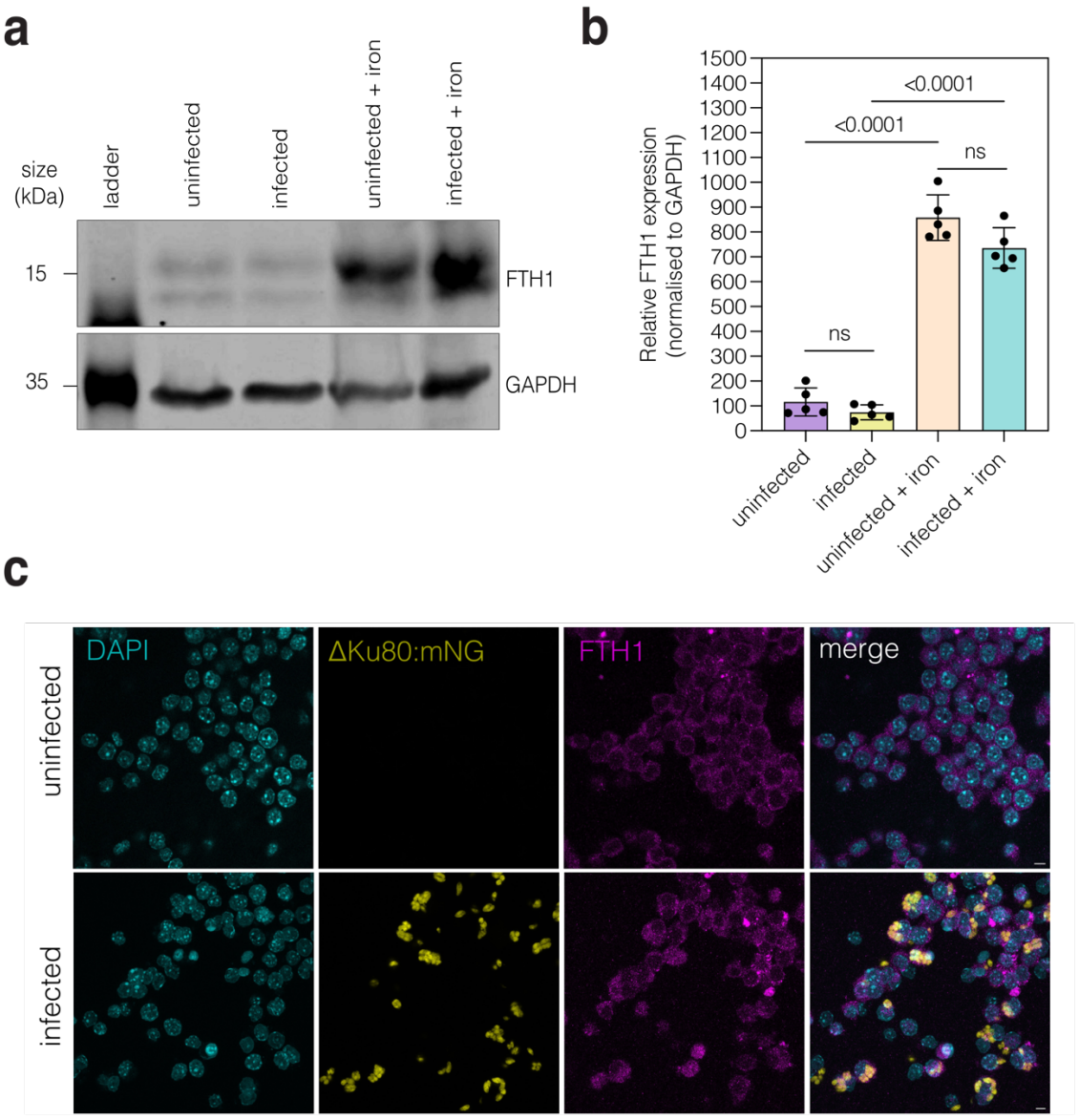


Figure 4.14 – FTH1 expression in RAW 264.7 murine macrophages does not significantly change following *T. gondii* infection at 24 h, however, FTH1 significantly increases in macrophages pretreated with excess iron.

a. Western blot analysis of FTH1 expression in uninfected and RHΔKu80 infected RAW 264.7 murine macrophages in both untreated and high iron (500 μM FAC) conditions at 24 h. GAPDH used as a loading control. **b.** Quantification of FTH1 expression levels in uninfected and infected macrophages in both untreated and high iron (500 μM FAC) conditions at 24 h, relative to uninfected untreated, from five independent biological experiments. Bars are at mean ± SD. *p* values from ordinary one-way ANOVA, Tukey corrected for multiple comparisons. **c.** Immunofluorescence assay of uninfected and infected macrophages at 24 h showing no change in FTH1 expression upon *T. gondii* infection. Scale bar 5 μM.

I next aimed to investigate if FTH1 expression levels increase at a later time point following infection with *Toxoplasma*, however the results were the same as at 24 h, demonstrating no parasite-specific effects on FTH1 (Figure 4.15a, b).

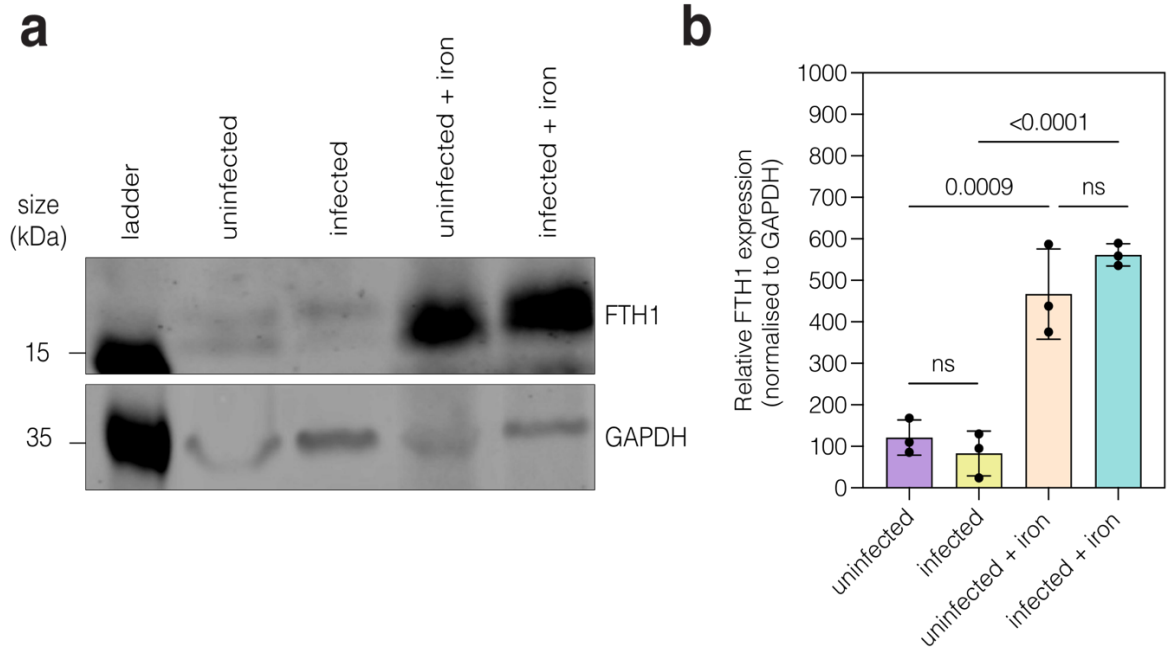


Figure 4.15 – FTH1 expression in RAW 264.7 murine macrophages does not significantly change following *T. gondii* infection at 48 h, however, FTH1 significantly increases in macrophages pretreated with excess iron.

a. Western blot analysis of FTH1 expression in uninfected and RHΔKu80 infected RAW 264.7 murine macrophages in both untreated and high iron (500 μM FAC) conditions at 48 h. GAPDH used as a loading control. **b.** Quantification of FTH1 expression levels in uninfected and infected macrophages in both untreated and high iron (500 μM FAC) conditions at 48 h, relative to uninfected untreated, from three independent biological experiments. Bars are at mean ± SD. *p* values from ordinary one-way ANOVA, Tukey corrected for multiple comparisons.

4.3.4 The *zft* 3' UTR confers iron responsiveness in fibroblasts, but not in macrophages

Previous studies by the lab have shown that the predicted iron responsive element (IRE) in the *zft* transcript confers iron responsivity (Sloan et al., 2025). To improve on the published system, the *zft* 3' UTR was cloned downstream of nanoLuciferase (nanoLuc$_{zft}$). The *dhfr* 3' UTR – which does not contain any IRE-like sequence - was cloned as a control (nanoLuc$_{dhfr}$). Both of these cell lines were generated by Lucia Mvrova. To investigate whether the *zft* 3' UTR confers iron responsivity in fibroblasts and macrophages, the nanoLuciferase assay was performed on extracellular parasites, grown for 24 h in HFFs and RAW 264.7 murine macrophages in untreated and low iron (100 µM DFO) conditions. I also treated cells with 0.5 µM CISMBI, a specific inhibitor of DMT1 (Montalbetti et al., 2015), for 24 h, to reduce the availability of host labile iron to the parasite to assess how the nanoluciferase reporter lines respond to this condition. Although the data demonstrated an increase in luminescence in nanoLuc$_{zft}$ parasites from HFFs under DFO conditions compared to untreated conditions (Figure 4.16a), there was no increase in parasite luminescence in nanoLuc$_{zft}$ parasites cultured in RAW 264.7 murine macrophages in the same DFO conditions, compared to untreated conditions (Figure 4.16b). Interestingly, in nanoLuc$_{zft}$ parasites infecting both fibroblasts and macrophages, the presence of the DMT1 inhibitor CISMBI did not affect parasite luminescence compared to untreated, supporting that DMT1 is not the only/main source of iron in both HFFs and macrophages (Figure 4.16a, b). However, as only two biological replicates were performed for this assay, these results are preliminary and should be repeated to obtain statistical significance.

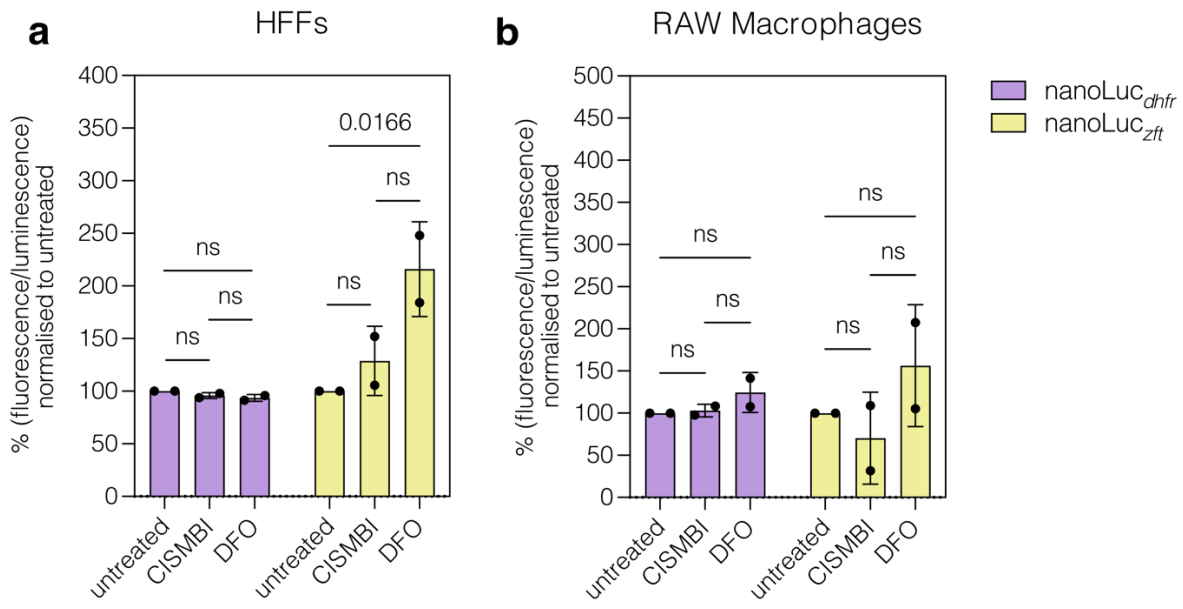


Figure 4.16 - The *zft* 3' UTR plays a role in iron responsiveness in iron deprivation conditions in fibroblasts but not in macrophages.

a. Bar graphs representing the percentage of fluorescence/luminescence of both nanoLuc$_{dhfr}$ and nanoLuc$_{zft}$ extracellular parasites which had infected HFF fibroblasts for 24 h in DMT1 inhibition (0.5 μM CISMBI) and iron deprivation (100 μM DFO) conditions, normalised to untreated conditions. Bars are at mean of two independent biological experiments, ± SD. *p* values from ordinary two-way ANOVA, Tukey corrected for multiple comparisons. **b.** Bar graphs representing the percentage of fluorescence/luminescence of both nanoLuc$_{dhfr}$ and nanoLuc$_{zft}$ extracellular parasites which had infected RAW 264.7 murine macrophages for 24 h in DMT1 inhibition (0.5 μM CISMBI) and iron deprivation (100 μM DFO) conditions, normalised to untreated conditions. Bars are at mean of two independent biological experiments, ± SD. *p* values from ordinary two-way ANOVA, Tukey corrected for multiple comparisons.

4.4 Discussion and summary

Nutritional immunity is a key strategy employed by cells to limit pathogen access to essential nutrients, including the transition metal iron. As iron is critical for the proliferation, survival and pathogenicity of many microbes, the tight regulation of iron and host cell iron restriction following infection poses a major challenge. Thus, many pathogens have developed mechanisms to subvert host iron homeostasis to their advantage, enabling them to acquire iron from their host to survive and replicate within these cells. However, despite the importance of iron in infection and immunity, the mechanisms by which the apicomplexan parasite *T. gondii* manipulates host iron homeostasis following infection remained unknown. In this chapter, I investigated how *T. gondii* subverts host iron stores following infection in both fibroblasts and macrophages, an immune cell that plays a critical role in controlling many pathogenic infections *in vivo* by sequestering iron stores.

4.4.1 Transferrin receptor expression is modulated following *T. gondii* infection in both fibroblasts and macrophages

Following IFNγ and/or LPS stimulation and an activation of a pro-inflammatory immune response, macrophages have been shown to sequester iron by reducing the expression of transferrin receptor (TfR), a principal iron uptake protein, preventing invading pathogens from acquiring iron and inhibiting their growth (Byrd and Horwitz, 1993; Mulero and Brock, 1999; Kim and Ponka, 2000; Zhong et al., 2001). To investigate the effect of *T. gondii* infection on host iron uptake, I first examined the expression of TfR in both fibroblasts and macrophages at 24 h and 48 h in uninfected and infected cells, in both untreated and high iron conditions. I found that TfR expression levels are significantly increased following *T. gondii* infection at both 24 h and 48 h in both fibroblast cells (Figure 4.1 and Figure 4.3 respectively) and murine macrophages at 24 h (Figure 4.9). This was further supported by the increased binding of transferrin to the surface of infected fibroblast and macrophage cells 24 h post infection (Figure 4.2 and Figure 4.10 respectively). The data also demonstrates that there was no significant difference in transferrin binding in IFNγ/LPS induced macrophages compared to uninfected cells (Figure 4.10b). Previous studies in phagocytic cells have shown that stimulation with IFNγ and/or LPS downregulates TfR expression levels while

upregulating FTH1 expression levels (Byrd and Horwitz, 1993; Mulero and Brock, 1999; Kim and Ponka, 2000). This shift reduces cellular iron uptake and enhances iron sequestration, restricting the availability of iron to inhibit microbial growth and survival. This suggests that the increase in TfR expression observed is likely a specific *T. gondii* response, rather than a general IFNγ/LPS response. This increase in TfR expression in macrophages is also observed following infection with other parasitic pathogens such as *Leishmania donovani* (Das et al., 2009) as well as the intracellular bacterial pathogen *Francisella tularensis* (Pan et al., 2010), and is critical for intracellular proliferation and survival. Studies have shown that the increase in TfR expression in *Leishmania* and *Francisella* infected macrophages is due to the increase in the binding of the eukaryotic iron response protein 1 and 2 (IRP1 and IRP2) to the iron-responsive elements (IREs) in the 3' UTR of the *TfR* mRNA. (Das et al., 2009; Pan et al., 2010). IRP1/2 sense changes in the labile iron pool within cells and post-translationally stabilises *TfR* mRNA by binding to the IREs in the 3' UTR of the transcript. This protects the transcript from endo-nucleolytic cleavage (Casey et al., 1988; Hentze et al., 1987) and results in an increased receptor expression on the surface of host cells following infection. This contrasts to macrophage infection with *Salmonella typhimurium*, which does not require the expression of TfR for survival, maintaining the labile iron pool at normal levels (Pan et al., 2010). Interestingly, at 48 h, there is no significant difference in TfR expression levels in *T. gondii* infected vs. uninfected macrophages (Figure 4.11). The data possibly suggests that iron uptake is more tightly regulated following infection at a later time points in the immune cell macrophages, which play an important role in iron sequestration following infection, compared to fibroblasts. Another possible explanation for this is that the macrophages are killing the parasites, however there is no direct evidence of this. It is also possible that the absence of a significant decrease in TfR expression levels following *T. gondii* infection in macrophages at 48 h may represent a tug of war and battle for iron between the parasite, driving increased TfR expression to increase iron availability for growth and persistence, compared to the host cell which may be decreasing TfR expression levels following infection to sequester iron stores and restrict pathogen replication and survival *in vitro*. In high iron conditions *in vivo*, the transferrin receptor triggers the cytokine IL-6 to induce hepcidin production from the liver, blocking the release of iron into the bloodstream and in turn the loading of iron onto transferrin, reducing iron

absorption. The opposite is observed in low iron conditions *in vivo*, where hepcidin production is reduced, increasing the release of iron into the blood and loading of iron onto transferrin, in turn increasing iron absorption and maintaining systemic iron homeostasis (Fillebeen et al., 2019).

Whether this increase in TfR expression levels upon *T. gondii* infection at 24 h *in vitro* is a host or parasite driven response is currently not known. The increase in TfR expression levels following infection could be a host cell response to increase the amount of iron in the cell to levels toxic enough kill the parasite, or it may be a parasite driven response to increase the availability of iron in the host cell for *T. gondii* proliferation and survival. To further examine the role of TfR in *T. gondii* infection, it would be interesting to assess the levels of IRP1 and IRP2 expression and mRNA binding in both fibroblasts and macrophages following infection, to determine how TfR expression is regulated. Further, the labile iron pool could be examined to assess if increased transferrin receptor expression, and transferrin binding, in infected cells alters the availability of iron within the cell. This can be done using calcein (Soe-Lin et al., 2006) as well as the fluorescent live cell indicator dye FerroOrange (Yambire et al., 2019). Moreover, determining the kinetics of host and parasite iron uptake would be important. To do so, infected, and uninfected cells can be treated with ^{55}Fe conjugated to Tf or citrate, and iron uptake in both parasites and host cells could be tracked over time. Furthermore, although TfR is the major route for iron uptake in mammalian cells, ZIP8/ZIP14 can also play a role in iron uptake (C.-Y. Wang et al., 2012). Future work could involve tagging these proteins in both fibroblasts and macrophages and quantifying their expression in the context of *T. gondii* infection, as well as high and low iron conditions. Answering these questions will assist in informing us on how infection with *Toxoplasma gondii* affects host iron uptake. It would be intriguing to further validate the increase in transferrin binding in infected cells by assessing radioactive transferrin uptake in both cell types upon infection. Finally, macrophages could be starved from iron using the iron chelator DFO for 24 h before infecting them with *T. gondii* and then supplementing them either with excess iron (FAC) or transferrin to assess whether supplementing the cells with transferrin restores growth of *T. gondii* in iron deprived macrophages.

Studies have previously also shown an inverse correlation with the expression of TfR and cellular iron levels. TfR expression levels are high in low iron conditions,

compared to high iron conditions where TfR expression is lower (Anderson et al., 2012; Kühn, 2015). To support this, I demonstrated in this chapter that TfR expression levels are significantly reduced in uninfected cells pretreated with excess iron compared to untreated cells at both 24 and 48 h in murine macrophages (Figure 4.9 and Figure 4.11 respectively). Interestingly however, this was only observed in macrophages and not in fibroblasts, where there was no significant difference in TfR expression levels in uninfected cells pretreated with excess iron compared to untreated cells at both 24 and 48 h (Figure 4.1 and Figure 4.3 respectively). This sheds light to differences between the two cell types, particularly in the context of iron in infection conditions. This may suggest that iron is more tightly regulated in immune cells such as macrophages compared to fibroblasts. In the context of high iron conditions and infection, TfR expression levels in both HFFs and macrophages at both 24 and 48 h significantly decrease compared to untreated infected cells. A possible explanation for this would be that in the presence of excess iron, there is no longer a demand for increased iron uptake, particularly because for both the host cell and the parasite, excess iron could be toxic. In these conditions, both the host cell and *T. gondii* have sufficient iron, thus downregulating transferrin receptor expression levels. However, whether this is a host- or parasite-driven response following infection currently remains unknown.

Another strategy used by intracellular pathogens is the acquisition of iron from iron-transporting proteins such as transferrin or lactoferrin. Lactoferrin is a high affinity iron-binding glycoprotein that belongs to the transferrin family protein and also plays an important role in the innate immune system exhibiting anti-inflammatory properties by restricting iron and inhibiting microbial survival (Kanwar et al., 2015; Kell et al., 2020). The presence of such receptors that bind mammalian iron-carrier proteins such as transferrin and lactoferrin have previously been reported in *Leishmania* (Voyiatzaki and Soteriadou, 1992, 1990), *Trypanosoma brucei* (Steverding et al., 1995; Kariuki et al., 2019; Kabiri and Steverding, 2021) as well as *Trichomonas vaginalis* (Lehker and Alderete, 1992). A study has also found that *T. gondii* tachyzoites bind bovine transferrin, lactoferrin and ovotransferrin (Tanaka et al., 2003). However, there is currently no supporting evidence that *Toxoplasma* uses human iron-transporting proteins such as TfR and FTH1 as a potential source of iron for growth and survival. Further,

a study has shown that *T. gondii* is able to bind human lactoferrin, but not transferrin (Dziadek et al., 2005). Although *Toxoplasma* is an intracellular pathogen and most likely relies on intracellular host iron stores, it would be interesting to investigate whether lactoferrin is a possible iron acquisition strategy by extracellular parasites by examining if the *T. gondii* genome encodes any receptors that may bind lactoferrin, and if supplementing host cells with lactoferrin or provided by serum supplementation increases levels of intracellular iron within the parasite.

4.4.2 DMT1 expression is modified in both fibroblasts and macrophages upon infection with *T. gondii*

Mammalian cells can also acquire non-transferrin bound iron from the extracellular environment through the action of DMT1. DMT1 also plays a role in the release of transferrin-bound iron from early endosomes into the cytoplasm within cells (Yanatori and Kishi, 2019). In low iron conditions, IRPs bind to IREs to regulate and increase the expression of DMT1 expression, increasing the availability of iron (Eisenstein and Blemings, 1998; Gunshin et al., 2001; Kato et al., 2007; Kühn, 2015). Previous studies have shown that DMT1 expression increases following infection with *Salmonella typhimurium,* in turn reducing the availability of iron within phagosomes in which *Salmonella* reside in, impairing the proliferation and persistence of the intracellular bacteria within macrophages (Grander et al., 2022). This was further supported by an increase in bacteria burden in the absence of DMT1 (Grander et al., 2022). Another study has shown that DMT1 mRNA expression increases in phagosomes following infection with *Mycobacterium avium*, whilst also seeing a decrease in TfR expression, restricting the availability of iron and inhibiting pathogen growth (Zhong et al., 2001). Studies have also found that pro-inflammatory cytokines such as tumour necrosis factor (TNF)-α and IFNγ as well as LPS stimulate an increase in DMT1 mRNA and protein expression levels in epithelial cells *in vitro* and *in vivo* (Wang et al., 2005). In this chapter, I show that DMT1 protein expression levels increase in both fibroblasts and macrophages after 24 h (Figure 4.4 and Figure 4.12 respectively) and 48 h (Figure 4.5 and Figure 4.12 respectively) of *T. gondii* infection. However, as previously discussed with the transferrin receptor, whether this is a host- or parasite-driven response is currently unknown. It is possible that the increase in DMT1 expression is a strategy employed by the host cell to increase iron

availability to a level toxic enough to kill the parasite, or that this is the parasite manipulating host DMT1 expression to ensure sufficient iron is available for its replication and survival within the host. Interestingly, in both fibroblast and macrophage cells, DMT1 expression levels is not significantly altered in the presence of excess iron in uninfected cells compared to untreated uninfected cells. A possible explanation for this would be that in the presence of excess iron, there is no longer a demand to increase the availability of iron, particularly as too much iron is toxic to the cell, so DMT1 levels are maintained. Cells pretreated with excess iron are able to sense and store iron more readily by increasing FTH1 expression without the need to downregulate DMT1 expression levels. This is indeed what was observed when investigating the expression of FTH1 in both fibroblasts and macrophages in high iron conditions at both 24 h (Figure 4.7 and Figure 4.8 respectively) and 48 h (Figure 4.14 and Figure 4.15 respectively). It is also plausible that in high iron conditions, cells upregulate the expression of iron exporters such as ferroportin, to maintain the levels of iron within the cell and avoid iron toxicity. However, future work is required to assess the levels of ferroportin under high iron conditions in fibroblasts and macrophages.

I previously demonstrated that TfR expression is reduced in uninfected fibroblasts and macrophages in high iron conditions compared to untreated, suggesting that although DMT1 expression levels are not significantly reduced, cells are maintaining iron homeostasis by reducing the uptake of iron through reducing TfR expression. Moreover, in the context of infection, DMT1 expression is significantly increased in infected fibroblast cells in high iron conditions compared to untreated infected cells at both 24 h and 48 h (Figure 4.4 and Figure 4.5 respectively). A possible explanation for this is that although DMT1 is not increased in high iron conditions, this response may be a parasite-driven modulation of host iron homeostasis. As *T. gondii* requires iron for replication and survival, a plausible explanation is that even in high environmental iron conditions, the parasite is actively manipulating host iron homeostasis and increasing DMT1 expression to maximise host iron availability and ensuring the parasite has sufficient iron access in endosomal compartments, overriding the host's IRP/IRE regulatory response to high iron conditions. This is observed in bacteria such as *Burkholderia pseudomallei* infection which induces the expression of DMT1 following infection

to increase iron accumulation in macrophages to facilitate its intracellular survival (Schmidt et al., 2018).

Under high iron conditions, FTH1 expression levels are also significantly increased. It is therefore possible that although DMT1 expression levels are significantly increased under high iron conditions, iron is sequestered and stored into ferritin to avoid iron toxicity. In these circumstances, it is possible that the host senses a low availability of iron and therefore upregulating the IRP/IRE system which would in turn increase the expression of DMT1. Another explanation could be that with an increase in iron availability, *T. gondii* may be replicating more efficiently and utilising/depleting iron stores in the host at a faster rate, and the host is responding by increasing iron importers such as DMT1 in order to compensate for the possible low iron availability. It will be essential to assess the quantity of iron within both the parasite and the host under these conditions either by FerroOrange, ICP-MS, or XFM. However, in contrast to fibroblasts, DMT1 expression in macrophages pretreated with excess iron is not significantly different following *T. gondii* infection at 24 h compared to uninfected cells pretreated with excess iron (Figure 4.12). This suggests that at this timepoint, macrophages most likely regulate DMT1 more steadily in high iron conditions than fibroblasts following infection either by storing iron in the form of ferritin in the cytoplasm, or by increasing the expression of iron exporters such as ferroportin, which may be more tightly regulated in immune cells to avoid iron toxicity. Interestingly, at 48 h, DMT1 expression in macrophages pretreated with excess iron and infected with *T. gondii* are significantly higher than that in uninfected macrophages pretreated with excess iron (Figure 4.13), supporting that the increase in DMT1 expression observed in infected macrophages pretreated with high iron is most likely a parasite-driven response rather than a host response to high iron conditions.

Previous studies have demonstrated that in the absence of DMT1, the availability for iron increases which in turn leads to increased proliferation and persistence of *Salmonella* in macrophages (Grander et al., 2022). To further examine the role of DMT1 in *T. gondii* infection, DMT1 knockdown lines in mammalian cells could be generated by siRNA and parasite replication in these cell lines could be quantified by fluorescence. This would further allow us to understand whether the change in DMT1 expression is host- or parasite-driven. Growth could attempt to be rescued with exogenous iron (FAC) to ensure that any growth phenotype observed is due

to iron deprivation rather than a general stress response. Iron-bound transferrin could be used as a control to ensure the rescue is a specific response. Furthermore, DMT1 activation could be induced using the pharmacological activator, nifedipine (Yu et al., 2017), and assess whether this rescues the growth of *T. gondii* in the DMT1 knockdown lines. This would particularly be interesting as studies both *in vitro* and *in vivo* have shown that the activation of DMT1 by nifedipine mediated host resistance to *Salmonella* infection, resulting in induction of the iron exporter ferroportin (FPN1), and limiting access of iron to the intracellular bacteria (Mair et al., 2011). DMT1 could also be inhibited by CISMBI (Montalbetti et al., 2015) and parasite growth could be examined to further validate the role that DMT1 plays in iron acquisition by *T. gondii*. Levels of parasite associated iron could then be measured by ICP-MS and XFM. The effect of knocking out DMT1 on the distribution of iron within the host cell could be explored by mapping iron by XFM in both uninfected and infected cells. The expression levels of FTH1 and FPN1 could also be quantified in these DMT1 knockdown lines in the context of *Toxoplasma* infection as well as excess iron and iron chelation conditions. Moreover, whether DMT1 expression is stabilised under high iron conditions is due to an increase in iron export could be investigated by assessing the expression of DMT1 in a cell line that overexpresses ferroportin. In addition to DMT1, iron and other cations can also be exported from lysosomes by TRPML1 (transient receptor potential mucolipin 1) (Dong et al., 2008; Fernández et al., 2022; Weber et al., 2020). In the situation that the knockdown of DMT1 does not inhibit parasite replication, the role of TRPML1 can be examined. These studies will further establish how iron is released from lysosomes and the important role that this plays for the parasite.

DMT1 often localises to the plasma membrane of mammalian cells, as well as late endosomes and lysosomes, colocalising with the LAMP-1/2 (lysosome-associated membrane protein 1/2) marker and supporting the role of mobilising iron from lysosomal compartments within the cell (Gruenheid et al., 1999; Tabuchi et al., 2000). Studies have also shown that DMT1 localisation is dynamic and can be recruited to the phagosomal membrane in macrophages following phagocytosis of particles such as beads (Jabado et al., 2002), suggesting a possibility that during infection, DMT1 can localise to the pathogen-containing vacuoles, modulating their access to iron. In this chapter I demonstrate that in uninfected fibroblasts,

DMT1 seems to localise near the nucleus, particularly near the ER and the Golgi apparatus. However, after infection with *T. gondii*, DMT1 localisation seems to change and is now being redirected and recruited to around the parasitophorous vacuole. It is possible that in addition to increasing the expression of DMT1, *T. gondii* may also be manipulating and hijacking host trafficking pathways to pull iron in by recruiting DMT1 closer to the vacuole. However, the possibility of this change in localisation also being a host-driven response to kill the parasite should not be ignored. I further demonstrated that although there was no obvious change observed in DMT1 localisation following infection with *T. gondii* at 24 h in macrophages, DMT1 expression appears to increase following infection by IFA (Figure 4.12). Future work is needed to further validate and quantify this.

As described above, the increase in DMT1 expression levels following infection may be host- or parasite-driven. Previous studies have shown that intracellular pathogens such as *Legionella pneumophila* and *Leishmania* manipulate host iron stores via secreted proteins (Christenson et al., 2019; Sen et al., 2022). I therefore hypothesise that it is more likely that *T. gondii* is actively manipulating host iron stores and lysosomal function in the host cell following infection to ensure sufficient availability of iron for replication and survival. To determine if the upregulation of DMT1 following infection is triggered by secreted proteins, DMT1 expression in fibroblasts was quantified following infection with parasites defective in effector secretion (ΔMYR1). MYR1 is a secreted protein important for the transfer of effector molecules to regulate important signalling pathways. Here, I found that DMT1 expression levels in fibroblast cells are not significantly altered when infected with ΔMYR1 compared to RHΔKu80 parasites (Figure 4.6), suggesting that a MYR1-depnedent protein is not involved in this response. It would have been intriguing to perform an IFA with fibroblasts infected with ΔMYR1 parasites and assess if DMT1 is still being recruited to the parasitophorous vacuole following infection or if any change in localisation of DMT1 is observed compared to fibroblasts infected with parental RHΔKu80 parasites.

Although no difference in DMT1 expression was observed in fibroblasts following infection with ΔMYR1 parasites, this does not completely rule out the role that MYR1-independent secreted effector proteins play in modulating host iron stores and homeostasis. *Toxoplasma gondii* constitutively secretes approximately over

70 dense granule proteins during replication to modulate host transcription (Ulahannan et al., 2022) as well as to prevent the destruction of the vacuole (Nadipuram et al., 2016). Despite their importance, the function of many of these dense granule proteins are currently not known. Studies in the lab have shown that the dense granule protein Gra76 mRNA is stabilised in iron deprivation conditions (Sloan et al., 2025), and proteomic analysis demonstrated that Gra76 is upregulated under iron chelation conditions (Hanna et al., 2025). Studies have demonstrated that knocking out Gra76 resulted in a delayed replication of the parasite (Zheng et al., 2024), although the mechanisms of this has not yet been investigated. It is possible that Gra76 may play a role in iron acquisition by the parasite, and thus knocking out this gene and assessing the sensitivity of the parasites to iron deprivation conditions would be interesting.

4.4.3 Iron storage is not modulated in *T. gondii* infected host cells

To prevent iron toxicity, iron is stored in protein cages of ferritin in the cytoplasm of cells (D. J. R. Lane et al., 2015). When iron is required, it is then released via the lysosomes by autophagic degradation (James E. Cassat and Skaar, 2013; Mancias et al., 2014). The expression of this iron storage protein in turn reduces the labile iron pool, restricting the availability of iron and making it inaccessible to many pathogens, being one of the most recognised mechanisms of iron sequestration during infection (Kumagai et al., 1992; Nairz et al., 2015; Siegert et al., 2015). This is critical as a low labile iron pool then goes on to induce important transcription factors including nuclear factor interleukin 6 and hypoxia-inducible factor 1a (HIF1a), which play a role in activating anti-microbial immune effector pathways (Siegert et al., 2015). In the context of nutritional immunity, macrophages restrict iron availability by increasing ferritin heavy chain 1 (FTH1) expression. The increase in FTH1 expression levels is also common in response to inflammation (Ganz, 2009; Weiss and Goodnough, 2005; Ganz and Nemeth, 2015). Previous studies have also shown that intracellular pathogens including *Salmonella* exploit these host iron stores to promote their pathogenicity and survival within macrophages (Nairz et al., 2007; Van Santen et al., 2013). Interestingly, in this chapter I show that at both 24 h and 48 h, infection with *T. gondii* does not change FTH1 expression levels in both fibroblasts (Figure 4.7 and Figure 4.8 respectively) and macrophages (Figure 4.14 and Figure 4.15 respectively). This is in contrast to other pathogens; for example *Burkholderia pseudomallei* infection causes an

increase in ferritin heavy chain 1 expression levels and iron accumulation in macrophages to facilitate its intracellular survival (Schmidt et al., 2018).

Further, a study has shown that the bacterial pathogen *Neisseria meningitidis* utilises host cell FTH1 as an iron source by indirectly decreasing the uptake of transferrin, inducing an iron starvation response within the cell by degrading FTH1 for the host cell to meet its own iron needs. The released iron is then accessed by *Neisseria* for its own proliferation and growth within the host cell (Larson et al., 2004). It is a possibility that this highlights the tug of war between the host and the pathogen where host cells may aim to increase FTH1 expression levels to sequester more iron and restrict *T. gondii* access. On the other hand, *T. gondii* may be manipulating the host to reduce FTH1 expression to ensure sufficient iron for replication. The increase in both TfR and DMT1 expression levels, and the absence of change in FTH1 expression levels, could emphasise and support that the effects observed to changes in host iron homeostasis is likely a parasite-driven response. I hypothesise that *T. gondii* mainly manipulates host iron uptake mechanisms through TfR and DMT1 to ensure sufficient iron availability. It is possible that instead of increasing iron storage following infection to respond to an increased flux of iron due to an increase in TfR and DMT1 expression levels, the host cells may increase the expression of the iron exporter ferroportin. However, this needs to be further investigated to elucidate if there are any changes in iron export following infection with *Toxoplasma gondii*.

As anticipated, FTH1 expression is highly upregulated in excess iron conditions. This is most likely the host cells responding to high iron concentrations and avoiding iron overload and toxicity by increasing iron storage. I would have been intrigued to also assess the expression of the iron exporter ferroportin in high iron conditions to assess if cells respond to iron overload by also increasing iron export. Interestingly, FTH1 expression is almost four times as much at 48 h compared to 24 h in high iron conditions, but only in fibroblasts, highlighting potentially disparate roles in iron regulation between the cell types.

A recent study has demonstrated that FTH1 plays a key role in conferring host defence against infection with the obligate intracellular pathogen *Mycobacterium tuberculosis*, and infection with this pathogen enhanced the NCOA4-mediated degradation of ferritin (Dai et al., 2023). This in turn results in an increased

availability of iron within the macrophages, thus promoting bacteria proliferation and survival. However, in *Toxoplasma gondii* infection, the role of ferritinophagy has not yet been explored. Future work could involve quantifying the levels of both PCBP1 (the chaperone which delivers iron to ferritin) and NCOA4 by western blot analysis. In the case that infection changes the loading of ferritin, this could potentially be followed up by infecting cells lacking such components and parasite replication as well as iron status could then be quantified to determine the role that they play in *T. gondii* infection. To summarise, future work is required to define the mechanisms of host ferritin utilisation by *T. gondii* following infection, particularly as different pathogens employ multiple and unique mechanisms to promote their survival in the mammalian host, which serves to actively limit the availability of iron.

4.4.4 What about iron export to maintain homeostasis?

Previous studies in macrophages infected with *Leishmania amazonensis* have been shown to increase the LIP by downregulating ferroportin, an iron export transporter, promoting parasite replication and survival in macrophages (Ben-Othman et al., 2014). In contrast, infection of macrophages with the intravacuolar bacterium *Salmonella typhimurium*, led to upregulation of ferroportin, reducing the LIP and preventing bacterial growth (Nairz et al., 2007). However, due to technical difficulties with visualising ferroportin expression both by western blotting and IFA as well as time restrictions, I was unable to examine the expression of ferroportin in both fibroblasts and macrophages following *T. gondii* infection. I hypothesise that the host cell will attempt to upregulate ferroportin levels to reduce LIP and in turn inhibit parasite proliferation and survival, as well as to reduce levels of iron influx caused by the increase in both TfR and DMT1 expression following infection as previously demonstrated in this chapter. However, it is also equally plausible that *T. gondii* could also trigger the downregulation of ferroportin to reduce iron export and increase the labile iron pool within the cell to support the survival and proliferation of the parasite. Future work is required to optimise antibody conditions to define host ferroportin expression levels following *T. gondii* infection, particularly as different pathogens employ multiple and unique mechanisms in different cell types to promote intracellular survival.

4.4.5 The role of the *zft* 3' UTR in iron responsiveness is dependent on cell type

Although the data demonstrated a significant increase in luminescence in nanoLuc$_{zft}$ parasites from fibroblasts under iron deprivation conditions compared to untreated conditions (Figure 4.16a), there was no significant increase in parasite luminescence in nanoLuc$_{zft}$ parasites cultured in RAW 264.7 murine macrophages (Figure 4.16b). This may suggest differences in iron handling between macrophages and fibroblasts. Interestingly, the presence of the DMT1 inhibitor CISMBI did not significantly affect nanoLuc$_{zft}$ parasites luminescence compared to untreated in both fibroblasts and macrophages. This suggests and supports that that DMT1 is not the only/main source of iron in both these cell types. Following DMT1 inhibition, functional redundancy could occur to ensure sufficient iron availability by upregulating the expression of the transferrin receptor, or downregulating the expression of the iron storage protein ferritin to compensate for the inhibition of DMT1. Further work is required to verify the activity of CISMBI activity in macrophages and fibroblasts by measuring host iron either by radioactive iron uptake assays or calcein quenching assays. A functional host readout of cellular labile iron following DMT1 inhibition could also be measured using FerroOrange to assess if CISMBI significantly reduces the LIP, or if cells compensate by upregulating iron uptake pathways via TfR or by reducing iron storage by downregulating FTH1 expression levels.

4.4.6 How is iron internalised at the parasitophorous vacuolar membrane (PVM)?

Finally, although ZFT has been identified as the major iron and zinc importer in *Toxoplasma*, it currently remains unknown how iron is internalised at the parasitophorous vacuolar membrane (PVM). Studies have shown that *T. gondii* is capable of internalising vesicles, including lysosomes, through the PVM, degrading them and then the contents are released into the intravacuolar space (Coppens et al., 2006; Romano et al., 2017). A hypothesis is that iron-loaded vesicles are internalised by *T. gondii* into the intravacuolar network where they are then degraded, allowing for the parasite to take up iron. The intravacuolar network is a complex tubular and vesicular network within the parasitophorous vacuolar space. Previous studies have observed LAMP-1 staining within the parasitophorous vacuole, supporting this hypothesis (Coppens et al., 2006). To further support this,

XFM can be performed to investigate iron distribution and localisation within the vacuole and assess whether there is any iron localisation external to the parasite. Moreover, studies have found that secreted Gra proteins play a role in constructing the intravacuolar network (Mayoral et al., 2022; Romano et al., 2017), and that the uptake and degradation of vesicles by *T. gondii* is also dependent on the endosomal sorting complex required for transport ESCRT pathways as well as the host cell tubulin cytoskeleton. This could further be examined by assessing if the loss of the intravacuolar network, through the deletion of Gra proteins such as Gra2 and Gra6, would lead to an increase in sensitivity to iron removal. This would further support the role that the intravacuolar network plays in parasite iron acquisition and internalisation at the PV.

4.4.7 Limitations of the study

This study focuses on examining iron-related proteins in both human fibroblast cells as well as murine macrophages. However, the direct comparison of protein expression levels between these two cell types is challenging, and there are some factors that need to be taken into consideration. A major limitation is that there may be species-specific differences between mouse and human cell types, particularly in relation to the regulation of gene expression, metabolism, and immune signalling. The differences observed between these two cell types may therefore not necessarily be due to the cell type itself (professional immune cell vs. structural cell). The possibility of these differences arising due to differences in species (mouse vs. human) should not be ruled out at this point.

Moreover, HFFs used in this study are primary cells, isolated directly from tissue and have a limited life span, compared to RAW 264.7 murine macrophages which are an immortalised cell line that can proliferate indefinitely. It is important to consider that although cell lines such as RAW 264.7 murine macrophages are easier to grow and maintain in culture, they are often less biologically relevant and can lose key characteristics, accumulate higher mutation rates and are more prone to genetic changes over time. However, although primary cells have a lower mutation rate and retain their genetic makeup and tissue characteristics more efficiently compared to immortalised cell lines, they are also more inconsistent and present batch-to-batch variability depending on the donor from which the tissue came from. Immortalised cell lines in contrast are often more reproducible.

Primary cells can also lose their *in vivo* characteristics over multiple passages in cell culture. Future work could use bone marrow derived macrophages (BMDMs), a primary cell line that is derived directly from living tissue from a mouse, or Tohoku Hospital Pediatrics-1 (THP-1) cells, a human immortalised monocyte cell line, to increase physiological relevance of this study.

Another limitation of this study is the absence of a systemic *in vivo* model. Although cellular *in vitro* systems are more straightforward, do not require ethical approval, and are more cost-effective, they are focused on a more isolated portion rather than examining biological systems as part of a wider network with complex interactions between different components. *In vitro* systems lack the complex systemic biological interactions that would be present between different organs and tissues as well as the interplay of the immune system and endocrine signalling in response to infection. For example, *in vitro* culture systems lack hepcidin, a central hormone and master regulator of systemic iron homeostasis, regulated by the liver and triggered by inflammation/infection linking organ-to-organ communication. The liver senses iron body levels and regulates dietary iron absorption (e.g. in the intestine) as well as iron recycling in macrophages and plasma iron levels through the control of the iron exporter ferroportin. *In vitro* systems lack this multi-organ and whole-organism hepcidin-driven iron sequestration which is critical in shaping the availability of iron following infection. Another limitation may be timing, as all experiments were performed at least 24 h following infection and no earlier time points were assessed. It is possible that at this time point, the transient dynamics that occur early on in infection are lost. Although the effects observed at 24 h may be direct, the possibility of the effects being a result of a downstream consequence to infection or a compensatory response should not be ruled out however could be explored by examining earlier time points. Further, cells in *in vitro* systems are maintained in “artificial” conditions, including culture media as well as availability and composition of nutrients which do not necessarily mimic the complex systemic environment. The behaviour of parasites is dependent on the chemical environment that they are in, and thus any results observed in *in vitro* studies may not be applicable directly in i*n vivo* studies at the whole-organism level.

4.4.8 Final summary and concluding remarks

Here, I show that following infection with *T. gondii*, both TfR and DMT1 expression levels significantly increase in both fibroblasts and macrophages at 24 h compared to uninfected cells. DMT1 upregulation is maintained at 48 h in both cell types, however, TfR upregulation is lost at 48 h in macrophages (but not fibroblasts). The increase in TfR expression at 24 h was further supported by flow cytometry which demonstrated an increase in surface transferrin binding. Furthermore, the increase in both TfR and DMT1 expression levels was seen by IFA, which also demonstrates a change in localisation of DMT1. Interestingly, there was no significant differences in DMT1 expression upon infection with ΔMYR1 parasites (compared to RHΔKu80), suggesting that changes in DMT1 expression are not mediated by MYR1-dependent effector secretory proteins. Finally, I found that there is no significant change in FTH1 upon infection. The changes in expression of these iron-related proteins following infection with *T. gondii* in both human fibroblasts and murine macrophages at 24 h compared to uninfected cells are represented in the schematic in Figure 4.17.

Upon treatment with high iron, the changes in macrophage iron responses (reduced TfR expression) suggests that macrophages are more specialised cells in controlling iron homeostasis in high iron conditions compared to fibroblasts, although as expected, FTH1 expression increased in both cell types.

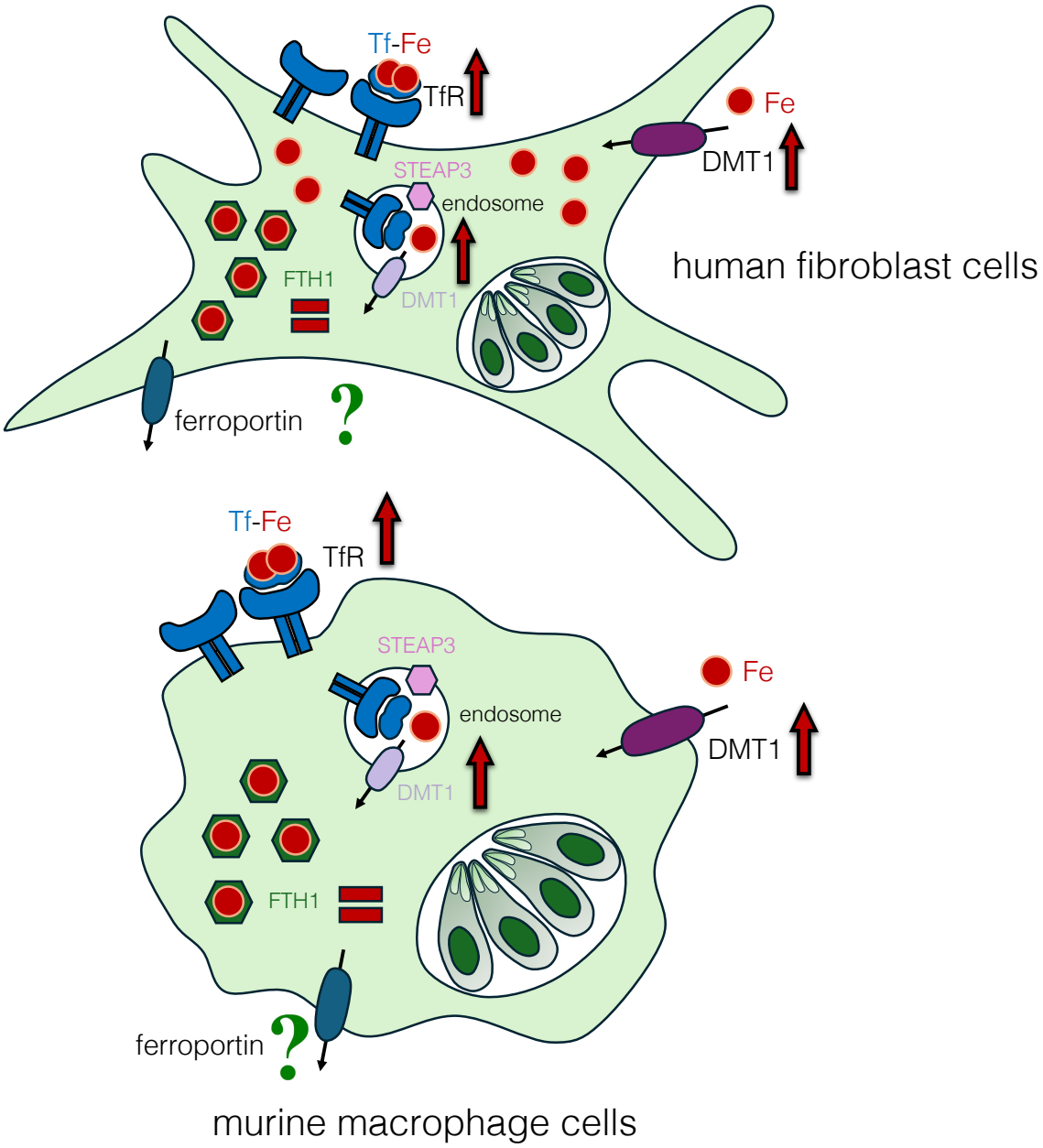


Figure 4.17 – Schematic representation of the changes in expression of iron-related proteins in both human fibroblasts and murine macrophages following infection with *Toxoplasma gondii* at 24 h compared to uninfected cells.

Schematic diagram demonstrating a significant increase (indicated by the red arrow) in both TfR and DMT1 expression levels in both human fibroblasts and murine macrophages following infection with *T. gondii* at 24 h compared to uninfected cells. No significant change (demonstrated by the red equal symbol) was observed in ferritin expression levels in both cell types following infection with *T. gondii* at 24 h compared to uninfected cells.

Upon infection under high iron, TfR expression reduces (compared to infected and untreated cells) in both fibroblasts and macrophages, but is significantly increased in fibroblasts when compared to uninfected, iron-treated cells. This suggests that even in high iron conditions, *T. gondii* is most likely driving the increase in TfR expression to ensure sufficient iron availability and counteract the host response of reducing TfR expression levels in high iron conditions. Contrary to fibroblasts, TfR levels upon infection and high iron conditions are maintained in macrophages when compared to uninfected, iron-treated cells. This suggests the possibility that *T. gondii* is counteracting the reduction of TfR expression level employed by macrophages to sequester iron stores following infection to support its survival and persistence. However, the different responses under high iron between cell types highlights that iron handling in macrophages is more tightly regulated compared to fibroblasts.

These results further support the findings from 2001 which showed an upregulation of TfR levels in infected fibroblasts by a gene-array hybridisation assay (Gail et al., 2001) and later studies in 2004 which attributed this increase in expression to an increased activity of IRP1, stabilising transferrin receptor mRNA and preventing it from degradation following infection with *T. gondii* (Gail et al., 2004). This increase in TfR expression is also observed upon *Leishmania* infection, where it was shown to be required for the intracellular growth and the survival of the parasite in macrophages (Das et al., 2009) as well as the intracellular bacterial pathogen *Francisella tularensis* (Pan et al., 2010). This highlights the manipulation of host transferrin receptor expression levels as a key strategy used by intracellular pathogens to subvert host iron restriction and suggests that *T. gondii* may be exploiting the same mechanisms to ensure sufficient iron availability for growth and survival within the host cell.

Upon infection under high iron, DMT1 expression significantly increases in fibroblasts when compared to uninfected, iron treated cells. This suggests that together with TfR, *T. gondii* is likely driving the increase in DMT1 expression to ensure sufficient iron availability. Contrary to fibroblasts, DMT1 levels upon infection and high iron conditions are maintained at 24 h in macrophages when compared to uninfected, iron treated cells, however, significantly increases at 48 h. This increase in DMT1 expression has also been observed in macrophages of patients with cutaneous leishmaniasis (Dighal et al., 2020). Further, the

expression of both TfR and DMT1 increase in macrophages following infection with the intracellular bacteria *Francisella tularensis*, resulting in a sustained increase in the labile iron pool within macrophages and in turn supporting the growth and survival of the pathogen (Fortier et al., 1995; Pan et al., 2010). Collectively, these studies highlight the manipulation of iron uptake pathways by pathogens as an important strategy to subvert host iron sequestration and suggests that the changes in TfR and DMT1 expression observed following *T. gondii* infection are likely to be parasite-driven.

Finally, there is no significant difference in FTH1 expression levels in both fibroblasts and macrophages when exposed to excess iron and *T. gondii* infection when compared to uninfected cells pretreated with excess iron. FTH1 levels do not change in infection, although do rise as expected upon iron treatment. This suggests that unlike *Leishmania* which intervenes in the host cell's ability to load iron into ferritin (Sen et al., 2022), *Toxoplasma gondii* does not directly impact iron storage in the host cell.

However, the maintenance of FTH1 upon the upregulation of TfR and DMT1 suggests that infection with *T. gondii* alters host iron homeostasis via iron uptake pathways instead of increasing the availability of iron within the cell by releasing iron stores. Schematics of the changes in expression of these iron-related proteins following *T. gondii* infection in high iron conditions in both human fibroblasts and murine macrophages at 24 h are represented in Figure 4.18 (compared to infected cells) and Figure 4.19 (compared to uninfected cells exposed to excess iron).

Overall, the findings from this study suggest that changes in iron uptake pathways in the host observed upon *Toxoplasma gondii* infection are most likely parasite-driven responses, by increasing the uptake of iron via TfR and DMT1 to guarantee sufficient iron availability for parasite survival. The findings from this study further emphasise the key differences in iron handling and infection control between the two cell types. They highlight the ability of *T. gondii* to manipulate host iron uptake pathways in fibroblasts more readily compared to macrophages and/or that fibroblasts are less specialised in iron-handling and sequestration following infection compared to macrophages. This highlights the tug-of-war for iron between specialised phagocytic cells and the parasite.

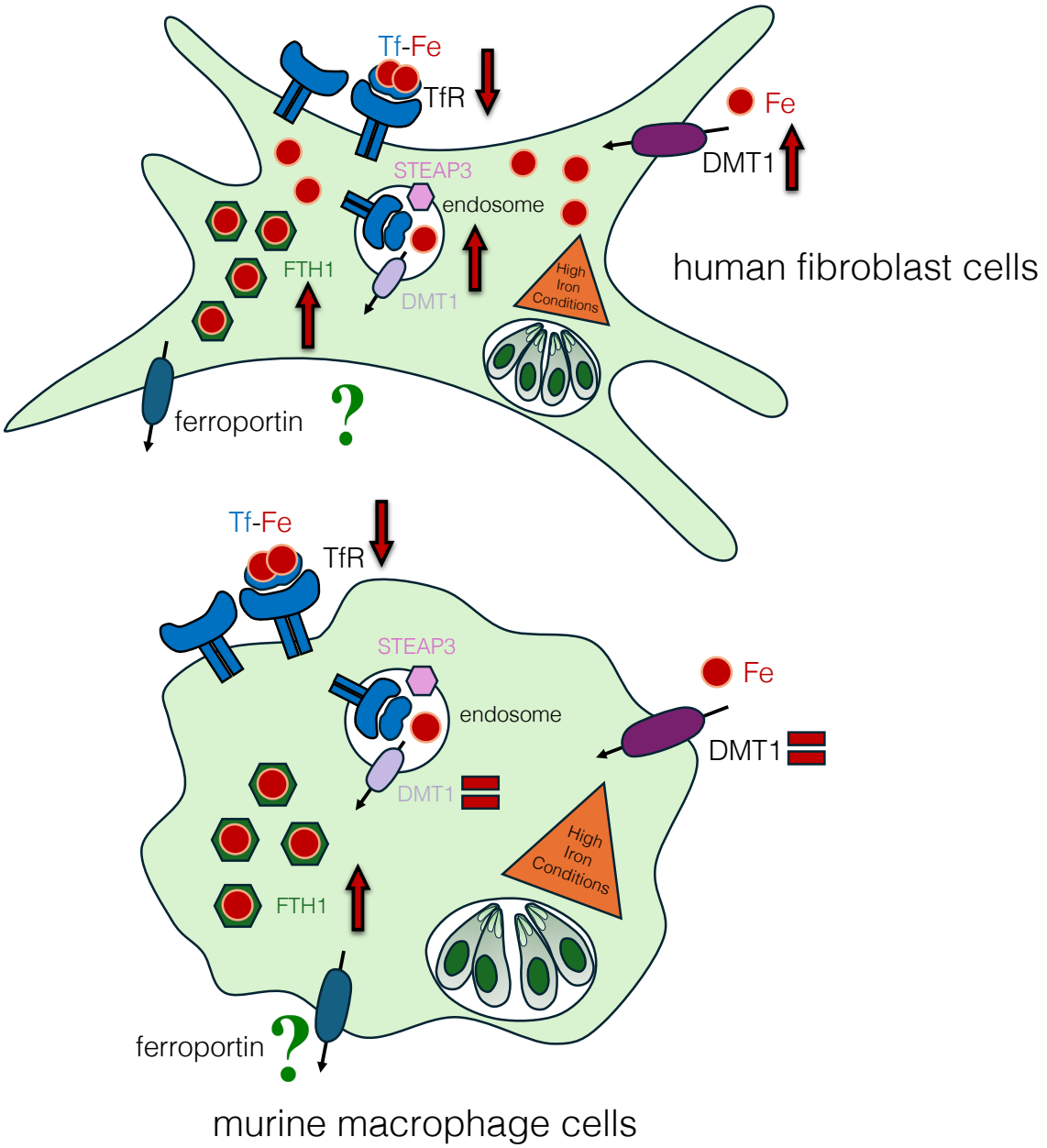


Figure 4.18 - Schematic representation of changes in the expression of iron-related proteins in fibroblasts and macrophages following *T. gondii* infection in excess iron conditions at 24 h compared to infected cells.

Schematic diagram demonstrating a significant decrease (indicated by the red arrow) in TfR expression levels in both human fibroblasts and murine macrophages following both *T. gondii* infection and high iron conditions (500 μM) at 24 h. In fibroblasts, there is an increase in DMT1 expression levels in both human fibroblasts and murine macrophages following exposure to both *T. gondii* infection and high iron conditions at 24 h. No significant difference (demonstrated by the red equal symbol) in DMT1 expression level is observed in macrophages in these conditions. A significant increase in FTH1 expression levels is observed in both human fibroblasts and murine macrophages exposed to *T. gondii* infection and excess iron at 24 h. All data is compared to infected untreated cells.

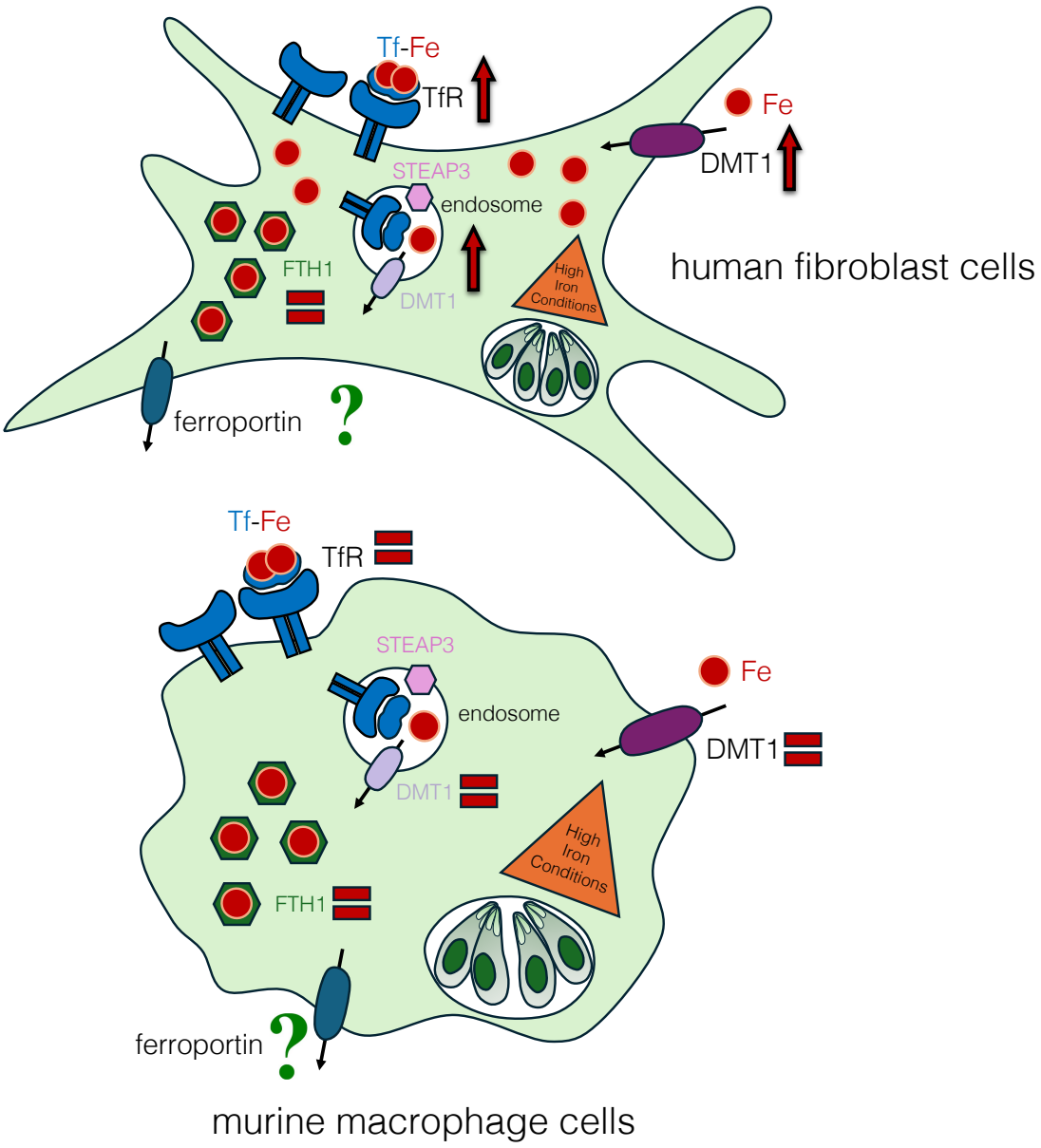


Figure 4.19 - Schematic representation of changes in the expression of iron-related proteins in fibroblasts and macrophages following *T. gondii* infection in excess iron conditions at 24 h compared to uninfected iron-treated cells.

Schematic diagram demonstrating a significant increase (indicated by the red arrow) in TfR and DMT1 expression levels human fibroblasts following both *T. gondii* infection and high iron conditions (500 μM) at 24 h. No significant difference (demonstrated by the red equal symbol) in FTH1 is observed in both cell types in these conditions. In macrophages, no significant difference in both TfR and DMT1 expression levels are observed following exposure to both *T. gondii* infection and high iron conditions at 24 h. All data is compared to uninfected cells exposed to excess iron.

Chapter 5 Final discussion, summary, and future outlooks

Trace elements including iron and zinc are essential for almost all life, including the ubiquitous obligate intracellular apicomplexan parasite *Toxoplasma gondii*. At the start of my PhD, the mechanisms by which these parasites acquired metals from the environment were not known. Moreover, very little was known about the strategies by which *T. gondii* hijacked and manipulated host iron homeostasis and trafficking to ensure growth and survival. The aim of my PhD was to answer two questions. Firstly, how does *Toxoplasma gondii* acquire iron and zinc? Secondly, how does host iron homeostasis change following infection with *T. gondii*?

In this thesis, I have identified and characterised the first iron and zinc uptake transporter, named ZFT, in *Toxoplasma gondii*, demonstrating its essential role in the parasite. Future work could involve identifying the metal binding sites of ZFT to start to understand the substrate specificity of this transporter. Understanding how ZFT is regulated and modified, particularly in the context of different iron conditions, and further examining the strategies behind the dynamic localisation observed are also of great interest. Moreover, I show that the expression of iron-related proteins, including the iron uptake proteins TfR and DMT1, increase following infection with *T. gondii*. However, future work is required to elucidate whether the changes in protein expression levels are host- or parasite-driven and how the expression of these iron-related proteins are regulated in the context of infection.

Putting this research in a broader context, the results of this thesis highlight the importance of iron in apicomplexan parasites, which actively import the divalent metal via dedicated transporter pathways on the plasma membrane of the parasite. The study further suggests that apicomplexan parasites sense the availability of iron, tightly regulating and controlling the uptake of iron and metal homeostasis. This is also likely tightly linked to parasite energy metabolism and developmental lifecycle stage progression. This is supported by changes observed in mitochondrial respiration which highlights the importance of iron-dependent enzymes including Fe-S cluster proteins, and a switch to a more quiescent lifecycle stage in the absence of the major iron importer ZFT in *T. gondii*. I show that

Toxoplasma actively acquires iron from its environment, potentially competing with the host cell for iron. This highlights a role for metal transporters as virulence determinants in infection.

Obligate intracellular apicomplexan parasites have evolved over time from free-living photosynthetic alveolate ancestors which lived independently and directly obtained iron from their marine environment. This suggests a transition in the strategies of iron acquisition as well as metabolic dependency. As they shifted from the free-living algae to endosymbionts to parasites, apicomplexan parasites have an increased reliance on nutrients from the host cell and possibly require fewer but functionally specialised, fine-tuned, and conserved iron importers to specifically exploit host iron stores, rather than multiple redundant or broad-spectrum metal transporters which acquired iron from the environment. Evidence of both iron and zinc transport by ZFT possibly suggests that the ancestral protein possibly transported a broad spectrum of divalent cations and has evolved over time to become a more specialised metal transporter with increased substrate specificity towards iron and zinc which are available in niche intracellular environments. This is further supported by the lack of ferrireductases encoded by apicomplexans. This emphasises that these intracellular parasites rely on the host cell reducing ferric iron, making ferrous iron available for the parasites to take up via dedicated iron transporters that take up iron already in the reduced form. The evolution of iron uptake highlights that iron has always been central to biological processes and energy metabolism, however the uptake mechanisms and source has shifted over time as these parasites evolved from being independent and free-living to becoming obligate and intracellular, relying on the host cell for survival.

This co-evolution between the host and the parasite sheds light onto whether changes in host iron handing are due to host- or parasite-driven processes. I hypothesise that both play a role and interact dynamically, but at different stages and for different purposes. I predict that during the initial stages of infection, iron homeostasis is controlled by host-driven processes which aim to restrict nutrient availability and thus trigger a nutritional immunity response following infection to limit parasite growth. In response to this and to directly counteract the iron sequestration by host cells, I hypothesise that *T. gondii* initiates parasite-driven modulation, such as an increase in TfR and DMT1 expression levels, to ensure sufficient iron availability, thus overriding the host defences. Like many biological

systems, I postulate that this interplay and interaction is not straightforward and is instead highly dynamic and based on a feedback loop. This highlights the tug-of-war or push-and-pull equilibrium between the host cell and the parasite and suggests that the outcome of infection depends on what side dominates – whether that is the host cell's ability to restrict, sequester and withhold iron, or the ability of *T. gondii* to subvert this control and ensure sufficient nutrient availability for parasite survival.

Overall, this study highlights the importance of iron and zinc for the survival of *Toxoplasma gondii* through the functional characterisation of the first iron and zinc importer in the parasite. It further emphasises the importance of controlling iron homeostasis both by the host cell to control infection, but also by the parasite which may be manipulating host iron trafficking and homeostasis to ensure sufficient availability of this nutrient for growth and persistence.

References

Abboud, S., Haile, D.J., 2000. A Novel Mammalian Iron-regulated Protein Involved in Intracellular Iron Metabolism. Journal of Biological Chemistry 275, 19906–19912. https://doi.org/10.1074/jbc.M000713200

Abdulai-Saiku, S., Vyas, A., 2017. Loss of predator aversion in female rats after Toxoplasma gondii infection is not dependent on ovarian steroids. Brain, Behavior, and Immunity 65, 95–98. https://doi.org/10.1016/j.bbi.2017.04.005

Abreu, R., Essler, L., Giri, P., Quinn, F., 2020. Interferon-gamma promotes iron export in human macrophages to limit intracellular bacterial replication. PLoS One 15, e0240949. https://doi.org/10.1371/journal.pone.0240949

Adl, S.M., Bass, D., Lane, C.E., Lukeš, J., Schoch, C.L., Smirnov, A., Agatha, S., Berney, C., Brown, M.W., Burki, F., Cárdenas, P., Čepička, I., Chistyakova, L., Del Campo, J., Dunthorn, M., Edvardsen, B., Eglit, Y., Guillou, L., Hampl, V., Heiss, A.A., Hoppenrath, M., James, T.Y., Karnkowska, A., Karpov, S., Kim, E., Kolisko, M., Kudryavtsev, A., Lahr, D.J.G., Lara, E., Le Gall, L., Lynn, D.H., Mann, D.G., Massana, R., Mitchell, E.A.D., Morrow, C., Park, J.S., Pawlowski, J.W., Powell, M.J., Richter, D.J., Rueckert, S., Shadwick, L., Shimano, S., Spiegel, F.W., Torruella, G., Youssef, N., Zlatogursky, V., Zhang, Q., 2019. Revisions to the Classification, Nomenclature, and Diversity of Eukaryotes. J Eukaryotic Microbiology 66, 4–119. https://doi.org/10.1111/jeu.12691

Adl, S.M., Leander, B.S., Simpson, A.G.B., Archibald, J.M., Anderson, O.Roger., Bass, D., Bowser, S.S., Brugerolle, G., Farmer, M.A., Karpov, S., Kolisko, M., Lane, C.E., Lodge, D.J., Mann, D.G., Meisterfeld, R., Mendoza, L., Moestrup, Ø., Mozley-Standridge, S.E., Smirnov, A.V., Spiegel, F., 2007. Diversity, Nomenclature, and Taxonomy of Protists. Systematic Biology 56, 684–689. https://doi.org/10.1080/10635150701494127

Adl, S.M., Simpson, A.G.B., Farmer, M.A., Andersen, R.A., Anderson, O.R., Barta, J.R., Bowser, S.S., Brugerolle, G., Fensome, R.A., Fredericq, S., James, T.Y., Karpov, S., Kugrens, P., Krug, J., Lane, C.E., Lewis, L.A., Lodge, J., Lynn, D.H., Mann, D.G., Mccourt, R.M., Mendoza, L., Moestrup, O., Mozley-Standridge, S.E., Nerad, T.A., Shearer, C.A., Smirnov, A.V., Spiegel, F.W., Taylor, M.F.J.R., 2005. The New Higher Level Classification of Eukaryotes with Emphasis on the Taxonomy of Protists. J Eukaryotic Microbiology 52, 399–451. https://doi.org/10.1111/j.1550-7408.2005.00053.x

Aghabi, D., Sloan, M., Gill, G., Hartmann, E., Antipova, O., Dou, Z., Guerra, A.J., Carruthers, V.B., Harding, C.R., 2023. The vacuolar iron transporter mediates iron detoxification in Toxoplasma gondii. Nat Commun 14, 3659. https://doi.org/10.1038/s41467-023-39436-y

Agrawal, S., van Dooren, G.G., Beatty, W.L., Striepen, B., 2009. Genetic evidence that an endosymbiont-derived endoplasmic reticulum-associated protein degradation (ERAD) system functions in import of apicoplast proteins. J Biol Chem 284, 33683–33691. https://doi.org/10.1074/jbc.M109.044024

Ahern, M.E., Bafaro, E.M., Cowan, A., Dempski, R.E., 2020. Quantifying the Oligomeric State of hZIP4 on the Surface of Cells.

Aisen, P., 2001. Chemistry and biology of eukaryotic iron metabolism. The International Journal of Biochemistry & Cell Biology 33, 940–959. https://doi.org/10.1016/S1357-2725(01)00063-2

Ajeesh Krishna, T.P., Maharajan, T., Victor Roch, G., Ignacimuthu, S., Antony Ceasar, S., 2020. Structure, Function, Regulation and Phylogenetic Relationship of ZIP Family Transporters of Plants. Front. Plant Sci. 11, 662. https://doi.org/10.3389/fpls.2020.00662

Akuh, O.-A., Elahi, R., Prigge, S.T., Seeber, F., 2022. The ferredoxin redox system – an essential electron distributing hub in the apicoplast of Apicomplexa. Trends in Parasitology 38, 868–881. https://doi.org/10.1016/j.pt.2022.08.002

Alday, H., Doggett, J., 2017. Drugs in development for toxoplasmosis: advances, challenges, and current status. DDDT Volume11, 273–293. https://doi.org/10.2147/DDDT.S60973

Allahyari, M., Mohabati, R., Vatanara, A., Golkar, M., 2020. In-vitro and in-vivo comparison of rSAG1-loaded PLGA prepared by encapsulation and adsorption methods as an efficient vaccine against Toxoplasma gondii". Journal of Drug Delivery Science and Technology 55, 101327. https://doi.org/10.1016/j.jddst.2019.101327

Al-sandaqchi, A.T., Brignell, C., Collingwood, J.F., Geraki, K., Mirkes, E.M., Kong, K., Castellanos, M., May, S.T., Stevenson, C.W., Elsheikha, H.M., 2018. Metallome of cerebrovascular endothelial cells infected with *Toxoplasma gondii* using μ-XRF imaging and inductively coupled plasma mass spectrometry. Metallomics 10, 1401–1414. https://doi.org/10.1039/c8mt00136g

Alyssa B., M., Tolunay Beker, A., Gregory J., G., Don A., S., Shou-Mei, C., Robert J., C., 2013. Gastric and Colonic Zinc Transporter ZIP11 (Slc39a11) in Mice Responds to Dietary Zinc and Exhibits Nuclear Localization. The Journal of Nutrition 143, 1882–1888. https://doi.org/10.3945/jn.113.184457

Ambroise-Thomas, P., Pelloux, H., 1993. Toxoplasmosis — congenital and in immunocompromised patients: A parallel. Parasitology Today 9, 61–63. https://doi.org/10.1016/0169-4758(93)90038-H

Amos, B., Aurrecoechea, C., Barba, M., Barreto, A., Basenko, E.Y., Bażant, W., Belnap, R., Blevins, A.S., Böhme, U., Brestelli, J., Brunk, B.P., Caddick, M., Callan, D., Campbell, L., Christensen, M.B., Christophides, G.K., Crouch, K., Davis, K., DeBarry, J., Doherty, R., Duan, Y., Dunn, M., Falke, D., Fisher, S., Flicek, P., Fox, B., Gajria, B., Giraldo-Calderón, G.I., Harb, O.S., Harper, E., Hertz-Fowler, C., Hickman, M.J., Howington, C., Hu, S., Humphrey, J., Iodice, J., Jones, A., Judkins, J., Kelly, S.A., Kissinger, J.C., Kwon, D.K., Lamoureux, K., Lawson, D., Li, W., Lies, K., Lodha, D., Long, J., MacCallum, R.M., Maslen, G., McDowell, M.A., Nabrzyski, J., Roos, D.S., Rund, S.S.C., Schulman, S.W., Shanmugasundram, A., Sitnik, V., Spruill, D., Starns, D., Stoeckert, C.J., Tomko, S.S., Wang, H., Warrenfeltz, S., Wieck, R., Wilkinson, P.A., Xu, L., Zheng, J., 2022. VEuPathDB: the eukaryotic pathogen, vector and host bioinformatics resource center. Nucleic Acids Research 50, D898–D911. https://doi.org/10.1093/nar/gkab929

Anderson, C.P., Shen, M., Eisenstein, R.S., Leibold, E.A., 2012. Mammalian iron metabolism and its control by iron regulatory proteins. Biochimica et Biophysica Acta (BBA) - Molecular Cell Research 1823, 1468–1483. https://doi.org/10.1016/j.bbamcr.2012.05.010

Andreini, C., Banci, L., Bertini, I., Rosato, A., 2006a. Counting the Zinc-Proteins Encoded in the Human Genome. J. Proteome Res. 5, 196–201. https://doi.org/10.1021/pr050361j

Andreini, C., Banci, L., Bertini, I., Rosato, A., 2006b. Zinc through the Three Domains of Life. J. Proteome Res. 5, 3173–3178. https://doi.org/10.1021/pr0603699

Andreini, C., Bertini, I., Rosato, A., 2009. Metalloproteomes: A Bioinformatic Approach. Acc. Chem. Res. 42, 1471–1479. https://doi.org/10.1021/ar900015x

Andreini, C., Putignano, V., Rosato, A., Banci, L., 2018. The human iron-proteome†. Metallomics 10, 1223–1231. https://doi.org/10.1039/c8mt00146d

Andrews, S.C., Robinson, A.K., Rodríguez-Quiñones, F., 2003. Bacterial iron homeostasis. FEMS Microbiol Rev 27, 215–237. https://doi.org/10.1016/S0168-6445(03)00055-X

Antala, S., Dempski, R.E., 2012. The Human ZIP4 Transporter Has Two Distinct Binding Affinities and Mediates Transport of Multiple Transition Metals. Biochemistry 51, 963–973. https://doi.org/10.1021/bi201553p

Antala, S., Ovchinnikov, S., Kamisetty, H., Baker, D., Dempski, R.E., 2015. Computation and Functional Studies Provide a Model for the Structure of the Zinc Transporter hZIP4. Journal of Biological Chemistry 290, 17796–17805. https://doi.org/10.1074/jbc.M114.617613

Apell, H.-J., 2004. How do P-Type ATPases transport ions? Bioelectrochemistry 63, 149–156. https://doi.org/10.1016/j.bioelechem.2003.09.021

Arango Duque, G., Descoteaux, A., 2014. Macrophage cytokines: involvement in immunity and infectious diseases. Front Immunol 5, 491. https://doi.org/10.3389/fimmu.2014.00491

Archibald, F., 1983. *Lactobacillus plantarum* , an organism not requiring iron. FEMS Microbiology Letters 19, 29–32. https://doi.org/10.1111/j.1574-6968.1983.tb00504.x

Archibald, J.M., 2015. Endosymbiosis and Eukaryotic Cell Evolution. Current Biology 25, R911–R921. https://doi.org/10.1016/j.cub.2015.07.055

Arosio, P., Ingrassia, R., Cavadini, P., 2009. Ferritins: A family of molecules for iron storage, antioxidation and more. Biochimica et Biophysica Acta (BBA) - General Subjects 1790, 589–599. https://doi.org/10.1016/j.bbagen.2008.09.004

Atri, C., Guerfali, F.Z., Laouini, D., 2018. Role of Human Macrophage Polarization in Inflammation during Infectious Diseases. IJMS 19, 1801. https://doi.org/10.3390/ijms19061801

Augusto, L., Martynowicz, J., Amin, P.H., Carlson, K.R., Wek, R.C., Sullivan, W.J., 2021. TgIF2K-B Is an eIF2α Kinase in Toxoplasma gondii That Responds to Oxidative Stress and Optimizes Pathogenicity. mBio 12, e03160-20. https://doi.org/10.1128/mBio.03160-20

Aw, Y.T.V., Seidi, A., Hayward, J.A., Lee, J., Makota, F.V., Rug, M., Van Dooren, G.G., 2021. A key cytosolic iron–sulfur cluster synthesis protein localizes to the mitochondrion of *Toxoplasma gondii*. Molecular Microbiology 115, 968–985. https://doi.org/10.1111/mmi.14651

Aydemir, T.B., Cousins, R.J., 2018. The Multiple Faces of the Metal Transporter ZIP14 (SLC39A14). The Journal of Nutrition 148, 174–184. https://doi.org/10.1093/jn/nxx041

Aydemir, T.B., Liuzzi, J.P., McClellan, S., Cousins, R.J., 2009. Zinc transporter ZIP8 (SLC39A8) and zinc influence IFN-γ expression in activated human T cells. Journal of Leukocyte Biology 86, 337–348. https://doi.org/10.1189/jlb.1208759

Bafaro, E.M., Maciejewski, M.W., Hoch, J.C., Dempski, R.E., 2019. Concomitant disorder and high-affinity zinc binding in the human zinc- and iron-regulated transport protein 4 intracellular loop. Protein Science 28, 868–880. https://doi.org/10.1002/pro.3591

Baker, N., Patel, J., Khacho, M., 2019. Linking mitochondrial dynamics, cristae remodeling and supercomplex formation: How mitochondrial structure can regulate bioenergetics. Mitochondrion 49, 259–268. https://doi.org/10.1016/j.mito.2019.06.003

Baldwin, S.A. (Ed.), 2000. Membrane Transport: A Practical Approach. Oxford University PressOxford. https://doi.org/10.1093/oso/9780199637058.001.0001

Banerjee, S., Datta, R., 2020. *Leishmania* infection triggers hepcidin-mediated proteasomal degradation of Nramp1 to increase phagolysosomal iron availability. Cellular Microbiology 22. https://doi.org/10.1111/cmi.13253

Barona-Gómez, F., Wong, U., Giannakopulos, A.E., Derrick, P.J., Challis, G.L., 2004. Identification of a Cluster of Genes that Directs Desferrioxamine Biosynthesis in *Streptomyces c oelicolor* M145. J. Am. Chem. Soc. 126, 16282–16283. https://doi.org/10.1021/ja045774k

Barrangou, R., Fremaux, C., Deveau, H., Richards, M., Boyaval, P., Moineau, S., Romero, D.A., Horvath, P., 2007. CRISPR Provides Acquired Resistance Against Viruses in Prokaryotes. Science 315, 1709–1712. https://doi.org/10.1126/science.1138140

Barthelme, D., Scheele, U., Dinkelaker, S., Janoschka, A., MacMillan, F., Albers, S.-V., Driessen, A.J.M., Stagni, M.S., Bill, E., Meyer-Klaucke, W., Schuönemann, V., Tampé;, R., 2007. Structural Organization of Essential Iron-Sulfur Clusters in the Evolutionarily Highly Conserved ATP-binding Cassette Protein ABCE1. Journal of Biological Chemistry 282, 14598–14607. https://doi.org/10.1074/jbc.M700825200

Barylyuk, K., Koreny, L., Ke, H., Butterworth, S., Crook, O.M., Lassadi, I., Gupta, V., Tromer, E., Mourier, T., Stevens, T.J., Breckels, L.M., Pain, A., Lilley, K.S., Waller, R.F., 2020. A Comprehensive Subcellular Atlas of the Toxoplasma Proteome via hyperLOPIT Provides Spatial Context for Protein Functions. Cell Host & Microbe 28, 752-766.e9. https://doi.org/10.1016/j.chom.2020.09.011

Beckers, C.J., Roos, D.S., Donald, R.G., Luft, B.J., Schwab, J.C., Cao, Y., Joiner, K.A., 1995. Inhibition of cytoplasmic and organellar protein synthesis in Toxoplasma gondii. Implications for the target of macrolide antibiotics. J. Clin. Invest. 95, 367–376. https://doi.org/10.1172/JCI117665

Beker Aydemir, T., Chang, S.-M., Guthrie, G.J., Maki, A.B., Ryu, M.-S., Karabiyik, A., Cousins, R.J., 2012. Zinc Transporter ZIP14 Functions in Hepatic Zinc, Iron and Glucose Homeostasis during the Innate Immune Response (Endotoxemia). PLoS ONE 7, e48679. https://doi.org/10.1371/journal.pone.0048679

Belli, S.I., Smith, N.C., Ferguson, D.J.P., 2006. The coccidian oocyst: a tough nut to crack! Trends in Parasitology 22, 416–423. https://doi.org/10.1016/j.pt.2006.07.004

Bellotti, D., Remelli, M., 2021. Deferoxamine B: A Natural, Excellent and Versatile Metal Chelator. Molecules 26, 3255. https://doi.org/10.3390/molecules26113255

Ben-Othman, R., Flannery, A.R., Miguel, D.C., Ward, D.M., Kaplan, J., Andrews, N.W., 2014. Leishmania-Mediated Inhibition of Iron Export Promotes

Parasite Replication in Macrophages. PLoS Pathog 10, e1003901. https://doi.org/10.1371/journal.ppat.1003901

Bergmann, A., Floyd, K., Key, M., Dameron, C., Rees, K.C., Thornton, L.B., Whitehead, D.C., Hamza, I., Dou, Z., 2020a. Toxoplasma gondii requires its plant-like heme biosynthesis pathway for infection. PLoS Pathog 16, e1008499. https://doi.org/10.1371/journal.ppat.1008499

Bergmann, A., Floyd, K., Key, M., Dameron, C., Rees, K.C., Thornton, L.B., Whitehead, D.C., Hamza, I., Dou, Z., 2020b. Toxoplasma gondii requires its plant-like heme biosynthesis pathway for infection. PLOS Pathogens 16, e1008499. https://doi.org/10.1371/journal.ppat.1008499

Besecker, B., Bao, S., Bohacova, B., Papp, A., Sadee, W., Knoell, D.L., 2008. The human zinc transporter SLC39A8 (Zip8) is critical in zinc-mediated cytoprotection in lung epithelia. American Journal of Physiology-Lung Cellular and Molecular Physiology 294, L1127–L1136. https://doi.org/10.1152/ajplung.00057.2008

Beyersmann, D., Haase, H., 2001. Functions of zinc in signaling, proliferation and differentiation of mammalian cells. Biometals 14, 331–341. https://doi.org/10.1023/A:1012905406548

Bin, B.-H., Fukada, T., Hosaka, T., Yamasaki, S., Ohashi, W., Hojyo, S., Miyai, T., Nishida, K., Yokoyama, S., Hirano, T., 2011. Biochemical Characterization of Human ZIP13 Protein. Journal of Biological Chemistry 286, 40255–40265. https://doi.org/10.1074/jbc.M111.256784

Björkman, A., Gil, P., Alifrangis, M., 2024. Alarming Plasmodium falciparum resistance to artemisinin-based combination therapy in Africa: the critical role of the partner drug. The Lancet Infectious Diseases 24, e540–e541. https://doi.org/10.1016/S1473-3099(24)00427-4

Blaby-Haas, C.E., Merchant, S.S., 2013. Iron sparing and recycling in a compartmentalized cell. Current Opinion in Microbiology 16, 677–685. https://doi.org/10.1016/j.mib.2013.07.019

Black, M.W., Boothroyd, J.C., 2000. Lytic Cycle of *Toxoplasma gondii*. Microbiol Mol Biol Rev 64, 607–623. https://doi.org/10.1128/MMBR.64.3.607-623.2000

Blader, I.J., Coleman, B.I., Chen, C.-T., Gubbels, M.-J., 2015. Lytic Cycle of *Toxoplasma gondii*: 15 Years Later. Annu. Rev. Microbiol. 69, 463–485. https://doi.org/10.1146/annurev-micro-091014-104100

Blake, D.P., Tomley, F.M., 2014. Securing poultry production from the ever-present Eimeria challenge. Trends in Parasitology 30, 12–19. https://doi.org/10.1016/j.pt.2013.10.003

Blume, M., Rodriguez-Contreras, D., Landfear, S., Fleige, T., Soldati-Favre, D., Lucius, R., Gupta, N., 2009. Host-derived glucose and its transporter in the obligate intracellular pathogen *Toxoplasma gondii* are dispensable by glutaminolysis. Proc. Natl. Acad. Sci. U.S.A. 106, 12998–13003. https://doi.org/10.1073/pnas.0903831106

Bogdan, A.R., Miyazawa, M., Hashimoto, K., Tsuji, Y., 2016. Regulators of Iron Homeostasis: New Players in Metabolism, Cell Death, and Disease. Trends Biochem Sci 41, 274–286. https://doi.org/10.1016/j.tibs.2015.11.012

Bohne, W., Heesemann, J., Gross, U., 1994. Reduced replication of Toxoplasma gondii is necessary for induction of bradyzoite-specific antigens: a possible role for nitric oxide in triggering stage conversion. Infect Immun 62, 1761–1767. https://doi.org/10.1128/iai.62.5.1761-1767.1994

Bohne, W., Heesemann, J., Gross, U., 1993. Induction of bradyzoite-specific Toxoplasma gondii antigens in gamma interferon-treated mouse macrophages. Infect Immun 61, 1141–1145. https://doi.org/10.1128/iai.61.3.1141-1145.1993

Botein, E.F., Darwish, A., El-Tantawy, N.L., EL-baz, R., Eid, M.I., Shaltot, A.M., 2019. Serological and molecular screening of umbilical cord blood for *Toxoplasma gondii* infection. Transplant Infectious Dis 21, e13117. https://doi.org/10.1111/tid.13117

Bougdour, A., Durandau, E., Brenier-Pinchart, M.-P., Ortet, P., Barakat, M., Kieffer, S., Curt-Varesano, A., Curt-Bertini, R.-L., Bastien, O., Coute, Y., Pelloux, H., Hakimi, M.-A., 2013. Host Cell Subversion by Toxoplasma GRA16, an Exported Dense Granule Protein that Targets the Host Cell Nucleus and Alters Gene Expression. Cell Host & Microbe 13, 489–500. https://doi.org/10.1016/j.chom.2013.03.002

Bouzid, M., Hunter, P.R., Chalmers, R.M., Tyler, K.M., 2013. Cryptosporidium Pathogenicity and Virulence. Clin Microbiol Rev 26, 115–134. https://doi.org/10.1128/CMR.00076-12

Braymer, J.J., Freibert, S.A., Rakwalska-Bange, M., Lill, R., 2021. Mechanistic concepts of iron-sulfur protein biogenesis in Biology. Biochimica et Biophysica Acta (BBA) - Molecular Cell Research 1868, 118863. https://doi.org/10.1016/j.bbamcr.2020.118863

Brown, K.M., Long, S., Sibley, L.D., 2017. Plasma Membrane Association by N-Acylation Governs PKG Function in *Toxoplasma gondii*. mBio 8, e00375-17. https://doi.org/10.1128/mBio.00375-17

Bublitz, M., Morth, J.P., Nissen, P., 2011. P-type ATPases at a glance. Journal of Cell Science 124, 2515–2519. https://doi.org/10.1242/jcs.088716

Bunnik, E.M., Venkat, A., Shao, J., McGovern, K.E., Batugedara, G., Worth, D., Prudhomme, J., Lapp, S.A., Andolina, C., Ross, L.S., Lawres, L., Brady, D., Sinnis, P., Nosten, F., Fidock, D.A., Wilson, E.H., Tewari, R., Galinski, M.R., Ben Mamoun, C., Ay, F., Le Roch, K.G., 2019. Comparative 3D genome organization in apicomplexan parasites. Proc Natl Acad Sci U S A 116, 3183–3192. https://doi.org/10.1073/pnas.1810815116

Burgess-Brown, N.A., Sharma, S., Sobott, F., Loenarz, C., Oppermann, U., Gileadi, O., 2008. Codon optimization can improve expression of human genes in Escherichia coli: A multi-gene study. Protein Expression and Purification 59, 94–102. https://doi.org/10.1016/j.pep.2008.01.008

Byrd, T.F., Horwitz, M.A., 1993. Regulation of transferrin receptor expression and ferritin content in human mononuclear phagocytes. Coordinate upregulation by iron transferrin and downregulation by interferon gamma. J Clin Invest 91, 969–976. https://doi.org/10.1172/JCI116318

Cairo, G., Bernuzzi, F., Recalcati, S., 2006. A precious metal: Iron, an essential nutrient for all cells. Genes Nutr 1, 25–39. https://doi.org/10.1007/BF02829934

Carme, B., Bissuel, F., Ajzenberg, D., Bouyne, R., Aznar, C., Demar, M., Bichat, S., Louvel, D., Bourbigot, A.M., Peneau, C., Neron, P., Dardé, M.L., 2002. Severe Acquired Toxoplasmosis in Immunocompetent Adult Patients in French Guiana. J Clin Microbiol 40, 4037–4044. https://doi.org/10.1128/JCM.40.11.4037-4044.2002

Carruthers, V.B., 2002. Host cell invasion by the opportunistic pathogen Toxoplasma gondii. Acta Tropica 81, 111–122. https://doi.org/10.1016/S0001-706X(01)00201-7

Carvalho, S., Barreira Da Silva, R., Shawki, A., Castro, H., Lamy, M., Eide, D., Costa, V., Mackenzie, B., Tomás, A.M., 2015. *Li* ZIP 3 is a cellular zinc transporter that mediates the tightly regulated import of zinc in *L eishmania infantum* parasites. Molecular Microbiology 96, 581–595. https://doi.org/10.1111/mmi.12957

Carvalho, S., Silva, R., Shawki, A., Mackenzie, B., Castro, H., Eide, D., Costa, V., Tomás, A.M., 2012. *Leishmania infantum* ZIP3 is a zinc transporter that is tightly regulated by zinc status. The FASEB Journal 26. https://doi.org/10.1096/fasebj.26.1_supplement.1112.4

Casey, J.L., Hentze, M.W., Koeller, D.M., Caughman, S.W., Rouault, T.A., Klausner, R.D., Harford, J.B., 1988. Iron-Responsive Elements: Regulatory RNA Sequences That Control mRNA Levels and Translation. Science 240, 924–928. https://doi.org/10.1126/science.2452485

Cassat, James E., Skaar, E.P., 2013. Iron in infection and immunity. Cell Host Microbe 13, 509–519. https://doi.org/10.1016/j.chom.2013.04.010

Cassat, James E., Skaar, E.P., 2013. Iron in Infection and Immunity. Cell Host & Microbe 13, 509–519. https://doi.org/10.1016/j.chom.2013.04.010

Cavalier-Smith, T., 1993. Kingdom protozoa and its 18 phyla. Microbiol Rev 57, 953–994. https://doi.org/10.1128/mr.57.4.953-994.1993

Cerasi, M., Liu, J.Z., Ammendola, S., Poe, A.J., Petrarca, P., Pesciaroli, M., Pasquali, P., Raffatellu, M., Battistoni, A., 2014. The ZupT transporter plays an important role in zinc homeostasis and contributes to Salmonella enterica virulence. Metallomics 6, 845–853. https://doi.org/10.1039/c3mt00352c

Cerutti, A., Blanchard, N., Besteiro, S., 2020. The Bradyzoite: A Key Developmental Stage for the Persistence and Pathogenesis of Toxoplasmosis. Pathogens 9, 234. https://doi.org/10.3390/pathogens9030234

Chalmers, R.M., Robinson, G., Elwin, K., Elson, R., 2019. Analysis of the Cryptosporidium spp. and gp60 subtypes linked to human outbreaks of cryptosporidiosis in England and Wales, 2009 to 2017. Parasit Vectors 12, 95. https://doi.org/10.1186/s13071-019-3354-6

Chang, Y., Dickinson, D.J., 2022. Non-invasive chimeric HaloTag labeling to study clustering and diffusion of membrane proteins. STAR Protocols 3, 101857. https://doi.org/10.1016/j.xpro.2022.101857

Chasen, N.M., Stasic, A.J., Asady, B., Coppens, I., Moreno, S.N.J., 2019. The Vacuolar Zinc Transporter TgZnT Protects Toxoplasma gondii from Zinc Toxicity. mSphere 4, e00086-19. https://doi.org/10.1128/mSphere.00086-19

Chasteen, N.D., 1998. Ferritin. Uptake, storage, and release of iron. Met Ions Biol Syst 35, 479–514.

Chaudhry, S.A., Gad, N., Koren, G., 2014. Toxoplasmosis and pregnancy. Can Fam Physician 60, 334–336.

Checkley, W., White, A.C., Jaganath, D., Arrowood, M.J., Chalmers, R.M., Chen, X.-M., Fayer, R., Griffiths, J.K., Guerrant, R.L., Hedstrom, L., Huston, C.D., Kotloff, K.L., Kang, G., Mead, J.R., Miller, M., Petri, W.A., Priest, J.W., Roos, D.S., Striepen, B., Thompson, R.C.A., Ward, H.D., Van Voorhis, W.A., Xiao, L., Zhu, G., Houpt, E.R., 2015. A review of the global burden, novel diagnostics, therapeutics, and vaccine targets for cryptosporidium. The Lancet Infectious Diseases 15, 85–94. https://doi.org/10.1016/S1473-3099(14)70772-8

Chen, A.L., Kim, E.W., Toh, J.Y., Vashisht, A.A., Rashoff, A.Q., Van, C., Huang, A.S., Moon, A.S., Bell, H.N., Bentolila, L.A., Wohlschlegel, J.A., Bradley, P.J., 2015. Novel Components of the Toxoplasma Inner Membrane Complex Revealed by BioID. mBio 6, e02357-14. https://doi.org/10.1128/mBio.02357-14

Chen, B., Yu, P., Chan, W.N., Xie, F., Zhang, Y., Liang, L., Leung, K.T., Lo, K.W., Yu, J., Tse, G.M.K., Kang, W., To, K.F., 2024. Cellular zinc metabolism and zinc signaling: from biological functions to diseases and therapeutic targets. Sig Transduct Target Ther 9, 6. https://doi.org/10.1038/s41392-023-01679-y

Chen, S., Saeed, A.F.U.H., Liu, Q., Jiang, Q., Xu, H., Xiao, G.G., Rao, L., Duo, Y., 2023. Macrophages in immunoregulation and therapeutics. Sig Transduct Target Ther 8, 207. https://doi.org/10.1038/s41392-023-01452-1

Chen, W., Paradkar, P.N., Li, L., Pierce, E.L., Langer, N.B., Takahashi-Makise, N., Hyde, B.B., Shirihai, O.S., Ward, D.M., Kaplan, J., Paw, B.H., 2009. Abcb10 physically interacts with mitoferrin-1 (Slc25a37) to enhance its stability and function in the erythroid mitochondria. Proc. Natl. Acad. Sci. U.S.A. 106, 16263–16268. https://doi.org/10.1073/pnas.0904519106

Chiang, C.-W., Carter, N., Sullivan, W.J., Donald, R.G.K., Roos, D.S., Naguib, F.N.M., El Kouni, M.H., Ullman, B., Wilson, C.M., 1999. The Adenosine Transporter of Toxoplasma gondii. Journal of Biological Chemistry 274, 35255–35261. https://doi.org/10.1074/jbc.274.49.35255

Chlosta, S., Fishman, D.S., Harrington, L., Johnson, E.E., Knutson, M.D., Wessling-Resnick, M., Cherayil, B.J., 2006. The Iron Efflux Protein Ferroportin Regulates the Intracellular Growth of *Salmonella enterica*. Infect Immun 74, 3065–3067. https://doi.org/10.1128/IAI.74.5.3065-3067.2006

Cho, S.-Y., Jung, S.-J., Kim, K.-D., Roe, J.-H., 2021. Non-mitochondrial aconitase regulates the expression of iron-uptake genes by controlling the RNA turnover process in fission yeast. J Microbiol. 59, 1075–1082. https://doi.org/10.1007/s12275-021-1438-4

Cho, Y.-E., Lomeda, R.-A.R., Ryu, S.-H., Lee, J.-H., Beattie, J.H., Kwun, I.-S., 2007. Cellular Zn depletion by metal ion chelators (TPEN, DTPA and chelex resin) and its application to osteoblastic MC3T3-E1 cells. Nutr Res Pract 1, 29–35. https://doi.org/10.4162/nrp.2007.1.1.29

Choi, D.W., Koh, J.Y., 1998. ZINC AND BRAIN INJURY. Annu. Rev. Neurosci. 21, 347–375. https://doi.org/10.1146/annurev.neuro.21.1.347

Chou, C.J., Wisedchaisri, G., Monfeli, R.R., Oram, D.M., Holmes, R.K., Hol, W.G.J., Beeson, C., 2004. Functional Studies of the Mycobacterium tuberculosis Iron-dependent Regulator. Journal of Biological Chemistry 279, 53554–53561. https://doi.org/10.1074/jbc.M407385200

Chowanadisai, W., Graham, D.M., Keen, C.L., Rucker, R.B., Messerli, M.A., 2013. Neurulation and neurite extension require the zinc transporter ZIP12 (*slc39a12*). Proc. Natl. Acad. Sci. U.S.A. 110, 9903–9908. https://doi.org/10.1073/pnas.1222142110

Christenson, E.T., Isaac, D.T., Yoshida, K., Lipo, E., Kim, J.-S., Ghirlando, R., Isberg, R.R., Banerjee, A., 2019. The iron-regulated vacuolar *Legionella pneumophila* MavN protein is a transition-metal transporter. Proc. Natl. Acad. Sci. U.S.A. 116, 17775–17785. https://doi.org/10.1073/pnas.1902806116

Chun, H., Korolnek, T., Lee, C.-J., Coyne, H.J., Winge, D.R., Kim, B.-E., Petris, M.J., 2019. An extracellular histidine-containing motif in the zinc

transporter ZIP4 plays a role in zinc sensing and zinc-induced endocytosis in mammalian cells. J Biol Chem 294, 2815–2826. https://doi.org/10.1074/jbc.RA118.005203

Clark, M., Fisher, N.C., Kasthuri, R., Cerami Hand, C., 2013. Parasite maturation and host serum iron influence the labile iron pool of erythrocyte stage *Plasmodium falciparum*. Br J Haematol 161, 262–269. https://doi.org/10.1111/bjh.12234

Coleman, J.E., 1992. ZINC PROTEINS: Enzymes, Storage Proteins, Transcription Factors, and Replication Proteins. Annu. Rev. Biochem. 61, 897–946. https://doi.org/10.1146/annurev.bi.61.070192.004341

Connolly, E.L., Fett, J.P., Guerinot, M.L., 2002. Expression of the IRT1 Metal Transporter Is Controlled by Metals at the Levels of Transcript and Protein Accumulation. Plant Cell 14, 1347–1357. https://doi.org/10.1105/tpc.001263

Conte, S.S., Walker, E.L., 2011. Transporters Contributing to Iron Trafficking in Plants. Molecular Plant 4, 464–476. https://doi.org/10.1093/mp/ssr015

Contopoulos-Ioannidis, D.G., Gianniki, M., Ai-Nhi Truong, A., Montoya, J.G., 2022. Toxoplasmosis and Schizophrenia: A Systematic Review and Meta-Analysis of Prevalence and Associations and Future Directions. PRCP 4, 48–60. https://doi.org/10.1176/appi.prcp.20210041

Coppens, I., 2014. Exploitation of auxotrophies and metabolic defects in Toxoplasma as therapeutic approaches. International Journal for Parasitology 44, 109–120. https://doi.org/10.1016/j.ijpara.2013.09.003

Coppens, I., Dunn, J.D., Romano, J.D., Pypaert, M., Zhang, H., Boothroyd, J.C., Joiner, K.A., 2006. Toxoplasma gondii Sequesters Lysosomes from Mammalian Hosts in the Vacuolar Space. Cell 125, 261–274. https://doi.org/10.1016/j.cell.2006.01.056

Corezzi, S., Urbanelli, L., Cloetens, P., Emiliani, C., Helfen, L., Bohic, S., Elisei, F., Fioretto, D., 2009. Synchrotron-based X-ray fluorescence imaging of human cells labeled with CdSe quantum dots. Analytical Biochemistry 388, 33–39. https://doi.org/10.1016/j.ab.2009.01.044

Costello, L.C., Liu, Y., Zou, J., Franklin, R.B., 1999. Evidence for a Zinc Uptake Transporter in Human Prostate Cancer Cells Which Is Regulated by Prolactin and Testosterone. Journal of Biological Chemistry 274, 17499–17504. https://doi.org/10.1074/jbc.274.25.17499

Couturier, L., Luna, J., Mazouni, K., Mestdagh, C., Phan, M.-S., Corson, F., Schweisguth, F., 2022. HaloTag-based reporters for sparse labeling and cell tracking. Fly 16, 360–366. https://doi.org/10.1080/19336934.2022.2142460

Cowen, D., 1942. TOXOPLASMIC ENCEPHALOMYELITIS: VI. CLINICAL DIAGNOSIS OF INFANTILE OR CONGENITAL TOXOPLASMOSIS; SURVIVAL BEYOND INFANCY. Arch NeurPsych 48, 689. https://doi.org/10.1001/archneurpsyc.1942.02290110009001

Cowman, A.F., Crabb, B.S., 2006. Invasion of Red Blood Cells by Malaria Parasites. Cell 124, 755–766. https://doi.org/10.1016/j.cell.2006.02.006

Crawford, M.J., Thomsen-Zieger, N., Ray, M., Schachtner, J., Roos, D.S., Seeber, F., 2006. Toxoplasma gondii scavenges host-derived lipoic acid despite its de novo synthesis in the apicoplast. EMBO J 25, 3214–3222. https://doi.org/10.1038/sj.emboj.7601189

Czachorowski, M., Lam-Yuk-Tseung, S., Cellier, M., Gros, P., 2009. Transmembrane topology of the mammalian Slc11a2 iron transporter. Biochemistry 48, 8422–8434. https://doi.org/10.1021/bi900606y

Dai, Y., Zhu, C., Xiao, W., Huang, K., Wang, X., Shi, C., Lin, D., Zhang, H., Liu, X., Peng, B., Gao, Y., Liu, C.H., Ge, B., Kaufmann, S.H.E., Feng, C.G., Chen, X., Cai, Y., 2023. Mycobacterium tuberculosis hijacks host TRIM21- and NCOA4-dependent ferritinophagy to enhance intracellular growth. Journal of Clinical Investigation 133, e159941. https://doi.org/10.1172/JCI159941

Das, N.K., Biswas, S., Solanki, S., Mukhopadhyay, C.K., 2009. *Leishmania donovani* depletes labile iron pool to exploit iron uptake capacity of macrophage for its intracellular growth. Cellular Microbiology 11, 83–94. https://doi.org/10.1111/j.1462-5822.2008.01241.x

Das, N.K., Sandhya, S., G., V.V., Kumar, R., Singh, A.K., Bal, S.K., Kumari, S., Mukhopadhyay, C.K., 2018. *Leishmania donovani* inhibits ferroportin translation by modulating FBXL5-IRP2 axis for its growth within host macrophages. Cellular Microbiology 20, e12834. https://doi.org/10.1111/cmi.12834

Dautry-Varsat, A., 1986. Receptor-mediated endocytosis: The intracellular journey of transferrin and its receptor. Biochimie 68, 375–381. https://doi.org/10.1016/S0300-9084(86)80004-9

De Domenico, I., McVey Ward, D., Kaplan, J., 2008. Regulation of iron acquisition and storage: consequences for iron-linked disorders. Nat Rev Mol Cell Biol 9, 72–81. https://doi.org/10.1038/nrm2295

De Domenico, I., Ward, D.M., Di Patti, M.C.B., Jeong, S.Y., David, S., Musci, G., Kaplan, J., 2007. Ferroxidase activity is required for the stability of cell surface ferroportin in cells expressing GPI-ceruloplasmin. EMBO J 26, 2823–2831. https://doi.org/10.1038/sj.emboj.7601735

De Domenico, I., Ward, D.M., Kaplan, J., 2009. Specific iron chelators determine the route of ferritin degradation. Blood 114, 4546–4551. https://doi.org/10.1182/blood-2009-05-224188

de Jesus, J.R., Aragão, A.Z.B., Arruda, M.A.Z., Ramos, C.H.I., 2019. Optimization of a Methodology for Quantification and Removal of Zinc Gives Insights Into the Effect of This Metal on the Stability and Function of the Zinc-Binding Co-chaperone Ydj1. Front Chem 7, 416. https://doi.org/10.3389/fchem.2019.00416

De Koning, H.P., Al-Salabi, M.I., Cohen, A.M., Coombs, G.H., Wastling, J.M., 2003. Identification and characterisation of high affinity nucleoside and nucleobase transporters in Toxoplasma gondii. International Journal for Parasitology 33, 821–831. https://doi.org/10.1016/S0020-7519(03)00091-2

De Moura, L., Bahia-Oliveira, L.M.G., Wada, M.Y., Jones, J.L., Tuboi, S.H., Carmo, E.H., Ramalho, W.M., Camargo, N.J., Trevisan, R., Graça, R.M.T., Da Silva, A.J., Moura, I., Dubey, J.P., Garrett, D.O., 2006. Waterborne Toxoplasmosis, Brazil, from Field to Gene. Emerg. Infect. Dis. 12, 326–329. https://doi.org/10.3201/eid1202.041115

De Souza Giassi, K., Costa, A.N., Apanavicius, A., Teixeira, F.B., Fernandes, C.J.C., Helito, A.S., Kairalla, R.A., 2014. Tomographic findings of acute pulmonary toxoplasmosis in immunocompetent patients. BMC Pulm Med 14, 185. https://doi.org/10.1186/1471-2466-14-185

Deffieu, M.S., Alayi, T.D., Slomianny, C., Tomavo, S., 2019. The *Toxoplasma gondii* dense granule protein TgGRA3 interacts with host Golgi and

dysregulates anterograde transport. Biology Open bio.039818. https://doi.org/10.1242/bio.039818

Del Campo, J., Heger, T.J., Rodríguez-Martínez, R., Worden, A.Z., Richards, T.A., Massana, R., Keeling, P.J., 2019. Assessing the Diversity and Distribution of Apicomplexans in Host and Free-Living Environments Using High-Throughput Amplicon Data and a Phylogenetically Informed Reference Framework. Front. Microbiol. 10, 2373. https://doi.org/10.3389/fmicb.2019.02373

de-la-Torre, A., Sauer, A., Pfaff, A.W., Bourcier, T., Brunet, J., Speeg-Schatz, C., Ballonzoli, L., Villard, O., Ajzenberg, D., Sundar, N., Grigg, M.E., Gomez-Marin, J.E., Candolfi, E., 2013. Severe South American Ocular Toxoplasmosis Is Associated with Decreased Ifn-γ/Il-17a and Increased Il-6/Il-13 Intraocular Levels. PLoS Negl Trop Dis 7, e2541. https://doi.org/10.1371/journal.pntd.0002541

Desmonts, G., Couvreur, J., 1974. Congenital Toxoplasmosis: A Prospective Study of 378 Pregnancies. N Engl J Med 290, 1110–1116. https://doi.org/10.1056/NEJM197405162902003

Di Cristina, M., Carruthers, V.B., 2018. New and emerging uses of CRISPR/Cas9 to genetically manipulate apicomplexan parasites. Parasitology 145, 1119–1126. https://doi.org/10.1017/S003118201800001X

Dick, C.F., Rocco-Machado, N., Dos-Santos, A.L.A., Carvalho-Kelly, L.F., Alcantara, C.L., Cunha-E-Silva, N.L., Meyer-Fernandes, J.R., Vieyra, A., 2022. An Iron Transporter Is Involved in Iron Homeostasis, Energy Metabolism, Oxidative Stress, and Metacyclogenesis in Trypanosoma cruzi. Front. Cell. Infect. Microbiol. 11, 789401. https://doi.org/10.3389/fcimb.2021.789401

Dighal, A., Mukhopadhyay, D., Sengupta, R., Moulik, S., Mukherjee, S., Roy, S., Chaudhuri, S.J., Das, N.K., Chatterjee, M., 2020. Iron trafficking in patients with Indian Post kala-azar dermal leishmaniasis. PLoS Negl Trop Dis 14, e0007991. https://doi.org/10.1371/journal.pntd.0007991

Dimier, Bout, 1998. Interferon-γ-activated primary enterocytes inhibit *Toxoplasma gondii* replication: a role for intracellular iron. Immunology 94, 488–495. https://doi.org/10.1046/j.1365-2567.1998.00553.x

Dixon, S.J., Stockwell, B.R., 2014. The role of iron and reactive oxygen species in cell death. Nat Chem Biol 10, 9–17. https://doi.org/10.1038/nchembio.1416

Donald, R.G., Roos, D.S., 1995. Insertional mutagenesis and marker rescue in a protozoan parasite: cloning of the uracil phosphoribosyltransferase locus from Toxoplasma gondii. Proc. Natl. Acad. Sci. U.S.A. 92, 5749–5753. https://doi.org/10.1073/pnas.92.12.5749

Donald, R.G., Roos, D.S., 1993. Stable molecular transformation of Toxoplasma gondii: a selectable dihydrofolate reductase-thymidylate synthase marker based on drug-resistance mutations in malaria. Proc. Natl. Acad. Sci. U.S.A. 90, 11703–11707. https://doi.org/10.1073/pnas.90.24.11703

Donald, R.G.K., Carter, D., Ullman, B., Roos, D.S., 1996. Insertional Tagging, Cloning, and Expression of the Hypoxanthine-Xanthine-Guanine Phosphoribosyltransferase Gene. Journal of Biological Chemistry 271, 14010–14019. https://doi.org/10.1074/jbc.271.24.14010

Dong, X.-P., Cheng, X., Mills, E., Delling, M., Wang, F., Kurz, T., Xu, H., 2008. The type IV mucolipidosis-associated protein TRPML1 is an endolysosomal

iron release channel. Nature 455, 992–996. https://doi.org/10.1038/nature07311

Donovan, A., Lima, C.A., Pinkus, J.L., Pinkus, G.S., Zon, L.I., Robine, S., Andrews, N.C., 2005. The iron exporter ferroportin/Slc40a1 is essential for iron homeostasis. Cell Metabolism 1, 191–200. https://doi.org/10.1016/j.cmet.2005.01.003

Dou, Z., McGovern, O.L., Di Cristina, M., Carruthers, V.B., 2014. Toxoplasma gondii Ingests and Digests Host Cytosolic Proteins. mBio 5, e01188-14. https://doi.org/10.1128/mBio.01188-14

Dubeaux, G., Neveu, J., Zelazny, E., Vert, G., 2018. Metal Sensing by the IRT1 Transporter-Receptor Orchestrates Its Own Degradation and Plant Metal Nutrition. Molecular Cell 69, 953-964.e5. https://doi.org/10.1016/j.molcel.2018.02.009

Dubey, J.P., 2020. The history and life cycle of Toxoplasma gondii, in: Toxoplasma Gondii. Elsevier, pp. 1–19. https://doi.org/10.1016/B978-0-12-815041-2.00001-3

Dubey, J.P., 2010. Toxoplasmosis of animals and humans, 2. ed. ed. CRC, Taylor & Francis, Boca Raton.

Dubey, J.P., 2009. History of the discovery of the life cycle of Toxoplasma gondii. International Journal for Parasitology 39, 877–882. https://doi.org/10.1016/j.ijpara.2009.01.005

Dubey, J.P., Frenkel, J.K., 1976. Feline Toxoplasmosis from Acutely Infected Mice and the Development of *Toxoplasma* Cysts*. The Journal of Protozoology 23, 537–546. https://doi.org/10.1111/j.1550-7408.1976.tb03836.x

Dubey, J.P., Lindsay, D.S., Speer, C.A., 1998. Structures of Toxoplasma gondii tachyzoites, bradyzoites, and sporozoites and biology and development of tissue cysts. Clin Microbiol Rev 11, 267–299. https://doi.org/10.1128/CMR.11.2.267

Dubey, J.P., Miller, N.L., Frenkel, J.K., 1970. THE TOXOPLASMA GONDII OOCYST FROM CAT FECES. The Journal of Experimental Medicine 132, 636–662. https://doi.org/10.1084/jem.132.4.636

Dubey, J.P., Pena, H.F.J., Cerqueira-Cézar, C.K., Murata, F.H.A., Kwok, O.C.H., Yang, Y.R., Gennari, S.M., Su, C., 2020. Epidemiologic significance of *Toxoplasma gondii* infections in chickens (*Gallus domesticus*): the past decade. Parasitology 147, 1263–1289. https://doi.org/10.1017/S0031182020001134

Dufner-Beattie, J., Langmade, S.J., Wang, F., Eide, D., Andrews, G.K., 2003a. Structure, Function, and Regulation of a Subfamily of Mouse Zinc Transporter Genes. Journal of Biological Chemistry 278, 50142–50150. https://doi.org/10.1074/jbc.M304163200

Dufner-Beattie, J., Wang, F., Kuo, Y.-M., Gitschier, J., Eide, D., Andrews, G.K., 2003b. The Acrodermatitis Enteropathica Gene ZIP4 Encodes a Tissue-specific, Zinc-regulated Zinc Transporter in Mice. Journal of Biological Chemistry 278, 33474–33481. https://doi.org/10.1074/jbc.M305000200

Dunay, I.R., Gajurel, K., Dhakal, R., Liesenfeld, O., Montoya, J.G., 2018. Treatment of Toxoplasmosis: Historical Perspective, Animal Models, and Current Clinical Practice. Clin Microbiol Rev 31, e00057-17. https://doi.org/10.1128/CMR.00057-17

Dunn, D., Wallon, M., Peyron, F., Petersen, E., Peckham, C., Gilbert, R., 1999. Mother-to-child transmission of toxoplasmosis: risk estimates for clinical

counselling. The Lancet 353, 1829–1833. https://doi.org/10.1016/S0140-6736(98)08220-8

Durham, A.C.H., 1983. A survey of readily available chelators for buffering calcium ion concentrations in physiological solutions. Cell Calcium 4, 33–46. https://doi.org/10.1016/0143-4160(83)90047-7

Dziadek, B., Dzitko, K., Dlugonska, H., 2005. Toxoplasma gondii binds human lactoferrin but not transferrin. Experimental Parasitology 110, 165–167. https://doi.org/10.1016/j.exppara.2005.03.019

Eide, D., Broderius, M., Fett, J., Guerinot, M.L., 1996. A novel iron-regulated metal transporter from plants identified by functional expression in yeast. Proc Natl Acad Sci U S A 93, 5624–5628. https://doi.org/10.1073/pnas.93.11.5624

Eide, D.J., 2020. Transcription factors and transporters in zinc homeostasis: lessons learned from fungi. Critical Reviews in Biochemistry and Molecular Biology 55, 88–110. https://doi.org/10.1080/10409238.2020.1742092

Eide, D.J., 2006. Zinc transporters and the cellular trafficking of zinc. Biochimica et Biophysica Acta (BBA) - Molecular Cell Research 1763, 711–722. https://doi.org/10.1016/j.bbamcr.2006.03.005

Eide, D.J., 2004. The SLC39 family of metal ion transporters. Pfl□gers Archiv European Journal of Physiology 447, 796–800. https://doi.org/10.1007/s00424-003-1074-3

Eisenstein, R.S., Blemings, K.P., 1998. Iron Regulatory Proteins, Iron Responsive Elements and Iron Homeostasis. The Journal of Nutrition 128, 2295–2298. https://doi.org/10.1093/jn/128.12.2295

Elati, H.A.A., Goerner, A.L., Martorelli Di Genova, B., Sheiner, L., De Koning, H.P., 2023. Pyrimidine salvage in Toxoplasma gondii as a target for new treatment. Front. Cell. Infect. Microbiol. 13, 1320160. https://doi.org/10.3389/fcimb.2023.1320160

Epelman, S., Lavine, K.J., Randolph, G.J., 2014. Origin and Functions of Tissue Macrophages. Immunity 41, 21–35. https://doi.org/10.1016/j.immuni.2014.06.013

Erlitzki, R., Long, J.C., Theil, E.C., 2002. Multiple, Conserved Iron-responsive Elements in the 3′-Untranslated Region of Transferrin Receptor mRNA Enhance Binding of Iron Regulatory Protein 2. Journal of Biological Chemistry 277, 42579–42587. https://doi.org/10.1074/jbc.M207918200

Etheridge, R.D., Alaganan, A., Tang, K., Lou, H.J., Turk, B.E., Sibley, L.D., 2014. The Toxoplasma Pseudokinase ROP5 Forms Complexes with ROP18 and ROP17 Kinases that Synergize to Control Acute Virulence in Mice. Cell Host & Microbe 15, 537–550. https://doi.org/10.1016/j.chom.2014.04.002

Fairweather, S.J., Rajendran, E., Blume, M., Javed, K., Steinhöfel, B., McConville, M.J., Kirk, K., Bröer, S., Van Dooren, G.G., 2021. Coordinated action of multiple transporters in the acquisition of essential cationic amino acids by the intracellular parasite Toxoplasma gondii. PLoS Pathog 17, e1009835. https://doi.org/10.1371/journal.ppat.1009835

Fan, B., Qin, B., Li, M., Zhu, Y., Fan, F., Xu, H., Xue, L., Chen, Y., Pan, M., Shen, B., 2025. The critical role of Toxoplasma gondii GRA1 in nutrient salvage. mBio 16, e0124225. https://doi.org/10.1128/mbio.01242-25

Fentress, S.J., Behnke, M.S., Dunay, I.R., Mashayekhi, M., Rommereim, L.M., Fox, B.A., Bzik, D.J., Taylor, G.A., Turk, B.E., Lichti, C.F., Townsend, R.R., Qiu, W., Hui, R., Beatty, W.L., Sibley, L.D., 2010. Phosphorylation of Immunity-Related GTPases by a Toxoplasma gondii-Secreted Kinase Promotes

Macrophage Survival and Virulence. Cell Host & Microbe 8, 484–495. https://doi.org/10.1016/j.chom.2010.11.005

Ferguson, D.J.P., 2009. Toxoplasma gondii: 1908-2008, homage to Nicolle, Manceaux and Splendore. Mem. Inst. Oswaldo Cruz 104, 133–148. https://doi.org/10.1590/S0074-02762009000200003

Ferguson, D.J.P., Hutchison, W.M., Siim, J.Chr., 1975. THE ULTRASTRUCTURAL DEVELOPMENT OF THE MACROGAMETE AND FORMATION OF THE OOCYST WALL OF *TOXOPLASMA GONDII*. Acta Pathologica Microbiologica Scandinavica Section B Microbiology 83B, 491–505. https://doi.org/10.1111/j.1699-0463.1975.tb00130.x

Fernández, B., Olmedo, P., Gil, F., Fdez, E., Naaldijk, Y., Rivero-Ríos, P., Bracher, F., Grimm, C., Churchill, G.C., Hilfiker, S., 2022. Iron-induced cytotoxicity mediated by endolysosomal TRPML1 channels is reverted by TFEB. Cell Death Dis 13, 1047. https://doi.org/10.1038/s41419-022-05504-2

Fernández-Escobar, M., Schares, G., Maksimov, P., Joeres, M., Ortega-Mora, L.M., Calero-Bernal, R., 2022. Toxoplasma gondii Genotyping: A Closer Look Into Europe. Front Cell Infect Microbiol 12, 842595. https://doi.org/10.3389/fcimb.2022.842595

Fernández-Martín, K.G., Alvarez-Sánchez, M.E., Arana-Argáez, V.E., Alvarez-Sánchez, L.C., Lara-Riegos, J.C., Torres-Romero, J.C., 2017. Genome-wide identification, in silico characterization and expression analysis of ZIP-like genes from Trichomonas vaginalis in response to Zinc and Iron. Biometals 30, 663–675. https://doi.org/10.1007/s10534-017-0034-x

Ferreira, I.M.R., Vidal, J.E., De Mattos, C.D.C.B., De Mattos, L.C., Qu, D., Su, C., Pereira-Chioccola, V.L., 2011. Toxoplasma gondii isolates: Multilocus RFLP-PCR genotyping from human patients in Sao Paulo State, Brazil identified distinct genotypes. Experimental Parasitology 129, 190–195. https://doi.org/10.1016/j.exppara.2011.06.002

Ferrer, P., Tripathi, A.K., Clark, M.A., Hand, C.C., Rienhoff, H.Y., Sullivan, D.J., 2012. Antimalarial Iron Chelator, FBS0701, Shows Asexual and Gametocyte Plasmodium falciparum Activity and Single Oral Dose Cure in a Murine Malaria Model. PLoS ONE 7, e37171. https://doi.org/10.1371/journal.pone.0037171

Fichera, M.E., Roos, D.S., 1997. A plastid organelle as a drug target in apicomplexan parasites. Nature 390, 407–409. https://doi.org/10.1038/37132

Fillebeen, C., Charlebois, E., Wagner, J., Katsarou, A., Mui, J., Vali, H., Garcia-Santos, D., Ponka, P., Presley, J., Pantopoulos, K., 2019. Transferrin receptor 1 controls systemic iron homeostasis by fine-tuning hepcidin expression to hepatocellular iron load. Blood 133, 344–355. https://doi.org/10.1182/blood-2018-05-850404

Flannery, A.R., Huynh, C., Mittra, B., Mortara, R.A., Andrews, N.W., 2011. LFR1 Ferric Iron Reductase of Leishmania amazonensis Is Essential for the Generation of Infective Parasite Forms. Journal of Biological Chemistry 286, 23266–23279. https://doi.org/10.1074/jbc.M111.229674

Flegr, J., Prandota, J., Sovičková, M., Israili, Z.H., 2014. Toxoplasmosis – A Global Threat. Correlation of Latent Toxoplasmosis with Specific Disease Burden in a Set of 88 Countries. PLoS ONE 9, e90203. https://doi.org/10.1371/journal.pone.0090203

Fleming, R.E., Migas, M.C., Zhou, X., Jiang, J., Britton, R.S., Brunt, E.M., Tomatsu, S., Waheed, A., Bacon, B.R., Sly, W.S., 1999. Mechanism of

increased iron absorption in murine model of hereditary hemochromatosis: Increased duodenal expression of the iron transporter DMT1. Proc. Natl. Acad. Sci. U.S.A. 96, 3143–3148. https://doi.org/10.1073/pnas.96.6.3143

Fortier, A.H., Leiby, D.A., Narayanan, R.B., Asafoadjei, E., Crawford, R.M., Nacy, C.A., Meltzer, M.S., 1995. Growth of Francisella tularensis LVS in macrophages: the acidic intracellular compartment provides essential iron required for growth. Infect Immun 63, 1478–1483. https://doi.org/10.1128/iai.63.4.1478-1483.1995

Fox, B.A., Falla, A., Rommereim, L.M., Tomita, T., Gigley, J.P., Mercier, C., Cesbron-Delauw, M.-F., Weiss, L.M., Bzik, D.J., 2011. Type II Toxoplasma gondii *KU80* Knockout Strains Enable Functional Analysis of Genes Required for Cyst Development and Latent Infection. Eukaryot Cell 10, 1193–1206. https://doi.org/10.1128/EC.00297-10

Fox, B.A., Gigley, J.P., Bzik, D.J., 2004. Toxoplasma gondii lacks the enzymes required for de novo arginine biosynthesis and arginine starvation triggers cyst formation. International Journal for Parasitology 34, 323–331. https://doi.org/10.1016/j.ijpara.2003.12.001

Fox, B.A., Ristuccia, J.G., Gigley, J.P., Bzik, D.J., 2009. Efficient Gene Replacements in *Toxoplasma gondii* Strains Deficient for Nonhomologous End Joining. Eukaryot Cell 8, 520–529. https://doi.org/10.1128/EC.00357-08

Franceschelli, A., Bonadonna, L., Cacciò, S.M., Sannella, A.R., Cintori, C., Gargiulo, R., Coccia, A.M., Paradiso, R., Iaconelli, M., Briancesco, R., Tripodi, A., 2022. An outbreak of cryptosporidiosis associated with drinking water in north-eastern Italy, August 2019: microbiological and environmental investigations. Euro Surveill 27, 2200038. https://doi.org/10.2807/1560-7917.ES.2022.27.35.2200038

Franco, M., Panas, M.W., Marino, N.D., Lee, M.-C.W., Buchholz, K.R., Kelly, F.D., Bednarski, J.J., Sleckman, B.P., Pourmand, N., Boothroyd, J.C., 2016. A Novel Secreted Protein, MYR1, Is Central to *Toxoplasma* 's Manipulation of Host Cells. mBio 7, e02231-15. https://doi.org/10.1128/mBio.02231-15

Franklin, R.B., Ma, J., Zou, J., Guan, Z., Kukoyi, B.I., Feng, P., Costello, L.C., 2003. Human ZIP1 is a major zinc uptake transporter for the accumulation of zinc in prostate cells. J Inorg Biochem 96, 435–442. https://doi.org/10.1016/s0162-0134(03)00249-6

Franz, M.C., Pujol-Giménez, J., Montalbetti, N., Fernandez-Tenorio, M., DeGrado, T.R., Niggli, E., Romero, M.F., Hediger, M.A., 2018. Reassessment of the Transport Mechanism of the Human Zinc Transporter SLC39A2. Biochemistry 57, 3976–3986. https://doi.org/10.1021/acs.biochem.8b00511

Frénal, K., Polonais, V., Marq, J.-B., Stratmann, R., Limenitakis, J., Soldati-Favre, D., 2010. Functional Dissection of the Apicomplexan Glideosome Molecular Architecture. Cell Host & Microbe 8, 343–357. https://doi.org/10.1016/j.chom.2010.09.002

Frenkel, J.K., Dubey, J.P., Miller, N.L., 1970. *Toxoplasma gondii* in Cats: Fecal Stages Identified as Coccidian Oocysts. Science 167, 893–896. https://doi.org/10.1126/science.167.3919.893

Frenkel, J.K., Ruiz, A., Chinchilla, M., 1975. Soil Survival of Toxoplasma Oocysts in Kansas and Costa Rica. The American Journal of Tropical Medicine and Hygiene 24, 439–443. https://doi.org/10.4269/ajtmh.1975.24.439

Frenkel, J.K., Smith, D.D., 2003. Determination of the genera of cyst-forming coccidia. Parasitology Research 91, 384–389. https://doi.org/10.1007/s00436-003-0969-4

Frey, P.A., Reed, G.H., 2012. The Ubiquity of Iron. ACS Chem. Biol. 7, 1477–1481. https://doi.org/10.1021/cb300323q

Fuentes, I., Rubio, J.M., Ramírez, C., Alvar, J., 2001. Genotypic Characterization of *Toxoplasma gondii* Strains Associated with Human Toxoplasmosis in Spain: Direct Analysis from Clinical Samples. J Clin Microbiol 39, 1566–1570. https://doi.org/10.1128/JCM.39.4.1566-1570.2001

Fujishiro, H., Miyamoto, S., Sumi, D., Kambe, T., Himeno, S., 2022. Effects of individual amino acid mutations of zinc transporter ZIP8 on manganese- and cadmium-transporting activity. Biochemical and Biophysical Research Communications 616, 26–32. https://doi.org/10.1016/j.bbrc.2022.05.068

Fukada, T., Asada, Y., Mishima, K., Shimoda, S., Saito, I., 2011. Slc39a13/Zip13: A Crucial Zinc Transporter Involved in Tooth Development and Inherited Disorders. Journal of Oral Biosciences 53, 1–12. https://doi.org/10.1016/S1349-0079(11)80030-7

Fukada, T., Kambe, T., 2011. Molecular and genetic features of zinc transporters in physiology and pathogenesis. Metallomics 3, 662. https://doi.org/10.1039/c1mt00011j

Gail, M., Gross, U., Bohne, W., 2004. Transferrin receptor induction in Toxoplasma gondii-infected HFF is associated with increased iron-responsive protein 1 activity and is mediated by secreted factors. Parasitol Res 94, 233–239. https://doi.org/10.1007/s00436-004-1209-2

Gail, M., Gross, U., Bohne, W., 2001. Transcriptional profile of Toxoplasma gondii-infected human fibroblasts as revealed by gene-array hybridization. Mol Gen Genomics 265, 905–912. https://doi.org/10.1007/s004380100487

Gaither, L.A., Eide, D.J., 2001a. Eukaryotic zinc transporters and their regulation. Biometals 14, 251–270. https://doi.org/10.1023/A:1012988914300

Gaither, L.A., Eide, D.J., 2001b. The Human ZIP1 Transporter Mediates Zinc Uptake in Human K562 Erythroleukemia Cells. Journal of Biological Chemistry 276, 22258–22264. https://doi.org/10.1074/jbc.M101772200

Gaither, L.A., Eide, D.J., 2000. Functional Expression of the Human hZIP2 Zinc Transporter. Journal of Biological Chemistry 275, 5560–5564. https://doi.org/10.1074/jbc.275.8.5560

Gajria, B., Bahl, A., Brestelli, J., Dommer, J., Fischer, S., Gao, X., Heiges, M., Iodice, J., Kissinger, J.C., Mackey, A.J., Pinney, D.F., Roos, D.S., Stoeckert, C.J., Wang, H., Brunk, B.P., 2007. ToxoDB: an integrated Toxoplasma gondii database resource. Nucleic Acids Research 36, D553–D556. https://doi.org/10.1093/nar/gkm981

Galaris, D., Barbouti, A., Pantopoulos, K., 2019. Iron homeostasis and oxidative stress: An intimate relationship. Biochimica et Biophysica Acta (BBA) - Molecular Cell Research 1866, 118535. https://doi.org/10.1016/j.bbamcr.2019.118535

Ganz, T., 2013. Systemic Iron Homeostasis. Physiological Reviews 93, 1721–1741. https://doi.org/10.1152/physrev.00008.2013

Ganz, T., 2009. Iron in innate immunity: starve the invaders. Current Opinion in Immunology 21, 63–67. https://doi.org/10.1016/j.coi.2009.01.011

Ganz, T., Nemeth, E., 2015. Iron homeostasis in host defence and inflammation. Nat Rev Immunol 15, 500–510. https://doi.org/10.1038/nri3863

Gao, F., Dubos, C., 2021. Transcriptional integration of plant responses to iron availability. Journal of Experimental Botany 72, 2056–2070. https://doi.org/10.1093/jxb/eraa556

Gardner, M.J., Hall, N., Fung, E., White, O., Berriman, M., Hyman, R.W., Carlton, J.M., Pain, A., Nelson, K.E., Bowman, S., Paulsen, I.T., James, K., Eisen, J.A., Rutherford, K., Salzberg, S.L., Craig, A., Kyes, S., Chan, M.-S., Nene, V., Shallom, S.J., Suh, B., Peterson, J., Angiuoli, S., Pertea, M., Allen, J., Selengut, J., Haft, D., Mather, M.W., Vaidya, A.B., Martin, D.M.A., Fairlamb, A.H., Fraunholz, M.J., Roos, D.S., Ralph, S.A., McFadden, G.I., Cummings, L.M., Subramanian, G.M., Mungall, C., Venter, J.C., Carucci, D.J., Hoffman, S.L., Newbold, C., Davis, R.W., Fraser, C.M., Barrell, B., 2002. Genome sequence of the human malaria parasite Plasmodium falciparum. Nature 419, 498–511. https://doi.org/10.1038/nature01097

Garza, K.R., Clarke, S.L., Ho, Y.-H., Bruss, M.D., Vasanthakumar, A., Anderson, S.A., Eisenstein, R.S., 2020. Differential translational control of 5′ IRE-containing mRNA in response to dietary iron deficiency and acute iron overload. Metallomics 12, 2186–2198. https://doi.org/10.1039/D0MT00192A

Gasiunas, G., Barrangou, R., Horvath, P., Siksnys, V., 2012. Cas9–crRNA ribonucleoprotein complex mediates specific DNA cleavage for adaptive immunity in bacteria. Proc. Natl. Acad. Sci. U.S.A. 109. https://doi.org/10.1073/pnas.1208507109

Gastens, M.H., Fischer, H.-G., 2002. Toxoplasma gondii eukaryotic translation initiation factor 4A associated with tachyzoite virulence is down-regulated in the bradyzoite stage. International Journal for Parasitology 32, 1225–1234. https://doi.org/10.1016/S0020-7519(02)00096-6

Gazanion, E., Vergnes, B., 2018. Protozoan Parasite Auxotrophies and Metabolic Dependencies, in: Silvestre, R., Torrado, E. (Eds.), Metabolic Interaction in Infection, Experientia Supplementum. Springer International Publishing, Cham, pp. 351–375. https://doi.org/10.1007/978-3-319-74932-7_9

Gerner, R.R., Nuccio, S.-P., Raffatellu, M., 2020. Iron at the host-microbe interface. Molecular Aspects of Medicine 75, 100895. https://doi.org/10.1016/j.mam.2020.100895

Ghosh, S., Chandra, N., Vishveshwara, S., 2015. Mechanism of Iron-Dependent Repressor (IdeR) Activation and DNA Binding: A Molecular Dynamics and Protein Structure Network Study. PLoS Comput Biol 11, e1004500. https://doi.org/10.1371/journal.pcbi.1004500

Gietz, R.D., Schiestl, R.H., 2007. High-efficiency yeast transformation using the LiAc/SS carrier DNA/PEG method. Nat Protoc 2, 31–34. https://doi.org/10.1038/nprot.2007.13

Gilbert, R.E., Freeman, K., Lago, E.G., Bahia-Oliveira, L.M.G., Tan, H.K., Wallon, M., Buffolano, W., Stanford, M.R., Petersen, E., for The European Multicentre Study on Congenital Toxoplasmosis (EMSCOT), 2008. Ocular Sequelae of Congenital Toxoplasmosis in Brazil Compared with Europe. PLoS Negl Trop Dis 2, e277. https://doi.org/10.1371/journal.pntd.0000277

Giles, J.R., Peterson, A.T., Busch, J.D., Olafson, P.U., Scoles, G.A., Davey, R.B., Pound, J.M., Kammlah, D.M., Lohmeyer, K.H., Wagner, D.M., 2014. Invasive potential of cattle fever ticks in the southern United States. Parasites Vectors 7, 189. https://doi.org/10.1186/1756-3305-7-189

Girijashanker, K., He, L., Soleimani, M., Reed, J.M., Li, H., Liu, Z., Wang, B., Dalton, T.P., Nebert, D.W., 2008. Slc39a14 Gene Encodes ZIP14, A

Metal/Bicarbonate Symporter: Similarities to the ZIP8 Transporter. Molecular Pharmacology 73, 1413–1423. https://doi.org/10.1124/mol.107.043588

Gissot, M., Hovasse, A., Chaloin, L., Schaeffer-Reiss, C., Van Dorsselaer, A., Tomavo, S., 2017. An evolutionary conserved zinc finger protein is involved in *Toxoplasma gondii* mRNA nuclear export: A zinc finger protein is involved in mRNA nuclear export. Cellular Microbiology 19, e12644. https://doi.org/10.1111/cmi.12644

Glasner, P.D., Silveira, C., Kruszon-Moran, D., Martins, M.C., Burnier, M., Silveira, S., Camargo, M.E., Nussenblatt, R.B., Kaslow, R.A., Belfort, R., 1992. An Unusually High Prevalence of Ocular Toxoplasmosis in Southern Brazil. American Journal of Ophthalmology 114, 136–144. https://doi.org/10.1016/S0002-9394(14)73976-5

Glickstein, H., Ben El, R., Shvartsman, M., Cabantchik, Z.I., 2005. Intracellular labile iron pools as direct targets of iron chelators: a fluorescence study of chelator action in living cells. Blood 106, 3242–3250. https://doi.org/10.1182/blood-2005-02-0460

Gold, D.A., Kaplan, A.D., Lis, A., Bett, G.C.L., Rosowski, E.E., Cirelli, K.M., Bougdour, A., Sidik, S.M., Beck, J.R., Lourido, S., Egea, P.F., Bradley, P.J., Hakimi, M.-A., Rasmusson, R.L., Saeij, J.P.J., 2015. The Toxoplasma Dense Granule Proteins GRA17 and GRA23 Mediate the Movement of Small Molecules between the Host and the Parasitophorous Vacuole. Cell Host & Microbe 17, 642–652. https://doi.org/10.1016/j.chom.2015.04.003

Gopalakrishnan, A.M., Aly, A.S.I., Aravind, L., Kumar, N., 2017. Multifunctional Involvement of a C2H2 Zinc Finger Protein (PbZfp) in Malaria Transmission, Histone Modification, and Susceptibility to DNA Damage Response. mBio 8, e01298-17. https://doi.org/10.1128/mBio.01298-17

Goswitz, V.C., Brooker, R.J., 1995. Structural features of the uniporter/symporter/antiporter superfamily. Protein Sci 4, 534–537. https://doi.org/10.1002/pro.5560040319

Goto, Y., Ito, T., Ghosh, S., Mukherjee, B., 2024. Access and utilization of host-derived iron by *Leishmania* parasites. The Journal of Biochemistry 175, 17–24. https://doi.org/10.1093/jb/mvad082

Graf, E., Mahoney, J.R., Bryant, R.G., Eaton, J.W., 1984. Iron-catalyzed hydroxyl radical formation. Stringent requirement for free iron coordination site. J Biol Chem 259, 3620–3624.

Grander, M., Hoffmann, A., Seifert, M., Demetz, E., Grubwieser, P., Pfeifhofer-Obermair, C., Haschka, D., Weiss, G., 2022. DMT1 Protects Macrophages from Salmonella Infection by Controlling Cellular Iron Turnover and Lipocalin 2 Expression. Int J Mol Sci 23, 6789. https://doi.org/10.3390/ijms23126789

Grass, G., Franke, S., Taudte, N., Nies, D.H., Kucharski, L.M., Maguire, M.E., Rensing, C., 2005. The metal permease ZupT from Escherichia coli is a transporter with a broad substrate spectrum. J Bacteriol 187, 1604–1611. https://doi.org/10.1128/JB.187.5.1604-1611.2005

Grass, G., Wong, M.D., Rosen, B.P., Smith, R.L., Rensing, C., 2002. ZupT Is a Zn(II) Uptake System in *Escherichia coli*. J Bacteriol 184, 864–866. https://doi.org/10.1128/JB.184.3.864-866.2002

Gray, M.W., 2012. Mitochondrial Evolution. Cold Spring Harbor Perspectives in Biology 4, a011403–a011403. https://doi.org/10.1101/cshperspect.a011403

Grigg, M.E., Boothroyd, J.C., 2001. Rapid Identification of Virulent Type I Strains of the Protozoan Pathogen *Toxoplasma gondii* by PCR-Restriction Fragment Length Polymorphism Analysis at the *B1* Gene. J Clin Microbiol 39, 398–400. https://doi.org/10.1128/JCM.39.1.398-400.2001

Grotz, N., Fox, T., Connolly, E., Park, W., Guerinot, M.L., Eide, D., 1998. Identification of a family of zinc transporter genes from *Arabidopsis* that respond to zinc deficiency. Proc. Natl. Acad. Sci. U.S.A. 95, 7220–7224. https://doi.org/10.1073/pnas.95.12.7220

Grubwieser, P., Hilbe, R., Gehrer, C.M., Grander, M., Brigo, N., Hoffmann, A., Seifert, M., Berger, S., Theurl, I., Nairz, M., Weiss, G., 2023. Klebsiella pneumoniae manipulates human macrophages to acquire iron. Front. Microbiol. 14, 1223113. https://doi.org/10.3389/fmicb.2023.1223113

Gruenheid, S., Canonne-Hergaux, F., Gauthier, S., Hackam, D.J., Grinstein, S., Gros, P., 1999. The Iron Transport Protein NRAMP2 Is an Integral Membrane Glycoprotein That Colocalizes with Transferrin in Recycling Endosomes. The Journal of Experimental Medicine 189, 831–841. https://doi.org/10.1084/jem.189.5.831

Gruenheid, S., Cellier, M., Vidal, S., Gros, P., 1995. Identification and characterization of a second mouse Nramp gene. Genomics 25, 514–525. https://doi.org/10.1016/0888-7543(95)80053-O

Guan, F., Wang, R., Yi, Z., Luo, P., Liu, W., Xie, Y., Liu, Z., Xia, Z., Zhang, H., Cheng, Q., 2025. Tissue macrophages: origin, heterogenity, biological functions, diseases and therapeutic targets. Sig Transduct Target Ther 10, 93. https://doi.org/10.1038/s41392-025-02124-y

Guerinot, M.L., 2000. The ZIP family of metal transporters. Biochimica et Biophysica Acta (BBA) - Biomembranes 1465, 190–198. https://doi.org/10.1016/S0005-2736(00)00138-3

Gunshin, H., Allerson, C.R., Polycarpou-Schwarz, M., Rofts, A., Rogers, J.T., Kishi, F., Hentze, M.W., Rouault, T.A., Andrews, N.C., Hediger, M.A., 2001. Iron-dependent regulation of the divalent metal ion transporter. FEBS Lett 509, 309–316. https://doi.org/10.1016/s0014-5793(01)03189-1

Gunshin, H., Mackenzie, B., Berger, U.V., Gunshin, Y., Romero, M.F., Boron, W.F., Nussberger, S., Gollan, J.L., Hediger, M.A., 1997. Cloning and characterization of a mammalian proton-coupled metal-ion transporter. Nature 388, 482–488. https://doi.org/10.1038/41343

Gustafsson, C., Govindarajan, S., Minshull, J., 2004. Codon bias and heterologous protein expression. Trends in Biotechnology 22, 346–353. https://doi.org/10.1016/j.tibtech.2004.04.006

Gutiérrez-Expósito, D., Tejerina, F., Gutiérrez, J., Fernández-Escobar, M., Ortega-Mora, L.M., Mantecón, A.R., Dagleish, M.P., Pérez, V., Benavides, J., 2021. Direct economic losses of Toxoplasma gondii abortion outbreaks in two Spanish sheep flocks. Veterinary Parasitology: Regional Studies and Reports 26, 100623. https://doi.org/10.1016/j.vprsr.2021.100623

Gyimesi, G., Albano, G., Fuster, D.G., Hediger, M.A., Pujol-Giménez, J., 2019. Unraveling the structural elements of pH sensitivity and substrate binding in the human zinc transporter SLC39A2 (ZIP2). Journal of Biological Chemistry 294, 8046–8063. https://doi.org/10.1074/jbc.RA118.006113

Hackett, S., Hamzah, J., Davis, T.M.E., St Pierre, T.G., 2009. Magnetic susceptibility of iron in malaria-infected red blood cells. Biochimica et Biophysica Acta (BBA) - Molecular Basis of Disease 1792, 93–99. https://doi.org/10.1016/j.bbadis.2008.11.001

Haldar, K., Bhattacharjee, S., Safeukui, I., 2018. Drug resistance in Plasmodium. Nat Rev Microbiol 16, 156–170. https://doi.org/10.1038/nrmicro.2017.161

Hanboonkunupakarn, B., White, N.J., 2016. The threat of antimalarial drug resistance. Trop Dis Travel Med Vaccines 2, 10. https://doi.org/10.1186/s40794-016-0027-8

Hanna, J.C., Shikha, S., Sloan, M.A., Harding, C.R., 2025. Global translational and metabolic remodelling during iron deprivation in *Toxoplasma gondii*. https://doi.org/10.1101/2025.08.11.669662

Hara, T., Takeda, T., Takagishi, T., Fukue, K., Kambe, T., Fukada, T., 2017. Physiological roles of zinc transporters: molecular and genetic importance in zinc homeostasis. The Journal of Physiological Sciences 67, 283–301. https://doi.org/10.1007/s12576-017-0521-4

Harb, O.S., Roos, D.S., 2020. ToxoDB: Functional Genomics Resource for Toxoplasma and Related Organisms, in: Tonkin, C.J. (Ed.), Toxoplasma Gondii, Methods in Molecular Biology. Springer US, New York, NY, pp. 27–47. https://doi.org/10.1007/978-1-4939-9857-9_2

Hare, D., Austin, C., Doble, P., 2012. Quantification strategies for elemental imaging of biological samples using laser ablation-inductively coupled plasma-mass spectrometry. Analyst 137, 1527. https://doi.org/10.1039/c2an15792f

Harrison, P.M., Arosio, P., 1996. The ferritins: molecular properties, iron storage function and cellular regulation. Biochimica et Biophysica Acta (BBA) - Bioenergetics 1275, 161–203. https://doi.org/10.1016/0005-2728(96)00022-9

Hartley, W.J., Marshall, S.C., 1957. Toxoplasmosis as a cause of ovine perinatal mortality. New Zealand Veterinary Journal 5, 119–124. https://doi.org/10.1080/00480169.1957.33275

Haschka, D., Hoffmann, A., Weiss, G., 2021a. Iron in immune cell function and host defense. Seminars in Cell & Developmental Biology 115, 27–36. https://doi.org/10.1016/j.semcdb.2020.12.005

Haschka, D., Tymoszuk, P., Petzer, V., Hilbe, R., Heeke, S., Dichtl, S., Skvortsov, S., Demetz, E., Berger, S., Seifert, M., Mitterstiller, A.-M., Moser, P., Bumann, D., Nairz, M., Theurl, I., Weiss, G., 2021b. Ferritin H deficiency deteriorates cellular iron handling and worsens Salmonella typhimurium infection by triggering hyperinflammation. JCI Insight 6, e141760. https://doi.org/10.1172/jci.insight.141760

Haynes, J.D., Diggs, C.L., Hines, F.A., Desjardins, R.E., 1976. Culture of human malaria parasites Plasmodium falciparum. Nature 263, 767–769. https://doi.org/10.1038/263767a0

Hayward, J., Rajendran, E., Makota, F., Bassett, B., Devoy, M., Neeman, T., Van Dooren, G., 2022. Real-Time Analysis of Mitochondrial Electron Transport Chain Function in Toxoplasma gondii Parasites Using a Seahorse XFe96 Extracellular Flux Analyzer. BIO-PROTOCOL 12. https://doi.org/10.21769/BioProtoc.4288

Hayward, J.A., Rajendran, E., Zwahlen, S.M., Faou, P., Van Dooren, G.G., 2021. Divergent features of the coenzyme Q:cytochrome c oxidoreductase complex in Toxoplasma gondii parasites. PLoS Pathog 17, e1009211. https://doi.org/10.1371/journal.ppat.1009211

Hayward, J.A., Van Dooren, G.G., 2019. Same same, but different: Uncovering unique features of the mitochondrial respiratory chain of apicomplexans.

Molecular and Biochemical Parasitology 232, 111204. https://doi.org/10.1016/j.molbiopara.2019.111204

He, L., Girijashanker, K., Dalton, T.P., Reed, J., Li, H., Soleimani, M., Nebert, D.W., 2006. ZIP8, Member of the Solute-Carrier-39 (SLC39) Metal-Transporter Family: Characterization of Transporter Properties. Molecular Pharmacology 70, 171–180. https://doi.org/10.1124/mol.106.024521

Henkel, S., Frohnecke, N., Maus, D., McConville, M.J., Laue, M., Blume, M., Seeber, F., 2022. Toxoplasma gondii apicoplast-resident ferredoxin is an essential electron transfer protein for the MEP isoprenoid-biosynthetic pathway. Journal of Biological Chemistry 298, 101468. https://doi.org/10.1016/j.jbc.2021.101468

Hentze, M.W., Muckenthaler, M.U., Andrews, N.C., 2004. Balancing Acts: Molecular Control of Mammalian Iron Metabolism. Cell 117, 285–297. https://doi.org/10.1016/S0092-8674(04)00343-5

Hentze, M.W., Muckenthaler, M.U., Galy, B., Camaschella, C., 2010. Two to Tango: Regulation of Mammalian Iron Metabolism. Cell 142, 24–38. https://doi.org/10.1016/j.cell.2010.06.028

Hentze, M.W., Rouault, T.A., Caughman, S.W., Dancis, A., Harford, J.B., Klausner, R.D., 1987. A cis-acting element is necessary and sufficient for translational regulation of human ferritin expression in response to iron. Proc. Natl. Acad. Sci. U.S.A. 84, 6730–6734. https://doi.org/10.1073/pnas.84.19.6730

Hershko, C., Konijn, A.M., Nick, H.P., Breuer, W., Cabantchik, Z.I., Link, G., 2001. ICL670A: a new synthetic oral chelator: evaluation in hypertransfused rats with selective radioiron probes of hepatocellular and reticuloendothelial iron stores and in iron-loaded rat heart cells in culture. Blood 97, 1115–1122. https://doi.org/10.1182/blood.V97.4.1115

Hill, D.E., Chirukandoth, S., Dubey, J.P., 2005. Biology and epidemiology of *Toxoplasma gondii* in man and animals. Anim. Health. Res. Rev. 6, 41–61. https://doi.org/10.1079/AHR2005100

Hiszczyńska-Sawicka, E., Li, H., Xu, J.B., Holec-Gąsior, L., Kur, J., Sedcole, R., Bickerstaffe, R., Stankiewicz, M., 2011. Modulation of immune response to Toxoplasma gondii in sheep by immunization with a DNA vaccine encoding ROP1 antigen as a fusion protein with ovine CD154. Veterinary Parasitology 183, 72–78. https://doi.org/10.1016/j.vetpar.2011.06.010

Hoch, E., Levy, M., Hershfinkel, M., Sekler, I., 2020. Elucidating the H+ Coupled Zn2+ Transport Mechanism of ZIP4; Implications in Acrodermatitis Enteropathica. IJMS 21, 734. https://doi.org/10.3390/ijms21030734

Hogstrand, C., Kille, P., Ackland, M.L., Hiscox, S., Taylor, K.M., 2013. A mechanism for epithelial–mesenchymal transition and anoikis resistance in breast cancer triggered by zinc channel ZIP6 and STAT3 (signal transducer and activator of transcription 3). Biochemical Journal 455, 229–237. https://doi.org/10.1042/BJ20130483

Hohlfeld, P., Daffos, F., Thulliez, P., Aufrant, C., Couvreur, J., MacAleese, J., Descombey, D., Forestier, F., 1989. Fetal toxoplasmosis: Outcome of pregnancy and infant follow-up after in utero treatment. The Journal of Pediatrics 115, 765–769. https://doi.org/10.1016/S0022-3476(89)80660-2

Hojyo, S., Fukada, T., 2016a. Roles of Zinc Signaling in the Immune System. Journal of Immunology Research 2016, 1–21. https://doi.org/10.1155/2016/6762343

Hojyo, S., Fukada, T., 2016b. Zinc transporters and signaling in physiology and pathogenesis. Archives of Biochemistry and Biophysics 611, 43–50. https://doi.org/10.1016/j.abb.2016.06.020

Hojyo, S., Miyai, T., Fujishiro, H., Kawamura, M., Yasuda, T., Hijikata, A., Bin, B.-H., Irié, T., Tanaka, J., Atsumi, T., Murakami, M., Nakayama, M., Ohara, O., Himeno, S., Yoshida, H., Koseki, H., Ikawa, T., Mishima, K., Fukada, T., 2014. Zinc transporter SLC39A10/ZIP10 controls humoral immunity by modulating B-cell receptor signal strength. Proc. Natl. Acad. Sci. U.S.A. 111, 11786–11791. https://doi.org/10.1073/pnas.1323557111

Holmes, M.J., Augusto, L.D.S., Zhang, M., Wek, R.C., Sullivan, W.J., 2017. Translational Control in the Latency of Apicomplexan Parasites. Trends in Parasitology 33, 947–960. https://doi.org/10.1016/j.pt.2017.08.006

Holmes, M.J., Bastos, M.S., Dey, V., Severo, V., Wek, R.C., Sullivan, W.J., 2024. mRNA cap-binding protein eIF4E1 is a novel regulator of *Toxoplasma gondii* latency. mBio 15, e02954-23. https://doi.org/10.1128/mbio.02954-23

Hong, D.-P., Radke, J.B., White, M.W., 2017. Opposing Transcriptional Mechanisms Regulate Toxoplasma Development. mSphere 2, e00347-16. https://doi.org/10.1128/mSphere.00347-16

Hood, M.I., Skaar, E.P., 2012. Nutritional immunity: transition metals at the pathogen–host interface. Nat Rev Microbiol 10, 525–537. https://doi.org/10.1038/nrmicro2836

Hortua Triana, M.A., Márquez-Nogueras, K.M., Vella, S.A., Moreno, S.N.J., 2018. Calcium signaling and the lytic cycle of the Apicomplexan parasite Toxoplasma gondii. Biochim Biophys Acta Mol Cell Res 1865, 1846–1856. https://doi.org/10.1016/j.bbamcr.2018.08.004

Howe, D.K., Sibley, L.D., 1995. Toxoplasma gondii Comprises Three Clonal Lineages: Correlation of Parasite Genotype with Human Disease. Journal of Infectious Diseases 172, 1561–1566. https://doi.org/10.1093/infdis/172.6.1561

Hsu, H.H.T., Anderson, H.C., 1995. Effects of zinc and divalent cation chelators on ATP hydrolysis and Ca deposition by rachitic rat matrix vesicles. Bone 17, 473–477. https://doi.org/10.1016/8756-3282(95)00331-0

Hu, J., 2021. Toward unzipping the ZIP metal transporters: structure, evolution, and implications on drug discovery against cancer. The FEBS Journal 288, 5805–5825. https://doi.org/10.1111/febs.15658

Hu, J., Jiang, Y., 2024. Evolution, classification, and mechanisms of transport, activity regulation, and substrate specificity of ZIP metal transporters. Critical Reviews in Biochemistry and Molecular Biology 59, 245–266. https://doi.org/10.1080/10409238.2024.2405476

Huang, L., Kirschke, C.P., Zhang, Y., Yu, Y.Y., 2005. The ZIP7 Gene (Slc39a7) Encodes a Zinc Transporter Involved in Zinc Homeostasis of the Golgi Apparatus. Journal of Biological Chemistry 280, 15456–15463. https://doi.org/10.1074/jbc.M412188200

Hubert, N., Hentze, M.W., 2002. Previously uncharacterized isoforms of divalent metal transporter (DMT)-1: implications for regulation and cellular function. Proc Natl Acad Sci U S A 99, 12345–12350. https://doi.org/10.1073/pnas.192423399

Huet, D., Rajendran, E., Van Dooren, G.G., Lourido, S., 2018. Identification of cryptic subunits from an apicomplexan ATP synthase. eLife 7, e38097. https://doi.org/10.7554/eLife.38097

Hunter, C.A., Sibley, L.D., 2012. Modulation of innate immunity by Toxoplasma gondii virulence effectors. Nat Rev Microbiol 10, 766–778. https://doi.org/10.1038/nrmicro2858

Hutchison, W.M., 1965. Experimental Transmission of Toxoplasma gondii. Nature 206, 961–962. https://doi.org/10.1038/206961a0

Hutchison, W.M., Dunachie, J.F., Siim, J.Chr., Work, K., 1970. Coccidian-like Nature of Toxoplasma gondii. BMJ 1, 142–144. https://doi.org/10.1136/bmj.1.5689.142

Huynh, C., Sacks, D.L., Andrews, N.W., 2006. A *Leishmania amazonensis* ZIP family iron transporter is essential for parasite replication within macrophage phagolysosomes. The Journal of Experimental Medicine 203, 2363–2375. https://doi.org/10.1084/jem.20060559

Huynh, M.-H., Carruthers, V.B., 2009. Tagging of Endogenous Genes in a *Toxoplasma gondii* Strain Lacking Ku80. Eukaryot Cell 8, 530–539. https://doi.org/10.1128/EC.00358-08

Imlay, J.A., Chin, S.M., Linn, S., 1988. Toxic DNA Damage by Hydrogen Peroxide Through the Fenton Reaction in Vivo and in Vitro. Science 240, 640–642. https://doi.org/10.1126/science.2834821

Ingram, W.M., Goodrich, L.M., Robey, E.A., Eisen, M.B., 2013. Mice Infected with Low-Virulence Strains of Toxoplasma gondii Lose Their Innate Aversion to Cat Urine, Even after Extensive Parasite Clearance. PLoS ONE 8, e75246. https://doi.org/10.1371/journal.pone.0075246

Jabado, N., Canonne-Hergaux, F., Gruenheid, S., Picard, V., Gros, P., 2002. Iron transporter Nramp2/DMT-1 is associated with the membrane of phagosomes in macrophages and Sertoli cells. Blood 100, 2617–2622. https://doi.org/10.1182/blood-2002-04-1182

Jacot, D., Daher, W., Soldati-Favre, D., 2013. Toxoplasma gondii myosin F, an essential motor for centrosomes positioning and apicoplast inheritance. EMBO J 32, 1702–1716. https://doi.org/10.1038/emboj.2013.113

Jacques, I., Andrews, N.W., Huynh, C., 2010. Functional characterization of LIT1, the Leishmania amazonensis ferrous iron transporter. Molecular and Biochemical Parasitology 170, 28–36. https://doi.org/10.1016/j.molbiopara.2009.12.003

Janouškovec, J., Horák, A., Oborník, M., Lukeš, J., Keeling, P.J., 2010. A common red algal origin of the apicomplexan, dinoflagellate, and heterokont plastids. Proc. Natl. Acad. Sci. U.S.A. 107, 10949–10954. https://doi.org/10.1073/pnas.1003335107

Jeffers, V., Tampaki, Z., Kim, K., Sullivan, W.J., 2018. A latent ability to persist: differentiation in Toxoplasma gondii. Cell. Mol. Life Sci. 75, 2355–2373. https://doi.org/10.1007/s00018-018-2808-x

Jelenska, J., Crawford, M.J., Harb, O.S., Zuther, E., Haselkorn, R., Roos, D.S., Gornicki, P., 2001. Subcellular localization of acetyl-CoA carboxylase in the apicomplexan parasite *Toxoplasma gondii*. Proc. Natl. Acad. Sci. U.S.A. 98, 2723–2728. https://doi.org/10.1073/pnas.051629998

Jelenska, J., Sirikhachornkit, A., Haselkorn, R., Gornicki, P., 2002. The Carboxyltransferase Activity of the Apicoplast Acetyl-CoA Carboxylase of Toxoplasma gondii Is the Target of Aryloxyphenoxypropionate Inhibitors. Journal of Biological Chemistry 277, 23208–23215. https://doi.org/10.1074/jbc.M200455200

Jenkitkasemwong, S., Wang, C.-Y., Mackenzie, B., Knutson, M.D., 2012. Physiologic implications of metal-ion transport by ZIP14 and ZIP8. Biometals 25, 643–655. https://doi.org/10.1007/s10534-012-9526-x

Jeong, J., Eide, D.J., 2013. The SLC39 family of zinc transporters. Molecular Aspects of Medicine 34, 612–619. https://doi.org/10.1016/j.mam.2012.05.011

Jeong, J., Walker, J.M., Wang, F., Park, J.G., Palmer, A.E., Giunta, C., Rohrbach, M., Steinmann, B., Eide, D.J., 2012. Promotion of vesicular zinc efflux by ZIP13 and its implications for spondylocheiro dysplastic Ehlers–Danlos syndrome. Proc. Natl. Acad. Sci. U.S.A. 109. https://doi.org/10.1073/pnas.1211775110

Jeong, S.Y., David, S., 2003. Glycosylphosphatidylinositol-anchored Ceruloplasmin Is Required for Iron Efflux from Cells in the Central Nervous System. Journal of Biological Chemistry 278, 27144–27148. https://doi.org/10.1074/jbc.M301988200

Jiang, Y., Li, Z., Sui, D., Sharma, G., Wang, T., MacRenaris, K., Takahashi, H., Merz, K., Hu, J., 2023. Rational engineering of an elevator-type metal transporter ZIP8 reveals a conditional selectivity filter critically involved in determining substrate specificity. Commun Biol 6, 778. https://doi.org/10.1038/s42003-023-05146-w

Jiang, Y., MacRenaris, K., O'Halloran, T.V., Hu, J., 2024. Determination of metal ion transport rate of human ZIP4 using stable zinc isotopes. Journal of Biological Chemistry 300, 107661. https://doi.org/10.1016/j.jbc.2024.107661

Jin, Q., Paunesku, T., Lai, B., Gleber, S., Chen, S., Finney, L., Vine, D., Vogt, S., Woloschak, G., Jacobsen, C., 2017. Preserving elemental content in adherent mammalian cells for analysis by synchrotron-based x-ray fluorescence microscopy. Journal of Microscopy 265, 81–93. https://doi.org/10.1111/jmi.12466

Jinek, M., Chylinski, K., Fonfara, I., Hauer, M., Doudna, J.A., Charpentier, E., 2012. A Programmable Dual-RNA–Guided DNA Endonuclease in Adaptive Bacterial Immunity. Science 337, 816–821. https://doi.org/10.1126/science.1225829

Jones, J.L., Dubey, J.P., 2012. Foodborne Toxoplasmosis. Clinical Infectious Diseases 55, 845–851. https://doi.org/10.1093/cid/cis508

Kabiri, M., Steverding, D., 2021. Trypanosoma brucei transferrin receptor: Functional replacement of the GPI anchor with a transmembrane domain. Molecular and Biochemical Parasitology 242, 111361. https://doi.org/10.1016/j.molbiopara.2021.111361

Kamal, Ahmed M., Kamal, Amany M., Abd El-Fatah, A.S., Rizk, M.M., Hassan, E.E., 2022. Latent Toxoplasmosis is Associated with Depression and Suicidal Behavior. Archives of Suicide Research 26, 819–830. https://doi.org/10.1080/13811118.2020.1838368

Kambe, T., Hashimoto, A., Fujimoto, S., 2014. Current understanding of ZIP and ZnT zinc transporters in human health and diseases. Cell. Mol. Life Sci. 71, 3281–3295. https://doi.org/10.1007/s00018-014-1617-0

Kambe, T., Matsunaga, M., Takeda, T., 2017. Understanding the Contribution of Zinc Transporters in the Function of the Early Secretory Pathway. IJMS 18, 2179. https://doi.org/10.3390/ijms18102179

Kambe, T., Taylor, K.M., Fu, D., 2021. Zinc transporters and their functional integration in mammalian cells. Journal of Biological Chemistry 296, 100320. https://doi.org/10.1016/j.jbc.2021.100320

Kannan, G., Di Cristina, M., Schultz, A.J., Huynh, M.-H., Wang, F., Schultz, T.L., Lunghi, M., Coppens, I., Carruthers, V.B., 2019. Role of *Toxoplasma gondii* Chloroquine Resistance Transporter in Bradyzoite Viability and Digestive Vacuole Maintenance. mBio 10, e01324-19. https://doi.org/10.1128/mBio.01324-19

Kanwar, J., Anand, N., Kanwar, R., Dubey, M., Sehgal, R., Verma, A., Vahishta, R.K., 2015. Effect of lactoferrin protein on red blood cells and macrophages: mechanism of parasite–host interaction. DDDT 3821. https://doi.org/10.2147/DDDT.S77860

Kariuki, C.K., Stijlemans, B., Magez, S., 2019. The Trypanosomal Transferrin Receptor of Trypanosoma Brucei-A Review. Trop Med Infect Dis 4, 126. https://doi.org/10.3390/tropicalmed4040126

Karlinsey, J.E., Maguire, M.E., Becker, L.A., Crouch, M.V., Fang, F.C., 2010. The phage shock protein PspA facilitates divalent metal transport and is required for virulence of *Salmonella enterica* sv. Typhimurium. Molecular Microbiology 78, 669–685. https://doi.org/10.1111/j.1365-2958.2010.07357.x

Kato, J., Kobune, M., Ohkubo, S., Fujikawa, K., Tanaka, M., Takimoto, R., Takada, K., Takahari, D., Kawano, Y., Kohgo, Y., Niitsu, Y., 2007. Iron/IRP-1-dependent regulation of mRNA expression for transferrin receptor, DMT1 and ferritin during human erythroid differentiation. Experimental Hematology 35, 879–887. https://doi.org/10.1016/j.exphem.2007.03.005

Kazemi, F., Sayyah, M., Tavalla, M., Arjmand, R., 2022. Toxoplasmosis in Treatment-Resistant Obsessive–Compulsive Disorder Patients. Acta Parasit. 67, 356–361. https://doi.org/10.1007/s11686-021-00471-8

Keeran, N.S., Usha, B., Ganesan, G., 2021. P-type ATPases and their role in metal homeostasis in plants, in: Metal and Nutrient Transporters in Abiotic Stress. Elsevier, pp. 33–54. https://doi.org/10.1016/B978-0-12-817955-0.00002-8

Kell, D.B., Heyden, E.L., Pretorius, E., 2020. The Biology of Lactoferrin, an Iron-Binding Protein That Can Help Defend Against Viruses and Bacteria. Front Immunol 11, 1221. https://doi.org/10.3389/fimmu.2020.01221

Kelleher, S.L., Velasquez, V., Croxford, T.P., McCormick, N.H., Lopez, V., MacDavid, J., 2012. Mapping the zinc-transporting system in mammary cells: Molecular analysis reveals a phenotype-dependent zinc-transporting network during lactation. Journal Cellular Physiology 227, 1761–1770. https://doi.org/10.1002/jcp.22900

Khan, A., Dubey, J.P., Su, C., Ajioka, J.W., Rosenthal, B.M., Sibley, L.D., 2011. Genetic analyses of atypical Toxoplasma gondii strains reveal a fourth clonal lineage in North America. International Journal for Parasitology 41, 645–655. https://doi.org/10.1016/j.ijpara.2011.01.005

Khan, A., Fux, B., Su, C., Dubey, J.P., Darde, M.L., Ajioka, J.W., Rosenthal, B.M., Sibley, L.D., 2007. Recent transcontinental sweep of *Toxoplasma gondii* driven by a single monomorphic chromosome. Proc. Natl. Acad. Sci. U.S.A. 104, 14872–14877. https://doi.org/10.1073/pnas.0702356104

Khan, A., Taylor, S., Ajioka, J.W., Rosenthal, B.M., Sibley, L.D., 2009. Selection at a Single Locus Leads to Widespread Expansion of Toxoplasma gondii Lineages That Are Virulent in Mice. PLoS Genet 5, e1000404. https://doi.org/10.1371/journal.pgen.1000404

Khan, A., Taylor, S., Su, C., Mackey, A.J., Boyle, J., Cole, R., Glover, D., Tang, K., Paulsen, I.T., Berriman, M., Boothroyd, J.C., Pfefferkorn, E.R., Dubey, J.P., Ajioka, J.W., Roos, D.S., Wootton, J.C., Sibley, L.D., 2005. Composite genome map and recombination parameters derived from three archetypal lineages of *Toxoplasma gondii*. Nucleic Acids Research 33, 2980–2992. https://doi.org/10.1093/nar/gki604

Khojah, H.M., Ahmed, S., Abdel-Rahman, M.S., Hamza, A.-B., 2016. Reactive oxygen and nitrogen species in patients with rheumatoid arthritis as potential biomarkers for disease activity and the role of antioxidants. Free Radical Biology and Medicine 97, 285–291. https://doi.org/10.1016/j.freeradbiomed.2016.06.020

Kiara, H., Steinaa, L., Nene, V., Svitek, N., 2018. Theileria in Ruminants, in: Florin-Christensen, M., Schnittger, L. (Eds.), Parasitic Protozoa of Farm Animals and Pets. Springer International Publishing, Cham, pp. 187–213. https://doi.org/10.1007/978-3-319-70132-5_8

Kicic, A., Chua, A.C.G., Baker, E., 2001. Effect of iron chelators on proliferation and iron uptake in hepatoma cells. Cancer 92, 3093–3110. https://doi.org/10.1002/1097-0142(20011215)92:12%253C3093::AID-CNCR10107%253E3.0.CO;2-B

Kijlstra, A., Petersen, E., 2014. Epidemiology, Pathophysiology, and the Future of Ocular Toxoplasmosis. Ocular Immunology and Inflammation 22, 138–147. https://doi.org/10.3109/09273948.2013.823214

Kim, A.H., Sheline, C.T., Tian, M., Higashi, T., McMahon, R.J., Cousins, R.J., Choi, D.W., 2000. L-type Ca2+ channel-mediated Zn2+ toxicity and modulation by ZnT-1 in PC12 cells11Published on the World Wide Web on 12 October 2000. Brain Research 886, 99–107. https://doi.org/10.1016/S0006-8993(00)02944-9

Kim, B.-E., Wang, F., Dufner-Beattie, J., Andrews, G.K., Eide, D.J., Petris, M.J., 2004. Zn2+-stimulated Endocytosis of the mZIP4 Zinc Transporter Regulates Its Location at the Plasma Membrane. Journal of Biological Chemistry 279, 4523–4530. https://doi.org/10.1074/jbc.M310799200

Kim, K., Soldati, D., Boothroyd, J.C., 1993. Gene Replacement in *Toxoplasma gondii* with Chloramphenicol Acetyltransferase as Selectable Marker. Science 262, 911–914. https://doi.org/10.1126/science.8235614

Kim, K., Weiss, L.M., 2004. Toxoplasma gondii: the model apicomplexan. International Journal for Parasitology 34, 423–432. https://doi.org/10.1016/j.ijpara.2003.12.009

Kim, S., Ponka, P., 2000. Effects of Interferon-γ and Lipopolysaccharide on Macrophage Iron Metabolism Are Mediated by Nitric Oxide-induced Degradation of Iron Regulatory Protein 2. Journal of Biological Chemistry 275, 6220–6226. https://doi.org/10.1074/jbc.275.9.6220

Kissinger, J.C., 2003. ToxoDB: accessing the Toxoplasma gondii genome. Nucleic Acids Research 31, 234–236. https://doi.org/10.1093/nar/gkg072

Klevar, S., 2007. Tissue cyst forming coccidia; Toxoplasma gondii and Neospora caninum as a cause of disease in farm animals. Acta Vet Scand 49, S1. https://doi.org/10.1186/1751-0147-49-S1-S1

Kloehn, J., Harding, C.R., Soldati-Favre, D., 2021. Supply and demand—heme synthesis, salvage and utilization by Apicomplexa. The FEBS Journal 288, 382–404. https://doi.org/10.1111/febs.15445

Knies, K.A., Li, Y.V., 2021. Zinc cytotoxicity induces mitochondrial morphology changes in hela cell line. Int J Physiol Pathophysiol Pharmacol 13, 43–51.

Koeller, D.M., Casey, J.L., Hentze, M.W., Gerhardt, E.M., Chan, L.N., Klausner, R.D., Harford, J.B., 1989. A cytosolic protein binds to structural elements within the iron regulatory region of the transferrin receptor mRNA. Proc. Natl. Acad. Sci. U.S.A. 86, 3574–3578. https://doi.org/10.1073/pnas.86.10.3574

Kořený, L., Oborník, M., Lukeš, J., 2013. Make It, Take It, or Leave It: Heme Metabolism of Parasites. PLoS Pathog 9, e1003088. https://doi.org/10.1371/journal.ppat.1003088

Korshunova, Y.O., Eide, D., Gregg Clark, W., Lou Guerinot, M., Pakrasi, H.B., 1999. The IRT1 protein from Arabidopsis thaliana is a metal transporter with a broad substrate range. Plant Mol Biol 40, 37–44. https://doi.org/10.1023/A:1026438615520

Krężel, A., Maret, W., 2016. The biological inorganic chemistry of zinc ions. Archives of Biochemistry and Biophysics 611, 3–19. https://doi.org/10.1016/j.abb.2016.04.010

Krishnan, A., Kloehn, J., Lunghi, M., Chiappino-Pepe, A., Waldman, B.S., Nicolas, D., Varesio, E., Hehl, A., Lourido, S., Hatzimanikatis, V., Soldati-Favre, D., 2020. Functional and Computational Genomics Reveal Unprecedented Flexibility in Stage-Specific Toxoplasma Metabolism. Cell Host & Microbe 27, 290-306.e11. https://doi.org/10.1016/j.chom.2020.01.002

Kühn, L.C., 2015. Iron regulatory proteins and their role in controlling iron metabolism. Metallomics 7, 232–243. https://doi.org/10.1039/C4MT00164H

Kühn, L.C., McClelland, A., Ruddle, F.H., 1984. Gene transfer, expression, and molecular cloning of the human transferrin receptor gene. Cell 37, 95–103. https://doi.org/10.1016/0092-8674(84)90304-0

Kumagai, T., Awai, M., Okada, S., 1992. Mobilization of Iron and Iron-related Proteins in Rat Spleen after Intravenous Injection of Lipopolysaccharides (LPS). Pathology - Research and Practice 188, 931–941. https://doi.org/10.1016/S0344-0338(11)80254-2

Kwiatkowski, J.L., 2011. Real-World Use of Iron Chelators. Hematology 2011, 451–458. https://doi.org/10.1182/asheducation-2011.1.451

Lacombe, A., Maclean, A.E., Ovciarikova, J., Tottey, J., Mühleip, A., Fernandes, P., Sheiner, L., 2019. Identification of the *Toxoplasma gondii* mitochondrial ribosome, and characterisation of a protein essential for mitochondrial translation. Molecular Microbiology 112, 1235–1252. https://doi.org/10.1111/mmi.14357

Lane, D., Bae, D.-H., Merlot, A., Sahni, S., Richardson, D., 2015. Duodenal Cytochrome b (DCYTB) in Iron Metabolism: An Update on Function and Regulation. Nutrients 7, 2274–2296. https://doi.org/10.3390/nu7042274

Lane, D.J.R., Merlot, A.M., Huang, M.L.-H., Bae, D.-H., Jansson, P.J., Sahni, S., Kalinowski, D.S., Richardson, D.R., 2015. Cellular iron uptake, trafficking and metabolism: Key molecules and mechanisms and their roles in disease. Biochimica et Biophysica Acta (BBA) - Molecular Cell Research 1853, 1130–1144. https://doi.org/10.1016/j.bbamcr.2015.01.021

Larson, J.A., Howie, H.L., So, M., 2004. *Neisseria meningitidis* accelerates ferritin degradation in host epithelial cells to yield an essential iron source. Molecular Microbiology 53, 807–820. https://doi.org/10.1111/j.1365-2958.2004.04169.x

Lau, Y.-L., Lee, W.-C., Gudimella, R., Zhang, G., Ching, X.-T., Razali, R., Aziz, F., Anwar, A., Fong, M.-Y., 2016. Deciphering the Draft Genome of

Toxoplasma gondii RH Strain. PLoS ONE 11, e0157901. https://doi.org/10.1371/journal.pone.0157901

Lawen, A., Lane, D.J.R., 2013. Mammalian Iron Homeostasis in Health and Disease: Uptake, Storage, Transport, and Molecular Mechanisms of Action. Antioxidants & Redox Signaling 18, 2473–2507. https://doi.org/10.1089/ars.2011.4271

Lawrence, C.M., Ray, S., Babyonyshev, M., Galluser, R., Borhani, D.W., Harrison, S.C., 1999. Crystal Structure of the Ectodomain of Human Transferrin Receptor. Science 286, 779–782. https://doi.org/10.1126/science.286.5440.779

Le, Y., Liu, Q., Yang, Y., Wu, J., 2024. The emerging role of nuclear receptor coactivator 4 in health and disease: a novel bridge between iron metabolism and immunity. Cell Death Discov 10, 312. https://doi.org/10.1038/s41420-024-02075-3

Leal, F.E., Cavazzana, C.L., Andrade, H.F.D., Galisteo, A.J., Mendonca, J.S.D., Kallas, E.G., 2007. Toxoplasma gondii Pneumonia in Immunocompetent Subjects: Case Report and Review. Clinical Infectious Diseases 44, e62–e66. https://doi.org/10.1086/511871

Lee, P.L., Gelbart, T., West, C., Halloran, C., Beutler, E., 1998. The Human Nramp2 Gene: Characterization of the Gene Structure, Alternative Splicing, Promoter Region and Polymorphisms. Blood Cells, Molecules, and Diseases 24, 199–215. https://doi.org/10.1006/bcmd.1998.0186

Lee, S., Lee, J., Ricachenevsky, F.K., Punshon, T., Tappero, R., Salt, D.E., Guerinot, M.L., 2021. Redundant roles of four ZIP family members in zinc homeostasis and seed development in *Arabidopsis thaliana*. The Plant Journal 108, 1162–1173. https://doi.org/10.1111/tpj.15506

Lee, W., Ha, J., Sugiyama, Y., 2020. Post-translational regulation of the major drug transporters in the families of organic anion transporters and organic anion–transporting polypeptides. Journal of Biological Chemistry 295, 17349–17364. https://doi.org/10.1074/jbc.REV120.009132

Lehker, M.W., Alderete, J.F., 1992. Iron regulates growth of *Trichomonas vaginalis* and the expression of immunogenic trichomonad proteins. Molecular Microbiology 6, 123–132. https://doi.org/10.1111/j.1365-2958.1992.tb00844.x

Leonard, R.A., Tian, Y., Tan, F., Van Dooren, G.G., Hayward, J.A., 2023. An essential role for an Fe-S cluster protein in the cytochrome c oxidase complex of Toxoplasma parasites. PLoS Pathog 19, e1011430. https://doi.org/10.1371/journal.ppat.1011430

Leung, K.W., Gvritishvili, A., Liu, Y., Tombran-Tink, J., 2012. ZIP2 and ZIP4 Mediate Age-Related Zinc Fluxes Across the Retinal Pigment Epithelium. J Mol Neurosci 46, 122–137. https://doi.org/10.1007/s12031-011-9536-0

Levine, N.D., 1988. Progress in Taxonomy of the Apicomplexan Protozoa. The Journal of Protozoology 35, 518–520. https://doi.org/10.1111/j.1550-7408.1988.tb04141.x

Levine, N.D., 1973. Protozoan parasites of domestic animals and of man, 2. ed. ed. Burgess, Minneapolis, Minn.

Levine, N.D., Corliss, J.O., Cox, F.E.G., Deroux, G., Grain, J., Honigberg, B.M., Leedale, G.F., Loeblich, A.R., Lom, Iii.J., Lynn, D., Merinfeld, E.G., Page, F.C., Poljansky, G., Sprague, V., Vavra, J., Wallace, F.G., 1980. A Newly Revised Classification of the Protozoa*: THE COMMITTEE ON SYSTEMATICS EVOLUTION OF THE SOCIETY OF PROTOZOOLOGISTS†. The Journal of

Protozoology 27, 37–58. https://doi.org/10.1111/j.1550-7408.1980.tb04228.x

Li, L., Kaplan, J., 1998. Defects in the Yeast High Affinity Iron Transport System Result in Increased Metal Sensitivity because of the Increased Expression of Transporters with a Broad Transition Metal Specificity. Journal of Biological Chemistry 273, 22181–22187. https://doi.org/10.1074/jbc.273.35.22181

Li, L., Murdock, G., Bagley, D., Jia, X., Ward, D.M., Kaplan, J., 2010. Genetic Dissection of a Mitochondria-Vacuole Signaling Pathway in Yeast Reveals a Link between Chronic Oxidative Stress and Vacuolar Iron Transport. Journal of Biological Chemistry 285, 10232–10242. https://doi.org/10.1074/jbc.M109.096859

Li, L.-Y., Zhou, C.-X., Han, B., Elsheikha, H.M., Qiu, H.-J., An, X.-D., Zeng, T., Liu, D.-A., Yang, Q., Zhu, X.-Q., Zhou, H.-Y., 2025. Ferroptosis is important for *Toxoplasma gondii* replication and virulence *in vitro* and *in vivo*. Virulence 16. https://doi.org/10.1080/21505594.2025.2530164

Li, Y., Shi, J., Wu, X., Luo, Z., Wang, F., Guo, Q., 2009. Tracing of intracellular zinc(II) fluorescence flux to monitor cell apoptosis by using FluoZin-3AM. Cell Biochemistry & Function 27, 417–423. https://doi.org/10.1002/cbf.1598

Licon, M.H., Giuliano, C.J., Chan, A.W., Chakladar, S., Eberhard, J.N., Shallberg, L.A., Chandrasekaran, S., Waldman, B.S., Koshy, A.A., Hunter, C.A., Lourido, S., 2023. A positive feedback loop controls Toxoplasma chronic differentiation. Nat Microbiol 8, 889–904. https://doi.org/10.1038/s41564-023-01358-2

Lill, R., 2009. Function and biogenesis of iron–sulphur proteins. Nature 460, 831–838. https://doi.org/10.1038/nature08301

Lill, R., Srinivasan, V., Mühlenhoff, U., 2014. The role of mitochondria in cytosolic-nuclear iron–sulfur protein biogenesis and in cellular iron regulation. Curr Opin Microbiol 22, 111–119. https://doi.org/10.1016/j.mib.2014.09.015

Lin, W., Chai, J., Love, J., Fu, D., 2010. Selective Electrodiffusion of Zinc Ions in a Zrt-, Irt-like Protein, ZIPB*. Journal of Biological Chemistry 285, 39013–39020. https://doi.org/10.1074/jbc.M110.180620

Lin, Y., Liang, H., Yang, S., Boch, A., Clemens, S., Chen, C., Wu, J., Huang, J., Yeh, K., 2009. Arabidopsis IRT3 is a zinc-regulated and plasma membrane localized zinc/iron transporter. New Phytologist 182, 392–404. https://doi.org/10.1111/j.1469-8137.2009.02766.x

Lin, Z., Fernández-Robledo, J.-A., Cellier, M.F.M., Vasta, G.R., 2011. The Natural Resistance-Associated Macrophage Protein from the Protozoan Parasite *Perkinsus marinus* Mediates Iron Uptake. Biochemistry 50, 6340–6355. https://doi.org/10.1021/bi200343h

Liu, J., Pace, D., Dou, Z., King, T.P., Guidot, D., Li, Z., Carruthers, V.B., Moreno, S.N.J., 2014. A vacuolar- H^+ -pyrophosphatase (TgVP 1) is required for microneme secretion, host cell invasion, and extracellular survival of *T oxoplasma gondii*. Molecular Microbiology 93, 698–712. https://doi.org/10.1111/mmi.12685

Liu, X., Hill, P., Haile, D.J., 2002. Role of the Ferroportin Iron-Responsive Element in Iron and Nitric Oxide Dependent Gene Regulation. Blood Cells, Molecules, and Diseases 29, 315–326. https://doi.org/10.1006/bcmd.2002.0572

Liu, Y., Bafaro, E.M., Cowan, A.E., Dempski, R.E., 2022. The transmembrane domains mediate oligomerization of the human ZIP4 transporter in vivo. Sci Rep 12, 21083. https://doi.org/10.1038/s41598-022-24782-6

Liu, Z., Li, H., Soleimani, M., Girijashanker, K., Reed, J.M., He, L., Dalton, T.P., Nebert, D.W., 2008. Cd2+ versus Zn2+ uptake by the ZIP8 HCO 3 - - dependent symporter: Kinetics, electrogenicity and trafficking. Biochemical and Biophysical Research Communications 365, 814–820. https://doi.org/10.1016/j.bbrc.2007.11.067

Liu, Z., Wang, H., Zhang, Z., Ma, Y., Jing, Q., Zhang, S., Han, J., Chen, J., Xiang, Y., Kou, Y., Wei, Y., Wang, L., Wang, Y., 2024. Fam96a is essential for the host control of Toxoplasma gondii infection by fine-tuning macrophage polarization via an iron-dependent mechanism. PLoS Negl Trop Dis 18, e0012163. https://doi.org/10.1371/journal.pntd.0012163

Liuzzi, J.P., Aydemir, F., Nam, H., Knutson, M.D., Cousins, R.J., 2006. Zip14 (Slc39a14) mediates non-transferrin-bound iron uptake into cells. Proc. Natl. Acad. Sci. U.S.A. 103, 13612–13617. https://doi.org/10.1073/pnas.0606424103

Lloyd, J.B., Cable, H., Rice-Evans, C., 1991. Evidence that desferrioxamine cannot enter cells by passive diffusion. Biochemical Pharmacology 41, 1361–1363. https://doi.org/10.1016/0006-2952(91)90109-I

Loveridge, K.M., Sigala, P.A., 2024. Identification of a divalent metal transporter required for cellular iron metabolism in malaria parasites. Proc. Natl. Acad. Sci. U.S.A. 121, e2411631121. https://doi.org/10.1073/pnas.2411631121

Lu, Q., Haragopal, H., Slepchenko, K.G., Stork, C., Li, Y.V., 2016. Intracellular zinc distribution in mitochondria, ER and the Golgi apparatus. Int J Physiol Pathophysiol Pharmacol 8, 35–43.

Ludwiczek, S., Aigner, E., Theurl, I., Weiss, G., 2003. Cytokine-mediated regulation of iron transport in human monocytic cells. Blood 101, 4148–4154. https://doi.org/10.1182/blood-2002-08-2459

Lykens, J.E., Terrell, C.E., Zoller, E.E., Divanovic, S., Trompette, A., Karp, C.L., Aliberti, J., Flick, M.J., Jordan, M.B., 2010. Mice with a Selective Impairment of IFN-γ Signaling in Macrophage Lineage Cells Demonstrate the Critical Role of IFN-γ–Activated Macrophages for the Control of Protozoan Parasitic Infections In Vivo. The Journal of Immunology 184, 877–885. https://doi.org/10.4049/jimmunol.0902346

Lymboussaki, A., Pignatti, E., Montosi, G., Garuti, C., Haile, D.J., Pietrangelo, A., 2003. The role of the iron responsive element in the control of ferroportin1/IREG1/MTP1 gene expression. Journal of Hepatology 39, 710–715. https://doi.org/10.1016/S0168-8278(03)00408-2

MacDiarmid, C.W., Gaither, L.A., Eide, D., 2000. Zinc transporters that regulate vacuolar zinc storage in Saccharomyces cerevisiae. EMBO J 19, 2845–2855. https://doi.org/10.1093/emboj/19.12.2845

Maclean, A.E., Bridges, H.R., Silva, M.F., Ding, S., Ovciarikova, J., Hirst, J., Sheiner, L., 2021. Complexome profile of Toxoplasma gondii mitochondria identifies divergent subunits of respiratory chain complexes including new subunits of cytochrome bc1 complex. PLoS Pathog 17, e1009301. https://doi.org/10.1371/journal.ppat.1009301

Maclean, A.E., Sloan, M.A., Renaud, E.A., Argyle, B.E., Lewis, W.H., Ovciarikova, J., Demolombe, V., Waller, R.F., Besteiro, S., Sheiner, L., 2024. The *Toxoplasma gondii* mitochondrial transporter ABCB7L is essential for the

biogenesis of cytosolic and nuclear iron-sulfur cluster proteins and cytosolic translation. mBio 15, e00872-24. https://doi.org/10.1128/mbio.00872-24

Maenz, M., Schlüter, D., Liesenfeld, O., Schares, G., Gross, U., Pleyer, U., 2014. Ocular toxoplasmosis past, present and new aspects of an old disease. Progress in Retinal and Eye Research 39, 77–106. https://doi.org/10.1016/j.preteyeres.2013.12.005

Maertens, B., Spriestersbach, A., von Groll, U., Roth, U., Kubicek, J., Gerrits, M., Graf, M., Liss, M., Daubert, D., Wagner, R., Schäfer, F., 2010. Gene optimization mechanisms: a multi-gene study reveals a high success rate of full-length human proteins expressed in Escherichia coli. Protein Sci 19, 1312–1326. https://doi.org/10.1002/pro.408

Maharana, B.R., Tewari, A.K., Saravanan, B.C., Sudhakar, N.R., 2016. Important hemoprotozoan diseases of livestock: Challenges in current diagnostics and therapeutics: An update. Vet World 9, 487–495. https://doi.org/10.14202/vetworld.2016.487-495

Mahmoud, M.S., 1999. Effect of deferoxamine alone and combined with pyrimethamine on acute toxoplasmosis in mice. J Egypt Soc Parasitol 29, 791–803.

Mair, S.M., Nairz, M., Bellmann-Weiler, R., Muehlbacher, T., Schroll, A., Theurl, I., Moser, P.L., Talasz, H., Fang, F.C., Weiss, G., 2011. Nifedipine Affects the Course of Salmonella enterica Serovar Typhimurium Infection by Modulating Macrophage Iron Homeostasis. The Journal of Infectious Diseases 204, 685–694. https://doi.org/10.1093/infdis/jir395

Mallo, N., Ovciarikova, J., Martins-Duarte, E.S., Baehr, S.C., Biddau, M., Wilde, M.-L., Uboldi, A.D., Lemgruber, L., Tonkin, C.J., Wideman, J.G., Harding, C.R., Sheiner, L., 2021. Depletion of a *Toxoplasma* porin leads to defects in mitochondrial morphology and contacts with the endoplasmic reticulum. Journal of Cell Science 134, jcs255299. https://doi.org/10.1242/jcs.255299

Mamaghani, A.J., Fathollahi, A., Arab-Mazar, Z., Kohansal, K., Fathollahi, M., Spotin, A., Bashiri, H., Bozorgomid, A., 2023. Toxoplasma gondii vaccine candidates: a concise review. Ir J Med Sci 192, 231–261. https://doi.org/10.1007/s11845-022-02998-9

Mancias, J.D., Pontano Vaites, L., Nissim, S., Biancur, D.E., Kim, A.J., Wang, X., Liu, Y., Goessling, W., Kimmelman, A.C., Harper, J.W., 2015. Ferritinophagy via NCOA4 is required for erythropoiesis and is regulated by iron dependent HERC2-mediated proteolysis. eLife 4, e10308. https://doi.org/10.7554/eLife.10308

Mancias, J.D., Wang, X., Gygi, S.P., Harper, J.W., Kimmelman, A.C., 2014. Quantitative proteomics identifies NCOA4 as the cargo receptor mediating ferritinophagy. Nature 509, 105–109. https://doi.org/10.1038/nature13148

Mao, X., Kim, B.-E., Wang, F., Eide, D.J., Petris, M.J., 2007. A Histidine-rich Cluster Mediates the Ubiquitination and Degradation of the Human Zinc Transporter, hZIP4, and Protects against Zinc Cytotoxicity. Journal of Biological Chemistry 282, 6992–7000. https://doi.org/10.1074/jbc.M610552200

Maret, W., 2017. Zinc in Cellular Regulation: The Nature and Significance of "Zinc Signals." IJMS 18, 2285. https://doi.org/10.3390/ijms18112285

Maret, W., 2013. Zinc Biochemistry: From a Single Zinc Enzyme to a Key Element of Life. Advances in Nutrition 4, 82–91. https://doi.org/10.3945/an.112.003038

Maret, W., 2009. Molecular aspects of human cellular zinc homeostasis: redox control of zinc potentials and zinc signals. Biometals 22, 149–157. https://doi.org/10.1007/s10534-008-9186-z

Maret, W., 2005. Zinc coordination environments in proteins determine zinc functions. Journal of Trace Elements in Medicine and Biology 19, 7–12. https://doi.org/10.1016/j.jtemb.2005.02.003

Marino, N.D., Boothroyd, J.C., 2017. Toxoplasma growth in vitro is dependent on exogenous tyrosine and is independent of AAH2 even in tyrosine-limiting conditions. Experimental Parasitology 176, 52–58. https://doi.org/10.1016/j.exppara.2017.02.018

Marino, N.D., Panas, M.W., Franco, M., Theisen, T.C., Naor, A., Rastogi, S., Buchholz, K.R., Lorenzi, H.A., Boothroyd, J.C., 2018. Identification of a novel protein complex essential for effector translocation across the parasitophorous vacuole membrane of Toxoplasma gondii. PLoS Pathog 14, e1006828. https://doi.org/10.1371/journal.ppat.1006828

Markus, B.M., Bell, G.W., Lorenzi, H.A., Lourido, S., 2019. Optimizing Systems for Cas9 Expression in Toxoplasma gondii. mSphere 4, e00386-19. https://doi.org/10.1128/mSphere.00386-19

Martinez, F.O., Gordon, S., 2014. The M1 and M2 paradigm of macrophage activation: time for reassessment. F1000Prime Rep 6, 13. https://doi.org/10.12703/P6-13

Martins, R., Carlos, A.R., Braza, F., Thompson, J.A., Bastos-Amador, P., Ramos, S., Soares, M.P., 2019. Disease Tolerance as an Inherent Component of Immunity. Annu. Rev. Immunol. 37, 405–437. https://doi.org/10.1146/annurev-immunol-042718-041739

Marvin, R.G., Wolford, J.L., Kidd, M.J., Murphy, S., Ward, J., Que, E.L., Mayer, M.L., Penner-Hahn, J.E., Haldar, K., O'Halloran, T.V., 2012. Fluxes in "free" and total zinc are essential for progression of intraerythrocytic stages of Plasmodium falciparum. Chem Biol 19, 731–741. https://doi.org/10.1016/j.chembiol.2012.04.013

Mathur, V., Wakeman, K.C., Keeling, P.J., 2021. Parallel functional reduction in the mitochondria of apicomplexan parasites. Current Biology 31, 2920-2928.e4. https://doi.org/10.1016/j.cub.2021.04.028

Matsuura, W., Yamazaki, T., Yamaguchi-Iwai, Y., Masuda, S., Nagao, M., Andrews, G.K., Kambe, T., 2009. SLC39A9 (ZIP9) Regulates Zinc Homeostasis in the Secretory Pathway: Characterization of the ZIP Subfamily I Protein in Vertebrate Cells. Bioscience, Biotechnology, and Biochemistry 73, 1142–1148. https://doi.org/10.1271/bbb.80910

Mayoral, J., Guevara, R.B., Rivera-Cuevas, Y., Tu, V., Tomita, T., Romano, J.D., Gunther-Cummins, L., Sidoli, S., Coppens, I., Carruthers, V.B., Weiss, L.M., 2022. Dense Granule Protein GRA64 Interacts with Host Cell ESCRT Proteins during *Toxoplasma gondii* Infection. mBio 13, e01442-22. https://doi.org/10.1128/mbio.01442-22

Mazumdar, J., H Wilson, E., Masek, K., A Hunter, C., Striepen, B., 2006. Apicoplast fatty acid synthesis is essential for organelle biogenesis and parasite survival in Toxoplasma gondii. Proc Natl Acad Sci U S A 103, 13192–13197. https://doi.org/10.1073/pnas.0603391103

McAuley, J.B., 2014. Congenital Toxoplasmosis. Journal of the Pediatric Infectious Diseases Society 3, S30–S35. https://doi.org/10.1093/jpids/piu077

McClelland, A., Kühn, L.C., Ruddle, F.H., 1984. The human transferrin receptor gene: genomic organization, and the complete primary structure of the

receptor deduced from a cDNA sequence. Cell 39, 267–274. https://doi.org/10.1016/0092-8674(84)90004-7

McFadden, G.I., Yeh, E., 2017. The apicoplast: now you see it, now you don't. International Journal for Parasitology 47, 137–144. https://doi.org/10.1016/j.ijpara.2016.08.005

McKie, A.T., Marciani, P., Rolfs, A., Brennan, K., Wehr, K., Barrow, D., Miret, S., Bomford, A., Peters, T.J., Farzaneh, F., Hediger, M.A., Hentze, M.W., Simpson, R.J., 2000. A Novel Duodenal Iron-Regulated Transporter, IREG1, Implicated in the Basolateral Transfer of Iron to the Circulation. Molecular Cell 5, 299–309. https://doi.org/10.1016/S1097-2765(00)80425-6

McRae, R., Lai, B., Vogt, S., Fahrni, C.J., 2006. Correlative microXRF and optical immunofluorescence microscopy of adherent cells labeled with ultrasmall gold particles. Journal of Structural Biology 155, 22–29. https://doi.org/10.1016/j.jsb.2005.09.013

Mead, P.S., Slutsker, L., Dietz, V., McCaig, L.F., Bresee, J.S., Shapiro, C., Griffin, P.M., Tauxe, R.V., 1999. Food-Related Illness and Death in the United States. Emerg. Infect. Dis. 5, 607–625. https://doi.org/10.3201/eid0505.990502

Meissner, M., Schlüter, D., Soldati, D., 2002. Role of *Toxoplasma gondii* Myosin A in Powering Parasite Gliding and Host Cell Invasion. Science 298, 837–840. https://doi.org/10.1126/science.1074553

Mendoza, F.J., Pérez-Écija, A., Kappmeyer, L.S., Suarez, C.E., Bastos, R.G., 2024. New insights in the diagnosis and treatment of equine piroplasmosis: pitfalls, idiosyncrasies, and myths. Front. Vet. Sci. 11, 1459989. https://doi.org/10.3389/fvets.2024.1459989

Mévélec, M.-N., Lakhrif, Z., Dimier-Poisson, I., 2020. Key Limitations and New Insights Into the Toxoplasma gondii Parasite Stage Switching for Future Vaccine Development in Human, Livestock, and Cats. Front. Cell. Infect. Microbiol. 10, 607198. https://doi.org/10.3389/fcimb.2020.607198

Miller, S., Ralle, M., 2024. Sample Preparation for X-Ray Fluorescence Microscopy of Iron Distribution in Biological Specimen. Methods Mol Biol 2839, 43–52. https://doi.org/10.1007/978-1-0716-4043-2_3

Milner, M.J., Seamon, J., Craft, E., Kochian, L.V., 2013. Transport properties of members of the ZIP family in plants and their role in Zn and Mn homeostasis. EXBOTJ 64, 369–381. https://doi.org/10.1093/jxb/ers315

Milon, B., Wu, Q., Zou, J., Costello, L.C., Franklin, R.B., 2006. Histidine residues in the region between transmembrane domains III and IV of hZip1 are required for zinc transport across the plasma membrane in PC-3 cells. Biochimica et Biophysica Acta (BBA) - Biomembranes 1758, 1696–1701. https://doi.org/10.1016/j.bbamem.2006.06.005

Miranda, K., Pace, D.A., Cintron, R., Rodrigues, J.C.F., Fang, J., Smith, A., Rohloff, P., Coelho, E., de Haas, F., de Souza, W., Coppens, I., Sibley, L.D., Moreno, S.N.J., 2010. Characterization of a novel organelle in Toxoplasma gondii with similar composition and function to the plant vacuole. Mol Microbiol 76, 1358–1375. https://doi.org/10.1111/j.1365-2958.2010.07165.x

Moncada, P.A., Montoya, J.G., 2012. Toxoplasmosis in the fetus and newborn: an update on prevalence, diagnosis and treatment. Expert Review of Anti-infective Therapy 10, 815–828. https://doi.org/10.1586/eri.12.58

Montalbetti, N., Simonin, A., Simonin, C., Awale, M., Reymond, J.-L., Hediger, M.A., 2015. Discovery and characterization of a novel non-competitive

inhibitor of the divalent metal transporter DMT1/SLC11A2. Biochemical Pharmacology 96, 216–224. https://doi.org/10.1016/j.bcp.2015.05.002

Montazeri, M., Mehrzadi, S., Sharif, M., Sarvi, S., Tanzifi, A., Aghayan, S.A., Daryani, A., 2018. Drug Resistance in Toxoplasma gondii. Front. Microbiol. 9, 2587. https://doi.org/10.3389/fmicb.2018.02587

Monteith, A.J., Skaar, E.P., 2021. The impact of metal availability on immune function during infection. Trends in Endocrinology & Metabolism 32, 916–928. https://doi.org/10.1016/j.tem.2021.08.004

Montoya, J., Liesenfeld, O., 2004. Toxoplasmosis. The Lancet 363, 1965–1976. https://doi.org/10.1016/S0140-6736(04)16412-X

Moreira, D., Estaquier, J., Cordeiro-da-Silva, A., Silvestre, R., 2018. Metabolic Crosstalk Between Host and Parasitic Pathogens, in: Silvestre, R., Torrado, E. (Eds.), Metabolic Interaction in Infection, Experientia Supplementum. Springer International Publishing, Cham, pp. 421–458. https://doi.org/10.1007/978-3-319-74932-7_12

Morrison, D.A., 2009. Evolution of the Apicomplexa: where are we now? Trends in Parasitology 25, 375–382. https://doi.org/10.1016/j.pt.2009.05.010

Morrison, W.I., 2015. The aetiology, pathogenesis and control of theileriosis in domestic animals: -EN- -FR- Étiologie, pathogénie et contrôle de la theilériose chez les animaux domestiques -ES- Etiología, patogénesis y control de la teileriosis en animales domésticos. Rev. Sci. Tech. OIE 34, 599–611. https://doi.org/10.20506/rst.34.2.2383

Morrissette, N.S., Sibley, L.D., 2002. Cytoskeleton of Apicomplexan Parasites. Microbiol Mol Biol Rev 66, 21–38. https://doi.org/10.1128/MMBR.66.1.21-38.2002

Muckenthaler, M., Gray, N.K., Hentze, M.W., 1998. IRP-1 Binding to Ferritin mRNA Prevents the Recruitment of the Small Ribosomal Subunit by the Cap-Binding Complex eIF4F. Molecular Cell 2, 383–388. https://doi.org/10.1016/S1097-2765(00)80282-8

Mulero, V., Brock, J.H., 1999. Regulation of iron metabolism in murine J774 macrophages: role of nitric oxide-dependent and -independent pathways following activation with gamma interferon and lipopolysaccharide. Blood 94, 2383–2389.

Musto, H., Romero, H., Zavala, A., Jabbari, K., Bernardi, G., 1999. Synonymous Codon Choices in the Extremely GC-Poor Genome of Plasmodium falciparum: Compositional Constraints and Translational Selection. J Mol Evol 49, 27–35. https://doi.org/10.1007/PL00006531

Nadipuram, S.M., Kim, E.W., Vashisht, A.A., Lin, A.H., Bell, H.N., Coppens, I., Wohlschlegel, J.A., Bradley, P.J., 2016. *In Vivo* Biotinylation of the *Toxoplasma* Parasitophorous Vacuole Reveals Novel Dense Granule Proteins Important for Parasite Growth and Pathogenesis. mBio 7, e00808-16. https://doi.org/10.1128/mBio.00808-16

Nairz, M., Ferring-Appel, D., Casarrubea, D., Sonnweber, T., Viatte, L., Schroll, A., Haschka, D., Fang, F.C., Hentze, M.W., Weiss, G., Galy, B., 2015. Iron Regulatory Proteins Mediate Host Resistance to Salmonella Infection. Cell Host & Microbe 18, 254–261. https://doi.org/10.1016/j.chom.2015.06.017

Nairz, M., Fritsche, G., Brunner, P., Talasz, H., Hantke, K., Weiss, G., 2008. Interferon-γ limits the availability of iron for intramacrophage *Salmonella typhimurium*. Eur J Immunol 38, 1923–1936. https://doi.org/10.1002/eji.200738056

Nairz, M., Haschka, D., Demetz, E., Weiss, G., 2014. Iron at the interface of immunity and infection. Front. Pharmacol. 5. https://doi.org/10.3389/fphar.2014.00152

Nairz, M., Schroll, A., Sonnweber, T., Weiss, G., 2010. The struggle for iron - a metal at the host-pathogen interface: Iron at the host-pathogen interface. Cellular Microbiology 12, 1691–1702. https://doi.org/10.1111/j.1462-5822.2010.01529.x

Nairz, M., Theurl, I., Ludwiczek, S., Theurl, M., Mair, S.M., Fritsche, G., Weiss, G., 2007. The co-ordinated regulation of iron homeostasis in murine macrophages limits the availability of iron for intracellular *Salmonella typhimurium*. Cellular Microbiology 9, 2126–2140. https://doi.org/10.1111/j.1462-5822.2007.00942.x

Nairz, M., Theurl, I., Swirski, F.K., Weiss, G., 2017. "Pumping iron"—how macrophages handle iron at the systemic, microenvironmental, and cellular levels. Pflugers Arch - Eur J Physiol 469, 397–418. https://doi.org/10.1007/s00424-017-1944-8

Nasirpour, S., Kheirandish, F., Fallahi, S., 2020. Depression and Toxoplasma gondii infection: assess the possible relationship through a seromolecular case-control study. Arch Microbiol 202, 2689–2695. https://doi.org/10.1007/s00203-020-01993-x

Nathan, C.F., Murray, H.W., Wiebe, M.E., Rubin, B.Y., 1983. Identification of interferon-gamma as the lymphokine that activates human macrophage oxidative metabolism and antimicrobial activity. The Journal of experimental medicine 158, 670–689. https://doi.org/10.1084/jem.158.3.670

Nayeri Chegeni, T., Sarvi, S., Amouei, A., Moosazadeh, M., Hosseininejad, Z., A Aghayan, S., Daryani, A., 2019. Relationship between toxoplasmosis and obsessive compulsive disorder: A systematic review and meta-analysis. PLoS Negl Trop Dis 13, e0007306. https://doi.org/10.1371/journal.pntd.0007306

Nayeri, T., Sarvi, S., Sharif, M., Daryani, A., 2021. Toxoplasma gondii: A possible etiologic agent for Alzheimer's disease. Heliyon 7, e07151. https://doi.org/10.1016/j.heliyon.2021.e07151

Nelson, N., Harvey, W.R., 1999. Vacuolar and Plasma Membrane Proton-Adenosinetriphosphatases. Physiological Reviews 79, 361–385. https://doi.org/10.1152/physrev.1999.79.2.361

Nemeth, E., Ganz, T., 2009. The Role of Hepcidin in Iron Metabolism. Acta Haematol 122, 78–86. https://doi.org/10.1159/000243791

Netz, D.J.A., Mascarenhas, J., Stehling, O., Pierik, A.J., Lill, R., 2014. Maturation of cytosolic and nuclear iron–sulfur proteins. Trends in Cell Biology 24, 303–312. https://doi.org/10.1016/j.tcb.2013.11.005

Ngwana-Joseph, G.C., Phelan, J.E., Manko, E., Dombrowski, J.G., Da Silva Santos, S., Suarez-Mutis, M., Vélez-Tobón, G., Tobón Castaño, A., Machado, R.L.D., Marinho, C.R.F., Nolder, D., Nosten, F., Sutherland, C.J., Campino, S., Clark, T.G., 2024. Genomic analysis of global Plasmodium vivax populations reveals insights into the evolution of drug resistance. Nat Commun 15, 10771. https://doi.org/10.1038/s41467-024-54964-x

Nicolle, C., Manceaux, L., 1908. Sur une infection à corps de Leishman (ou organismes voisins) du gondi. Comptes Rendus Hebdomadaires des Séances de l'Académie des Sciences 147, 763–766.

Nicolle, C., Manceaux, L.H., 2009. On a Leishman body infection (or related organisms) of the gondi. International Journal for Parasitology 39, 863–864. https://doi.org/10.1016/j.ijpara.2009.02.001

Nimmanon, T., Ziliotto, S., Morris, S., Flanagan, L., Taylor, K.M., 2017. Phosphorylation of zinc channel ZIP7 drives MAPK, PI3K and mTOR growth and proliferation signalling. Metallomics 9, 471–481. https://doi.org/10.1039/C6MT00286B

Nolan, S.J., Romano, J.D., Coppens, I., 2017. Host lipid droplets: An important source of lipids salvaged by the intracellular parasite Toxoplasma gondii. PLoS Pathog 13, e1006362. https://doi.org/10.1371/journal.ppat.1006362

Notredame, C., Higgins, D.G., Heringa, J., 2000. T-coffee: a novel method for fast and accurate multiple sequence alignment 1 1Edited by J. Thornton. Journal of Molecular Biology 302, 205–217. https://doi.org/10.1006/jmbi.2000.4042

Ochoa Tufiño, V., Almira Casellas, M., van Duynhoven, A., Flis, P., Salt, D.E., Schat, H., Aarts, M.G.M., 2025. Arabidopsis thaliana Zn transporter genes ZIP3 and ZIP5 provide the main Zn uptake route and act redundantly to face Zn deficiency. Plant J 121, e17251. https://doi.org/10.1111/tpj.17251

Ohashi, W., Kimura, S., Iwanaga, T., Furusawa, Y., Irié, T., Izumi, H., Watanabe, T., Hijikata, A., Hara, T., Ohara, O., Koseki, H., Sato, T., Robine, S., Mori, H., Hattori, Y., Watarai, H., Mishima, K., Ohno, H., Hase, K., Fukada, T., 2016. Zinc Transporter SLC39A7/ZIP7 Promotes Intestinal Epithelial Self-Renewal by Resolving ER Stress. PLoS Genet 12, e1006349. https://doi.org/10.1371/journal.pgen.1006349

Ohgami, R.S., Campagna, D.R., Greer, E.L., Antiochos, B., McDonald, A., Chen, J., Sharp, J.J., Fujiwara, Y., Barker, J.E., Fleming, M.D., 2005. Identification of a ferrireductase required for efficient transferrin-dependent iron uptake in erythroid cells. Nat Genet 37, 1264–1269. https://doi.org/10.1038/ng1658

Olea-Flores, M., Kan, J., Carlson, A., Syed, S.A., McCann, C., Mondal, V., Szady, C., Ricker, H.M., McQueen, A., Navea, J.G., Caromile, L.A., Padilla-Benavides, T., 2022. ZIP11 Regulates Nuclear Zinc Homeostasis in HeLa Cells and Is Required for Proliferation and Establishment of the Carcinogenic Phenotype. Front. Cell Dev. Biol. 10, 895433. https://doi.org/10.3389/fcell.2022.895433

Ortiz, J.F., Millhouse, P.W., Morillo Cox, Á., Campoverde, L., Kaur, A., Wirth, M., Atoot, A., 2020. Babesiosis: Appreciating the Pathophysiology and Diverse Sequela of the Infection. Cureus 12, e11085. https://doi.org/10.7759/cureus.11085

Pamukcu, S., Cerutti, A., Bordat, Y., Hem, S., Rofidal, V., Besteiro, S., 2021. Differential contribution of two organelles of endosymbiotic origin to iron-sulfur cluster synthesis and overall fitness in Toxoplasma. PLoS Pathog 17, e1010096. https://doi.org/10.1371/journal.ppat.1010096

Pan, X., Tamilselvam, B., Hansen, E.J., Daefler, S., 2010. Modulation of iron homeostasis in macrophages by bacterial intracellular pathogens. BMC Microbiol 10, 64. https://doi.org/10.1186/1471-2180-10-64

Pandey, S., Kant, S., Khawary, M., Tripathi, D., 2022. Macrophages in Microbial Pathogenesis: Commonalities of Defense Evasion Mechanisms. Infect Immun 90, e00291-21. https://doi.org/10.1128/iai.00291-21

Pang, C., Chai, J., Zhu, P., Shanklin, J., Liu, Q., 2023. Structural mechanism of intracellular autoregulation of zinc uptake in ZIP transporters. Nat Commun 14, 3404. https://doi.org/10.1038/s41467-023-39010-6

Pantopoulos, K., 2004. Iron Metabolism and the IRE/IRP Regulatory System: An Update. Annals of the New York Academy of Sciences 1012, 1–13. https://doi.org/10.1196/annals.1306.001

Pappas, G., Roussos, N., Falagas, M.E., 2009. Toxoplasmosis snapshots: Global status of Toxoplasma gondii seroprevalence and implications for pregnancy and congenital toxoplasmosis. International Journal for Parasitology 39, 1385–1394. https://doi.org/10.1016/j.ijpara.2009.04.003

Park, J., Hunter, C.A., 2020. The role of macrophages in protective and pathological responses to *Toxoplasma gondii*. Parasite Immunology 42, e12712. https://doi.org/10.1111/pim.12712

Parker, K.E.R., Fairweather, S.J., Rajendran, E., Blume, M., McConville, M.J., Bröer, S., Kirk, K., Van Dooren, G.G., 2019. The tyrosine transporter of Toxoplasma gondii is a member of the newly defined apicomplexan amino acid transporter (ApiAT) family. PLoS Pathog 15, e1007577. https://doi.org/10.1371/journal.ppat.1007577

Parussini, F., Coppens, I., Shah, P.P., Diamond, S.L., Carruthers, V.B., 2010. Cathepsin L occupies a vacuolar compartment and is a protein maturase within the endo/exocytic system of Toxoplasma gondii: Cathepsin L in a vacuolar compartment. Molecular Microbiology 76, 1340–1357. https://doi.org/10.1111/j.1365-2958.2010.07181.x

Patel, S.J., Protchenko, O., Shakoury-Elizeh, M., Baratz, E., Jadhav, S., Philpott, C.C., 2021. The iron chaperone and nucleic acid–binding activities of poly(rC)-binding protein 1 are separable and independently essential. Proc. Natl. Acad. Sci. U.S.A. 118, e2104666118. https://doi.org/10.1073/pnas.2104666118

Paunesku, T., Gordon, A.C., White, S., Harris, K., Antipova, O., Maxey, E., Vogt, S., Smith, A., Daddario, L., Procissi, D., Larson, A., Woloschak, G.E., 2021. Use of X-Ray Fluorescence Microscopy for Studies on Research Models of Hepatocellular Carcinoma. Front. Public Health 9, 711506. https://doi.org/10.3389/fpubh.2021.711506

Peters, M.L., Shukla, A., Gotthold, Z.A., McCormick, D.M., Xiang, K., Bartel, D.P., Lourido, S., 2025. 5′ untranslated regions tune *Toxoplasma* translation. https://doi.org/10.1101/2025.07.14.664749

Pfaffl, M.W., 2001. A new mathematical model for relative quantification in real-time RT-PCR. Nucleic Acids Res 29, e45. https://doi.org/10.1093/nar/29.9.e45

Pfefferkorn, E.R., 1984. Interferon gamma blocks the growth of Toxoplasma gondii in human fibroblasts by inducing the host cells to degrade tryptophan. Proc. Natl. Acad. Sci. U.S.A. 81, 908–912. https://doi.org/10.1073/pnas.81.3.908

Pfefferkorn, E.R., Rebhun, S., Eckel, M., 1986. Characterization of an Indoleamine 2,3-Dioxygenase Induced by Gamma-Interferon in Cultured Human Fibroblasts. Journal of Interferon Research 6, 267–279. https://doi.org/10.1089/jir.1986.6.267

Pinilla-Tenas, J.J., Sparkman, B.K., Shawki, A., Illing, A.C., Mitchell, C.J., Zhao, N., Liuzzi, J.P., Cousins, R.J., Knutson, M.D., Mackenzie, B., 2011. Zip14 is a complex broad-scope metal-ion transporter whose functional properties support roles in the cellular uptake of zinc and nontransferrin-bound iron.

Am J Physiol Cell Physiol 301, C862-871. https://doi.org/10.1152/ajpcell.00479.2010

Pinkerton, H., Weinman, D., 1944. TOXOPLASMA INFECTION IN MAN. Ann Intern Med 20, 832–836. https://doi.org/10.7326/0003-4819-20-5-832

Pinto-Ferreira, F., Caldart, E.T., Pasquali, A.K.S., Mitsuka-Breganó, R., Freire, R.L., Navarro, I.T., 2019. Patterns of Transmission and Sources of Infection in Outbreaks of Human Toxoplasmosis. Emerg. Infect. Dis. 25, 2177–2182. https://doi.org/10.3201/eid2512.181565

Plaza, J., Dámek, F., Villena, I., Innes, E.A., Katzer, F., Hamilton, C.M., 2020. Detection of Toxoplasma gondii in retail meat samples in Scotland. Food and Waterborne Parasitology 20, e00086. https://doi.org/10.1016/j.fawpar.2020.e00086

Plikus, M.V., Wang, X., Sinha, S., Forte, E., Thompson, S.M., Herzog, E.L., Driskell, R.R., Rosenthal, N., Biernaskie, J., Horsley, V., 2021. Fibroblasts: Origins, definitions, and functions in health and disease. Cell 184, 3852–3872. https://doi.org/10.1016/j.cell.2021.06.024

Plotkin, J.B., Kudla, G., 2011. Synonymous but not the same: the causes and consequences of codon bias. Nat Rev Genet 12, 32–42. https://doi.org/10.1038/nrg2899

Pocanschi, C.L., Ehsani, S., Mehrabian, M., Wille, H., Reginold, W., Trimble, W.S., Wang, H., Yee, A., Arrowsmith, C.H., Bozóky, Z., Kay, L.E., Forman-Kay, J.D., Rini, J.M., Schmitt-Ulms, G., 2013. The ZIP5 Ectodomain Co-Localizes with PrP and May Acquire a PrP-Like Fold That Assembles into a Dimer. PLoS ONE 8, e72446. https://doi.org/10.1371/journal.pone.0072446

Pollack, Y., Katzen, A.L., Spira, D.T., Golenser, J., 1982. The genome of Plasmodium falciparum. I: DNA base composition. Nucl Acids Res 10, 539–546. https://doi.org/10.1093/nar/10.2.539

Poncet, A.F., Blanchard, N., Marion, S., 2019. Toxoplasma and Dendritic Cells: An Intimate Relationship That Deserves Further Scrutiny. Trends in Parasitology 35, 870–886. https://doi.org/10.1016/j.pt.2019.08.001

Posey, J.E., Gherardini, F.C., 2000. Lack of a Role for Iron in the Lyme Disease Pathogen. Science 288, 1651–1653. https://doi.org/10.1126/science.288.5471.1651

Potocki, S., Valensin, D., Kozlowski, H., 2014. The specificity of interaction of Zn^{2+} , Ni^{2+} and Cu^{2+} ions with the histidine-rich domain of the TjZNT1 ZIP family transporter. Dalton Trans. 43, 10215–10223. https://doi.org/10.1039/C4DT00903G

Poulos, T.L., 2014. Heme Enzyme Structure and Function. Chem. Rev. 114, 3919–3962. https://doi.org/10.1021/cr400415k

Protchenko, O., Baratz, E., Jadhav, S., Li, F., Shakoury-Elizeh, M., Gavrilova, O., Ghosh, M.C., Cox, J.E., Maschek, J.A., Tyurin, V.A., Tyurina, Y.Y., Bayir, H., Aron, A.T., Chang, C.J., Kagan, V.E., Philpott, C.C., 2021. Iron Chaperone Poly rC Binding Protein 1 Protects Mouse Liver From Lipid Peroxidation and Steatosis. Hepatology 73, 1176–1193. https://doi.org/10.1002/hep.31328

Qian, Z.M., Tang, P.L., 1995. Mechanisms of iron uptake by mammalian cells. Biochimica et Biophysica Acta (BBA) - Molecular Cell Research 1269, 205–214. https://doi.org/10.1016/0167-4889(95)00098-X

Qian, Z.M., Tang, P.L., Wang, Q., 1997. Iron crosses the endosomal membrane by a carrier-mediated process. Progress in Biophysics and Molecular Biology 67, 1–15. https://doi.org/10.1016/S0079-6107(97)00009-6

Radke, J.B., Lucas, O., De Silva, E.K., Ma, Y., Sullivan, W.J., Weiss, L.M., Llinas, M., White, M.W., 2013. ApiAP2 transcription factor restricts development of the *Toxoplasma* tissue cyst. Proc. Natl. Acad. Sci. U.S.A. 110, 6871–6876. https://doi.org/10.1073/pnas.1300059110

Rajapakse, D., Curtis, T., Chen, M., Xu, H., 2017. Zinc Protects Oxidative Stress-Induced RPE Death by Reducing Mitochondrial Damage and Preventing Lysosome Rupture. Oxidative Medicine and Cellular Longevity 2017, 6926485. https://doi.org/10.1155/2017/6926485

Rajapakse, S., Chrishan Shivanthan, M., Samaranayake, N., Rodrigo, C., Deepika Fernando, S., 2013. Antibiotics for human toxoplasmosis: a systematic review of randomized trials. Pathogens and Global Health 107, 162–169. https://doi.org/10.1179/2047773213Y.0000000094

Rajendran, E., Clark, M., Goulart, C., Steinhöfel, B., Tjhin, E.T., Gross, S., Smith, N.C., Kirk, K., Van Dooren, G.G., 2021. Substrate-mediated regulation of the arginine transporter of Toxoplasma gondii. PLoS Pathog 17, e1009816. https://doi.org/10.1371/journal.ppat.1009816

Raventos-Suarez, C., Pollack, S., Nagel, R.L., 1982. Plasmodium Falciparum: Inhibition of in Vitro Growth by Desferrioxamine. The American Journal of Tropical Medicine and Hygiene 31, 919–922. https://doi.org/10.4269/ajtmh.1982.31.919

Recalcati, S., Cairo, G., 2021. Macrophages and Iron: A Special Relationship. Biomedicines 9, 1585. https://doi.org/10.3390/biomedicines9111585

Remington, J.S., 1974. Toxoplasmosis in the adult. Bull N Y Acad Med 50, 211–227.

Renaud, E.A., Maupin, A.J.M., Besteiro, S., 2025. Iron-sulfur cluster biogenesis and function in Apicomplexa parasites. Biochimica et Biophysica Acta (BBA) - Molecular Cell Research 1872, 119876. https://doi.org/10.1016/j.bbamcr.2024.119876

Renaud, E.A., Maupin, A.J.M., Bordat, Y., Graindorge, A., Berry, L., Besteiro, S., 2024. Iron depletion has different consequences on the growth and survival of *Toxoplasma gondii* strains. Virulence 15, 2329566. https://doi.org/10.1080/21505594.2024.2329566

Renaud, E.A., Pamukcu, S., Cerutti, A., Berry, L., Lemaire-Vieille, C., Yamaryo-Botté, Y., Botté, C.Y., Besteiro, S., 2022. Disrupting the plastidic iron-sulfur cluster biogenesis pathway in Toxoplasma gondii has pleiotropic effects irreversibly impacting parasite viability. Journal of Biological Chemistry 298, 102243. https://doi.org/10.1016/j.jbc.2022.102243

Richardson, D.R., Ponka, P., 1997. The molecular mechanisms of the metabolism and transport of iron in normal and neoplastic cells. Biochimica et Biophysica Acta (BBA) - Reviews on Biomembranes 1331, 1–40. https://doi.org/10.1016/S0304-4157(96)00014-7

Riley, L.G., Cowley, M.J., Gayevskiy, V., Roscioli, T., Thorburn, D.R., Prelog, K., Bahlo, M., Sue, C.M., Balasubramaniam, S., Christodoulou, J., 2017. A *SLC39A8* variant causes manganese deficiency, and glycosylation and mitochondrial disorders. J of Inher Metab Disea 40, 261–269. https://doi.org/10.1007/s10545-016-0010-6

Rivera-Cuevas, Y., Mayoral, J., Di Cristina, M., Lawrence, A.-L.E., Olafsson, E.B., Patel, R.K., Thornhill, D., Waldman, B.S., Ono, A., Sexton, J.Z., Lourido, S., Weiss, L.M., Carruthers, V.B., 2021. Toxoplasma gondii exploits the host ESCRT machinery for parasite uptake of host cytosolic proteins. PLoS Pathog 17, e1010138. https://doi.org/10.1371/journal.ppat.1010138

Robe, K., Lefebvre-Legendre, L., Cleard, F., Barberon, M., 2025. Four ZIPs contribute to Zn, Fe, Cu and Mn acquisition at the outer root domain. PLoS Genet 21, e1011796. https://doi.org/10.1371/journal.pgen.1011796

Robert-Gangneux, F., Dardé, M.-L., 2012. Epidemiology of and Diagnostic Strategies for Toxoplasmosis. Clin Microbiol Rev 25, 264–296. https://doi.org/10.1128/CMR.05013-11

Rogers, E.E., Eide, D.J., Guerinot, M.L., 2000. Altered selectivity in an *Arabidopsis* metal transporter. Proc. Natl. Acad. Sci. U.S.A. 97, 12356–12360. https://doi.org/10.1073/pnas.210214197

Romana-Souza, B., Chen, L., Leonardo, T.R., Chen, Z., DiPietro, L.A., 2021. Dermal fibroblast phagocytosis of apoptotic cells: A novel pathway for wound resolution. The FASEB Journal 35, e21443. https://doi.org/10.1096/fj.202002078R

Romano, J.D., Mayoral, J., Guevara, R.B., Rivera-Cuevas, Y., Carruthers, V.B., Weiss, L.M., Coppens, I., 2023. *Toxoplasma gondii* scavenges mammalian host organelles through the usurpation of host ESCRT-III and Vps4A. Journal of Cell Science 136, jcs260159. https://doi.org/10.1242/jcs.260159

Romano, J.D., Nolan, S.J., Porter, C., Ehrenman, K., Hartman, E.J., Hsia, R., Coppens, I., 2017. The parasite *Toxoplasma* sequesters diverse Rab host vesicles within an intravacuolar network. Journal of Cell Biology 216, 4235–4254. https://doi.org/10.1083/jcb.201701108

Roos, D.S., 1999. The Apicoplast as a Potential Therapeutic Target in Toxoplasma and Other Apicomplexan Parasites: Some Additional Thoughts. Parasitology Today 15, 41. https://doi.org/10.1016/S0169-4758(98)01367-2

Rosenzweig, A.C., 2002. Metallochaperones. Chemistry & Biology 9, 673–677. https://doi.org/10.1016/S1074-5521(02)00156-4

Rosenzweig, A.C., Argüello, J.M., 2012. Toward a molecular understanding of metal transport by P(1B)-type ATPases. Curr Top Membr 69, 113–136. https://doi.org/10.1016/B978-0-12-394390-3.00005-7

Rouault, T.A., 2006. The role of iron regulatory proteins in mammalian iron homeostasis and disease. Nat Chem Biol 2, 406–414. https://doi.org/10.1038/nchembio807

Ruggiero, M.A., Gordon, D.P., Orrell, T.M., Bailly, N., Bourgoin, T., Brusca, R.C., Cavalier-Smith, T., Guiry, M.D., Kirk, P.M., 2015. A higher level classification of all living organisms. PLoS One 10, e0119248. https://doi.org/10.1371/journal.pone.0119248

Sabine, D.B., Vaselekos, J., 1967. Trace Element Requirements of Lactobacillus acidophilus. Nature 214, 520–520. https://doi.org/10.1038/214520a0

Sabri, M., Houle, S., Dozois, C.M., 2009. Roles of the Extraintestinal Pathogenic *Escherichia coli* ZnuACB and ZupT Zinc Transporters during Urinary Tract Infection. Infect Immun 77, 1155–1164. https://doi.org/10.1128/IAI.01082-08

Sadée, W., Drübbisch, V., Amidon, G.L., 1995. Biology of Membrane Transport Proteins. Pharm Res 12, 1823–1837. https://doi.org/10.1023/A:1016211015926

Sahu, T., Boisson, B., Lacroix, C., Bischoff, E., Richier, Q., Formaglio, P., Thiberge, S., Dobrescu, I., Ménard, R., Baldacci, P., 2014. ZIPCO , a putative metal ion transporter, is crucial for *Plasmodium* liver-stage development. EMBO Mol Med 6, 1387–1397. https://doi.org/10.15252/emmm.201403868

Sanchez, M., Galy, B., Schwanhaeusser, B., Blake, J., Bähr-Ivacevic, T., Benes, V., Selbach, M., Muckenthaler, M.U., Hentze, M.W., 2011. Iron regulatory protein-1 and -2: transcriptome-wide definition of binding mRNAs and shaping of the cellular proteome by iron regulatory proteins. Blood 118, e168–e179. https://doi.org/10.1182/blood-2011-04-343541

Sanchez, S.G., Pouzet, E., Guimbaud, L., Graindorge, A., Berry, L., Besteiro, S., 2025. TgGloL is an atypical glyoxalase/VOC domain-containing apicoplast protein that is important for the growth of *Toxoplasma*. MBoC 36, ar32. https://doi.org/10.1091/mbc.E24-09-0391

Santana-Codina, N., Mancias, J.D., 2018. The Role of NCOA4-Mediated Ferritinophagy in Health and Disease. Pharmaceuticals (Basel) 11, 114. https://doi.org/10.3390/ph11040114

Sayers, C.P., Mollard, V., Buchanan, H.D., McFadden, G.I., Goodman, C.D., 2018. A genetic screen in rodent malaria parasites identifies five new apicoplast putative membrane transporters, one of which is essential in human malaria parasites. Cellular Microbiology 20. https://doi.org/10.1111/cmi.12789

Schaefer-Ramadan, S., Barlog, M., Roach, J., Al-Hashimi, M., Bazzi, H.S., Machaca, K., 2019. Synthesis of TPEN variants to improve cancer cells selective killing capacity. Bioorganic Chemistry 87, 366–372. https://doi.org/10.1016/j.bioorg.2019.03.045

Schindelin, J., Arganda-Carreras, I., Frise, E., Kaynig, V., Longair, M., Pietzsch, T., Preibisch, S., Rueden, C., Saalfeld, S., Schmid, B., Tinevez, J.-Y., White, D.J., Hartenstein, V., Eliceiri, K., Tomancak, P., Cardona, A., 2012. Fiji: an open-source platform for biological-image analysis. Nat Methods 9, 676–682. https://doi.org/10.1038/nmeth.2019

Schlüter, D., Däubener, W., Schares, G., Groß, U., Pleyer, U., Lüder, C., 2014. Animals are key to human toxoplasmosis. International Journal of Medical Microbiology 304, 917–929. https://doi.org/10.1016/j.ijmm.2014.09.002

Schmidt, I.H.E., Gildhorn, C., Böning, M.A.L., Kulow, V.A., Steinmetz, I., Bast, A., 2018. Burkholderia pseudomallei modulates host iron homeostasis to facilitate iron availability and intracellular survival. PLoS Negl Trop Dis 12, e0006096. https://doi.org/10.1371/journal.pntd.0006096

Schneider, C., Owen, M.J., Banville, D., Williams, J.G., 1984. Primary structure of human transferrin receptor deduced from the mRNA sequence. Nature 311, 675–678. https://doi.org/10.1038/311675b0

Schoondermark-Van De Ven, E., Melchers, W., Camps, W., Eskes, T., Meuwissen, J., Galama, J., 1994. Effectiveness of spiramycin for treatment of congenital Toxoplasma gondii infection in rhesus monkeys. Antimicrob Agents Chemother 38, 1930–1936. https://doi.org/10.1128/AAC.38.9.1930

Schröder, N., Schmidtmann, M., Christoffers, J., 2021. Diaminoterephthalate-EDTA and -EGTA Conjugates – "Turn on" Fluorescence Sensors for Zinc Ions. Eur J Org Chem 2021, 4260–4268. https://doi.org/10.1002/ejoc.202100641

Schwab, J.C., Beckers, C.J., Joiner, K.A., 1994. The parasitophorous vacuole membrane surrounding intracellular Toxoplasma gondii functions as a molecular sieve. Proc. Natl. Acad. Sci. U.S.A. 91, 509–513. https://doi.org/10.1073/pnas.91.2.509

Seeber, F., Limenitakis, J., Soldati-Favre, D., 2008. Apicomplexan mitochondrial metabolism: a story of gains, losses and retentions. Trends in Parasitology 24, 468–478. https://doi.org/10.1016/j.pt.2008.07.004

Seeber, F., Soldati-Favre, D., 2010. Metabolic Pathways in the Apicoplast of Apicomplexa, in: International Review of Cell and Molecular Biology. Elsevier, pp. 161–228. https://doi.org/10.1016/S1937-6448(10)81005-6

Segura, M., Madrid, Y., Cámara, C., 2003. Elimination of calcium and argon interferences in iron determination by ICP-MS using desferrioxamine chelating agent immobilized in sol–gel and cold plasma conditions. J. Anal. At. Spectrom. 18, 1103–1108. https://doi.org/10.1039/B301719M

Semenovskaya, K., Lévêque, M.F., Berry, L., Bordat, Y., Dubremetz, J., Lebrun, M., Besteiro, S., 2020. TgZFP2 is a novel zinc finger protein involved in coordinating mitosis and budding in *Toxoplasma*. Cellular Microbiology 22. https://doi.org/10.1111/cmi.13120

Sen, S., Bal, S.K., Yadav, S., Mishra, P., G, V.V., Rastogi, R., Mukhopadhyay, C.K., 2022. Intracellular pathogen Leishmania intervenes in iron loading into ferritin by cleaving chaperones in host macrophages as an iron acquisition strategy. Journal of Biological Chemistry 298, 102646. https://doi.org/10.1016/j.jbc.2022.102646

Shapiro, K., Bahia-Oliveira, L., Dixon, B., Dumètre, A., de Wit, L.A., VanWormer, E., Villena, I., 2019. Environmental transmission of Toxoplasma gondii: Oocysts in water, soil and food. Food Waterborne Parasitol 15, e00049. https://doi.org/10.1016/j.fawpar.2019.e00049

Sharma, G., Merz, K.M., 2021. Formation of the Metal-Binding Core of the ZRT/IRT-like Protein (ZIP) Family Zinc Transporter. Biochemistry 60, 2727–2738. https://doi.org/10.1021/acs.biochem.1c00415

Sharma, S., Schiller, M.R., 2019. The carboxy-terminus, a key regulator of protein function. Critical Reviews in Biochemistry and Molecular Biology 54, 85–102. https://doi.org/10.1080/10409238.2019.1586828

Sharman, P.A., Smith, N.C., Wallach, M.G., Katrib, M., 2010. Chasing the golden egg: vaccination against poultry coccidiosis. Parasite Immunology 32, 590–598. https://doi.org/10.1111/j.1365-3024.2010.01209.x

Shaw, G.C., Cope, J.J., Li, L., Corson, K., Hersey, C., Ackermann, G.E., Gwynn, B., Lambert, A.J., Wingert, R.A., Traver, D., Trede, N.S., Barut, B.A., Zhou, Y., Minet, E., Donovan, A., Brownlie, A., Balzan, R., Weiss, M.J., Peters, L.L., Kaplan, J., Zon, L.I., Paw, B.H., 2006. Mitoferrin is essential for erythroid iron assimilation. Nature 440, 96–100. https://doi.org/10.1038/nature04512

Sheiner, L., Demerly, J.L., Poulsen, N., Beatty, W.L., Lucas, O., Behnke, M.S., White, M.W., Striepen, B., 2011a. A Systematic Screen to Discover and Analyze Apicoplast Proteins Identifies a Conserved and Essential Protein Import Factor. PLoS Pathog 7, e1002392. https://doi.org/10.1371/journal.ppat.1002392

Sheiner, L., Demerly, J.L., Poulsen, N., Beatty, W.L., Lucas, O., Behnke, M.S., White, M.W., Striepen, B., 2011b. A Systematic Screen to Discover and Analyze Apicoplast Proteins Identifies a Conserved and Essential Protein Import Factor. PLoS Pathog 7, e1002392. https://doi.org/10.1371/journal.ppat.1002392

Sheline, C.T., Behrens, M.M., Choi, D.W., 2000. Zinc-Induced Cortical Neuronal Death: Contribution of Energy Failure Attributable to Loss of NAD^+ and Inhibition of Glycolysis. J. Neurosci. 20, 3139–3146. https://doi.org/10.1523/JNEUROSCI.20-09-03139.2000

Shen, B., Brown, K.M., Lee, T.D., Sibley, L.D., 2014. Efficient Gene Disruption in Diverse Strains of Toxoplasma gondii Using CRISPR/CAS9. mBio 5, e01114-14. https://doi.org/10.1128/mBio.01114-14

Shi, H., Bencze, K.Z., Stemmler, T.L., Philpott, C.C., 2008. A Cytosolic Iron Chaperone That Delivers Iron to Ferritin. Science 320, 1207–1210. https://doi.org/10.1126/science.1157643

Shrivastava, D., Jha, A., Kabrambam, R., Vishwakarma, J., Mitra, K., Ramachandran, R., Habib, S., 2024. *Plasmodium falciparum* ZIP1 Is a Zinc-Selective Transporter with Stage-Dependent Targeting to the Apicoplast and Plasma Membrane in Erythrocytic Parasites. ACS Infect. Dis. 10, 155–169. https://doi.org/10.1021/acsinfecdis.3c00426

Sibley, L.D., Khan, A., Ajioka, J.W., Rosenthal, B.M., 2009. Genetic diversity of *Toxoplasma gondii* in animals and humans. Phil. Trans. R. Soc. B 364, 2749–2761. https://doi.org/10.1098/rstb.2009.0087

Sidik, S.M., Hackett, C.G., Tran, F., Westwood, N.J., Lourido, S., 2014. Efficient Genome Engineering of Toxoplasma gondii Using CRISPR/Cas9. PLoS ONE 9, e100450. https://doi.org/10.1371/journal.pone.0100450

Sidik, S.M., Huet, D., Ganesan, S.M., Huynh, M.-H., Wang, T., Nasamu, A.S., Thiru, P., Saeij, J.P.J., Carruthers, V.B., Niles, J.C., Lourido, S., 2016. A Genome-wide CRISPR Screen in Toxoplasma Identifies Essential Apicomplexan Genes. Cell 166, 1423-1435.e12. https://doi.org/10.1016/j.cell.2016.08.019

Siegert, I., Schödel, J., Nairz, M., Schatz, V., Dettmer, K., Dick, C., Kalucka, J., Franke, K., Ehrenschwender, M., Schley, G., Beneke, A., Sutter, J., Moll, M., Hellerbrand, C., Wielockx, B., Katschinski, D.M., Lang, R., Galy, B., Hentze, M.W., Koivunen, P., Oefner, P.J., Bogdan, C., Weiss, G., Willam, C., Jantsch, J., 2015. Ferritin-Mediated Iron Sequestration Stabilizes Hypoxia-Inducible Factor-1α upon LPS Activation in the Presence of Ample Oxygen. Cell Reports 13, 2048–2055. https://doi.org/10.1016/j.celrep.2015.11.005

Sigala, P.A., Goldberg, D.E., 2014. The Peculiarities and Paradoxes of *Plasmodium* Heme Metabolism. Annu. Rev. Microbiol. 68, 259–278. https://doi.org/10.1146/annurev-micro-091313-103537

Silva, M.D., Teixeira, C., Gomes, P., Borges, M., 2021. Promising Drug Targets and Compounds with Anti-Toxoplasma gondii Activity. Microorganisms 9, 1960. https://doi.org/10.3390/microorganisms9091960

Silva, M.F., Douglas, K., Sandalli, S., Maclean, A.E., Sheiner, L., 2023. Functional and biochemical characterization of the Toxoplasma gondii succinate dehydrogenase complex. PLoS Pathog 19, e1011867. https://doi.org/10.1371/journal.ppat.1011867

Singer, M., Simon, K., Forné, I., Meissner, M., 2023. A central CRMP complex essential for invasion in Toxoplasma gondii. PLoS Biol 21, e3001937. https://doi.org/10.1371/journal.pbio.3001937

Skuza, L., Szućko-Kociuba, I., Filip, E., Bożek, I., 2022. Natural Molecular Mechanisms of Plant Hyperaccumulation and Hypertolerance towards Heavy Metals. IJMS 23, 9335. https://doi.org/10.3390/ijms23169335

Slepchenko, K.G., Lu, Q., Li, Y.V., 2017. Cross talk between increased intracellular zinc (Zn^{2+}) and accumulation of reactive oxygen species in chemical ischemia. American Journal of Physiology-Cell Physiology 313, C448–C459. https://doi.org/10.1152/ajpcell.00048.2017

Sloan, M.A., Scott, A., Aghabi, D., Mrvova, L., Harding, C.R., 2025a. Iron-mediated post-transcriptional regulation in Toxoplasma gondii. PLoS Pathog 21, e1012857. https://doi.org/10.1371/journal.ppat.1012857

Sloan, M.A., Scott, A., Aghabi, D., Mrvova, L., Harding, C.R., 2025b. Iron-mediated post-transcriptional regulation in Toxoplasma gondii. PLOS Pathogens 21, e1012857. https://doi.org/10.1371/journal.ppat.1012857

Soares, M.P., Hamza, I., 2016. Macrophages and Iron Metabolism. Immunity 44, 492–504. https://doi.org/10.1016/j.immuni.2016.02.016

Soe-Lin, S., Buss, J.L., Tang, E., Ponka, P., 2006. Calcein and the Labile Iron Pool. Blood 108, 1546–1546. https://doi.org/10.1182/blood.V108.11.1546.1546

Soete, M., Camus, D., Dubrametz, J.F., 1994. Experimental Induction of Bradyzoite-Specific Antigen Expression and Cyst Formation by the RH Strain of Toxoplasma gondii in Vitro. Experimental Parasitology 78, 361–370. https://doi.org/10.1006/expr.1994.1039

Soete, M., Fortier, B., Camus, D., Dubremetz, J.F., 1993. Toxoplasma gondii : Kinetics of Bradyzoite-Tachyzoite Interconversion in vitro. Experimental Parasitology 76, 259–264. https://doi.org/10.1006/expr.1993.1031

Soldati, D., Boothroyd, J.C., 1995. A selector of transcription initiation in the protozoan parasite Toxoplasma gondii. Mol Cell Biol 15, 87–93. https://doi.org/10.1128/MCB.15.1.87

Solé, V.A., Papillon, E., Cotte, M., Walter, Ph., Susini, J., 2007. A multiplatform code for the analysis of energy-dispersive X-ray fluorescence spectra. Spectrochimica Acta Part B: Atomic Spectroscopy 62, 63–68. https://doi.org/10.1016/j.sab.2006.12.002

Soleymani, E., Faizi, F., Heidarimoghadam, R., Davoodi, L., Mohammadi, Y., 2020. Association of T. gondii infection with suicide: a systematic review and meta-analysis. BMC Public Health 20, 766. https://doi.org/10.1186/s12889-020-08898-w

Solioz, M., Vulpe, C., 1996. CPx-type ATPases: a class of P-type ATPases that pump heavy metals. Trends in Biochemical Sciences 21, 237–241. https://doi.org/10.1016/S0968-0004(96)20016-7

Song, X., Yang, X., Ying, Z., Wu, K., Liu, J., Liu, Q., 2023. Regulation of Mitochondrial Energy Metabolism by Glutaredoxin 5 in the Apicomplexan Parasite Neospora caninum. Microbiol Spectr 11, e03091-22. https://doi.org/10.1128/spectrum.03091-22

Sorour, M.H., Hani, H.A., Shaalan, H.F., El-Sayed, M.M.H., 2016. Experimental screening of some chelating agents for calcium and magnesium removal from saline solutions. Desalination and Water Treatment 57, 22799–22808. https://doi.org/10.1080/19443994.2015.1111595

Splendore, A., 1908. Un nuovo protozoa parassita deconigli incontrato nelle lesioni anatomiche d'une malattia che ricorda in molti punti il Kala-azar dell'uoma. Nota preliminare pel. Nota preliminare pel Rev Soc Sci Sao Paulo, 109–112.

Stasic, A.J., Chasen, N.M., Dykes, E.J., Vella, S.A., Asady, B., Starai, V.J., Moreno, S.N.J., 2019. The Toxoplasma Vacuolar H+-ATPase Regulates Intracellular pH and Impacts the Maturation of Essential Secretory Proteins. Cell Reports 27, 2132-2146.e7. https://doi.org/10.1016/j.celrep.2019.04.038

Stasic, A.J., Moreno, S.N.J., Carruthers, V.B., Dou, Z., 2022. The *Toxoplasma* plant-like vacuolar compartment (PLVAC). J Eukaryotic Microbiology 69, e12951. https://doi.org/10.1111/jeu.12951

Stelzer, S., Basso, W., Benavides Silván, J., Ortega-Mora, L.M., Maksimov, P., Gethmann, J., Conraths, F.J., Schares, G., 2019. Toxoplasma gondii infection and toxoplasmosis in farm animals: Risk factors and economic impact. Food and Waterborne Parasitology 15, e00037. https://doi.org/10.1016/j.fawpar.2019.e00037

Steverding, D., Stierhof, Y.D., Fuchs, H., Tauber, R., Overath, P., 1995. Transferrin-binding protein complex is the receptor for transferrin uptake in Trypanosoma brucei. The Journal of cell biology 131, 1173–1182. https://doi.org/10.1083/jcb.131.5.1173

Stillwell, W., 2016. Membrane Transport, in: An Introduction to Biological Membranes. Elsevier, pp. 423–451. https://doi.org/10.1016/B978-0-444-63772-7.00019-1

Stork, C.J., Li, Y.V., 2016. Elevated Cytoplasmic Free Zinc and Increased Reactive Oxygen Species Generation in the Context of Brain Injury, in: Applegate, R.L., Chen, G., Feng, H., Zhang, J.H. (Eds.), Brain Edema XVI, Acta Neurochirurgica Supplement. Springer International Publishing, Cham, pp. 347–353. https://doi.org/10.1007/978-3-319-18497-5_60

Striepen, B., 2013. Parasitic infections: Time to tackle cryptosporidiosis. Nature 503, 189–191. https://doi.org/10.1038/503189a

Striepen, B., 2011. The apicoplast: a red alga in human parasites. Essays in Biochemistry 51, 111–125. https://doi.org/10.1042/bse0510111

Su, C., Evans, D., Cole, R.H., Kissinger, J.C., Ajioka, J.W., Sibley, L.D., 2003. Recent Expansion of *Toxoplasma* Through Enhanced Oral Transmission. Science 299, 414–416. https://doi.org/10.1126/science.1078035

Su, Y., Gao, J., Kaur, P., Wang, Z., 2020. Neutrophils and Macrophages as Targets for Development of Nanotherapeutics in Inflammatory Diseases. Pharmaceutics 12, 1222. https://doi.org/10.3390/pharmaceutics12121222

Suárez-Quintana, C., Navarro-Padilla, M., Chorostecki, U., Sanchez, M., 2025. SIREs 3.0, an improved RNA prediction tool for iron-responsive elements. Nucleic Acids Research 53, W520–W527. https://doi.org/10.1093/nar/gkaf390

Sullivan, W.J., Jeffers, V., 2012. Mechanisms of *Toxoplasma gondii* persistence and latency. FEMS Microbiol Rev 36, 717–733. https://doi.org/10.1111/j.1574-6976.2011.00305.x

Suzuki, Y., Orellana, M.A., Schreiber, R.D., Remington, J.S., 1988. Interferon-γ: the Major Mediator of Resistance Against *Toxoplasma gondii*. Science 240, 516–518. https://doi.org/10.1126/science.3128869

Tabuchi, M., Tanaka, N., Nishida-Kitayama, J., Ohno, H., Kishi, F., 2002. Alternative Splicing Regulates the Subcellular Localization of Divalent Metal Transporter 1 Isoforms. MBoC 13, 4371–4387. https://doi.org/10.1091/mbc.e02-03-0165

Tabuchi, M., Yoshimori, T., Yamaguchi, K., Yoshida, T., Kishi, F., 2000. Human NRAMP2/DMT1, Which Mediates Iron Transport across Endosomal Membranes, Is Localized to Late Endosomes and Lysosomes in HEp-2 Cells. Journal of Biological Chemistry 275, 22220–22228. https://doi.org/10.1074/jbc.M001478200

Takács, A.C., Swierzy, I.J., Lüder, C.G.K., 2012. Interferon-γ Restricts Toxoplasma gondii Development in Murine Skeletal Muscle Cells via Nitric Oxide Production and Immunity-Related GTPases. PLoS ONE 7, e45440. https://doi.org/10.1371/journal.pone.0045440

Takagishi, T., Hara, T., Fukada, T., 2017. Recent Advances in the Role of SLC39A/ZIP Zinc Transporters In Vivo. IJMS 18, 2708. https://doi.org/10.3390/ijms18122708

Tanaka, T., Abe, Y., Kim, W.-S., Xuan, X., Nagasawa, H., Igarashi, I., Kumura, H., Shimazaki, K., 2003. The Detection of Bovine Lactoferrin Binding Protein on Toxoplasma gondii. J. Vet. Med. Sci. 65, 1377–1380. https://doi.org/10.1292/jvms.65.1377

Taniguchi, M., Fukunaka, A., Hagihara, M., Watanabe, K., Kamino, S., Kambe, T., Enomoto, S., Hiromura, M., 2013. Essential Role of the Zinc Transporter ZIP9/SLC39A9 in Regulating the Activations of Akt and Erk in B-Cell Receptor Signaling Pathway in DT40 Cells. PLoS ONE 8, e58022. https://doi.org/10.1371/journal.pone.0058022

Taylor, K.M., 2023. The LIV-1 Subfamily of Zinc Transporters: From Origins to Present Day Discoveries. IJMS 24, 1255. https://doi.org/10.3390/ijms24021255

Taylor, K.M., Hiscox, S., Nicholson, R.I., Hogstrand, C., Kille, P., 2012. Protein Kinase CK2 Triggers Cytosolic Zinc Signaling Pathways by Phosphorylation of Zinc Channel ZIP7. Sci. Signal. 5. https://doi.org/10.1126/scisignal.2002585

Taylor, K.M., Morgan, H.E., Johnson, A., Nicholson, R.I., 2005. Structure–function analysis of a novel member of the LIV-1 subfamily of zinc transporters, ZIP14. FEBS Letters 579, 427–432. https://doi.org/10.1016/j.febslet.2004.12.006

Taylor, K.M., Morgan, H.E., Johnson, A., Nicholson, R.I., 2004. Structure-function analysis of HKE4, a member of the new LIV-1 subfamily of zinc transporters. Biochemical Journal 377, 131–139. https://doi.org/10.1042/bj20031183

Taylor, K.M., Muraina, I.A., Brethour, D., Schmitt-Ulms, G., Nimmanon, T., Ziliotto, S., Kille, P., Hogstrand, C., 2016. Zinc transporter ZIP10 forms a heteromer with ZIP6 which regulates embryonic development and cell migration. Biochemical Journal 473, 2531–2544. https://doi.org/10.1042/BCJ20160388

Taylor, K.M., Nicholson, R.I., 2003. The LZT proteins; the LIV-1 subfamily of zinc transporters. Biochimica et Biophysica Acta (BBA) - Biomembranes 1611, 16–30. https://doi.org/10.1016/S0005-2736(03)00048-8

Taylor, S., Barragan, A., Su, C., Fux, B., Fentress, S.J., Tang, K., Beatty, W.L., Hajj, H.E., Jerome, M., Behnke, M.S., White, M., Wootton, J.C., Sibley, L.D., 2006. A Secreted Serine-Threonine Kinase Determines Virulence in the Eukaryotic Pathogen *Toxoplasma gondii*. Science 314, 1776–1780. https://doi.org/10.1126/science.1133643

Teh, M.R., Armitage, A.E., Drakesmith, H., 2024. Why cells need iron: a compendium of iron utilisation. Trends in Endocrinology & Metabolism 35, 1026–1049. https://doi.org/10.1016/j.tem.2024.04.015

Tenter, A.M., Heckeroth, A.R., Weiss, L.M., 2000. Toxoplasma gondii: from animals to humans. International Journal for Parasitology 30, 1217–1258. https://doi.org/10.1016/S0020-7519(00)00124-7

Theurl, I., Fritsche, G., Ludwiczek, S., Garimorth, K., Bellmann-Weiler, R., Weiss, G., 2005. The Macrophage: A Cellular Factory at the Interphase Between Iron and Immunity for the Control of Infections. Biometals 18, 359–367. https://doi.org/10.1007/s10534-005-3710-1

Thingholm, T.E., Rönnstrand, L., Rosenberg, P.A., 2020. Why and how to investigate the role of protein phosphorylation in ZIP and ZnT zinc

transporter activity and regulation. Cell. Mol. Life Sci. 77, 3085–3102. https://doi.org/10.1007/s00018-020-03473-3

Tjhin, E.T., Hayward, J.A., McFadden, G.I., Van Dooren, G.G., 2020. Characterization of the apicoplast-localized enzyme TgUroD in Toxoplasma gondii reveals a key role of the apicoplast in heme biosynthesis. Journal of Biological Chemistry 295, 1539–1550. https://doi.org/10.1074/jbc.RA119.011605

Tomavo, S., Boothroyd, J.C., 1995. Interconnection between organellar functions, development and drug resistance in the protozoan parasite, Toxoplasma gondii. International Journal for Parasitology 25, 1293–1299. https://doi.org/10.1016/0020-7519(95)00066-B

Tomita, T., Bzik, D.J., Ma, Y.F., Fox, B.A., Markillie, L.M., Taylor, R.C., Kim, K., Weiss, L.M., 2013. The Toxoplasma gondii Cyst Wall Protein CST1 Is Critical for Cyst Wall Integrity and Promotes Bradyzoite Persistence. PLoS Pathog 9, e1003823. https://doi.org/10.1371/journal.ppat.1003823

Torrey, E.F., Yolken, R.H., 2013. Toxoplasma oocysts as a public health problem. Trends in Parasitology 29, 380–384. https://doi.org/10.1016/j.pt.2013.06.001

Trager, W., Jenson, J.B., 1978. Cultivation of malarial parasites. Nature 273, 621–622. https://doi.org/10.1038/273621a0

Trees, A.J., Davison, H.C., Innes, E.A., Wastling, J.M., 1999. Towards evaluating the economic impact of bovine neosporosis. International Journal for Parasitology 29, 1195–1200. https://doi.org/10.1016/S0020-7519(99)00093-4

Tsuji, Y., 2020. Transmembrane protein western blotting: Impact of sample preparation on detection of SLC11A2 (DMT1) and SLC40A1 (ferroportin). PLoS ONE 15, e0235563. https://doi.org/10.1371/journal.pone.0235563

Turan, B., Billur, D., Tuncay, E., 2024. Toxic Effects of Intracellular Free Zinc Ion in Cardiomyocytes via Zinc-Transporters: Structural and Functional Changes in Mitochondria, in: Djuric, D.M., Agrawal, D.K. (Eds.), Environmental Factors in the Pathogenesis of Cardiovascular Diseases, Advances in Biochemistry in Health and Disease. Springer Nature Switzerland, Cham, pp. 259–281. https://doi.org/10.1007/978-3-031-62806-1_10

Ulahannan, N., Cutler, R., Doña-Termine, R., Simões-Pires, C.A., Wijetunga, N.A., Croken, M.M., Johnston, A.D., Kong, Y., Maqbool, S.B., Suzuki, M., Greally, J.M., 2022. Genomic insights into host and parasite interactions during intracellular infection by Toxoplasma gondii. PLoS ONE 17, e0275226. https://doi.org/10.1371/journal.pone.0275226

Ullah, I., Wang, Y., Eide, D.J., Dunwell, J.M., 2018. Evolution, and functional analysis of Natural Resistance-Associated Macrophage Proteins (NRAMPs) from Theobroma cacao and their role in cadmium accumulation. Sci Rep 8, 14412. https://doi.org/10.1038/s41598-018-32819-y

Unlu, G., Prizer, B., Erdal, R., Yeh, H.-W., Bayraktar, E.C., Birsoy, K., 2022. Metabolic-scale gene activation screens identify SLCO2B1 as a heme transporter that enhances cellular iron availability. Molecular Cell 82, 2832-2843.e7. https://doi.org/10.1016/j.molcel.2022.05.024

Vallochi, A.L., Muccioli, C., Martins, M.C., Silveira, C., Belfort, R., Rizzo, L.V., 2005. The genotype of Toxoplasma gondii strains causing ocular toxoplasmosis in humans in Brazil. American Journal of Ophthalmology 139, 350–351. https://doi.org/10.1016/j.ajo.2004.07.040

Van Dooren, G.G., Kennedy, A.T., McFadden, G.I., 2012. The Use and Abuse of Heme in Apicomplexan Parasites. Antioxidants & Redox Signaling 17, 634–656. https://doi.org/10.1089/ars.2012.4539

Van Dooren, G.G., McConville, M.J., 2025. Nutrient acquisition by intracellular parasitic protists. Cell Host & Microbe 33, 854–868. https://doi.org/10.1016/j.chom.2025.05.016

Van Dooren, G.G., Striepen, B., 2013. The Algal Past and Parasite Present of the Apicoplast. Annu. Rev. Microbiol. 67, 271–289. https://doi.org/10.1146/annurev-micro-092412-155741

Van Santen, S., De Mast, Q., Swinkels, D.W., Van Der Ven, A.J.A.M., 2013. The iron link between malaria and invasive non-typhoid Salmonella infections. Trends in Parasitology 29, 220–227. https://doi.org/10.1016/j.pt.2013.03.006

Varegg, M.S., Woolsey, I.D., Robertson, L.J., Jiménez-Meléndez, A., 2025. Rapid review: Recent advances in in vitro models for the study of Cryptosporidium parvum. Current Research in Parasitology & Vector-Borne Diseases 7, 100269. https://doi.org/10.1016/j.crpvbd.2025.100269

Vert, G., Briat, J., Curie, C., 2001. *Arabidopsis IRT2* gene encodes a root-periphery iron transporter. The Plant Journal 26, 181–189. https://doi.org/10.1046/j.1365-313x.2001.01018.x

Vert, G., Grotz, N., Dédaldéchamp, F., Gaymard, F., Guerinot, M.L., Briat, J.-F., Curie, C., 2002. IRT1, an Arabidopsis Transporter Essential for Iron Uptake from the Soil and for Plant Growth. Plant Cell 14, 1223–1233. https://doi.org/10.1105/tpc.001388

Victor, T.W., O'Toole, K.H., Easthon, L.M., Ge, M., Smith, R.J., Huang, X., Yan, H., Chu, Y.S., Chen, S., Gursoy, D., Ralle, M., Imperiali, B., Allen, K.N., Miller, L.M., 2020. Lanthanide-Binding Tags for 3D X-ray Imaging of Proteins in Cells at Nanoscale Resolution. J. Am. Chem. Soc. 142, 2145–2149. https://doi.org/10.1021/jacs.9b11571

Vieira, F.P., Alves, M. da G., Martins, L.M., Rangel, A.L.P., Dubey, J.P., Hill, D., Bahia-Oliveira, L.M.G., 2015. Waterborne toxoplasmosis investigated and analysed under hydrogeological assessment: new data and perspectives for further research. Mem Inst Oswaldo Cruz 110, 929–935. https://doi.org/10.1590/0074-02760150262

Voyiatzaki, C.S., Soteriadou, K.P., 1992. Identification and isolation of the Leishmania transferrin receptor. J Biol Chem 267, 9112–9117.

Voyiatzaki, C.S., Soteriadou, K.P., 1990. Evidence of transferrin binding sites on the surface of Leishmania promastigotes. J Biol Chem 265, 22380–22385.

Vyas, A., 2015. Mechanisms of Host Behavioral Change in Toxoplasma gondii Rodent Association. PLoS Pathog 11, e1004935. https://doi.org/10.1371/journal.ppat.1004935

Vyas, A., Kim, S.-K., Giacomini, N., Boothroyd, J.C., Sapolsky, R.M., 2007. Behavioral changes induced by *Toxoplasma* infection of rodents are highly specific to aversion of cat odors. Proc. Natl. Acad. Sci. U.S.A. 104, 6442–6447. https://doi.org/10.1073/pnas.0608310104

Waldman, B.S., Schwarz, D., Wadsworth, M.H., Saeij, J.P., Shalek, A.K., Lourido, S., 2020. Identification of a Master Regulator of Differentiation in Toxoplasma. Cell 180, 359-372.e16. https://doi.org/10.1016/j.cell.2019.12.013

Wallander, M.L., Leibold, E.A., Eisenstein, R.S., 2006. Molecular control of vertebrate iron homeostasis by iron regulatory proteins. Biochimica et

Biophysica Acta (BBA) - Molecular Cell Research 1763, 668–689. https://doi.org/10.1016/j.bbamcr.2006.05.004

Wallbank, B.A., Dominicus, C.S., Broncel, M., Legrave, N., Kelly, G., MacRae, J.I., Staines, H.M., Treeck, M., 2019. Characterisation of the *Toxoplasma gondii* tyrosine transporter and its phosphorylation by the calcium-dependent protein kinase 3. Molecular Microbiology 111, 1167–1181. https://doi.org/10.1111/mmi.14156

Wang, C., Xie, L., Xing, Y., Liu, M., Yang, J., Gao, N., Cai, Y., 2023. Iron-overload-induced ferroptosis in mouse cerebral toxoplasmosis promotes brain injury and could be inhibited by Deferiprone. PLoS Negl Trop Dis 17, e0011607. https://doi.org/10.1371/journal.pntd.0011607

Wang, C.-Y., Jenkitkasemwong, S., Duarte, S., Sparkman, B.K., Shawki, A., Mackenzie, B., Knutson, M.D., 2012. ZIP8 Is an Iron and Zinc Transporter Whose Cell-surface Expression Is Up-regulated by Cellular Iron Loading. Journal of Biological Chemistry 287, 34032–34043. https://doi.org/10.1074/jbc.M112.367284

Wang, F., 2004. Acrodermatitis enteropathica mutations affect transport activity, localization and zinc-responsive trafficking of the mouse ZIP4 zinc transporter. Human Molecular Genetics 13, 563–571. https://doi.org/10.1093/hmg/ddh049

Wang, F., Dufner-Beattie, J., Kim, B.-E., Petris, M.J., Andrews, G., Eide, D.J., 2004a. Zinc-stimulated Endocytosis Controls Activity of the Mouse ZIP1 and ZIP3 Zinc Uptake Transporters. Journal of Biological Chemistry 279, 24631–24639. https://doi.org/10.1074/jbc.M400680200

Wang, F., Holmes, M.J., Hong, H.J., Thaprawat, P., Kannan, G., Huynh, M.-H., Schultz, T.L., Licon, M.H., Lourido, S., Dong, W., Brito Querido, J., Sullivan, W.J., O'Leary, S.E., Carruthers, V.B., 2024. Translation initiation factor eIF1.2 promotes Toxoplasma stage conversion by regulating levels of key differentiation factors. Nat Commun 15, 4385. https://doi.org/10.1038/s41467-024-48685-4

Wang, F., Kim, B.-E., Petris, M.J., Eide, D.J., 2004b. The Mammalian Zip5 Protein Is a Zinc Transporter That Localizes to the Basolateral Surface of Polarized Cells. Journal of Biological Chemistry 279, 51433–51441. https://doi.org/10.1074/jbc.M408361200

Wang, H., Wang, M., Wang, B., Li, M., Chen, H., Yu, X., Yang, K., Chai, Z., Zhao, Y., Feng, W., 2012. Immunogold labeling and X-ray fluorescence microscopy reveal enrichment ratios of Cu and Zn, metabolism of APP and amyloid-ß plaque formation in a mouse model of Alzheimer's disease. Metallomics 4, 1113. https://doi.org/10.1039/c2mt20056b

Wang, N., Liang, H., Zen, K., 2014. Molecular Mechanisms That Influence the Macrophage M1â€“M2 Polarization Balance. Front. Immunol. 5. https://doi.org/10.3389/fimmu.2014.00614

Wang, X., Garrick, M.D., Yang, F., Dailey, L.A., Piantadosi, C.A., Ghio, A.J., 2005. TNF, IFN-γ, and endotoxin increase expression of DMT1 in bronchial epithelial cells. American Journal of Physiology-Lung Cellular and Molecular Physiology 289, L24–L33. https://doi.org/10.1152/ajplung.00428.2003

Wang, X., Lorenz, C.D., Hogstrand, C., Maret, W., 2025. Structures and zinc ion transport pathways of the human SLC39A family of metal transporters. https://doi.org/10.1101/2025.08.09.669477

Wang, Z.-D., Wang, S.-C., Liu, H.-H., Ma, H.-Y., Li, Z.-Y., Wei, F., Zhu, X.-Q., Liu, Q., 2017. Prevalence and burden of Toxoplasma gondii infection in HIV-

infected people: a systematic review and meta-analysis. The Lancet HIV 4, e177–e188. https://doi.org/10.1016/S2352-3018(17)30005-X

Weaver, B.P., Dufner-Beattie, J., Kambe, T., Andrews, G.K., 2007. Novel zinc-responsive post-transcriptional mechanisms reciprocally regulate expression of the mouse Slc39a4 and Slc39a5 zinc transporters (*Zip4* and *Zip5*). bchm 388, 1301–1312. https://doi.org/10.1515/BC.2007.149

Weber, R.A., Yen, F.S., Nicholson, S.P.V., Alwaseem, H., Bayraktar, E.C., Alam, M., Timson, R.C., La, K., Abu-Remaileh, M., Molina, H., Birsoy, K., 2020. Maintaining Iron Homeostasis Is the Key Role of Lysosomal Acidity for Cell Proliferation. Molecular Cell 77, 645-655.e7. https://doi.org/10.1016/j.molcel.2020.01.003

Webster, J.P., 2001. Rats, cats, people and parasites: the impact of latent toxoplasmosis on behaviour. Microbes and Infection 3, 1037–1045. https://doi.org/10.1016/S1286-4579(01)01459-9

Weiss, G., Carver, P.L., 2018. Role of divalent metals in infectious disease susceptibility and outcome. Clinical Microbiology and Infection 24, 16–23. https://doi.org/10.1016/j.cmi.2017.01.018

Weiss, G., Goodnough, L.T., 2005. Anemia of Chronic Disease. N Engl J Med 352, 1011–1023. https://doi.org/10.1056/NEJMra041809

Weiss, L.M., Dubey, Jitender.P., 2009. Toxoplasmosis: A history of clinical observations. International Journal for Parasitology 39, 895–901. https://doi.org/10.1016/j.ijpara.2009.02.004

Weiss, L.M., Laplace, D., Takvorian, P.M., Tanowitz, H.B., Cali, A., Wittner, M., 1995. A Cell Culture System for Study of the Development of *Toxoplasma gondii* Bradyzoites. J Eukaryotic Microbiology 42, 150–157. https://doi.org/10.1111/j.1550-7408.1995.tb01556.x

Wessling-Resnick, M., 2015. Nramp1 and Other Transporters Involved in Metal Withholding during Infection. J Biol Chem 290, 18984–18990. https://doi.org/10.1074/jbc.R115.643973

Willemetz, A., Beatty, S., Richer, E., Rubio, A., Auriac, A., Milkereit, R.J., Thibaudeau, O., Vaulont, S., Malo, D., Canonne-Hergaux, F., 2017. Iron- and Hepcidin-Independent Downregulation of the Iron Exporter Ferroportin in Macrophages during Salmonella Infection. Front. Immunol. 8, 498. https://doi.org/10.3389/fimmu.2017.00498

Winterbourn, C.C., 1995. Toxicity of iron and hydrogen peroxide: the Fenton reaction. Toxicology Letters 82–83, 969–974. https://doi.org/10.1016/0378-4274(95)03532-X

Wiuf, A., Steffen, J.H., Becares, E.R., Grønberg, C., Mahato, D.R., Rasmussen, S.G.F., Andersson, M., Croll, T., Gotfryd, K., Gourdon, P., 2022. The two-domain elevator-type mechanism of zinc-transporting ZIP proteins. Sci. Adv. 8, eabn4331. https://doi.org/10.1126/sciadv.abn4331

Wolf, A., Cowen, D., Paige, B.H., 1939. Toxoplasmic encephalomyelitis: III. A new case of granulomatous encephalomyelitis due to a protozoon. Am J Pathol 15, 657-694.11.

Wolff, N.A., Garrick, L.M., Zhao, L., Garrick, M.D., Thévenod, F., 2014. Mitochondria represent another locale for the divalent metal transporter 1 (DMT1). Channels 8, 458–466. https://doi.org/10.4161/19336950.2014.956564

Wong, S.-Y., Remington, J.S., 1994. Toxoplasmosis in Pregnancy. Clinical Infectious Diseases 18, 853–862. https://doi.org/10.1093/clinids/18.6.853

Work, K., Hutchison, W.M., 1969. THE NEW CYST OF TOXOPLASMA GONDII. Acta Pathologica Microbiologica Scandinavica 77, 414–424. https://doi.org/10.1111/j.1699-0463.1969.tb04248.x

Wu, Y., Ying, Z., Liu, J., Sun, Z., Li, S., Liu, Q., 2022. Depletion of Toxoplasma adenine nucleotide translocator leads to defects in mitochondrial morphology. Parasites Vectors 15, 185. https://doi.org/10.1186/s13071-022-05295-7

Wunderlich, J., Kotov, V., Votborg-Novél, L., Ntalla, C., Geffken, M., Peine, S., Portugal, S., Strauss, J., 2024. Iron transport pathways in the human malaria parasite Plasmodium falciparum revealed by RNA-sequencing. Front. Cell. Infect. Microbiol. 14, 1480076. https://doi.org/10.3389/fcimb.2024.1480076

Xu, Z., Wang, P., Wang, H., Yu, Z.H., Au-Yeung, H.Y., Hirayama, T., Sun, H., Yan, A., 2019. Zinc excess increases cellular demand for iron and decreases tolerance to copper in Escherichia coli. Journal of Biological Chemistry 294, 16978–16991. https://doi.org/10.1074/jbc.RA119.010023

Yamamoto, N., Urabe, K., Takaoka, M., Nakazawa, K., Gotoh, A., Haga, M., Fuchigami, H., Kimata, I., Iseki, M., 2000. Outbreak of Cryptosporidiosis after Contamination of the Public Water Supply in Saitama Prefecture, Japan, in 1996. kansenshogakuzasshi 74, 518–526. https://doi.org/10.11150/kansenshogakuzasshi1970.74.518

Yamasaki, S., Sakata-Sogawa, K., Hasegawa, A., Suzuki, T., Kabu, K., Sato, E., Kurosaki, T., Yamashita, S., Tokunaga, M., Nishida, K., Hirano, T., 2007. Zinc is a novel intracellular second messenger. The Journal of Cell Biology 177, 637–645. https://doi.org/10.1083/jcb.200702081

Yambire, K.F., Rostosky, C., Watanabe, T., Pacheu-Grau, D., Torres-Odio, S., Sanchez-Guerrero, A., Senderovich, O., Meyron-Holtz, E.G., Milosevic, I., Frahm, J., West, A.P., Raimundo, N., 2019. Impaired lysosomal acidification triggers iron deficiency and inflammation in vivo. eLife 8, e51031. https://doi.org/10.7554/eLife.51031

Yan, N., 2015. Structural Biology of the Major Facilitator Superfamily Transporters. Annu. Rev. Biophys. 44, 257–283. https://doi.org/10.1146/annurev-biophys-060414-033901

Yanatori, I., Kishi, F., 2019. DMT1 and iron transport. Free Radical Biology and Medicine 133, 55–63. https://doi.org/10.1016/j.freeradbiomed.2018.07.020

Yang, H.-Y., Chien, W.-C., Chung, C.-H., Su, R.-Y., Lai, C.-Y., Yang, C.-C., Tzeng, N.-S., 2021. Risk of dementia in patients with toxoplasmosis: a nationwide, population-based cohort study in Taiwan. Parasites Vectors 14, 435. https://doi.org/10.1186/s13071-021-04928-7

Yang, L., Wang, B., Yang, Z., Zheng, S., Xin, Z., Wu, S., Zou, W., Peng, H., 2024. Toxoplasma gondii infection positively associated with schizophrenia: Evidences from UK Biobank cohort and case-controlled studies. Journal of Psychiatric Research 175, 243–250. https://doi.org/10.1016/j.jpsychires.2024.05.025

Yang, N., Farrell, A., Niedelman, W., Melo, M., Lu, D., Julien, L., Marth, G.T., Gubbels, M.-J., Saeij, J.P., 2013. Genetic basis for phenotypic differences between different Toxoplasma gondii type I strains. BMC Genomics 14, 467. https://doi.org/10.1186/1471-2164-14-467

Yang, Y., Chen, S., Liu, H., Chen, H., Lu, Z., Qiao, G., Xu, J., Qiu, W., Zhuo, R., Han, X., 2025. Plant ZIP transporter: functional analysis on metal uptake,

transport, and homeostasis. Plant Physiology and Biochemistry 229, 110336. https://doi.org/10.1016/j.plaphy.2025.110336

Yang, Y., Wang, P., Guo, J., Ma, T., Hu, Y., Huang, L., Xing, B., He, Y., Xi, J., 2023. Zinc Overload Induces Damage to H9c2 Cardiomyocyte Through Mitochondrial Dysfunction and ROS-Mediated Mitophagy. Cardiovasc Toxicol 23, 388–405. https://doi.org/10.1007/s12012-023-09811-8

Yarovinsky, F., 2014. Innate immunity to Toxoplasma gondii infection. Nat Rev Immunol 14, 109–121. https://doi.org/10.1038/nri3598

Ybañez, R.H.D., Ybañez, A.P., Nishikawa, Y., 2020. Review on the Current Trends of Toxoplasmosis Serodiagnosis in Humans. Front. Cell. Infect. Microbiol. 10, 204. https://doi.org/10.3389/fcimb.2020.00204

Yeh, K., Yeh, M., Mims, L., Glass, J., 2009. Iron feeding induces ferroportin 1 and hephaestin migration and interaction in rat duodenal epithelium. American Journal of Physiology-Gastrointestinal and Liver Physiology 296, G55–G65. https://doi.org/10.1152/ajpgi.90298.2008

Yilmaz, S.M., Hopkins, S.H., 1972. Effects of Different Conditions on Duration of Infectivity of Toxoplasma gondii Oocysts. The Journal of Parasitology 58, 938. https://doi.org/10.2307/3286589

Ying, Z., Yin, M., Zhu, Z., Shang, Z., Pei, Y., Liu, J., Liu, Q., 2024. Iron Stress Affects the Growth and Differentiation of Toxoplasma gondii. IJMS 25, 2493. https://doi.org/10.3390/ijms25052493

Yılmaz, A., Yazıcı, E., Turk, C., 2021. Assessment of seroprevalence of Toxoplasma gondii in blood donors applied to the blood center of Gazi University Hospital. IJM. https://doi.org/10.18502/ijm.v13i2.5986

Yu, F., Zhang, Q., Liu, H., Liu, J., Yang, S., Luo, X., Liu, W., Zheng, H., Liu, Q., Cui, Y., Chen, G., Li, Y., Huang, X., Yan, X., Zhou, J., Chen, Q., 2022. Dynamic O-GlcNAcylation coordinates ferritinophagy and mitophagy to activate ferroptosis. Cell Discov 8, 40. https://doi.org/10.1038/s41421-022-00390-6

Yu, S.-S., Jiang, L.-R., Ling, Y., Qian, Z.-M., Zhou, Y.-F., Li, J., Ke, Y., 2017. Nifedipine Increases Iron Content in WKPT-0293 Cl.2 Cells via Up-Regulating Iron Influx Proteins. Front. Pharmacol. 8. https://doi.org/10.3389/fphar.2017.00060

Yucesan, B., Guldemir, D., Babur, C., Kilic, S., Cakmak, A., 2021. Whole-genome sequencing of a Toxoplasma gondii strain from a Turkish isolate using next-generation sequencing technology. Acta Tropica 218, 105907. https://doi.org/10.1016/j.actatropica.2021.105907

Zackular, J.P., Knippel, R.J., Lopez, C.A., Beavers, W.N., Maxwell, C.N., Chazin, W.J., Skaar, E.P., 2020. ZupT Facilitates Clostridioides difficile Resistance to Host-Mediated Nutritional Immunity. mSphere 5, e00061-20. https://doi.org/10.1128/mSphere.00061-20

Zaidi, A., Singh, K.P., Ali, V., 2017. Leishmania and its quest for iron: An update and overview. Molecular and Biochemical Parasitology 211, 15–25. https://doi.org/10.1016/j.molbiopara.2016.12.004

Zhang, D.-L., Hughes, R.M., Ollivierre-Wilson, H., Ghosh, M.C., Rouault, T.A., 2009. A Ferroportin Transcript that Lacks an Iron-Responsive Element Enables Duodenal and Erythroid Precursor Cells to Evade Translational Repression. Cell Metabolism 9, 461–473. https://doi.org/10.1016/j.cmet.2009.03.006

Zhang, D.-L., Wu, J., Shah, B.N., Greutélaers, K.C., Ghosh, M.C., Ollivierre, H., Su, X., Thuma, P.E., Bedu-Addo, G., Mockenhaupt, F.P., Gordeuk, V.R.,

Rouault, T.A., 2018. Erythrocytic ferroportin reduces intracellular iron accumulation, hemolysis, and malaria risk. Science 359, 1520–1523. https://doi.org/10.1126/science.aal2022

Zhang, T., Kuliyev, E., Sui, D., Hu, J., 2019. The histidine-rich loop in the extracellular domain of ZIP4 binds zinc and plays a role in zinc transport. Biochemical Journal 476, 1791–1803. https://doi.org/10.1042/BCJ20190108

Zhang, T., Liu, J., Fellner, M., Zhang, C., Sui, D., Hu, J., 2017. Crystal structures of a ZIP zinc transporter reveal a binuclear metal center in the transport pathway. Sci. Adv. 3, e1700344. https://doi.org/10.1126/sciadv.1700344

Zhang, T., Sui, D., Hu, J., 2016. Structural insights of ZIP4 extracellular domain critical for optimal zinc transport. Nat Commun 7, 11979. https://doi.org/10.1038/ncomms11979

Zhang, T., Sui, D., Zhang, C., Cole, L., Hu, J., 2020. Asymmetric functions of a binuclear metal center within the transport pathway of a human zinc transporter ZIP4. FASEB J 34, 237–247. https://doi.org/10.1096/fj.201902043R

Zhang, X., Zhang, D., Sun, W., Wang, T., 2019. The Adaptive Mechanism of Plants to Iron Deficiency via Iron Uptake, Transport, and Homeostasis. Int J Mol Sci 20, 2424. https://doi.org/10.3390/ijms20102424

Zhang, Y., Jiang, Y., Gao, K., Sui, D., Yu, P., Su, M., Wei, G.-W., Hu, J., 2023. Structural insights into the elevator-type transport mechanism of a bacterial ZIP metal transporter. Nat Commun 14, 385. https://doi.org/10.1038/s41467-023-36048-4

Zhao, H, Eide, D., 1996. The yeast ZRT1 gene encodes the zinc transporter protein of a high-affinity uptake system induced by zinc limitation. Proc. Natl. Acad. Sci. U.S.A. 93, 2454–2458. https://doi.org/10.1073/pnas.93.6.2454

Zhao, Hui, Eide, D., 1996. The Gene Encodes the Low Affinity Zinc Transporter in. Journal of Biological Chemistry 271, 23203–23210. https://doi.org/10.1074/jbc.271.38.23203

Zhao, M., Zhou, B., 2020. A distinctive sequence motif in the fourth transmembrane domain confers ZIP13 iron function in Drosophila melanogaster. Biochimica et Biophysica Acta (BBA) - Molecular Cell Research 1867, 118607. https://doi.org/10.1016/j.bbamcr.2019.118607

Zhao, N., Gao, J., Enns, C.A., Knutson, M.D., 2010. ZRT/IRT-like Protein 14 (ZIP14) Promotes the Cellular Assimilation of Iron from Transferrin. Journal of Biological Chemistry 285, 32141–32150. https://doi.org/10.1074/jbc.M110.143248

Zheng, X.-N., Sun, L.-X., Elsheikha, H.M., Li, T.-T., Gao, J., Wu, X.-J., Zhang, Z.-W., Wang, M., Fu, B.-Q., Zhu, X.-Q., Wang, J.-L., 2024. A newly characterized dense granule protein (GRA76) is important for the growth and virulence of Toxoplasma gondii. International Journal for Parasitology 54, 109–121. https://doi.org/10.1016/j.ijpara.2023.09.001

Zhitnitsky, D., Lewinson, O., 2014. Identification of functionally important conserved trans-membrane residues of bacterial P_{IB} -type ATPases. Molecular Microbiology 91, 777–789. https://doi.org/10.1111/mmi.12495

Zhong, M., Zhou, B., 2023. Plasmodium yoelii iron transporter PyDMT1 interacts with host ferritin and is required in full activity for malarial pathogenesis. BMC Biol 21, 279. https://doi.org/10.1186/s12915-023-01776-y

Zhong, W., Lafuse, W.P., Zwilling, B.S., 2001. Infection with Mycobacterium avium differentially regulates the expression of iron transport protein mRNA in

murine peritoneal macrophages. Infect Immun 69, 6618–6624. https://doi.org/10.1128/IAI.69.11.6618-6624.2001

Zhu, Q., Zhai, J., Chen, Z., Guo, Z., Wang, N., Zhang, C., Deng, H., Wang, S., Yang, G., 2024. Ferritinophagy: Molecular mechanisms and role in disease. Pathology - Research and Practice 262, 155553. https://doi.org/10.1016/j.prp.2024.155553

Zohn, I.E., De Domenico, I., Pollock, A., Ward, D.M., Goodman, J.F., Liang, X., Sanchez, A.J., Niswander, L., Kaplan, J., 2007. The flatiron mutation in mouse ferroportin acts as a dominant negative to cause ferroportin disease. Blood 109, 4174–4180. https://doi.org/10.1182/blood-2007-01-066068